

RESEARCH ARTICLE

Influence of Ocean Acidification on a Natural Winter-to-Summer Plankton Succession: First Insights from a Long-Term Mesocosm Study Draw Attention to Periods of Low Nutrient Concentrations

Lennart T. Bach^{1*}, Jan Taucher¹, Tim Boxhammer¹, Andrea Ludwig¹, The Kristineberg KOSMOS Consortium¹, Eric P. Achterberg¹, María Algueró-Muñiz², Leif G. Anderson³, Jessica Bellworthy^{1,4}, Jan Büdenbender¹, Jan Czerny¹, Ylva Ericson⁵, Mario Esposito^{1,4}, Matthias Fischer¹, Mathias Haunost¹, Dana Hellemann^{1,6}, Henriette G. Horn², Thomas Hornick⁷, Jana Meyer¹, Michael Sswat¹, Maren Zark⁸, Ulf Riebesell¹

1 GEOMAR Helmholtz Centre for Ocean Research Kiel, Kiel, Germany, **2** Alfred-Wegener-Institut Helmholtz-Zentrum für Polar- und Meeresforschung, Biologische Anstalt Helgoland, Helgoland, Germany, **3** Department of Marine Sciences, University of Gothenburg, Gothenburg, Sweden, **4** Ocean and Earth Sciences, University of Southampton, Southampton, United Kingdom, **5** The University Centre in Svalbard (UNIS), Longyearbyen, Norway, **6** Department of Environmental Sciences, University of Helsinki, Helsinki, Finland, **7** Leibniz Institute of Freshwater Ecology and Inland Fisheries (IGB), Experimental Limnology, Stechlin, Germany, **8** Institute for Chemistry and Biology of the Marine Environment (ICBM), Research Group for Marine Geochemistry (ICBM-MPI Bridging Group), Carl von Ossietzky University, Oldenburg, Germany

[†] Membership of The Kristineberg KOSMOS Consortium is provided in the Acknowledgments.

* lbach@geomar.de



OPEN ACCESS

Citation: Bach LT, Taucher J, Boxhammer T, Ludwig A, The Kristineberg KOSMOS Consortium, Achterberg EP, et al. (2016) Influence of Ocean Acidification on a Natural Winter-to-Summer Plankton Succession: First Insights from a Long-Term Mesocosm Study Draw Attention to Periods of Low Nutrient Concentrations. PLoS ONE 11(8): e0159068. doi:10.1371/journal.pone.0159068

Editor: Arga Chandrashekar Anil, CSIR-National Institute of Oceanography, INDIA

Received: February 3, 2016

Accepted: June 27, 2016

Published: August 15, 2016

Copyright: © 2016 Bach et al. This is an open access article distributed under the terms of the [Creative Commons Attribution License](https://creativecommons.org/licenses/by/4.0/), which permits unrestricted use, distribution, and reproduction in any medium, provided the original author and source are credited.

Data Availability Statement: All relevant data are within the paper and its Supporting Information files.

Funding: Support was provided by the German Federal Ministry of Science and Education (BMBF) in the framework of the BIOACID II project (FKZ 03F06550). U. Riebesell received funding from the Leibniz Award 2012 by the German Science Foundation (DFG). The carbonate chemistry measurements were supported by a grant from the Hasselblad Foundation. M. Zark and T. Hornick were

Abstract

Every year, the oceans absorb about 30% of anthropogenic carbon dioxide (CO₂) leading to a re-equilibration of the marine carbonate system and decreasing seawater pH. Today, there is increasing awareness that these changes—summarized by the term ocean acidification (OA)—could differentially affect the competitive ability of marine organisms, thereby provoking a restructuring of marine ecosystems and biogeochemical element cycles. In winter 2013, we deployed ten pelagic mesocosms in the Gullmar Fjord at the Swedish west coast in order to study the effect of OA on plankton ecology and biogeochemistry under close to natural conditions. Five of the ten mesocosms were left unperturbed and served as controls (~380 μatm pCO₂), whereas the others were enriched with CO₂-saturated water to simulate realistic end-of-the-century carbonate chemistry conditions (~760 μatm pCO₂). We ran the experiment for 113 days which allowed us to study the influence of high CO₂ on an entire winter-to-summer plankton succession and to investigate the potential of some plankton organisms for evolutionary adaptation to OA in their natural environment. This paper is the first in a PLOS collection and provides a detailed overview on the experimental design, important events, and the key complexities of such a “long-term mesocosm” approach. Furthermore, we analyzed whether simulated end-of-the-century carbonate chemistry

supported by the association of European marine biological laboratories (ASSEMBLE, grant no. 227799). E. P. Achterberg received funding from the UK Ocean Acidification research programme (grant no. NE/H017348/1). The funders had no role in study design, data collection and analysis, decision to publish, or preparation of the manuscript.

Competing Interests: The authors have declared that no competing interests exist.

conditions could lead to a significant restructuring of the plankton community in the course of the succession. At the level of detail analyzed in this overview paper we found that CO₂-induced differences in plankton community composition were non-detectable during most of the succession except for a period where a phytoplankton bloom was fueled by remineralized nutrients. These results indicate: (1) Long-term studies with pelagic ecosystems are necessary to uncover OA-sensitive stages of succession. (2) Plankton communities fueled by regenerated nutrients may be more responsive to changing carbonate chemistry than those having access to high inorganic nutrient concentrations and may deserve particular attention in future studies.

1 Introduction

The oceans absorb currently about 2 gigatons carbon as anthropogenic CO₂ per year [1]. In seawater, most of the anthropogenic CO₂ reacts with H₂O to form carbonic acid. The subsequent dissociation of carbonic acid causes a prominent decline in the seawater pH and major shifts in the marine carbonate system—a process called “ocean acidification” [2,3]. Studies investigating the consequences of ocean acidification (OA) for marine life have primarily focused on physiological processes of individual organisms and the experiments were usually conducted with OA-acclimated rather than OA-adapted individuals [4]. However, OA takes place in natural ecosystems with complex species interactions and occurs on timescales long enough to provide the opportunity for evolutionary adaptation [5,6]. Hence, our understanding of OA effects on marine biota must advance from a single species to a whole ecosystem level and our experimental design should ideally consider timescales which cover the entire plankton succession and are long enough to include evolutionary adaptation [7].

So far, OA studies comprising entire ecosystems were primarily focused on benthic habitats near volcanic CO₂ vent sites [8–11] whereas fewer studies have been made in pelagic ecosystems which are more difficult to study due to local displacement of the plankton community [12]. Therefore, much of our understanding on the impacts of OA on plankton communities derives from (short-term) incubation experiments with relatively small volume [13]. These experiments are particularly valuable when aiming to investigate physiological and ecological changes on the lowest trophic levels. However, the duration of such experiments is limited due to technical restrictions with small incubation volumes and they are therefore in most cases inadequate to study an entire plankton succession. Furthermore, they are limited when aiming to unravel the potential consequences of OA-induced changes in the plankton community on key biogeochemical traits such as organic matter export as these investigations require large sample volumes generated by plankton communities representative of the study site. *In-situ* mesocosm experiments with large incubation volumes are one option to bridge this gap as plankton communities can be sustained for long enough time to study the seasonal succession of natural plankton communities in their natural habitat [14] without too much bias towards smaller functional groups [15]. However, *in-situ* long-term studies with large incubation volumes are technically, logistically, and financially challenging and thus require strong institutional support and a well-coordinated collaborative effort of many scientists and technicians. From January to July 2013 we faced this challenge and conducted the “BIOACID II long-term mesocosm study” hosted by the Sven Lovén Centre for Marine Sciences, Kristineberg located on the Skagerrak coast (west coast of Sweden). In total, 55 scientists and technicians from 11 different institutes participated actively in this study with the aim to investigate the impact of

OA on physiological, ecological, evolutionary [16], and biogeochemical processes in a natural winter-to-summer plankton succession.

The present paper is the first within this PLOS collection and has two primary intentions. First, we aim to provide a detailed overview on the study site, starting conditions, background data, and key events during the study, thereby setting the scene for the more specialized papers published within the framework of this mesocosm experiment (a summary of intended publications is provided in [S1 Table](#)). Second, we will investigate on a relatively coarse functional/taxonomic resolution (in this overview paper) whether realistic end of the century carbonate chemistry conditions (i.e. $p\text{CO}_2 = 760 \mu\text{atm}$; [17]) can restructure plankton community composition over the course of a natural winter-to-summer plankton succession. This will help to uncover the critical phases where CO₂ is particularly influential.

2 Materials and Methods

In this study we added herring eggs (*Clupea harengus*) to the mesocosms. Animal welfare was assured according to the ethical permission (number 332–2012), where it is stated that the species used is not endangered and that sacrificed specimens were anaesthetized beforehand with MS-222, so stress was reduced to a minimum.

2.1 The study site

The Gullmar Fjord is located approximately 100 km north of Gothenburg on the Swedish west coast ([Fig 1A](#)). It extends 28 km inland in a north-easterly direction and is about 1–2 km wide ([Fig 1B](#)). It was shaped by a seaward moving glacier which formed the 116 m deep inner basin and the shallower sill (43 m) at the entrance of the fjord ([Fig 1C](#); [18,19]). Water below sill level in the inner basin is filled with relatively saline ($S > 33$) North Sea and/or North Atlantic water which has a prolonged residence time of about one year due to entrapment by the sill barrier ([20]; [Fig 1C](#)). The exchange of water above sill level is considerably faster (16–40 days; [21]). It is primarily driven by wind stress since tidal forcing is usually below 0.2 m in this region [18]. The water column above sill level is composed of three major water bodies: (1) a thin low-salinity top layer (usually less than 1 m) primarily due to freshwater discharge from the Örekil River located at the landward end of the fjord ([Fig 1B](#)); (2) a brackish seawater ($S < 30$) layer fed by the northward moving Baltic current which transports low salinity water from the Baltic proper along the Swedish coast through the Kattegat where it gradually mixes with North Sea water; (3) a marine ($S > 30$) layer fed by North Atlantic and/or North Sea water from the Skagerrak which constitutes the majority of the water on top of the sill and the entrapped basin water. The halocline, separating brackish surface water from underlying marine water, is usually between 5–20 m [18,21,22].

2.2 Mesocosm deployment and initiation of the experiment

On the 29th of January 2013, ten “Kiel Off-Shore Mesocosms for Future Ocean Simulations” (KOSMOS, M1–M10; [23]) were deployed by research vessel *Alkor* close to the fjord entrance at the inner edge of the sill (58° 15.981' N, 11° 28.699' E; [Fig 1](#)) at a water depth of ~60–80 m ([Fig 1](#), [Table 1](#), [Table 2](#)). The cylindrical but initially folded mesocosm bags (2 m diameter) made of thermoplastic polyurethane foil were mounted in 8 m high flotation frames ([Fig 1E](#)). The bags were unfolded immediately after deployment in such a way that the lower opening of the bags reached a depth of 19 m, while the upper opening was positioned 1 m below surface. Both the upper and lower openings were covered with meshes (3 mm mesh size) in order to exclude patchily distributed nekton and large zooplankton like fish larvae or jelly fish from the enclosed water body. On the 12th of February, divers replaced the meshes at the bottom of

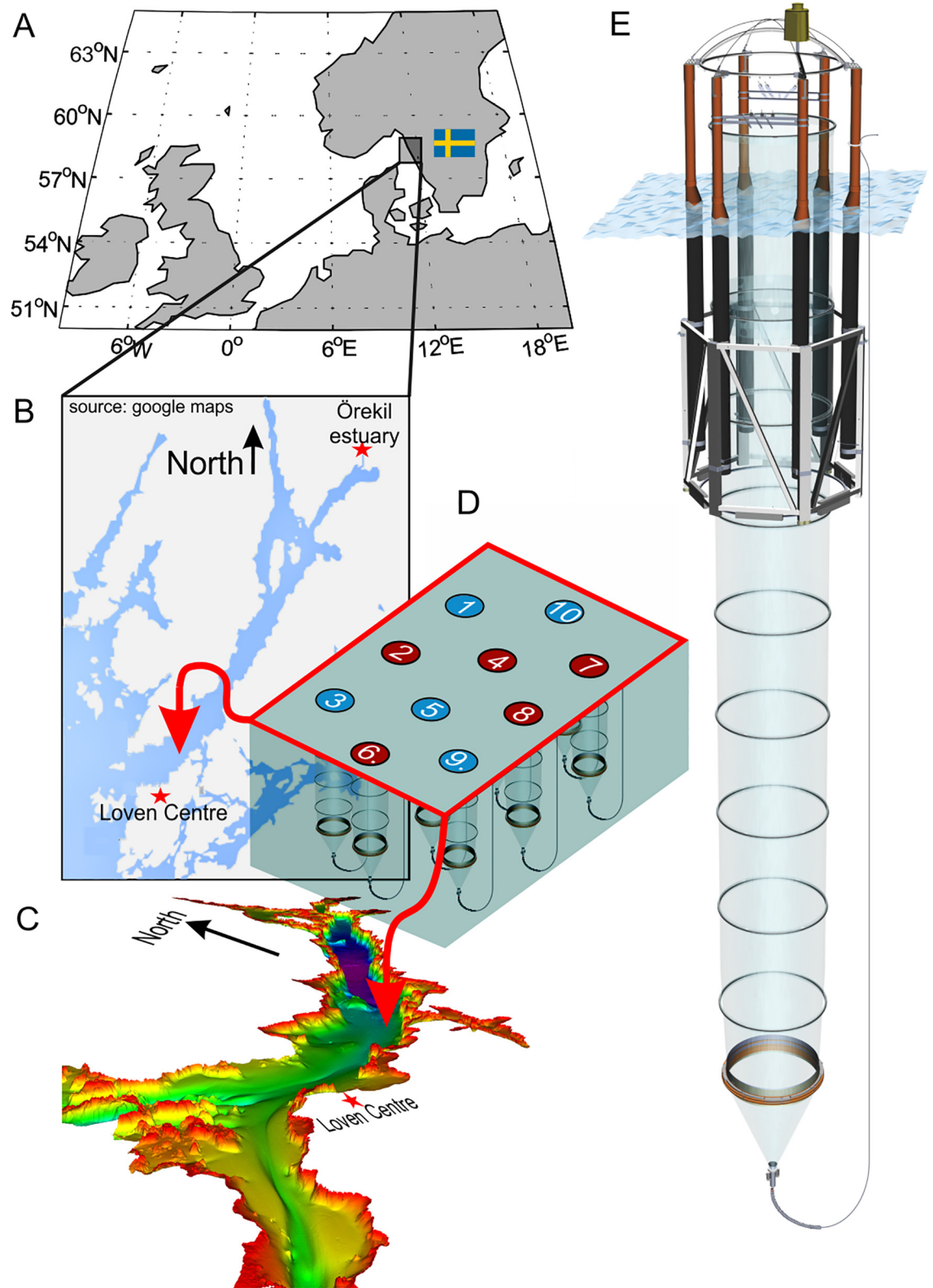


Fig 1. Study site and mesocosm deployment. (A) Map of north-western Europe. The small black square marks the study site off the Swedish west coast. (B) Close-up on the Gullmar Fjord region. (C) Bathymetric map of Gullmar Fjord [19]. The mesocosm deployment site was on the inner edge of the sill, close to the fjord mouth (marked on (B) and (C) by the red arrows). (D) Arrangement of the 10 mesocosms at deployment site (see Table 2 for coordinates). Small numbers inside the circles show mesocosm arrangement (M1-M10) whereas blue and red represent ambient and high CO₂ replicates, respectively. (E) Schematic drawing of a mesocosm unit. The floatation frame is 8 m high. The bag without sediment trap extends 17 m below sea surface and has a diameter of 2 m. The sediment trap is attached to the bag with a flange ring and reaches down to 19 m water depth.

doi:10.1371/journal.pone.0159068.g001

mesocosm bags with 2 m long conical sediment traps thereby sealing the bottom of the mesocosms. Simultaneously, the boat crew pulled the upper part of the bags above the sea surface so that the water body within mesocosms was isolated from this time onwards (Fig 1E) and the experiment started (Table 1). Mesocosm closing lasted for less than 1 hour in total, thereby minimizing differences between the enclosed water in each mesocosm.

On the 3rd of March we had to stop the experiment and recover the sediment traps due to technical problems (see section 3.1.1 for reasons and 3.2.1 for biological consequences). Therefore, mesocosm bags were lowered below surface to allow water exchange with the fjord. After repairing the sediment traps they were re-installed and all mesocosms were closed again on the 7th of March as described above but without the use of the 3 mm meshes. Instead, a mesh with 1 mm mesh size was attached to the cleaning ring on day 6 (Table 1; cleaning ring application described in section 2.4) and passed through the mesocosms to remove large and often patchily distributed zooplankton and nekton. Very few organisms were caught, however, in this operation. The 7th of March marks the beginning of the second experiment, which lasted for 113 days from t-2 until t111 (Table 1).

2.3 Mesocosm CO₂ manipulations and salt additions

Five of the ten mesocosms (M1, M3, M5, M9, M10) were untreated controls while the other five (M2, M4, M6, M7, M8) were manipulated by adding CO₂-saturated seawater [23]. In this manipulation technique, a filtered (20 μm) Gullmar Fjord surface water volume of about 1500 L is aerated with pure CO₂ gas for about 1 hour to reach pH_{NBS} ~4 and subsequently transferred into smaller bottles of ~25 L which are closed airtight, without headspace, to avoid degassing. These bottles were transported to the mesocosms by boat where the aerated water was pumped into the high CO₂ mesocosms through a distribution device which we call “the spider” as it has multiple small tubes which disperse the volume evenly within a radius of ~1 m. By pulling the spider up and down within each mesocosm, we ensured homogenous CO₂ enrichment throughout the entire water column. Target pCO₂ was reached initially by CO₂ additions on four consecutive days with the first one being on the 8th of March (t-1). Further CO₂ additions in the course of the experiment were made on a regular basis to account for CO₂ loss through outgassing (Table 1).

Adding precise known amounts of saturated NaCl brine to the mesocosms can be used to determine their volume as it is proportional to the measurable change in salinity [24]. Saturated NaCl brine was generated by dissolving 300 kg of NaCl in 1000 L of filtered (20 μm) Gullmar Fjord surface water. The brine was subsequently filled into 25 L bottles and evenly dispersed in the mesocosms on the 24th of April (t46) with the spider as described above. For a detailed description of the procedure please refer to Czerny et al. [24].

2.4 Mesocosm cleaning

The mesocosm bags had to be cleaned from the in- and outside on a regular basis to avoid growth of a benthic community on the bags, which consume nutrients and reduce photon flux

Table 1. Sampling and maintenance schedule during the mesocosm study.

Date	t day	STS	WCS	CTD	net haul	CLEAN	seed	Event
23/01/2013	t-45							Arrival of RV Alkor on study site
29/01/2013	t-39							Deployment of all 10 mesocosms in Gullmar Fjord (exact location shown in Fig 1)
12/02/2013	t-25							Closing all 10 mesocosms (i.e. start of the failed experiment)
03/03/2013	t-6							Opening all 10 mesocosms (i.e. end of the failed experiment)
06/03/2013	t-3					█		Cleaning of mesocosm bags and servicing of sediment traps on shore
07/03/2013	t-2			█				Closing all 10 mesocosms (i.e. start of the successful experiment), mixing water column (5 minutes), hole detected in M1
08/03/2013	t-1	█	█	█	█ 1			1 st CO ₂ enrichment
09/03/2013	t0			█				Mixing water column (4 minutes), 2 nd CO ₂ enrichment, N ₂ O tracer addition (M3, M5, M7, M8)
10/03/2013	t1	█	█	█	█ 2			Hole detected in M8
11/03/2013	t2							Sampling (15 L) for nutrients and microzooplankton grazing incubations, 3 rd CO ₂ enrichment, mixing M8 for 5 minutes with subsequent CTD cast to spot the hole, hole detected in M1
12/03/2013	t3	█	█	█	█ 1			Diving with rebreather inside M1 and M8 and fixing holes of both mesocosms from the outside.
13/03/2013	t4							4 th CO ₂ enrichment
14/03/2013	t5	█	█	█				
15/03/2013	t6					█		While cleaning a 1 mm mesh was attached to the cleaning ring to remove fish larvae and jelly fish, outside cleaning (0–1.5 m)
16/03/2013	t7	█	█	█			█	
17/03/2013	t8							
18/03/2013	t9	█	█	█	█ 1			
19/03/2013	t10							
20/03/2013	t11	█	█	█	█ 1		█	
21/03/2013	t12							Deployment of benthos and biofilm plates in all mesocosms, diving with rebreather inside M6 to recover lost device
22/03/2013	t13	█	█	█				
23/03/2013	t14					█		Outside cleaning (1.5–8 m)
24/03/2013	t15	█	█	█			█	
25/03/2013	t16							
26/03/2013	t17	█	█	█	█ 2			5 th CO ₂ enrichment
27/03/2013	t18							Outside cleaning (0–1.5 m), sampling for microzooplankton grazing experiments

(Continued)

Table 1. (Continued)

Date	t day	STS	WCS	CTD	net haul	CLEAN	seed	Event
28/03/2013	t19				2			
29/03/2013	t20							
30/03/2013	t21							
31/03/2013	t22							
01/04/2013	t23							
02/04/2013	t24							
03/04/2013	t25				3			
04/04/2013	t26							Biofilm sampling
05/04/2013	t27				1			
06/04/2013	t28							Outside cleaning (3–5 m)
07/04/2013	t29							
08/04/2013	t30							
09/04/2013	t31							Installation of light and temperature loggers in M4 and M10
10/04/2013	t32							Sampling of 40 L for light stress experiments, recovery of light and temperature loggers
11/04/2013	t33				3			
12/04/2013	t34							Sampling for microzooplankton grazing incubations (15 L)
13/04/2013	t35							Sediment trap collector of M5 was opened for ~1 min to recover a lost device
14/04/2013	t36							
15/04/2013	t37							Establishment of thermal stratification (Fig 5)
16/04/2013	t38							N ₂ O tracer addition to M3, M5, M7, and M8
17/04/2013	t39				1			
18/04/2013	t40							
19/04/2013	t41							Sediment trap collector of M2 was opened for ~1 min to remove clogging
20/04/2013	t42							
21/04/2013	t43							Biofilm sampling
22/04/2013	t44							Outside cleaning (6–8 m)

(Continued)

Table 1. (Continued)

Date	t day	STS	WCS	CTD	net haul	CLEAN	seed	Event
23/04/2013	t45							
24/04/2013	t46							6 th CO ₂ enrichment, 1 st brine (NaCl) addition to all mesocosms for volume determination, hole detected in M2
25/04/2013	t47							Hole fixed in M2
26/04/2013	t48							7 th CO ₂ enrichment, addition of herring egg incubators at 3 m depth
27/04/2013	t49				2			
28/04/2013	t50							
29/04/2013	t51							
30/04/2013	t52							
01/05/2013	t53							Lowering herring egg incubators from 3 to 6 m depth, hole detected in M9
02/05/2013	t54							
03/05/2013	t55							
04/05/2013	t56							Addition of sea urchin larvae, biofilm sampling
05/05/2013	t57				2			
06/05/2013	t58							Hole fixed in M9
07/05/2013	t59				2			
08/05/2013	t60							Outside cleaning (5–7 m)
09/05/2013	t61							
10/05/2013	t62							Biofilm sampling
11/05/2013	t63							Peak hatch of herring larvae
12/05/2013	t64							Recovery of herring egg incubators
13/05/2013	t65				2			
14/05/2013	t66							Diving with rebreather in M9, deployment of temperature and light loggers in M4 and M10
15/05/2013	t67							
16/05/2013	t68							Biofilm sampling, 8 th CO ₂ enrichment
17/05/2013	t69							
18/05/2013	t70							

(Continued)

Table 1. (Continued)

Date	t day	STS	WCS	CTD	net haul	CLEAN	seed	Event
19/05/2013	t71							
20/05/2013	t72							Outside cleaning (0–1.5 m)
21/05/2013	t73				2			
22/05/2013	t74							
23/05/2013	t75							
24/05/2013	t76				1			Outside cleaning (15–17 m)
25/05/2013	t77							
26/05/2013	t78							Biofilm sampling
27/05/2013	t79							
28/05/2013	t80							Outside cleaning (3–5 m)
29/05/2013	t81				2			Biofilm sampling
30/05/2013	t82							Outside cleaning (5–10 m)
31/05/2013	t83							
01/06/2013	t84							Outside cleaning (10–12 m)
02/06/2013	t85							
03/06/2013	t86							Outside cleaning (12–14 m)
04/06/2013	t87							
05/06/2013	t88							9 th CO ₂ enrichment
06/06/2013	t89				2			
07/06/2013	t90							
08/06/2013	t91							
09/06/2013	t92							
10/06/2013	t93							
11/06/2013	t94							
12/06/2013	t95							
13/06/2013	t96				2			Net hauls with a 10 µm net, biofilm sampling

(Continued)

Table 1. (Continued)

Date	t day	STS	WCS	CTD	net haul	CLEAN	seed	Event
14/06/2013	t97				2			
15/06/2013	t98							Outside cleaning (8–10 m)
16/06/2013	t99							
17/06/2013	t100							
18/06/2013	t101							
19/06/2013	t102							Cleaning inner part of the sediment traps from the outside with magnetic brushes
20/06/2013	t103				1		μ	One net haul with 10 μm net
21/06/2013	t104							A 1 mm mesh was attached to the cleaning ring to recover herring larvae
22/06/2013	t105							Hole detected in M8 and M9
23/06/2013	t106							Hole fixed in M8 but not in M9
24/06/2013	t107				2			
25/06/2013	t108				8			All net hauls with 10 μm net
26/06/2013	t109							
27/06/2013	t110							Biofilm sampling
28/06/2013	t111							End of the experiment

Days of experiment (t days) relate to the day where the water column was fully homogeneous after mixing (t0). Filled grey areas are events of: Sediment trap sampling (STS), water column sampling (WCS), CTD casts, net hauls (with the number indicating how many net hauls were done), cleaning the inside of the mesocosm bags (CLEAN), and water column seeding (seed).

doi:10.1371/journal.pone.0159068.t001

density inside the mesocosms. The outside of the bags was cleaned on a regular basis (Table 1) with brushes, either by boat crews (0–1 m depth) or by divers (1–19 m). The inside was cleaned down to the last segment of the bag with a cleaning ring specifically designed for this purpose [23]. Inside cleaning of the bags was conducted approximately every eighth day (Table 1) to disturb fouling by benthic organisms in very early stage of their succession. The inner side of the lowest segment and of the sediment trap was only cleaned at the very end of the experiment (t102). Note, however, that fouling by algae and epiphytes is reduced at this depth as the photon flux density reaching the sediment trap is fairly low and most large heterotrophs like mussels or barnacles do not attach to the flexible bag material.

2.5 Addition of organisms

Some organisms, characteristic for a winter-to-summer succession in this region may not have been present in the water column by the time the mesocosms were closed. We accounted for this problem by adding fjord water to the mesocosms every fourth day (Table 1) allowing

Table 2. Overview of mesocosm setup.

Mesocosm	mooring position		Enclosed water mass		Mean pCO ₂ (µatm)				
	North	East	weight (ton)	estimated influx through holes (% of total volume)	phase I	phase II	phase III	phase IV	total
M1	58° 16.008'	11° 28.680'	51.3	2.4 (t-1—t3)	370	318	341	425	365
M2	58° 15.995'	11° 28.659'	55.9	2.8 (t39—t45)	745	629	759	864	759
M3	58° 15.983'	11° 28.639'	47.5		365	342	385	472	398
M4	58° 15.981	11° 28.699'	51.6		754	615	719	865	744
M5	58° 15.969'	11° 28.678'	47.9		366	346	393	481	404
M6	58° 15.955'	11° 28.660'	51.4		765	640	731	857	753
M7	58° 15.972'	11° 28.767'	49.1		779	637	745	876	765
M8	58° 15.961'	11° 28.745'	53.1	3 (t0—t5), 0.2 (t105)	765	686	754	865	773
M9	58° 15.949'	11° 28.727'	50.0	1.9 (t53—t63), 0.3 (t105—t111)	361	321	374	471	389
M10	58° 15.993'	11° 28.720'	49.6		367	316	335	423	362

The volume of water enclosed in each mesocosm was determined on t46 of the experiment. pCO₂ values are averages of the four phases and means over the entire study (total).

doi:10.1371/journal.pone.0159068.t002

plankton organisms to enter the mesocosm community. Seeding water was collected at deployment site with a submersible pump which was lowered steadily to 19 m depth in about 5 minutes, thereby transferring about 300 L of seawater into a large container placed on the sampling boat. The collected seawater was subsequently stirred carefully so that all organisms were distributed homogeneously within the 300 L batch. 22 L of the stirred seawater (i.e. ~0.44 % of the total mesocosm volume) was then added to each mesocosm with a bucket which was lowered to the water surface inside the mesocosms and emptied carefully. In total, 550 L fjord water was added to each mesocosm on 25 occasions (Table 1) which sums up to ~1% of the mesocosms' volume.

Next to smaller planktonic organisms, we also added herring (*Clupea harengus*) and green sea-urchin (*Strongylocentrotus droebachiensis*) larvae to each mesocosm. Both species were released in relatively low densities (~90 herring eggs and 110 sea urchin larvae per m³) to minimize potential top-down-effects. Herring eggs were stuck on plastic plates and mounted in the middle of the cylindrical bags at 3 m depth from day 48 until peak hatching on day 63. Herring larvae started feeding on (most likely) copepod-nauplii and ciliates after the yolk-sac stage at around day 71, switching to bigger prey with growing size. Larvae of the green sea urchin were grown in the laboratory following Dorey et al. [25] until reaching the swimming gastrula stage and then gently added to the mesocosms on day 56 with a bucket in the same way as the seeding water.

2.6 Sampling and CTD operations

Sinking detritus was collected in the sediment traps at the bottom of the mesocosms. To avoid resuspension of the material we emptied the sediment traps before water column sampling

using a vacuum system connected to a tube which was attached to the collecting cups following Boxhammer et al. [26].

Water column samples were collected every second day at 9 a.m. (local time) with “integrating water samplers” (IWS, Hydrobios) that sample a total volume of 5 L from 0–17 m depth evenly through the water column. The number of IWS hauls per mesocosm varied between sampling days but generally ranged between 4 and 8. More volume was needed on days when incubation experiments were conducted on shore. The volume of 2–4 IWS hauls was pooled in 1–2 ten liter carboys per mesocosm onboard the sampling boat. This water was later used for particulate matter (PM) analysis, pigment analysis, flow cytometry, and phytoplankton/microzooplankton microscopy. All carboys were stored in the dark on the boats until sampling was finished (usually between 10 and 12 a.m. local time) and then transferred into a temperature-controlled room on shore (set to in-situ temperature) where subsamples were taken (section 2.7). The volume of the remaining IWS hauls was used for gas or easily contaminable samples, which were transferred into separate sampling bottles on the sampling boats. These sensitive samples were: dissolved inorganic carbon (DIC), pH, halocarbons, nitrous oxide (N₂O), inorganic nutrients (nitrate (NO₃⁻), nitrite (NO₂⁻), dissolved silicate (Si(OH)₄), ammonium (NH₄⁺), phosphate (PO₄³⁻), dissolved organic carbon/nitrogen (DOC, DON), and water for all *in vitro* incubation experiments such as primary production (¹⁴C) or bacterial protein production assays.

Gas and incubation samples were carefully transferred from the IWS into gas tight sampling bottles with TYGON tubes placed at the bottom of the bottle. Sample bottles were then filled bottom to top avoiding air bubbles and allowing an overflow of twice the bottle volume before they were closed without headspace. All bottles were rinsed with sample water before the actual sample was taken. Inorganic nutrient samples were filled into 200 mL acid washed (10% HCl) PVC bottles. Samples for DOC and DON determination were transferred from IWS into pre-combusted (400°C, 4 h) glass vials (Whatman), after filtration through pre-combusted glass fibre filters (GF/F, nominal pore size 0.7 μm, Whatman). All samples tapped from the IWS on board were stored in boxes and in the shade until sampling was finished.

Zooplankton samples were collected around 3 p.m. (local time) with an Apstein net (0.17 m diameter opening, 55 μm mesh size except for two occasions with 10 μm mesh size; Table 1) on a weekly basis. The maximum sampling depth was 17 m to avoid contact of the Apstein net with the sediment traps. Sampling frequency was restricted to low numbers (usually 1–3) of net hauls per sampling day (usually every 8th day) to avoid overfishing (Table 1). Zooplankton hauls were transported to shore directly after sampling where they were preserved with sodium tetraborate-buffered formalin (4% v/v) for counting and taxonomic analyses.

Depth profiles of salinity, temperature, pH, chlorophyll *a* (chl_a), and photosynthetically active radiation (PAR) were measured with a CTD60M (Sea & Sun Technologies) on every sampling day. CTD casts within each mesocosm were typically conducted after sediment trap and water column sampling between 11 a.m and 3 p.m. (local time, Table 1). Sensor details of the CTD60M and data analysis procedures for salinity, temperature, and density were described by Schulz and Riebesell [27]. Correction of pH CTD data is described in the following section.

2.7 Sample processing, measurement, and analysis

Inorganic nutrient samples were filtered (cellulose acetate filters, pore size 0.45 μm; Whatman) directly after sampling and analyzed on the same day to avoid any possibility of concentration changes due to biological growth or decay. NO₃⁻ + NO₂⁻ (= NO₃⁻/NO₂⁻), Si(OH)₄, and PO₄³⁻ concentrations were measured with a SEAL Analytical QuAAtro AutoAnalyzer connected to

JASCO Model FP-2020 Intelligent Fluorescence Detector and a SEAL Analytical XY2 autosampler. When NO₃⁻/NO₂⁻ and PO₄³⁻ concentrations dropped below 0.1 μM during the phytoplankton bloom we switched to using the nanomolar system with a detection limit of 0.8 nM PO₄³⁻ and 1.5 nM NO₃⁻/NO₂⁻, as reported by Patey et al. [28]. Both methods were used in parallel during the transition phase (days 31–41) for inter-comparison (average deltas of the measurements were ±4.5 nM for NO₃⁻/NO₂⁻ and ±2.9 nM for PO₄³⁻). Both measurement approaches are based on spectrophotometric techniques developed by Murphy and Riley [29] and Hansen and Grasshoff [30]. Ammonium concentrations were determined fluorometrically following Holmes et al. [31]. Instrument precision was calculated from the average standard deviation (1σ) of triplicate samples (±0.02 μM for NO₃⁻/NO₂⁻, ±0.01 μM for PO₄³⁻, ±0.05 μM for Si(OH)₄ and ±0.01 μM for NH₄⁺). Analyzer performance was monitored by recording baseline, calibration coefficients and slopes of the nutrient species over time. The variations observed throughout the experiment were within the analytical error of the methods.

DOC and total dissolved nitrogen (TDN) concentrations were measured by high-temperature catalytic oxidation on a Shimadzu TOC-VCPH analyzer with ASI-V auto sampler as described by Zark et al. [32]. The DON concentration was calculated as TDN–(NO₃⁻/NO₂⁻ + NH₄⁺).

Carbonate chemistry samples were sterile-filtered (0.2 μm) with syringe filters into two separate 300 mL Schott DURAN glass bottles (pH, DIC) allowing an overflow of twice the bottle volumes. Sterile-filtered subsamples were stored at 4°C in the dark for a maximum of three days until analysis. DIC was determined by the colorimetric titration method established by Johnson et al. [33], with a precision of 3.0 μmol kg⁻¹ (estimated from duplicates). The accuracy was set by calibration against certified reference materials, supplied by A. Dickson, Scripps Institution of Oceanography (USA). pH_T (total scale) was determined by a spectrophotometric method, based on the absorption ratio of the sulfonephthalein dye, *m*-cresol purple [34], with a precision of ~0.002 pH_T units and accuracy set by the equilibrium constants of the indicator. *p*CO₂ and aragonite saturation state (Ω_{aragonite}), were calculated from the combination of pH_T and DIC using CO2SYS (excel version 2.1 [35]) with the carbonate dissociation constants (K₁ and K₂) of Lueker et al. [36]. Input data included salinity, temperature, PO₄³⁻ and Si(OH)₄ data, where the latter two were from the previous sampling day in the few cases of missing nutrient data. For calculation of [HCO₃⁻]/[H⁺] (proton concentration on free scale), measured pH_T was converted to the free scale using CO2SYS. pH profiles measured with the CTD were originally on the NBS scale. Thus, the mean pH_{NBS} averaged over the whole water column had an offset compared to spectrophotometrically measured pH_T values. We corrected this offset and recalibrated the CTD probe to the total pH scale by means of daily linear correlation between averaged water column pH_{NBS} measured in-situ and pH_T measured in the laboratory.

The PM samples were filtered using 200 mbar on cellulose acetate (biogenic silica (BSi)) or glass fiber filters (total particulate carbon (TPC), total particulate nitrogen (TPN)). All glass fiber filters and glass petri dishes for filter storage were precombusted (450°C, 6 h) prior to use, in order to remove residual organic matter. The PM samples were stored at -20°C in plastic (BSi) or glass Petri dishes (TPC, TPN) until analyses. Filters for BSi analysis were heated in 0.1 M NaOH (85°C, 135 minutes) to leach the particulate silica from the filters. After neutralizing with 0.05 M H₂SO₄, samples were analysed as dissolved silicate by spectrophotometry according to Hansen and Koroleff [37]. TPC and TPN samples were dried (60°C) over night and wrapped in tin foil before measurement with an elemental CN analyzer following Sharp [38].

Samples for pigment analysis were filtered on glass fibre filters (800 mL, gentle vacuum of ~200 mbar), carefully folded, and immediately frozen and stored at -80°C in cryovials. Pigments were extracted 4–7 months after sampling in acetone (90%) as described by Paul et al. [14]. Pigment extracts were used for analysis by means of reverse phase high performance liquid chromatography (HPLC, [39]) and their concentrations were calibrated with commercial

standards. Contributions of individual phytoplankton groups to total *chl a* concentrations were calculated with CHEMTAX [40].

Flow cytometry samples for phytoplankton, bacteria, and virus abundances as well as microzooplankton samples (20–200 μm; mostly ciliates) were taken from the 10 L carboys directly after the boats returned from mesocosm sampling. Care was taken that the volume within the 10 L carboys was gently mixed before sub-sampling in order to avoid sinking bias. Bacteria and virus samples were immediately fixed with glutaraldehyde (0.5% v/v; 30 minutes), flash-frozen in liquid nitrogen, and stored at -80°C until analysis 4–7 months later with an Accuri C6 flow cytometer (BD Biosciences). For more details on the applied preservation and measurement procedures please refer to the protocols by Marie et al. [41] Larsen et al. [42], and Brussaard [43]. Phytoplankton samples were measured within three hours after sub-sampling with the Accuri C6 flow cytometer. Gates were set based on the forward scatter signal or red fluorescence signals except for the *Synechococcus* and cryptophyte-like groups where the orange instead of the red fluorescence signal was used to distinguish them from bulk phytoplankton. The size of different phytoplankton groups was determined by fractionation with a variety of polycarbonate filters (0.2, 0.8, 2, 3, 5, 8 μm) following Veldhuis and Kraay [44]. We distinguished between picoeukaryotes (Pico; 0.2–2 μm), small nanoautotrophs (Nano I; 0.2–8 μm), *Synechococcus*-like autotrophs (Syneco; 0.2–2 μm), and cryptophyte-like autotrophs (Crypto; 0.2–8 μm). Note that larger species like chain-forming diatoms which could potentially interfere with flow cytometry measurements were almost absent in the water column (as determined by light microscopy). It is therefore safe to assume that the flow cytometry measurements are representative for the size spectrum <200 μm. Autotrophs larger >200 μm, represented by the large diatom *Coscinodiscus* sp. were present in this experiment in considerable quantity. Their abundance was determined by photographing TPC/TPN and BSi, filters and counting cells manually using ImageJ. Microzooplankton samples were immediately fixed after sub-sampling with acidic Lugol solution and stored in 250 mL brown glass bottles until analysis. Based on *chl a* data it was decided to evaluate microzooplankton samples on a weekly basis until t73 and every second week thereafter (t73 –t103). Metazoan abundances (mostly copepods) from net haul samples (> 55 μm) were counted with a binocular microscope. Both microzooplankton and metazoan abundance were determined 3–12 months after sampling.

2.8 Data analyses

We applied ANalysis Of SIMilarity (ANOSIM; [45]) to determine whether significant differences in the plankton community composition were present between ambient (M1, M3, M5, M9, M10) and high CO₂ mesocosms (M2, M4, M6, M7, M8). To account for the different scales in abundance of different organism groups, ranging from viruses to mesozooplankton, ANOSIM input data was “range normalized” as:

$$N_{normalized} = \frac{N}{N_{max} - N_{min}} \quad (1)$$

where N is the abundance of the individual groups, and max and min refer to the highest and lowest abundance measurement among the 10 mesocosms, respectively. The normalized data from 4 selected stages of succession was then used to generate four different Bray-Curtis dissimilarity matrices. The selected stages of succession were: (1) the beginning of the study (Table 3); (2) the individual peak *chl a* concentration for each mesocosm between t27 and t35 (S2 Table); (3) the individual peak *chl a* concentration for each mesocosm between t45 and t59 (S3 Table). Note that the days of highest *chl a* concentration (i.e. bloom peak) differed slightly among mesocosms so that plankton abundances used in the analysis were not always from the

Table 3. Chemical and biological conditions at the beginning of the experiment.

parameter	average of	low CO ₂								high CO ₂								T-test	correlation with salinity (p-value)
		M1	M3	M5	M9	M10	mean low CO ₂	S.D. low CO ₂	M2	M4	M6	M7	M8	mean high CO ₂	S.D. high CO ₂				
salinity	10, 11	29.03	29.16	29.26	29.26	29.91	29.12	0.15	29.16	29.96	29.11	29.16	29.19	29.12	0.09	0.93			
⁹ DIC (μmol kg ⁻¹)	t-1	2072.2	2073.4	2079.3	2065.2	2073.4	2072.7	5.0	2066.0	2077.4	2075.7	2080.3	2075.9	2075.1	5.4	0.49	0.713		
⁹ pH _{total} (spectrophotometer)	t-1	8.096	8.059	8.046	8.038	8.063	8.061	0.022	8.058	8.063	8.062	8.046	8.037	8.053	0.011	0.51	0.046		
NO ₃ ⁻ + NO ₂ ⁻ (μmol L ⁻¹)	12–111	6.89	6.70	6.81	6.73	6.80	6.79	0.07	6.73	6.68	6.75	6.76	6.69	6.72	0.04	0.12	0.605		
Si(OH) ₄ (μmol L ⁻¹)	12–111	10.33	10.01	9.80	9.68	9.57	9.88	0.30	9.94	9.84	9.78	9.65	9.75	9.79	0.11	0.57	0.833		
PO ₄ ³⁻ (μmol L ⁻¹)	12–111	0.76	0.76	0.76	0.76	0.77	0.76	0.007	0.74	0.74	0.76	0.76	0.75	0.75	0.010	0.11	0.915		
DOC (μmol L ⁻¹)	t-1–111	185	180	173	179	200	184	10	191	182	182	184	184	185	4	0.85	0.033		
DON (μmol L ⁻¹)	13–111	16	16	16	15	15	15.6	0.4	15	16	16	16	16	15.7	0.4	0.96	0.873		
POC (μmol L ⁻¹)	t-1–13	13.8	14.2	16.1	14.7	13.3	14.4	1.1	13.2	14.3	14.4	15.7	15.5	14.6	1.0	0.77	0.056		
PON (μmol L ⁻¹)	t-1–13	2.0	2.1	2.3	1.8	1.9	2.0	0.2	2.0	2.0	2.0	2.3	2.1	2.1	0.2	0.56	0.331		
chlorophyll a (ng L ⁻¹)	t-1	315	322	271	304	317	306	21	282	303	299	314	324	304	16	0.89	0.324		
*Coccolinodiscus (cells L ⁻¹)	t-1–17	0.9	1.7	1.5	0.9	1.1	1.21	0.35	1.3	1.6	1.7	1.4	1.1	1.44	0.24	0.26	0.973		
Prasinophytes (ng chl a L ⁻¹)	t-1	175	165	154	157	154	161	9	150	167	161	169	181	166	12	0.52	0.822		
Dinophytes (ng chl a L ⁻¹)	t-1	26	19	17	16	16	19	4	16	19	22	14	18	18	3	0.75	0.410		
Diatoms (ng chl a L ⁻¹)	t-1	35	43	21	52	63	43	16	30	35	29	48	51	39	10	0.65	0.467		
Cryptophytes (ng chl a L ⁻¹)	t-1	75	92	76	74	82	80	8	83	78	84	79	70	79	5	0.81	0.640		
Chrysophytes (ng chl a L ⁻¹)	t-1	4	4	3	5	3	4	1	3	3	4	4	4	3	0	0.50	0.273		
*Pico (cells mL ⁻¹)	t-1	16980	18155	16980	18428	17750	17659	665	18942	19578	18393	19494	19472	19176	505	0.00	0.976		
*Nano (cells mL ⁻¹)	t-1	1606	1333	1606	1520	1586	1530	116	1526	1779	1598	1882	1805	1718	150	0.06	0.692		
*Crypto (cells mL ⁻¹)	t-1	178	160	178	170	152	167	12	190	181	166	271	193	200	41	0.15	0.502		
*Syneco (cells mL ⁻¹)	t-1	887	916	887	951	834	895	43	828	934	834	891	1003	898	73	0.93	0.348		
*Bacteria (cells mL ⁻¹)	t-1	817580	832881	869058	862507	895435	85452	30767	838855	881913	873826	870391	902652	873528	23080	0.32	0.693		
*Virus like particles (ind mL ⁻¹)	t-1	10245000	8855714	10220714	9600714	12061429	10196714	1186756	9945000	8600714	9195000	10329286	10530714	9720143	807394	0.48	0.518		
<i>Pseudocalanus</i> (male) (ind m ⁻³)	t1	3752	2107	2742	4012	5772	3677	1401	2511	3203	3001	3679	4012	3261	570	0.56	0.152		
* <i>Pseudocalanus</i> (female) (ind m ⁻³)	t1	7071	3810	5339	6955	9380	6511	2086	5166	6898	5281	5743	6955	6009	865	0.63	0.072		
* <i>Pseud</i> Copepodites (ind m ⁻³)	t1	3001	2559	2597	2039	3925	2824	704	2732	2771	2386	2771	2039	2540	323	0.43	0.008		
*Nauplii (ind m ⁻³)	t1	1655	2097	1924	1655	1732	1812	194	1597	2347	1789	1501	1655	1778	335	0.85	0.408		
*Ciliates (cells mL ⁻¹)	t-1	2.9	3.1	2.5	3.5	1.9	2.8	0.6	2.5	2.9	3.1	2.0	2.2	2.5	0.5	0.46	0.477		

Values are either the first measurements or an average of measurements from the first couple of days. For the community-based analysis we generally included functional groups rather than species. For copepods, we only included *Pseudocalanus* sp. here since this species strongly dominated the copepod community both in abundance and biomass (note, however, that “nauplii” includes copepod nauplii from all species since they were not distinguished taxonomically). Parameters marked with an asterisk were used in the ANOSIM/NMDS analysis (Fig 8A). Bold values indicate statistical significance (p = <0.05).

^a prior to the first CO₂ addition

doi:10.1371/journal.pone.0159068.t003

same days (see [S2](#) and [S3](#) Tables). (4) The post-bloom period for which we calculated the average values of plankton abundances for the period from t81 to t111 ([S4 Table](#)). A significant ANOSIM result ($p < 0.05$) indicates an effect of CO₂ on the composition of the entire plankton community, i.e. that communities within the ambient CO₂ mesocosms were more similar to each other than to the communities in the high CO₂ mesocosms. Nonmetric multidimensional scaling (NMDS) was performed with the same Bray-Curtis dissimilarity matrices as the ANOSIM tests in order to visualize mesocosm clustering. Bray-Curtis dissimilarity matrices, NMDS results, ANOSIM results, and subsequent similarity percentage analysis (SIMPER, which point towards the components in the community that primarily drive the clustering) were assessed with the Fathom Matlab toolbox provided by Jones [46].

In addition to these multivariate tests, we performed Student's *t*-tests for each measured variable separately. These were done with MS excel where we tested for equality of variance and normal distribution and then used an independent sample *t*-test (type 2 in case of homogeneity in variance, else type 3) to assess statistical significance (threshold *p*-value = 0.05).

3 Results and Discussion

3.1 Overview of important events, developments, and perturbations during the mesocosm study

3.1.1 Restart of experiments due to technical difficulties. The conditions at our arrival in the fjord were challenging due to the presence of sea ice and its potential to damage the mesocosms. Prevailing easterly winds during the end of January and February led to stable air temperatures below 0°C ([Fig 2A](#)) and thus to continuing ice formation and drift. An upwelling event around the 10th of February brought relatively warm (~5°C) and saline (~32) North Atlantic water to the surface melted the ice. We used this opportunity to close the mesocosms and start the experiment on February 12th, 2013 (t-25). However, the upwelling event was a curse and a blessing at the same time because the water entrapped in the mesocosm bags was effectively 300–600 kg heavier than the usual mixture of Baltic Sea and North Atlantic water (mean salinity ~25) which returned a few days after the upwelling. Even though we were aware of this problem and added extra buoyancy aids to the mesocosm floatation frames, we could not prevent the water from accumulating at the bottom of the bags. Consequently the mesocosm bags took on a pear-like shape and water was pressed out of the bags into the fjord through a weak point in the connection between the bags and the sediment traps. Thus, we had to stop the experiment on the 3rd of March (t-6) and fix the sediment traps on shore because the mesocosm bags had lost a large fraction of the initially enclosed water ([S1 Fig](#)).

3.1.2 Changes in the enclosed water mass. The second experiment started four days after the end of the first on 7th March (t-2) and lasted for 113 days until the 28th June (t111). The enclosed water mass had an average salinity of 29.12 (±0.11) which is close to the upper limit typically measured for the 0–19 m depth range in Gullmar Fjord [21]. Thus, we once more enclosed a water mass of primarily marine (North Sea) origin. This time, however, the relatively heavy water did not cause trouble as we were able to sustainably repair the leaking weak point of the sediment traps. Almost complete water exchange occurred between the opened mesocosm bags and the fjord during the period between the failed experiment and our second approach (t-6 –t-2). Only a rather small, yet unquantifiable, amount of water in the middle of the submersed mesocosm bags was not flushed out and was carried over into the successful second try. The influence of this carry over of water from the first experiment into the second one will be discussed in detail in section 3.2.1.

Water exchange with the surrounding fjord stopped as soon as the sediment traps were attached and the upper part of the mesocosm bags pulled above the surface as explained in

section 2.2. However, by cleaning the mesocosm bags with the cleaning ring we unfortunately created small cuts in the bags on 6 occasions during the experiment so that there was unintentional water exchange with the fjord until the cuts were repaired (Fig 3). Holes were sealed by divers with small rubber patches glued onto the outer side of the mesocosm bags. Detection of holes was difficult and sometimes took us several days of intense diving activity. In some instances they could not be detected from the outside so that it became necessary to dive into the mesocosm because it is much easier to spot the holes from the inside (inside diving events recorded in Table 1). Diving equipment was thoroughly cleaned before entering a mesocosm and we only used rebreathers in combination with dry suits and full face masks to minimize contamination and mixing of the enclosed water bodies.

Water exchange through holes was quantified by changes in mesocosm salinity. In the most extreme case (M8 between t0 and t5) it accounted for 3% of the total volume (all estimates

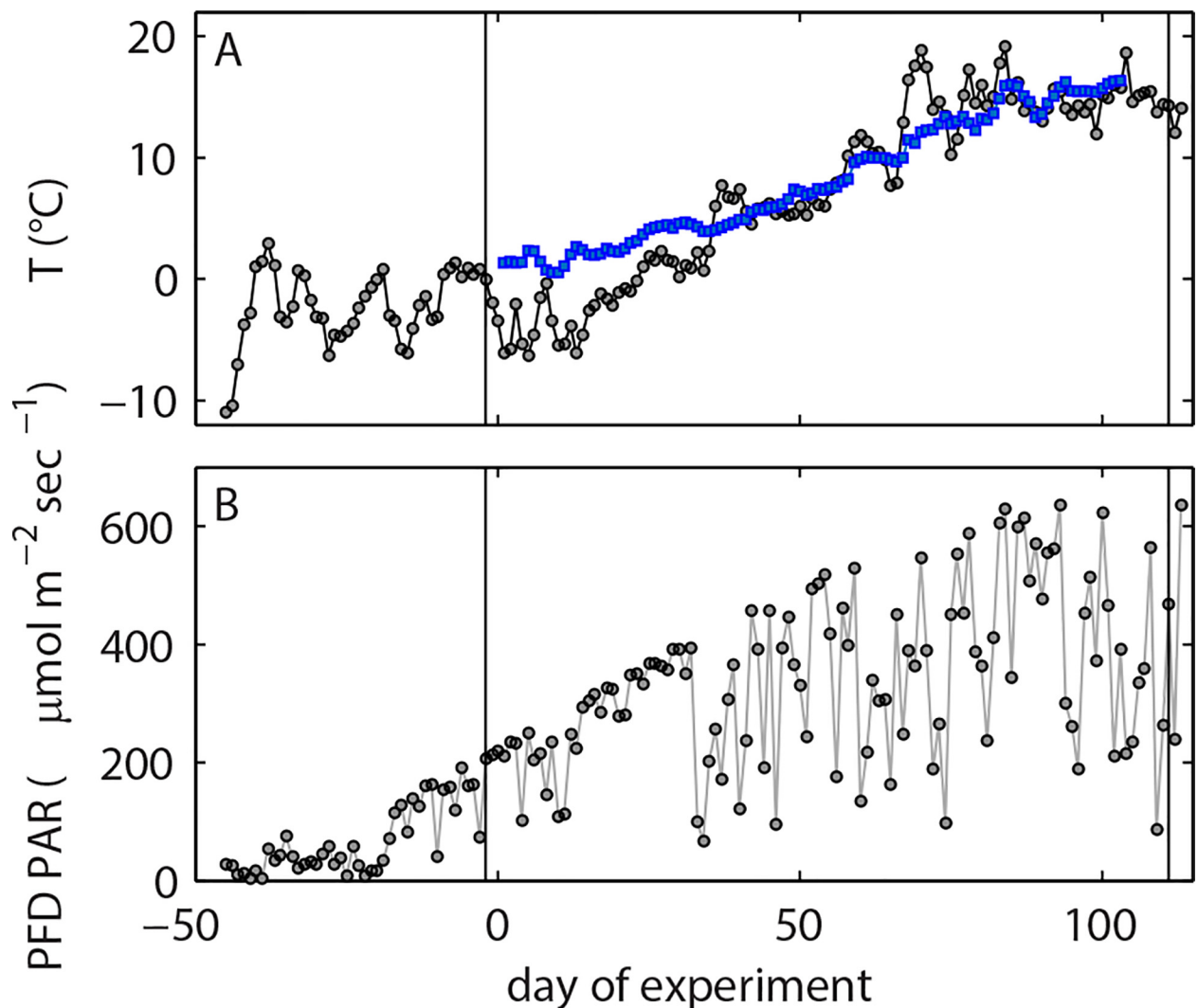


Fig 2. Daily averaged (A) air temperature (grey), surface water temperature (blue) and (B) photon flux density (PAR) of photosynthetic active radiation (PAR). Air temperature and PAR data were recorded on the roof of the Sven Lovén Centre (~3 km distance from the mesocosm deployment site) and downloaded from <http://www.weather.loven.gu.se/kristineberg/data.shtml>. Surface water temperature was recorded with HOBO pro v2 data logger mounted at 0.1 m depth in M2. Note that temperature development was quasi identical in all mesocosms (S3 Fig). The timeline starts with the arrival of research vessel *Alkor* at Gullmar Fjord on the 23rd of January, 2013 (t-45). Grey vertical lines indicate the start (7th of March; t-2) and the end (28th of June; t111) of the successful experiment.

doi:10.1371/journal.pone.0159068.g002

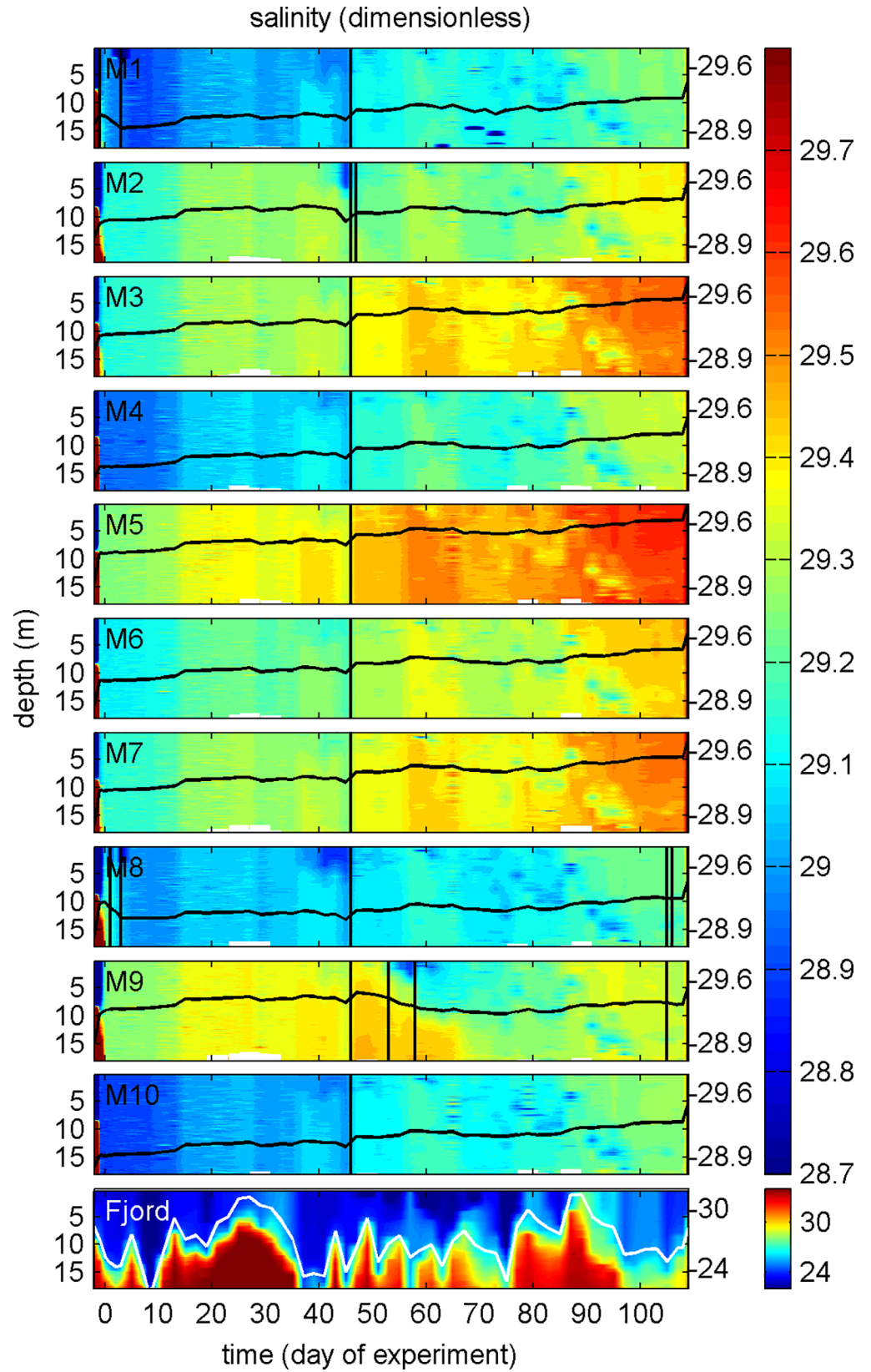


Fig 3. Salinity profiles over the course of the study. Note the different color coding for the fjord contour plot. Change of salinity averaged over the entire water column is represented by the black (or white in the case of the fjord) line plots on top of the contours with the corresponding additional y-axes on the right side. The vertical black lines on t46 mark the volume determination by brine (NaCl) addition. The other vertical black lines frame periods where we had small holes in the mesocosm bags (influx estimates given in [Table 2](#)).

doi:10.1371/journal.pone.0159068.g003

given in [Table 2](#)). The impact of the water influx is difficult to assess but we did not observe anomalies in any of the measured parameters during or after these damages. Furthermore, mesocosms which were damaged did not have any fundamental differences in community succession ([Fig 4](#)). Hence, we tentatively conclude that the unintentional water influxes had a limited influence on the results presented here.

The water column was mixed immediately after the second closing procedure on t-2 in order to break down the existing halocline. The salinity homogenization initiated a strong convective mixing inside the bags, as the deeper water in the fjord (North Atlantic water) was warmer than the fresher top layer thereby constantly heating the lower parts of the mesocosms ([Fig 5](#)). Since the salinity stratification was absent inside the mesocosms after mixing, the water at the bottom of the mesocosm, warmed by the adjacent fjord, could rise to the surface where it was cooled by the cold, low salinity fjord water ([Fig 5](#)). This convection cell thoroughly homogenized the water column ([Figs 3 and 6](#)) until mid-April (t37), the time when surface water temperatures exceeded those of the bottom water, and established a thermocline which prevailed until the end of the experiment ([Fig 5](#)).

The masses of the water enclosed within the ten mesocosms were determined on t46. On this particular date, masses ranged from 55.9 tons in M2 to 47.5 tons in M3 ([Table 2](#)). Note, however, that mass changed slightly over the course of the experiment due to evaporation, rain, sampling, seeding and the unintentional water exchange through holes.

3.1.3 Different phases of bloom development. Surface irradiance at the beginning of the study was relatively low ([Fig 2B](#)) and convective water column mixing homogenized phytoplankton distribution over the entire water column. The lack of stratification did, however, not inhibit the growth of phytoplankton. Chl a concentrations increased steadily from the first day until t10 where a short depression was observed before growth regained momentum and led to the first chl a peak between t29 to t35 with mesocosm-specific intensity (highest in M10 and lowest in M3; [Fig 4A](#)). Scanning electron microscopy samples revealed that the most important species contributing to the chl a build-up were the small (2–5 μm) silicifying species *Arcocellulus* sp., *Minidiscus* sp. (both diatoms), and *Tetraparma* sp. (Chrysophyte) as well as the very large (>200 μm) diatom *Coscinodiscus* sp. The first bloom was fueled by inorganic nutrients upwelled during winter and enclosed in the mesocosms at the beginning of the study. Initial concentrations of NO₃⁻/NO₂⁻, PO₄³⁻, and Si(OH)₄ were ~6.8, ~0.7 and 9.85 $\mu\text{mol L}^{-1}$, respectively ([Table 3](#); [Fig 7](#)), which is within the range typically observed in this region before the spring bloom [47]. The collapse of the phytoplankton spring bloom was not initiated by the abrupt end of convective mixing on t37 as chl a decrease began 2 to 7 days earlier. Instead, it is most likely attributable to aggregation and subsequent sedimentation as well as ongoing grazing pressure at the point where NO₃⁻/NO₂⁻ concentrations ran into limitation ([Fig 7A](#)). PO₄³⁻ was also low at peak bloom but concentrations remained far above the detection limit (0.8 nmol L⁻¹) and fluctuated at a low level (max 0.2 $\mu\text{mol L}^{-1}$) from around t35 onwards ([Fig 7B](#)). The Si(OH)₄ decline was more linear than that of NO₃⁻/NO₂⁻ and PO₄³⁻ ([Fig 7C](#)). Detection limit was reached quite shortly after peak bloom in some mesocosms (e.g. M3, M5), while it took up to forty days longer in others (e.g. M10).

A second phytoplankton bloom developed directly after the first collapsed. Bloom magnitude was on average slightly lower than in the first bloom with peak1/peak2 chl a ratios ranging

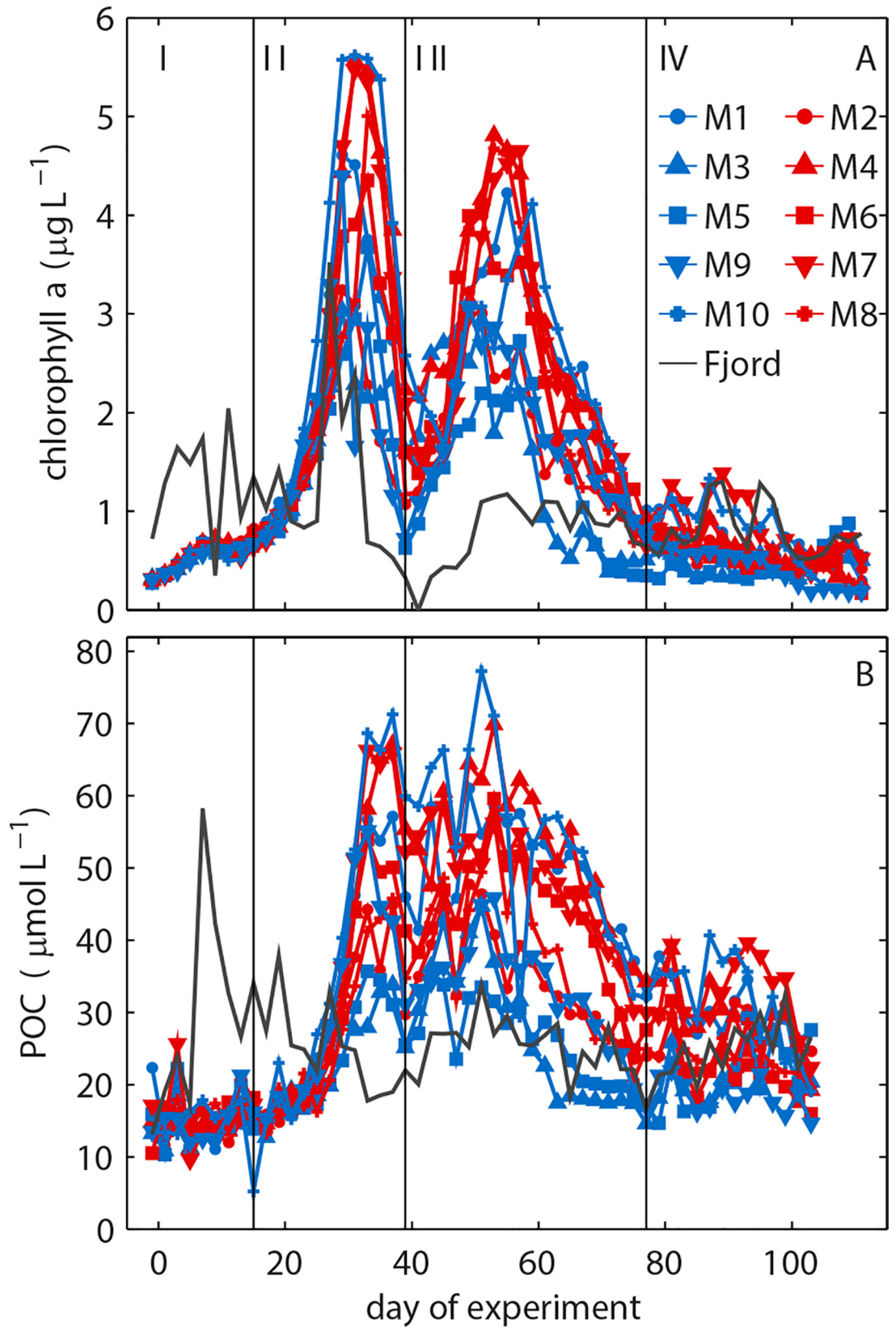


Fig 4. Development of (A) chl a and (B) POC concentrations over the course of the experiment. Roman numbers denote the different phases of the experiment.

doi:10.1371/journal.pone.0159068.g004

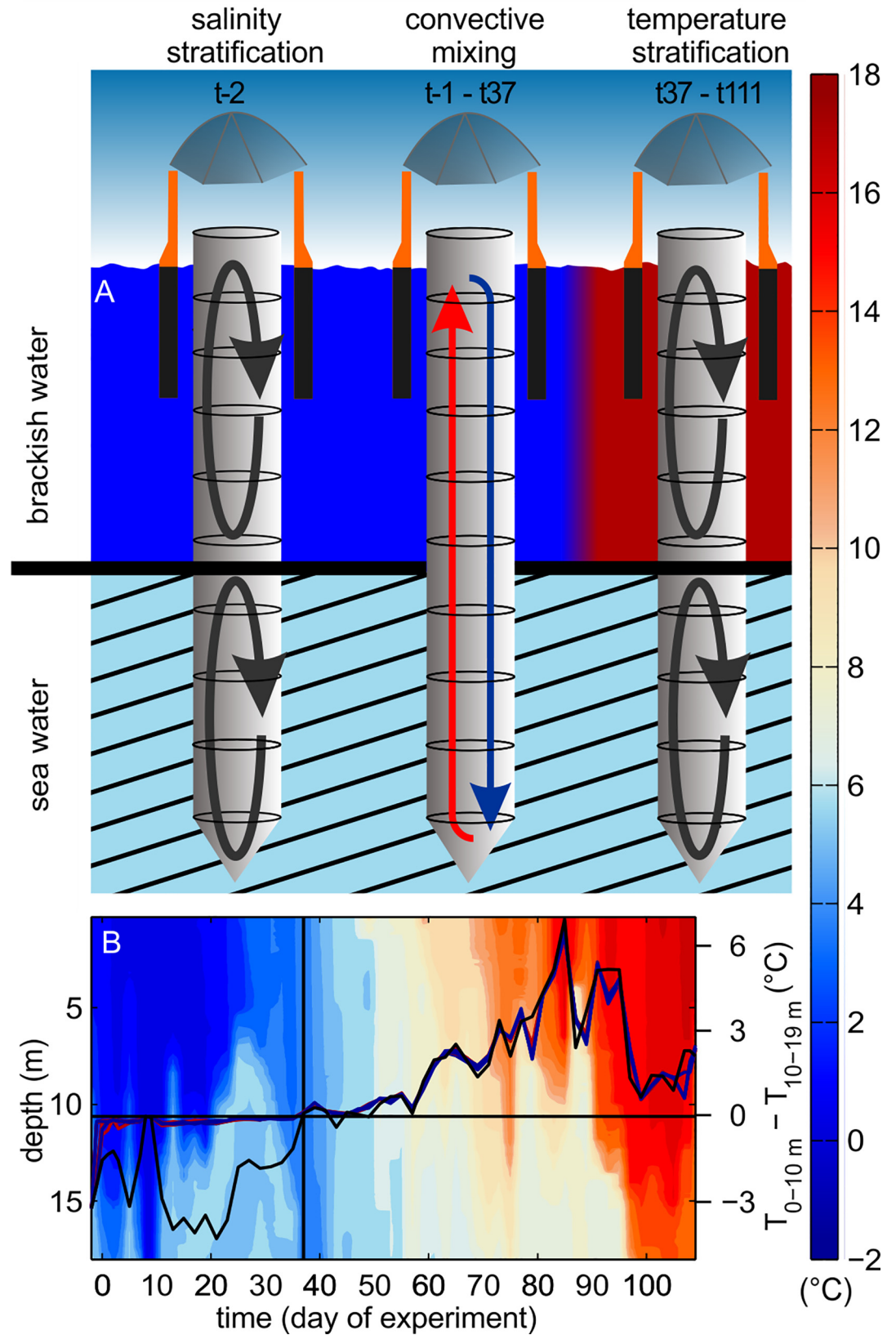


Fig 5. Changes in water column mixing in the course of the experiment. A salinity stratification prevented water column mixing at the beginning of the study (t-2). Convective mixing was initiated after homogenizing water column salinity. Convection was sustained until t37 by saline North Sea water which was warmer than the fresher surface water. (B) Surface water temperature rose above that of the deep water after t37 thereby establishing temperature stratification and terminating convective mixing.

doi:10.1371/journal.pone.0159068.g005

from 1.5 (M10) to 0.9 (M3). The most important taxa contributing to the second bloom were small (2–5 μm) diatoms (*Minidiscus* sp., *Arcocellulus* sp.), a large variety of small green flagellates (0.8–5 μm) and *Coscinodiscus* sp. Chla build-up was fueled by remineralized nutrients as new nutrients upwelled by winter mixing and available at the beginning of the experiment were depleted at this time point. DON and NH₄⁺ concentrations did not noticeably change during the second bloom suggesting that nutrients required for bloom development were remineralized and directly transferred into phytoplankton biomass without transient accumulation in the dissolved organic and inorganic nutrient pools (Fig 7D; [32]). Stable post-bloom conditions were established in the aftermath of the second bloom. They were characterized by low chla concentrations and an intensifying temperature stratification of the water column (Figs 4A and 5B).

POC concentrations increased with chla during the first bloom but did not follow its decline thereafter (Fig 4B). Instead, POC remained at elevated levels and bridged the chla gap between the two blooms (compare Fig 4A and 4B). This suggests that most POC generated by phytoplankton was retained in the water column in the form of senescent phytoplankton detritus and/or routed in heterotrophic biomass. The chla decline after the second bloom and the low level stagnation during the post-bloom period was reflected in POC concentrations (Fig 4B). Similar to chla, there was also a noticeable variance in POC trends between mesocosms. In the first bloom between t30 and t40, for example, POC increased to up to 71 μmol L⁻¹ in M10 but only reached a maximum of 34 μmol L⁻¹ in M3. Reasons for such large differences in chla and POC development between mesocosms are unclear at present but there is some evidence that they originate from differences in the plankton community enclosed at the beginning of the study (see section 3.2.1 for further details).

Based on the development in chla concentrations described above we define four major phases of the winter-to-summer succession in the mesocosms (Fig 4). Phase I lasted from the beginning of the experiment until t16 and encompasses the period before the major chla build-up of the spring bloom. Phase II lasted from t17 until t40 and includes the major chla build-up and decline of the spring bloom. Phase III started on t41 and ends after the second chla peak has gone on t77. Phase IV covers the post-bloom phase and ends with the experiment on t111.

3.1.4 Carbonate chemistry conditions. Injections of CO₂ enriched seawater into the designated high CO₂ mesocosms (M2, M4, M6, M7, M8) on t-1 and t0 elevated the DIC concentration from 2075 (±5) to 2186 (±3) μmol kg⁻¹ (Fig 7E). This change increased pCO₂ from 385 (±9) to 960 (±10) μatm (Fig 7E) and reduced pH_T from 8.045 (±0.009) to 7.674 (±0.004) (Fig 6). Ω_{aragonite} and the substrate-inhibitor ratio for calcification ([HCO₃⁻]/[H⁺]) are two specifically relevant carbonate chemistry parameters for calcifying organisms as they control post-production dissolution of aragonite (Ω_{aragonite}) and characterize the ability of the carbonate system to support high CaCO₃ formation rates ([HCO₃⁻]/[H⁺]; [48]). Ω_{aragonite} dropped below 1 (~0.6) upon CO₂ addition so that seawater in the low pH treatments was corrosive for aragonite (Fig 7G). [HCO₃⁻]/[H⁺] declined from ~0.25 to ~0.12 mol/μmol (Fig 7H) suggesting that biotic formation of CaCO₃ was more challenging under high CO₂.

The mesocosms were an open system and gas exchange occurred at the air-sea boundary layer [49]. Thus, DIC concentrations needed to be readjusted in the high CO₂ treatment on 5 occasions during the experiment in order to compensate for CO₂ loss to the atmosphere (Fig 6;

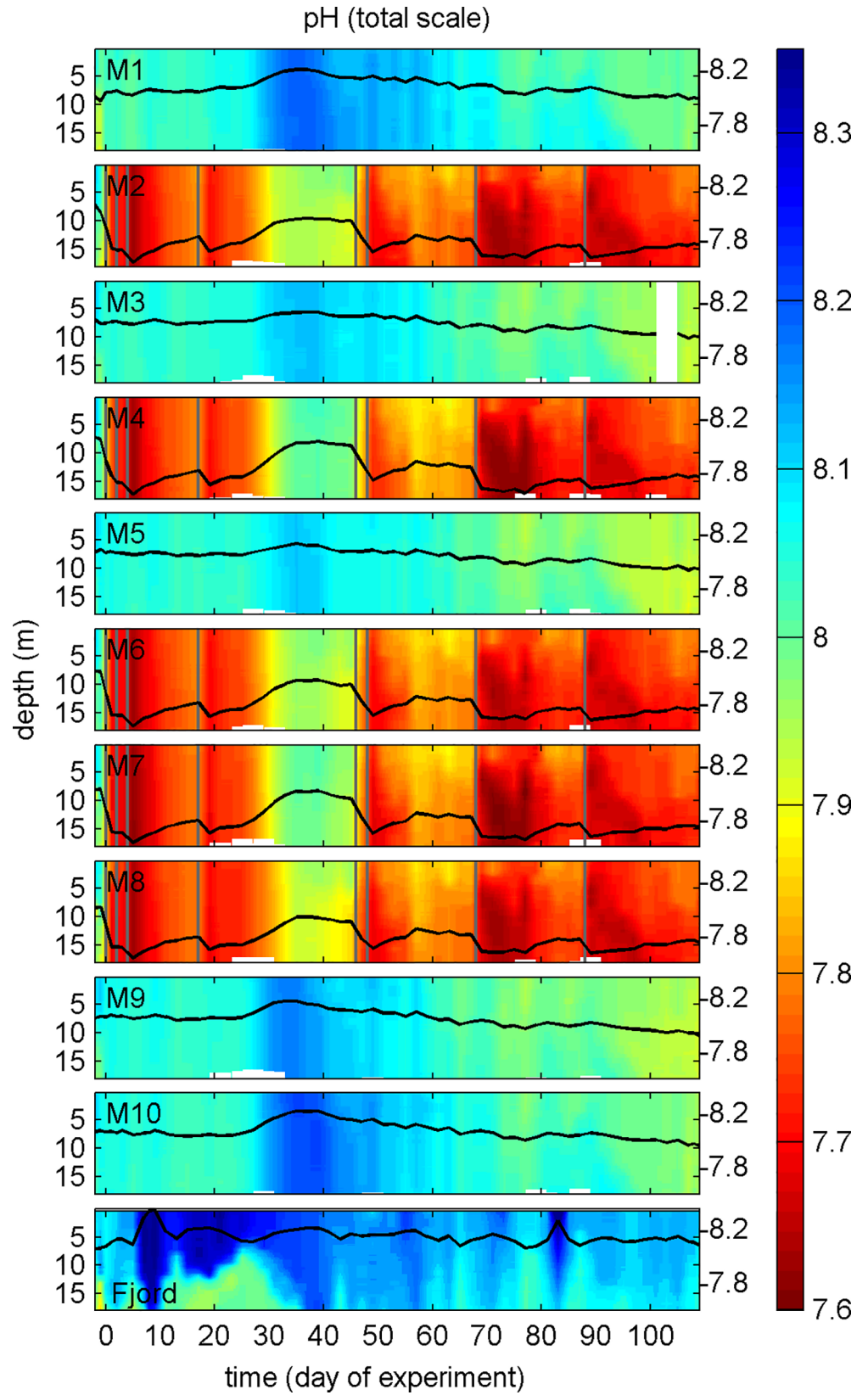


Fig 6. pH_T depth profiles at *in-situ* temperature over the course of the study. Change of pH_T averaged over the entire water column is represented by the black line plot on top of the contours with the corresponding y-axes on the right side. The vertical grey lines signify days of carbonate chemistry manipulation by additions of CO₂-aerated water.

doi:10.1371/journal.pone.0159068.g006

(Table 1). The differences in carbonate chemistry conditions between the high and ambient CO₂ treatment were variable in the course of the experiment but at no point overlapped (Fig 7). DIC concentrations declined in both treatments during the spring bloom in phase II primarily due to DIC uptake by photoautotrophs. In the aftermath of the bloom, DIC remained

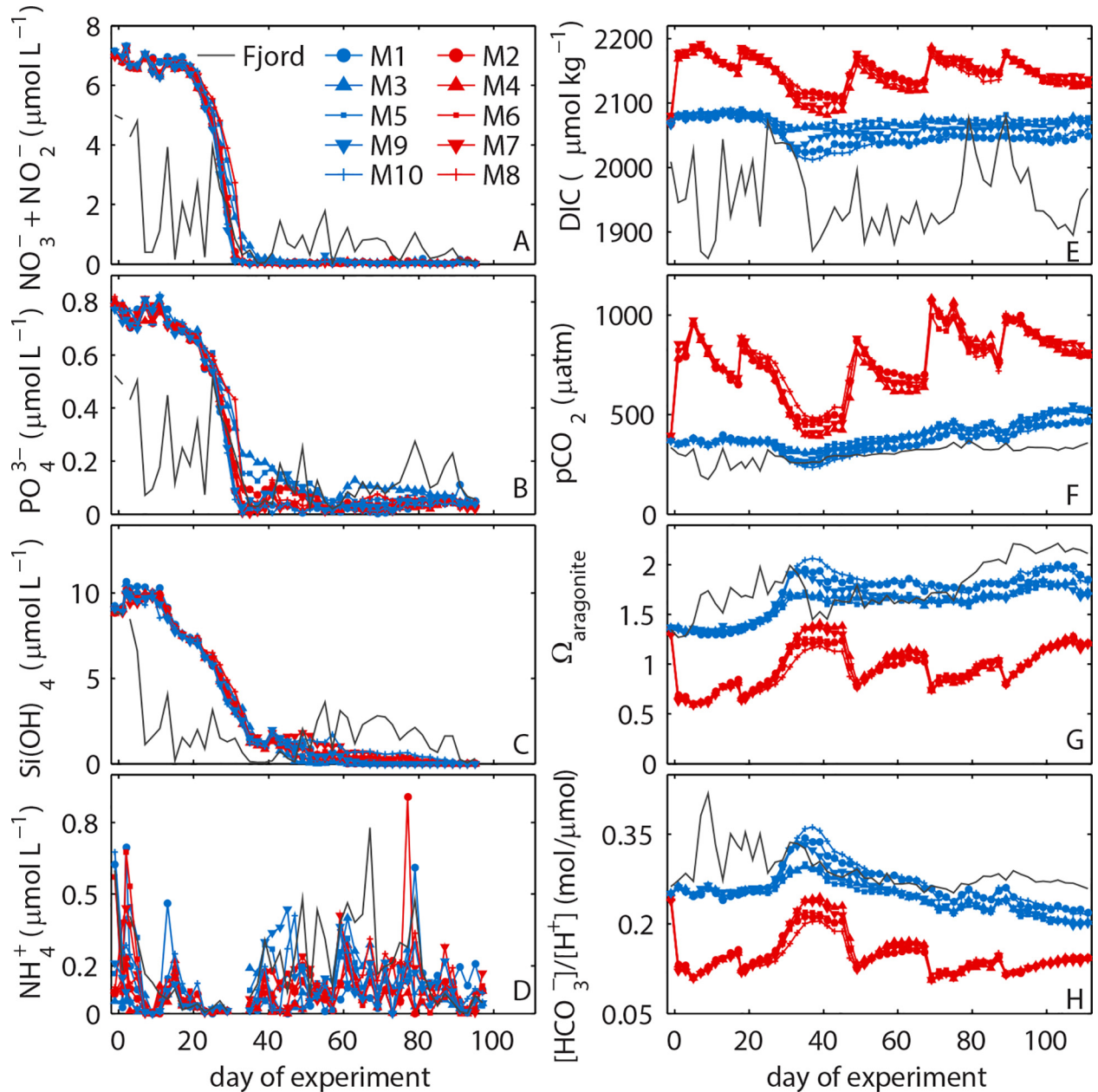


Fig 7. Water column integrated (0–17 m) inorganic nutrient concentrations and carbonate chemistry conditions inside the mesocosms and in the surrounding fjord water.

doi:10.1371/journal.pone.0159068.g007

relatively stable with only some gas-exchange driven fluctuations in the high CO₂ treatment. The absence of a DIC decrease in the ambient CO₂ treatment during the second bloom suggests that inorganic carbon used for autotroph growth in phase III probably originated from respired biomass and thus was supplied by heterotrophs. The $p\text{CO}_2$ trends reflect the changes in DIC with the exception of a continuous increase in the second half of the study caused by the warming of water inside the mesocosms. $\Omega_{\text{aragonite}}$ and $[\text{HCO}_3^-]/[\text{H}^+]$ increase until the peak of the spring bloom. $\Omega_{\text{aragonite}}$ remained relatively stable thereafter because the influence of increasing DIC is counterbalanced by increasing temperature. Corrosive conditions for aragonite were present during most of the time in the high CO₂ treatment (Fig 7G). In contrast to $\Omega_{\text{aragonite}}$, $[\text{HCO}_3^-]/[\text{H}^+]$ is insensitive to changing temperature but becomes smaller with decreasing pH [48]. It therefore constantly decreases after the spring bloom (Fig 7H) suggesting that carbonate chemistry conditions for calcification deteriorated from spring to summer.

Vertically, carbonate chemistry conditions were homogenous until the end of convective mixing on t37 (Fig 6). Mildly stratified conditions developed thereafter with generally higher pH_T (lower $p\text{CO}_2$) in the upper mixed layer of the high CO₂ treatment and generally lower pH_T (higher $p\text{CO}_2$) in the upper mixed layer of the ambient CO₂ treatment (Fig 7). Differences in vertical pH zonation between the two treatments were due to the opposing direction of air-to-sea gas exchange; net CO₂ outgassing was dominant in the high CO₂ mesocosms while net in-gassing was persistent under ambient CO₂ conditions except for phase IV.

3.2 Plankton community structure

3.2.1 Influence of initial differences in the plankton community upon their succession. The composition of the plankton community enclosed at the beginning of an experiment influences its subsequent succession. A detailed summary of the initial conditions revealed broadly similar conditions in most biogeochemical and community-related parameters at the level of detail investigated here (Table 3). Heterogeneity among the ten mesocosms was primarily found in those parameters with lower measurement precision or where measurements were close to detection limit (e.g. copepod and diatom abundance; Table 3). Correlations between biogeochemical or community-based parameters and salinity were used to assess whether differences at the beginning of the study could be due to enclosure of different water masses. These correlations were only in 3 out of 27 cases significant (Table 3) indicating that there seems to be no systematic difference among mesocosms related to differential water exchange before closing. Variability among mesocosms was generally larger in the ambient CO₂ treatment than in the high CO₂ treatment, with the standard deviation (SD) being higher in 22 out of 28 measured parameters (Table 3). This is also reflected in NMDS analysis where the spread among ambient CO₂ mesocosms looks higher than in the high CO₂ treatment (Fig 8A).

Results from the ANOSIM test suggested that there was no significant difference between the plankton communities in the high CO₂ and low CO₂ mesocosms at the beginning of the study ($R = 0.13$; $p = 0.2$). To support the ANOSIM results we performed t -tests with each of the measured parameters separately. The t -tests generally support the ANOSIM result (no significant difference among treatments in 27 out of 28 parameters) with the exception of picoeukaryotes where the t -test implied significantly ($p = 0.0018$) higher abundance in the high CO₂ treatment (Table 3). The initial difference in picoeukaryote abundance uncovered by the t -test can be explained by the outcome of the first (failed) experiment which was terminated after 19 days due to technical problems (section 3.1.1). In this preceding experiment, we observed a strong positive effect of CO₂ on the abundance of picoeukaryotes (S2A Fig). This outcome was partially transferred into the second experiment because of the incomplete water exchange

within the mesocosms during the four days between the two studies (S2B Fig, see also section 3.1.1). Based on this evidence we refrain from using the ANOSIM result (which is based on multivariate analysis of all community parameters) and follow the univariate *t*-test analysis which suggested that both mesocosm treatments showed no significant difference at the beginning of the study except for the picoeukaryote abundance.

Some of the patterns recorded at the beginning of the study seemed to diminish over the course of the experiment whereas others were conserved. For instance, the higher variability of community structure in the ambient CO₂ treatment (higher SD in 22 out of 28 measured parameters, see above) was still present during the first bloom (SD higher in 9 out of 12 parameters, S2 Table, Fig 8B) but this pattern vanished in the second bloom (SD higher in 6 out of 12 parameters, S3 Table, Fig 8C) and in the post-bloom period (SD higher in 5 out of 12 parameters, S4 Table, Fig 8D). The initially large difference between M3 and M10 (both ambient CO₂ replicates; Fig 8) seemed to be conserved, a feature which was also observed during the peak of the bloom in phase II and then again in the post-bloom period, after having a short interval of relatively similar conditions in phase III. These two mesocosms also had a particularly different development in *chl a* concentrations (Fig 4A), POC concentrations (Fig 4B), and many other measured parameters (shown in the more specialized publications of this PLOS collection; S1 Table) which strengthens the impression that differences in the plankton community enclosed at the beginning of the study may in part explain the variability observed during its subsequent succession.

A critical aspect in this context is the above-mentioned significant higher abundance of picoeukaryotes in the high CO₂ treatment. Due to this remnant from the first experiment we cannot fully clarify to what extent the picoeukaryote response in the second experiment was preset by the initial conditions and to what extent the response developed over the course of the experiment. Several lines of evidence, however, suggest that initial difference was of minor importance for the responses later in the succession. Initial differences were on average ~1500 cells mL⁻¹ which is less than 9% of the total population (Table 3). Thus, only 9% of the population in the ambient CO₂ mesocosms would have needed to divide in order to equalize the initial difference. This could be achieved within hours since picoeukaryotes are able to divide more than twice per day [50]. Therefore, it is not surprising that this significant difference between ambient and high CO₂ treatment is lost already within phase I (indicated by a switch of a *t*-test *p*-value from 0.04 on t15 to 0.23 on t17). A loss of the initial difference in picoeukaryotes during phase I strongly suggests that the re-establishment of a positive CO₂ effect during phase III (S3 Table) was formed by processes taking place during the succession and not as a result of initial differences. However, even in the unlikely case that the phase III observations were caused by the initial differences, they would still be CO₂-induced (S2 Fig). Thus, the carry-over of the positive CO₂ effect on picoeukaryote abundance would not negate the conclusions made in this study.

3.2.2 Restructuring of the plankton community by ocean acidification. A major motivation of this study was to test whether simulated end of the century CO₂ concentrations can restructure entire plankton communities on a natural winter-to-summer succession. Succession patterns can be investigated at different degrees of functional or taxonomic resolution. The present analysis included various plankton types with a relatively broad functional spectrum but did not account for CO₂ effects within functional groups. CO₂ effects on or within specific functional groups (e.g. picoautotrophs) or taxonomic entities (e.g. crustaceans) will be investigated in more targeted studies presented within the framework of this special issue (S1 Table). At the level of detail investigated in the present work, a significant CO₂ effect on plankton community structure was subtle and only detectable during the second phytoplankton bloom (phase III). Here, the main drivers of the CO₂-induced community restructuring were nauplii, bacteria, and picoeukaryote abundances (Fig 8C; S3 Table). No CO₂ effects were

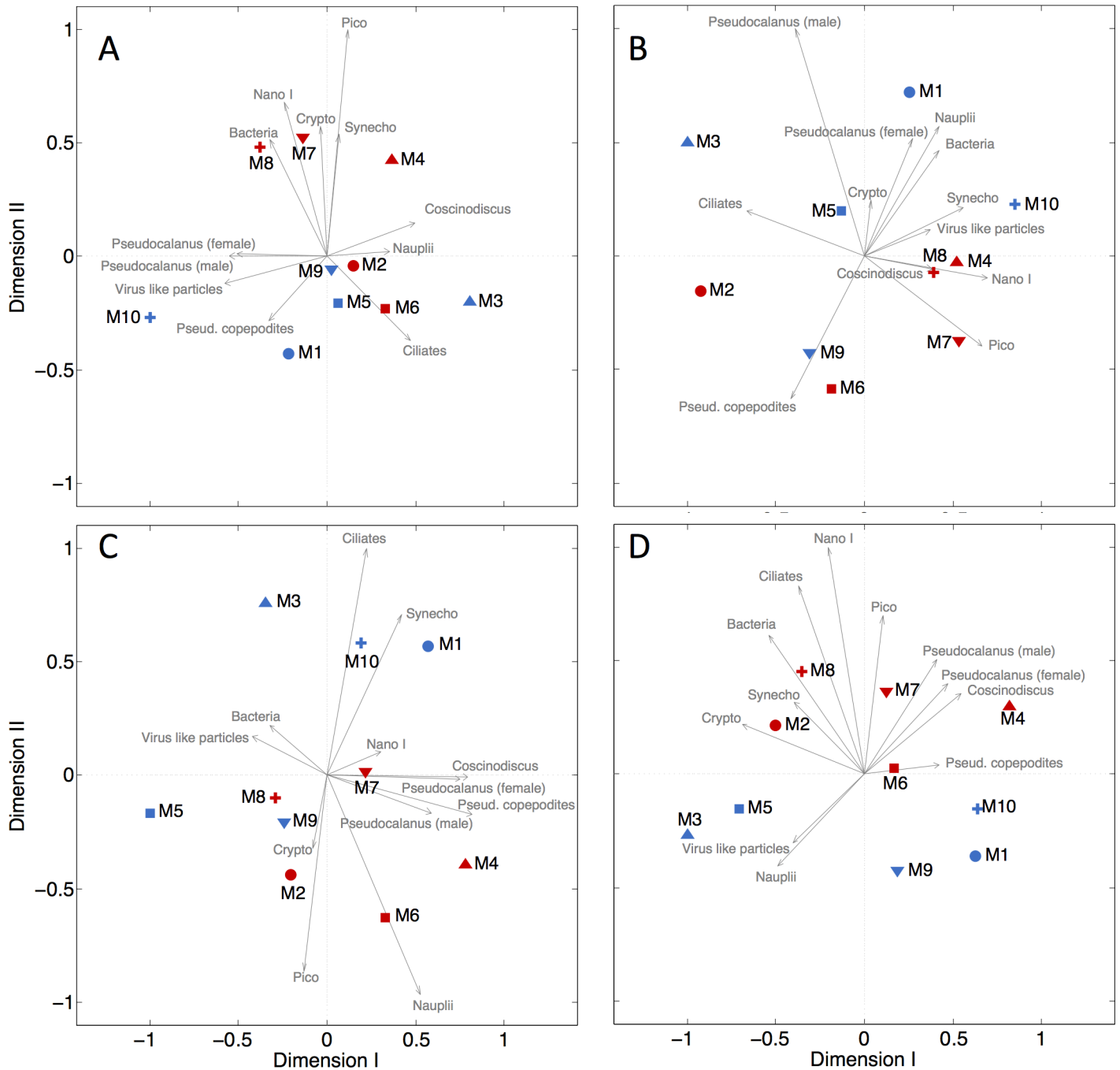


Fig 8. NMDS analysis of plankton community composition based on Bray-Curtis dissimilarities from (A) the beginning of the experiment (Stress = 0.0452), (B) peak chl_a concentrations during the first bloom (Stress = 0.0269), (C) peak chl_a concentrations during the second bloom (Stress = 0.0831), and (D) during the post-bloom period (Stress = 0.0138). Significant clustering (ANOSIM $p = 0.039$) between ambient and high CO₂ mesocosms was only observed during the second bloom (C). The underlying data implemented in the analysis are shown in [Table 3](#) and [S2](#), [S3](#) and [S4](#) Tables.

doi:10.1371/journal.pone.0159068.g008

detected in any of the three other stages of succession (phase I, II, IV; [Fig 8](#)) which leads to two key questions: Why was the CO₂ effect restricted to phase III? And, how was this CO₂ effect on community composition generated?

To answer this we need to characterize the stage of succession at which the CO₂ effect occurred. The second phytoplankton bloom was profoundly different to the first one as it was fueled by remineralized nutrients (section 3.1.2). Thus, essential resources for autotrophic growth needed to be provided by, or extracted from, various sources within the food-web. In contrast, no upstream ecosystem processes were necessary during the first bloom where upwelled inorganic nutrients were naturally available. A putatively more complex ecosystem structure during the second bloom may consequently have provided more “contact points” for altered carbonate chemistry to induce community restructuring. Conversely, a comparatively low ecosystem complexity during the first bloom where a few dominant phytoplankton species outgrew the others may have led to a fairly one-dimensional nutrient flux through the food-web. In such a bloom setting, altered CO₂ conditions may be less likely to significantly affect bloom development because only a few (often only one) fast growing species are involved.

The obvious problem with this line of reasoning is the inconsistency of results between phase III and phase IV (the post-bloom phase) where the plankton community was similarly fueled by regenerated nutrients. However, the absence of a detectable CO₂ effect during phase IV (Fig 8D) is probably not surprising due to the following. In phase III we analyzed a defined event (peak of the second bloom) whereas we averaged each parameter over the entire post-bloom period in phase IV (S4 Table). Averaging over phase IV was necessary because there was no clear event suitable for a more focused analysis. Hence, we may have missed a potential CO₂-induced community restructuring due to the averaging of a large time period. Furthermore, we also noticed that fluctuations of taxonomic group or species abundances over time seemed to increasingly desynchronize among replicates the longer the experiment lasted. Accordingly, later in the experiment it became more and more difficult to uncover CO₂ effects because even if they were present they may have occurred at different days in the five replicates. Uncovering such temporal mismatches seems to be one of the major challenges in long-term mesocosm studies but being able to resolve this problem is essential in order to avoid an inflation of type II errors (concluding there is no CO₂ effect on the plankton community even though there is one).

4 Conclusion and Outlook

In this experiment we investigated the influence of realistic end-of-the-century carbonate chemistry conditions on a natural winter-to-summer plankton succession in a coastal pelagic ecosystem for a period of 113 days. An examination of key biogeochemical variables and the plankton community composition before CO₂ treatment revealed broadly similar starting conditions among replicates. However, some of the variability present at the beginning seemed to be conserved in the succession pattern, which suggests that consideration of starting conditions is necessary to understand the temporal dynamics of plankton community composition. Furthermore, we noticed that initial differences in combination with the variability introduced in the course of the succession makes it increasingly difficult to detect CO₂-induced effects later in the experiment which is a considerable complication of these kinds of long-term studies.

At the level of detail investigated in this study we found that CO₂-induced changes in plankton community composition were generally subtle and detected only in a succession stage where a phytoplankton bloom was fueled by remineralized nutrients. This finding agrees with two other recent studies in different oceanographic regimes which also reported the most noticeable CO₂ effects to occur at limiting inorganic nutrient concentrations [14,51]. Since most published OA experiments with plankton communities were conducted in relatively eutrophic settings, we may thus far have missed many potential CO₂ effects. We should therefore focus on settings where plankton communities are fueled by regenerated nutrients in future OA studies.

Supporting Information

S1 Fig. Underwater photograph (~8 m depth) of a mesocosm at the end of the first (failed) experiment where we enclosed seawater with a considerably higher salinity than usually experienced in the fjord. The heavy water was accumulating at the bottom of the mesocosm and leaked out of the bags into the fjord through a weak point in the connection between the bag and the sediment trap. Seen here is the upper part of the bag that became compressed as a consequence of water leakage at the bottom. Sampling was impossible at that point because the sampling gear no longer fitted into the mesocosm bag.

(DOCX)

S2 Fig. (A) Development of picoeukaryote abundance in the first experiment (12th February until the 3rd March). The two grey lines frame the period of CO₂ addition. High CO₂ mesocosms (warm colors: M2, M4, M6, M7, M8) reached an average $p\text{CO}_2$ of 1063 (± 15) μatm on t-16. Ambient CO₂ mesocosms (cold colors: M1, M3, M5, M9, M10) were left unperturbed with an average $p\text{CO}_2$ of 371 (± 1.5) μatm . A pronounced positive effect of elevated $p\text{CO}_2$ emerged after t-13. (B) pH_{NBS} CTD profiles from the very beginning of the second study (7th of March, t-2), directly after closing the mesocosms but before mixing them with compressed air. pH_{NBS} profiles reveal that some of the high CO₂ water from the first experiment was still present in some mesocosms (mainly M7 and M8) at the beginning of the second approach, even though mesocosm bags were completely under water and the sediment traps were removed during the 4 days in between the two studies.

(DOCX)

S3 Fig. Temperature profiles over the course of the study. Changes in temperature averaged over the entire water column are represented by the white line plots on top of the contours with the corresponding y-axes on the right side. The black lines at t37 mark the end of convective mixing (See also [Fig 5](#)).

(DOCX)

S1 Table. Contributions intended to be published within the framework of the BIOACID II long-term mesocosm study. Note that two studies [[16,32](#)] have already been published before initiating the PLOS collection.

(DOCX)

S2 Table. Abundance of individual plankton groups during peak *chl a* concentrations in phase II. For the community-based analysis we generally included functional groups rather than species. For copepods, we only included *Pseudocalanus* sp. here since this species strongly dominated the copepod community both, numerically and in terms of biomass. (Note, however, that “nauplii” includes copepod nauplii from all species since they were not distinguished taxonomically). This data was used for ANOSIM/NMDS analysis ([Fig 8B](#)).

(DOCX)

S3 Table. Abundance of individual plankton groups during peak *chl a* concentrations in phase III. For the community-based analysis we generally included functional groups rather than species. For copepods, we only included *Pseudocalanus* sp. here since this species strongly dominated the copepod community both, numerically and in terms of biomass. (Note, however, that “nauplii” includes copepod nauplii from all species since they were not distinguished taxonomically). This data was used for ANOSIM/NMDS analysis ([Fig 8C](#)).

(DOCX)

S4 Table. Abundance of individual plankton groups during the post bloom period in phase IV. For the community-based analysis we generally included functional groups rather than

species. For copepods, we only included *Pseudocalanus* sp. here since this species strongly dominated the copepod community both, numerically and in terms of biomass. (Note, however, that “nauplii” includes copepod nauplii from all species since they were not distinguished taxonomically). This data was used for ANOSIM/NMDS analysis (Fig 8D). (DOCX)

Acknowledgments

We thank the Sven Lovén Centre for Marine Sciences, Kristineberg for giving us access to their facilities and the warm hospitality. We also gratefully acknowledge the captain and crew of RV *ALKOR* for their work transporting, deploying and recovering the mesocosms during cruises AL406 and AL420. This project was funded by the German Federal Ministry of Science and Education (BMBF) in the framework of the BIOACID II project (FKZ 03F06550). U. Riebesell received additional funding from the Leibniz Award 2012 by the German Science Foundation (DFG). The carbonate chemistry measurements were supported by a grant from the Hasselblad Foundation. M. Zark and T. Hornick were supported by the association of European marine biological laboratories (ASSEMBLE, grant no. 227799), M. Algueró-Muñoz and H. G. Horn by the Swedish Academy of Sciences, and E. P. Achterberg received funding from the UK Ocean Acidification research programme (grant no. NE/H017348/1). This manuscript profited from the helpful comments of four anonymous reviewers.

Members of The Kristineberg KOSMOS Consortium: Nicole Aberle-Malzahn, Katarina Abrahamsson, Anna-Karin Almén, Maria E. Asplund, Saskia Audritz, Maarten Boersma, Eike Breitbarth, Christopher Bridges, Corina Brussaard, Andreas Brutemark, Catriona Clemmesen, Sinead Collins, Kate Crawford, Flemming Dahlke, Mario Deckelnick, Thorsten Dittmar, Ralf Doose, Sam Dupont, Tim Eberlein, Sonja Endres, Anja Engel, Jonna Engström-Öst, Sarah Febiri, Dirk Fleischer, Peter Fritsche, Martha Gledhill, Gwendolin Göttler, Maria Granberg, Hans-Peter Grossart, Amy Grifos, Linn Hoffmann, Anders Karlsson, Michael Klages, Uwe John, Fredrik Jutfelt, Irina Köster, Julia Lange, Elettra Leo, Silke Lischka, Kai Lohbeck, Bengt Lundve, Felix Christopher Mark, Michael Meyerhöfer, Maike Nicolai, Christian Pansch, Berne Petersson, Thorsten Reusch, Karlos Ribeiro de Moraes, Markus Schartau, Matias Scheinin, Kai G. Schulz, Ursula Schwarz, Marcus Stenegren, Martina Stiasny, Daniela Storch, Annegret Stuhr, Lennart Sswat, Maria Svensson, Peter Thor, Maren Voss, Dedmer van de Waal, Nicola Wannicke, Sylke Wohlrab, Angela Wulff

Author Contributions

Conceived and designed the experiments: UR LTB TB JC AL MS.

Performed the experiments: LTB TB AL MAM J. Bellworthy J. Büdenbender JC ME MF MH DH HGH TH JM MS MZ UR.

Analyzed the data: LTB JT TB AL EPA MAM LGA YE ME DH HGH TH JM MZ.

Contributed reagents/materials/analysis tools: UR EPA LGA.

Wrote the paper: LTB.

References

1. Le Quéré C, Raupach MR, Canadell JG, Marland G, Bopp L, Ciais P, et al. Trends in the sources and sinks of carbon dioxide. *Nat Geosci.* 2009; 2: 831–836. doi: [10.1038/ngeo689](https://doi.org/10.1038/ngeo689)

2. Wolf-Gladrow DA, Riebesell U, Burkhardt S, Bijma J. Direct effects of CO₂ concentration on growth and isotopic composition of marine plankton. *Tellus b*. 1999; 51B: 461–476.
3. Caldeira K, Wickett ME. Anthropogenic carbon and ocean pH. *Nature*. 2003; 425: 365. PMID: [14508477](#)
4. Kroeker KJ, Kordas RL, Crim RN, Singh GG. Meta-analysis reveals negative yet variable effects of ocean acidification on marine organisms. *Ecol Lett*. 2010; 13: 1419–1434. doi: [10.1111/j.1461-0248.2010.01518.x](#) PMID: [20958904](#)
5. Collins S, Rost B, Rynearson TA. Evolutionary potential of marine phytoplankton under ocean acidification. *Evol Appl*. 2014; 7: 140–55. doi: [10.1111/eva.12120](#) PMID: [24454553](#)
6. Dam HG. Evolutionary Adaptation of Marine Zooplankton to Global Change. *Annu Rev Mar Sci*. 2013; 5: 349–370. doi: [10.1146/annurev-marine-121211-172229](#)
7. Riebesell U, Gattuso J-P. Lessons learned from ocean acidification research. *Nat Clim Chang*. 2015; 5: 12–14. doi: [10.1038/nclimate2456](#)
8. Hall-Spencer JM, Rodolfo-Metalpa R, Martin S, Ransome E, Fine M, Turner SM, et al. Volcanic carbon dioxide vents show ecosystem effects of ocean acidification. *Nature*. 2008; 454: 96–99. doi: [10.1038/nature07051](#) PMID: [18536730](#)
9. Fabricius KE, Langdon C, Uthicke S, Humphrey C, Noonan S, De'ath G, et al. Losers and winners in coral reefs acclimatized to elevated carbon dioxide concentrations. *Nat Clim Chang*. 2011; 1: 165–169. doi: [10.1038/nclimate1122](#)
10. Calosi P, Rastrick SPS, Lombardi C, de Guzman HJ, Davidson L, Jahnke M, et al. Adaptation and acclimatization to ocean acidification in marine ectotherms: an in situ transplant experiment with polychaetes at a shallow CO₂ vent system. *Philos Trans Biol Sci*. 2013; 368: 1–15. doi: [10.1098/rstb.2012.0444](#)
11. Pettit LR, Hart MB, Medina-Sánchez AN, Smart CW, Rodolfo-Metalpa R, Hall-Spencer JM, et al. Benthic foraminifera show some resilience to ocean acidification in the northern Gulf of California, Mexico. *Mar Pollut Bull*. 2013; 73: 452–462. doi: [10.1016/j.marpolbul.2013.02.011](#) PMID: [23473095](#)
12. Ziveri P, Passaro M, Incarbona A, Milazzo M, Rodolfo-Metalpa R, Hall-Spencer JM. Decline in coccolithophore diversity and impact on coccolith morphogenesis along a natural CO₂ gradient. *Biol Bull*. 2014; 226: 282–290. PMID: [25070871](#)
13. Riebesell U, Tortell PD. Effects of ocean acidification on pelagic organisms and ecosystems. In: Gattuso J-P, Hansson L, editors. *Ocean acidification*. Oxford: Oxford University Press; 2011. pp. 99–121.
14. Paul AJ, Bach LT, Schulz K-G, Boxhammer T, Czerny J, Achterberg EP, et al. Effect of elevated CO₂ on organic matter pools and fluxes in a summer Baltic Sea plankton community. *Biogeosciences*. 2015; 12: 6181–6203. doi: [10.5194/bg-12-6181/2015/](#)
15. Sswat M, Boxhammer T, Jutfelt F, Bach LT, Nicolai M, Riebesell U. Video of a plankton community enclosed in a “Kiel Off-Shore Mesocosm for future Ocean Simulations” (KOSMOS) during the long-term study in Gullmar Fjord (Sweden) 2013. 2015. doi: [10.3289/KOSMOS_PLANKTON_SWEDEN_2013](#)
16. Scheinin M, Riebesell U, Rynearson TA, Lohbeck KT, Collins S. Experimental evolution gone wild. *J R Soc Interface*. 2015; 12: 1–5. doi: [10.1098/rsif.2015.0056](#)
17. Stocker TF, Qin D, Plattner G-K, Tignor M, Allen SK, Boschung J, et al. *Climate Change 2013: The Physical Science Basis. Contribution of Working Group I to the Fifth Assessment Report of the Intergovernmental Panel on Climate Change*. Cambridge; 2013 p. 1535 pp. doi: [10.1017/CBO9781107415324](#)
18. Arneborg L, Liljebladh B. The Internal Seiches in Gullmar Fjord. Part II: Contribution to Basin Water Mixing. *J Phys Oceanogr*. 2001; 31: 2549–2566. doi: [10.1175/1520-0485\(2001\)031<2567:TISIGF>2.0.CO;2](#)
19. Kilnäs M, Harlen A, Mättetnik M, Oskarsson O, Wikmar M, Sundin H, et al. Sjömätning i Gullmarsfjorden. 2006 pp. 1–24. Available: [www.o.lst.se](#)
20. Arneborg L, Erlandsson CP, Liljebladh B, Stigebrandt A. The rate of inflow and mixing during deep-water renewal in a sill fjord. *Limnol Oceanogr*. 2004; 49: 768–777. doi: [10.4319/lo.2004.49.3.0768](#)
21. Arneborg L. Turnover times for the water above sill level in Gullmar Fjord. *Cont Shelf Res*. 2004; 24: 443–460. doi: [10.1016/j.csr.2003.12.005](#)
22. Lindahl O, Belgrano A, Davidsson L, Hernroth B. Primary production, climatic oscillations, and physico-chemical processes: the Gullmar Fjord time-series data set (1985–1996). *ICES J Mar Sci*. 1998; 55: 723–729. doi: [10.1006/jmsc.1998.0379](#)
23. Riebesell U, Czerny J, von Bröckel K, Boxhammer T, Büdenbender J, Deckelnick M, et al. Technical Note: A mobile sea-going mesocosm system—new opportunities for ocean change research. *Biogeosciences*. 2013; 10: 1835–1847. doi: [10.5194/bg-10-1835-2013](#)

24. Czerny J, Schulz KG, Krug SA, Ludwig A, Riebesell U. Technical note: The determination of enclosed water volume in large flexible-wall mesocosms "KOSMOS." *Biogeosciences*. 2013; 10: 1937–1941. doi: [10.5194/bg-10-1937-2013](https://doi.org/10.5194/bg-10-1937-2013)
25. Dorey N, Lançon P, Thorndyke M, Dupont S. Assessing physiological tipping point of sea urchin larvae exposed to a broad range of pH. *Glob Chang Biol*. 2013; 19: 3355–3367. doi: [10.1111/gcb.12276](https://doi.org/10.1111/gcb.12276) PMID: [23744556](https://pubmed.ncbi.nlm.nih.gov/23744556/)
26. Boxhammer T, Bach LT, Czerny J, Riebesell U. Technical Note: Sampling and processing of mesocosm sediment trap material for quantitative biogeochemical analysis. *Biogeosciences*. 2016; 13: 2. doi: [10.5194/bgd-12-18693-2015](https://doi.org/10.5194/bgd-12-18693-2015)
27. Schulz KG, Riebesell U. Diurnal changes in seawater carbonate chemistry speciation at increasing atmospheric carbon dioxide. *Mar Biol*. 2013; 160: 1889–1899. doi: [10.1007/s00227-012-1965-y](https://doi.org/10.1007/s00227-012-1965-y) PMID: [24391286](https://pubmed.ncbi.nlm.nih.gov/24391286/)
28. Patey MD, Rijkenberg MJA, Statham PJ, Stinchcombe MC, Achterberg EP, Mowlem M. Determination of nitrate and phosphate in seawater at nanomolar concentrations. *TrAC Trends Anal Chem*. 2008; 27: 169–182. doi: [10.1016/j.trac.2007.12.006](https://doi.org/10.1016/j.trac.2007.12.006)
29. Murphy J, Riley JP. A modified single solution method for the determination of phosphate in natural waters. *Analytica Chimica Acta*. 1962. pp. 31–36. doi: [10.1016/S0003-2670\(00\)88444-5](https://doi.org/10.1016/S0003-2670(00)88444-5)
30. Hansen HP, Grasshoff K. Automated chemical analysis. In: Grasshoff K, Kremling K, Ehrhardt M, editors. *Methods of Seawater Analysis* Verlag Chemie, Weinheim. Wiley-VCH; 1983. pp. 347–379.
31. Holmes RM, Aminot A, K erouel R, Hooker BA, Peterson BJ. A simple and precise method for measuring ammonium in marine and freshwater ecosystems. *Can J Fish Aquat Sci*. 1999; 56: 1801–1808. doi: [10.1139/f99-128](https://doi.org/10.1139/f99-128)
32. Zark M, Riebesell U, Dittmar T. Effects of ocean acidification on marine dissolved organic matter are not detectable over the succession of phytoplankton blooms. *Sci Adv*. 2015; 1: e1500531. doi: [10.1126/sciadv.1500531](https://doi.org/10.1126/sciadv.1500531) PMID: [26601292](https://pubmed.ncbi.nlm.nih.gov/26601292/)
33. Johnson K, Sieburth JM, Williams PJ, Br andstr om L. Coulometric total carbon dioxide analysis for marine studies: automation and calibration. *Mar Chem*. 1987; 21: 117–133. doi: [10.1016/0304-4203\(87\)90033-8](https://doi.org/10.1016/0304-4203(87)90033-8)
34. Clayton TD, Byrne RH. Spectrophotometric seawater pH measurements: total hydrogen ion concentration scale calibration of m-cresol purple and at-sea results. *Deep Sea Res Part I Oceanogr Res Pap*. 1993; 40: 2115–2129.
35. Pierrot D, Lewis E, Wallace DWR. MS excel program developed for CO₂ system calculations. ORNL/CDIAC-105a Carbon Dioxide Inf Anal Center, Oak Ridge Natl Lab US Dep Energy, Oak Ridge, Tennessee. 2006;
36. Lueker TJ, Dickson AG, Keeling CD. Ocean pCO₂ calculated from dissolved inorganic carbon, alkalinity, and equations for K₁ and K₂: Validation based on laboratory measurements of CO₂ in gas and seawater at equilibrium. *Mar Chem*. 2000; 70: 105–119. doi: [10.1016/S0304-4203\(00\)00022-0](https://doi.org/10.1016/S0304-4203(00)00022-0)
37. Hansen HP, Koroleff F. Determination of nutrients. In: Grasshoff K, Kremling K, Ehrhardt M, editors. *Methods of Seawater Analysis*. Weinheim: Wiley-VCH; 1999. pp. 159–226.
38. Sharp JH. Improved analysis for "particulate" organic carbon and nitrogen from seawater. *Limnol Oceanogr*. 1974; 19: 984–989.
39. Barlow RG, Cummings DG, Gibb SW. Improved resolution of mono- and divinyl chlorophylls a and b and zeaxanthin and lutein in phytoplankton extracts using reverse phase C-8 HPLC. *Mar Ecol Prog Ser*. 1997; 161: 303–307. doi: [10.3354/meps161303](https://doi.org/10.3354/meps161303)
40. Mackey MD, Mackey DJ, Higgins HW, Wright SW. CHEMTAX- a program for estimating class abundances from chemical markers: application to HPLC measurements of phytoplankton. *Mar Ecol Prog Ser*. 1996; 144: 265–283.
41. Marie D, Partensky F, Vaulot D, Brussaard CPD. Enumeration of phytoplankton, bacteria, and viruses in marine samples. In: Robinson JPEA, editor. *Current protocols in cytometry*. New York: John Wiley and sons; 2001. pp. 1–14. doi: [10.1002/0471142956.cy1111s10](https://doi.org/10.1002/0471142956.cy1111s10)
42. Larsen A, Castberg T, Sandaa RA, Brussaard CPD, Egge J, Heldal M, et al. Population dynamics and diversity of phytoplankton, bacteria and viruses in a seawater enclosure. *Mar Ecol Prog Ser*. 2001; 221: 47–57. doi: [10.3354/meps221047](https://doi.org/10.3354/meps221047)
43. Brussaard CPD. Optimization of Procedures for Counting Viruses by Flow Cytometry. *Appl Environ Microbiol*. 2004; 70: 1506–1513. doi: [10.1128/AEM.70.3.1506](https://doi.org/10.1128/AEM.70.3.1506) PMID: [15006772](https://pubmed.ncbi.nlm.nih.gov/15006772/)
44. Veldhuis MJW, Kraay GW. Application of flow cytometry in marine phytoplankton research: current applications and future perspectives. *Sci Mar*. 2000; 64: 121–134.
45. Clarke KR. Non-parametric multivariate analyses of changes in community structure. *Aust J Ecol*. 1993; 18: 117–143. doi: [10.1111/j.1442-9993.1993.tb00438.x](https://doi.org/10.1111/j.1442-9993.1993.tb00438.x)

46. Jones DL. Fathom Toolbox for Matlab: software for multivariate ecological and oceanographic data analysis. College of Marine Science, University of South Florida, St. Petersburg, FL, USA; 2015.
47. Calliari D, Tiselius P. Organic carbon fluxes through the mesozooplankton and their variability at different time-scales in the Gullmarsfjord, Sweden. *Estuar Coast Shelf Sci.* 2009; 85: 107–117. doi: [10.1016/j.ecss.2009.06.016](https://doi.org/10.1016/j.ecss.2009.06.016)
48. Bach LT. Reconsidering the role of carbonate ion concentration in calcification by marine organisms. *Biogeosciences.* 2015; 12: 4939–4951. doi: [10.5194/bg-12-4939-2015](https://doi.org/10.5194/bg-12-4939-2015)
49. Czerny J, Schulz KG, Ludwig A, Riebesell U. Technical Note: A simple method for air-sea gas exchange measurements in mesocosms and its application in carbon budgeting. *Biogeosciences.* 2013; 10: 1379–1390. doi: [10.5194/bg-10-1379-2013](https://doi.org/10.5194/bg-10-1379-2013)
50. Schaum E, Rost B, Millar AJ, Collins S. Variation in plastic responses of a globally distributed picoplankton species to ocean acidification. *Nat Clim Chang.* 2012; 3: 298–302. doi: [10.1038/nclimate1774](https://doi.org/10.1038/nclimate1774)
51. Sala MM, Aparicio FL, Balagué V, Boras JA, Borrull E, Cardelús C, et al. Contrasting effects of ocean acidification on the microbial food web under different trophic conditions. *Ices J Mar Sci.* 2015; 73: 670–679. doi: [10.1093/icesjms/fsv130](https://doi.org/10.1093/icesjms/fsv130)



Molecular evidence for abiotic sulfurization of dissolved organic matter in marine shallow hydrothermal systems

Gonzalo V. Gomez-Saez^{a,*}, Jutta Niggemann^b, Thorsten Dittmar^b,
Anika M. Pohlabein^b, Susan Q. Lang^{c,d}, Ann Noowong^e, Thomas Pichler^f,
Lars Wörmer^g, Solveig I. Bühring^a

^a Hydrothermal Geomicrobiology Group, MARUM – Center for Marine Environmental Sciences, University of Bremen, PO Box 330440, 28334 Bremen, Germany

^b Research Group for Marine Geochemistry (ICBM – MPI Bridging Group), Institute for Chemistry and Biology of the Marine Environment (ICBM), University of Oldenburg, Carl-von-Ossietzky-Str. 9-11, 26129 Oldenburg, Germany

^c Department of Earth Sciences, Swiss Federal Institute of Technology ETH Zürich, 8092 Zürich, Switzerland

^d Earth and Ocean Sciences, 701 Sumter Street, EWS 617, University of South Carolina, Columbia, SC 29208, USA

^e Department of Physics and Earth Sciences, Jacobs University Bremen, Campus Ring 1, 28759 Bremen, Germany

^f Geochemistry and Hydrogeology Group, University of Bremen, PO Box 330440, 28334 Bremen, Germany

^g Organic Geochemistry Group, MARUM – Center for Marine Environmental Sciences, Department of Geosciences, University of Bremen, 28359 Bremen, Germany

Received 28 October 2015; accepted in revised form 19 June 2016; available online 23 June 2016

Abstract

Shallow submarine hydrothermal systems are extreme environments with strong redox gradients at the interface of hot, reduced fluids and cold, oxygenated seawater. Hydrothermal fluids are often depleted in sulfate when compared to surrounding seawater and can contain high concentrations of hydrogen sulfide (H₂S). It is well known that sulfur in its various oxidation states plays an important role in processing and transformation of organic matter. However, the formation and the reactivity of dissolved organic sulfur (DOS) in the water column at hydrothermal systems are so far not well understood. We investigated DOS dynamics and its relation to the physicochemical environment by studying the molecular composition of dissolved organic matter (DOM) in three contrasting shallow hydrothermal systems off Milos (Eastern Mediterranean), Dominica (Caribbean Sea) and Iceland (North Atlantic). We used ultra-high resolution Fourier transform ion cyclotron resonance mass spectrometry (FT-ICR-MS) to characterize the DOM on a molecular level. The molecular information was complemented with general geochemical data, quantitative dissolved organic carbon (DOC) and DOS analyses as well as isotopic measurements ($\delta^2\text{H}$, $\delta^{18}\text{O}$ and F^{14}C). In contrast to the predominantly meteoric fluids from Dominica and Iceland, hydrothermal fluids from Milos were mainly fed by recirculating seawater. The hydrothermal fluids from Milos were enriched in H₂S and DOS, as indicated by high DOS/DOC ratios and by the fact that >90% of all assigned DOM formulas that were exclusively present in the fluids contained sulfur. In all three systems, DOS from hydrothermal fluids had on average lower O/C ratios (0.26–0.34) than surrounding surface seawater DOS (0.45–0.52), suggesting shallow hydrothermal systems as a source of reduced DOS, which will likely get oxidized upon contact with oxygenated seawater. Evaluation of hypothetical sulfurization reactions suggests DOM reduction and sulfurization during seawater recirculation in Milos seafloor. The four most effective potential sulfurization reactions were those exchanging an O atom by one S atom in the formula or the equivalent + H₂S reaction, correspondingly exchanging H₂O, H₂ and/or O₂ by a H₂S molecule. Our study reveals novel insights into DOS

* Corresponding author at: Research Group for Marine Geochemistry (ICBM – MPI Bridging Group), Institute for Chemistry and Biology of the Marine Environment (ICBM), University of Oldenburg, Carl-von-Ossietzky-Str. 9-11, 26129 Oldenburg, Germany.

E-mail address: gonzalo.gomez@uni-oldenburg.de (G.V. Gomez-Saez).

dynamics in marine hydrothermal environments and provides a conceptual framework for molecular-scale mechanisms in organic sulfur geochemistry.

© 2016 Elsevier Ltd. All rights reserved.

Keywords: Marine shallow hydrothermal systems; Dissolved organic matter (DOM); Dissolved organic sulfur (DOS); FT-ICR-MS; Milos (Eastern Mediterranean); Dominica (Caribbean Sea); Iceland (North Atlantic)

1. INTRODUCTION

Dissolved organic matter (DOM) is defined as the organic components in water that pass through a $\leq 0.7 \mu\text{m}$ filter. The importance of DOM in global geochemistry relies on the enormous amount of carbon that is dissolved in the oceans, quantified as more than 200 times the carbon of all living marine biomass (Hansell et al., 2009) and being similar to all atmospheric CO_2 (Hedges, 1992). Thus, changes in DOM dynamics may have implications for local and global carbon cycling processes (Battin et al., 2009; Dittmar and Stubbins, 2014; German et al., 2015). While molecular DOM characterization of a range of marine habitats has become available in the last years (e.g. Lechtenfeld et al., 2014; Hansman et al., 2015), there exists a striking scarcity of studies targeting specifically the role of organic sulfur species in DOM (e.g. Lechtenfeld et al., 2011; Pohlabein and Dittmar, 2015). Sulfur plays a considerable role in the various transformations of organic matter, from early diagenesis to the late stage of catagenesis, due to its ability to exist in many different oxidation states (Aizenshtat et al., 1995; Sleighter et al., 2014). In marine sediments, organic sulfur is quantitatively the second most important sulfur pool only behind pyrite, frequently accounting for 35% of total sedimentary sulfur in many marine environments (Zaback and Pratt, 1992; Cutter and Kluckhohn, 1999; Werne et al., 2004; Zhu et al., 2014). Abiotic sulfurization can contribute to the stabilization of organic matter (Sinninghe Damsté et al., 1989; Sinninghe Damsté and de Leeuw, 1990) but whether it also contributes to the stability of DOM in the oceans is still an open research question (Dittmar, 2015).

A significant contribution to the understanding of dissolved organic sulfur (DOS) origin and fate may be achieved through the investigation of DOS biogeochemistry at hydrothermal systems. Hydrothermal activity has been operating for most of the Earth's history, occurring over a wide depth range in the oceans, from intertidal to the abyss (Sander and Koschinsky, 2011). Hydrothermal vents have been postulated as possible sites for the first steps of organic chemical evolution, where sulfur reduction might have played a role in prebiotic chemical processes occurring in sulfide-rich environments (Russell and Hall, 1997; Cody et al., 2000; Hebling et al., 2006; McCollom and Seewald, 2007). The hydrothermal vents located at less than 200 m water depth are categorized as shallow-water hydrothermal systems (Tarasov et al., 2005). They are easily accessible extreme environments with strong redox gradients and unique biogeochemical conditions due to the interaction of hot, reduced fluids and cold, oxygenated seawater (e.g. Dando et al., 1999; Tarasov et al., 2005). The main group

of solid phase extractable (SPE) DOS in the open ocean was recently identified as unreactive sulfonic acids (Pohlabein and Dittmar, 2015). In hydrothermal systems, reduced sulfur compounds are expected to be released and quickly oxidized to form sulfonic acids once they reach the oxic sediment surface or water column. Some functional groups like thiols and thioethers could be produced by reaction of reduced inorganic sulfur compounds with organic matter (Sinninghe Damsté et al., 1989; Aizenshtat et al., 1995; Schneckenburger et al., 1998; Hertkorn et al., 2013; Sleighter et al., 2014) and then be rapidly oxidized to sulfonic acids as well (Pohlabein and Dittmar, 2015). However, neither the pathways of sulfurization nor of oxidation of DOS at hydrothermal systems are well understood (Zhu et al., 2014; Pohlabein and Dittmar, 2015).

Recent advances in mass spectrometry allow characterization of the complex mixture of DOM at a molecular level. Fourier transform ion cyclotron resonance mass spectrometry (FT-ICR-MS) in combination with soft ionization techniques such as electrospray ionization (ESI) provides molecular information on individual compounds without prior chromatographic separation. Thousands of molecular formulas containing C, H, O, N, S or P can be attributed to a single water sample (e.g. Marshall et al., 1998; Kujawinski et al., 2002; Kujawinski and Behn, 2006; Schmidt et al., 2014; Zark et al., 2015), providing unique data sets to study the multitude of processes that affect the composition of the DOM pool in the oceans. The aim of this paper is to characterize at a molecular level DOS variations at the interface between hot, reduced hydrothermal fluids and cold, oxygenated seawater in three contrasting marine shallow-water hydrothermal systems off the coast of Milos (Eastern Mediterranean), Dominica (Caribbean Sea) and Iceland (North Atlantic) (Fig. 1). We hypothesize that in shallow hydrothermal systems (1) the reduced DOS released from hydrothermal fluids is oxidized upon contact with oxygenated seawater and (2) there is DOM reduction and sulfurization during seawater recirculation through the subsurface. Therefore, within a robust geochemical data set we specifically investigated (1) the impact of physicochemical properties on the DOM signature and (2) the molecular similarities and differences in DOS between shallow hydrothermal fluids and surrounding surface seawater samples.

2. STUDY SITES

2.1. Milos

Milos Island is located in the tectonically active region of the Hellenic Volcanic Arc in the Eastern Mediterranean

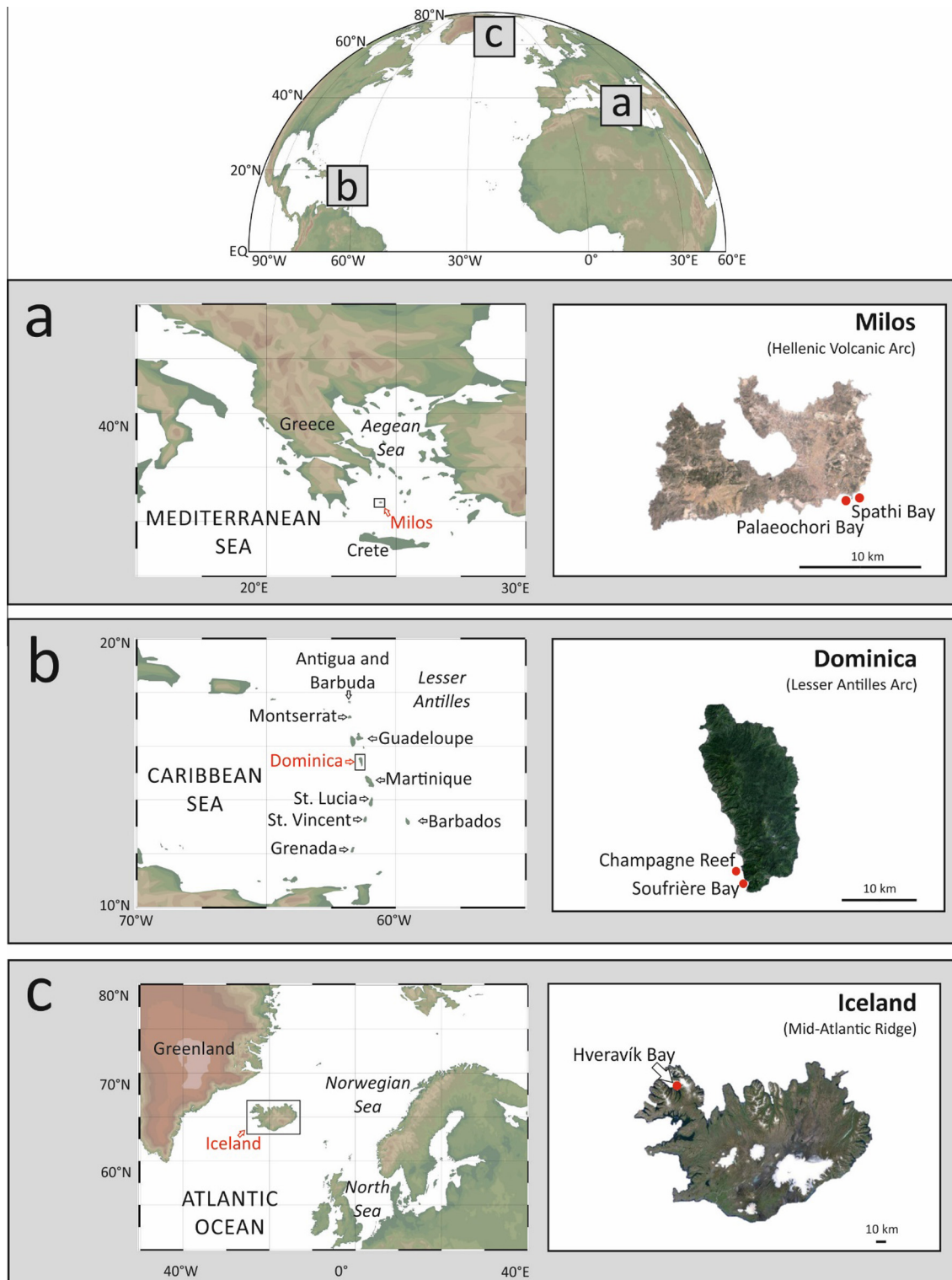


Fig. 1. Shallow-water hydrothermal systems studied: (a) Milos (Hellenic Volcanic Arc, Eastern Mediterranean), (b) Dominica (Lesser Antilles Arc, Caribbean Sea) and (c) Iceland (Mid-Atlantic Ridge, North Atlantic). Maps were created using Ocean Data View (R. Schlitzer, <http://odv.awi.de>) and Google Earth (<http://earth.google.com>).

(Dando et al., 1999; Fig. 1a). The volcanism of the Hellenic Volcanic Arc is linked to the subduction of the African plate beneath the Aegean micro plate. It started during

the Early to Middle Pliocene and the last eruption occurred 90,000 years ago (McKenzie, 1972). Milos hydrothermal activity occurs on shore but also in the shallow waters off

the coast (Kleint et al., 2015). The marine shallow hydrothermal vents off Milos cover an area of about 35 km² and hot fluids can reach temperatures up to 150 °C (Dando et al., 1995, 1999). Two types of venting activity are observed in Milos hydrothermal system: a gas-dominated focused flow with visible gas bubbles, containing mainly CO₂, plus minor contributions from H₂, H₂S and CH₄, and a brine-rich fluid seep enriched in Ca, Na, K, SiO₂, Mn and NH₃ (Dando et al., 1995; Fitzsimmons et al., 1997; Yücel et al., 2013). Abundant yellow, white and orange patches appear in Milos sediment as a result of elemental sulfur or arsenic sulfide precipitates (Price et al., 2013). In this study, the hydrothermal fluids released at the most intense submarine venting area in the south-east of Milos, at Palaeochori and Spathi bays (Fig. 1a), were investigated.

2.2. Dominica

Dominica has been the volcanically most productive island in the Lesser Antilles arc over the last 100,000 years and one of the most productive worldwide (Wadge, 1984; Lindsay et al., 2005). It belongs to the Lesser Antilles archipelago, between the Atlantic Ocean and the Caribbean Sea, which represents one of only two active arc systems in the Atlantic Ocean (Fig. 1b). Most of the Lesser Antilles islands in the Caribbean Sea only have a single vent, but Dominica has nine potentially active volcanic centres (Lindsay et al., 2005; Joseph et al., 2011). Quaternary volcanic activity on Dominica has been dominated by intermediate to felsic magmas, erupted as large-volume ignimbrites and dome complexes (Lindsay et al., 2005; Kleint et al., 2015). Dominica submarine hydrothermal venting occurs mainly along the submerged flank of the Plat Pays Volcanic Complex in the south-west of the island, with fluid temperatures ranging between 44 and 75 °C (McCarthy et al., 2005; Gomez-Saez et al., 2015). The hydrothermal fluids are characterised by high concentrations of ferrous iron, which is immediately oxidized upon contact with oxygenated seawater, leading to the formation of orange patches in the sediment composed of hydrous ferric oxide precipitates (McCarthy et al., 2005; Gomez-Saez et al., 2015). For this study, the hydrothermal fluids released at Champagne Reef and Soufrière Bay submarine venting systems in the south-west of Dominica (Fig. 1b) were investigated.

2.3. Iceland

Iceland is located on the volcanically active Mid-Atlantic ridge system and represents the largest area of sub-aerially exposed mid-ocean ridge on Earth (Höskuldsson et al., 2007). In northern Iceland, several localities are known with submarine geothermal activity in basaltic lava of 6–12 million years of age (Marteinsson et al., 2001). The low-temperature systems in Iceland have by definition a reservoir temperature below 150 °C at 1 km depth and are mainly located outside the volcanic zone that passes through Iceland (Axelsson et al., 2010). The hot springs in the north-west region of the Reykjanes

peninsula are considered as one of the most extreme microbial environments on Earth (Hobel et al., 2005). The Reykjanes geothermal system is supplied with deep fresh and slightly alkaline groundwater, with low sulfide concentrations and fluid temperatures ranging between 45 and 95 °C (Kristjansson et al., 1986). Freshwater hot springs have been described on the seashore, from the tidal zone to about 100 m off the coast (Hobel et al., 2005). The hydrothermal vents in this area are influenced by tides as high as 4 m, leading to almost 100 °C temperature fluctuations implying severe changes in salinity, light penetration and oxygen concentration (Hobel et al., 2005). In this study, the Hveravík Bay hydrothermal system in the Reykjanes peninsula in north-west Iceland was investigated (Fig. 1c). We sampled a shallow vent, which was air-exposed under low tide conditions (Hveravík-1) and another permanently submerged vent (Hveravík-2).

3. MATERIALS AND METHODS

3.1. Field work

The hydrothermal fluids and seawater samples for this study were taken during field expeditions to Milos (11th–30th of May 2012), Dominica (9th–24th of April 2013) and Iceland (15th–30th of June 2014). Identification of hot-fluid spots in the area were carried out by SCUBA diving using the same *in situ* temperature probes as in previous studies (e.g. Price et al., 2013; Gomez-Saez et al., 2015). Fluid samples were collected with a funnel placed on the vent orifice which opened into food-grade large volume nylon bags. On shore, 2 L polycarbonate bottles (Nalgene, USA), previously cleaned with ultrapure pH 2 water, were filled with the hydrothermal fluids up to the top to prevent headspace, immediately closed and kept in the dark until filtration and acidification. Surface seawater samples were taken directly into the 2 L bottles. Samples were filtered using pre-combusted glass microfiber filters (GF/F, pore size: 0.7 µm, diameter: 47 mm; Whatman), acidified to pH 2 (HCl 25% p.a., Carl Roth, Germany) and kept at 4 °C in the dark until extraction.

3.2. Geochemical parameters

Temperature, pH and salinity were measured directly in the field. The pH and salinity were determined using a WTW pH meter 3210 with Mic-D electrode. Aliquots of 4 mL filtered (0.2 µm, GHP Pall Acrodisc) vent fluids were kept sealed in cold storage at 4 °C for transport to the laboratory. Analyses of inorganic geochemical parameters of Milos and Dominica samples were performed at the University of Bremen (Germany) and in the case of Iceland samples at Jacobs University (Germany), following established procedures for hydrothermal fluids from marine shallow-water hydrothermal systems (e.g. McCarthy et al., 2005; Price et al., 2013; Gomez-Saez et al., 2015; Kleint et al., 2015). Aliquots for H₂S analysis were preserved by precipitation of ZnS and analyzed using a Merck photometer at a wavelength of 670 nm (e.g. Price et al., 2013). The anions Br, Cl, F and SO₄ were determined by

ion chromatography using a Metrohm system (Switzerland). The cations of As, Ca, Fe, K, Li, Mg, Mn, Na, Si and Sr were measured by inductively coupled plasma-optical emission spectroscopy (ICP-OES) using a Perkin Elmer Optima 7300 (USA). Oxygen and deuterium isotopic analyses were performed on filtered samples (0.2 μm , GHP Pall Acrodisc) using a LGR liquid water isotope analyzer (LWIA-24d) at the University of Bremen (Germany) (e.g. McCarthy et al., 2005; Price et al., 2013). All isotopic values are reported using the standard delta notation. Both $\delta^{18}\text{O}$ and $\delta^2\text{H}$ are expressed relative to Vienna Standard Mean Ocean Water (VSMOW; Craig, 1961).

3.3. Dissolved organic matter

Aliquots of 20 mL (triplicates per sample), filtered (0.7 μm ; GF/F; Whatman) and acidified to pH 2, were analyzed for dissolved organic carbon (DOC) concentration via high temperature catalytic combustion using a Shimadzu TOC-VCPH/CPN Total Organic Carbon Analyzer at the University of Oldenburg (Germany). Accuracy of DOC determination was checked daily by analyzing the deep-sea reference provided by D. Hansell (University of Miami, USA). DOM was extracted from filtered and acidified samples by solid phase extraction (SPE) using divinyl benzene polymer in pre-packed cartridges (1 g PPL, Agilent, USA) according to Dittmar et al. (2008). Acidification of the sample to pH 2 is recommended for DOM extraction of natural water samples in FT-ICR-MS analysis, because the majority of natural DOM is assumed to consist of organic acids (Dittmar et al., 2008). Although low pH may decrease binding strengths, protonation of the binding sites is not high enough to completely dissociate metals like iron from acid-stable metal–organic complexes (Waska et al., 2015). Prior to extraction, the cartridges were soaked with methanol for 24 h and rinsed afterwards twice each, with ultrapure water, methanol (VWR, USA) and ultrapure water at pH 2. After loading DOM onto the adsorbing resin (PPL) of the SPE cartridge, the remaining salts were removed by rinsing with ultrapure water at pH 2 and dried by pressing air through the cartridge with a clean air-syringe (20 mL, Braun, Germany). DOM was eluted with 6 mL of methanol (HPLC-grade, Sigma–Aldrich, USA) and the SPE-DOM extracts were stored in amber vials at $-20\text{ }^\circ\text{C}$. The extraction efficiency of PPL adsorber is on average 62% for marine samples (Dittmar et al., 2008). However, high-temperature fluid samples usually have lower SPE-DOC concentrations and lower extraction volumes (Hawkes et al., 2015, 2016; Rossel et al., 2015). Accordingly, we found on average lower SPE extraction efficiencies in hydrothermal fluids ($35 \pm 5\%$) than in surface seawater samples ($45 \pm 31\%$). Aliquots of the SPE-DOM extracts were used to determine the SPE-DOS concentration and ^{14}C content. Sulfur concentrations were measured using an ICP-OES (iCAP 6000, Thermo, Bremen, Germany) at the University of Oldenburg (Germany) according to Pohlabeln and Dittmar (2015). The radiocarbon analyses of Milos SPE-DOC were carried out by Accelerator Mass Spectrometry (AMS) at the Institute of Particle Physics and the Geological Institute of the ETH Zürich

(Zürich, Switzerland). Aliquots of the SPE-DOM extracts were transferred to pre-combusted quartz tubes ($850\text{ }^\circ\text{C}$, 5 h), dried under high purity helium, and flame sealed with combusted CuO under vacuum. CO_2 was cryogenically captured and measured using a microscale radiocarbon dating system and gas feeding system (MICADAS; Synal et al., 2007; Ruff et al., 2007, 2010; Wacker et al., 2010). Processing blanks, where ultrapure water was solid phase extracted in an identical manner, were also analyzed but contained insufficient carbon for ^{14}C analysis. Data are reported as fraction modern ($F^{14}\text{C}$) after Reimer et al. (2004) to differentiate between dead ($F^{14}\text{C} = 0$) and modern ($F^{14}\text{C} = 1$) radiocarbon. The total measured $F^{14}\text{C}$ value is a mixture of the sample and blank contributions: $F_T * C_T = F_S * C_S + F_{EX} * C_{EX}$, where F is the $F^{14}\text{C}$ fraction modern radiocarbon content and C is the amount of carbon of the total measurement (subscript T), the sample (subscript S), and the extraneous carbon (subscript EX) (Lang et al., 2013).

For characterization of DOM molecular composition, mass spectra were obtained in negative ionization mode using the 15 Tesla FT-ICR-MS (Solarix, Bruker Daltonik, Bremen, Germany) at the University of Oldenburg (Germany) combined with an ESI device (Bruker Apollo II) with a needle voltage set to -4 kV . A total of 500 scans were accumulated per run. The mass-to-charge window was set to 150–2000 Da. For control of overall mass spectrometry quality and reproducibility, twice a day an in-house reference of DOM from North Equatorial Pacific Intermediate Water (NEqPIW) was analyzed (Green et al., 2014; Riedel and Dittmar, 2014). A common detection limit on the relative signal intensity scale was applied to facilitate maximum comparability among samples (Riedel and Dittmar, 2014), and this explains the relatively low number of compounds detected in NEqPIW compared to previous studies (Table 2). Internal calibration of the spectra was performed using the Bruker Daltonics Data Analysis software package with help of an established calibration list for marine DOM, consisting of >100 mass calibration points of known molecular formulas. The data were processed using in-house Matlab routines (Riedel et al., 2012) and molecular formulas with $\text{C}_{1-100}\text{H}_{1-250}\text{O}_{1-100}\text{N}_{0-4}\text{S}_{0-2}$ or P_{0-1} were assigned to peaks with a minimum signal-to-noise ratio of four according to Koch et al. (2007). For the Iceland samples, where duplicates or triplicates were available, only those molecular formulas detected in all analytical replicates were accepted (80–91% of total formulas), which decreased the number of formulas but efficiently removed non-analytes from the data set that only result from noise in the mass spectra (Riedel and Dittmar, 2014). Additionally, we analyzed blank samples and all of the DOM formulas detected in the blanks were removed from our DOM dataset. Since the hydrothermal fluids sampling methodology was identical for the three study sites (Milos, Dominica and Iceland), the exclusive DOM or DOS fraction from the hydrothermal fluids was unlikely affected by the sampling procedure (food-grade large volume nylon bags).

The molecular formulas were used to calculate two indexes: the Double Bond Equivalence Index ($\text{DBE} = 1$

Table 1

Physicochemical composition of Milos, Dominica and Iceland surface seawater and shallow hydrothermal vent fluids. Being “n.a.” not analyzed and “b.d.” below detection limit. The Na – K geothermometer is in the form from Fournier (1979): $T (^{\circ}\text{C}) = (1217/\log(\text{Na}/\text{K}) + 1.483) - 273.15$; The Na – K – Ca geothermometer equation is in the form from Henley et al., (1984): $T (^{\circ}\text{C}) = (1647/(\log(\text{Na}/\text{K}) + 0.33 (\log(\text{Ca}) 1/2\text{Na}) + 2.06) + 2.47)) - 273.15$. Concentrations in geothermometer calculations are in mg/L.

	Seawater			Hydrothermal fluids						
	Milos	Dominica	Iceland	Milos		Dominica		Iceland		
				Palaeochori	Spathi	Champagne	Soufrière	Hveravík-1	Hveravík-2	
Water depth (m)	0	0	0	5	12	5	5	0	2	
Temperature ($^{\circ}\text{C}$)	20	28	11	81	65	75	55	86	80	
pH	8.2	7.9	8.2	4.9	5.7	6.3	6.3	8.0	8.3	
Salinity	38	34	31	56	33	17	11	2	5	
$\delta^2\text{H}$	8.6	6.3	-7.9	5.0	8.9	-1.9	-5.5	-76.6	-67.6	
$\delta^{18}\text{O}$	1.3	0.8	-0.4	2.6	1.2	-1.0	-1.3	-10.3	-9.4	
$\text{F}^{14}\text{C}_{\text{SPE}}$	1.02–1.03	n.a.	n.a.	0.78–0.81	0.77–0.79	n.a.	n.a.	n.a.	n.a.	
DOC (μM)	60	99	183	21	41	22	27	112	142	
DOS (μM)	1.8	0.2	0.5	0.8	1.3	0.1	0.1	0.1	0.2	
DOS/DOC ratio	0.0296	0.0024	0.0030	0.0375	0.0317	0.0026	0.0051	0.0009	0.0013	
Major elements and molecules (mM)	Br	0.97	0.83	0.98	1.23	0.92	0.40	0.20	0.01	0.06
	Ca	10.7	11.0	7.86	31.8	20.1	12.2	3.97	4.64	5.19
	Cl	664.0	569.6	623.1	947.8	633.6	273.5	141.8	22.4	85.0
	K	10.8	10.6	4.40	75.1	19.4	6.55	3.19	0.09	0.67
	Mg	57.2	60.3	48.1	25.9	99.8	29.4	18.2	0.10	6.37
	Na	503.2	513.6	397.6	673.7	893.8	314.3	149.3	13.9	65.3
	SO_4	29.9	26.1	26.7	8.36	29.7	10.4	7.42	0.95	5.43
Trace elements and molecules (μM)	B	463.3	409.7	586.5	2434.9	457.9	1119.5	543.2	321.9	414.4
	Fe	b.d.	b.d.	b.d.	229.7	24.2	88.2	214.7	b.d.	b.d.
	F	36.8	b.d.	239.5	52.6	31.6	b.d.	b.d.	14.3	19.7
	H_2S	b.d.	b.d.	b.d.	498.0	255.6	0.3	1.3	1.4	1.4
	Li	47.2	45.5	15.8	5296.8	129.6	256.8	64.3	1.15	4.03
	Mn	7.22	b.d.	b.d.	57.4	17.7	b.d.	b.d.	b.d.	b.d.
	Si	b.d.	b.d.	294.8	274.8	639.4	226.2	665.9	1438.2	1324.3
Sr	84.1	88.3	69.5	236.3	80.1	71.2	26.4	4.79	12.7	
Geothermometers ($^{\circ}\text{C}$)	Na/K	–	–	–	279	144	142	143	78	102
	Na – K – Ca	–	–	–	276	179	164	162	79	115

Table 2
Summary of molecular composition of the DOM as characterized by FT-ICR-MS, given in percentages of the relative abundances of all identified formulas, and as intensity-weighted average values, where indicated.

	Seawater			Hydrothermal fluids						Exclusive DOM of hydrothermal fluids			
	NEqPIW	Milos	Dominica	Iceland	Milos		Dominica		Iceland		Milos	Dominica	Iceland
					Palaeochori	Spathi	Champagne	Soufrière	Hveravfk-1	Hveravfk-2			
Total formulas	2418	3266	2538	1815	3430	3505	2840	2001	2127	322	223	124	
H/C ratio _{average}	1.25	1.25	1.25	1.20	1.25	1.25	1.18	1.13	1.20	1.37	1.03	1.51	
O/C ratio _{average}	0.49	0.49	0.49	0.49	0.43	0.47	0.43	0.43	0.47	0.32	0.32	0.25	
S/C ratio _{average}	0.003	0.003	0.002	0.003	0.009	0.007	0.005	0.005	0.005	0.062	0.022	0.013	
DBE index _{average}	8.9	8.4	8.4	8.8	7.9	8.1	9.3	9.4	8.9	6.3	11.0	7.7	
AI _{mod} index _{average}	0.2	0.2	0.2	0.3	0.3	0.3	0.3	0.3	0.3	0.2	0.4	0.2	
Aromatics %	7	6	9	13	6	6	12	21	15	5	35	9	
Condensed aromatics %	<1	<1	1	4	<1	<1	2	5	3	0	5	0	

+ \emptyset (2C – H + N + P)) in order to assess the degree of unsaturation, and the modified Aromaticity Index (AI_{mod} = (1 + C – \emptyset O – S – \emptyset (N + P + H))/(C – \emptyset O – S – N – P)) to estimate the presence and abundance of aromatics (AI_{mod} \geq 0.5) and condensed aromatics (AI_{mod} \geq 0.66), taking into consideration the abundance of carboxyl groups in natural organic matter (Koch and Dittmar, 2006). Condensed aromatics containing nitrogen, sulfur or phosphorus were excluded for data interpretation as they were not specifically confirmed by the presence of the respective ¹³C isotopologs due to their low abundance in the mass spectra. Signal intensities of individual signals were converted into percentages relative to total signal intensity of each sample. These relative signal intensities were used to calculate intensity-weighted averages of DBE, AI_{mod} and molar ratios (H/C, O/C, S/C) (e.g. Schmidt et al., 2009; Seidel et al., 2014).

Potential sulfurization reactions were tested in the FT-ICR-MS dataset on the basis of relationships of molecular formulas and the geochemical context (e.g. Schmidt et al., 2014). The following nine possibilities of S addition while adding/removing H and/or O were tested with 27 potential reactions (Table 3), differentiating between oxidative and reductive ones: oxidative sulfurization reactions structure: + S₁; + S₁/ – H_n; + H_nS₁O_n; + S₁O_n; + S₁O_n/ – H_n; reductive sulfurization reactions structure: + H_nS₁; + S₁/ – H_nO_n; + S₁/ – O_n; + H_nS₁/ – O_n. The effectiveness of the potential sulfurization reactions was considered as a percentage of mono-S compounds (CHOS₁) exclusively present in hydrothermal fluids that can be considered the product of a seawater DOM precursor (CHO) following the corresponding reaction of S addition. All the reactions with >50% of potential precursors in seawater were proposed as the equivalent + H₂S reaction. They were exchanging H₂O, H₂ and/or O₂ by a H₂S molecule and accordingly an exclusive CHOS₁ formula from the hydrothermal fluids was obtained.

4. RESULTS

4.1. Hydrothermal fluids imprint on general geochemistry

Hydrothermal fluids and seawater differed substantially in temperature and pH. Hydrothermal fluid temperatures ranged from 55 to 86 °C and seawater from 11 to 28 °C at the three sampling sites (Table 1). Fluids in Milos and Dominica were acidic compared to seawater, in contrast to Iceland hydrothermal fluids that were slightly alkaline (Table 1). Trace elements and molecules that were likely of hydrothermal origin, as they were detected in the fluids but not in the surrounding seawater, were H₂S in Milos and dissolved Fe and Si in both Milos and Dominica (Table 1).

Salinity, major element concentrations and isotopic composition indicated substantial differences in the origin of the fluids at the three sites. Salinity and major element concentrations were similar or higher in Milos fluids as compared to seawater, but lower in Dominica and Iceland hydrothermal fluids (Table 1). The isotopic composition of the fluids (δ^2 H and δ^{18} O) from Milos, mainly from Palaeochori Bay,

Table 3

Theoretical sulfurization reactions tested in this study, differentiating between oxidative (blue) and reductive (red) reactions. The nine possibilities of adding one S-atom and adding/removing H and/or O were tested. The effectiveness of the potential reactions was considered as a percentage of mono-S compounds (CHOS_1) exclusive in hydrothermal fluids that can be considered the product of a seawater DOM precursor following the corresponding reaction. The reactions with $>50\%$ of precursors found in seawater are highlighted in light green, $>75\%$ in green and $>85\%$ in dark green. All the reactions giving at least $>50\%$ were potential $+ \text{H}_2\text{S}$ incorporation reactions, correspondingly exchanging H_2O , H_2 and/or O_2 by a H_2S molecule. For example, the reductive reaction of substituting one O atom by one S atom is equivalent to the reaction substituting one H_2O by one H_2S molecule and could provide a precursor in seawater DOM formulas to 87% of Milos CHOS_1 -compounds exclusive from hydrothermal fluids. An example of this procedure is visualized in Fig. 6.

	+ S reactions	% of precursors in seawater			equivalent + H_2S reactions	- H_2	- O_2	- H_2O
		Milos	Dominica	Iceland				
OXIDATIVE reactions	+ S	87	21	8	+ $\text{H}_2\text{S} / - \text{H}_2$			
	+ S/ - H_2	84	21	3	+ $\text{H}_2\text{S} / - 2\text{H}_2$			
	+ S/ - H_4	70	20	0	+ $\text{H}_2\text{S} / - 4\text{H}_2$			
	+ H_2OS	82	44	20	+ $\text{H}_2\text{S} + \text{H}_2\text{O} / - \text{H}_2$			
	+ H_2SO_2	60	48	13	+ $\text{H}_2\text{S} + \text{O}_2$			
	+ H_2SO_4	9	20	13				
	+ SO	82	26	13	+ $\text{H}_2\text{S} + \text{H}_2\text{O} / - 2\text{H}_2$			
	+ SO_2	64	42	10	+ $\text{H}_2\text{S} + \text{O}_2 / - \text{H}_2$			
	+ SO_3	33	49	23				
	+ SO_4	15	31	15				
	+ SO_5	4	10	5				
	+ SO/ - H_2	66	30	0	+ $\text{H}_2\text{S} + \text{O}_2 / - (\text{H}_2 + \text{H}_2\text{O})$			
	+ $\text{SO}_2 / - \text{H}_2$	60	43	0	+ $\text{H}_2\text{S} + \text{O}_2 / - 2\text{H}_2$			
	+ $\text{SO}_4 / - \text{H}_2$	16	25	5				
REDUCTIVE reactions	+ H_2S	86	32	18	+ H_2S			
	+ H_4S	74	33	20	+ $\text{H}_2\text{S} + \text{H}_2$			
	+ S/ - H_2O	83	16	8	+ $\text{H}_2\text{S} / - (\text{H}_2\text{O} + \text{H}_2)$			
	+ S/ - H_2O_2	82	24	10	+ $\text{H}_2\text{S} / - 2 (\text{H}_2\text{O})$			
	+ S/ - H_2O_4	76	62	30	+ $\text{H}_2\text{S} / - 2 (\text{H}_2 + \text{O}_2)$			
	+ S/ - O	87	21	10	+ $\text{H}_2\text{S} / - \text{H}_2\text{O}$			
	+ S/ - O_2	87	33	18	+ $\text{H}_2\text{S} / - (\text{H}_2 + \text{O}_2)$			
	+ S/ - O_3	85	41	23	+ $\text{H}_2\text{S} / - (\text{H}_2\text{O} + \text{O}_2)$			
	+ S/ - O_4	82	58	35	+ $\text{H}_2\text{S} / - (\text{H}_2 + 2\text{O}_2)$			
	+ S/ - O_5	76	70	48	+ $\text{H}_2\text{S} / - (\text{H}_2\text{O} + 2\text{O}_2)$			
	+ $\text{H}_2\text{S} / - \text{O}$	80	28	23	+ $\text{H}_2\text{S} + \text{H}_2\text{O} / - (\text{O}_2 + \text{H}_2)$			
	+ $\text{H}_2\text{S} / - \text{O}_2$	75	32	18	+ $\text{H}_2\text{S} / - \text{O}_2$			
	+ $\text{H}_2\text{S} / - \text{O}_4$	80	56	45	+ $\text{H}_2\text{S} / - 2\text{O}_2$			

> 85% of precursors in seawater

> 75% of precursors in seawater

> 50% of precursors in seawater

was far off from the estimated Mediterranean Sea meteoric water line, whereas Dominica and Iceland fluids plotted close to the global and the estimated Caribbean Sea meteoric water line (Fig. 2; Table 1). Dominica and Iceland hydrothermal fluids thus seem to be composed mainly of meteoric water, while Milos hydrothermal fluids were predominantly fed by recirculating seawater.

The hydrothermal fluids had lower DOC concentrations than corresponding surface seawater in all three systems. The DOC of hydrothermal fluids was 21–41 μM in Milos, 22–27 μM in Dominica and 112–142 μM in Iceland, and seawater DOC concentrations were 60 μM , 99 μM and 183 μM in Milos, Dominica and Iceland, respectively (Table 1). The Milos SPE-DOC contained less ^{14}C than

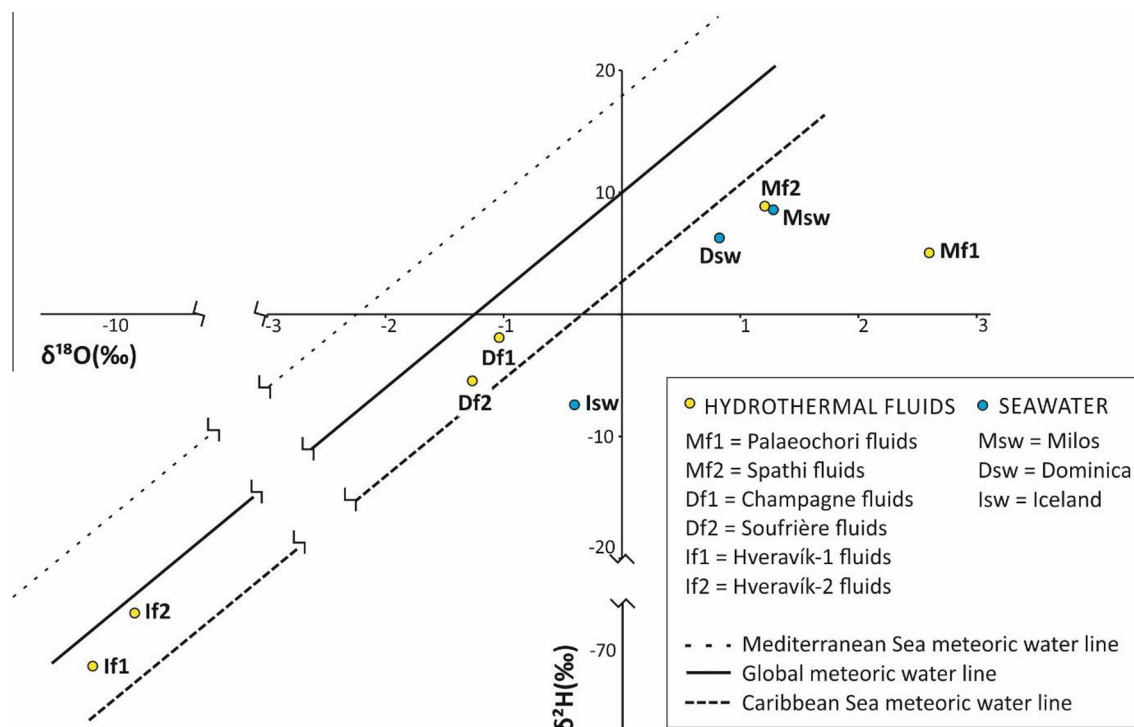


Fig. 2. Diagram of $\delta^2\text{H}$ and $\delta^{18}\text{O}$ isotopic values of shallow hydrothermal fluids (yellow) and surface seawater (blue) samples. Both $\delta^{18}\text{O}$ and $\delta^2\text{H}$ are expressed relative to Vienna Standard Mean Ocean Water (VSMOW; Craig, 1961). Caribbean Sea meteoric water line adapted from McCarthy et al. (2005) and Mediterranean Sea meteoric water line from Price et al. (2013). (For interpretation of the references to colour in this figure legend, the reader is referred to the web version of this article.)

near-by seawater. Samples had 77–167 $\mu\text{g C}$ while SPE process blanks contained $<2 \mu\text{g C}$. Because the AMS requires at least 5 $\mu\text{g C}$ for analysis, the ^{14}C content of the SPE process blank was not obtained. The sample SPE data are therefore reported as a range that reflects the possibility that the contribution of 2 $\mu\text{g C}$ of extraneous carbon from the blank was either entirely modern ($F^{14}\text{C} = 1$) or entirely ^{14}C free ($F^{14}\text{C} = 0$). Even with this extreme assumption, the data clearly demonstrate that Milos seawater contains organic matter with a modern $F^{14}\text{C}$ signature (1.02–1.03) while the fluids from the Palaeochori (0.78–0.81) and Spathi (0.77–0.79) vents contain material that has less ^{14}C (Table 1). The isotopic results were consistent with the estimated reservoir temperature of the fluids, showing the highest values in Milos fluids from Palaeochori (276–279 $^{\circ}\text{C}$) as compared to rest of the samples ($<180 \text{ }^{\circ}\text{C}$; Table 1). Assuming the same extraction efficiency for SPE-DOS as for SPE-DOC (e.g. Lechtenfeld et al., 2011; Pohlmann and Dittmar, 2015), the DOS concentrations in the hydrothermal fluids were 0.8–1.3 μM in Milos, 0.1 μM in Dominica and 0.1–0.2 μM in Iceland; and seawater DOS concentrations were 1.8 μM in Milos, 0.2 μM in Dominica and 0.5 μM in Iceland. Accordingly, molar DOS/DOC ratios were one order of magnitude higher in Milos compared to Dominica and Iceland (Table 1).

4.2. Hydrothermal fluids imprint on DOM signature

Using FT-ICR-MS, more formulas were found in hydrothermal fluids than in surrounding seawater: a total

of 3266–3505 molecular formulas were identified in Milos samples, 2538–2852 in Dominica, 1815–2127 in Iceland and 2418 formulas in the NEqPIW sample included as DOM reference (Table 2). The DOM of the hydrothermal fluids was on average more reduced than seawater DOM (O/C ratio; Table 2). The degree of unsaturation of the DOM molecules, as assessed by weighted averages of H/C ratios, DBE, and the relative abundance of aromatics, differed at the three sites (Table 2). On Milos, seawater and hydrothermal fluids showed a similar degree of unsaturation, whereas on Dominica, lower H/C ratio, higher DBE and higher abundances of aromatics indicated more unsaturated molecules in the hydrothermal fluids than in the seawater. On Iceland, a similar degree of unsaturation was found for seawater and fluids from the permanently submerged hydrothermal vent (Hveravík-2), while more unsaturated molecules were found in the air-exposed hydrothermal vent (Hveravík-1).

Another characteristic feature was the high weight averaged S/C ratio in the DOM of Milos hydrothermal fluids (Table 2). The most obvious difference in molecular DOM composition between hydrothermal fluids and seawater on Milos was the number of sulfur containing formulas (CHOS; Fig. 3). Hydrothermal fluids from Milos contained 8% more CHOS compounds than the corresponding seawater (hydrothermal fluids 23%; seawater 15%; Fig. 3). In the other two systems, molecular composition of hydrothermal fluids and seawater were relatively similar regarding CHOS compounds. On Dominica, the dominant groups of formulas were CHO ($\sim 50\%$) and

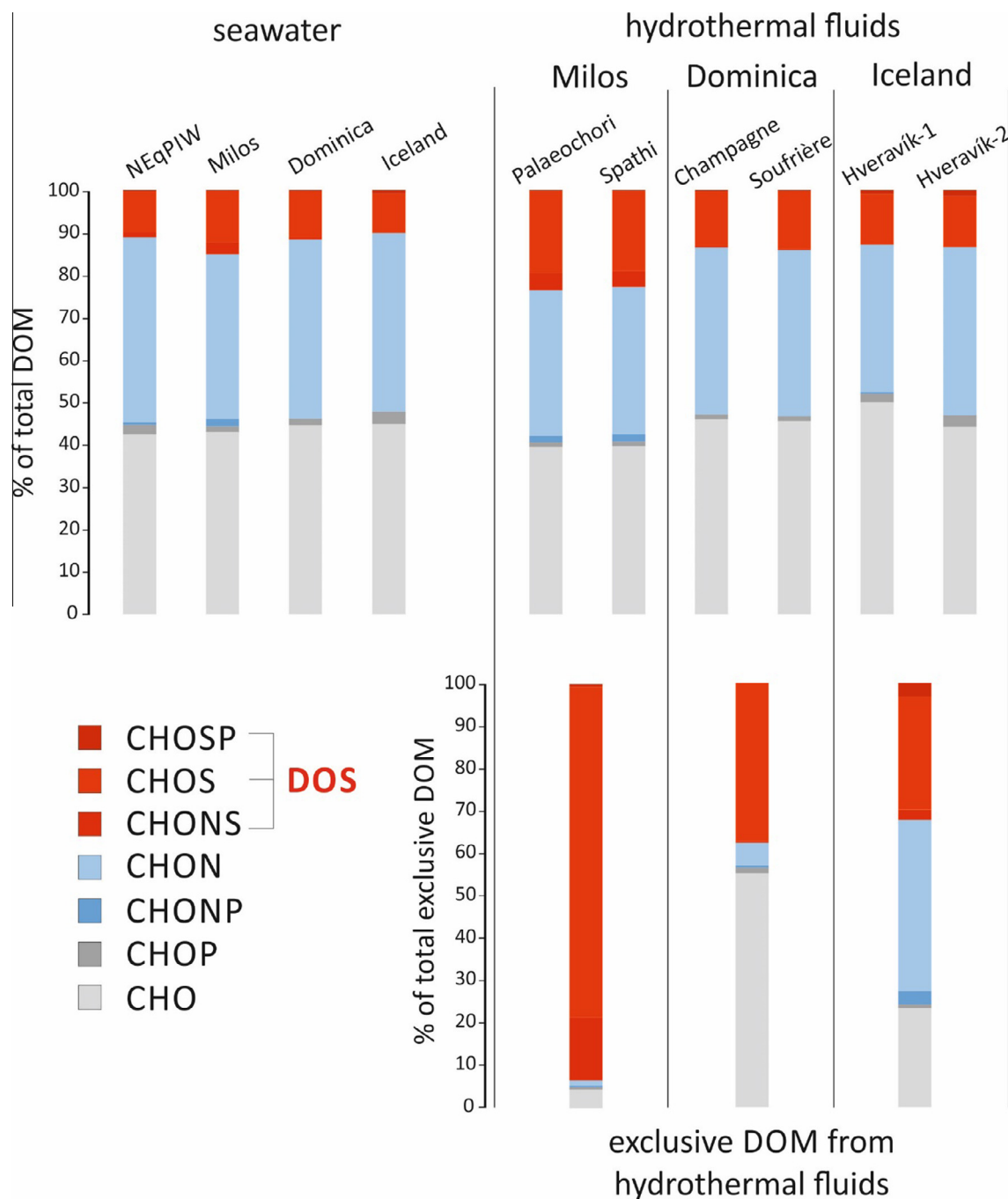


Fig. 3. DOM molecular compounds identified by FT-ICR-MS as a percentage of all molecular formulas detected for the respective sample: surface seawater samples (upper left), hydrothermal fluids (upper right) and exclusive formulas in hydrothermal fluids DOM (down right). Formulas containing sulfur (DOS) are highlighted in red and included CHOS, CHONS and CHOSP formulas. (For interpretation of the references to colour in this figure legend, the reader is referred to the web version of this article.)

CHON (~40%), while CHOS accounted for ~11% and CHOP for <2%. On Iceland, CHO and CHON formulas were also similarly abundant (~40%), while CHOS contributed ~14% and CHOP ~5% to the identified formulas. Besides the higher number of CHOS formulas in Milos fluids, the sum of intensities of these CHOS compounds was also highest in these systems (11–14% of total intensities; Fig. 4). In the seawater samples of Milos and Dominica,

CHOS compounds summed up to only 5% of total intensity, in Iceland seawater to 7%, respectively. The hydrothermal fluids of Dominica (5–7% of total intensity) and Iceland (8%) were only slightly enriched in CHOS compounds compared to seawater (Fig. 4).

The differences in molecular DOM composition of hydrothermal fluids and seawater were also manifested in occurrence of exclusive formulas only present in the

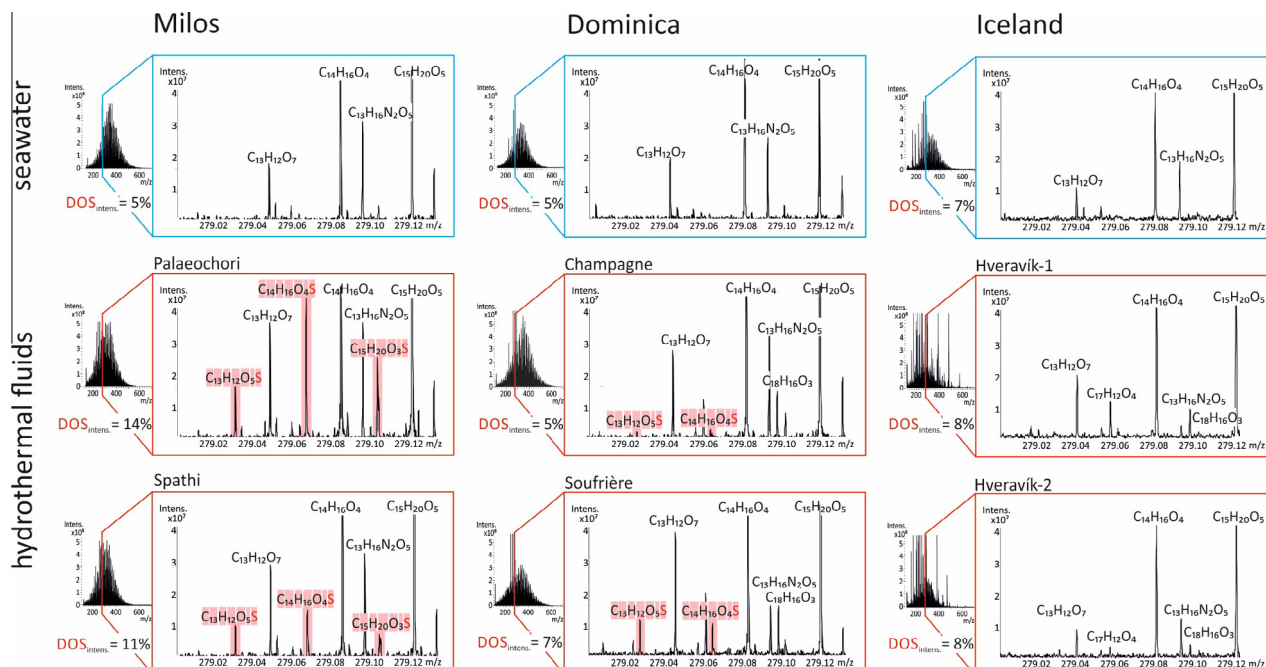


Fig. 4. FT-ICR mass spectra (ESI negative mode) of seawater (blue) and hydrothermal fluids (red) samples. Expanded section of the mass spectra at 279.00–279.14 Da with the identified molecular formulas. DOS formulas highlighted in red provide evidence for the relevance of S-containing compounds in Milos hydrothermal fluids. $\text{DOS}_{\text{intens.}}$ gives the percentage of summed intensities of all DOS compounds relative to total intensity of the respective sample. (For interpretation of the references to colour in this figure legend, the reader is referred to the web version of this article.)

hydrothermal fluids. On Milos, these exclusive formulas accounted for 9% (322 formulas) of the formulas in the hydrothermal fluids, in Dominica for 8% (223 formulas) and in Iceland for 6% (124 formulas), respectively (Table 2). Regarding their molecular composition, major differences were observed between sites. The exclusive formulas represented mainly reduced compounds with very low O/C ratio (0.25–0.32; Table 2; Fig. 5a), predominantly saturated in Milos and Iceland, but mainly unsaturated in Dominica with more than one third being aromatics (Table 2; Fig. 5a). The exclusive formulas of all hydrothermal fluids were on average strongly enriched in sulfur (S/C 0.013–0.062) when compared to total DOM of both fluids and seawater (maximum 0.009; Table 2). On Milos, almost all exclusive formulas in the hydrothermal DOM contained sulfur (>90%; Fig. 3), for Dominica and Iceland the respective percentages were considerably lower but still elevated (~38% and ~30%, respectively; Fig. 3).

4.3. Molecular variations of exclusive DOS from hydrothermal fluids

The molecular composition of the exclusive DOS from hydrothermal fluids (Fig. 5b) was substantially different from the DOS compounds from seawater (Fig. 5c). These differences were most evident from the degree of oxidation. In the three systems, the specific DOS of hydrothermal fluids had lower O/C ratios on average (0.26–0.34; Fig. 5b) than the surrounding surface seawater or NEqPIW DOS (0.45–0.52; Fig. 5c). A closer look into the exclusive DOS

from hydrothermal fluids was then obtained by searching for the presence of potential precursors for the individual CHOS_1 formulas in the seawater DOM (Fig. 6). Potential precursors were identified according to the 27 hypothetical sulfurization reactions shown in Table 3. On Dominica, only four reductive reactions provided potential precursors for more than 50% of exclusive mono-S compounds (CHOS_1) from hydrothermal fluids. None of the 27 potential sulfurization reactions achieved this 50% threshold value on Iceland. In the DOS-enriched system of Milos, almost all potential sulfurization reactions provided precursors for more than 50% of exclusive CHOS_1 compounds, many of them for more than 75% and up to 87% (Table 3; Fig. 6). Furthermore, a clear trend was observed regarding these reactions. All those that could be categorized as reductive ones provided a potential precursor for at least 74% of all specific CHOS_1 compounds from Milos fluids (Table 3). The four most effective potential sulfurization reactions (precursors for over 85% of exclusive formulas) were those exchanging an O atom by one S atom in the formula or the equivalent + H_2S reaction, correspondingly exchanging H_2O , H_2 and/or O_2 by a H_2S molecule (Table 3; Fig. 6).

5. DISCUSSION

5.1. Origin of the hydrothermal fluids

Understanding the origin of hydrothermal fluids is an essential step to decipher potential subsurface processes

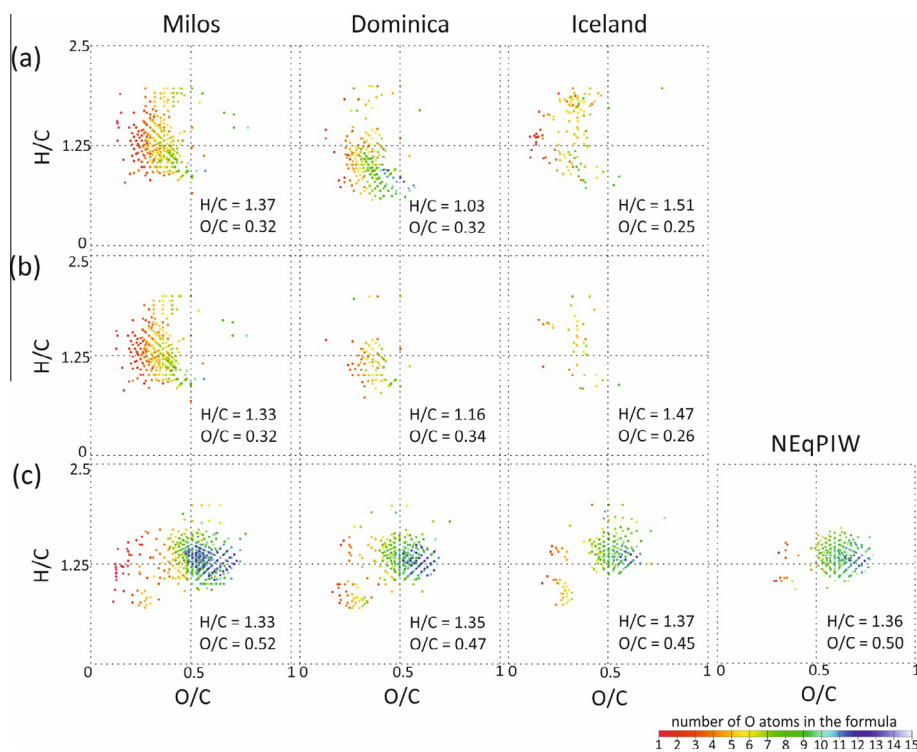


Fig. 5. Van Krevelen diagrams representing the O/C (oxygen-to-carbon ratio) and H/C (hydrogen-to-carbon ratio) in Milos, Dominica, Iceland and NEqPIW DOM samples: (a) exclusive DOM compounds from hydrothermal fluids, (b) exclusive DOS compounds from hydrothermal fluids (those formulas of “a” containing one or two S atoms) and (c) seawater DOS compounds (formulas containing S atoms in Milos, Dominica, Iceland and NEqPIW surface seawater samples). Every dot represents a specific molecular formula in the FT-ICR-MS dataset. The color scale illustrates the number of O atoms in every formula providing visual evidence of more oxidized compounds (blue dots) in seawater DOS (c) than in exclusive hydrothermal DOS (b), as represented also by the O/C and H/C intensity-weighted averages in each diagram. (For interpretation of the references to colour in this figure legend, the reader is referred to the web version of this article.)

(McCarthy et al., 2005). Fluids in a shallow-water hydrothermal system may be derived from one or from a combination of the following sources: meteoric water, seawater and/or magmatic water (Pichler, 2005). While deep-sea hydrothermal systems most likely derive all of their fluids from seawater, on-land hydrothermal fluids are originated mainly from meteoric sources along with possible magmatic contributions (Giggenbach, 1992). The three shallow-water systems in this study have hydrothermal fluids with different geochemical and isotopic composition indicating different potential sources.

Dominica and Iceland hydrothermal fluids were a mixture of mainly meteoric water and seawater. Meteoric waters are generally depleted in the heavy isotopic species of hydrogen and oxygen relative to ocean waters (Craig, 1961). In our study, the $\delta^2\text{H}$ and $\delta^{18}\text{O}$ isotopic values of Dominica and Iceland fluids were depleted and closely aligned between the global meteoric water line and the estimated Caribbean Sea meteoric water line (McCarthy et al., 2005; Fig. 2; Table 1), suggesting local meteoric origin, although discharging in a submarine environment (Pichler, 2005). Similar isotopic values were observed in a global marine precipitation survey (IAWA/WMO since 1961) at the station closest to the Dominica hydrothermal vents ($-1.0 \delta^2\text{H}$, $-0.9 \delta^{18}\text{O}$ in Barbados, Lesser Antilles; Rozanski et al., 1993). The low salinity and major element

concentrations were also consistent with a mainly meteoric origin of Dominica and Iceland fluids.

In contrast, the fluids discharging on Milos were predominantly recirculating seawater, as evidenced by the high salinity and major element concentrations and by the isotopic values of $\delta^2\text{H}$ and $\delta^{18}\text{O}$ that were far off from the estimated Mediterranean Sea meteoric water line (Price et al., 2013; Fig. 2; Table 1), as well as from values of the closest station in the global precipitation survey ($-6.3 \delta^2\text{H}$, $-32.8 \delta^{18}\text{O}$ in Heraklion, Aegean Sea; Rozanski et al., 1993). This is consistent with a higher estimated reservoir temperature obtained for Milos samples (Table 1), suggesting that the endmember fluids were likely a mixture of seawater and andesitic water with minor meteoric water content (e.g. Yamanaka et al., 2013). Potentially high temperature of Milos reservoir might imply abiotic origin of H_2S during the final stages of kerogen formation (temperature required between 150 and 200 °C; McCarthy et al., 2011a). Magmatic contribution in Milos hydrothermal fluids composition was previously confirmed by stable isotope studies on the released gases (Botz et al., 1996) and potentially hot magma was indicated by direct drilling of the underlying hydrothermal reservoir, detecting 318 °C at 1200 m depth (Vrouzi, 1985; Dando et al., 1999) as well as reservoir temperature estimations of up to 325 °C (Fitzsimmons et al., 1997). Consequently, subsurface seawater recirculation

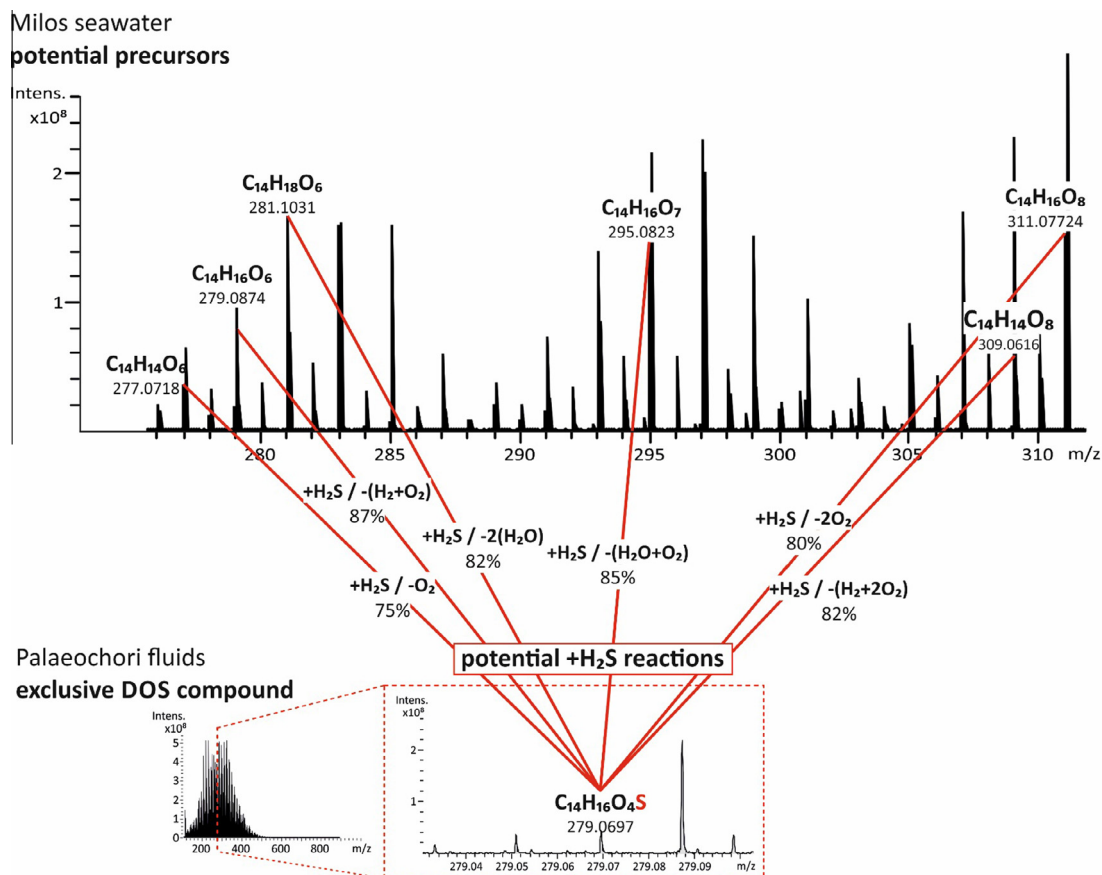


Fig. 6. Example of potential sulfurization reactions tested in this study (Table 3), showing an exclusive DOS compound of Milos hydrothermal fluids from Palaeochori Bay (down) and the potential precursors in the FT-ICR mass spectra of Milos seawater DOM (up). Neutral molecular formulas of detected ions are presented. The potential proposed reactions as $+H_2S$ incorporation reactions, correspondingly exchanging H_2O , H_2 and/or O_2 by a H_2S molecule, are represented in red including the percentage of precursors found in seawater following the corresponding reaction.

may have been favored by magmatic input, because heat makes the water less buoyant, driving the water flow. Our ^{14}C isotopic analysis of the SPE-DOM indicated a contribution of non-modern carbon. One possible source is the desorption of pre-aged organics from the sediments (Schillawski and Petsch, 2008). Alternatively, primary production could convert CO_2 with a non-modern signature, such as ^{14}C -free mantle CO_2 or pre-aged CO_2 remineralized from the sediment, into organic molecules. The seawater at Milos was entirely modern. If the only other SPE-DOM carbon contribution to the Milos hydrothermal fluids was ^{14}C -free, then the organics were composed of approximately 80% modern and 20% dead radiocarbon material (Table 1). If the sediments contributed significant carbon to the fluids they would have also have this mixed radiocarbon signature. Similar observations have been made in deep hydrothermal systems, for example, the $F^{14}C$ values of ultra-filtrated (>1000 Da) DOC in axial diffuse hydrothermal fluids from the Juan de Fuca Ridge ranged from 0.48 to 0.55, comparable to local deep seawater with an $F^{14}C$ of 0.56 (McCarthy et al., 2011b). The fact that Milos fluids may be more influenced by magmatic contributions than Dominica and Iceland is also relevant to the potential

sulfurization of seawater DOM and other subsurface processes. In contrast, the higher meteoric content in Dominica and Iceland fluids likely favor processes occurring in terrestrial environments that may subsequently affect the DOM molecular composition.

5.2. DOC depletion in the fluids and DOS enrichment in Milos

Bulk DOC concentrations provide an integrated view of sources and processes in hydrothermal venting sites (Lang et al., 2006; McCarthy et al., 2011b). In the three systems included in this study, DOC concentrations in hydrothermal fluids were lower than in surface seawater (Table 1). The surface seawater DOC concentration in Milos was within the range of regular open ocean surface water (40–80 μM ; Hansell et al., 2009). In case of Dominica and Iceland it was higher but still representative for coastal regions (Dittmar and Stubbins, 2014) where shallow-water hydrothermal vents are located. Given the close proximity to the island, an input of terrigenous organic matter is a likely explanation for the enhanced DOC concentrations in the surface seawater samples through rivers,

rain-washing or submarine groundwater discharge via aquifers (Pichler, 2005). This is supported by a higher percentage of aromatics in Dominica and Iceland surface seawater DOM signature than in the reference DOM from the deep ocean (NEqPIW), which might reflect terrestrial plant derived compounds like lignin-phenols (Dittmar and Stubbins, 2014). Alternatively, increased DOC concentrations might be derived from recent primary production, which is the biggest source of organic carbon in the oceanic epipelagic zone (0–200 m water depth; Dittmar and Stubbins, 2014). Our three study sites were located in the shallow, euphotic and continuously mixed water column, with close benthic–pelagic coupling, and typically high rates of primary production (Behrenfeld et al., 2005; Cloern et al., 2014). Therefore, higher DOC concentrations in surface seawater of Milos, Dominica and Iceland as compared to the hydrothermal fluids could be explained by both terrestrial input and/or autochthonous production in the coastal waters.

The most likely explanation for the low DOC concentrations (Table 1) in Dominica and Iceland hydrothermal fluids may be the strong contribution of low-DOC meteoric water. In addition, different abiotic and biotic processes during seawater recirculation might contribute to DOC depletion in hydrothermal fluids. In the deep ocean, seawater DOC can be removed by hydrothermal circulation within Earth's crust (Lang et al., 2006; Lin et al., 2012; Hansell, 2013; Hawkes et al., 2015). Potential explanations are microbial consumption driven by vent communities, interactions with minerals in the subsurface leading to DOC sorption or direct abiotic thermal degradation of DOC (Lang et al., 2006; Santelli et al., 2008; Hawkes et al., 2015, 2016). The possibilities of heterotrophic consumption and organic matter adsorption to mineral surfaces may be favored by high availability of organic carbon in shallow hydrothermal systems (e.g. Svensson et al., 2004) and high porosity of Milos and Dominica sediment, respectively. In addition, co-precipitation of DOM with minerals can occur at the redox interface and subsequently remove a DOC fraction from the fluids (Riedel et al., 2013; Gomez-Saez et al., 2015). However, thermal degradation of SPE-DOM was recently detected at temperatures above 68 °C (Hawkes et al., 2016) and therefore represents, together with the low-DOC meteoric water input, the most likely explanation of the lower DOC concentration detected in Milos, Dominica and Iceland shallow hydrothermal fluids compared to surface seawater.

Information on DOS concentrations in marine systems is still scarce (Lechtenfeld et al., 2011; Pohlabein and Dittmar, 2015). Compared to the few published data, the DOS concentrations in the Milos hydrothermal system were distinctly higher (0.8–1.8 μM) than in other marine environments, (0.8 μM North Sea; 0.3–0.9 μM South Atlantic central water; 0.4–1.2 μM Antarctic surface water; Lechtenfeld et al., 2011; Pohlabein and Dittmar, 2015), whereas Dominica and Iceland DOS concentrations were similar to values reported for open ocean waters (Cutter et al., 2004; Lechtenfeld et al., 2011; Pohlabein and Dittmar, 2015). Accordingly, the molar DOS/DOC ratio in Milos was one order of magnitude higher than in the

other studied marine systems. FT-ICR-MS data were consistent with the ICP-OES based quantification. Nearly all DOM molecular formulas exclusively present in the Milos fluids contained sulfur. Moreover, the percentage of CHOS-compounds in total DOM on Milos was one of the highest ever observed through DOM characterization by FT-ICR-MS analysis of natural samples (e.g. Riedel et al., 2013) and distinctly higher than the sum of CHOS intensities observed for Dominica and Iceland. Our findings thereby support FT-ICR-MS as a capable technique to semi-quantitatively characterize the fraction of DOM containing DOS and identify potential DOS-enriched scenarios in marine environments.

5.3. Redox transformations of hydrothermal DOM

Our data identify shallow-water hydrothermal fluids as a source of reduced DOM and reduced DOS to the oceans. On Milos, where seawater recirculation through the sediment accounted for most of the fluids composition, variations in O/C ratios suggested DOM reduction during recirculation and subsequent oxidation upon contact with oxygenated seawater. Formation of organically bound sulfur is promoted by the availability of reactive organic matter, an excess of reduced sulfur species and a limited supply of reactive iron (Eglinton and Repeta, 2014). In hydrothermal fluids from Palaeochori Bay (Milos) and Soufrière Bay (Dominica), dissolved iron was much higher than in the vents from Spathi Bay (Milos) and Champagne Reef (Dominica). In Iceland fluids, dissolved iron was below detection limit (Table 1). Nevertheless, DOS concentration and CHOS-compounds abundance was similarly high in both Milos fluids and lower in Dominica and Iceland fluid samples, respectively. Thus, in our study dissolved iron apparently was not linked to DOS abundance.

In contrast, clear trends were observed in H₂S concentration and DOS abundance. In Milos hydrothermal fluids, we detected high H₂S concentration together with high abundance of DOS, and vice versa in Dominica and Iceland. High DOS content in DOM from pore water in anoxic coastal sediments enriched in H₂S and reduced sulfur species has been demonstrated before (Schmidt et al., 2009; Seidel et al., 2014). Elevated H₂S concentration in interstitial water coinciding with increasing abundance of DOS compounds (in number and intensity), probably resulted from sulfurization reactions during the early stages of sedimentary diagenesis (e.g. Black Sea; Schmidt et al., 2014). This could suggest that the exclusive fraction of DOS detected in our hydrothermal fluid samples may be at least partially originated from sedimentary organic matter. On the other hand, our results indicated endmember fluids in Milos to be highly influenced by seawater recirculation and sulfurization reactions have been detected even at the sediment–water interface (Sinninghe Damsté and de Leeuw, 1990; Wakeham et al., 1995). Therefore, potential DOS origin in DOM sulfurization processes during seawater recirculation may be reasonable in our study and we discuss potential sulfurization reactions at a molecular level.

Some organic compounds can react with reduced sulfur species as hydrogen sulfides or polysulfides binding to

carbon-carbon double bonds by nucleophilic addition (Vairavamurthy and Mopper, 1987; Kohnen et al., 1989; Sleighter et al., 2014). Unequivocal precursor-product relationships cannot be established without detailed structural information, but potential reactions can be explored on the basis of relationships of molecular formulas and the geochemical context. For example, Schmidt et al. (2014) tested in a FT-ICR-MS dataset the possible sulfurization reaction of exchanging one O atom by one S atom and two H atoms. In our study, we observed reductive sulfurization of seawater DOM recirculating through Milos sediment, most likely substituting one O atom by one S atom or correspondingly exchanging H₂O, H₂ and/or O₂ by a H₂S molecule (Table 3). Hydrothermal vents have been postulated as possible sites for the first steps of organic chemical evolution, where sulfur reduction might have played a role in prebiotic chemistry occurring in sulfide-rich environments (Russell and Hall, 1997; Cody et al., 2000; Hebbing et al., 2006). McCollom and Seewald (2007) described a potential mechanism to convert simple organic compounds to complex organic matter in sulfur-rich hydrothermal environments, by progressive elongation of alkyl carbon chains and formation of complex organic compounds through involvement of a thiol intermediate. Our results from natural environments support the last step of their hypothetical reaction which was the addition of a H₂S molecule instead of H₂O (McCollom and Seewald, 2007).

In the water column, the main compound group in DOS was recently identified as unreactive sulfonic acids, which are fully oxidized molecules with low reactivity and a component of the long-time persistent fraction of DOM in the oceans (Pohlabein and Dittmar, 2015). This is consistent with the O/C ratio variations that we observed in our study. While our surface seawater samples contained only oxidized DOS compounds with high O/C ratios, the hydrothermal fluids not only contained higher percentages of DOS (Fig. 3), but included oxidized DOS compounds and a fraction of reduced DOS exclusive from the fluids (Fig. 5). Therefore, our results suggested potential transformation of reduced DOS molecules exclusively from the fluids to more oxidized DOS compounds abundant in seawater, which were not removed during hydrothermal circulation through the subsurface. At the same time, a new pool of reduced DOS was generated either through sulfurization of seawater DOM or release of DOS from sedimentary organic matter. This supports the scenario that functional groups like thiols and thioethers could be produced in hydrothermal systems by reactions of reduced inorganic sulfur compounds with organic matter (Sinninghe Damsté et al., 1989; Aizenshtat et al., 1995; Schneckenburger et al., 1998; Hertkorn et al., 2013; Sleighter et al., 2014) and then be rapidly oxidized to unreactive sulfonic acids once exposed to oxygenated seawater (Pohlabein and Dittmar, 2015).

From a biotic perspective, organic matter can react with H₂S and other reduced sulfur species (e.g. Cutter and Kluckhohn, 1999; Schmidt et al., 2009, 2014) produced from the activity of sulfate-reducing bacteria (SRB) or dissimilatory iron-reducing bacteria (DIRB), which were

found in relatively large number in Palaeochori Bay (Sievert et al., 1999). Furthermore, the reduced inorganic sulfur compounds in Milos hydrothermal fluids, mainly H₂S, would provide the necessary electron donor for sulfur-oxidizing bacteria (SOB), which contribute to primary production in the Milos system (Sievert et al., 1999). Analysis of the structural information (e.g. Pohlabein and Dittmar, 2015) of the reduced organosulfur compounds that were detected in hydrothermal fluids prior to oxidation upon contact with oxygenated seawater, isotopic investigation (e.g. δ³⁴S; Raven et al., 2015) to provide insights into the CHOS-compounds origin and also research on sulfur-related microbes and their linkage to molecular DOM composition (e.g. Osterholz et al., 2016) in marine shallow hydrothermal systems will further improve our understanding of the underlying mechanisms that control global organic sulfur biogeochemistry.

6. CONCLUSION

We investigated DOS dynamics and its relation to the physicochemical environment by studying the molecular composition of DOM in three contrasting shallow hydrothermal systems off the coast of Milos (Eastern Mediterranean), Dominica (Caribbean Sea) and Iceland (North Atlantic). In all three systems, exclusive DOS from hydrothermal fluids had on average lower O/C ratios (0.26–0.34) than surrounding surface seawater or NEqPIW DOS (0.45–0.52). Therefore, shallow-hydrothermal systems can be considered a source of reduced DOS, which will get oxidized upon contact with oxygenated seawater. Our results suggested that the more oxidized DOS compounds abundant in seawater were not removed during hydrothermal circulation through the subsurface. At the same time, a new pool of reduced DOS was generated either through sulfurization of seawater DOM or release of DOS from sedimentary organic matter. This supports the scenario that functional groups like thiols and thioethers could be produced in hydrothermal systems and then be rapidly oxidized to form unreactive sulfonic acids, which were recently reported as the main group of DOS in the oceans and part of the long-time persistent fraction of marine DOM.

In contrast to the predominantly low-DOC meteoric fluids from Dominica and Iceland, the hydrothermal fluids from Milos were mainly fed by recirculating seawater. Furthermore, the hydrothermal fluids from Milos were enriched in H₂S and DOS, as indicated by DOS/DOC ratio one order of magnitude higher than for Dominica and Iceland systems, and by the fact that >90% of all assigned DOM formulas exclusively present in the fluids contained sulfur. Evaluation of hypothetical sulfurization reactions during seawater recirculation in Milos sediments suggested DOM reduction and sulfurization. The four most effective potential sulfurization reactions (precursors for over 85% of exclusive DOS formulas) were those exchanging an O atom by one S atom in the formula or the equivalent + H₂S reaction, correspondingly exchanging H₂O, H₂ and/or O₂ by a H₂S molecule. Our results thereby support the last step of hypothetical abiotic reactions proposed

earlier for sulfide-rich hydrothermal systems, which was the replacement of a H₂O molecule by H₂S. In conclusion, our study reveals novel insights into DOS dynamics in marine hydrothermal environments and provides a conceptual framework for molecular-scale mechanisms in organic sulfur geochemistry.

ACKNOWLEDGMENTS

The authors would like to thank all members of scientific expeditions to Milos (May 2012), Dominica (April 2013) and Iceland (June 2014). Special thanks to A. Koschinsky (Jacobs University, Bremen) for laboratory assistance in Iceland geochemical analyses, A. Cording for her help in Milos sampling campaign and S.M. Sievert (WHOI, USA) for DOM filtration support in Dominica. Thanks to A. Magloire (Dominican Department of Fisheries) for granting permission and E. Reynisson, P. Vannier and V.T. Marteinsson (Matís, Reykjavík) for logistical support in DOM extraction in Iceland. Thanks to I. Ulber, M. Friebe, B. Schnetger, E. Gründken (University of Oldenburg) and L. Knigge (University of Bremen) for laboratory assistance and F. Lechleitner, C. McIntyre and T.I. Eglinton (ETH, Zürich) for AMS data analysis and guidance. Special thanks to K. Klaproth (ICBM-MPI, Oldenburg) for FT-ICR-MS continuous supervision. We also thank the editor and three anonymous reviewers whose comments helped to improve an earlier version of this manuscript. This work was financed through the DFG Emmy Noether Grant BU 2606/1-1 and MARUM grant 44110593 given to S.I.B.

REFERENCES

- Aizenshtat Z., Krein E. B., Vairavamurthy M. A. and Goldstein T. P. (1995) Role of sulfur in the transformations of sedimentary organic matter: a mechanistic overview. In *Geochemical Transformations of Sedimentary Sulfur*, Vol. 612 (eds. M. A. Vairavamurthy, M. A. A. Schoonen, T. I. Eglinton, W. Luther and B. Manowitz), pp. 16–37. ACS Symposium Series.
- Axelsson G., Gunnlaugsson E., Jónasson T. and Ólafsson M. (2010) Low-temperature geothermal utilization in Iceland – Decades of experience. *Geothermics* **39**, 329–338.
- Battin T. J., Luysaert S., Kaplan L. A., Aufdenkampe A. K., Richter A. and Tranvik L. (2009) The boundless carbon cycle. *Nat. Geosci.* **2**, 598–600.
- Behrenfeld M. J., Boss E., Siegel D. A. and Shea D. M. (2005) Carbon-based ocean productivity and phytoplankton physiology from space. *Global Biogeochem. Cycles* **19**, 1–14.
- Botz R., Stüben D., Winckler G., Bayer R., Schmitt M. and Faber E. (1996) Hydrothermal gases from offshore Milos Island, Greece. *Chem. Geol.* **130**, 161–173.
- Cody G. D., Boctor N. Z., Filley T. R., Hazen R. M., Scott J. H., Sharma A. and Yoder H. S. (2000) Primordial carbonylated iron-sulfur compounds and the synthesis of pyruvate. *Science* **289**, 1337.
- Cloern J. E., Foster S. Q. and Kleckner A. E. (2014) Phytoplankton primary production in the world's estuarine-coastal ecosystems. *Biogeosciences* **11**, 2477–2501.
- Craig H. (1961) Isotopic variations in meteoric waters. *Science* **133** (3465), 1702–1703.
- Cutter G. A. and Kluckhohn R. S. (1999) The cycling of particulate carbon, nitrogen, sulfur, and sulfur species (iron monosulfide, greigite, pyrite, and organic sulfur) in the water columns of Framvaren Fjord and the Black Sea. *Mar. Chem.* **67**, 149–160.
- Cutter G. A., Cutter L. S. and Filippino K. C. (2004) Sources and cycling of carbonyl sulfide in the Sargasso Sea. *Limnol. Oceanogr.* **49**, 555–565.
- Dando P. R., Hughes J. A., Leahy Y., Niven S. J., Taylor L. J. and Smith C. (1995) Gas venting rates from submarine hydrothermal areas around the island of Milos, Hellenic Volcanic Arc. *Cont. Shelf Res.* **15**(8), 913–929.
- Dando P. R., Stüben D. and Varnavas S. P. (1999) Hydrothermalism in the Mediterranean Sea. *Progr. Oceanogr.* **44**, 333–367.
- Dittmar T. (2015) Reasons behind the long-term stability of marine dissolved organic matter. In *The Biogeochemistry of Marine Dissolved Organic Matter* (eds. D. A. Hansell and C. A. Carlson). Elsevier, The Netherlands, pp. 369–388.
- Dittmar T., Koch B., Hertkorn N. and Kattner G. (2008) A simple and efficient method for the solid-phase extraction of dissolved organic matter (SPE-DOM) from seawater. *Limnol. Oceanogr. Methods* **6**, 230–235.
- Dittmar T. and Stubbins A. (2014) Dissolved organic matter in aquatic systems. In *Treatise of Geochemistry* (eds. B. Birrer, P. Falkowski and K. Freeman). Elsevier, pp. 125–156.
- Eglinton T. I. and Repeta D. J. (2014) Organic matter in the contemporary ocean. In *Treatise on Geochemistry* (eds. K. Turekian and H. Holland). Elsevier, Amsterdam, pp. 151–189.
- Fitzsimmons M. F., Dando P. R., Hughes J. A., Thiermann F., Akoumianaki I. and Pratt S. M. (1997) Submarine hydrothermal brine seeps off Milos, Greece: Observations and geochemistry. *Mar. Chem.* **57**, 325–340.
- Fournier R. O. (1979) A revised equation for the Na/K geothermometer. *Geotherm. Resour. Counc. Trans.* **3**, 221–224.
- German C. R., Legendre L. L., Sander S. G., Niquil N., Luther, G. W., Bharati L., Han X. and Le Bris N. (2015) Hydrothermal Fe cycling and deep ocean organic carbon scavenging: Model-based evidence for significant POC supply to seafloor sediments. *Earth Planet. Sci. Lett.* **419**, 143–153.
- Giggenbach W. F. (1992) Isotopic shifts in waters from geothermal and volcanic systems along convergent plate boundaries and their origin. *Earth Planet. Sci. Lett.* **113**(4), 495–510.
- Gomez-Saez G. V., Riedel T., Niggemann J., Pichler T., Dittmar T. and Bühring S. I. (2015) Interaction between iron and dissolved organic matter in a marine shallow hydrothermal system off Dominica Island (Lesser Antilles). *Mar. Chem.* **177**, 677–686.
- Green N. W., Perdue E. M., Aiken G. R., Butler K. D., Chen H., Dittmar T., Niggemann J. and Stubbins A. (2014) An intercomparison of three methods for the large-scale isolation of oceanic dissolved organic matter. *Mar. Chem.* **161**, 14–19.
- Hansman R. L., Dittmar T. and Herndl G. J. (2015) Conservation of dissolved organic matter molecular composition during mixing of the deep water masses of the northeast Atlantic Ocean. *Mar. Chem.* **177**, 288–297.
- Hansell D. A. (2013) Recalcitrant dissolved organic carbon fractions. *Annu. Rev. Mater. Sci.* **5**, 421–445.
- Hansell D. A., Carlson C. A., Repeta D. J. and Schlitzer R. (2009) Dissolved organic matter in the ocean: a controversy stimulates new insights. *Oceanography* **22**, 202–211.
- Hawkes J. A., Rossel P. E., Stubbins A., Butterfield D., Connelly D. P., Achterberg E. P., Koschinsky A., Chavagnac V., Hansen C., Bach W. and Dittmar T. (2015) Efficient removal of recalcitrant deep-ocean dissolved organic matter during hydrothermal circulation. *Nat. Geosci.* **8**, 856–860.
- Hawkes J. A., Hansen C. T., Goldhammer T., Bach W. and Dittmar T. (2016) Molecular alteration of marine dissolved organic matter under experimental hydrothermal conditions. *Geochim. Cosmochim. Acta* **175**, 68–85.
- Hebting Y., Schaeffer P., Behrens A., Adam P., Schmitt G., Schneckeburger P., Bernasconi S. M. and Albrecht P. (2006)

- Biomarker evidence for a major preservation pathway of sedimentary organic carbon. *Science* **312**, 1627.
- Hedges J. I. (1992) Global biogeochemical cycles – progress and problems. *Mar. Chem.* **39**, 67–93.
- Henley R. W., Truesdell A. H., Barton P. B. and Whitney J. A. (1984) Fluid-mineral equilibria in hydrothermal systems. *Rev. Econ. Geol.* **1**, 267.
- Hertkorn N., Harir M., Koch B. P., Michalke B. and Schmitt-Kopplin P. (2013) High-field NMR spectroscopy and FTICR mass spectrometry: powerful discovery tools for the molecular level characterization of marine dissolved organic matter. *Biogeosciences* **10**, 1583–1624.
- Hobel C. F. V., Marteinson V. T., Hreggvidsson G. O. and Kristjansson J. K. (2005) Investigation of the microbial ecology of intertidal hot springs by using diversity analysis of 16S rRNA and chitinase genes. *Appl. Environ. Microbiol.* **71**(5), 2771.
- Höskuldsson A., Hey R., Kjartansson E. and Gudmundsson G. B. (2007) The Reykjanes Ridge between 63°10'N and Iceland. *J. Geodyn.* **43**, 73–86.
- Joseph E. P., Fournier N., Lindsay J. M. and Fischer T. P. (2011) Gas and water geochemistry of geothermal systems in Dominica, Lesser Antilles island arc. *J. Volcanol. Geotherm. Res.* **206**, 1–14.
- Kleint C., Kuzmanovski S., Powell Z., Bühring S. I., Sander S. G. and Koschinsky A. (2015) Organic Cu-complexation at the shallow marine hydrothermal vent fields off the coast of Milos (Greece), Dominica (Lesser Antilles) and the Bay of Plenty (New Zealand). *Mar. Chem.* **173**, 244–252.
- Koch B. P. and Dittmar T. (2006) From mass to structure: an aromaticity index for high resolution mass data of natural organic matter. *Rapid Commun. Mass Spectrom.* **20**, 926–932.
- Koch B. P., Dittmar T., Witt M. and Kattner G. (2007) Fundamentals of molecular formula assignment to ultrahigh resolution mass data of natural organic matter. *Anal. Chem.* **79**, 1758–1763.
- Kohnen M. E. L., Sinninghe Damsté J. S. S., ten Haven H. L. and de Leeuw J. W. (1989) Early incorporation of polysulphides in sedimentary organic matter. *Nature* **341**, 640–641.
- Kristjansson J. K., Hreggvidsson G. O. and Alfredsson G. A. (1986) Isolation of halotolerant *Thermus* spp. from submarine hot springs in Iceland. *Appl. Environ. Microbiol.* **52**, 1313–1316.
- Kujawinski E. B. and Behn M. D. (2006) Automated analysis of electrospray ionization Fourier transform ion cyclotron resonance mass spectra of natural organic matter. *Anal. Chem.* **78**, 4363–4373.
- Kujawinski E. B., Freitas M. A., Zang X., Hatcher P. G., Green-Church K. B. and Jones R. B. (2002) The application of electrospray ionization mass spectrometry (ESI MS) to the structural characterization of natural organic matter. *Org. Geochem.* **33**, 171–180.
- Lang S. Q., Butterfield D. A., Lilley M. D., Paul Johnson. H. and Hedges J. I. (2006) Dissolved organic carbon in ridge-axis and ridge-flank hydrothermal systems. *Geochim. Cosmochim. Acta* **70**, 3830–3842.
- Lang S. Q., Früh-Green G. L., Bernasconi S. M. and Wacker L. (2013) Isotopic ($\delta^{13}\text{C}$, $\Delta^{14}\text{C}$) analysis of organic acids in marine samples using wet chemical oxidation. *Limnol. Oceanogr. Methods* **11**, 161–175.
- Lechtenfeld O. J., Koch B. P., Geibert W., Ludwiczowski K.-U. and Kattner G. (2011) Inorganics in organics: quantification of organic phosphorus and sulfur and trace element speciation in natural organic matter using HPLC-ICPMS. *Anal. Chem.* **83**, 8968–8974.
- Lechtenfeld O. J., Kattner G., Flerus R., Leigh Mc. Callister. S., Schmitt-Kopplin P. and Koch B. P. (2014) Molecular transformation and degradation of refractory dissolved organic matter in the Atlantic and Southern Ocean. *Geochim. Cosmochim. Acta* **126**, 312–337.
- Lin H.-T., Cowen J. P., Olson E. J., Amend J. P. and Lilley M. D. (2012) Inorganic chemistry, gas compositions and dissolved organic carbon in fluids from sedimented young basaltic crust on the Juan de Fuca Ridge flanks. *Geochim. Cosmochim. Acta* **85**, 213–227.
- Lindsay J. M., Trumbull R. B. and Siebel W. (2005) Geochemistry and petrogenesis of late Pleistocene to Recent volcanism in Southern Dominica, Lesser Antilles. *J. Volcanol. Geotherm. Res.* **148**, 253–294.
- Marshall A. G., Hendrickson C. L. and Jackson G. S. (1998) Fourier transform ion cyclotron resonance mass spectrometry: a primer. *Mass Spectrom. Rev.* **17**, 1–35.
- Marteinson V. T., Hauksdottir S., Hobel C. F. V., Kristmannsdottir H., Hreggvidsson G. O. and Kristjansson J. K. (2001) Phylogenetic diversity analysis of subterranean hot springs in Iceland. *Appl. Environ. Microbiol.* **67**, 4242–4248.
- McCarthy K. T., Pichler T. and Price R. E. (2005) Geochemistry of Champagne Hot Springs shallow hydrothermal vent field and associated sediments, Dominica, Lesser Antilles. *Chem. Geol.* **224**, 55–68.
- McCarthy K., Rojas K., Niemann M., Palmowski D., Peters K. and Stankiewicz A. (2011a) Basic petroleum geochemistry for source rock evaluation. *Oilfield Rev.* **23**, 32–43.
- McCarthy M. D., Beaupré S. R., Walker B. D., Voparil I., Guilderson T. P. and Druffel E. R. M. (2011b) Chemosynthetic origin of ^{14}C -depleted dissolved organic matter in a ridge-flank hydrothermal system. *Nat. Geosci.* **4**, 32–36.
- McCollom T. M. and Seewald J. S. (2007) Abiotic synthesis of organic compounds in deep-sea hydrothermal environments. *Chem. Rev.* **107**, 382–401.
- McKenzie D. (1972) Active tectonics of the Mediterranean Region. *Geophys. J. Int.* **30**, 109–185.
- Osterholz H., Singer G., Wemheuer B., Daniel R., Simon M., Niggemann J. and Dittmar T. (2016) Deciphering associations between dissolved organic molecules and bacterial communities in a pelagic marine system. *ISME J.* <http://dx.doi.org/10.1038/ismej.2015.231>.
- Pichler T. (2005) Stable and radiogenic isotopes as tracers for the origin, mixing and subsurface history of fluids in shallow-water hydrothermal systems. *J. Volcanol. Geotherm. Res.* **139**(3–4), 211–226.
- Pohlabein A. M. and Dittmar T. (2015) Novel insights into the molecular structure of non-volatile marine dissolved organic sulfur. *Mar. Chem.* **168**, 86–94.
- Price R. E., Savov I., Planer-Friedrich B., Bühring S. I., Amend J. and Pichler T. (2013) Processes influencing extreme As enrichment in shallow-sea hydrothermal fluids of Milos Island, Greece. *Chem. Geol.* **348**, 15–26.
- Raven M. R., Adkins J. F., Werne J. P., Lyons T. W. and Sessions A. L. (2015) Sulfur isotopic composition of individual organic compounds from Cariaco Basin sediments. *Org. Geochem.* **80**, 53–59.
- Reimer P. J., Brown T. A. and Reimer R. W. (2004) Discussion: Reporting and calibration of post-bomb ^{14}C data. *Radiocarbon* **46**(3), 1299–1304.
- Riedel T., Biester H. and Dittmar T. (2012) Molecular fractionation of dissolved organic matter with metal salts. *Environ. Sci. Technol.* **46**, 4419–4426.
- Riedel T., Zak D., Biester H. and Dittmar T. (2013) Iron traps terrestrially derived dissolved organic matter at redox interfaces. *Proc. Natl. Acad. Sci. U.S.A.* **110**, 10101–10105.
- Riedel T. and Dittmar T. (2014) A method detection limit for the analysis of natural organic matter via Fourier Transform Ion

- Cyclotron Resonance Mass Spectrometry. *Anal. Chem.* **86**(16), 8376–8382.
- Rossel P. E., Stubbins A., Hach P. F. and Dittmar T. (2015) Bioavailability and molecular composition of dissolved organic matter from a diffuse hydrothermal system. *Mar. Chem.* **177**, 257–266.
- Rozanski K., Araguás-Araguás L. and Gonfiantini R. (1993) Isotopic patterns in modern global precipitation. *Geophys. Monogr. Series* **78**, 1–36.
- Ruff M., Wacker L., Gäggeler H. W., Suter M., Sinal H.-A. and Szidat S. (2007) A gas ion source for radiocarbon measurements at 200 kV. *Radiocarbon* **49**, 307–314.
- Ruff M., Fahrni S., Gäggeler H. W., Hajdas I., Suter M., Sinal H.-A., Szidat S. and Wacker L. (2010) On-line radiocarbon measurements of small samples using elemental analyzer and MICADAS gas ion source. *Radiocarbon* **52**, 1645–1656.
- Russell M. J. and Hall A. J. (1997) The emergence of life from iron monosulphide bubbles at a submarine hydrothermal redox and pH front. *J. Geol. Soc. London* **154**(3), 377–402.
- Sander S. G. and Koschinsky A. (2011) Metal flux from hydrothermal vents increased by organic complexation. *Nat. Geosci.* **4**, 145–150.
- Santelli C. M., Orcutt B. N., Banning E., Bach W., Moyer C. L., Sogin M. L., Staudigel H. and Edwards K. J. (2008) Abundance and diversity of microbial life in ocean crust. *Nature* **453**, 653–656.
- Schillawski S. and Petsch S. (2008) Release of biodegradable dissolved organic matter from ancient sedimentary rocks. *Global Biogeochem. Cycles* **22**, GB3002. <http://dx.doi.org/10.1029/2007GB002980>.
- Schmidt F., Elvert M., Koch B. P., Witt M. and Hinrichs K.-U. (2009) Molecular characterization of dissolved organic matter in pore water of continental shelf sediments. *Geochim. Cosmochim. Acta* **73**, 3337–3358.
- Schmidt F., Koch B. P., Witt M. and Hinrichs K.-U. (2014) Extending the analytical window for water-soluble organic matter in sediments by aqueous Soxhlet extraction. *Geochim. Cosmochim. Acta* **141**, 83–96.
- Schneckenburger P., Adam P. and Albrecht P. (1998) Thioketones as key intermediates in the reduction of ketones to thiols by HS⁻ in natural environments. *Tetrahedron Lett.* **39**, 447–450.
- Seidel M., Beck M., Riedel T., Waska H., Suryaputra I. G. N. A., Schnetger B., Niggemann J., Simon M. and Dittmar T. (2014) Biogeochemistry of dissolved organic matter in an anoxic intertidal creek bank. *Geochim. Cosmochim. Acta* **140**, 418–434.
- Sievert S. M., Brinkhoff T., Muyzer G., Ziebis W. and Kuever J. (1999) Spatial heterogeneity of bacterial populations along an environmental gradient at a shallow submarine hydrothermal vent near Milos Island (Greece). *Appl. Environ. Microbiol.* **65** (9), 3834–3842.
- Sleighter R. L., Chin Y.-P., Arnold W. A., Hatcher P. G., McCabe A. J., McAdams B. C. and Wallace G. C. (2014) Evidence of incorporation of abiotic S and N into prairie wetland dissolved organic matter. *Environ. Sci. Technol. Lett.* **1**, 345–350.
- Sinninghe Damsté J. S. and de Leeuw J. W. (1990) Analysis, structure and geochemical significance of organically-bound sulphur in the geosphere: State of the art and future research. *Org. Geochem.* **16**, 1077–1101.
- Sinninghe Damsté J. S., Rijpstra W. I. C., Kock-van Dalen A. C., de Leeuw J. W. and Schenck P. A. (1989) Quenching of labile functionalized lipids by inorganic sulphur species: evidence for the formation of sedimentary organic sulphur compounds at the early stages of diagenesis. *Geochim. Cosmochim. Acta* **53**, 1343–1355.
- Svensson E., Skoog A. and Amend J. P. (2004) Concentration and distribution of dissolved amino acids in a shallow hydrothermal system, Vulcano Island (Italy). *Org. Geochem.* **35**(9), 1001–1014.
- Sinal H.-A., Stocker M. and Suter M. (2007) MICADAS: A new compact radiocarbon AMS system. *Nucl. Instrum. Methods Phys. Res., Sect. B* **259**, 7–13.
- Tarasov V. G., Gebruk A. V., Mironov A. N. and Moskalev L. I. (2005) Deep-sea and shallow water hydrothermal vent communities: two different phenomena? *Chem. Geol.* **224**, 5–39.
- Vairavamurthy A. and Mopper K. (1987) Geochemical formation of organosulphur compounds (thiols) by addition of H₂S to sedimentary organic matter. *Nature* **329**, 623–625.
- Vrouzi F. (1985) Research and development of geothermal resources in Greece: present status and future prospects. *Geothermics* **14**, 213–227.
- Wacker L., Christl M. and Sinal H. A. (2010) Bats: A new tool for AMS data reduction. *Nucl. Instrum. Methods Phys. Res., Sect. B* **268**, 976–979.
- Wadge G. (1984) Comparison of volcanic production rates and subduction rates in the Lesser Antilles and Central America. *Geology* **12**, 555–558.
- Wakeham S. G., Sinninghe Damsté J. S., Kohnen M. E. L. and de Leeuw J. W. (1995) Organic sulfur compounds formed during early diagenesis in Black Sea sediments. *Geochim. Cosmochim. Acta* **59**, 521–533.
- Werne J. P., Hollander D. J., Lyons T. W. and Sinninghe Damsté J. S. (2004) Organic sulfur biogeochemistry: recent advances and future research directions. In *Sulfur Biogeochemistry – Past and Present* (eds. J. P. Amend, K. J. Edwards and T. W. Lyons). Geological Society of America, Boulder, Colorado, pp. 117–134.
- Waska H., Koschinsky A., Ruiz-Chancho M. J. and Dittmar T. (2015) Investigating the potential of solid-phase extraction and Fourier-transform ion cyclotron resonance mass spectrometry (FT-ICR-MS) for the isolation and identification of dissolved metal-organic complexes from natural waters. *Mar. Chem.* **173**, 78–92.
- Yamanaka T., Maeto K., Akashi H., Ishibashi J. I., Miyoshi Y., Okamura K., Noguchi T., Kuwahara Y., Toki T., Tsunogai U., Ura T., Nakatani T., Maki T., Kubokawa K. and Chiba H. (2013) Shallow submarine hydrothermal activity with significant contribution of magmatic water producing talc chimneys in the Wakamiko Crater of Kagoshima Bay, southern Kyushu, Japan. *J. Volcanol. Geotherm. Res.* **258**, 74–84.
- Yücel M., Sievert S. M., Vetrani C., Foustoukos D. I., Giovannelli D. and Le Bris N. (2013) Eco-geochemical dynamics of a shallow-water hydrothermal vent system at Milos Island, Aegean Sea (Eastern Mediterranean). *Chem. Geol.* **356**, 11–20.
- Zaback D. A. and Pratt L. M. (1992) Isotopic composition and speciation of sulfur in the Miocene Monterey Formation: reevaluation of sulfur reactions during early diagenesis in marine environments. *Geochim. Cosmochim. Acta* **56**, 763–774.
- Zark M., Riebesell U. and Dittmar T. (2015) Effects of ocean acidification on marine dissolved organic matter are not detectable over the succession of phytoplankton blooms. *Sci. Adv.* **1** e1500531.
- Zhu M.-X., Chen L.-J., Yang G.-P., Huang X.-L. and Ma C.-Y. (2014) Humic sulfur in eutrophic bay sediments: characterization by sulfur stable isotopes and K-edge XANES spectroscopy. *Estuarine Coastal Shelf Sci.* **138**, 121–129.

Evaluation of the Orbitrap Mass Spectrometer for the Molecular Fingerprinting Analysis of Natural Dissolved Organic Matter

Jeffrey A. Hawkes,^{*,†} Thorsten Dittmar,[‡] Claudia Patriarca,[†] Lars Tranvik,[§] and Jonas Bergquist[†]

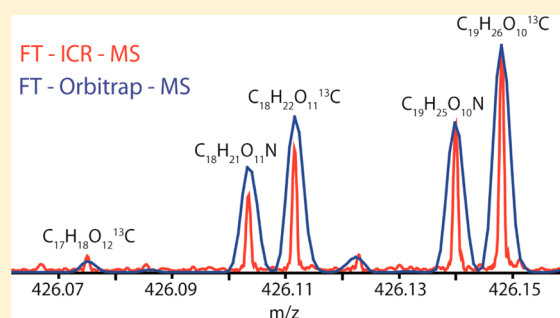
[†]Analytical Chemistry, Department of Chemistry - BMC, Uppsala University, 751 24 Uppsala, Sweden

[‡]Research Group for Marine Geochemistry, Institute for Chemistry and Biology of the Marine Environment, Carl von Ossietzky University of Oldenburg, 26129 Oldenburg, Germany

[§]Department of Limnology, Uppsala University, 752 36 Uppsala, Sweden

S Supporting Information

ABSTRACT: We investigated the application of the LTQ-Orbitrap mass spectrometer (LTQ-Velos Pro, Thermo Fisher) for resolving complex mixtures of natural aquatic dissolved organic matter (DOM) and compared this technique to the more established state-of-the-art technique, Fourier transform ion cyclotron resonance mass spectrometry (FTICR-MS, Bruker Daltonics), in terms of the distribution of molecular masses detected and the reproducibility of the results collected. The Orbitrap was capable of excellent reproducibility: Bray–Curtis dissimilarity between duplicate measurements was $2.85 \pm 0.42\%$ (mean \pm standard deviation). The Orbitrap was also capable of the detection of most major ionizable organic molecules in typical aquatic mixtures, with the exception of most sulfur and phosphorus containing masses. This result signifies that the Orbitrap is an appropriate technique for the investigation of very subtle biogeochemical processing of bulk DOM. The lower costs (purchase and maintenance) and wider availability of Orbitrap mass spectrometers in university departments means that the tools necessary for research into DOM processing at the molecular level should be accessible to a much wider group of scientists than before. The main disadvantage of the technique is that substantially fewer molecular formulas can be resolved from a complex mixture (roughly one third as many), meaning some loss of information. In balance, most biogeochemical studies that aim at molecularly fingerprinting the source of natural DOM could be satisfactorily carried out with Orbitrap mass spectrometry. For more targeted metabolomic studies where individual compounds are traced through natural systems, FTICR-MS remains advantageous.



Recent advances in ultrahigh-resolution mass spectrometry have played a key role in the investigation of dissolved organic matter (DOM) in aquatic environments.^{1–5} Discerning and comparing the signal intensity from the mass spectrometric detector of individual molecular formulas from immensely complex natural DOM mixtures has given new molecular-level information that has been critical in numerous research themes in biogeochemistry, such as the investigation of microbial or ecosystem functioning,^{6–9} DOM fluxes across marine environments,^{10–16} mechanisms of DOM alteration and removal from aquatic environments,^{17–20} and DOM persistence in the environment.^{21–23}

Organic molecules with the same nominal mass but a different molecular formula can be resolved from each other by their mass defect, the sum of the atomic mass defects (Δm) of their constituent elements (e.g., $^1\text{H} = 1.007825$ Da, $\Delta m = 7.825$ mDa; $^{16}\text{O} = 15.994915$ Da, $\Delta m = -5.085$ mDa). The mass resolving power (mass divided by full width at half-maximum height, $m/z/\text{fwhm}$) of the instrument determines whether two peaks in a spectra may be separated by mass, and resolving power has improved from ~ 3000 at m/z 400 in low-resolution mass analysers to $>100\,000$ in ultrahigh-resolution techniques.

This is sufficient to separate molecules with a mass difference of <5 mDa at a mass range of 200–600 Da³ and allows resolution of several thousand distinct molecular formulas from natural DOM.

Ultrahigh-resolution techniques, in particular high-field-strength Fourier transform ion cyclotron resolution mass spectrometry (>7 T FTICR-MS), are extremely limited in their availability, with only a handful of laboratories worldwide regularly analyzing environmental samples and offering resolving power in excess of 100 000 at m/z 400. This is mainly due to the purchase and running costs of 7–21 T FTICR-MS instruments, which require a large supply of liquid helium and often a dedicated engineer. The Orbitrap (Thermo Scientific) is a potential alternative to FTICR-MS that uses an electrostatic field rather than a magnetic field for separation of accumulated ions.^{24,25} A detailed comparison of the physical theory and engineering of the two techniques can be found elsewhere.³ Because the Orbitrap does not involve a large

Received: April 25, 2016

Accepted: July 12, 2016

Published: July 12, 2016

cryogenic magnet, the running costs are considerably lower and instruments are much more widely available in university departments.

The latest Orbitraps have resolving powers of 100 000–600 000 (ref 3), with mass accuracy and precision comparable to 7 T FTICR-MS,² and show some promise as an alternative or complementary technique for investigating natural DOM.^{26–30} The Orbitrap has not yet been rigorously compared with a state-of-the-art FTICR-MS for the investigation of biogeochemical processing of DOM, where the precision of the intensity distribution of ions, and not just the mass accuracy and resolution, becomes critically important.

Both FTICR-MS and Orbitrap mass analysers can be coupled to electrospray ionization (ESI) in commercial instruments, meaning that the mixture of ions that is analyzed by both techniques can be closely controlled and the resulting data critically compared. In this study, we assessed the similarity between the data resulting from ESI-FTICR-MS and ESI-FT-Orbitrap-MS, the latter at two software-controlled resolution settings (“100 000” and “30 000”) on samples isolated from aquatic environments. We evaluated the performance of the Orbitrap at different resolution settings as a “molecular fingerprinting” tool of aquatic DOM and will present recommendations in the use of lower-resolving power instruments in biogeochemical research.

■ EXPERIMENTAL SECTION

Reagents and Instrumentation. We used ultrapure ULC/MS grade methanol (Biosolve BV, Netherlands), ultrapure water (Sartorius Stedim Arium 611VF), and high-purity hydrochloric acid (AnalaR Normapur 25%, VWR, Germany). All glassware was muffled at 450 °C for at least 4 h prior to use. The Orbitrap was a LTQ-Velos-Pro (Thermo Scientific, Germany), hosted at Uppsala University, Sweden. The FTICR-MS was a SolariX 15 T (Bruker Daltonics, U.S.A.), hosted at the University of Oldenburg, Germany.

Sample Collection. Samples were isolated from marine and lake settings for this study. The marine samples were taken from the North Pacific Ocean (~0.5 ppm DOC) at two depths (NEqPIW; 21 m “surface” and 674 m “intermediate”) at the Natural Energy Laboratory of Hawaii Authority (NELHA). The seawater samples were acidified (0.01 M HCl), then desalted and concentrated by solid-phase extraction on divinylbenzene adsorber (PPL, Varian) to a final concentration in methanol of 9000 ppm DOC as described elsewhere.³¹ The lake sample was taken from a brown water lake, Lake Plåten, Sweden (59.8627° N, 18.5426° E; ~20 ppm DOC). The sample was concentrated by a factor of about 11 to a final concentration of 225 ppm DOC by reverse osmosis, and then further concentrated on PPL sorbent after acidification, as described for the seawater sample, to a final concentration in methanol of 3991 ppm DOC. These samples were stored at –20 °C until the day of analysis, when they were filtered through a precleaned 0.2 µm pore size syringe filter (PTFE; Carl Roth Rotilabo) and diluted with 50% ultrapure methanol in ultrapure water before analysis.

Preanalysis Treatment of Samples. In order to test the sensitivity of the two mass spectrometers to slight changes in the organic mixture, the intermediate depth marine sample and lake sample were diluted to 20 ppm DOC in 50% ultrapure methanol in ultrapure water and then mixed together to final percentages of 0%, 5%, 10%, 20%, 50%, 80%, 90%, 95%, 100% lake DOM in marine DOM. Each mixed sample was analyzed twice (not sequentially) in random order on both instruments.

The marine sample was analyzed twice at the start, once in the middle, and twice at the end of the set of analysis on the Orbitrap, and three times in total on the FTICR-MS. All analyses were completed in one working day per instrument to minimize the effect of long-term instrumental variability.

FTICR-MS Analysis. Samples were continuously infused into the FTICR-MS by ESI in negative mode (–4 kV, 3 µL min^{–1}) using a nebulized gas flow at a temperature of 220 °C. Ions were accumulated in a hexapole ion trap for 0.2 s before being transferred into the ICR cell. Broad-band mass spectra were recorded between 150 and 2000 *m/z*. A total of 300 scans were summed, and the spectra were internally calibrated with a list of 51 expected compounds over the relevant mass/charge range using the Bruker Daltonics Data Analysis software package. Peaks were identified by the manufacturer’s software, and *m/z*, signal intensity, and resolution data for all peaks above a signal-to-noise ratio of 4 were exported to individual mass lists. The sample infusion syringe (Hamilton, 500 µL) and poly(ether ether ketone) (PEEK) tubing were rinsed with 1–2 mL of 50:50 ultrapure MeOH/H₂O between samples.

FT-Orbitrap-MS Analysis. The Orbitrap was externally calibrated for mass accuracy on the day of analysis using the manufacturer’s guidelines and negative calibration solution. The ion optics and ESI source settings were tuned to maximize the intensity of the peak at *m/z* 431 in low-resolution linear ion trap mode. The resulting settings were as follows: ESI spray voltage, –3.1 kV; sheath gas flow rate, 28; capillary temperature, 275 °C; S-lens rf level, 68.7%; syringe pump flow rate, 8 µL min^{–1}. Complete details of the instrumental tuning can be found in the [Supporting Information](#). It is important to note that the settings between the instruments are not directly comparable, e.g., capillary and dry gas temperature can differ even though the samples were exposed to similar temperatures. Therefore, fine-tuning of the two instruments was done individually with the goal to optimize performance and comparability. Samples were loaded to the ESI by Hamilton syringe (500 µL), using the instrument’s built-in syringe pusher, through PEEK tubing to the ESI source. The ions then transferred by octopole and square quadrupole lenses into a linear ion trap, before being transferred into a curved linear trap (C-Trap) and finally into the Orbitrap cell. Ions were accumulated until 1 × 10⁶ ions had been trapped, as set by the “automatic gain control” setting. Broad-band mass spectra were then recorded between 150 and 2000 *m/z*. Each scan was internally calibrated in lock mass mode using a list of 18 expected compounds covering the mass/charge range of 173–625 *m/z*, using the Xcalibur software package (Thermo Electron Corporation). A total of 300 scans were accumulated, and peaks were identified by the manufacturer’s software, and *m/z*, intensity, and resolution data for all peaks were exported to individual mass lists. Two resolution modes were used to collect data, “30 000” and “100 000”. The actual resolution differs from these values.

Detection Limit, Formula Assignment, and Spectrum Interpretation. Each sample mass list was individually processed in the software package *R* to remove noise peaks which occurred below a mass-dependent detection limit. This variable detection limit was calculated by considering the first 99th percentile of peaks with a mass defect between 0.4 and 0.8 Da (no organic formulas can fall in this range within our mass window) and calculating the linear dependence of their intensity with *m/z*. The resulting noise level generally does not change across the mass range of 150–2000 Da for the

Orbitrap, but increases with mass by about 70% on the FTICR-MS.

Formulas were assigned using an in-house MATLAB routine. First, all peaks from the internally calibrated mass list produced by the 15 T FTICR-MS were aligned to ~26 000 measured masses using a clustering approach. Masses which only occurred in one sample (a total of 6320) were removed, and the remaining masses were then assigned to formulas where possible using an in-house MATLAB routine, allowing a maximum average mass difference of 300 ppb from the negatively charged ($-1H^+$) assigned formula and the measured mass. Formulas were considered over the ranges of $C_{1-40}H_{1-82}O_{1-40}N_{0-4}S_{0-1}P_{0-1}$ under the conditions $O \leq C$, $0.3C \leq H \leq 2C + 2$, $O > (2P + S)$, and formulas with certain arrangements of heteroatoms were not considered, as they are difficult to resolve even by 15 T FTICR-MS. These were $[CHO]N_{2-4}S$, $[CHO]N_{2-4}P$, $[CHO]NSP$, and $[CHO]SP$, where the term $[CHO]$ means any allowed combination of these three atoms.

The resulting list of 9054 formulas was then used to match peaks detected at lower resolution by FT-Orbitrap-MS using a routine that will be published elsewhere. We only allowed formulas to be assigned if the mass difference to the nearest large peak was high enough to be resolved at the instrumental resolution in question, in order to minimize false assignments (see Supporting Information for complete formula lists used at each resolution). These techniques were combined to cluster and align peaks and assign carefully screened molecular formulas to one large data set. All intensities remaining after noise removal and formula assignment were normalized, I_{norm} , so that the sum of the top 100 intensities in each sample ($\sum I_{100}$) equaled 10 000. Contaminant masses which were detected in the wash solution (50% ultrapure methanol in ultrapure water) with $I_{norm} > 5$ and all unassigned masses were then removed from the data set. Some “false negatives”—true analytes—would have been removed with the contaminant ^{13}C -containing and other unassigned masses due to the presence of noncontaminant structural isotopes or molecular formulas which were not considered in our formula assignment routine. This issue is commonplace, and further discussion is outside of the scope of this study.

The large data set was imported into the statistical programming software *R*, where sample data were intercompared by a Bray–Curtis dissimilarity test (eq 1). The dissimilarities were compiled into a matrix and used as the basis for a principle coordinate analysis.

% Bray–Curtis dissimilarity calculation: signal intensity I is compared between sample p and q for each molecular mass k (from k_1 to k_n)

$$\%B-C \text{ dissimilarity} = 100 \frac{\sum_{k=1}^n |I_{p,k} - I_{q,k}|}{\sum_{k=1}^n (I_{p,k} + I_{q,k})} \quad (1)$$

RESULTS AND DISCUSSION

Mass Accuracy. All three techniques (15 T FTICR-MS, Orbitrap at setting 100 000, and Orbitrap at setting 30 000) had mass accuracy better than 0.8 mDa for the 18 common molecular masses which were used as “lock masses” in the Orbitrap. The FTICR-MS had consistently less than 0.02 mDa offset from the calculated exact negative mass across the entire mass range. The Orbitrap was more variable, and 90% of the

assigned masses had mass inaccuracy < 1 ppm (i.e., 0.5 mDa at m/z 500; Figure S13), similar to a recent assessment of an Orbitrap for petroleomics.³⁰ We found that the mass accuracy was sufficient for formula assignment, as long as we accounted for the resolution of the data set in the formula assignment algorithm (Figure 1). Attempts to use the complete formula list

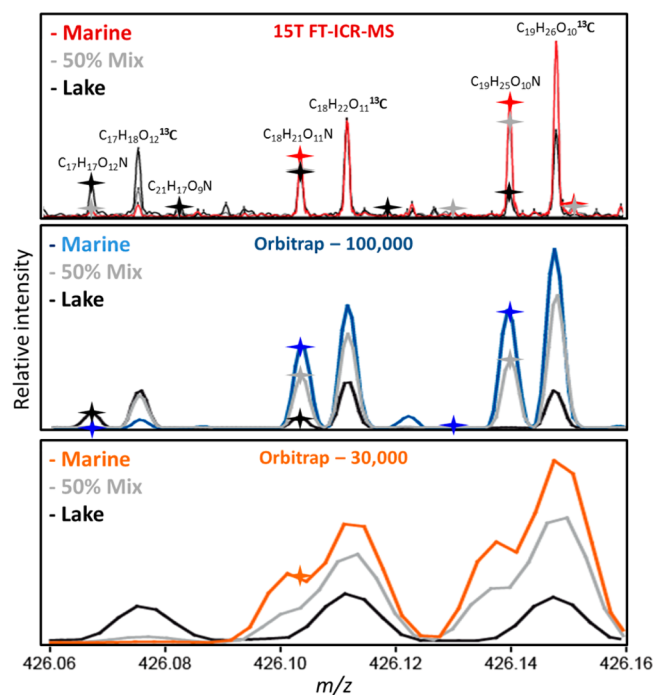


Figure 1. Comparison of raw mass spectra over a mass window of 0.1 Da. Assigned molecular formulas at the exact (not measured) mass are indicated by four-pointed stars. The data are displayed for an even nominal mass, meaning that nitrogen-containing formulas need to be resolved from ^{13}C -containing formulas. Note that the nitrogen-containing peak at ~ 426.14 is not assigned in the Orbitrap 30 000 data set, as it was not resolvable from the ^{13}C -containing formula at this resolution. ^{13}C -containing formulas are not explicitly assigned, as they are already in the data set as the respective ^{12}C -isotopologue.

generated from the 15 T FTICR-MS for assignment of the lower-resolution data led to an unacceptable and variable number of false positive assignments to low-intensity sulfur and nitrogen containing peaks which occur next to larger CHO peaks (as confirmed by 15 T FTICR-MS), or unwanted assignment of ^{13}C -containing formula peaks to other potential formulas. Future studies should be similarly cautious in constraining the allowed formulas in this type of complex mixture at low resolutions. Furthermore, the Orbitrap mass accuracy drifted out of an acceptable range over a time scale of weeks during our investigation so that internal mass calibration was not possible anymore. Therefore, external mass calibration on the Orbitrap at least once a week is necessary.

Peak Resolution and Detection Limit. At higher resolving power, narrower peaks allow the resolution of many additional analytes at each nominal mass (Figure 1). The median peak width at half-maximum height of peaks with nominal mass 401 Da was 0.8 mDa using 15 T FTICR-MS and 3.1 mDa and 13.6 mDa using Orbitrap in resolution modes 100 000 and 30 000, respectively (Table 1). As a result, the total number of molecular masses identified in the intermediate depth marine sample increased from ~ 1000 at resolution mode

Table 1. Main Features of the Different Techniques Used

	15 T FTICR-MS	Orbitrap LTQ Velos	Orbitrap at 30 000 setting
mass accuracy—median (interquartile range) all assigned formulas	0.04 (0.09) ppm	0.29 (0.47) ppm	1.09 (1.81) ppm
resolution—median of all peaks at m/z 401	0.8 mDa ($R = 484\,620$)	3.1 mDa ($R = 136\,951$)	13.6 mDa ($R = 28\,865$)
Bray–Curtis dissimilarity between replicates (mean \pm SD)	$6.89 \pm 3.94\%$	$2.85 \pm 0.42\%$	$3.48 \pm 0.94\%$
data acquisition time (300 scans)	~ 8 min	~ 8 min	~ 2 min
major benefits	best resolution and accuracy, detection of more molecular masses	better availability, lower purchase and running costs	faster: better for coupled chromatography applications and very large data sets
major disadvantages	expensive, not widely available	loss of potentially important information including most small peaks and many N and S containing formulas	loss of almost all N, S, P containing formulas

30 000 (Orbitrap) to ~ 1600 at resolution mode 100 000 (Orbitrap) to ~ 4600 using the 15 T FTICR-MS (Table S11). In total, over 3000 peaks were detected by FTICR-MS and not by Orbitrap (100 000 mode) in the intermediate depth marine sample. Some of these were not determined because of resolution, but the majority were not detected for other reasons, likely including differences in response factor (e.g., ionization efficiency) and detection limit. The dynamic range of the Orbitrap is on the order of 10^3 – 10^4 , which is comparable to the FTICR-MS,^{32,33} but due to the lower mass resolution of data acquisition and the apodization of the FT signal conducted by the software on the Orbitrap, many small peaks were not detected (see, for example, $C_{21}H_{17}O_9N$ in Figure 1). The FTICR-MS data has more intense noise peaks (Figure 1) because more subtle apodization settings were chosen compared to the settings on the Orbitrap in order to increase the detection limit for low-abundance compounds. This raises the absolute detection limit, but the increased mass sampling resolution means an increased number of small, narrow peaks can be resolved and determined.

Only the largest peaks were identified in the lowest resolution mode, generally meaning [CHO] formulas at odd nominal masses and [CHO]¹³C formulas at even masses. Nitrogen is not highly abundant in natural organic matter,³⁴ and due to the 1.1% natural abundance of ¹³C and the large number of carbon atoms (10–40) in DOM molecules, ¹³C-containing peaks often have similar intensities to nitrogen-containing peaks (Figure 1). The mass difference between [CHO]¹³CH and [CHO]N is 8.11 mDa, and these homologous series were not always successfully resolved from each other at resolution mode 30 000 on the Orbitrap (Figure 1). This is important, because all even m/z assignments (in negative mode) depend on this resolution. Nitrogen-containing formula therefore cannot be reliably considered at this lower-resolution mode, except at lower masses which have better resolution. Contrarily, these homologous series can be easily resolved at resolution mode 100 000 (Figure 1). Neither settings 30 000 nor 100 000 were able to resolve the pair [CHO]C₃ and [CHO]H₄S ($\Delta m = 3.34$ mDa), which can be similar in intensity at certain mass defects, leading to a single broad peak with peak intensity at an intermediate mass on the Orbitrap, which is then assigned to one peak or another, but not to both as it is by 15 T FTICR-MS. Another problematic set of peaks is the triplet [CHO]N₂O₂, [CHO]C₅ (+4.1 mDa), and [CHO]C₂H₄S (+3.2 mDa). It is important that these formula candidates are not included for consideration in lower-resolution methods, as they may lead to systematic artifacts in the data which may be misinterpreted as environmental trends.

The intensity ratios of the closely occurring peaks may vary across geochemical gradients or during a biogeochemical process, meaning that simply accepting the peak only containing C, H, and O in these cases, knowing that the others can occur, would be careless. The 15 T FTICR-MS data indicated that these doublets and triplets were only problematic at certain mass defects. The largest CHO or CHON peaks were much greater in intensity than their neighbors, meaning that they could be included for consideration at both of the resolution modes on the Orbitrap. This was the case for the marine and freshwater sample considered, and is likely to apply to all natural aquatic samples, given their low overall variability.⁵ Our formula list, along with exact masses and mass defects to the nearest neighbor, is included as Supporting Information.

The additional information provided by the “heteroatom-containing” molecular formulas, such as [CHO]N_{1–4} and [CHO]S, is therefore lost at resolutions somewhere around 100 000. Figure 2 shows the additional molecular formulas

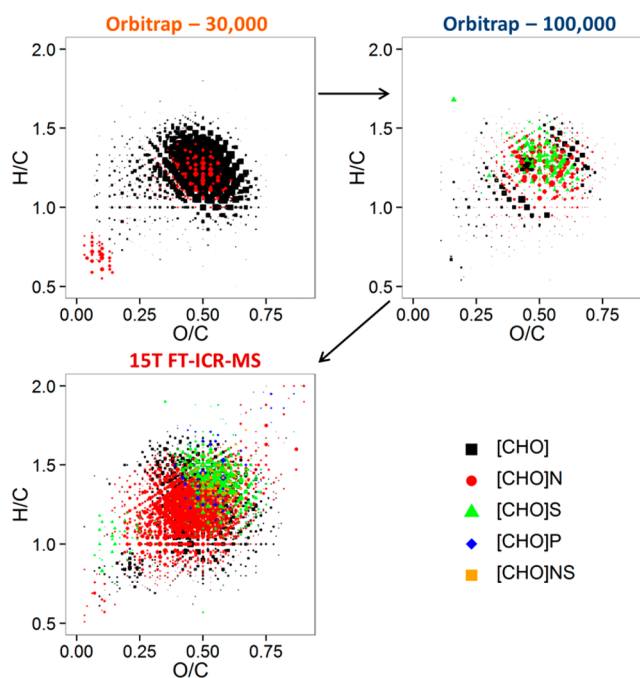


Figure 2. Van Krevelen diagrams (H/C vs O/C of detected molecular formulas) of additional formulas resolved at each setting or instrument tested. Most of the [CHO] formulas are detected at setting 30 000 on the Orbitrap, and greater detail is revealed with improved resolution on the Orbitrap or with FTICR-MS. The size of data point is proportional to the logarithm of the intensity.

obtained at each resolving power in Van Krevelen space (atomic ratio of H/C vs O/C for each assigned formula). The bulk [CHO] components and some nitrogen-containing formulas that are typically reported for natural DOM^{34,35} are resolved at reasonable intensity ratios in the lower-resolution mode, whereas the lower-intensity molecules as well as (most) nitrogen, sulfur, or phosphorus containing formulas are only resolved at higher resolutions (mostly only by FTICR-MS; Table S11). This resolution data, along with the apparent differences in detection limit, suggests that simple presence/absence questions, such as use of the recently proposed DOM lability index²³ or for drinking water quality monitoring^{26,36} can be approached with only moderate resolving power ($\sim 30\,000$) mass spectrometry, although less peaks will be considered (Figure 2).

Peak Intensity Distribution and Precision. The main focus of our study was the evaluation of the Orbitrap for more complex biogeochemical investigations that require precise and accurate formula intensity ratios. The broad-band mass spectrum produced by the Orbitrap appears quite different from that of the FTICR-MS (Figure 3), with a broad lowering

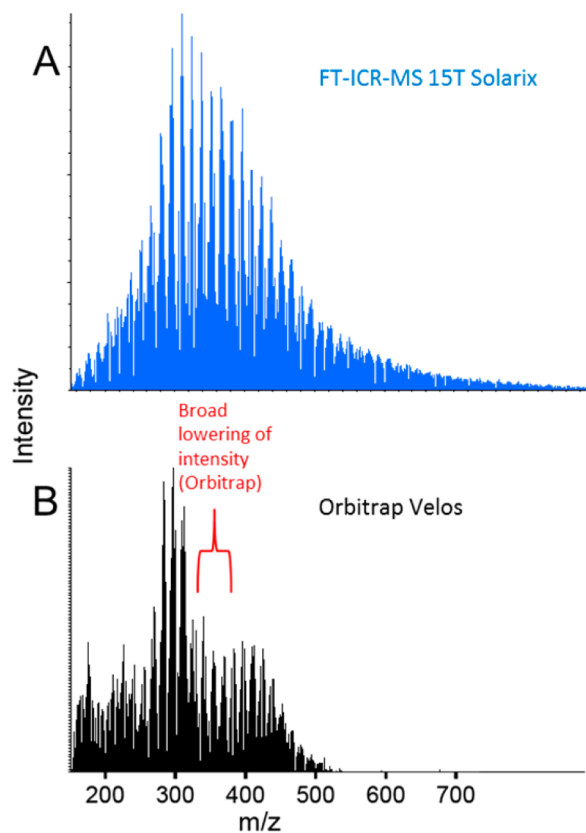


Figure 3. (A) Broad-band mass spectrum FTICR-MS. (B) Broad-band mass spectrum Orbitrap setting 100 000. A broad double hump was found in the lake extract by Orbitrap with intensity maxima at $m/z \sim 311$ and ~ 425 , whereas only the maximum at $m/z \sim 311$ was found by FTICR-MS, accompanied by a gradual high-mass tail to $m/z \sim 850$. The chosen tune mass was not found to affect the broad shape of the mass spectrum (tested tune masses: 311.11, 355.01, 431.06).

of peak intensities around m/z 350. This obviously had an important effect on the overall intensity of certain nominal masses, but did not have an obvious effect on the intensity distribution within each nominal mass (Figure 1). The result of this effect is that the calculated intensity-weighted average H/C

ratio (H/C_{wa}) is similar, whereas the calculated intensity-weighted molecular weight (MW_{wa}) is strongly influenced (Figure S11). In order to assess the importance of this effect, we compared these calculated variables for the Orbitrap (100 000) and FTICR-MS for corresponding samples, and found that the average ratio (\pm SD) of $H/C_{wa,Orbitrap}/H/C_{wa,FTICRMS}$ was 0.99 ± 0.01 , whereas $MW_{wa,Orbitrap}/MW_{wa,FTICRMS}$ was much less comparable at 0.91 ± 0.03 (Figure S11). This broad mass bias has a large effect on the calculated overall dissimilarity between the marine and lake samples (Figure 4) and should be

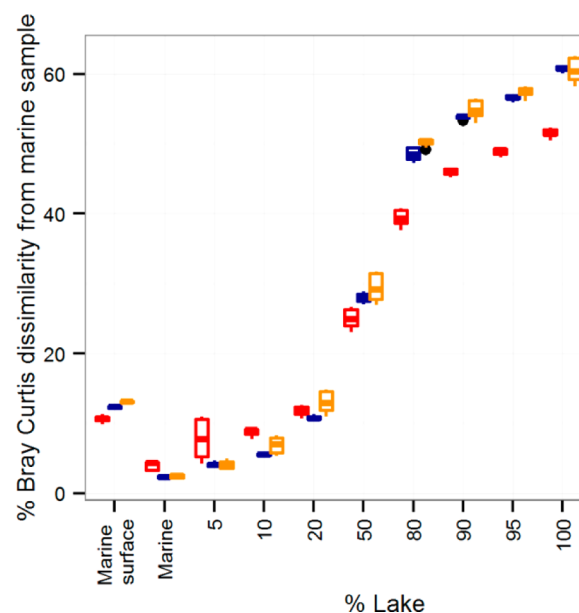


Figure 4. Boxplots showing variability in Bray–Curtis dissimilarity between all samples and the marine samples. The marine samples were analyzed 3–5 times, and all other samples were analyzed in duplicate, so there are 6–10 [(3 × 2)–(5 × 2)] distances summarized in each boxplot. Red is 15 T FTICR-MS, blue is Orbitrap 100 000, orange is Orbitrap 30 000. All detected formulas were used for this statistical analysis, and the increased number of molecular formulas being considered at higher resolutions (Table S11) leads to more random variability.

contemplated when broad mass distribution changes appear to be an important characteristic of a study.¹⁸ Overall, as the fine scale detail (Figure 1) and geochemical results (Figures 4–6) were essentially unaffected by this feature, we consider it to be of minor importance and simply an artifact that researchers should be aware of. It does not appear as an obvious feature when analyzing marine DOM samples.

All three methods were capable of detecting as little as 5% of lake sample mixed into the intermediate depth sample (or vice versa), as demonstrated by Bray–Curtis dissimilarity (Figures 4 and 5). The marine sample contained more saturated molecular formulas (higher H/C ratio) than the lake sample, resulting in a difference in intensity distribution toward higher mass defects at each nominal mass (Figures 1 and 6). This geochemical gradient was highly reproducible between the techniques and across all samples, leading to a first-principle coordinate that explained 59% of all data variability. This gradient therefore outweighed instrumental differences, which accounted for a further 31% of data variability (Figure 5). The detection of the geochemical gradient was not apparently affected by the broad-band mass bias of the Orbitrap, and was clear enough to detect

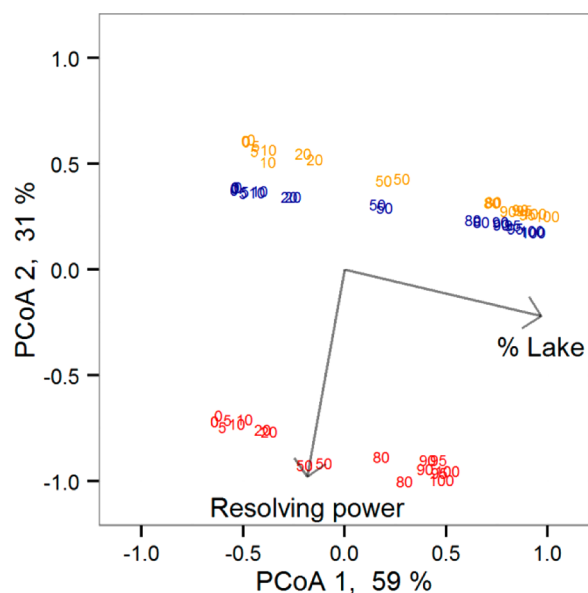


Figure 5. Principle coordinate diagram showing position of each sample in the mixing experiment on the first two eigenvectors, which made up ~90% of the total variability in the data set of 9044 molecular intensities. Red is 15 T FTICR-MS, blue is Orbitrap 100 000, orange is Orbitrap 30 000. The data points indicate the percent of lake extract in the analyzed sample. The first PCoA axis correlates to the percent of lake DOM in the sample, while instrumental differences are reflected on the second axis. Thus, instrumental bias had much less influence on the results than molecular composition of the samples. As in Figure 4, it is clear that small changes (>5%) in the sample mixture can be detected by all three methods.

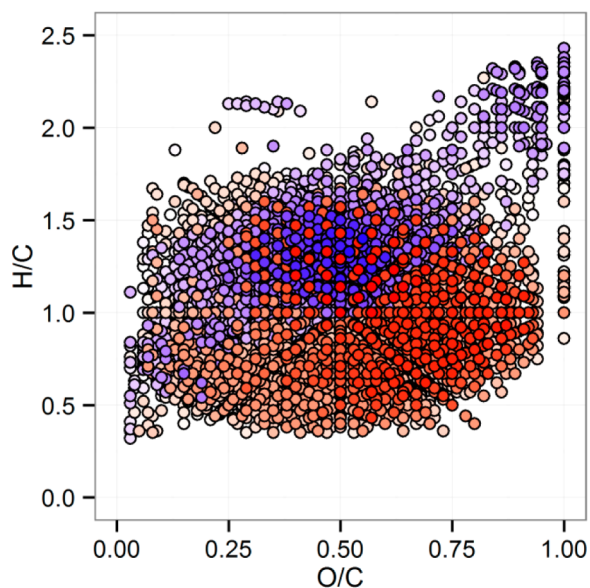


Figure 6. Van Krevelen diagram showing all detected molecular formulas by their H/C and O/C atomic ratios. Each point is colored according to its correlation with PCoA 1, with red colors correlating positively (more terrestrial) and blue colors correlating negatively (more marine). These trends were reproducible by all three methods.

at resolution setting 30 000, which is very encouraging for the use of this level of resolving power for the investigation of freshwater–seawater geochemical gradients.^{15,16} It also suggests that this resolving power would be sufficient to detect and study molecular alterations which are specific to certain

functional or molecular groups, such as the changes subjected by UV irradiation,^{17,20,37} coprecipitation with metal salts,^{19,38,39} or hydrothermal degradation.¹⁸ It is unclear whether other mass spectrometers with this level of resolution would be appropriate for DOM fingerprinting analysis, as variability in peak intensity and peak ratios would still need to be assessed.

Differences between surface and deep seawater samples were also clearly detectable in all three methods (Figure 5), which is very encouraging. The reproducibility found for replicate analysis was for some samples apparently better than that found for FTICR-MS (Figure 5, Table 1). This is because more independent variables (molecular formulas) were included in the statistics for FTICR-MS data. Most of the additional molecular formulas exclusively detected via FTICR-MS have low signal intensities and are close to the instrumental noise; thus, the analytical variability is intrinsically higher for these compounds. The excellent reproducibility achieved suggests that the Orbitrap would be suitable for investigating even subtle changes within a marine or freshwater sample set,^{11,22,40} assuming that these changes affected the compounds that are resolvable by this method. Overall, we have found that the Orbitrap, when correctly tuned and calibrated, is a very promising alternative to high-field-strength FTICR-MS for the molecular fingerprinting of DOM in the environment.

■ FURTHER CONSIDERATIONS AND CONCLUSIONS

The Orbitrap has a different mass range than typical FTICR-MS instruments, and masses down to 50 Da can be detected (cf. Solarix 15 T FTICR-MS ≥ 120 Da), whereas higher masses (>500 Da) in the organic mixture are generally not detected. Analysis over the mass window of 50–2000 Da leads to a significant low mass bias that has previously been revealed in published figures without much discussion.^{26,28} Data acquired over different mass ranges must not be directly compared with each other, as systematic errors in interpretation of factors such as average molecular mass are inevitable, even under the same instrumental tune settings (e.g., Figure S12).

The vast majority of molecular-level studies of environmental DOM to date have used FTICR-MS as the means of resolving individual molecular formulas from the complex natural mixture. Until recently, other mass spectrometry techniques were not capable of resolving powers as high as FTICR-MS (>80 000), but recent advances to time-of-flight (TOF) mass spectrometers³ and the introduction of the Orbitrap mass spectrometer^{24,25,41} may now allow a greater number of laboratories to participate in the characterization of DOM from the environment. These instruments are currently being heavily utilized for biomedical and food sciences, but are not being as well-exploited as they should be for environmental science despite their widespread availability in university departments.

■ ASSOCIATED CONTENT

Supporting Information

The Supporting Information is available free of charge on the ACS Publications website at DOI: 10.1021/acs.analchem.6b01624.

Numbers of categorized molecular masses detected by different techniques, average molecular mass and H/C of detected formulas, demonstration of the mass bias effect on the Orbitrap when changing broad-band mass range,

and mass error of all assigned formulas in one marine sample for the three methods (PDF)
Tuning file for the Orbitrap (TXT)
Complete mass list of detected formulas (TXT)

AUTHOR INFORMATION

Corresponding Author

*Phone: +46 184713681. E-mail: jeffrey.hawkes@kemi.uu.se.

Notes

The authors declare no competing financial interest.

ACKNOWLEDGMENTS

The authors are grateful to Katrin Klaproth for FTICR-MS assistance, Benjamin Jacob for sharing his MATLAB routines, the Knut and Alice Wallenberg Foundation for funding (Grant KAW 2013.0091), and to David C. Podgorski and two anonymous reviewers for their helpful contributions.

REFERENCES

- (1) Stenson, A. C.; Landing, W. M.; Marshall, A. G.; Cooper, W. T. *Anal. Chem.* **2002**, *74* (17), 4397–4409.
- (2) Cortés-Francisco, N.; Flores, C.; Moyano, E.; Caixach, J. *Anal. Bioanal. Chem.* **2011**, *400* (10), 3595–3606.
- (3) Xian, F.; Hendrickson, C. L.; Marshall, A. G. *Anal. Chem.* **2012**, *84* (2), 708–719.
- (4) Marshall, A. G.; Hendrickson, C. L.; Jackson, G. S. *Mass Spectrom. Rev.* **1998**, *17* (1), 1–35.
- (5) Dittmar, T.; Stubbins, A. Dissolved Organic Matter In Aquatic Systems. In *Treatise of Geochemistry*, 2nd ed., Vol. 12; Birrer, B., Falkowski, P., Freeman, K., Eds.; Elsevier: Oxford, U.K., 2014.
- (6) Roth, V.-N.; Dittmar, T.; Gaupp, R.; Gleixner, G. *Vadose Zone J.* **2014**, *13* (7), 0162.
- (7) Rossel, P. E.; Vähätalo, A. V.; Witt, M.; Dittmar, T. *Org. Geochem.* **2013**, *60*, 62–71.
- (8) Osterholz, H.; Niggemann, J.; Giebel, H.-A.; Simon, M.; Dittmar, T. *Nat. Commun.* **2015**, *6* (May), 7422.
- (9) Romano, S.; Dittmar, T.; Bondarev, V.; Weber, R. J. M.; Viant, M. R.; Schulz-Vogt, H. N. *PLoS One* **2014**, *9* (5), e96038.
- (10) Sleighter, R. L.; Hatcher, P. G. *Mar. Chem.* **2008**, *110* (3–4), 140–152.
- (11) Lechtenfeld, O. J.; Kattner, G.; Flerus, R.; McCallister, S. L.; Schmitt-Kopplin, P.; Koch, B. P. *Geochim. Cosmochim. Acta* **2014**, *126*, 321–337.
- (12) Flerus, R.; Koch, B. P.; Schmitt-Kopplin, P.; Witt, M.; Kattner, G. *Mar. Chem.* **2011**, *124* (1–4), 100–107.
- (13) Hansman, R. L.; Dittmar, T.; Herndl, G. J. *Mar. Chem.* **2015**, *177* (2), 288–297.
- (14) Dittmar, T.; Koch, B. P. *Mar. Chem.* **2006**, *102* (3–4), 208–217.
- (15) Seidel, M.; Beck, M.; Riedel, T.; Waska, H.; Suryaputra, I. G. N. a.; Schmetger, B.; Niggemann, J.; Simon, M.; Dittmar, T. *Geochim. Cosmochim. Acta* **2014**, *140*, 418–434.
- (16) Medeiros, P. M.; Seidel, M.; Ward, N. D.; Carpenter, E. J.; Gomes, H. R.; Niggemann, J.; Krusche, A. V.; Richey, J. E.; Yager, P. L.; Dittmar, T. *Global Biogeochem. Cycles* **2015**, *29*, 677–690.
- (17) Stubbins, A.; Dittmar, T. *Mar. Chem.* **2015**, *177*, 318–324.
- (18) Hawkes, J. A.; Hansen, C. T.; Goldhammer, T.; Bach, W.; Dittmar, T. *Geochim. Cosmochim. Acta* **2016**, *175*, 68–85.
- (19) Riedel, T.; Biester, H.; Dittmar, T. *Environ. Sci. Technol.* **2012**, *46*, 4419–4426.
- (20) Gonsior, M.; Peake, B. M.; Cooper, W. T.; Podgorski, D.; D'Andrilli, J.; Cooper, W. J. *Environ. Sci. Technol.* **2009**, *43* (3), 698–703.
- (21) Reemtsma, T.; These, A.; Linscheid, M.; Leenheer, J.; Spitzky, A. *Environ. Sci. Technol.* **2008**, *42* (5), 1430–1437.
- (22) Kellerman, A. M.; Dittmar, T.; Kothawala, D. N.; Tranvik, L. J. *Nat. Commun.* **2014**, *5*, 3804.
- (23) D'Andrilli, J.; Cooper, W. T.; Foreman, C. M.; Marshall, A. G. *Rapid Commun. Mass Spectrom.* **2015**, *29* (24), 2385–2401.
- (24) Hu, Q.; Noll, R. J.; Li, H.; Makarov, A.; Hardman, M.; Cooks, R. G. *J. Mass Spectrom.* **2005**, *40* (4), 430–443.
- (25) Makarov, A. *Anal. Chem.* **2000**, *72* (6), 1156–1162.
- (26) Cortés-Francisco, N.; Caixach, J. *Environ. Sci. Technol.* **2013**, *47*, 9619–9627.
- (27) Danger, G.; Orthous-Daunay, F. R.; de Marcellus, P.; Modica, P.; Vuitton, V.; Duvernay, F.; Flandinet, L.; Le Sergeant d'Hendecourt, L.; Thissen, R.; Chiavassa, T. *Geochim. Cosmochim. Acta* **2013**, *118*, 184–201.
- (28) Remucal, C. K.; Cory, R. M.; Sander, M.; McNeill, K. *Environ. Sci. Technol.* **2012**, *46* (17), 9350–9359.
- (29) Cortés-Francisco, N.; Caixach, J. *Anal. Bioanal. Chem.* **2015**, *407* (9), 2455–2462.
- (30) Zhurov, K. O.; Kozhinov, A. N.; Tsybin, Y. O. *Energy Fuels* **2013**, *27* (6), 2974–2983.
- (31) Green, N. W.; Perdue, E. M.; Aiken, G. R.; Butler, K. D.; Chen, H.; Dittmar, T.; Niggemann, J.; Stubbins, A. *Mar. Chem.* **2014**, *161*, 14–19.
- (32) Makarov, A.; Denisov, E.; Kholomeev, A.; Balschun, W.; Lange, O.; Strupat, K.; Horning, S. *Anal. Chem.* **2006**, *78* (7), 2113–2120.
- (33) Makarov, A.; Denisov, E.; Lange, O.; Horning, S. *J. Am. Soc. Mass Spectrom.* **2006**, *17* (7), 977–982.
- (34) Koch, B. P.; Dittmar, T.; Witt, M.; Kattner, G. *Anal. Chem.* **2007**, *79* (4), 1758–1763.
- (35) D'Andrilli, J.; Dittmar, T.; Koch, B. P.; Purcell, J. M.; Marshall, A. G.; Cooper, W. T. *Rapid Commun. Mass Spectrom.* **2010**, *24*, 643–650.
- (36) Cortés-Francisco, N.; Harir, M.; Lucio, M.; Ribera, G.; Martínez-Lladó, X.; Rovira, M.; Schmitt-Kopplin, P.; Hertkorn, N.; Caixach, J. *Water Res.* **2014**, *67*, 154–165.
- (37) Medeiros, P.; Seidel, M.; Powers, L. C.; Dittmar, T.; Hansell, D. A.; Miller, W. L. *Geophys. Res. Lett.* **2015**, *42*, 863–870.
- (38) Riedel, T.; Zak, D.; Biester, H.; Dittmar, T. *Proc. Natl. Acad. Sci. U. S. A.* **2013**, *110*, 10101–10105.
- (39) Gomez-Saez, G. V.; Riedel, T.; Niggemann, J.; Pichler, T.; Dittmar, T.; Bühring, S. I. *Mar. Chem.* **2015**, *177*, 677–686.
- (40) Zark, M.; Riebesell, U.; Dittmar, T. *Sci. Adv.* **2015**, *1* (9), e1500531–e1500531.
- (41) Zubarev, R. a.; Makarov, A. *Anal. Chem.* **2013**, *85* (11), 5288–5296.

REPLY TO PRINCE ET AL.:

Ability of chemical dispersants to reduce oil spill impacts remains unclear

Sara Kleindienst^{a,1}, Michael Seidel^{a,2}, Kai Ziervogel^b, Sharon Grim^{c,3}, Kathy Loftis^{a,4}, Sarah Harrison^a, Sairah Y. Malkin^a, Matthew J. Perkins^d, Jennifer Field^d, Mitchell L. Sogin^c, Thorsten Dittmar^{e,f}, Uta Passow^g, Patricia Medeiros^a, and Samantha B. Joye^{a,5}

Chemical dispersants are applied to oil-contaminated areas as a primary response to oceanic oil spills. The impacts of dispersants on microbial community composition and activity, particularly hydrocarbon turnover, are debated. Kleindienst et al. (1) demonstrated that Corexit 9500, a dispersant, can suppress the activity of oil-degrading microorganisms. Chemically enhanced water-accommodated fractions (CEWAFs) were used for these experiments because the deepwater plume that formed following the *Deepwater Horizon* (DWH) blowout consisted of the water-accommodated fraction: Roughly half of the discharged oil, along with dispersants applied at the wellhead, was entrained in the deepwater plume (2). Using CEWAFs assured an appropriate simulation of the DWH plume chemistry. Prince et al. (3) claim that the method used to produce CEWAFs would leave most of the added oil floating atop the surface in the bottles. Kleindienst et al. (1) followed standardized methods to produce CEWAFs, and only the dispersed oil fraction was used; no floating oil was present in the experiments (1).

The studies by Kleindienst et al. (1) and Prince et al. (4) revealed opposite effects of dispersants on oil biodegradation, but the results are not directly comparable. Prince et al. (4) used New Jersey shore near-surface seawater and Alaska North Slope crude, whereas Kleindienst et al. (1) used Gulf of Mexico deepwater and Macondo surrogate oil. Moreover, the two studies used a different procedure for oil and dispersant amendments. Kleindienst et al. (1) optimally simulated the physical and chemical conditions

of the DWH plume, whereas Prince et al. (4) added oil or dispersant or dispersed oil directly to samples, which were then mixed with a stir-bar over a 60-d incubation. Prince et al. (3) claimed comparing dispersed oil and a floating oil would be a better comparison. However, Kleindienst et al. (1) focused on deepwater oil dynamics, and because the deepwater plume contained only dissolved oil, the use of CEWAFs was essential. The results of Kleindienst et al. (1) are highly relevant to open ocean oil spill scenarios like the DWH, where dispersant was added directly to the discharging blown-out wellhead. Additionally, Kleindienst et al. (1) addressed the impacts of dispersants on microbial hydrocarbon turnover in surface water contaminated with oil from the sunken Taylor Energy oil platform. Those findings corroborated the deepwater microcosm results: Dispersants inhibited hydrocarbon turnover.

Prince et al. (3) stated that successful dispersant application would transfer all floating slick into the water column. In real-world scenarios, dispersant applications are not that efficient, as evidenced by the large amount of oil that remained on the surface during the DWH incident. Furthermore, chemically dispersed oil can still pollute coastlines and is more toxic to a variety of marine life forms than dispersed oil. Prince et al. (3) further claimed that dispersants exert only short-term impacts, but dispersants were still found in Gulf habitats ~4 y later (5). Because dispersants can slow microbial oil biodegradation and persist long term in the environment, challenges remain to fully understand their efficacy in a range of oil spill scenarios.

^aDepartment of Marine Sciences, University of Georgia, Athens, GA 30602; ^bDepartment of Marine Sciences, University of North Carolina at Chapel Hill, Chapel Hill, NC 27599; ^cJosephine Bay Paul Center, Marine Biological Laboratory, Woods Hole, MA 02543; ^dDepartment of Environmental and Molecular Toxicology, Oregon State University, Corvallis, OR 97331; ^eResearch Group for Marine Geochemistry, Institute for Chemistry and Biology of the Marine Environment (ICBM), Carl von Ossietzky University, 26129 Oldenburg, Germany; ^fMax Planck Institute for Marine Microbiology (MPI), 28359 Bremen, Germany; and ^gMarine Science Institute, University of California, Santa Barbara, CA 93106

Author contributions: S.K., M.S., K.Z., S.G., K.L., S.H., S.Y.M., M.J.P., J.F., M.L.S., T.D., U.P., P.M., and S.B.J. wrote the paper.

The authors declare no conflict of interest.

¹Present address: Center for Applied Geosciences, Eberhard Karls University Tuebingen, 72074 Tuebingen, Germany.

²Present address: Research Group for Marine Geochemistry, Institute for Chemistry and Biology of the Marine Environment (ICBM), Carl von Ossietzky University, 26129 Oldenburg, Germany.

³Present address: Department of Earth and Environmental Sciences, University of Michigan, Ann Arbor, MI 48109.

⁴Present address: Center for Applied Isotope Studies, University of Georgia, Athens, GA 30602.

⁵To whom correspondence should be addressed. Email: mjoye@uga.edu.

-
- 1 Kleindienst S, et al. (2015) Chemical dispersants can suppress the activity of natural oil-degrading microorganisms. *Proc Natl Acad Sci USA* 112(48):14900–14905.
 - 2 Joye SB (2015) Deepwater Horizon, 5 years on. *Science* 349(6248):592–593.
 - 3 Prince RC, Coolbaugh TS, Parkerton TF (2016) Oil dispersants do facilitate biodegradation of spilled oil. *Proc Natl Acad Sci USA* 113:E1421.
 - 4 Prince RC, et al. (2013) The primary biodegradation of dispersed crude oil in the sea. *Chemosphere* 90(2):521–526.
 - 5 White HK, et al. (2014) Long-term persistence of dispersants following the Deepwater Horizon oil spill. *Environ Sci Technol Lett* 1(7):295–299.

Molecular Fractionation of Dissolved Organic Matter in a Shallow Subterranean Estuary: The Role of the Iron Curtain

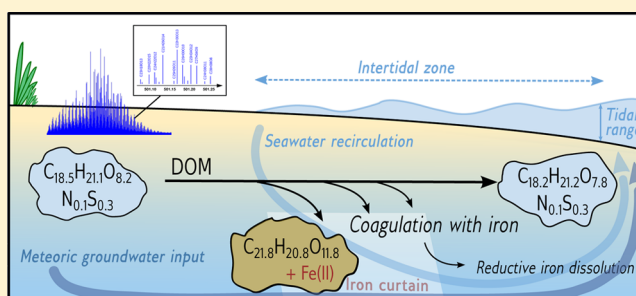
Annika Linkhorst,^{*,†,‡,§} Thorsten Dittmar,[‡] and Hannelore Waska^{*,‡}

[†]Institute of Biogeochemistry and Pollutant Dynamics, ETH Zurich, 8092 Zurich, Switzerland

[‡]Research Group for Marine Geochemistry (ICBM-MPI Bridging Group), Institute for Chemistry and Biology of the Marine Environment (ICBM), University of Oldenburg, 26129 Oldenburg, Germany

S Supporting Information

ABSTRACT: Iron that precipitates under aerobic conditions in natural aquatic systems scavenges dissolved organic matter (DOM) from solution. Subterranean estuaries (STEs) are of major importance for land–ocean biogeochemical fluxes. Their specific redox boundaries, coined the “iron curtain” due to the abundance of precipitated iron(III) (oxy)hydroxides, are hot spots for the removal and redissolution of iron, associated nutrients, and DOM. We used ultra-high-resolution electrospray ionization Fourier transform ion cyclotron resonance mass spectrometry to molecularly characterize the iron-coagulating fractions of 32 groundwater and seawater DOM samples along a salinity gradient from a shallow STE on Spiekeroog Island, North Sea, Germany, and linked our findings to trace metal and nutrient concentrations. We found systematic iron coagulation of large (>450 Da), oxygen-rich, and highly aromatic DOM molecules of terrestrial origin. The extent of coagulation increased with growing terrestrial influence along the salinity gradient. Our study is the first to show that the iron curtain may be capable of retaining terrigenous DOM fractions in marine sediments. We hypothesize that the iron curtain serves as an inorganic modulator for the supply of DOM from groundwaters to the sea, and that the STE has the potential to act as a temporal storage or even sink for terrigenous aromatic DOM compounds.



INTRODUCTION

Marine dissolved organic matter (DOM) is one of the largest active carbon pools on Earth and, thus, an important component of the global carbon cycle.¹ The Earth's continents are a major source of terrigenous DOM to the oceans, which is transported with other constituents such as iron (Fe) via riverine and submarine groundwater inputs. Groundwater-based fluxes, however, are not well constrained because before entering the coastal ocean, groundwater passes through a biogeochemically active environment, the subterranean estuary² (STE). While DOM has been found to coagulate with Fe(III) (oxy)hydroxides at redox boundaries in other environments, Fe–DOM coagulation processes in STEs have not yet been investigated, despite much already being known about Fe cycling in STEs.^{3–9} If Fe–DOM coagulation is prominent in STEs, which are characteristic of sandy shores that cover “up to two-thirds of the world's ice-free coastlines”,¹⁰ then such processes would be of global importance in terms of modulating the transport of terrigenous constituents from land to the ocean, with consequential implications on the global carbon cycle.

STEs are coastal aquifers where meteoric groundwater mixes with recirculating seawater. To date, no coherent database of the global coverage of STEs exists, but the occurrence of submarine groundwater discharge (SGD), the advective flux of terrestrial and marine groundwater into the ocean that

originates from the STE, has been reported worldwide.¹¹ It has been estimated that the annual discharge of freshwater via SGD amounts to ~2400 km³/year, with the majority of it passing through unconfined aquifers such as permeable beach sediments prior to entering the coastal ocean.¹¹ Because SGD can be highly enriched in nutrients, its constituent fluxes are estimated to be on the same order of magnitude as that of global surface runoffs, even though the freshwater volume flux amounts to only 6–10% as compared to rivers.¹² SGD is also a significant source of DOM to the coastal environment, as well as of Fe, a redox active trace metal and an important micronutrient for primary productivity in marine sediments.^{13–15}

In STEs, changes in redox potential are expected to serve as a main control for the removal or mobilization of Fe and other nutrients. Chambers and Odum¹⁶ first used the term iron curtain for an iron hydroxide precipitation zone on tidal freshwater marsh creekbanks, where reduced iron, Fe(II), from advectively discharged porewater was oxidized to Fe(III) upon coming into contact with the oxygenated surface waters of the tidal creeks and consequently scavenging dissolved phosphate.

Received: July 19, 2016

Revised: December 14, 2016

Accepted: December 15, 2016

Published: December 15, 2016

Later, Charette³ applied the expression to describe ferric hydroxide precipitates at redox interfaces within the STE. This iron curtain may vary spatially and temporally, depending on tidal amplitudes and long-term sea level changes, and acts as a barrier for chemical species such as phosphate and barium.^{3,5,6}

The iron curtain has mostly been investigated with regard to the retention of inorganic constituents from submarine groundwater; however, various studies have described oxidative Fe–DOM coagulation at different redox gradients. Riedel et al.,¹⁷ for instance, studied Fe–DOM coagulation in peat bog samples and found that highly aromatic, typically terrestrial DOM molecules are more likely to coagulate with iron than are aliphatic compounds typically found in aged marine DOM. Gomez-Saez et al.¹⁸ recently showed that iron from iron-rich hydrothermal vent fluids, as it coagulates with DOM, leads to a decrease in dissolved organic carbon (DOC) and changes in DOM molecular composition in the surrounding seawater. In addition to the molecular properties described by Riedel et al.¹⁷ and Gomez-Saez et al.,¹⁸ Lv et al.¹⁹ also reported an affinity of higher-molecular weight compounds (>500 Da) for coagulation with a variety of iron oxyhydroxides. They revealed that the extent of DOM coagulation was related to the type of iron substrate, with amorphous ferrihydrites scavenging more DOM than other iron oxyhydroxide minerals.

In their studies of the organic geochemistry of advective porewater systems of the German Wadden Sea, Seidel et al.^{20,21} recently postulated that Fe–DOM interactions had affected the observed molecular properties of DOM. However, to the best of our knowledge, no experimental data about the reactivity of DOM with iron within the STE exist, although STEs probably occur ubiquitously along coastal shorelines and may affect land–ocean fluxes of DOM and Fe on a global scale. In addition, dissolved Fe concentrations in the STE are often in the micromolar range,^{3,6,9,22} which are equal to or larger than normal DOC concentrations in STE porewaters,^{3,21} and DOM coagulation potentials of 50–80% can be achieved for Fe/DOM ratios between 0.8 and 1.2.²³ The iron curtain as a major biogeochemical barrier within the STE thus has the potential to modulate the global transport of terrigenous constituents from land to the ocean. Here, we hypothesize that the iron curtain affects the quality and quantity of advective porewater DOM fluxes from STEs into the coastal ocean by retaining specific molecular fractions of terrigenous DOM.

Fractionation of DOM can be investigated on a molecular level with new nontargeted analytical technologies, in particular ultra-high-resolution mass spectrometry using soft ionization [electrospray ionization Fourier transform ion cyclotron resonance mass spectrometry (ESI-FT-ICR-MS)]. Whereas traditional analytical methods target only small groups of compounds, ESI-FT-ICR-MS allows the identification of specific molecules on a broader scale.^{24,25} This method allowed researchers to determine molecular DOM fingerprints to track water masses,²⁴ follow the molecular succession of microbial remineralization,²⁶ and identify the molecular formulas of DOM subject to change under experimental conditions.^{17,27,28}

We studied coagulation of iron with DOM from a set of porewater samples from the northern beach of Spiekeroog Island, where an STE is formed by the terrestrial freshwater lens and the tidally recirculating seawater. We characterized both noncoagulating and coagulating fractions of DOM by molecular analysis with ESI-FT-ICR-MS.

■ EXPERIMENTAL SECTION

Overview. We collected porewater samples from three different sites along a transect perpendicular to the shoreline and one seawater sample as a reference. The stations were chosen to yield representative samples from the STE with varying amounts of fresh groundwater and recirculating seawater, and oxic to anoxic conditions. We performed precipitation experiments with samples that contained Fe²⁺ at micromolar concentrations, either naturally or through addition of an Fe²⁺ spike. We characterized the DOM molecular composition of all samples before and after their exposure to oxygen and subsequent precipitation of Fe(III) (oxy)-hydroxides, identifying both noncoagulating and coagulating DOM fractions. All samples were desalted via solid-phase extraction²⁹ prior to molecular analysis via ESI-FT-ICR-MS.

Study Site. Spiekeroog is one of the East Frisian Islands in the German North Sea and part of the UNESCO World Heritage area “Wadden Sea”. Peat and clay layers within the sand dunes confine its precipitation-fed fresh water lens at a depth of ~40 m.³⁰ Spiekeroog is exposed to a mesotidal regime (2–4 m tidal range). With its complex redox zonation, Spiekeroog has formerly proved to be a suitable sampling site for studies on the biogeochemistry of STEs.^{21,31–33} Previously, numerical models from Spiekeroog South Beach, a sheltered site facing the Wadden Sea, revealed that tidal pumping produced an upper saline plume (USP) with an ~100 m lateral extension and an ~20 m depth.²¹ Groundwater from the fresh water lens discharged near the low tide water line, forced to a narrow tube.²¹ The model data were backed up by in situ geochemical transects, which in addition indicated a complex redox zonation, for example, two Fe reduction zones associated with organic matter decomposition at the drift line as well as at the low tide water line (LWL).²¹ Transect data from a shallow subterranean estuary at Spiekeroog North Beach recently indicated the occurrence of a similar USP at this exposed beach site.²² Both studies from the north and south shores of Spiekeroog have described the STE as a biogeochemical reactor: They showed a succession of denitrification and iron and manganese reduction zones along the groundwater flow path from land to sea.^{21,22} Analogous to the south beach, a transition zone in the north beach STE with high Fe²⁺ concentrations was described near the LWL.²² The zone spanned a width of approximately 150–200 m and was bordered by sharply decreasing porewater Fe²⁺ concentrations, probably because of oxidation processes forming Fe(III) (oxy)hydroxide precipitates. A more detailed study of the north beach circulation system, including a numerical model, is currently in revision.³⁴ On the basis of these previous findings, samples were taken at the north beach site of the island, at 53°46′N, 07°43′E, in the vicinity of Umweltzentrum Wittbülten. Our sampling beach very likely represents the redox and iron gradients that are typical of many STEs worldwide.^{5,6,9}

Sampling. Samples were collected on December 10, 2013. Sites were selected on the basis of ref 22 and a preliminary study in November 2013 (see the [Supporting Information](#)), in which concentrations of nutrients and Fe²⁺³⁵ had been measured in porewaters over the range of the study site to define the Fe(II)/Fe(III) transition zone of the local STE. Sampling started at the LWL at low tide. Porewater (PW) samples were taken at three different sites along a transect perpendicular to the shoreline, with increasing distances from

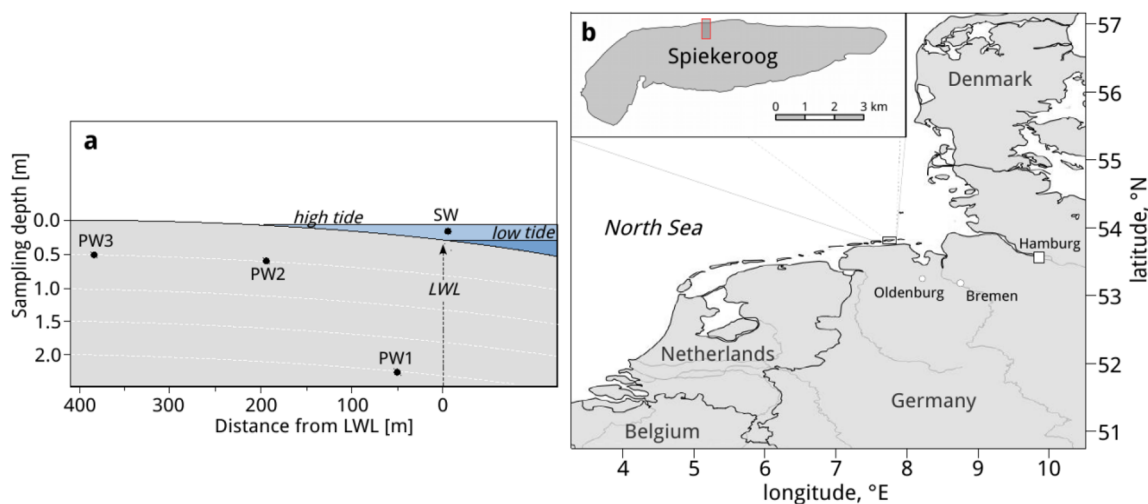


Figure 1. (a) Sampling scheme at 53°46'N, 07°43'E, where LWL is the low tide water line on the day of sampling. (b) Spiekeroog Island, with the sampling area as shown in panel a marked with a red box. PW denotes sites of porewater sampling and SW sites of seawater sampling.

the LWL toward the sand dunes (Figure 1): PW1–PW3, with distances from the LWL of 100, 250, and 450 m, respectively. PW1 and PW2 were located within the intertidal zone; PW1 was closest to the LWL and PW2 at the edge of the intertidal zone. PW3 was the most landward site and located outside the tidal zone, ~50 m from the beginning of the foredune belt colonized by marram grass. Two seawater samples (SW) were taken from the surf zone during high tide.

At each of the three beach sites, porewater was sampled at two spots less than 1 m apart. Viton tubes were attached to stainless steel push point samplers placed into the sediments at a depth of 0.5–2 m. At each spot prior to DOM sampling, small volumes of porewater were first sampled with a polyethylene syringe to determine salinity and Fe^{2+} concentrations. Salinity was measured with a standard Tetra-Con 925 Multi 3430 (WTW) conductivity measuring cell, and Fe^{2+} was detected by adding 1 mL of porewater to 1.5 mL clear safe-lock tubes (Eppendorf) containing 100 μL of a ferrozine solution.³⁵ Iron concentrations were then estimated in the field by visually comparing the emerging color from the ferrozine reaction with a color table. More precise Fe^{2+} determination was performed later in the laboratory (see below). Afterward, 2 L of porewater was taken from the selected spots by applying a gentle vacuum with a hand pump. The samples passed through an inline filter (a 3.0 μm Millipore Isopore polycarbonate membrane filter on top of a 0.2 μm Pall polyethersulfon membrane filter, both 47 mm in diameter) into acid-washed 2 L polycarbonate (PC) bottles (Nalgene). The bottles were fitted with vacuum caps and PC two-way valves and had been flushed and filled with Ar gas to a slight overpressure before sampling to prevent oxygen contamination and subsequent uncontrolled Fe(III) precipitation. The SW samples were also collected in acid-washed 2 L PC bottles but filtered approximately 2 h later back in the laboratory by vacuum as described above for PW1–PW3. After the first round of filtration, subsamples for DOC and trace metals were extracted from the PC bottles with acid-washed syringes attached to the vacuum valves. All subsamples were acidified with HCl (Merck, suprapur) to pH 2 and stored in acid-washed HDPE bottles at 4 °C in the dark. All PC bottles were soaked in 0.14 M nitric acid (HNO_3 p.a., Carl Roth, 1% in ultrapure water) and 0.01 M hydrochloric acid (suprapur) for 1 week each and rinsed repeatedly with ultrapure water prior to

use. All other nonglass material (filter membranes, filter holders, tubing, sampling bottle caps, etc.) were soaked in 0.14 M HNO_3 (p.a.) for several weeks and rinsed repeatedly with ultrapure water before being used. Samples for analyses of trace metals, DOC, and solid-phase extraction of DOM were acidified to a final concentration of 0.01 M HCl (suprapur).

Precipitation Experiments. Controls (one per site). To prevent any Fe in solution from precipitating, the filtered control samples in the PC bottles were acidified in situ to pH 2 with HCl. This is also the pH necessary for solid-phase extraction as described below.²⁹ The SW samples were filtered in the laboratory and thereafter split into two sets, with one of them being acidified to serve as a control and the other being prepared as a treatment sample as follows.

Treatment Samples (one per site). After all samples had been brought back to the laboratory, Fe^{2+} was roughly quantified in the ferrozine subsamples by visual comparison with an Fe^{2+} –ferrozine calibration series (5–100 μM) prepared prior to sampling. In the porewater closest to the LWL (PW1), natural Fe^{2+} was present as indicated by the in situ ferrozine test; in all other samples, no visible Fe(II)–ferrozine coloration was found. Fe^{2+} from an FeCl_2 (EMSURE, Merck) spike solution enriched with a suprapur hydroxylamine hydrochloride solution to prevent any Fe^{2+} from oxidizing ($\text{HONH}_2\cdot\text{HCl}$, Merck) was then added to all treatment samples of PW2, PW3, and SW in amounts approximating the concentrations of those estimated in PW1 (~80 μM). The hydroxylamine hydrochloride concentration was just high enough to keep the spike in solution. After a short exposure to atmospheric oxygen, the bottles were capped, shaken, and left standing for 24 h. The samples were then shaken again, and each of the treatment samples was filtered again (through an inline filter such as in the field), split into four acid-washed 2 L PC bottles, and acidified to pH 2 with suprapur HCl. These four replicates are hereafter termed filtrate samples. One filter served for the filtration of two replicates. After filtration, all filters were rinsed and desalted with ultrapure water and stored at 4 °C. The precipitates were later gently dissolved in 0.01 M HCl (pH 2) and are termed precipitate samples.

Analysis of DOC, Nutrient, Fe, and Mn. DOC concentrations were measured on a Shimadzu (TOC-VCPH and TNM-1) analyzer, using high-temperature catalytic

Table 1. Biogeochemical Characteristics of the Sampling Sites

site	latitude 07°43'	longitude 53°46'	depth (m)	Sal	DOC ^a (μM)	Fe ²⁺ ^b (μM)	Fe _{tot} ^c (μM)	Mn ^c (μM)	NH ₄ (μM)	NO _x (μM)	PO ₄ (μM)
SW			surf zone		193	nd ^d	0.09 ^e	0.04 ^e	12.1	15.3	0.3
				30.4	297	nd ^d	–	–			
					215	–	0.09 ^e	0.04 ^e	–	–	–
PW1			2		284	37.54	67.9	15.65	57.1	nd ^d	2.8
	41.3	57.6	2	29.7	132	80.44	–	–	17.9	nd ^d	3.3
					180	–	0.09 ^e	5.89	–	–	–
PW2			0.5		160	0.27	0.22	0.04 ^e	nd ^d	46.8	4.9
	37.4	53.2	0.5	24.0	182	nd ^d	–	–	1.4	47.4	21.1
					190	–	0.09 ^e	0.04 ^e	–	–	–
PW3			0.5		260	nd ^d	0.09 ^e	0.04 ^e	nd ^d	59.0	3.6
	33.6	47	0.5	9.0	235	nd ^d	–	–	nd ^d	27.2	4.6
					137	–	0.04 ^e	0.04 ^e	–	–	–

^aControl and pretreatment: after the first filtration, mean values of three injections. Post-treatment: after coagulation and the second filtration, mean values of duplicate samples, three injections each. ^bNatural reduced iron concentration according to the ferrozine test,³⁵ as measured at the sampling spot prior to taking the ESI-FT-ICR-MS samples. ^cTotal dissolved iron or manganese, as measured via ICP-MS directly from the ESI-FT-ICR-MS samples, after coagulation and filtration of the treatment samples. PW1 treatment samples were not measured via ICP-MS because of their high Fe and Mn concentrations; thus, ICP-OES results are given. ^dNot detected (below the detection limit). ^eAt the threshold of the detection limit.

oxidation, against a calibration series and a deep sea reference standard provided by D. Hansell (University of Miami, Miami, FL). The samples were measured via a low-volume hand-injection method.³⁶ Concentrations of nutrients [sum of nitrate and nitrite (NO_x), ammonium, and phosphate] and Fe²⁺ from ferrozine treatments of the porewater samples were measured by UV/vis microplate spectroscopy (Multiscan Spectrum, Thermo Scientific) at the ICBM Microbiogeochemistry Laboratory at the University of Oldenburg (Oldenburg, Germany). Nutrients were measured with a method modified from refs 37 and 38, and Fe²⁺ was measured according to ref 35. Total Fe and Mn were measured by inductively coupled plasma optical emission spectrometry (ICP-OES) (iCAP 6000, Thermo Scientific) coupled with an argon humidifier (T 2100 BR); resultant data were analyzed with iTEVA software. Calibration was performed with NIST traceable standard solutions and verified using SLEW-3 as reference material.³³

Solid-Phase Extraction. For ESI-FT-ICR-MS analysis, samples must be salt-free and concentrated to a carbon concentration of >10 mg L⁻¹. All samples were thus extracted via solid-phase extraction (SPE) according to the method described in ref 29; 1 g Varian Bond Elut PPL cartridges were used for extraction. Their solid phase is a modified styrene-divinylbenzene (SDBV) polymer that is capable of also retaining some polar analytes, including phenols.^{29,39} Prior to use, the cartridges were soaked with methanol (UPLC/MS grade, Biosolve BV) overnight and rinsed twice with ultrapure water, twice with methanol, and twice with 0.01 M HCl (suprapur). All samples were acidified to pH 2 with HCl prior to extraction to prevent Fe(III) precipitation outside of the control of the experimental setup and to increase the extraction efficiency for the organic acids and phenols that are present. After the samples had been passed over the SPE resin, the cartridges were rinsed with 100 mL of 0.01 M HCl and dried with Ar gas. The absorbed DOM samples on the cartridges were then immediately eluted with 6 mL of methanol into precombusted amber glass vials. The eluted extracts were stored in the dark at -18 °C. Prior to analysis by ESI-FT-ICR-MS, all extracts were diluted with ultrapure water and methanol to yield a 15 ppm solution in a 1/1 (v/v) methanol/water mixture. Extracts with lower DOC concentrations, such as the precipitate samples, were concentrated by evaporation and

redissolved with a 1/1 methanol/water mixture. Extraction efficiencies were calculated after determining DOC concentrations in both the original water samples and the extracts (after complete evaporation of the methanol and redissolution in ultrapure water) and were 43 ± 7% for all filtrate and control samples and 47 ± 12% for all precipitate samples.

Molecular Analysis. Samples were measured on a Bruker Solarix ESI-FT-ICR-MS instrument (Bruker Daltonik GmbH, Bremen, Germany), equipped with a 15 T magnet system. All samples were analyzed in negative electrospray ionization (ESI, Bruker Apollo II) mode. All instrument settings and data processing approaches, including molecular formula assignments, are described in detail in ref 21. All filtrate and control samples were measured over the course of 2 days in randomly mixed order. To test the reproducibility and stability of the ESI-FT-ICR-MS analysis, a DOM extract of North Equatorial Pacific Intermediate Water (NEQPIW) was used as a reference sample. This sample is an in-house reference material for aged, marine DOM.⁴⁰ On the basis of the suggestions made by Stenson et al.⁴¹ and Koch et al.,⁴² we used an element setting of ¹²C₁₋₁₃₀¹H₁₋₂₀₀¹⁶O₁₋₅₀¹⁴N₁₋₅₀⁰¹⁴N₀₋₄³²S₀₋₂ for molecular formula assignments. The double bond equivalence (DBE) was determined using the method described by Stenson et al.,⁴¹ and the aromaticity index was determined in its modified version using the method described by Koch and Dittmar.^{43,44} (Almod).

Statistics. After molecular formulas were assigned, data were further statistically analyzed by using the software package “R” (version 3.1.1, 2014-04-10). To test for differences in molecular composition between filtrate and control samples, a Mann–Whitney-U test ($\alpha = 0.05$) was applied, the non-parametric version of the *t* test for the determination of significant differences between two data sets with non-normally distributed residuals. The molecular formulas driving those differences were then further investigated. The precipitate samples were not included in the statistical analyses described above but were finally used to compare the presence and absence of molecular formulas between filtrate and precipitate fractions.

Table 2. Molecular Characterization of the DOM Samples As Determined by ESI-FT-ICR-MS^a

	control	treatment (present in filtrate) ^b	treatment (absent from filtrate) ^b	treatment (present in precipitate) ^c	NEqPIW ^d
total no. of molecules	2066	1829	217	114	1378
mean mass (Da)	380	395	470	409	406
average formula	C _{18.5} H _{21.1} O _{8.2} N _{0.1} S _{0.3}	C _{18.2} H _{21.2} O _{7.8} N _{0.1} S _{0.3}	C _{21.8} H _{20.8} O _{11.8} N _{0.0} S _{0.0}	C _{19.5} H _{17.5} O _{9.9} N _{0.0} S _{0.0}	C _{19.9} H _{24.0} O _{8.8} N _{0.0} S _{0.3}
average H/C atom ratio	1.1	1.2	0.9	0.9	1.2
average O/C atom ratio	0.4	0.4	0.5	0.5	0.4
average Almod ^e	0.4	0.4	0.4	0.5	0.3
average DBE ^f	9.1	8.8	12.4	11.7	9.0
percentage of combustion-derived polycyclic aromates (PCAs) (Almod > 0.66)	10.0	10.1	9.7	12.4	3.1
PCAs smaller than C ₁₅	7.0	7.4	3.7	7.0	2.4
PCAs larger than or equal to C ₁₅	3.0	2.6	6.0	5.3	0.7
PCAs rich in O (O/C > 0.5)	0.8	1.0	0.5	0.9	0.0
PCAs poor in O (O/C ≤ 0.5)	9.1	9.1	9.2	11.5	3.1
percentage of polyphenols (0.66 ≥ Almod > 0.5)	19.2	17.5	30.9	38.0	14.3
polyphenols rich in O (O/C > 0.5)	4.6	3.9	11.5	9.7	1.4
polyphenols poor in O (O/C ≤ 0.5)	14.6	13.7	19.4	28.3	12.9
percentage of highly unsaturated molecules (HU)	59.7	60.0	59.4	49.6	72.8
HU rich in O (O/C > 0.5)	24.4	21.9	48.8	37.2	28.0
HU poor in O (O/C ≤ 0.5)	35.3	38.1	10.6	12.4	44.8

^aMolecular classifications are from the work of Koch and Dittmar,^{43,44} Šantl Temkiv et al.,⁴⁵ and Seidel et al.²⁰ ^bAs obtained from Mann–Whitney–U statistics. ^cMissing molecules from the filtrate that were also found in the precipitate. ^dDOM extract of North Equatorial Pacific Intermediate Water, an in-house reference material for aged, marine DOM; here given as present in at least five of eight NEqPIW standard measurements. ^eAromaticity index in its modified version according to Koch and Dittmar.^{43,44} ^fDouble bond equivalence according to Stenson et al.⁴¹

RESULTS

General Biogeochemical Characteristics of the STE.

The studied system was highly heterogeneous (Table 1). Nutrient and DOC concentrations varied substantially within only 1 m sampling distance for control and treatment samples from the same station. In particular, DOC displayed no specific trend, as it varied more between close locations at a given station than between stations. In some of the experiments (PW1 and PW2), bulk DOC concentrations were higher after than before the precipitation treatments. We excluded these DOC data from further consideration because of the risk of contamination with volatile organics. The other porewater constituents showed a clear trend among sites. For example, the more landward PW2 and PW3 stations were enriched with NO_x, whereas station PW1 was clearly located in an iron reduction zone, with NH₄ being the dominant form of dissolved inorganic nitrogen. Total dissolved Fe was completely removed from the filtrate samples after the second filtration step, while we found precipitated Fe(III) (oxy)hydroxides in the precipitate samples. Thus, we investigated the molecular composition of solid-phase-extracted DOM in the Fe(III) (oxy)hydroxide precipitates, as well as in the filtered permeate, to track experimentally induced changes not evident in bulk DOC data.

Molecular Characteristics of DOM. We identified 2066 molecular formulas, representing 34% of all 6015 molecular masses detected by ESI-FT-ICR-MS. Unassigned masses are isotopologues of assigned molecular formulas or contain combinations of elements not considered in this study. By Mann–Whitney–U testing on all 6015 masses, we found that 423 compounds were responsible for significant differences between filtrate and control samples ($p < 0.05$); 267 of these 423 compounds were missing or had significantly lower

intensities in the mass spectra of the filtrate samples, suggesting that they coagulated with iron and were filtered out from the filtrate samples. To 217 of these 267 detected masses (4% of all 6015 compounds and 11% of all 2066 molecularly described compounds) we were able to assign molecular formulas. In the precipitate, 114 of these 217 missing compounds in the filtrate could be detected (2% of all 6015 compounds and 6% of all 2066 molecularly described compounds). It should be noted that we were not able to fully redissolve the precipitate from the filter holders by the acidification processing step.

We identified C_{18.5}H_{21.1}O_{8.2}N_{0.1}S_{0.3} as the average formula for all molecules present in the control samples and C_{21.8}H_{20.8}O_{11.8}N_{0.0}S_{0.0} for all molecules that were missing in the filtrate residual solution of the treatment, indicating that they had been removed during precipitation. C_{18.2}H_{21.2}O_{7.8}N_{0.1}S_{0.3} is the average formula for all compounds that remained in the residual filtrate after coagulation. The reference deep sea standard, NEqPIW, in comparison, had a molecular formula of C_{19.9}H_{24.0}O_{8.8}N_{0.0}S_{0.3} (Table 2).

Molecular Categories. We found that iron coagulation specifically affected large molecules with a relatively high oxygen content. The mean mass and oxygen content of the molecules that were removed from the filtrate samples (470 Da, 12 O) were substantially higher than the mean mass of all described molecules as found in the control samples (380 Da, 8 O) and the residual filtrate (395 Da, 8 O). DBE was much higher for the coagulated molecules (12) than for molecules in the control samples and the residual filtrate (both 9), suggesting a preferential coagulation of molecules with a higher content of unsaturated fractions. As another indicator for rather unsaturated, oxygenated molecules undergoing coagulation, coagulated molecules tended to have a relatively high O/C and low H/C ratio (0.5 and 0.9, respectively) as compared to all

identified molecules in the controls (0.4 and 1.1, respectively) and residual filtrates (0.4 and 1.2, respectively) (Figure 2).

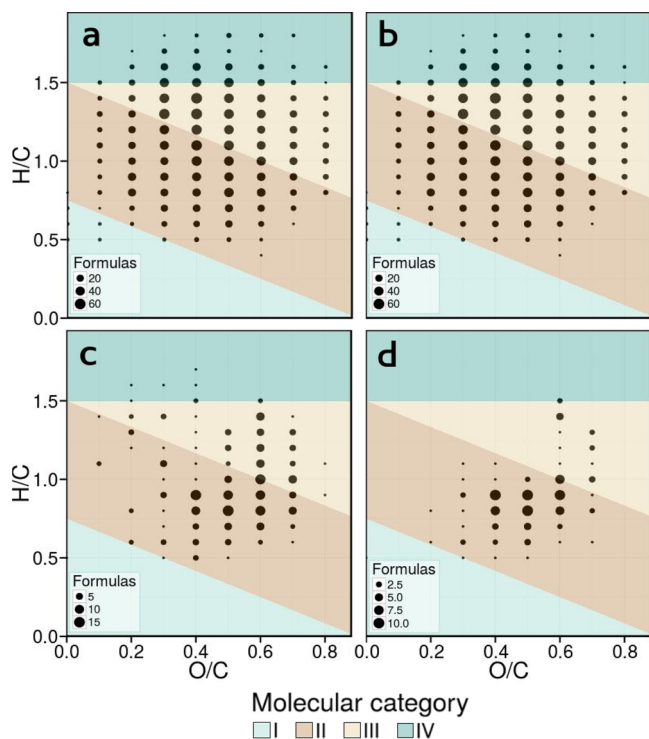


Figure 2. Abundance frequency plots of molecular formulas in categories of O/C and H/C element ratios (Van Krevelen diagrams), showing the distribution of all detected molecular formulas in the respective sample: (a) present in all controls, (b) retained in the filtrates, (c) with relative intensities in the filtrate samples statistically significantly lower than those in the control samples, i.e., thought to have coagulated with iron, and (d) the coagulating molecules from panel c that were also detected in the precipitate samples. All four diagrams include all sampling sites. The color code in the background shows the different molecular categories according to Šantl Temkiv et al.:⁴⁵ (I) combustion-derived polycyclic aromates (PCAs), (II) soil-derived polyphenols and PCAs with aliphatic chains, (III) soil-derived “humics” (i.e., phenolic and highly unsaturated compounds), and (IV) unsaturated aliphatic compounds.

DISCUSSION

Molecular Selectivity of Coagulation. Our findings of preferential coagulation of large, oxidized, aromatic molecules with a high content of unsaturated fractions are in general agreement with previous reports from a variety of different environmental and experimental setups.^{17–19} Contrary to Gomez-Saez et al.,¹⁸ who, in a similar experiment in a hydrothermal vent system, found a selective enrichment of sulfuric groups in their iron-DOM coagulate precipitate samples, we did not find preferential coagulation of nitric or sulfuric DOM; they were also not found missing in the filtrate or present in the precipitate samples. It should be noted though that Gomez-Saez et al.¹⁸ worked with samples naturally much higher in organic sulfur, and many terrigenous DOM fractions may have already been removed as they worked with seawater samples, which potentially leaves less competition for Fe oxide surfaces from remaining other (marine) organic matter fractions. We found no general preferential coagulation of molecules classified as combustion-derived (“black carbon”) or

highly saturated compounds, but it was the large, oxidized fraction within these compound groups that coagulated. In general, compounds that are characteristic of terrigenous DOM (categories II and III in Figure 2) preferentially coagulated. No evidence of the precipitation of compounds that share molecular formulas with sugars, peptides, or aliphatic molecules was found.

Like any analytical technique, SPE combined with FT-ICR-MS has its analytical window. Even though the analytical window of this combination of techniques is unsurpassed for molecular DOM analysis, not all compounds are detectable. In a study by Hawkes et al.,³⁹ experimental modifications of DOM moved a molecularly defined fraction out of the analytical window, which was clear evidence of substantial molecular modifications. We do not rule out this possibility in our study. Several past studies (e.g., Seidel et al.⁴⁶) have, however, shown that our approach is not selective toward marine or terrigenous (polyphenolic) compounds. Our extraction efficiencies are at the lower reported end for PPL-SPE but are still within the range of similar samples. Most importantly, there was no systematic difference between types of samples.

Land–Ocean Trends and STE Heterogeneity. Our findings for DOM fractions prone to coagulation with iron are consistent with previous descriptions from peat-bog samples by Riedel et al.¹⁷ We additionally show that these processes of preferential coagulation of terrigenous DOM work in terrestrial and marine environments. On the basis of our experimental setup, we were able to estimate the “coagulation potential” of all studied porewater samples at each sampling site. We achieved this by calculating the cumulative difference of relative molecular abundances between control and filtrate samples for each site. To present our data, we describe three molecular categories that coagulated most with iron: group II and III according to Šantl Temkiv et al.⁴⁵ and all molecules with an O/C ratio of >0.35 and a H/C ratio of <1.0 (Figures 2 and 3). Overall, the extent of coagulation decreased along the studied transect from land to sea (Figure 3). We suggest that, as DOM from terrestrial sources is transported through the STE, fractions more prone to iron coagulation (such as polyphenols, PCAs with aliphatic chains, and phenolic and highly unsaturated compounds) precipitate with iron, so that the extent of coagulation overall decreases with increasing distance from land to sea.

STEs are highly heterogeneous systems, and the observed land–ocean trends in the extent of coagulation contribute in a systematic way to the apparent heterogeneity of the STE. Compositional differences in DOM from the various groundwater end members may have contributed to the observed trend. Further, the retention of metal-sensitive DOM fractions in the STE is intrinsically linked to sediment redox chemistry, which is not directly dependent on salinity. For example, Seidel et al.²¹ found highly aromatic, terrigenous DOM in an intertidal porewater seepage zone on the southern shore of Spiekeroog, downstream of several iron oxidation–reduction zones in the STE. They suggested on the basis of their findings that Fe-DOM coagulation in the STE is a reversible process. Similarly, concomitant dissolution of Fe and DOC under anoxic conditions and fast subsequent flocculation after the re-establishment of oxic conditions were reported from incubation studies with boreal lake sediments.⁴⁷ Therefore, movements of the freshwater–saltwater boundary over tidal, seasonal, or even geological time scales, which influence advective flow rates and the supply of organic matter for microbial processes in the

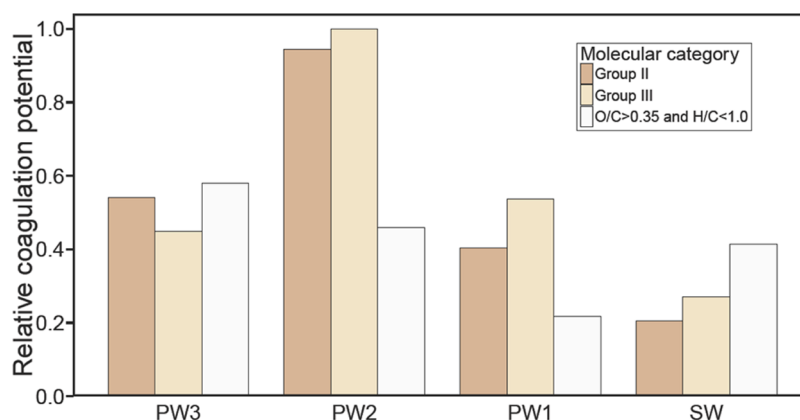


Figure 3. Relative coagulation potential for the four different sampling sites, from the dunes (PW3) to the sea (SW). Dark brown bars show data for group II, soil-derived polyphenols and PCAs with aliphatic chains. Light brown bars show data for group III, soil-derived “humics”, i.e., polyphenolic and highly unsaturated compounds, both as according to Šantl Temkiv et al.⁴⁵ Light gray bars show data for samples with an O/C of >0.35 and a H/C of <1.0, i.e., large unsaturated molecules with a high oxygen content. The coagulation potential is calculated as the cumulative difference in relative molecular abundances (ESI-FT-ICR-MS signal intensities) between control and filtrate samples per sampling site, each shown relative to the highest potential found (i.e., PW2 group III).

STE,^{8,48} will also impact the dynamics of the iron curtain. For example, microbial reduction of iron, triggered by the supply of fresh, labile marine DOM from a spring bloom, could trigger the release of older, more aromatic DOM of meteoric origin into the coastal water column. We therefore hypothesize that the STE has the potential to act as intermediate storage,¹⁷ rather than only as a net sink, for terrigenous aromatic DOM compounds.

Implications. In this study, we showed that Fe–DOM coagulation, a process previously studied on the molecular level only in terrestrial and hydrothermal vent systems, occurs at coastal beach sites, potentially on a global scale. We found preferential coagulation of Fe with DOM of a molecular composition typical for soil-derived DOM, such as highly oxidized polyphenols.

The discovery of Fe–DOM coagulation in STEs potentially has major implications as STEs occur globally, and DOM is an essential component of the global carbon cycle. Our study supports the hypothesis of the iron curtain selectively modulating the advective groundwater fluxes of organic carbon from land to sea. Whereas ESI-FT-ICR-MS allows for detailed qualitative molecular analyses, the quantitative relevance of iron–DOM coagulation in STEs should be further investigated by additional techniques; for example, terrestrial marker compounds can be used for quantification with liquid chromatography, or the sediments can be leached to quantify the attached DOM.

As we do not know the time scale on which coagulated DOM is buried in coastal and shelf sediments, we cannot determine if STEs act as a temporal storage or an effective long-term sink for terrigenous DOM. In this study, we investigated a shallow STE. Deep STEs might have different dynamics such as longer residence times, which may influence the forms of DOM that can potentially coagulate and the ultimate fate of sedimentary bound DOM. The role of iron in the preservation of organic matter in sediments is well-known.⁴⁹ Our study indicates that terrigenous DOM may also be trapped and preserved in the “rusty carbon sink”⁵⁰ on its subterranean way from land to ocean. Many open questions about the global relevance of this process and the relevant time scales involved for burial and potential remobilization remain and should be the focus of future studies.

■ ASSOCIATED CONTENT

📄 Supporting Information

The Supporting Information is available free of charge on the ACS Publications website at DOI: 10.1021/acs.est.6b03608.

Data from a preliminary study to define the sampling site (PDF)

■ AUTHOR INFORMATION

Corresponding Authors

*Phone: +46 18 471 6568. E-mail: liannika@alumni.ethz.ch.

*Phone: +49 441 798 3348. E-mail: hannelore.waska@uni-oldenburg.de.

ORCID

Annika Linkhorst: 0000-0002-3609-5107

Present Address

§A.L.: Department of Ecology and Genetics/Limnology, Uppsala University, 75236 Uppsala, Sweden.

Notes

The authors declare no competing financial interest.

■ ACKNOWLEDGMENTS

We thank Anja Reckhardt, Matthias Friebe, and Kevin Obermann for valuable field assistance, Katrin Klaproth, Matthias Friebe, Eleonore Gründken, and Ina Ulber for technical laboratory assistance, and Heike Simon for hand injection of the DOC samples. We are grateful to the associate editor and three anonymous reviewers for their constructive comments that significantly improved the manuscript. We gratefully acknowledge funding by the Deutsche Forschungsgemeinschaft (DFG, Eigene Stelle for H.W., WA3067/1-2) and an Erasmus student placement scholarship as provided to A.L. by ETH Zurich. A.L. acknowledges additional funding from the European Research Council under the European Union’s Seventh Framework Programme (FP7/2007-2013)/ERC Grant Agreement n° 336642. We further thank Umweltzentrum Wittbülten on Spiekeroog Island and the microbiogeochemistry group at ICBM Oldenburg for providing their facilities.

REFERENCES

- (1) Ridgwell, A.; Arndt, S. Why Dissolved Organics Matter: DOC in Ancient Oceans and Past Climate Change. In *Biogeochemistry of Marine Dissolved Organic Matter*, 2nd ed.; Hansell, D. A., Carlson, C. A., Eds.; Academic Press: New York, 2015; pp 1–20.
- (2) Moore, W. S. The subterranean estuary: a reaction zone of ground water and sea water. *Mar. Chem.* **1999**, *65* (1–2), 111–125.
- (3) Charette, M. A.; Sholkovitz, E. R. Oxidative precipitation of groundwater-derived ferrous iron in the subterranean estuary of a coastal bay. *Geophys. Res. Lett.* **2002**, *29* (10), 851–854.
- (4) Charette, M. A.; Sholkovitz, E. R.; Hansel, C. M. Trace element cycling in a subterranean estuary: Part 1. Geochemistry of the permeable sediments. *Geochim. Cosmochim. Acta* **2005**, *69* (8), 2095–2109.
- (5) Charette, M. A.; Sholkovitz, E. R. Trace element cycling in a subterranean estuary: Part 2. Geochemistry of the porewater. *Geochim. Cosmochim. Acta* **2006**, *70*, 811–826.
- (6) Roy, M.; Martin, J. B.; Cherrier, J.; Cable, J. E.; Smith, C. G. Influence of sea level rise on iron diagenesis in an east Florida subterranean estuary. *Geochim. Cosmochim. Acta* **2010**, *74*, 5560–5573.
- (7) Roy, M.; Martin, J. B.; Smith, C. G.; Cable, J. E. Reactive-transport modeling of iron diagenesis and associated organic carbon remineralization in a Florida (USA) subterranean estuary. *Earth Planet. Sci. Lett.* **2011**, *304* (1–2), 191–201.
- (8) Roy, M.; Martin, J. B.; Cable, J. E.; Smith, C. G. Variations of iron flux and organic carbon remineralization in a subterranean estuary caused by inter-annual variations in recharge. *Geochim. Cosmochim. Acta* **2013**, *103*, 301–315.
- (9) Snyder, M.; Taillefer, M.; Ruppel, C. Redox zonation at the saline-influenced boundaries of a permeable surficial aquifer: Effects of physical forcing on the biogeochemical cycling of iron and manganese. *J. Hydrol.* **2004**, *296*, 164–178.
- (10) McLachlan, A.; Brown, A. C. *The ecology of sandy shores*; Academic Press: Burlington, MA, 2006.
- (11) Zhang, J.; Mandal, A. K. Linkages between submarine groundwater systems and the environment. *Curr. Opin. Env. Sust.* **2012**, *4* (2), 219–226.
- (12) Burnett, W. C.; Bokuniewicz, H.; Huettel, M.; Moore, W. S.; Taniguchi, M. Groundwater and pore water inputs to the coastal zone. *Biogeochemistry* **2003**, *66*, 3–33.
- (13) Windom, H. L.; Moore, W. S.; Niencheski, L. F. H.; Jahnke, R. A. Submarine groundwater discharge: A large, previously unrecognized source of dissolved organic iron to the South Atlantic Ocean. *Mar. Chem.* **2006**, *102* (3–4), 252–266.
- (14) Rouxel, O.; Sholkovitz, E.; Charette, M. A.; Edwards, K. J. Iron isotope fractionation in subterranean estuaries. *Geochim. Cosmochim. Acta* **2008**, *72* (14), 3413–3430.
- (15) Kim, T. H.; Waska, H.; Kwon, E.; Suryaputra, I. G. N.; Kim, G. Production, degradation, and flux of dissolved organic matter in the subterranean estuary of a large tidal flat. *Mar. Chem.* **2012**, *142–144*, 1–10.
- (16) Chambers, R. M.; Odum, W. E. Porewater oxidation, dissolved phosphate and the iron curtain. Iron-phosphorus relations in tidal freshwater marshes. *Biogeochemistry* **1990**, *10* (1), 37–52.
- (17) Riedel, T.; Biester, H.; Dittmar, T. Molecular fractionation of dissolved organic matter with metal salts. *Environ. Sci. Technol.* **2012**, *46* (8), 4419–26.
- (18) Gomez-Saez, G. V.; Riedel, T.; Niggemann, J.; Pichler, T.; Dittmar, T.; Bühring, S. I. Interaction between iron and dissolved organic matter in a marine shallow hydrothermal system off Dominica Island (Lesser Antilles). *Mar. Chem.* **2015**, *177*, 677–686.
- (19) Lv, J.; Zhang, S.; Wang, S.; Luo, L.; Cao, D.; Christie, P. Molecular-Scale Investigation with ESI-FT-ICR-MS on Fractionation of Dissolved Organic Matter Induced by Adsorption on Iron Oxyhydroxides. *Environ. Sci. Technol.* **2016**, *50*, 2328–2336.
- (20) Seidel, M.; Beck, M.; Riedel, T.; Waska, H.; Suryaputra, I. G. N. A.; Schnetger, B.; Niggemann, J.; Simon, M.; Dittmar, T. Biogeochemistry of dissolved organic matter in an anoxic creek bank. *Geochim. Cosmochim. Acta* **2014**, *140*, 418–434.
- (21) Seidel, M.; Beck, M.; Greskowiak, J.; Riedel, T.; Waska, H.; Suryaputra, I. G. N. A.; Schnetger, B.; Niggemann, J.; Simon, M.; Dittmar, T. Benthic-pelagic coupling of nutrients and dissolved organic matter composition in an intertidal sandy beach. *Mar. Chem.* **2015**, *176*, 150–163.
- (22) Reckhardt, A.; Beck, M.; Seidel, M.; Riedel, T.; Wehrmann, A.; Bartholomä, A.; Schnetger, B.; Dittmar, T.; Brumsack, H.-J. Carbon, nutrient and trace metal cycling in sandy sediments: A comparison of high-energy beaches and backbarrier tidal flats. *Estuarine, Coastal Shelf Sci.* **2015**, *159*, 1–14.
- (23) Nierop, K. G. J.; Jansen, B.; Verstraten, J. M. Dissolved organic matter, aluminium, and iron interactions: precipitation induced by metal/carbon ratio, pH and competition. *Sci. Total Environ.* **2002**, *300*, 201–211.
- (24) Koch, B. P.; Witt, M.; Engbrodt, R.; Dittmar, T.; Kattner, G. Molecular formulae of marine and terrigenous dissolved organic matter detected by electrospray ionization Fourier transform ion cyclotron resonance mass spectrometry. *Geochim. Cosmochim. Acta* **2005**, *69* (13), 3299–3308.
- (25) Sosa, O. A.; Gifford, S. M.; Repeta, D. J.; DeLong, E. F. High molecular weight dissolved organic matter enrichment selects for methylotrophs in dilution to extinction cultures. *ISME J.* **2015**, *9*, 2725–2739.
- (26) Osterholz, H.; Niggemann, J.; Giebel, H.-A.; Simon, M.; Dittmar, T. Inefficient microbial production of refractory dissolved organic matter in the ocean. *Nat. Commun.* **2015**, *6*, 7422.
- (27) Stubbins, A.; Spencer, R. G. M.; Chen, H.; Hatcher, P. G.; Mopper, K.; Hernes, P. J.; Mwamba, V. L.; Mangangu, A. M.; Wabakanghanzi, J. N.; Six, J. Illuminated darkness: Molecular signatures of Congo River dissolved organic matter and its photochemical alteration as revealed by ultrahigh precision mass spectrometry. *Limnol. Oceanogr.* **2010**, *55* (4), 1467–1477.
- (28) Zark, M.; Riebesell, U.; Dittmar, T. Effects of ocean acidification on marine dissolved organic matter are not detectable over the succession of phytoplankton blooms. *Sci. Adv.* **2015**, *1* (9), e1500531.
- (29) Dittmar, T.; Koch, B.; Hertkorn, N.; Kattner, G. A simple and efficient method for the solid-phase extraction of dissolved organic matter (SPE-DOM) from seawater. *Limnol. Oceanogr.: Methods* **2008**, *6*, 230–235.
- (30) Röper, T.; Kröger, K. F.; Meyer, H.; Stülfenuss, J.; Greskowiak, J.; Massmann, G. Groundwater ages, recharge conditions, and hydrochemical evolution of a barrier island freshwater lens (Spiekeroog, Northern Germany). *J. Hydrol.* **2012**, *454–455*, 173–186.
- (31) Al-Raei, A. M.; Bosselmann, K.; Böttcher, M. E.; Hespeneheide, B.; Tauber, F. Seasonal dynamics of microbial sulfate reduction in temperate intertidal surface sediments: controls by temperature and organic matter. *Ocean Dynam.* **2009**, *59* (2), 351–370.
- (32) Beck, M.; Brumsack, H.-J. Biogeochemical cycles in sediment and water column of the Wadden Sea: The example Spiekeroog Island in a regional context. *Ocean Coast. Manage.* **2012**, *68*, 102–113.
- (33) Beck, M.; Dellwig, O.; Fischer, S.; Schnetger, B.; Brumsack, H.-J. Trace metal geochemistry of organic carbon-rich watercourses draining the NW German coast. *Estuarine, Coastal Shelf Sci.* **2012**, *104–105*, 66–79.
- (34) Beck, M.; Reckhardt, A.; Amelsberg, J.; Bartholomä, A.; Brumsack, H.-J.; Cypionka, H.; Dittmar, T.; Engelen, B.; Greskowiak, J.; Hillebrand, H.; Holtappels, M.; Neuholz, R.; Köster, J.; Kuypers, M. M. M.; Massmann, G.; Meier, D.; Niggemann, J.; Paffrath, R.; Pahnke, K.; Rovo, S.; Striebel, M.; Vandieken, V.; Wehrmann, A.; Zielinski, O. The drivers of biogeochemistry in beach ecosystems: A cross-shore transect from the dunes to the low water line. Submitted to *Marine Chemistry*, 2016.
- (35) Viollier, E.; Inglett, P. W.; Hunter, K.; Roychoudhury, A. N.; Van Cappellen, P. The ferrozine method revisited: Fe(II)/Fe(III) determination in natural waters. *Appl. Geochem.* **2000**, *15*, 785–790.
- (36) Stubbins, A.; Dittmar, T. Low volume quantification of dissolved organic carbon and dissolved nitrogen. *Limnol. Oceanogr.: Methods* **2012**, *10*, 347–352.

(37) Schnetger, B.; Lehnert, C. Determination of nitrate plus nitrite in small volume marine water samples using vanadium(III)chloride as a reduction agent. *Mar. Chem.* **2014**, *160*, 91–98.

(38) Grasshoff, K.; Kremling, K.; Ehrhardt, M. *Methods of seawater analysis*; Wiley-VCH: Weinheim, Germany, 1990.

(39) Hawkes, J. A.; Hansen, C. T.; Goldhammer, T.; Bach, W.; Dittmar, T. Molecular alteration of marine dissolved organic matter under experimental hydrothermal conditions. *Geochim. Cosmochim. Acta* **2016**, *175*, 68–85.

(40) Green, N. W.; Perdue, E. M.; Aiken, G. R.; Butler, K. D.; Chen, H.; Dittmar, T.; Niggemann, J.; Stubbins, A. An intercomparison of three methods for the large-scale isolation of oceanic dissolved organic matter. *Mar. Chem.* **2014**, *161*, 14–19.

(41) Stenson, A. C.; Marshall, A. G.; Cooper, W. T. Exact Masses and Chemical Formulas of Individual Suwannee River Fulvic Acids from Ultrahigh Resolution Electrospray Ionization Fourier Transform Ion Cyclotron Resonance Mass Spectra. *Anal. Chem.* **2003**, *75* (6), 1275–1284.

(42) Koch, B. P.; Dittmar, T.; Witt, M.; Kattner, G. Fundamentals of molecular formula assignment to ultrahigh resolution mass data of natural organic matter. *Anal. Chem.* **2007**, *79* (4), 1758–63.

(43) Koch, B. P.; Dittmar, T. From mass to structure: an aromaticity index for high-resolution mass data of natural organic matter. *Rapid Commun. Mass Spectrom.* **2006**, *20* (5), 926–932.

(44) Koch, B. P.; Dittmar, T. Corrigendum: From mass to structure: an aromaticity index for high-resolution mass data of natural organic matter. *Rapid Commun. Mass Spectrom.* **2016**, *30* (1), 250.

(45) Šantl Temkiv, T.; Finster, K.; Dittmar, T.; Hansen, B. M.; Thyraug, R.; Nielsen, N. W.; Karlson, U. G. Hailstones: a window into the microbial and chemical inventory of a storm cloud. *PLoS One* **2013**, *8* (1), e53550.

(46) Seidel, M.; Yager, P. L.; Ward, N. D.; Carpenter, E. J.; Gomes, H. R.; Krusche, A. V.; Richey, J. E.; Dittmar, T.; Medeiros, P. M. Molecular-level changes of dissolved organic matter along the Amazon River-to-ocean continuum. *Mar. Chem.* **2015**, *177*, 218–231.

(47) Peter, S.; Isidorova, A.; Sobek, S. Enhanced carbon loss from anoxic lake sediment through diffusion of dissolved organic carbon. *J. Geophys. Res.: Biogeosci.* **2016**, *121* (7), 1959–1977.

(48) Michael, H. A.; Mulligan, A. E.; Harvey, C. F. Seasonal oscillations in water exchange between aquifers and the coastal ocean. *Nature* **2005**, *436*, 1145–1148.

(49) Lalonde, K.; Mucci, A.; Ouellet, A.; Gélinas, Y. Preservation of organic matter in sediments promoted by iron. *Nature* **2012**, *483*, 198–200.

(50) Eglinton, T. I. Geochemistry: A rusty carbon sink. *Nature* **2012**, *483*, 165–166.



Short-Term Dynamics of North Sea Bacterioplankton-Dissolved Organic Matter Coherence on Molecular Level

Judith Lucas^{1*†}, Irina Koester^{2†}, Antje Wichels¹, Jutta Niggemann², Thorsten Dittmar², Ulrich Callies³, Karen H. Wiltshire^{1,4} and Gunnar Gerds¹

¹ Biological Station Helgoland, Shelf Sea Systems Ecology, Alfred-Wegener-Institute Helmholtz-Center for Polar and Marine Research, Helgoland, Germany, ² Research Group for Marine Geochemistry (ICBM-MPI Bridging Group), Institute for Chemistry and Biology of the Marine Environment, Carl von Ossietzky University Oldenburg, Oldenburg, Germany, ³ Helmholtz-Zentrum Geesthacht Centre for Materials and Coastal Research, Institute of Coastal Research, Modelling for the Assessment of Coastal Systems, Geesthacht, Germany, ⁴ Wattenmeerstation Sylt, Coastal Ecology, Alfred-Wegener-Institute Helmholtz-Center for Polar and Marine Research, List/Sylt, Germany

OPEN ACCESS

Edited by:

Hongyue Dang,
Xiamen University, China

Reviewed by:

Xavier Mayali,
Lawrence Livermore National
Laboratory, USA
Qiang Zheng,
Xiamen University, China

*Correspondence:

Judith Lucas
judith.lucas@awi.de

[†]These authors have contributed
equally to this work.

Specialty section:

This article was submitted to
Aquatic Microbiology,
a section of the journal
Frontiers in Microbiology

Received: 11 August 2015

Accepted: 29 February 2016

Published: 15 March 2016

Citation:

Lucas J, Koester I, Wichels A,
Niggemann J, Dittmar T, Callies U,
Wiltshire KH and Gerds G (2016)
Short-Term Dynamics of North Sea
Bacterioplankton-Dissolved Organic
Matter Coherence on Molecular Level.
Front. Microbiol. 7:321.
doi: 10.3389/fmicb.2016.00321

Remineralization and transformation of dissolved organic matter (DOM) by marine microbes shape the DOM composition and thus, have large impact on global carbon and nutrient cycling. However, information on bacterioplankton-DOM interactions on a molecular level is limited. We examined the variation of bacterial community composition (BCC) at Helgoland Roads (North Sea) in relation to variation of molecular DOM composition and various environmental parameters on short-time scales. Surface water samples were taken daily over a period of 20 days. Bacterial community and molecular DOM composition were assessed via 16S rRNA gene tag sequencing and ultrahigh resolution Fourier-transform ion cyclotron resonance mass spectrometry (FT-ICR-MS), respectively. Environmental conditions were driven by a coastal water influx during the first half of the sampling period and the onset of a summer phytoplankton bloom toward the end of the sampling period. These phenomena led to a distinct grouping of bacterial communities and DOM composition which was particularly influenced by total dissolved nitrogen (TDN) concentration, temperature, and salinity, as revealed by distance-based linear regression analyses. Bacterioplankton-DOM interaction was demonstrated in strong correlations between specific bacterial taxa and particular DOM molecules, thus, suggesting potential specialization on particular substrates. We propose that a combination of high resolution techniques, as used in this study, may provide substantial information on substrate generalists and specialists and thus, contribute to prediction of BCC variation.

Keywords: DOM, bacterioplankton community variation, short-term, FT-ICR-MS, 16S rRNA sequencing

INTRODUCTION

The global marine net primary production is estimated at 50 Gt C per year (Hedges, 1992). Part of this primary production is transferred to the marine dissolved organic matter (DOM) pool, making it one of the largest active carbon pool on earth (700 Gt), containing as much carbon as the Earth's atmospheric CO₂ or all land plant biomass (Hedges, 1992). Bacterial consumption and remineralization of DOM via the microbial loop, transfers energy to higher trophic levels and thus,

provides an important base for marine food webs (Azam et al., 1983; Azam, 1998). Between 30 and >90% of net primary production pass through the so-called labile dissolved organic carbon (DOC) fraction (Ducklow, 1999) and face rapid turnover by heterotrophic prokaryotes on a time scale of hours to days. Additionally, semi-labile DOC, which exhibits turnover times of months to years and can be followed as seasonal variability in DOC concentrations, provides support for the microbial loop (Hansell, 2013). Part of the DOC resists rapid bacterial degradation and as recalcitrant DOC, comprises a huge carbon pool of ~630 Gt, the largest part residing in the deep oceans. Since bacterial processing of DOM has large impact on global carbon and nutrient cycling, it is of great importance to understand how organic matter-bacteria interactions are controlled.

Different phylogenetic groups of bacteria tend to exploit different organic resources (e.g., Cottrell and Kirchman, 2000; Elifantz et al., 2005). This resource partitioning implies, that the DOM composition influences the bacterial community composition (BCC) and vice versa. Most studies that focus on DOM-bacterioplankton interactions are restricted to limited taxonomic resolution of microbial communities and selected compound classes of DOM. For instance, seasonal shifts of bulk DOC concentration and bacterial activity have been demonstrated over an annual cycle (Sintes et al., 2010). Venter et al. (2004) observed the tidal dynamics of DOC concentration and the bacterial community composition. McCarren et al. (2010) examined the genomic and transcriptional response of microbial communities to addition of high molecular weight DOM in microcosms over the course of 1 day. However, only few studies observed interactions of bacterial communities and molecular DOM composition in marine systems (Osterholz et al., 2014, 2016; Medeiros et al., 2015; Seidel et al., 2015) and to our knowledge there is no study investigating the interactions of bacterial community variation and molecular DOM composition on high resolutions and short time-scales such as day to day variation.

This study examines short-term dynamics in bacterial community and DOM composition at Helgoland Roads (North Sea, German Bight) on a daily basis over a period of 20 days including the onset of the summer phytoplankton bloom. We hypothesize that changes in the BCC are closely linked to patterns in DOM composition and vice versa. We assessed the BCC via 16S rRNA gene tag sequencing and the DOM composition via electro-spray ionization (ESI) coupled with Fourier-transform ion cyclotron resonance mass spectrometry (FT-ICR-MS). Multiple regression analyses were used to identify environmental parameters that have fundamental impact on the bacterial community and DOM compositions.

MATERIALS AND METHODS

Site Description and Sampling

From August 6 to 26, 2012 a total of 17 surface water samples were collected daily at Helgoland Roads (North Sea, German Bight, 54°18.31 N, 7°88.97 E). Due to contamination and technical problems, samples from August 11, 15, 19, and 24

are not included in the data set. Environmental data including water level, water temperature, salinity, dissolved O₂ and CO₂ concentrations, turbidity, pH, SiO₂, PO₄³⁻, NO₂⁻, NO₃⁻, and chlorophyll *a* (Chl *a*) were obtained as part of the Helgoland Roads Time Series (Wiltshire et al., 2008). Data were measured with a Ferry Box system installed at the eastern pier at Helgoland. Water intake is at about 2–4 m depth, depending on tides. Data are accessible via the open database PANGAEA 2004 (<http://www.pangaea.de>).

Surface seawater was sampled always at 1 pm with a bucket, (initially thoroughly rinsed with surface seawater) from the pier at the inflow site of the Ferry Box. Samples were transferred to glass bottles (cleaned with acidified pH 2, ultrapure water and rinsed with sample water before use), transported to the lab immediately and further processed within 1 h at the Biological Station Helgoland.

16S rRNA Gene Tag Sequencing of Bacterial Communities

Five hundred milliliters of surface seawater were vacuum filtered through 0.22 μm polycarbonate filters (GTTP, Ø 47 mm, Merck Millipore, USA) using bottletops cleaned with pH2, ultrapure water, and rinsed with sample water before use, to obtain bacterial biomass. Filters were stored at –20°C and further processed within 4 weeks. DNA extraction was carried out as described in Sapp et al. (2007). Briefly, lysozyme and sodium dodecyl sulfate were used for cell lysis followed by extraction with phenol-chloroform-isoamyl alcohol (25:24:1) and precipitation with isopropanol. DNA concentration per sample and purity were determined photometrically using a Tecan Infinite©200, NanoQuant microplate reader (Tecan, Switzerland).

16S rRNA gene tag sequencing was performed at LGC Genomics GmbH (Berlin, Germany). Community DNA samples were sent to LGC in a 96-well plate for generation of 16S V4 rRNA amplicon libraries for Illumina sequencing. Community DNA was amplified utilizing amplification primers targeting the V4 region of the 16S rRNA gene using 515F (5' GTGCCAGCMGCCGCGGTAA 3') and 806R (5' GGACTACHVGGGTWTCTAAT 3') (Caporaso et al., 2011). Primers also contained the Illumina sequencing adapter sequence and a unique barcode index. Sequencing was done on an Illumina MySeq platform using 2 × 250 bp chemistry. Raw paired-end reads were merged using the FLASH 1.2.4 software (<http://ccb.jhu.edu/software/FLASH/>) and processed through the SILVA pipeline (Quast et al., 2013). Sequences were de-replicated at 100% identity and then clustered within each individual sample at 98% similarity. Representative sequences from operational taxonomic unit clusters (OTUs) were classified up to genus level against the SILVA v119 database using BLAST as described by (Ionescu et al., 2012). Genus-level classifications were used in the final abundance matrix for downstream analyses. Each classification contained the sum of all sequences represented by OTUs with the same taxonomic path. For the purposes of this study we were not interested in diversity calculated at the level of 98% clustered OTUs but rather used BLAST identities as our OTU. From this point on, we define these taxa as OTUs

for simplicity. Eukaryotic, chloroplast and mitochondria-derived OTUs were removed from the resulting OTU matrix. Only OTUs with an average relative abundance $\geq 0.1\%$ were considered for further analysis.

Sequence data were deposited in the Sequence Read Archive (SRA) of the National Center for Biotechnology Information (NCBI) under accession number SRP058371.

Dissolved Organic Matter (DOM)

For DOM extraction, 2 l of each sample were filtered through 2 and 0.7 μm glass fiber filters (GMF and GF/F, Whatman, United Kingdom, combusted at 400°C, 4 h), acidified to pH 2 (HCl 32% p.a., Carl Roth, Germany), and stored at 4°C in the dark. Aliquots of the acidified 0.7 μm filtrate were sampled for quantification of DOC and total dissolved nitrogen (TDN). DOC and TDN concentrations were analyzed by high-temperature catalytic combustion using a TOC-VCPH/CPN Total Organic Carbon Analyzer equipped with an ASI-V autosampler and a TNM-1 module (Shimadzu, Japan). Prior to analysis, the acidified samples were purged with synthetic air to remove dissolved inorganic carbon. L-arginine solutions ranging from 5 to 500 $\mu\text{mol C l}^{-1}$ and 6.6 to 333.3 $\mu\text{mol N l}^{-1}$, respectively, were used for calibration and Deep Atlantic Seawater reference material (DSR, D. A. Hansell, University of Miami, Florida, USA) was measured during each run to control for instrumental precision and accuracy. Samples were measured in duplicates, average deviation of duplicate analysis was 4.4% for DOC and 1.6% for TDN.

DOM was extracted using modified styrene divinyl benzene polymer cartridges (PPL, Agilent, USA) as described in Dittmar et al. (2008). Cartridges were rinsed with two cartridge volumes of pH 2 ultrapure water to remove remaining salts, dried with inert pure argon gas and eluted with 6 ml methanol (ULC/MS grade, Biosolve, Netherland) into amber vials. The extract volume was determined by weight. Hundred microliters of the methanol extracts were evaporated overnight and re-dissolved in 10 ml ultrapure water at pH 2 for DOC analysis. The extraction efficiency was calculated as percentage DOC amount of the extract on the DOC amount of the original sample.

Mass spectra were obtained using a 15 T Solarix FT-ICR-MS (Bruker Daltonics, USA) equipped with an electrospray ionization source (Bruker Apollo II) applied in negative mode. Methanol extracts were diluted in a 1:1 ratio with ultrapure water to a final concentration of 20 mg C l^{-1} . A total of 500 scans were accumulated per run and mass spectra were evaluated in the range from 150 to 2000 Da. Mass spectra were calibrated with an internal calibration list of known molecular formulae mass peaks (Bruker Daltonics Data Analysis 4.0 SP 3 software package). Mass to charge ratios, peak intensities, and resolutions were exported and molecular formulae were assigned to the detected mass peaks with a minimum signal-to-noise ratio of 4, according to Koch et al. (2007). Masses were kept for further data analysis when detected in more than two samples. Masses present in less than 20% of the samples were allowed if the S/N ratio was >20 in at least one sample. Additionally, formulae were deleted that contained following combinations of heteroatoms: NSP, N₂S, N₃S, N₄S, N₂P, N₃P, N₄P, NS₂, N₂S₂, N₃S₂, N₄S₂, PS₂.

Remaining double assignments were removed. Peak intensities were normalized to the sum of peak intensities of all masses and considered as quantitative measure (relative abundances) of the respective DOM formulae. The ability of FT-ICR-MS peaks to be quantitative and reproducible has been evidenced by numerous studies (e.g., Riedel and Dittmar, 2014; Osterholz et al., 2015; Seidel et al., 2015; Zark et al., 2015). Masses which are listed as known contaminations including their homologous series and all isotopologs were removed. For each assigned formula the double bond equivalents [DBE = $1 + \frac{1}{2}(2C-H+N+P)$] as a measure for the degree of unsaturation (Koch and Dittmar, 2006) and the modified aromaticity index [$AI_{\text{mod}} = (1 + C - \frac{1}{2}O - S - \frac{1}{2}H)/(C - \frac{1}{2}O - S - N - P)$] were calculated to assess the presence and abundance of aromatic structures (Koch and Dittmar, 2006). Based on elemental ratios, AI_{mod} and heteroatom contents, molecular formulae can be categorized into compound groups (Seidel et al., 2014).

Statistical Analysis

Principal coordinates analyses (PCoA) were accomplished to reveal patterns in environmental parameters, BCC and DOM composition. Environmental variables were log transformed and normalized prior to analyses. PCoA for environmental parameters was carried out using Euclidean distances. Patterns in BCC were revealed by conducting PCoA of OTU read numbers using Hellinger distance (Legendre and Legendre, 1998), which uses square root transformed relative abundances for distance calculation. Patterns in DOM composition were observed based on Bray-Curtis distances, generated from square root transformed mass spectrometric data.

Samples were grouped via non-hierarchical group-average linkage clustering implemented in the non-parametric *k-R clustering* approach of the Primer v.7 software package (PRIMER-E, UK). In this approach, the classic idea of *k-means clustering*, which seeks to minimize within-group sums of squares about *k* group centroids, is generalized to non-parametric *k-R clustering* which analogously maximizes ANOSIM R and thus, allows the application of any resemblance measure desired. Based on the PCoA patterns the desired number of groups was specified as per authors discretion *a priori* to *k* = 3 for environmental data and *k* = 2 for 16S rRNA tag sequencing and DOM data. An iterative search then attempts to divide the samples into *k* groups in such a way that samples with greatest similarities (defined as the average of the pairwise similarities between a sample and all members of the same group) fall into one group. Significance of groups was confirmed using permutational multivariate analysis of variance (PERMANOVA) with fixed factors and 999 permutations at a significance level of $p < 0.05$ (see Table S3). Analysis of variance (ANOVA) was applied at a significance level of $p < 0.05$ using Statistica 11 (StatSoft, USA), to test for significant difference of single environmental parameters between groups of samples.

The linear discriminant analysis effect size method (LEfSe; Segata et al., 2011) was used to determine particular bacterial taxa and DOM molecules which were most likely to explain differences between the two groups of samples. LEfSe uses the non-parametric factorial Kruskal-Wallis sum-rank test to

detect features (OTUs or DOM molecules respectively) with significant differential abundance with respect to the groups of interest. Linear discriminant analysis (LDA) is then used to rank features according to their relative difference (effect size) among groups. Kruskal–Wallis tests were done on a significance level of $p < 0.05$. The threshold on the logarithmic LDA score for discriminative features was set at 2. An implementation of LEfSe including a convenient graphical interface incorporated in the Galaxy framework (Giardine et al., 2005; Blankenberg et al., 2010; Goecks et al., 2010) is provided online at <http://huttenhower.sph.harvard.edu/lefse/>.

Correlations between all environmental parameters were determined using Spearman rank order correlation (Statistica 11, StatSoft, USA) to reveal multicollinearities. Based on these correlations, environmental parameters were selected for multiple regression analysis to unravel their relationship with BCC and DOM composition. Multiple regression analyses were performed using distance-based linear modeling (DistLM). DistLM models were built using stepwise selection, adjusted R^2 and applying 999 permutations at a significance level of $p < 0.05$. Due to observed multicollinearity, the variables pH, turbidity and CO_2 were excluded from the analysis (see Results part for further explanation). Results were visualized via distance-based redundancy analysis (dbRDA). All multivariate analyses were performed using the Primer v.7 software package (PRIMER-E, UK). To further unravel the relationship of DOM molecules with specific environmental parameters, correlations of DOM molecules with salinity, temperature, and DOC were calculated using Pearson product-moment correlation (Statistica 11, StatSoft, USA).

To investigate the relationship between specific OTUs, DOM compounds and environmental parameters, pairwise correlations were calculated with R (R Development Core Team, 2014) using Pearson product-moment correlation at a significance level of $p < 0.05$. When considering several hypotheses in the same test the problem of multiple statistical inference arises (Holm, 1979). If one accounts for this family-wise error rate, e.g., via the Holm-Bonferroni correction (Holm, 1979), few of the apparent correlations would remain statistically significant. We compared raw data of OTU relative abundances and molecular formulae intensities to demonstrate that the observed correlations are plausible and consistent, and do not occur in a random fashion (Figure S2). High correlations ($r \leq -0.9$ or ≥ 0.9) were visualized in a network constructed using Cytoscape version 3.2.0 (Shannon et al., 2003).

RESULTS

Oceanographic Conditions at Sampling Site

Concurrent with water sampling, various physico-chemical parameters and nutrient concentrations were recorded (Table S1). Most striking was the high variation in salinity during the sampling period (Figure 1). During the first week of sampling, salinity decreased from 32.6 to 31.2 on August 12 2012, followed by an increase to 32.9 in the following week.

Additionally, TDN concentration and temperature increased over the sampling period (Figure 1). The Chl *a* concentration increased toward the end of the sampling period, indicating the onset of a summer phytoplankton bloom. Spearman rank order correlations revealed strong significant multicollinearity ($p < 0.5$, $r > 0.6$, Graham, 2003) among turbidity and Chl *a* ($R = 0.890$), salinity and pH ($R = -0.799$), salinity and DOC ($R = -0.600$), O_2 and CO_2 ($R = -0.807$), temperature and NO_2^- ($R = 0.645$), NO_3^- and SiO_2 ($R = 0.607$), and depth and pH ($R = -0.620$; Table S2). The power to detect a significant effect of a predictor on a response variable decreases nonlinearly with increasing multicollinearity (Graham, 2003). Therefore, we decided to drop collinear variables from further analysis, knowing that this might result in a substantial loss of overall explanatory power. Based on previous studies that uncovered Chl *a* (as proxy for phytoplankton abundance) and salinity as important driving factors for bacterial community dynamics (Fortunato et al., 2012; Lucas et al., 2015) we decided to treat pH, turbidity and CO_2 as functionally less important and excluded those variables from all further analyses.

PCoA of environmental data suggested that samples might cluster in three groups (Figure 2A), reflecting pronounced changes in environmental conditions during the sampling period. Non-hierarchical *k*-*R* clustering results, however, revealed that the third group was built by a single sample (13.8). Thus, a separation into two groups (group A and B) appeared more reasonable and the sample 13.8. was added to group A during all following analyses. ANOVA confirmed significant ($p < 0.05$) differences between both groups for TDN, temperature, salinity and Chl *a* (Table S3). Group A is characterized by lower average temperature (17.6°C), salinity (32.25), TDN ($14.61 \mu\text{M}$), and Chl *a* ($0.68 \mu\text{g l}^{-1}$) concentrations compared to group B where the average values were 18.13°C , 32.84, $17.98 \mu\text{M}$ TDN, and $0.79 \mu\text{g l}^{-1}$ Chl *a*.

Bacterial Community Composition, Variation, and Relation to Environmental Parameters

A total of 1,720,615 high quality sequences were obtained, clustering into 98 different taxonomically assigned OTUs (Table S4). During the sampling period the community was mainly composed of *Proteobacteria* (52.8%), *Bacteroidetes* (30.8%), and *Actinobacteria* (4.8%). On class level, *Flavobacteriia* was the predominant group (27.3%), closely followed by *Alphaproteobacteria* (26.8%) and *Gammaproteobacteria* (21.8%). Another highly abundant class was *Acidimicrobiia* (6.6%).

Prevailing OTUs within the *Flavobacteriia* were the NS5 marine group, *Tenacibaculum* and a *Cryomorphaceae* related cluster (Figure S1). *Alphaproteobacteria* were dominated by OTUs affiliated with the *Roseobacter* clade (*Candidatus Planktomarina*, NAC11-7 lineage, OCT lineage and *Sulfitobacter*). The prominent *Gammaproteobacteria* were OM60(NOR5) clade, *Oceanospirillales* related clone ZD0405 and SAR86 clade. Other OTUs with high relative abundances were *Candidatus Actinomarina*, Marine group II (*Euryarchaeota*).

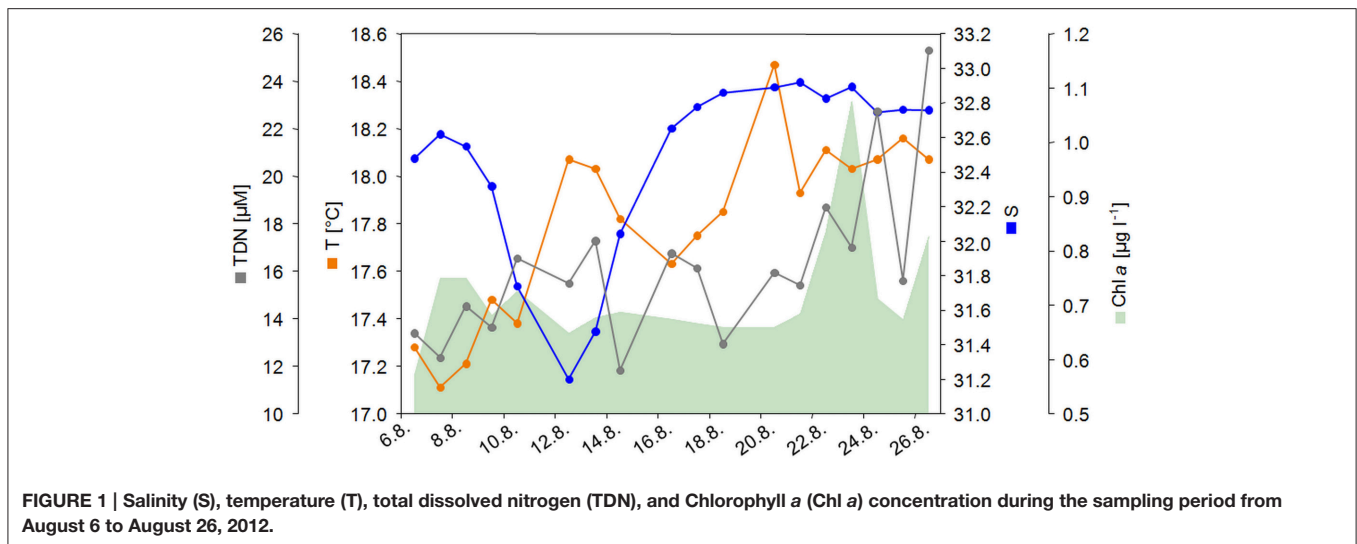


FIGURE 1 | Salinity (S), temperature (T), total dissolved nitrogen (TDN), and Chlorophyll a (Chl a) concentration during the sampling period from August 6 to August 26, 2012.

PCoA and non-hierarchical clustering of bacterial community tag data revealed a separation of samples into two groups (**Figure 2B**). DistLM analysis suggested that temperature, TDN, O_2 , PO_4^{3-} and DOC significantly influenced this group formation (**Figure 2D**, Table S5). To determine which bacterial taxa were most likely contributing to the differences in community composition between the two groups, linear discriminant effect size analysis (LEfSe) was performed (**Figures 3A,B**). In general, *Alpha-* and *Gammaproteobacteria* were dominating group A (25.2 and 26.8%). *Gammaproteobacteria* decreased in relative abundance in group B (19.1%), whereas *Alphaproteobacteria* increased slightly (27.6%). Most interestingly, *Flavobacteriia* reached a relative abundance of 30.1% in group B and became the dominating class. In particular the *Gammaproteobacteria* OTUs TBZ33 and BPS-CK174 (*Oceanospirillales*), *Chromohalobacter*, *Idiomarina*, *Salinisphaera*, *Marinobacter*, *Marinicella*, and SAR86 clade, the *Flavobacteriia* related OTUs *Formosa*, *Fluviicola*, *Crocinitomix*, NS2b, and NS7 marine group, and the *Alphaproteobacteria* related OTUs *Defluviococcus* and *Leisingera* contributed most to the differences between the groups A and B (**Figures 3A,B**).

DOM Composition, Variation, and Relation to Environmental Parameters

The average solid phase extraction efficiency was 44% (\pm 3.3%). A total of 4039 molecular formulae were assigned, ranging between 3842 and 3947 formulae per sample (average of all samples: 3892). The identified peaks covered a mass range from 159 to 809 Da with weighted average masses per sample between 370.2 and 385.4 Da (average of all samples: 377.1 Da).

As for BCC and for environmental parameters, PCoA and non-hierarchical clustering revealed a separation of samples into two groups (**Figure 2C**). DistLM analysis identified salinity and temperature as main influencing factors (**Figure 2E**, Table S5). However, temperature exhibited a significant ($p < 0.05$) correlation with TDN ($R = 0.508$) and NO_2^- ($R = 0.645$) and

salinity exhibited a significant correlation with DOC ($R = -0.6$) and O_2 ($R = -0.556$), thus, there might be a shared contribution to the explanation of variation in DOM composition. Elemental ratios of assigned molecular formulae provide information on molecular characteristics, which can be visualized in van Krevelen diagrams (Kim et al., 2003). Van Krevelen plots of all molecules that were significantly correlated ($p < 0.05$) with either salinity, temperature, or DOC revealed the nature of these relationships in more detail (**Figure 4**). Molecules that were positively correlated with salinity had higher H/C ratios and were clearly distinguished from molecules that were negatively correlated with salinity and showed lower H/C ratios (**Figure 4A**). Molecules that were positively correlated with temperature formed a dense cluster in the center of the van Krevelen diagram, whereas molecules negatively correlated with temperature were more scattered, showed higher H/C ratios and covered a broader range of O/C ratios (**Figure 4B**). The distribution of H/C and O/C ratios of molecules significantly correlated ($p < 0.5$) with DOC is depicted in **Figure 4C**. Molecules that were positively correlated with DOC showed low H/C ratios, while negatively correlated molecules exhibited higher H/C ratios.

LEfSe analysis identified few molecules that were significantly contributing to the differences in DOM composition between the two groups (**Figure 5**). Those molecules belonged mainly to the category of highly unsaturated compounds ($AI_{mod} \leq 0.5$ and $H/C < 1.5$) that increased in relative abundance from 80.9% in group A to 82.1% in group B and unsaturated aliphatics ($2.0 > H/C \geq 1.5$) that decreased slightly from group A (8.9%) compared to group B (8.1%).

Linking Bacterial Communities with Molecular DOM Composition

Although similar patterns in bacterial community structure and molecular DOM composition have been observed via PCoA, statistical analysis (PRIMER-E; RELATE subroutine, data not shown) failed to confirm co-variation of both;

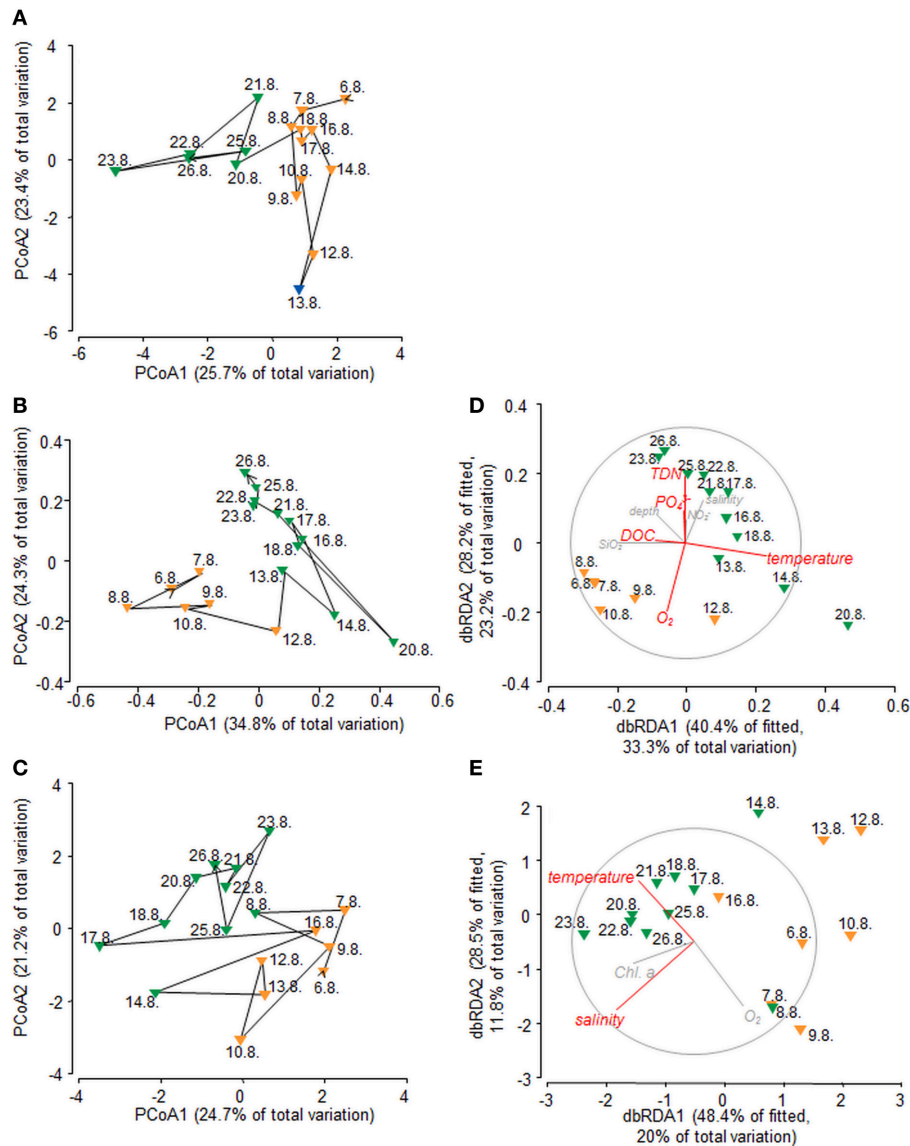


FIGURE 2 | Principal coordinates analyses (PCoA) of (A) environmental variables based on Euclidean distance, (B) bacterial communities based on Hellinger distance, and (C) molecular DOM composition based on Bray-Curtis similarity. Distance-based redundancy analysis (dbRDA) of (D) bacterial communities and (E) DOM composition, both based on Bray-Curtis similarities. Environmental parameters explaining the variation significantly ($p < 0.05$) are depicted in red, non-significant parameters are depicted in gray. Color code refers to group formation according to *k*-R Clustering. Orange, group A; Green, group B; Blue, group C.

i.e., among-sample relationships within the sequence data set differed from that within the DOM data set. Nevertheless, strong correlations between single OTUs and DOM molecules were detected. The majority of significant correlations ($p < 0.05$) exhibited correlation coefficients in the range of 0.5–0.6 (Table 1). As the coefficient increased, the number of significant correlations decreased to 56 with $R \geq 0.9$ of which 51 were exhibited between DOM molecules and OTUs. These strong correlations were formed between only seven OTUs and 36 DOM molecules (Figure 6, Figure S2). Five OTUs belonged to the *Gammaproteobacteria*, one OTU to the *Alphaproteobacteria* and one to the *Cytophagia*. Most of the

DOM compounds belonged to unsaturated aliphatics ($2.0 > H/C \geq 1.5$) or saturated fatty acids ($H/C \geq 2.0$ or $O/C \geq 0.9$). A group of seven distinct DOM compounds exhibited strong correlations ($R \geq 0.9$) with more than one OTU, whereas the remaining DOM compounds were correlated with either, *Defluviococcus*, *Idiomarina*, or *Glaciicola*. Strong correlations of *Defluviococcus* were restricted to unsaturated aliphatics, whereas strong correlations of *Idiomarina* occurred almost exclusively with saturated fatty acids. All OTUs exhibiting strong correlations also belonged to the ones contributing most to the differences between groups A and B as revealed by LefSe analyses (Figures 3, 5).

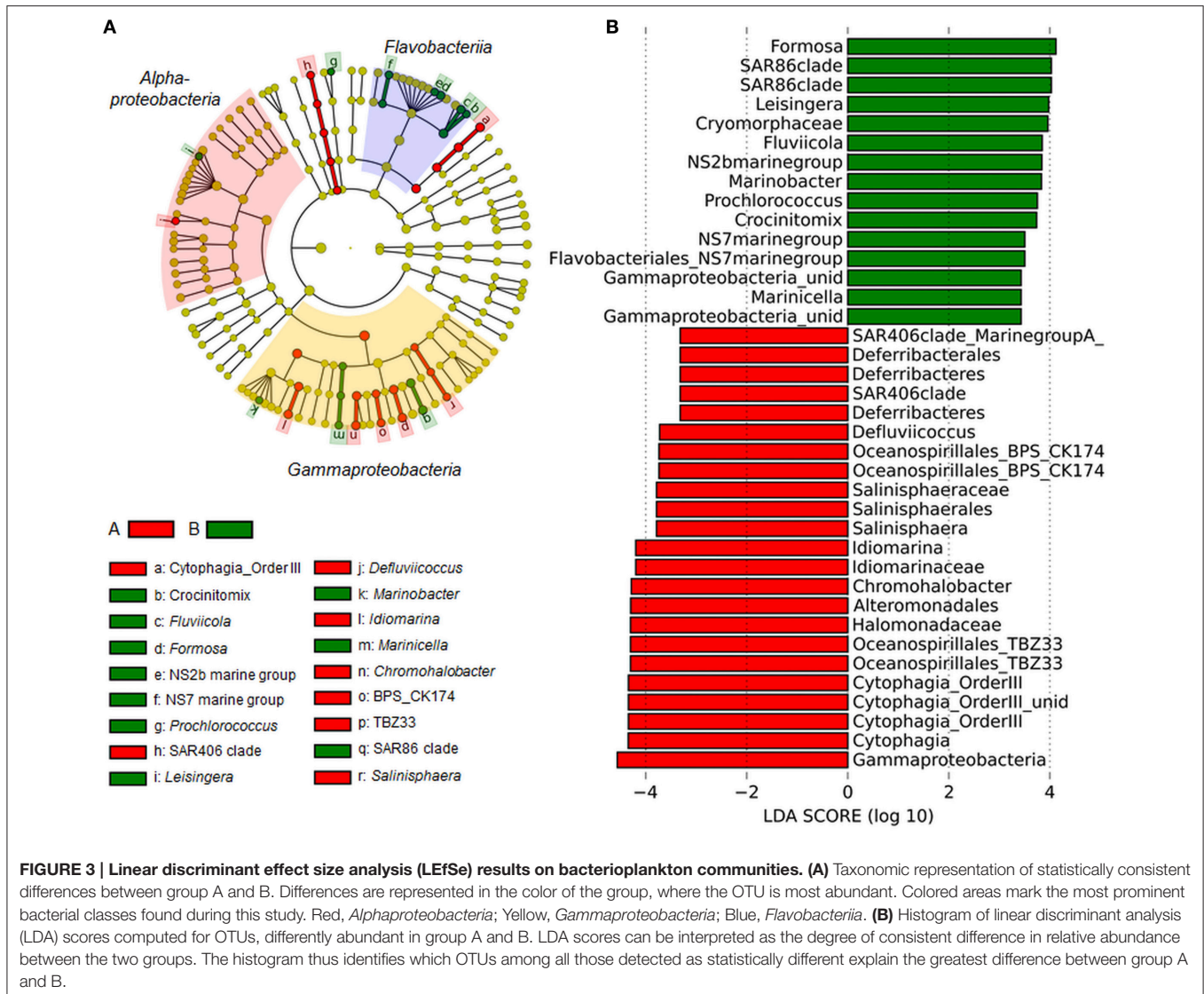


FIGURE 3 | Linear discriminant effect size analysis (LEfSe) results on bacterioplankton communities. (A) Taxonomic representation of statistically consistent differences between group A and B. Differences are represented in the color of the group, where the OTU is most abundant. Colored areas mark the most prominent bacterial classes found during this study. Red, *Alpha*proteobacteria; Yellow, *Gammaproteobacteria*; Blue, *Flavobacteria*. **(B)** Histogram of linear discriminant analysis (LDA) scores computed for OTUs, differently abundant in group A and B. LDA scores can be interpreted as the degree of consistent difference in relative abundance between the two groups. The histogram thus identifies which OTUs among all those detected as statistically different explain the greatest difference between group A and B.

DISCUSSION

Impact of Environmental Conditions on BCC

Salinity dynamics at Helgoland Roads are mainly controlled by hydrological and meteorological forces and by the huge runoff from the rivers Elbe and Weser (Atlas and Bartha, 1987). Long-term studies of oceanographic environmental parameters at Helgoland Roads reported mean annual salinities ranging between 31 and 33 (Raabe and Wiltshire, 2009). Transport of central North Sea water toward Helgoland Roads results in high salinities, whereas coastal water influx is related to lower salinities (Wiltshire et al., 2010). Low salinity events at Helgoland Roads presumably occur during winter months, especially in February, when the Elbe discharge is particularly high (Raabe and Wiltshire, 2009). During this study conducted in August 2012, the recorded salinity values exhibited a salinity shift of ~1.5 within 4 days which is exceptional during usually more stable hydrographic

conditions in summer and points to a strong short-term influence of coastal water masses.

The intermittent change of water masses during our study is confirmed by the results of tracer particle backtracking. Trajectories were simulated with PELETS-2D (Callies et al., 2011) based on pre-calculated near surface current velocity fields from the hydrodynamic model BSHcmod (Dick et al., 2001) operated by the Federal Maritime and Hydrographic Agency of Germany (Bundesamt für Seeschifffahrt und Hydrographie, BSH). Model results (Figure 7) help delineate regions of origin by analyzing the percentages of particle trajectories that crossed certain grid cells over the previous 3 weeks. We organized grid cells in a cobweb like structure centered at Helgoland Roads in order to take account of uncertainty increasing with distance. Figure 7 clearly documents an event with strong advection from the inner German Bight (near the Elbe estuary) toward Helgoland during the period around the 12th of August (Figure 7, right bottom panel) when salinity values at Helgoland were found to

TABLE 1 | Pivot-table for spearman rank order correlations between DOM molecules and environmental parameters, DOM molecules and OTUs, and OTUs and environmental parameters.

Coefficient	<0.5	0.5 – 0.6	0.6 – 0.7	0.7 – 0.8	0.8 – 0.9	0.9 – 1	Total
DOM and Env	789 (14.3)	2796 (50.5)	1296 (23.4)	517 (9.3)	130 (2.3)	5 (0.1)	5533
neg	462	1603	769	271	96	5	
pos	327	1193	527	246	34	0	
OTUs and DOM	4248 (16.6)	14,910 (58.2)	5087 (19.9)	1126 (4.4)	183 (0.7)	51 (0.2)	25,605
neg	2262	7912	2522	466	32	1	
pos	1986	6998	2565	660	151	50	
OTUs and Env	17 (10.1)	84 (50)	42 (25)	19 (11.3)	6 (3.6)	0 (0)	168
neg	7	34	18	12	3	0	
pos	10	50	24	7	3	0	
Sum	5054	17,790	6425	1662	319	56	31,306

Correlations are sorted according to correlation strength. Numbers of correlations are given. Numbers in brackets refer to percentage of correlations on total correlations within the corresponding group. Env, environmental parameter; neg, negative correlations; pos, positive correlations.

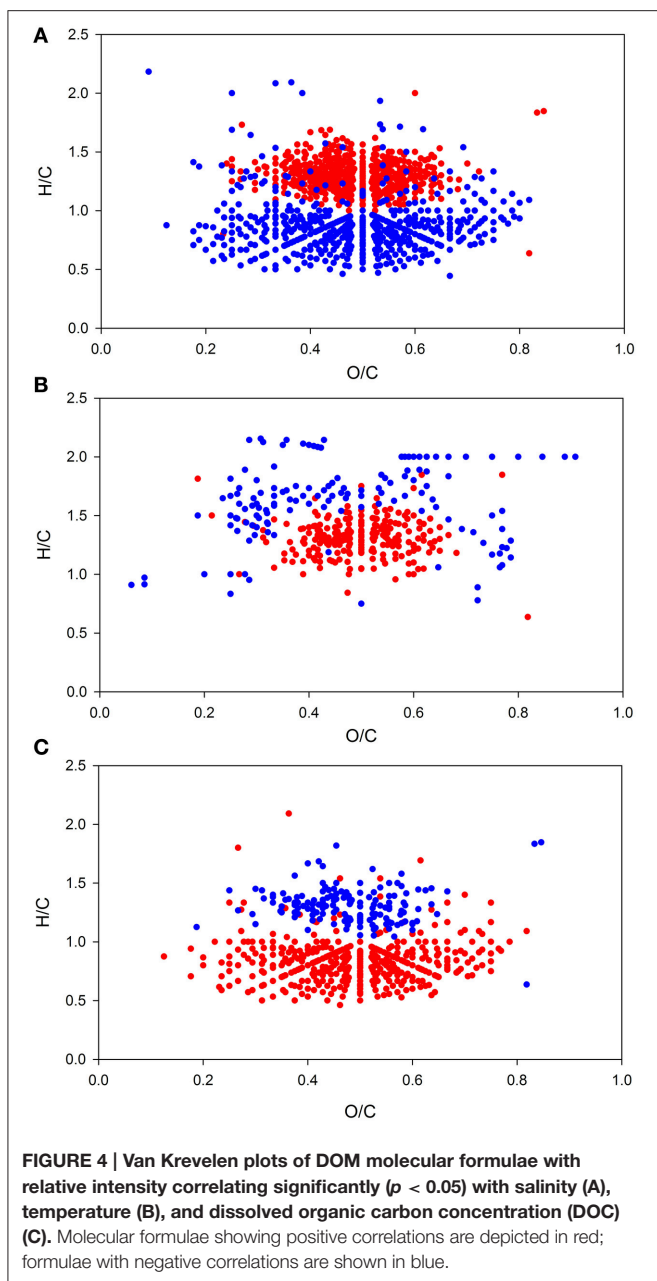
drop substantially. According to model simulations, this inshore origin of water masses did not exist (or was at least much less pronounced) at both the beginning and the end of the sampling period.

Statistical analysis on 16S rRNA tag data suggested a separation of samples into two groups that is particularly influenced by temperature, TDN, O₂, PO₄³⁻, and DOC. Multicollinearity of parameters describing ecological conditions might lead to biased interpretation of linear regression models (Graham, 2003). Correlation analysis confirmed multicollinearity of salinity with O₂ and DOC, which hints at a shared contribution of these parameters. In conjunction with the above mentioned coastal water inflow this leads to the assumption that salinity can be interpreted as a proxy for different water bodies with differing environmental conditions.

TDN is composed of dissolved inorganic nitrogen (DIN) and dissolved organic nitrogen (DON). DON comprises a large pool of fixed nitrogen in most aquatic systems, accounting for as much as 40–70% of the TDN pool in surface seawater (Bronk, 2002). It consists of labile, rapidly overturning proteins, amino polysaccharides, urea, and nucleic acids, but also includes more refractory compounds like humic acids (e.g., Bronk et al., 2007), most of which derive from primary producers but also from bacterial cell wall material (McCarthy et al., 1998). TDN concentrations measured during this study increased toward the end of the sampling period and reached highest concentrations shortly after the Chl *a* maximum. Thus, the increase in TDN concentration might reflect the permanent release of DOM by phytoplankton during its growth phase and additional release due to grazing or viral lysis that may affect the termination of the bloom (Beare et al., 2002; Wiltshire et al., 2010). However, it has to be noticed that DON concentration was not measured thus, this interpretation is speculative and needs to be evidenced.

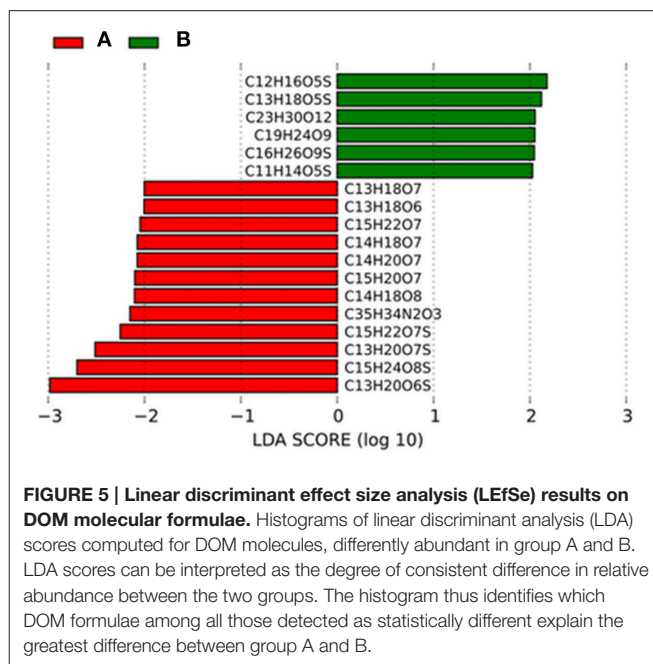
In general, the bacterial community observed in our study was dominated by *Flavobacteriia*, *Alpha*-, and *Gammaproteobacteria*. These classes have been consistently found to dominate bloom-associated bacterial communities as reviewed by Buchan et al. (2014). Also, the most abundant OTUs found during this study

are common members of the North Sea bacterial community during phytoplankton blooms (e.g., Giebel et al., 2011; Teeling et al., 2012; Wemheuer et al., 2014). Comparison of bacterial communities of group A, with low average TDN concentration (14.61 μM) and group B exhibiting higher TDN concentrations (19.98 μM) revealed that group B is characterized by higher relative abundance of *Flavobacteriia* (*Formosa*, *Fluviicola*, NS2b, *Crocinitomix*, and NS7 marine group) which are well known to be active in biopolymer degradation and reacting to phytoplankton blooms (e.g., Teeling et al., 2012; Buchan et al., 2014; Lucas et al., 2015). *Formosa* for instance has been found to be among the first taxa responding to a phytoplankton bloom and dominating the bacterial community at Helgoland Roads (Teeling et al., 2012). In contrast, some *Alpha*- and *Gammaproteobacteria* related OTUs decreased in relative abundance from group A to B. For instance *Defluviococcus* (*Alphaproteobacteria*) exhibited slightly higher relative abundances in Group A (0.3%) than in group B (0.1%). *Defluviococcus* is not a typical representative of marine *Alphaproteobacteria* and is usually found in wastewater treatment plants (Nobu et al., 2014), which might explain the occurrence of this OTU more frequently in coastal waters than in marine oceanic environments. Another OTU, *Idiomarina* (*Gammaproteobacteria*) showed increased relative abundances in group A (3.1%) compared to group B (0.3%). Also *Idiomarina* spp. is not a typical representative of the marine waters around Helgoland. It has been isolated from various marine environments such as deep-sea waters, hydrothermal vents, sediments, and reef building corals (e.g., Ivanova et al., 2000; Donachie et al., 2003; Chen et al., 2012; Zhang et al., 2012), but also from estuarine environments like Baltic Sea surface water (Brettar et al., 2003). The increased occurrence of these two OTUs at Helgoland Roads during the first half of the sampling period (group A), leads to the hypothesis that OTUs that are commonly associated with coastal marine environments have been passively transported to Helgoland Roads with the above mentioned coastal water inflow. Thus, *Defluviococcus* and *Idiomarina* reflect the short-term impact of coastal water inflows on the BCC at Helgoland Roads.



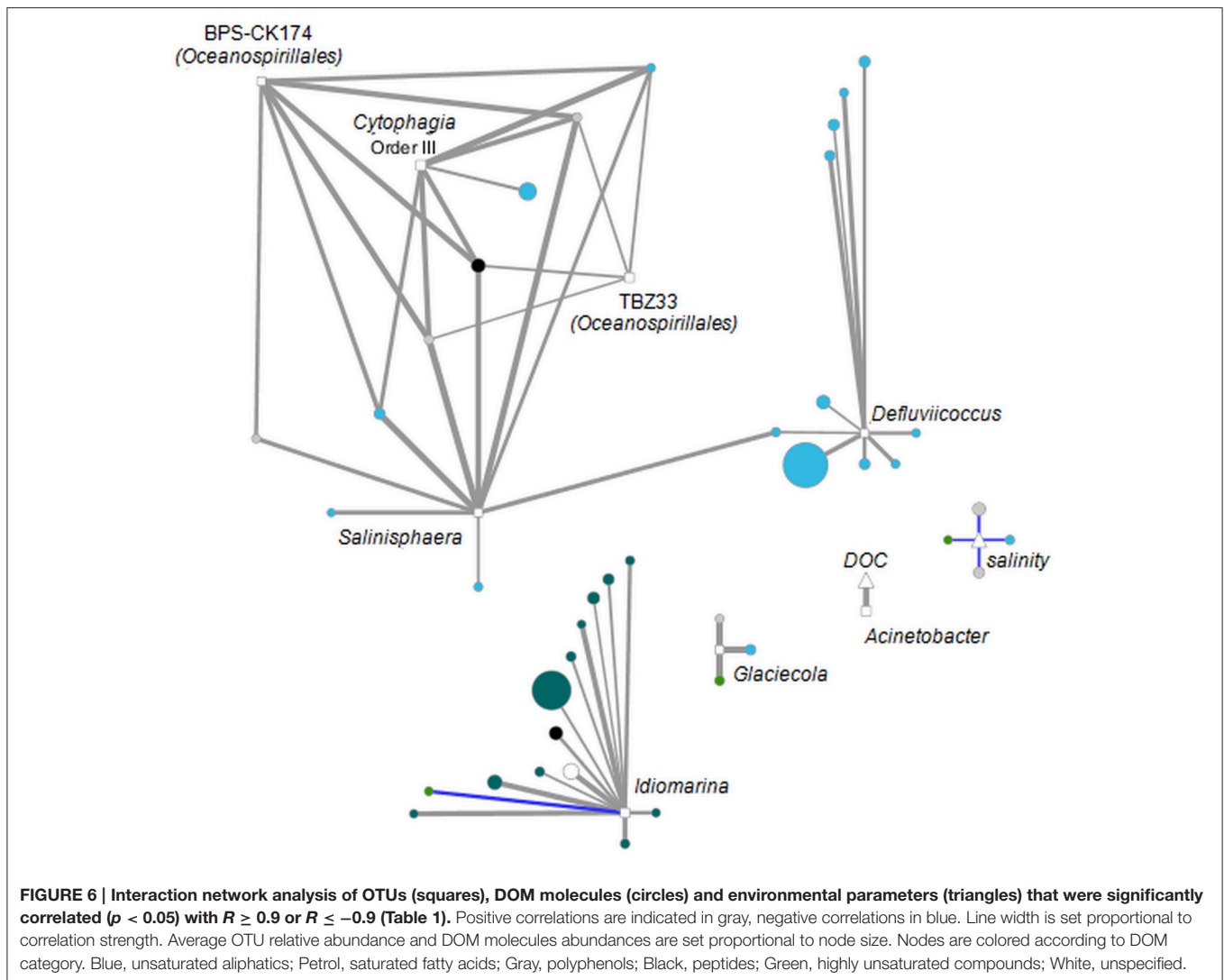
Impact of Environmental Conditions on Molecular DOM Composition

Variability in the DOM composition was mainly driven by salinity and temperature as revealed by DistLM (Figure 2E). The molecules that were positively correlated with salinity exhibited higher H/C ratios and were clearly separated from molecules that were negatively correlated with salinity and showed lower H/C values (Figure 4A). In general, marine DOM has higher H/C ratios, is more aliphatic and contains higher proportions of carbohydrates, amino acids, and lipids, whereas terrestrial DOM is more aromatic, contains carboxyl, and hydroxyl functionalities and has lower H/C ratios (Sleighter and Hatcher, 2008; Medeiros et al., 2015; Seidel et al., 2015).



Similar observations by Kim et al. (2003) and Koch et al. (2005) support the assumption that the molecules positively correlated with salinity are associated with marine DOM and those negatively correlated are associated with terrigenous DOM. This interpretation is also supported by our findings that on average unsaturated aliphatics ($2.0 > H/C \geq 1.5$) were most abundant during the coastal water inflow. Thus, we conclude that differences between the observed groups in this study can be partly explained by different water masses and thus origins of DOM.

Furthermore, we found that molecules negatively correlated with temperature had higher H/C ratios than positively correlated molecules (Figure 4B). Higher H/C ratios indicate higher saturation which is characteristic for compounds that are rapidly degradable, e.g., fatty acids and proteinaceous material. As temperature increased toward the end of the sampling period, molecules with high H/C ratio decreased. This observation could be explained by a scenario where microbial activity had increased with rising temperatures and as response to enhanced organic matter supply released by phytoplankton. Due to enhanced metabolism, the microbial community may have consumed more DOM (Pomeroy and Wiebe, 2001), which could have preferentially diminished the pool of labile DOM and thus, diminished the amount of molecules with high H/C ratio. The notion of enhanced microbial activity is also supported by the H/C ratios of molecules correlated with DOC. The simultaneous increase of compounds with low H/C ratios and DOC concentration (reflected in the positive correlation of these compounds with DOC) support the scenario of preferential consumption of rapidly degradable compounds with high H/C ratios leading to an increasing relative abundance of molecules with low H/C ratios.



Relation between Bacterial Community and Molecular DOM Composition

Linkage of bacterial relative abundances with DOM data revealed evidence for dependency of specific OTUs on particular DOM molecules. Especially *Gammaproteobacteria* showed strong positive correlations ($R \geq 0.9$) with unsaturated aliphatics and saturated fatty acids (Figure 6), all of which showed decreased relative abundances in group B compared to group A. *Gammaproteobacteria* are known to be typical marine bacteria, thus one would expect increasing relative abundances in group B, which exhibits higher salinity than group A, which was strongly influenced by a coastal freshwater inflow. A possible explanation for the observed predominance of *Bacteroidetes* in group B might be the onset of the summer phytoplankton bloom that occurred in group B and might have supported enhanced growth of *Bacteroidetes* by providing complex organic compounds. Thus *Gammaproteobacteria* relative abundances might have decreased due to increasing *Bacteroidetes* abundances.

Network analyses revealed few DOM compounds that were highly correlated ($R \geq 0.9$) with different bacteria taxa and thus seem to serve as a general substrate. On the other hand we observed strong correlations of *Defluviicoccus* (*Alphaproteobacteria*) with unsaturated aliphatics as the only substrate category (Figure 6), which might indicate that *Defluviicoccus* specialized on selected DOM compounds that are not as intensively consumed by other taxa and which might be important for defining its ecological niche. As already mentioned *Defluviicoccus* spp. is typically found in wastewater treatment plants (e.g., Nobu et al., 2014), and capable of taking up a narrow range of substrates such as acetate, propionate, pyruvate, and glucose (Burow et al., 2007), which supports our findings of strong correlations with unsaturated aliphatics. Another example for specialization on specific substrate classes is *Idiomarina* (*Gammaproteobacteria*), which is almost exclusively strongly correlated with specific saturated fatty acids (Figure 6). The notion of specific bacterial taxa specializing on selected DOM molecules is supported by previous studies that also suggested

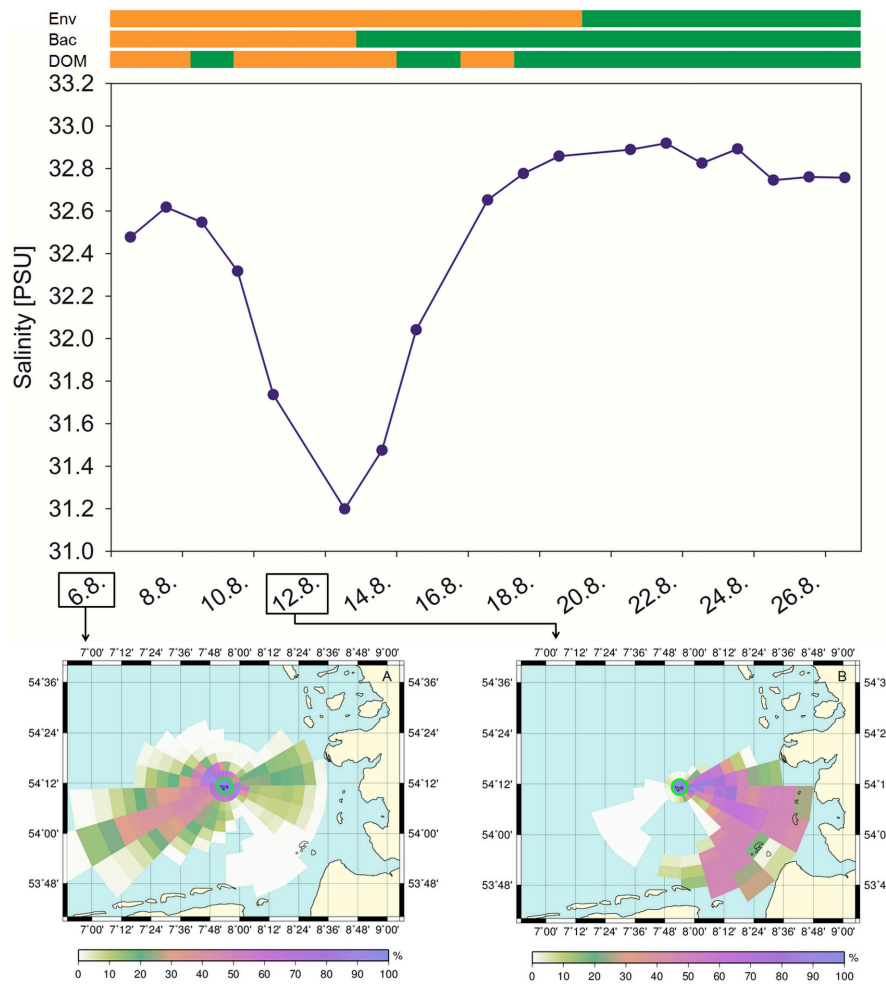


FIGURE 7 | Histories of water bodies observed at Helgoland Roads. Based on pre-calculated near surface current velocities from the hydrodynamic model BSHmod, 500 passive tracer particles were tracked backward in time. Referring to a cobweb like grid structure, the color scale reflects the percentage of particle trajectories that touched a given grid cell at any time within the past 3 weeks. Bars on top depict group formation for environmental parameters (Env), bacterial communities (Bac) and DOM. Orange, group A; Green, group B.

coordinated resource partitioning by bacterial specialists leading to a defined temporal succession of bacterial taxa (e.g., McCarren et al., 2010; Teeling et al., 2012). Nevertheless, as discussed above we hypothesize that relative abundances of *Defluviococcus* and *Idiomarina* at Helgoland Roads are influenced by the observed coastal water inflow. The same might be true for the different DOM compound classes. Thus, it has to be further analyzed whether the simultaneously decreasing relative abundances of unsaturated aliphatics and *Defluviococcus* and saturated fatty acids and *Idiomarina* represent real dependencies, or just reflect a simple co-occurrence in different water bodies. However, so far studies that dealt with resource partitioning by bacterial specialists analyzed the transcriptional responses of microbial communities to high-molecular-weight DOM amendment or enhanced substrate supply by phytoplankton blooms. Here, we demonstrate the possibility to link single bacterial taxa to specific DOM formulae rather than just molecule categories. Even though

FT-ICR-MS has, as any analytical technique, a defined analytical window, it is an important step to further unravel the specific microorganisms and metabolic pathways responsible for the degradation and transformation of DOM in the oceans.

Although we were able to relate single OTUs with specific DOM molecules, a direct general relationship between bacterial community structure and DOM composition could not be demonstrated. One possible explanation might be that freshly produced labile DOM that is accessible for microorganisms is rapidly turned over by the bacterial community as shown in several studies (Kirchman et al., 1991; Amon and Benner, 1996; Weiss and Simon, 1999). Thus, the pool of labile DOM compounds that could have a significant influence on bacterial community structure might not be detectable with the methods applied in this study. An instantaneous degradation of introduced fresh DOM by bacterioplankton is also proposed for arctic fjords (Svalbard), which results in a predominance of the

prevailing semi-refractory and refractory DOM pool Osterholz et al. (2014).

Furthermore, methodological limitations could have led to lacking evidence of a relation between the bacterial community structure and DOM composition. A previous study by Flerus et al. (2012) suggested that colloidal material and low molecular weight DOM (<250 Da) can be lost during solid phase extraction (SPE) as used in this study. Thus, labile DOM that might have an influence on bacterial community structure, escapes the analytical window. The low extraction efficiencies observed during our study might indicate that a substantial fraction of DOM was not extracted. Although the efficiencies were in the range described for marine samples (Dittmar et al., 2008), they were considerably lower than in more recent studies (Rossel et al., 2013; Osterholz et al., 2014). Despite these methodological limitations inherent to any analytical method, we identified significant variations in DOM composition and successfully linked them to environmental conditions and BCC.

To our knowledge this is the first time that dynamics of BCC and molecular DOM composition have been documented on high temporal and analytical resolution. We conclude that the bacterial community is highly influenced by freshly produced, labile DOM pulses as derived from phytoplankton blooms. Rapid transformation of labile DOM might lead to selective relative enrichment of more refractory DOM and thus hamper the detection of interdependencies between bacterial community structure and DOM composition. High resolution techniques like 16S rRNA tag sequencing and FT-ICR-MS provide substantial information on substrate generalists and specialists and may help to predict changes in BCC. To further unravel the relationship between bacteria and molecular DOM composition it has to be considered that metabolic capabilities are not restricted

to specific phylogenetic groups. Thus, for future analyses we suggest combining FT-ICR-MS analyses of DOM with functional approaches of bacterial communities rather than phylogenetic description.

AUTHOR CONTRIBUTIONS

GG, AW, TD, and JN conceived the study. IK and JN performed sampling. IK performed DOM-analysis. JL performed bacterial community and statistical analysis. UC performed tracer particle backtracking analysis. KW provided environmental parameters. All authors contributed to data interpretation. JL and IK wrote the manuscript with significant input from all co-authors.

ACKNOWLEDGMENTS

We would like to thank Kristine Carstens, Matthias Friebe, Ina Ulber, and Katrin Klaproth for their technical assistance. Many thanks to the “de.NBI Initiative” (www.denbi.de) that substantially supports the Arb SILVAngs project (www.arb-silva.de/ngs/). We are grateful for calculation of correlations between DOM, OTUs, and environmental factors with R by Stephan Frickenhaus. We gratefully acknowledge the provision of BSHcmod current velocity fields by the Federal Maritime and Hydrographic Agency of Germany (Bundesamt für Seeschifffahrt und Hydrographie, BSH) in Hamburg.

SUPPLEMENTARY MATERIAL

The Supplementary Material for this article can be found online at: <http://journal.frontiersin.org/article/10.3389/fmicb.2016.00321>

REFERENCES

- Amon, R. M. W., and Benner, R. (1996). Bacterial utilization of different size classes of dissolved organic matter. *Limnol. Oceanogr.* 41, 41–51. doi: 10.4319/lo.1996.41.1.0041
- Atlas, R. M., and Bartha, R. (1987). *Microbial Ecology: Fundamentals and Applications*. Menlo Park, CA: Benjamin/Cummings.
- Azam, F. (1998). Microbial control of oceanic carbon flux: the plot thickens. *Science* 280, 694–696. doi: 10.1126/science.280.5364.694
- Azam, F., Fenchel, T., Field, J. G., Gray, J. S., Meyer-Reil, L. A., and Thingstad, F. (1983). The ecological role of water-column microbes in the sea. *Mar. Ecol. Prog. Ser.* 10, 257–263. doi: 10.3354/meps010257
- Beare, D. J., Batten, S., Edwards, M., and Reid, D. G. (2002). Prevalence of boreal Atlantic, temperate Atlantic and neritic zooplankton in the North Sea between 1958 and 1998 in relation to temperature, salinity, stratification intensity and Atlantic inflow. *J. Sea Res.* 48, 29–49. doi: 10.1016/S1385-1101(02)00131-4
- Blankenberg, D., Kuster, G. V., Coraor, N., Ananda, G., Lazarus, R., Mangan, M., et al. (2010). Galaxy: A web-based genome analysis tool for experimentalists. *Curr. Protoc. Mol. Biol.* 89, 19.10.1–19.10.21. doi: 10.1002/0471142727.mb1910s89
- Brettar, I., Christen, R., and Höfle, M. G. (2003). *Idiomarina baltica* sp. nov., a marine bacterium with a high optimum growth temperature isolated from surface water of the central Baltic Sea. *Int. J. Syst. Evol. Microbiol.* 53, 407–413. doi: 10.1099/ijs.0.02399-0
- Bronk, D. A. (2002). “Dynamics of DON,” in *Biogeochemistry of Marine Dissolved Organic Matter*, eds D. A. Hansell and C. A. Carlson (San Diego, CA: Academic Press), 153–249.
- Bronk, D. A., See, J. H., Bradley, P., and Killberg, L. (2007). DON as a source of bioavailable nitrogen for phytoplankton. *Biogeosciences* 4, 283–296. doi: 10.5194/bg-4-283-2007
- Buchan, A., LeCleir, G. R., Gulvik, C. A., and González, J. M. (2014). Master recyclers: features and functions of bacteria associated with phytoplankton blooms. *Nat. Rev. Microbiol.* 12, 686–698. doi: 10.1038/nrmicro3326
- Burow, L. C., Kong, Y., Nielsen, J. L., Blackall, L. L., and Nielsen, P. H. (2007). Abundance and ecophysiology of *Deftluicoccus* spp., glycogen-accumulating organisms in full-scale wastewater treatment processes. *Microbiology* 153, 178–185. doi: 10.1099/mic.0.2006/001032-0
- Callies, U., Plüß, A., Kappenberg, J., and Kapitzka, H. (2011). Particle tracking in the vicinity of Helgoland, North Sea: a model comparison. *Ocean Dynamics* 61, 2121–2139. doi: 10.1007/s10236-011-0474-8
- Caporaso, J. G., Lauber, C. L., Walters, W. A., Berg-Lyons, D., Lozupone, C. A., Turnbaugh, P. J., et al. (2011). Global patterns of 16S rRNA diversity at a depth of millions of sequences per sample. *Proc. Natl. Acad. Sci. U.S.A.* 108, 4516–4522. doi: 10.1073/pnas.1000080107
- Chen, M.-H., Sheu, S.-Y., Chen, C. A., Wang, J.-T., and Chen, W.-M. (2012). *Idiomarina aquimaris* sp. nov., isolated from the reef-building coral *Isopora palifera*. *Int. J. Syst. Evol. Microbiol.* 62, 1536–1542. doi: 10.1099/ijs.0.035592-0
- Cottrell, M. T., and Kirchman, D. L. (2000). Natural assemblages of marine *Proteobacteria* and members of the *Cytophaga-Flavobacter* cluster consuming

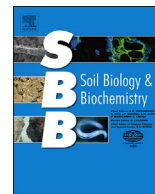
- low- and high-molecular-weight dissolved organic matter. *Appl. Environ. Microbiol.* 66, 1692–1697. doi: 10.1128/AEM.66.4.1692-1697.2000
- Dick, S., Kleine, E., Müller-Navarra, S. H., Klein, H., and Komo, H. (2001). “The operational circulation model of BSH (BSHcmod)-model description and validation,” in *Berichte Des Bundesamtes Für Seeschifffahrt Und Hydrographie* (Hamburg).
- Dittmar, T., Koch, B., Hertkorn, N., and Kattner, G. (2008). A simple and efficient method for the solid-phase extraction of dissolved organic matter (SPE-DOM) from seawater. *Limnol. Oceanogr. Methods* 6, 230–235. doi: 10.4319/lom.2008.6.230
- Donachie, S. P., Hou, S., Gregory, T. S., Malahoff, A., and Alam, M. (2003). *Idiomarina loihiensis* sp. nov., a halophilic γ -Proteobacterium from the Lō'ihi submarine volcano, Hawaii. *Int. J. Syst. Evol. Microbiol.* 53, 1873–1879. doi: 10.1099/ijs.0.02701-0
- Ducklow, H. W. (1999). The bacterial component of the oceanic euphotic zone. *FEMS Microbiol. Ecol.* 30, 1–10. doi: 10.1111/j.1574-6941.1999.tb00630.x
- Elifantz, H., Malmstrom, R. R., Cottrell, M. T., and Kirchman, D. L. (2005). Assimilation of polysaccharides and glucose by major bacterial groups in the Delaware Estuary. *Appl. Environ. Microbiol.* 71, 7799–7805. doi: 10.1128/AEM.71.12.7799-7805.2005
- Flerus, R., Lechtenfeld, O. J., Koch, B. P., McCallister, S. L., Schmitt-Kopplin, P., Benner, R., et al. (2012). A molecular perspective on the ageing of marine dissolved organic matter. *Biogeosciences* 9, 1935–1955. doi: 10.5194/bg-9-1935-2012
- Fortunato, C. S., Herfort, L., Zuber, P., Baptista, A. M., and Crump, B. C. (2012). Spatial variability overwhelms seasonal patterns in bacterioplankton communities across a river to ocean gradient. *ISME J.* 6, 554–563. doi: 10.1038/ismej.2011.135
- Giardine, B., Riemer, C., Hardison, R. C., Burhans, R., Eltnitski, L., Shah, P., et al. (2005). Galaxy: a platform for interactive large-scale genome analysis. *Genome Res.* 15, 1451–1455. doi: 10.1101/gr.4086505
- Giebel, H.-A., Kalhoefer, D., Lemke, A., Thole, S., Gahl-Jannsen, R., Simon, M., et al. (2011). Distribution of *Roseobacter* RCA and SAR11 lineages in the North Sea and characteristics of an abundant RCA isolate. *ISME J.* 5, 8–19. doi: 10.1038/ismej.2010.87
- Goecks, J., Nekrutenko, A., Taylor, J., and Team, T. G. (2010). Galaxy: a comprehensive approach for supporting accessible, reproducible, and transparent computational research in the life sciences. *Genome Biol.* 11:R86. doi: 10.1186/gb-2010-11-8-r86
- Graham, M. H. (2003). Confronting multicollinearity in ecological multiple regression. *Ecology* 84, 2809–2815. doi: 10.1890/02-3114
- Hansell, D. A. (2013). Recalcitrant dissolved organic carbon fractions. *Ann. Rev. Mar. Sci.* 5, 421–445. doi: 10.1146/annurev-marine-120710-100757
- Hedges, J. I. (1992). Global biogeochemical cycles: progress and problems. *Mar. Chem.* 39, 67–93. doi: 10.1016/0304-4203(92)90096-S
- Holm, S. (1979). A simple sequentially rejective multiple test procedure. *Scand. J. Stat.* 6, 65–70.
- Ionescu, D., Siebert, C., Polerecky, L., Munwes, Y. Y., Lott, C., Häusler, S., et al. (2012). Microbial and chemical characterization of underwater fresh water springs in the Dead Sea. *PLoS ONE* 7:e38319. doi: 10.1371/journal.pone.0038319
- Ivanova, E. P., Romanenko, L. A., Chun, J., Matte, M. H., Matte, G. R., Mikhailov, V. V., et al. (2000). *Idiomarina* gen. nov., comprising novel indigenous deep-sea bacteria from the Pacific Ocean, including descriptions of two species, *Idiomarina abyssalis* sp. nov. and *Idiomarina zobellii* sp. nov. *Int. J. Syst. Evol. Microbiol.* 50, 901–907. doi: 10.1099/00207113-50-2-901
- Kim, S., Kramer, R. W., and Hatcher, P. G. (2003). Graphical method for analysis of ultrahigh-resolution broadband mass spectra of natural organic matter, the Van Krevelen Diagram. *Anal. Chem.* 75, 5336–5344. doi: 10.1021/ac034415p
- Kirchman, D. L., Suzuki, Y., Garside, C., and Ducklow, H. W. (1991). High turnover rates of dissolved organic carbon during a spring phytoplankton bloom. *Nature* 352, 612–614. doi: 10.1038/352612a0
- Koch, B. P., and Dittmar, T. (2006). From mass to structure: an aromaticity index for high-resolution mass data of natural organic matter. *Rapid Commun. Mass Spec.* 20, 926–932. doi: 10.1002/rcm.2386
- Koch, B. P., Dittmar, T., Witt, M., and Kattner, G. (2007). Fundamentals of molecular formula assignment to ultrahigh resolution mass data of natural organic matter. *Anal. Chem.* 79, 1758–1763. doi: 10.1021/ac061949s
- Koch, B. P., Witt, M., Engbrodt, R., Dittmar, T., and Kattner, G. (2005). Molecular formulae of marine and terrigenous dissolved organic matter detected by electrospray ionization Fourier transform ion cyclotron resonance mass spectrometry. *Geochim. Cosmochim. Acta* 69, 3299–3308. doi: 10.1016/j.gca.2005.02.027
- Legendre, P., and Legendre, L. (1998). *Numerical Ecology*. San Diego, CA: Elsevier.
- Lucas, J., Wichels, A., Teeling, H., Chafee, M., Scharfe, M., and Gerdt, G. (2015). Annual dynamics of North Sea bacterioplankton: seasonal variability superimposes short-term variation. *FEMS Microbiol. Ecol.* 91:fiv099. doi: 10.1093/femsec/fiv099
- McCarren, J., Becker, J. W., Repeta, D. J., Shi, Y., Young, C. R., Malmstrom, R. R., et al. (2010). Microbial community transcriptomes reveal microbes and metabolic pathways associated with dissolved organic matter turnover in the sea. *Proc. Natl. Acad. Sci. U. S. A.* 107, 16420–16427. doi: 10.1073/pnas.1010732107
- McCarthy, M. D., Hedges, J. I., and Benner, R. (1998). Major bacterial contribution to marine dissolved organic nitrogen. *Science* 281, 231–234. doi: 10.1126/science.281.5374.231
- Medeiros, P. M., Seidel, M., Ward, N. D., Carpenter, E. J., Gomes, H. R., Niggemann, J., et al. (2015). Fate of the Amazon River dissolved organic matter in the tropical Atlantic Ocean. *Global Biogeochem. Cycles* 29, 677–690. doi: 10.1002/2015GB005115
- Nobu, M. K., Tamaki, H., Kubota, K., and Liu, W.-T. (2014). Metagenomic characterization of ‘*Candidatus Defluviicoccus tetraformis* strain TFO71’, a tetrad-forming organism, predominant in an anaerobic-aerobic membrane bioreactor with deteriorated biological phosphorus removal. *Environ. Microbiol.* 16, 2739–2751. doi: 10.1111/1462-2920.12383
- Osterholz, H., Dittmar, T., and Niggemann, J. (2014). Molecular evidence for rapid dissolved organic matter turnover in Arctic fjords. *Mar. Chem.* 160, 1–10. doi: 10.1016/j.marchem.2014.01.002
- Osterholz, H., Niggemann, J., Giebel, H.-A., Simon, M., and Dittmar, T. (2015). Inefficient microbial production of refractory dissolved organic matter in the ocean. *Nat. Commun.* 6:7422. doi: 10.1038/ncomms8422
- Osterholz, H., Singer, G., Wemheuer, B., Daniel, R., Simon, M., Niggemann, J., et al. (2016). Deciphering associations between dissolved organic molecules and bacterial communities in a pelagic marine system. *ISME J.* doi: 10.1038/ismej.2015.231. [Epub ahead of print].
- Pomeroy, L. R., and Wiebe, W. J. (2001). Temperature and substrates as interactive limiting factors for marine heterotrophic bacteria. *Aquat. Microb. Ecol.* 23, 187–204. doi: 10.3354/ame023187
- Quast, C., Pruesse, E., Yilmaz, P., Gerken, J., Schweer, T., Yarza, P., et al. (2013). The SILVA ribosomal RNA gene database project: improved data processing and web-based tools. *Nucleic Acids Res.* 41, D590–D596. doi: 10.1093/nar/gks1219
- Raabe, T., and Wiltshire, K. H. (2009). Quality control and analyses of the long-term nutrient data from Helgoland Roads, North Sea. *J. Sea Res.* 61, 3–16. doi: 10.1016/j.seares.2008.07.004
- R Development Core Team (2014). *R: A language and Environment for Statistical Computing*. Vienna: R Foundation for Statistical Computing.
- Riedel, T., and Dittmar, T. (2014). A method detection limit for the analysis of natural organic matter via fourier transform ion cyclotron resonance mass spectrometry. *Anal. Chem.* 86, 8376–8382. doi: 10.1021/ac501946m
- Rossel, P. E., Vähätalo, A. V., Witt, M., and Dittmar, T. (2013). Molecular composition of dissolved organic matter from a wetland plant (*Juncus effusus*) after photochemical and microbial decomposition (1.25 yr): common features with deep sea dissolved organic matter. *Org. Geochem.* 60, 62–71. doi: 10.1016/j.orggeochem.2013.04.013
- Sapp, M., Gerdt, G., Wiltshire, K. H., and Wichels, A. (2007). Bacterial community dynamics during the winter-spring transition in the North Sea. *FEMS Microbiol. Ecol.* 59, 622–637. doi: 10.1111/j.1574-6941.2006.00238.x
- Segata, N., Izard, J., Waldron, L., Gevers, D., Miropolsky, L., Garrett, W., et al. (2011). Metagenomic biomarker discovery and explanation. *Genome Biol.* 12:R60. doi: 10.1186/gb-2011-12-6-r60
- Seidel, M., Beck, M., Riedel, T., Waska, H., Suryaputra, I. G. N. A., Schnetger, B., et al. (2014). Biogeochemistry of dissolved organic matter in an anoxic intertidal creek bank. *Geochim. Cosmochim. Acta* 140, 418–434. doi: 10.1016/j.gca.2014.05.038
- Seidel, M., Yager, P. L., Ward, N. D., Carpenter, E. J., Gomes, H. R., Krusche, A. V., et al. (2015). Molecular-level changes of dissolved organic matter along the

- Amazon River-to-ocean continuum. *Mar. Chem.* 177, 218–231. doi: 10.1016/j.marchem.2015.06.019
- Shannon, P., Markiel, A., Ozier, O., Baliga, N. S., Wang, J. T., Ramage, D., et al. (2003). Cytoscape: a software environment for integrated models of biomolecular interaction networks. *Genome Res.* 13, 2498–2504. doi: 10.1101/gr.1239303
- Sintes, E., Stodereger, K., Parada, V., and Herndl, G. (2010). Seasonal dynamics of dissolved organic matter and microbial activity in the coastal North Sea. *Aquat. Microb. Ecol.* 60, 85–95. doi: 10.3354/ame01404
- Sleighter, R. L., and Hatcher, P. G. (2008). Molecular characterization of dissolved organic matter (DOM) along a river to ocean transect of the lower Chesapeake Bay by ultrahigh resolution electrospray ionization Fourier transform ion cyclotron resonance mass spectrometry. *Mar. Chem.* 110, 140–152. doi: 10.1016/j.marchem.2008.04.008
- Teeling, H., Fuchs, B. M., Becher, D., Klockow, C., Gardebrecht, A., Bennke, C. M., et al. (2012). Substrate-controlled succession of marine bacterioplankton populations induced by a Phytoplankton bloom. *Science* 336, 608–611. doi: 10.1126/science.1218344
- Venter, J. C., Remington, K., Heidelberg, J. F., Halpern, A. L., Rusch, D., Eisen, J. A., et al. (2004). Environmental genome shotgun sequencing of the Sargasso Sea. *Science* 304, 66–74. doi: 10.1126/science.1093857
- Weiss, M., and Simon, M. (1999). Consumption of labile dissolved organic matter by limnetic bacterioplankton: the relative significance of amino acids and carbohydrates. *Aquat. Microb. Ecol.* 17, 1–12. doi: 10.3354/ame017001
- Wemheuer, B., Güllert, S., Billerbeck, S., Giebel, H.-A., Voget, S., Simon, M., et al. (2014). Impact of a phytoplankton bloom on the diversity of the active bacterial community in the southern North Sea as revealed by metatranscriptomic approaches. *FEMS Microbiol. Ecol.* 87, 378–389. doi: 10.1111/1574-6941.12230
- Wiltshire, K., Kraberg, A., Bartsch, I., Boersma, M., Franke, H.-D., Freund, J., et al. (2010). Helgoland Roads, North Sea: 45 Years of Change. *Estuar. Coasts* 33, 295–310. doi: 10.1007/s12237-009-9228-y
- Wiltshire, K. H., Malzahn, A. M., Wirtz, K., Janisch, S., Mangelsdorf, P., and Manly, B. F. J. (2008). Resilience of North Sea phytoplankton spring bloom dynamics: an analysis of long-term data at Helgoland Roads. *Limnol. Oceanogr.* 53, 1294–1302. doi: 10.4319/lo.2008.53.4.1294
- Zark, M., Riebesell, U., and Dittmar, T. (2015). Effects of ocean acidification on marine dissolved organic matter are not detectable over the succession of phytoplankton blooms. *Sci. Adv.* 1:e1500531. doi: 10.1126/sciadv.1500531
- Zhang, Y.-J., Zhang, X.-Y., Zhao, H.-L., Zhou, M.-Y., Li, H.-J., Gao, Z.-M., et al. (2012). *Idiomarina maris* sp. nov., a marine bacterium isolated from sediment. *Int. J. Syst. Evol. Microbiol.* 62, 370–375. doi: 10.1099/ijs.0.027896-0

Conflict of Interest Statement: The authors declare that the research was conducted in the absence of any commercial or financial relationships that could be construed as a potential conflict of interest.

The reviewer QZ and handling Editor declared their shared affiliation, and the handling Editor states that the process nevertheless met the standards of a fair and objective review.

Copyright © 2016 Lucas, Koester, Wichels, Niggemann, Dittmar, Callies, Wiltshire and Gerds. This is an open-access article distributed under the terms of the Creative Commons Attribution License (CC BY). The use, distribution or reproduction in other forums is permitted, provided the original author(s) or licensor are credited and that the original publication in this journal is cited, in accordance with accepted academic practice. No use, distribution or reproduction is permitted which does not comply with these terms.



Linking molecular size, composition and carbon turnover of extractable soil microbial compounds



Ashish A. Malik^{a, b, *}, Vanessa-Nina Roth^a, Mathieu Hébert^c, Luc Tremblay^c, Thorsten Dittmar^d, Gerd Gleixner^a

^a Department of Biogeochemical Processes, Max Planck Institute for Biogeochemistry, Jena, Germany

^b Centre for Ecology & Hydrology, Wallingford, United Kingdom

^c Department of Chemistry and Biochemistry, Université de Moncton, Moncton, New Brunswick, Canada

^d Research Group for Marine Geochemistry (ICBM-MPI Bridging Group), Institute for Chemistry and Biology of the Marine Environment (ICBM), University of Oldenburg, Oldenburg, Germany

ARTICLE INFO

Article history:

Received 18 January 2016

Received in revised form

21 May 2016

Accepted 27 May 2016

Available online 5 June 2016

Keywords:

Soil carbon

Microbial biomass

Chloroform fumigation extraction

HPLC-FTIR

ESI-FT-ICR-MS

HPLC-IRMS

ABSTRACT

Microbial contribution to the maintenance and turnover of soil organic matter is significant. Yet, we do not have a thorough understanding of how biochemical composition of soil microbial biomass is related to carbon turnover and persistence of different microbial components. Using a suite of state-of-the-art analytical techniques, we investigated the molecular characteristics of extractable microbial biomass and linked it to its carbon turnover time. A ¹³C₂ plant pulse labelling experiment was used to trace plant carbon into rhizosphere soil microbial biomass, which was obtained by chloroform fumigation extraction (CFE). ¹³C content in molecular size classes of extracted microbial compounds was analysed using size exclusion chromatography (SEC) coupled online to high performance liquid chromatography–isotope ratio mass spectrometry (SEC-HPLC-IRMS). Molecular characterization of microbial compounds was performed using complementary approaches, namely SEC-HPLC coupled to Fourier transform infrared spectroscopy (SEC-HPLC-FTIR) and electrospray ionization Fourier transform ion cyclotron resonance mass spectrometry (ESI-FT-ICR-MS). SEC-HPLC-FTIR suggests that mid to high molecular weight (MW) microbial compounds were richer in aliphatic CH bonds, carbohydrate-like compounds and possibly P=O derivatives from phospholipids. On the contrary, the lower size range was characterized by more oxidised compounds with hydroxyl, carbonyl, ether and/or carboxyl groups. ESI-FT-ICR-MS suggests that microbial compounds were largely aliphatic and richer in N than the background detrital material. Both molecular characterization tools suggest that CFE derived microbial biomass was largely lipid, carbohydrate and protein derived. SEC-HPLC-IRMS analysis revealed that ¹³C enrichment decreased with increasing MW of microbial compounds and the turnover time was deduced as 12.8 ± 0.6, 18.5 ± 0.6 and 22.9 ± 0.7 days for low, mid and high MW size classes, respectively. We conclude that low MW compounds represent the rapidly turned-over metabolite fraction of extractable soil microbial biomass consisting of organic acids, alcohols, amino acids and sugars; whereas, larger structural compounds are part of the cell envelope (likely membrane lipids, proteins or polysaccharides) with a much lower renewal rate. This relation of microbial carbon turnover to its molecular size, structure and composition thus highlights the significance of cellular biochemistry in determining the microbial contribution to soil carbon cycling and specifically soil organic matter formation.

© 2016 Elsevier Ltd. All rights reserved.

* Corresponding author. Centre for Ecology & Hydrology, Maclean Building, Benson Lane, Crowmarsh Gifford, Wallingford, Oxfordshire, OX10 8BB, United Kingdom.

E-mail address: ashmalik@ceh.ac.uk (A.A. Malik).

1. Introduction

Microbial growth and activity largely control soil carbon cycling (Liang and Balser, 2011; Schimel and Schaeffer, 2012). It is readily accepted that the majority of plant organic carbon passes through the soil microorganisms, a fraction of which is used for cellular energy needs and the rest for biomass build-up; and that microbial

biomass forms soil organic matter (SOM) mostly from cell fragments (Gleixner, 2013; Kögel-Knabner, 2002; Miltner et al., 2012). The contribution of microbial biomass to maintenance and accumulation of SOM is significant, some estimates suggest it could be as high as 80% of organic carbon in soil (Kindler et al., 2009; Liang et al., 2011; Simpson et al., 2007; Six et al., 2006). The residence time of microbial compounds in soil has been attributed to its molecular structure and biochemical composition as well as ecosystem specific effects (Simpson et al., 2007; Throckmorton et al., 2012; Tremblay and Benner, 2006). However, we do not have a thorough understanding of the dependencies of C turnover and persistence of microbial compounds on their molecular size and composition.

A widely used method to obtain microbial biomass from soil is biocidal fumigation using chloroform that lyses microbial cells and releases their contents which is followed by its extraction using K_2SO_4 solution (Tate et al., 1988; Vance et al., 1987). It is likely that chloroform fumigation does not lyse certain microbial groups with tougher cell envelopes and that the K_2SO_4 extraction selectively extracts only specific molecular compounds out of the lysed cellular products (Malik et al., 2013). Notwithstanding these shortcomings, chloroform fumigation extraction (CFE) has been extensively used to estimate soil microbial biomass carbon (Franzluebbers, 1999; Philippot et al., 2012) and its source and turnover time when coupled with stable isotope analysis (Dijkstra et al., 2006; Ryan and Aravena, 1994). However, in spite of its popularity in soil biology there is still no knowledge of the molecular structure and composition of the CFE microbial fraction. One of the aims of this report is to provide this understanding that is essential in making reliable ecological interpretations from CFE results. We applied two state-of-the-art molecular profiling tools to characterize the extracted microbial compounds: size exclusion chromatography (SEC) high performance liquid chromatography coupled with Fourier transform infrared spectroscopy (SEC-HPLC-FTIR) and electrospray ionization Fourier transform ion cyclotron resonance mass spectrometry (ESI-FT-ICR-MS). While SEC-HPLC-FTIR quantifies different functional groups in size classes of the dissolved natural organic matter (Landry and Tremblay, 2012); ESI-FT-ICR-MS is able to identify the elemental formulae of thousands of molecular ions over a wide mass range (Reemtsma, 2009; Sleighter and Hatcher, 2007). A combination of these complementary tools allows detailed molecular profiling investigations by revealing different information. Relating this information to stable carbon isotope ratios ($^{13}C/^{12}C$) of size separated compounds, when a ^{13}C tracer is applied in an experimental system, allows one to associate the molecular fingerprints to inherent carbon turnover rates. SEC-HPLC-IRMS involves size exclusion chromatography coupled online with an SEC-HPLC-IRMS interface that enables molecular size-dependent separation of organic compounds followed by direct online stable carbon isotope analysis of the eluted size fractions (Malik et al., 2012).

The objective of this study was to link the molecular size and structure of extractable microbial compounds to their carbon turnover time. CFE derived soil microbial biomass from a plant $^{13}CO_2$ pulse-labelling experiment over a time series was analysed to estimate the turnover time of its molecular size classes and to gain the molecular profiles of both bulk microbial fraction as well as its size classes. The combination of analytical tools used here allowed us to profile the CFE-derived microbial compounds and ascertain if different compound size classes have variable turnover time. The methods also provide valuable information on the molecular characteristics of compounds in soil organic matter, which has been discussed in relation to the microbial contribution to SOM formation.

2. Materials and methods

2.1. Soil sampling and experimental setup

Soil from an arable field at the Jena Biodiversity Experiment located in Jena, Germany was used in a greenhouse experiment. *Dysphania ambrosioides* (formerly *Chenopodium ambrosioides*), a temperate herb, was grown in soil mesocosms and after 3 months of plant growth; a $^{13}CO_2$ pulse labelling was performed for 10 h at a CO_2 concentration of 350–400 ppm in an airtight glass chamber. The plants were returned to the greenhouse at the end of the labelling period and destructive soil sampling was performed at 1, 3, 12 and 24 h, then at 2, 4, 7, 14, 21 and 28 days after the pulse labelling. Rhizosphere soil from 3 mesocosms was sampled at each time point. Soil was then sieved to <2 mm, fine roots were extensively removed (this excludes mesofauna and plant residues) and stored at $-20\text{ }^\circ\text{C}$. Details about the experimental design and the sampling strategy are given elsewhere (Malik et al., 2015).

2.2. Microbial biomass extraction

Microbial biomass from soil was obtained using a slightly modified version of the CFE method (Vance et al., 1987; Malik et al., 2013). Soil (7 g wet weight) was fumigated in a desiccator with chloroform gas for 24 h followed by repeated (8 times) evacuation. Organic matter was extracted from fumigated and non-fumigated control soils with 0.05 M K_2SO_4 solution in a ratio of 1:4 (w/v). The mixture was homogenized on an orbital shaker (250 rev per min, 30 min), centrifuged for 5 min at 12,000 g and then filtered using prewashed Whatman filter paper. The resultant dissolved organic matter (DOM) was acidified and purged with nitrogen gas in order to remove the dissolved inorganic carbon (Scheibe et al., 2012). Fumigated and non-fumigated K_2SO_4 extracts from all time points and replicates ($n = 30$) were measured for stable carbon isotope ratios using SEC-HPLC-IRMS, whereas only two composite samples from ten randomly pooled K_2SO_4 extracts were used for the other detailed molecular analyses because as expected the microbial biomass content and composition did not change in our steady state experimental system (Malik et al., 2015). The K_2SO_4 extracts were directly measured on SEC-HPLC-IRMS without any further treatment but for the other analyses a solid phase extraction (SPE) was performed in order to concentrate and desalt the DOM. Fumigated and non-fumigated DOM was acidified to pH 2 and applied to activated SPE cartridges (Bond Elut PPL cartridge; 1 g, Agilent Technologies; Dittmar et al., 2008). CFE protocol blank (K_2SO_4 extract without any soil sample) and SPE cartridge blank were also maintained throughout the molecular fingerprinting analyses. CFE microbial biomass and background non-fumigated DOM represented approximately 1.2 and 0.3% of total organic carbon, respectively, in the studied soil system.

2.3. SEC-HPLC-FTIR analysis

The SPE extracts were dissolved in methanol in order to obtain a DOC concentration of $\sim 3\text{ mg mL}^{-1}$. 40 μL of this solution was injected into an Agilent 1200 HPLC system equipped with the Polymer standards service (PSS) SUPREMA analytical Linear S ($8 \times 300\text{ mm}$; $5\text{ }\mu\text{m}$) SEC column. Otherwise, the SEC-HPLC-FTIR technique and calibration used were the same as previously described (Landry and Tremblay, 2012). Before deposition and FTIR analysis, UV detection was carried out at a wavelength of 254 nm. SEC separated DOM was deposited as tracks onto a rotating germanium disk where a background spectrum was taken on a portion of the track where no DOM was eluting. Each band of every FTIR spectrum was integrated, valley-to-valley. The absolute

absorbance area of each band present in the protocol blank was subtracted from the absolute area of the same band in the samples. Concentration factors were considered for these subtractions. The corrected absorbance area of the band was normalized by the corrected total absorbance area of the spectrum to obtain the relative absorbance (%) for the band. These relative values enabled us to follow variations in the proportion of each peak present in different spectra (i.e., in different samples and for different MW).

2.4. ESI-FT-ICR-MS analysis

Mass spectral analyses were performed on a Bruker Solarix 15 T FT-ICR-MS (Bruker Daltonics, USA) in negative ionization mode. Prior to analysis the SPE DOM extracts were diluted to achieve a dissolved organic carbon concentration of 20 mg/L in a 1:1 mixture of methanol and water (v/v). The samples and blanks were injected into the ESI source with a flow rate of 120 $\mu\text{L}/\text{h}$ and an ESI needle voltage of -4 kV. The recorded m/z range was between m/z 150 and 2000. 500 transients with an ion accumulation time of 0.2 s were added up to one spectrum. A list of 67 compounds that covered the relevant m/z range was used for linear internal mass calibration with a maximum mass error of 0.1 ppm. Molecular formula assignment considered C, H, O, N, S and P using a self-written Matlab routine (Koch et al., 2007; Stenson et al., 2003).

To remove detected masses or peaks that were not measured significantly, several criteria were applied. First, m/z with a signal-to-noise ratio of the maximum of each m/z ($s/n_{\text{Max},i}$) ≤ 5 were discarded (Pohlabein and Dittmar, 2015 and references therein). The noise was defined as the minimum intensity across all detected masses without blanks. $s/n_{\text{Max},i}$ was defined for each m/z_i individually by dividing the maximum intensity of each m/z_i by the noise. Second, only detected masses that occurred more than one time in the set of measured samples were kept. Third, all detected masses with a s/n_{Blanks} ratio ≥ 20 were removed. To determine s/n_{Blanks} the average of signal intensity across all measured blanks was divided by noise. After removing detected masses according to these criteria, the remaining detected masses were normalized to the sum of intensities. For the following data analyses, only detected masses with assigned molecular formulae were considered. For the list of non-fumigated samples only formulae that were detected in both replicates were considered, the same was applied to the list of peaks in the fumigated samples. Identified molecular formulae were assigned to compound groups based on established molar ratios, aromaticity index and heteroatom contents (Seidel et al., 2015a, 2015b; Text S1). Formulae present in both fumigated and non-fumigated DOM extracts were considered as signatures of bulk SOM, whereas those unique to fumigated extracts were identified as microbial. In addition, a differential spectrum approach was used, wherein the relative intensities of non-fumigated samples were subtracted from those of the fumigated samples resulting in m/z with positive and negative values. Formulae that were present in higher abundance above a threshold (10% of the median intensity of the top 1% of formulae ranked according to intensity) in either fumigated (positive values) or non-fumigated (negative values) were considered and identified as microbial or bulk SOM-related, respectively. More details about the data analysis are given in Supporting Information, Text S1.

2.5. SEC-HPLC-IRMS analysis

Stable carbon isotope measurements were carried out using an HPLC system coupled to a Delta + XP IRMS through an LC IsoLink interface (Thermo Fisher Scientific, Germany). SEC was performed on a mixed bed analytical column (TSK-GEL GMPWXL-7.8 mm \times 30 cm; Tosoh Bioscience, Germany). 100 μL aliquot of soil

extracts was injected using an autosampler (Surveyor autosampler, Thermo Fisher Scientific) into the mobile phase that consisted of phosphate buffer 20 mM (pH 6.2) maintained at a constant flow rate of 500 $\mu\text{L min}^{-1}$ using a Surveyor MS pump. Apparent MW was obtained using a calibration curve plotted with standards having known MW (Malik et al., 2012, 2013 for technical details). Empirical C turnover time (synonymously referred to as mean residence time) of microbial size classes was obtained by estimating the pulse ^{13}C dilution rate using an exponential function in SigmaPlot (Malik et al., 2015).

3. Results

3.1. SEC-HPLC-FTIR

The SEC chromatograms obtained from UV detection shows the distribution of fumigated and non-fumigated DOM with molecular weight ranging from 300 to 6500 Da (Supporting Information, Fig. S1). The majority of fumigated and non-fumigated DOM was between 500 Da and 3500 Da with peak maxima around 1400 Da. Another peak was observed only in fumigated extracts between 300 Da and 480 Da with peak maxima around 400 Da. The same two peaks were seen in SEC chromatograms obtained with FTIR detection (total spectrum absorbance) but their relative intensities differed when compared with UV absorbance peaks (not shown). FTIR absorption bands at differing wavenumbers were assigned to functional groups on the basis of published literature on natural organic matter and related complex molecules (Landry and Tremblay, 2012 and references therein). Unique presence of functional groups in fumigated extracts or their increased abundance in fumigated relative to non-fumigated DOM was the criteria used to identify microbial molecular structures (Fig. 1). In general, fumigated DOM was richer in aliphatic CH bonds (3050–2830 cm^{-1}), carbohydrate-like compounds and possibly P=O derivatives (1080 cm^{-1}) (Fig. 1-B, G; Table 1; Davis and Mauer, 2010). The distribution with MW suggests that these functional groups or structures were more abundant in mid to high MW CFE-derived microbial compounds. OH (3700–2700 cm^{-1}), C–O/C–O–C or C–OH (1400–1200 cm^{-1}) and C–N or C–O bonds (1250 cm^{-1}) were more abundant in low MW fumigated DOM (Fig. 1-A, E, F; Table 1). The highest proportion of C–N or C–O groups in fumigated DOM was observed below 565 Da, which includes masses assigned to the low end of mid-MW and all the low MW.

3.2. ESI-FT-ICR-MS

Molecular formula assignment revealed that 59 formulae were unique to fumigated DOM and 112 formulae were more abundant in fumigated relative to non-fumigated extracts (Figure S2A–B). These 171 formulae were considered as signatures of microbial compounds. 659 formulae were present in both fumigated and non-fumigated extracts and therefore linked to the background SOM. Another 47 of them that were present in higher abundance in non-fumigated relative to fumigated DOM were also considered as SOM-derived (Figure S2C). Among the SOM related molecular formulae 80.6% (569) were characterized with no nitrogen (N), 17% (120) with 1 N and the rest 2.4% (17) with 2–4 N. On the contrary, molecular formulae identified as microbial were rich in N; 53.2% contained at least 1 N (Table 2). 17% (29) of microbial molecular formulae were linked to peptides, compared to a tiny 2.5% (18) of SOM-related formulae. Aromaticity index (AI) estimated for each formula identifies the molecules as non-aromatic (AI ≤ 0.5), aromatic (0.5 < AI < 0.67) or condensed aromatic (AI ≥ 0.67 ; (Koch and Dittmar, 2006). The percentage of non-aromatic formulae that were identified as microbial were higher (87.1%) than those identified as

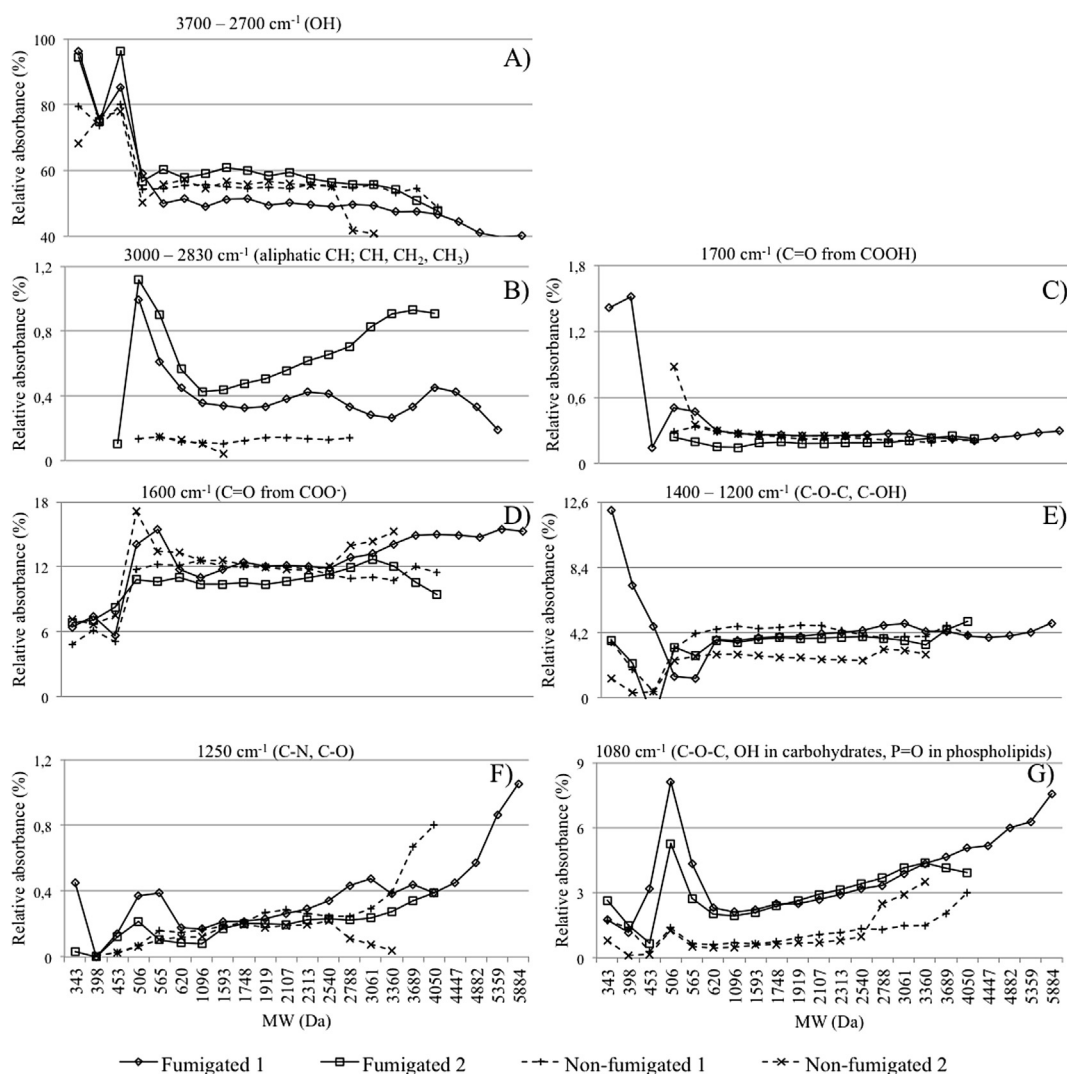


Fig. 1. FTIR relative absorbance of seven peaks (panels A to G) of size separated DOM in fumigated and non-fumigated samples. A greater proportion of a particular functional group in the microbial fraction is indicated by its higher relative absorbance in the fumigated fraction in comparison to the non-fumigated.

Table 1

Proportion of functional groups in different molecular weight (MW) size classes of microbial compounds as obtained by SEC-LC-FTIR analyses. Number of pluses signifies relative abundance in fumigated soil extracts in comparison to non-fumigated ones.

Functional group	Microbial compounds				Bulk
	Low MW 343–398 Da	Mid MW 453–620 Da	High MW 1593–2107 Da	High MW 2788–5844 Da	
Aliphatic CH	nd	++	+	++	++
Carbohydrate, P=O	+#	++	+	+	+
OH	++	+			
C–N, C–O	+#	+		#	
C–O–C, C–OH	++				
C=O (COOH)	+#				

= Relative absorbance values between replicates were variable, thus comparison was less reliable.

nd = Not determined because the signal was too low over the entire FTIR spectra for this part of the track.

SOM related (75.2%; Table 2). Unique insights were obtained when the extracted formulae were plotted in the H/C (hydrogen/carbon) versus O/C (oxygen/carbon) space called van Krevelen diagrams (Fig. 2; (Kim et al., 2003; Sleighter and Hatcher, 2007)). Comparing the van Krevelen analysis of microbial and SOM related molecular formulae with that of standard compound classes we could roughly

infer that most microbial compounds extracted using CFE were lipid, amino sugar or protein derived. Assigned compound groups varied in relative abundance in microbial and SOM-related fraction; polyphenols and highly unsaturated compounds dominated the SOM-related fraction whereas unsaturated aliphatic and peptide like compounds were present in a higher fraction in the microbial

Table 2

Absolute and relative abundance of ESI-FT-ICR-MS derived formulae identified as microbial and SOM related. Note: AI < 0.5: non-aromatic, AI > 0.5: aromatic and AI > 0.67: condensed aromatic.

	Microbial in%	SOM-related in %	Microbial absolute	SOM-related absolute
Total formulae			171	706
0 N	46.8	80.6	80	569
1 N	41.5	17	71	120
2–4 N	11.7	2.4	20	17
AI ≤ 0.5	87.1	75.2	149	531
0.5 < AI < 0.67	5.8	14.2	10	100
AI ≥ 0.67	7.1	10.6	12	75

extract (Fig. 2E–F, Table S1). The mass:charge ratio (m/z) provides an indication of the MW of the microbial compounds because they were singly charged, which allowed us to investigate the molecular size to structure relationship. Most of the microbial formulae with higher m/z ratio were devoid of N and fell in the van Krevelen space

for lipids, whereas those with relatively lower m/z ratio contained 1–2 N and fell in the protein and/or amino sugar van Krevelen space (Fig. 2A–D). SOM-related formulae with higher molecular weight fell in the lignin and tannin van Krevelen space where those on the lower range were widely distributed across the van Krevelen diagram.

3.3. SEC-HPLC-IRMS

When used in combination with stable carbon isotope analysis the CFE fraction can be used to track the source of microbial carbon. Fumigated and non-fumigated DOM separated using SEC was assigned into three size classes (Fig. S3) consistent with those used for SEC-HPLC-FTIR results: less than 408 Da (LMW/low MW), 408–2072 Da (MMW/mid MW) and 2072–10510 Da (HMW/high MW). ^{13}C enrichment in microbial compound size classes was estimated from the $\delta^{13}\text{C}$ values of fumigated and non-fumigated DOM size classes using a mass balance. ^{13}C enrichment in all size classes was highest immediately after the pulse labeling of plants

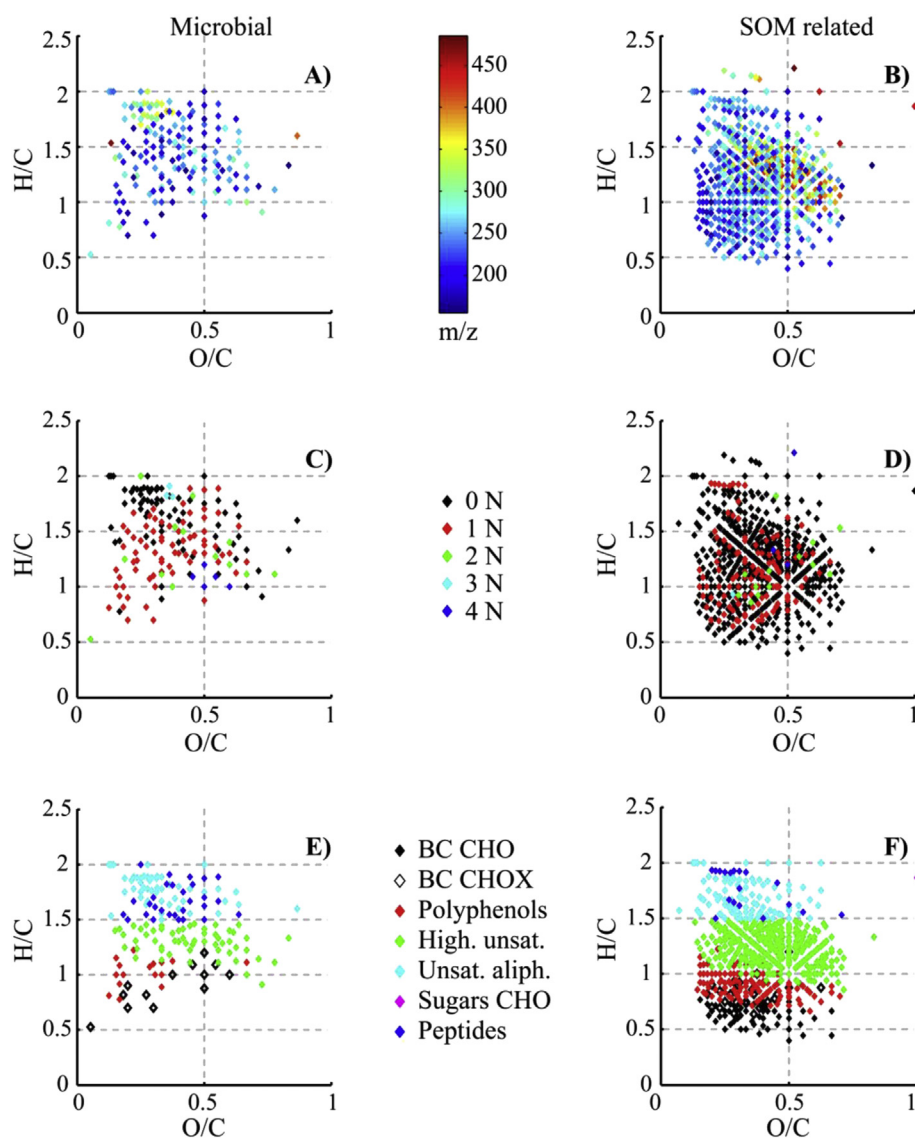


Fig. 2. Van Krevelen plots of ESI-FT-ICR-MS derived formulae over molecular weight (A,B), number of nitrogen (C,D) and compound classes (E,F) that are microbial- (unique to or in higher abundance in fumigated extracts) or soil organic matter (SOM) related (unique to or in higher abundance in non-fumigated extracts). van Krevelen diagrams plot the H/C (hydrogen/carbon) of each assigned molecular formula against its O/C (oxygen/carbon).

and remained so for at least 12 h after the pulse (Fig. 3). Among the size classes, highest enrichment was measured in the LMW fraction and it decreased with increasing MW. The mean $\Delta\delta^{13}\text{C}$ of LMW, MMW and HMW microbial compounds 1 h after pulse labeling was 151 ± 48.9 , 107.2 ± 16.5 and $81 \pm 29.9\%$; it decreased to 28.7 ± 8.1 , 29.3 ± 4.8 and $17.1 \pm 6.7\%$ by the final sampling point 4 weeks after pulse labelling. The ^{13}C enrichment was fitted into an exponential decay function and the fitted degradation rate constant (k) was used to calculate the turnover time of microbial compound size classes (Fig. 3). Empirical C turnover time was estimated at 12.8 ± 0.6 , 18.5 ± 0.6 and 22.9 ± 0.7 days for LMW, MMW and HMW size classes, respectively (Table 3).

4. Discussion

Chloroform fumigation extraction (CFE) is a widely used technique to quantify soil microbial biomass and although the

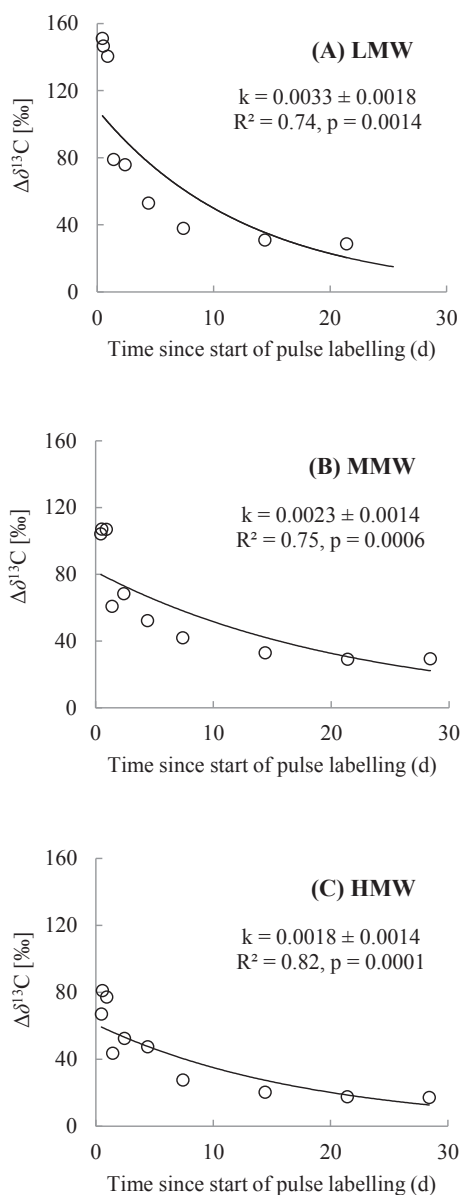


Fig. 3. ^{13}C isotope incorporation in different microbial size classes ($n = 3$) over the experimental period following $^{13}\text{CO}_2$ pulse labeling of plants (LMW: low molecular weight, MMW: mid molecular weight and HMW: high molecular weight).

Table 3

Estimated turnover time for the different molecular size fractions of soil microbial biomass. Also given is the empirical molecular size range and relative abundance of the size fractions.

Molecular size class	Turnover time (d)	Relative abundance (%)
Low MW (<408 Da)	12.8 ± 0.6	8
Mid MW (408–2072 Da)	18.5 ± 0.6	80.4
High MW (2072–10510 Da)	22.9 ± 0.7	11.6

extraction is incomplete and selective it is the easiest and fastest method of characterising soil microbial biomass. CFE gives lysed cellular components (living microbial biomass) in addition to K_2SO_4 -extractable SOM that includes microbial residues and necromass. Therefore, the non-fumigated extract has to be subtracted from the fumigated one in order to quantify and profile microbial organic matter. The high-resolution analytical tools reported here allowed us to characterize and decipher microbial molecular fingerprints from that of the background SOM. We observed some clear relationships between molecular size and structure of microbial compounds. However, SEC and mass spectrometry measure molecular size using different mechanisms and therefore the size, structure and carbon turnover relationships obtained from these techniques may not be entirely comparable. In addition, the starting material used in the molecular characterization techniques was DOM concentrated through SPE with approximately 60% recovery (Roth et al., 2015), while that used for isotope analyses was unprocessed fumigated and non-fumigated DOM. This means we are missing a fraction of DOM in the molecular characterization analyses.

SEC-HPLC-FTIR analysis revealed that low to mid MW compounds were more oxidised and rich in hydroxyl (OH and C–OH), carbonyl (C=O), amine (C–N), ether or carbohydrates (C–O/C–O–C) and/or carboxyl (COOH) groups suggesting that this is the ‘metabolite fraction’ of the microbial biomass (Baldock et al., 1990). ESI-FT-ICR-MS suggests that lower MW microbial compounds were enriched in N and fell in the peptide and highly unsaturated compounds’ space of van Krevelen analysis and ^{13}C analysis revealed that lower MW compounds have faster turnover. Thus we could conclude that the low MW microbial metabolite fraction consists of fast turnover components often monomers like amino acids, sugars, organic acids and alcohols (Ma et al., 2012). Towards the higher MW range, SEC-HPLC-FTIR observations suggest higher abundance of aliphatic compounds, carbohydrates and phosphate groups indicating the presence of larger cellular biosynthetic components (Simpson et al., 2007). ESI-FT-ICR-MS indicates that mid MW microbial compounds were unsaturated aliphatic compounds, devoid of N and possibly lipid-derived. It is clear from synthesis of data from all three techniques that the majority of microbial compounds were in the mid to high MW range and were polymeric or oligomeric biosynthetic cellular components of lipid, polysaccharide or protein origin (Hart et al., 2013; Spence et al., 2011). SEC-HPLC-IRMS analysis based turnover time estimates suggest that these cellular structural compounds have slower turnover in comparison to the metabolite fraction. These compounds can be degraded into smaller and more oxidised fragments, in agreement with the observation that O-rich functional groups were more abundant in low MW microbial extracts and in bulk SOM. Microorganisms appear to be important contributors of bulk low to mid MW SOM extractable fraction, while bulk high MW SOM seems mostly from plant-derived macromolecules such as lignin and tannin. Through this greenhouse based mesocosm experiment we clearly demonstrate the molecular size and structure relationship to turnover time of microbial compounds. A similar correlation of size and turnover time of microbial compounds has been

previously demonstrated in a C3–C4 vegetation change field experiment on two different soil types and this report validates the earlier results (Malik et al., 2013). However, the turnover time of high MW compounds was 22 days that appears to be rather small in the SOM context (Schmidt et al., 2011). This could mean that CFE microbial biomass is largely labile and/or many high turnover time compounds are not extracted (Malik et al., 2015).

The complementary molecular characterization tools reported here are neither exhaustive nor specific, but they allowed us for the first time to profile the molecular fingerprints of living microbial biomass as well as the SOM that is largely derived from microbial necromass. CFE is a popular technique in soil biology employed to measure microbial biomass, its source, turnover and fate in soil systems. It is often referred to as “quick and dirty” because there is not much information about the molecular composition of the fumigated and non-fumigated extracts. Assuming a strong dominance of microbial-derived material in the fumigated extracts and by constructing differential spectra, the molecular techniques used in this report suggest that CFE derived microbial biomass is largely lipid, carbohydrate and protein derived. This study sheds light on the hitherto unknown molecular characteristics of the CFE extractable soil microbial biomass.

Unique molecular signatures of the extracted SOM were also obtained by focussing on the non-fumigated DOM fraction. SEC-HPLC-FTIR observations suggest that hydroxyl, carboxyl and ester groups were abundant across the MW range in SOM derived extracts. Interestingly, aliphatic compounds, carbohydrates and phosphate groups were less abundant compared to the fumigated fraction. Complementary ESI-FT-ICR-MS analysis supports the lower abundance of aliphatic compounds and furthermore suggests the lack of nitrogen in most molecules detected. It also identified that SOM-related high MW compounds were likely lignin and tannin compounds, indicators of vascular plants. Those on the lower MW range were also lignin and tannin-related but in addition were also identified as lipid, carbohydrate and protein derived, which are all molecular signatures of microbial biomass (Hart et al., 2013; Kelleher et al., 2006; Malik and Gleixner, 2013; Mann et al., 2015; Spence et al., 2011). This overlap suggests contribution of microbial necromass or microbially processed or altered compounds to SOM formation. It is further substantiated by reports about marine sequestration of carbon in bacterial metabolites where a similar overlap between bacterial and surrounding DOM molecular formulae is observed (Lechtenfeld et al., 2015).

The turnover time relationship with molecular size and structure of microbial compounds highlights the importance of cellular biochemistry in determining the microbial contribution to soil C formation. This dependency could be altered in conditions of environmental change as a function of physiological adaptation of soil microorganisms. The latter could lead to change in the balance of microbial anabolic and catabolic processes that is often linked to the capacity of soil microorganisms to regulate the flow of C in soil systems. A more efficient metabolic pathway with higher anabolic fluxes could lead to increased microbial biomass and subsequently higher SOC storage. In this context, the molecular size-turnover time relationship could be useful in understanding the microbial physiological adaptations to climate change and help improving the mechanistic understanding of soil C cycling processes.

Acknowledgements

This truly collaborative project was funded by the Max-Planck-Gesellschaft (MPG)/Max Planck Society, the Natural Science and Engineering Research Council of Canada (NSERC), and the New Brunswick Innovation Foundation (NBIF). We acknowledge Deutsche Forschungsgemeinschaft (DFG)/German Research Foundation

for the PhD fellowship to A.A.M. in the research training group 1257 ‘Alteration and element mobility at microbe–mineral interface’. V.-N. R. received financial support from the foundation “Zwillenberg-Tietz Stiftung” and Deutsche Forschungsgemeinschaft (DFG)/German Research Foundation as part of the collaborative research centre (CRC) 1076 “AquaDiva”. A.A.M. has also received funding from the European Union’s Horizon 2020 research and innovation programme under the Marie Skłodowska-Curie grant agreement No 655240. We thank Steffen Ruelhrow for technical support with stable isotope analyses; Agnes Fastnacht, Karl Kuebler and Iris Kuhlmann for support in establishing the experimental setup and K. Klapproth for technical support with FT-ICR-MS measurements. We also thank the reviewers and the editor for constructive comments that helped improve the manuscript.

Appendix A. Supplementary data

Supplementary data related to this article can be found at <http://dx.doi.org/10.1016/j.soilbio.2016.05.019>.

References

- Baldock, J.A., Oades, J.M., Vassallo, A.M., Wilson, M.A., 1990. Solid-state CP/MAS ¹³C N.M.R. analysis of bacterial and fungal cultures isolated from a soil incubated with glucose. *Aust. J. Soil Res.* 28, 213–225.
- Davis, R., Mauer, L., 2010. Fourier transform infrared (FT-IR) spectroscopy: a rapid tool for detection and analysis of foodborne pathogenic bacteria. In: Méndez-Vilas, A. (Ed.), *Current Research, Technology and Education Topics in Applied Microbiology and Microbial Biotechnology*. FORMATEX, Spain, pp. 1582–1594.
- Dijkstra, P., Ishizu, A., Doucet, R., Hart, S.C., Schwartz, E., Menyailo, O.V., Hungate, B.A., 2006. ¹³C and ¹⁵N natural abundance of the soil microbial biomass. *Soil Biol. Biochem.* 38, 3257–3266. <http://dx.doi.org/10.1016/j.soilbio.2006.04.005>.
- Dittmar, T., Koch, B., Hertkorn, N., Kattner, G., 2008. A simple and efficient method for the solid-phase extraction of dissolved organic matter (SPE-DOM) from seawater. *Limnol. Oceanogr. Methods* 6, 230–235. <http://dx.doi.org/10.4319/lom.2008.6.230>.
- Franzluebbers, A.J., 1999. Introduction to symposium — microbial biomass. *Meas. Role Soil Qual.* 30677, 505–506.
- Gleixner, G., 2013. Soil organic matter dynamics: a biological perspective derived from the use of compound-specific isotopes studies. *Ecol. Res.* 28, 683–695. <http://dx.doi.org/10.1007/s11284-012-1022-9>.
- Hart, K.M., Kulakova, A.N., Allen, C.C.R., Simpson, A.J., Oppenheimer, S.F., Masoom, H., Courtier-Murias, D., Soong, R., Kulakov, L.A., Flanagan, P.V., Murphy, B.T., Kelleher, B.P., 2013. Tracking the fate of microbially sequestered carbon dioxide in soil organic matter. *Environ. Sci. Technol.* 47, 5128–5137. <http://dx.doi.org/10.1021/es3050696>.
- Kelleher, B.P., Simpson, M.J., Simpson, A.J., 2006. Assessing the fate and transformation of plant residues in the terrestrial environment using HR-MAS NMR spectroscopy. *Geochim. Cosmochim. Acta* 70, 4080–4094. <http://dx.doi.org/10.1016/j.gca.2006.06.012>.
- Kim, S., Kramer, R.W., Hatcher, P.G., 2003. Graphical method for analysis of ultrahigh-resolution broadband mass spectra of natural organic matter, the van Krevelen diagram. *Anal. Chem.* 75, 5336–5344. <http://dx.doi.org/10.1021/ac034415p>.
- Kindler, R., Miltner, A., Thullner, M., Richnow, H.-H., Kästner, M., 2009. Fate of bacterial biomass derived fatty acids in soil and their contribution to soil organic matter. *Org. Geochem.* 40, 29–37. <http://dx.doi.org/10.1016/j.orggeochem.2008.09.005>.
- Koch, B.P., Dittmar, T., 2006. From mass to structure: an aromaticity index for high-resolution mass data of natural organic matter. *Rapid Commun. Mass Spectrom.* 20, 926–932. <http://dx.doi.org/10.1002/rcm.2386>.
- Koch, B.P., Dittmar, T., Witt, M., Kattner, G., 2007. Fundamentals of molecular formula assignment to ultrahigh resolution mass data of natural organic matter. *Anal. Chem.* 79, 1758–1763. <http://dx.doi.org/10.1021/ac061949s>.
- Kögel-Knabner, I., 2002. The macromolecular organic composition of Plant and microbial residues as inputs to soil organic matter. *Soil Biol. Biochem.* 34, 139–162. [http://dx.doi.org/10.1016/S0038-0717\(01\)00158-4](http://dx.doi.org/10.1016/S0038-0717(01)00158-4).
- Landry, C., Tremblay, L., 2012. Compositional differences between size classes of dissolved organic matter from freshwater and seawater revealed by an HPLC-FTIR system. *Environ. Sci. Technol.* 46, 1700–1707. <http://dx.doi.org/10.1021/es203711v>.
- Lechtenfeld, O.J., Hertkorn, N., Shen, Y., Witt, M., Benner, R., 2015. Marine sequestration of carbon in bacterial metabolites. *Nat. Commun.* 6, 6711. <http://dx.doi.org/10.1038/ncomms7711>.
- Liang, C., Balseer, T.C., 2011. Microbial production of recalcitrant organic matter in global soils: implications for productivity and climate policy. *Nat. Rev. Microbiol.* 9 <http://dx.doi.org/10.1038/nrmicro2386-c1>, 75–75.

- Liang, C., Cheng, G., Wixon, D.L., Balsler, T.C., 2011. An Absorbing Markov Chain approach to understanding the microbial role in soil carbon stabilization. *Biogeochemistry* 106, 303–309. <http://dx.doi.org/10.1007/s10533-010-9525-3>.
- Ma, J., Ibekwe, A.M., Wang, H., Xu, J., Leddy, M., Yang, C.-H., Crowley, D.E., 2012. Assimilable organic carbon (AOC) in soil water extracts using vibrio harveyi BB721 and its implication for microbial biomass. *PLoS One* 7, e28519. <http://dx.doi.org/10.1371/journal.pone.0028519>.
- Malik, A., Blagodatskaya, E., Gleixner, G., 2013. Soil microbial carbon turnover decreases with increasing molecular size. *Soil Biol. Biochem.* 62, 115–118. <http://dx.doi.org/10.1016/j.soilbio.2013.02.022>.
- Malik, A., Gleixner, G., 2013. Importance of microbial soil organic matter processing in dissolved organic carbon production. *FEMS Microbiol. Ecol.* 86, 139–148. <http://dx.doi.org/10.1111/1574-6941.12182>.
- Malik, A., Scheibe, A., LokaBharathi, P.A., Gleixner, G., 2012. Online stable isotope analysis of dissolved organic carbon size classes using size exclusion chromatography coupled to an isotope ratio mass spectrometer. *Environ. Sci. Technol.* 46, 10123–10129. <http://dx.doi.org/10.1021/es302467y>.
- Malik, A.A., Dannert, H., Griffiths, R.I., Thomson, B.C., Gleixner, G., 2015. Rhizosphere bacterial carbon turnover is higher in nucleic acids than membrane lipids: implications for understanding soil carbon cycling. *Front. Microbiol.* 6, 268. <http://dx.doi.org/10.3389/fmicb.2015.00268>.
- Mann, B.F., Chen, H., Herndon, E.M., Chu, R.K., Tolic, N., Portier, E.F., Roy Chowdhury, T., Robinson, E.W., Callister, S.J., Wullschleger, S.D., Graham, D.E., Liang, L., Gu, B., 2015. Indexing permafrost soil organic matter degradation using high-resolution mass spectrometry. *PLoS One* 10, e0130557. <http://dx.doi.org/10.1371/journal.pone.0130557>.
- Miltner, A., Bombach, P., Schmidt-Brücken, B., Kästner, M., 2012. SOM genesis: microbial biomass as a significant source. *Biogeochemistry* 111, 41–55. <http://dx.doi.org/10.1007/s10533-011-9658-z>.
- Philippot, L., Ritz, K., Pandard, P., Hallin, S., Martin-Laurent, F., 2012. Standardisation of methods in soil microbiology: progress and challenges. *FEMS Microbiol. Ecol.* 82, 1–10. <http://dx.doi.org/10.1111/j.1574-6941.2012.01436.x>.
- Pohlabein, A.M., Dittmar, T., 2015. Novel insights into the molecular structure of non-volatile marine dissolved organic sulfur. *Mar. Chem.* 168, 86–94. <http://dx.doi.org/10.1016/j.marchem.2014.10.018>.
- Reemtsma, T., 2009. Determination of molecular formulas of natural organic matter molecules by (ultra-) high-resolution mass spectrometry. Status and needs. *J. Chromatogr. A* 1216, 3687–3701. <http://dx.doi.org/10.1016/j.chroma.2009.02.033>.
- Roth, V.-N., Dittmar, T., Gaupp, R., Gleixner, G., 2015. The Molecular composition of dissolved organic matter in forest soils as a function of pH and temperature. *PLoS One* 10, e0119188.
- Ryan, M.C., Aravena, R., 1994. Combining C-13 natural-abundance and fumigation extraction methods to investigate soil microbial biomass turnover. *Soil Biol. Biochem.* 26, 1583–1585. [http://dx.doi.org/10.1016/0038-0717\(94\)90101-5](http://dx.doi.org/10.1016/0038-0717(94)90101-5).
- Scheibe, A., Krantz, L., Gleixner, G., 2012. Simultaneous determination of the quantity and isotopic signature of dissolved organic matter from soil water using high-performance liquid chromatography/isotope ratio mass spectrometry. *Rapid Commun. Mass Spectrom.* 26, 173–180. <http://dx.doi.org/10.1002/rcm.5311>.
- Schimel, J.P., Schaeffer, S.M., 2012. Microbial control over carbon cycling in soil. *Front. Microbiol.* 3, 1–11. <http://dx.doi.org/10.3389/fmicb.2012.00348>.
- Schmidt, M.W.I., Torn, M.S., Abiven, S., Dittmar, T., Guggenberger, G., Janssens, I.A., Kleber, M., Kögel-Knabner, I., Lehmann, J., Manning, D.A.C., Nannipieri, P., Rasse, D.P., Weiner, S., Trumbore, S.E., 2011. Persistence of soil organic matter as an ecosystem property. *Nature* 478, 49–56. <http://dx.doi.org/10.1038/nature10386>.
- Seidel, M., Beck, M., Greskowiak, J., Riedel, T., Waska, H., Suryaputra, I.G.N.A., Schnetger, B., Niggemann, J., Simon, M., Dittmar, T., 2015a. Biogeochemistry of dissolved organic matter in an intertidal sandy beach. *Mar. Chem.* 176, 150–163. <http://dx.doi.org/10.1016/j.marchem.2015.08.011>.
- Seidel, M., Yager, P.L., Ward, N.D., Carpenter, E.J., Gomes, H.R., Krusche, A.V., Richey, J.E., Dittmar, T., Medeiros, P.M., 2015b. Molecular-level changes of dissolved organic matter along the Amazon river-to-ocean continuum. *Mar. Chem.* 177, 218–231. <http://dx.doi.org/10.1016/j.marchem.2015.06.019>.
- Simpson, A.J., Simpson, M.J., Smith, E., Kelleher, B.P., 2007. Microbially derived inputs to soil organic matter: are current estimates too low? *Environ. Sci. Technol.* 41, 8070–8076. <http://dx.doi.org/10.1021/es071217x>.
- Six, J., Frey, S.D., Thiet, R.K., Batten, K.M., 2006. Bacterial and fungal contributions to carbon sequestration in agroecosystems. *Soil Sci. Soc. Am. J.* 70, 555–569. <http://dx.doi.org/10.2136/sssaj2004.0347>.
- Sleighter, R.L., Hatcher, P.G., 2007. The application of electrospray ionization coupled to ultrahigh resolution mass spectrometry for the molecular characterization of natural organic matter. *J. Mass Spectrom.* 42, 559–574. <http://dx.doi.org/10.1002/jms.1221>.
- Spence, A., Simpson, A.J., McNally, D.J., Moran, B.W., McCaul, M.V., Hart, K., Paull, B., Kelleher, B.P., 2011. The degradation characteristics of microbial biomass in soil. *Geochim. Cosmochim. Acta* 75, 2571–2581. <http://dx.doi.org/10.1016/j.gca.2011.03.012>.
- Stenson, A.C., Marshall, A.G., Cooper, W.T., 2003. Exact masses and chemical formulas of individual Suwannee river fulvic acids from ultrahigh resolution electrospray ionization Fourier transform ion cyclotron resonance mass spectra. *Anal. Chem.* 75, 1275–1284. <http://dx.doi.org/10.1021/ac026106p>.
- Tate, K.R., Ross, D.J., Feltham, C.W., 1988. A direct extraction method to estimate soil microbial C: effects of experimental variables and some different calibration procedures. *Soil Biol. Biochem.* 20, 329–335. [http://dx.doi.org/10.1016/0038-0717\(88\)90013-2](http://dx.doi.org/10.1016/0038-0717(88)90013-2).
- Throckmorton, H.M., Bird, J.A., Dane, L., Firestone, M.K., Horwath, W.R., 2012. The source of microbial C has little impact on soil organic matter stabilisation in forest ecosystems. *Ecol. Lett.* 15, 1257–1265. <http://dx.doi.org/10.1111/j.1461-0248.2012.01848.x>.
- Tremblay, L., Benner, R., 2006. Microbial contributions to N-immobilization and organic matter preservation in decaying plant detritus. *Geochim. Cosmochim. Acta* 70, 133–146. <http://dx.doi.org/10.1016/j.gca.2005.08.024>.
- Vance, E.D., Brookes, P.C., Jenkinson, D.S., 1987. An extraction method for measuring soil microbial biomass C. *Soil Biol. Biochem.* 19, 703–707. [http://dx.doi.org/10.1016/0038-0717\(87\)90052-6](http://dx.doi.org/10.1016/0038-0717(87)90052-6).



Global Biogeochemical Cycles

RESEARCH ARTICLE

10.1002/2015GB005320

Key Points:

- 184 molecular formulae indicative of riverine inputs (t-Peaks) have been identified
- t-Peaks are correlated with tracers of terrigenous input and observed in multiple rivers worldwide
- t-Peaks revealed injection of terrigenous DOM into deep ocean by meridional overturning circulation

Supporting Information:

- Supporting Information S1

Correspondence to:

P. M. Medeiros,
medeiros@uga.edu

Citation:

Medeiros, P. M., M. Seidel, J. Niggemann, R. G. M. Spencer, P. J. Hernes, P. L. Yager, W. L. Miller, T. Dittmar, and D. A. Hansell (2016), A novel molecular approach for tracing terrigenous dissolved organic matter into the deep ocean, *Global Biogeochem. Cycles*, 30, 689–699, doi:10.1002/2015GB005320.

Received 4 NOV 2015

Accepted 12 APR 2016

Accepted article online 28 APR 2016

Published online 14 MAY 2016

A novel molecular approach for tracing terrigenous dissolved organic matter into the deep ocean

Patricia M. Medeiros¹, Michael Seidel^{1,2}, Jutta Niggemann², Robert G. M. Spencer³, Peter J. Hernes⁴, Patricia L. Yager¹, William L. Miller¹, Thorsten Dittmar², and Dennis A. Hansell⁵

¹Department of Marine Sciences, University of Georgia, Athens, Georgia, USA, ²Research Group for Marine Geochemistry (ICBM-MPI Bridging Group), University of Oldenburg, Oldenburg, Germany, ³Department of Earth, Ocean, and Atmospheric Science, Florida State University, Tallahassee, Florida, USA, ⁴Department of Land, Air, and Water Resources, University of California, Davis, California, USA, ⁵Rosenstiel School of Marine and Atmospheric Science, University of Miami, Miami, Florida, USA

Abstract Marine dissolved organic matter (DOM) contains one of the largest exchangeable organic carbon pools on Earth. Riverine input represents an important source of DOM to the oceans, yet much remains to be learned about the fate of the DOM linking terrestrial to oceanic carbon cycles through rivers at the global scale. Here we use ultrahigh-resolution mass spectrometry to identify 184 molecular formulae that are indicators of riverine inputs (referred to as t-Peaks) and to track their distribution in the deep North Atlantic and North Pacific Oceans. The t-Peaks were found to be enriched in the Amazon River, to be highly correlated with known tracers of terrigenous input, and to be observed in all samples from four different rivers characterized by vastly different landscapes and vegetation coverage spanning equatorial (Amazon and Congo), subtropical (Altamaha), and Arctic (Kolyma) regions. Their distribution reveals that terrigenous organic matter is injected into the deep ocean by the global meridional overturning circulation, indicating that a fraction of the terrigenous DOM introduced by rivers contributes to the DOM pool observed in the deep ocean and to the storage of terrigenous organic carbon. This novel molecular approach can be used to further constrain the transfer of DOM from land to sea, especially considering that Fourier transform ion cyclotron resonance mass spectrometer analysis is becoming increasingly frequent in studies characterizing the molecular composition of DOM in lakes, rivers, and the ocean.

1. Introduction

Marine dissolved organic matter (DOM) contains one of the largest active organic carbon pools on Earth (~662 Pg C), holding greater than 200 times the carbon inventory of marine biomass [Hansell *et al.*, 2009]. The pool is comparable in size to the organic carbon present in forest biomass (~450 Pg C [Pan *et al.*, 2011]) and rivals the size of the atmospheric CO₂ reservoir (~820 Pg C [Walther, 2013]). DOM forms a link between production and decay of organic matter in the oceanic water column [Dittmar and Paeng, 2009], playing a major role in biogeochemical processes and in carbon storage on scales of several thousand years [e.g., Flerus *et al.*, 2011]. Most marine DOM is released from photosynthetic plankton or through heterotrophic transformations occurring in the surface ocean [Carlson and Hansell, 2015], where intense decomposition and cycling of organic matter occur.

Global riverine discharge of organic matter also represents a substantial source of dissolved organic carbon (DOC) to the oceans [Hedges *et al.*, 1997; Raymond and Spencer, 2015], with riverine inputs alone being sufficient to support the turnover of DOC throughout the marine environment [Williams and Druffel, 1987]. The total DOC flux to the ocean is estimated at 250–260 Tg C yr⁻¹ [Hedges *et al.*, 1997; Raymond and Spencer, 2015], with the Amazon River exporting over 29 Tg C yr⁻¹ [Moreira-Turcq *et al.*, 2003; Raymond and Spencer, 2015], or almost 12% of the global riverine DOC flux. The Congo River, the largest in Africa, is the second largest exporter and is responsible for 5% of the global total flux [Coynel *et al.*, 2005]. A large amount of terrigenous DOM is also delivered to the Arctic Ocean [e.g., Amon *et al.*, 2012; Holmes *et al.*, 2012]. Indeed, a disproportionately large fraction of the global river discharge (~10%) is received by the Arctic Ocean [Aagaard and Carmack, 1989; Anderson and Amon, 2015], although it holds only 1% of the global ocean volume [Menard and Smith, 1966; Opsahl *et al.*, 1999]. Recent estimates of pan-Arctic riverine DOC flux to the ocean are in the range of 34–38 Tg C yr⁻¹ [Holmes *et al.*, 2012], although this may be an underestimate because of limited availability of data in northern high-latitude rivers characterized by high DOC yields [Raymond and Spencer, 2015].

Quantitative assessments indicate that despite such large inputs, terrestrial DOM experiences substantial alterations over relatively short time scales [e.g., Benner and Opsahl, 2001; Hernes and Benner, 2003; Hansell

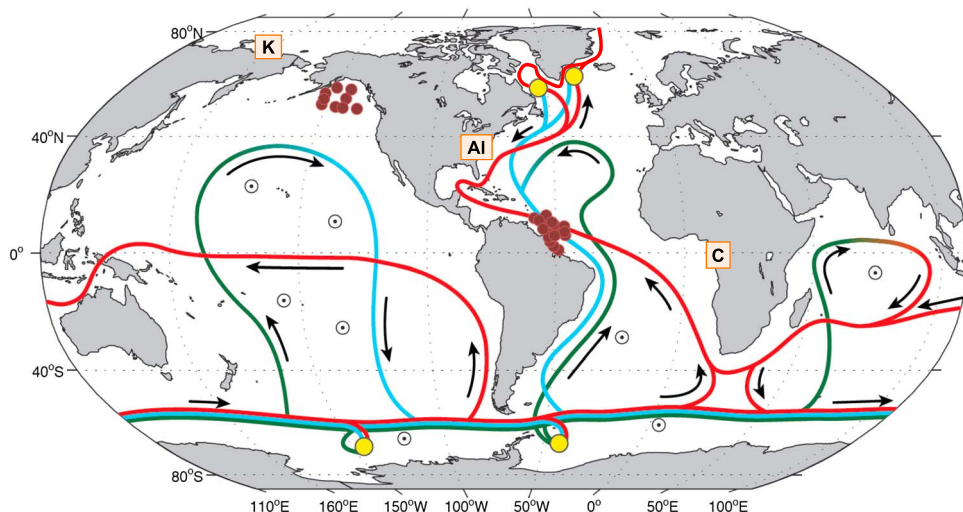


Figure 1. Location of stations where DOM samples were collected during cruises to the tropical North Atlantic and northern North Pacific Oceans. The brown circles show Amazon River, Amazon River plume, surface and deep North Atlantic, and surface and deep North Pacific. AI = Altamaha River [Medeiros *et al.*, 2015c], C = Congo River [Stubbins *et al.*, 2010], K = Kolyma River [Spencer *et al.*, 2015]. Simplified sketch of the meridional overturning circulation [Rahmstorf, 2002] is also shown. Surface flow is shown in red, while deep and bottom flows are sketched in light blue and dark green, respectively. The yellow circles at high latitudes indicate location of deep and bottom water formation. The black circles with dots indicate zones of wind-driven or mixing-driven upwelling [Kuhlbrodt *et al.*, 2007].

et al., 2004; Spencer *et al.*, 2009, 2015], with ocean margins acting as major sinks of terrigenous DOC [Letscher *et al.*, 2011; Fichot and Benner, 2014]. Several processes act as removal mechanisms of terrigenous DOC in the coastal ocean, including photo-oxidation, microbial degradation, and flocculation [e.g., Sholkovitz, 1978; Hernes and Benner, 2003]. Despite that, a fraction of the terrigenous DOC exported from rivers escapes the continental margin [e.g., Medeiros *et al.*, 2015b; Seidel *et al.*, 2015] and is transported to the open ocean, where it can be incorporated into the large scale ocean circulation, including deepwater formation. Terrigenous DOC of Arctic origin has been identified in North Atlantic Deep Water (NADW) [Benner *et al.*, 2005; Hernes and Benner, 2006], and lignin phenols, unique components of vascular terrestrial plants, have been observed in the deep Atlantic and Pacific Oceans [e.g., Opsahl and Benner, 1997; Hernes and Benner, 2002]. More recently, Follett *et al.* [2014] showed that $\delta^{13}\text{C}$ values of deep DOC have a range of at least 10‰, allowing for significant contributions from terrestrial organic matter. DOC exported to great depths can remain in the deepest portions of the ocean for many centuries, potentially contributing to carbon storage and sequestration of atmospheric CO_2 at those time scales.

Understanding transfer of organic matter from land to sea is an important link in the global carbon cycle. $\delta^{13}\text{C}$ values have been used to differentiate between terrigenous and marine sources in DOC samples [e.g., Bianchi *et al.*, 2004; McCallister *et al.*, 2006; Griffith *et al.*, 2012; Lalonde *et al.*, 2014; Medeiros *et al.*, 2015b]. However, stable carbon isotopic compositions alone may be insufficient to resolve a minor terrigenous component of marine DOM [Opsahl and Benner, 1997]. In those cases, integrating additional tracers of terrigenous DOM (e.g., lignin) is useful. Since Fourier transform ion cyclotron resonance mass spectrometer (FT-ICR MS) analysis is becoming increasingly frequent in studies characterizing the molecular composition of DOM in lakes, rivers, and the ocean [e.g., Sleighter and Hatcher, 2008; Kujawinski *et al.*, 2009; Sleighter *et al.*, 2010; Stubbins *et al.*, 2010; Flerus *et al.*, 2012; Hertkorn *et al.*, 2013; Kellerman *et al.*, 2014; Lechtenfeld *et al.*, 2014; Osterholz *et al.*, 2014; Medeiros *et al.*, 2015a, 2015b, 2015c], it is constructive to identify molecular formulae that can be potentially used to track the distribution of terrigenous material in the ocean.

The composition of DOM in the Amazon River-ocean continuum has been recently analyzed using FT-ICR MS [Medeiros *et al.*, 2015b]. Principal component analysis revealed a robust pattern of variability in DOM composition differentiating riverine and marine DOM, which was observed in three different years capturing both high and low discharge conditions. Here we build on Medeiros *et al.* [2015b] and compared the composition of DOM in the tropical North Atlantic and in the northern North Pacific Oceans to identify and track the

distribution of riverine inputs to the deep ocean. Samples from the North Atlantic captured both the surface and deep branches of the meridional overturning circulation [Rahmstorf, 2002] (Figure 1). Our sampling allowed for the characterization of DOM under direct influence of a large river plume (i.e., from the Amazon River [Medeiros et al., 2015b]), as well as of deep DOM in the NADW, a few decades after deepwater formation [Smethie et al., 2000]. After circumnavigating Antarctica, the bottom water runs northward in the Pacific Ocean [Rahmstorf, 2002]. Samples from the northern North Pacific Ocean allow for the characterization of very old DOM that has not been exposed to the ocean surface for at least 1000 years [Primeau, 2005], and thus represent an extreme end-member to examine persistence of riverine DOM inputs.

2. Methods

2.1. Sample Collection

DOM samples were collected in the tropical North Atlantic Ocean ($n = 101$) during research cruises to the Amazon River plume in 2010, 2011, and 2012 [Medeiros et al., 2015b; Seidel et al., 2015] and in the northern North Pacific Ocean ($n = 70$) during a research cruise to the Gulf of Alaska in August 2013 [Medeiros et al., 2015a] (Figure 1). At each station, samples were collected from the surface to depths of 2000 m in the North Atlantic and to as deep as 5040 m in the North Pacific. Immediately after collection, samples were filtered (sequentially through 0.7 μm Whatman GF/F filters precombusted at 450°C for 5 h and prewashed 0.2 μm Pall Supor membrane filters) and aliquots were collected for DOC analysis. Filtrates were acidified to pH 2 (concentrated HCl), and DOM was isolated using solid-phase extraction (SPE) cartridges (Agilent Bond Elut PPL) as in Dittmar et al. [2008].

2.2. Chemical Analyses

DOC concentrations from water samples and solid-phase extracts (i.e., dried and redissolved in ultrapure water) were measured with a Shimadzu TOC-V_{CPH} analyzer with daily potassium hydrogen phthalate (KHP) standard curves and regular analysis of Consensus Reference Materials obtained from the University of Miami [Hansell, 2005]. SPE efficiency was $61 \pm 7\%$ of the DOC for samples collected in the tropical North Atlantic and $58 \pm 6\%$ of the DOC for those collected in the northern North Pacific. Bulk $\delta^{13}\text{C}$ of extracted DOC (SPE-DOC) were analyzed with a Finnigan MAT 251 isotope ratio mass spectrometer after complete drying. All isotopic compositions were expressed relative to the standard Vienna Pee Dee Belemnite. Procedural blanks did not yield detectable amounts of carbon isotope contamination. Lignin phenols of the solid-phase extracts from the North Pacific Ocean were determined by alkaline CuO oxidation [Hedges and Ertel, 1982; Spencer et al., 2008]. Quantification of six lignin phenols was carried out by gas chromatography–mass spectrometry as described by Spencer et al. [2010].

The molecular composition of SPE-extracted DOM (15 mg CL⁻¹ in 1:1 water:methanol) was analyzed by ultrahigh-resolution mass spectrometry using a 15 T Fourier transform ion cyclotron resonance mass spectrometer (FT-ICR MS; Bruker Daltonics) with electrospray ionization (negative mode) as in Seidel et al. [2014]. Spectra were internally calibrated with >100 known C_xH_yO_z molecular formulae over the mass range in the samples. With this calibration procedure, a mass error of <0.1 ppm was achieved. Before each sample set, blank checks with methanol and ultrapure water were measured. Molecular formulae were calculated in the mass range between 150 and 850 Da by applying the following restrictions: ¹²C_{1–130}¹H_{1–200}¹⁶O_{1–150}¹⁴N_{0–4}³²S_{0–2}³¹P_{0–2}. Assignment of molecular formulae was done considering a maximum mass error of 0.5 ppm and using the criteria described by Rossel et al. [2013]. Only compounds with a signal-to-noise ratio of 4 or higher were used in the analysis to eliminate intersample variability based on peaks that were close to the limit of detection [Seidel et al., 2014]. Much of the global DOM pool is composed of a huge variety of relatively small molecules (200–800 Da [e.g., Kujawinski, 2011; Dittmar and Stubbins, 2014]), which are efficiently captured by the technique [Dittmar and Paeng, 2009]. Approximately 4000 molecular formulae were identified in the complex DOM mixture in each sample. As in previous studies [e.g., Flerus et al., 2012; Lechtenfeld et al., 2014], FT-ICR MS data evaluation was based on normalized peak magnitudes.

2.3. Tracers of Terrigenous Inputs in the Ocean

2.3.1. Molecular Formulae Indicator of Riverine Inputs (t-Peaks)

Medeiros et al. [2015b] identified a set of molecular formulae that were relatively enriched at the Amazon River mouth DOM (salinity $S = 0$) compared to the DOM from samples collected over the shelf and in the open ocean.

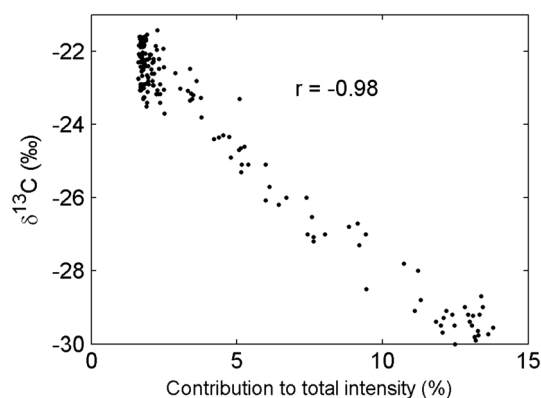


Figure 2. Scatterplot of percentage contribution of t-Peaks to the sum of the magnitude of all peaks with molecular formula assigned in FT-ICR MS spectra versus bulk $\delta^{13}\text{C}$ SPE-DOC for all 171 samples analyzed in this study.

In the Amazon River-ocean continuum, the relative abundances of those formulae were highly correlated negatively (significant at the 95% confidence level) with bulk $\delta^{13}\text{C}$ SPE-DOC and positively with concentrations of dissolved lignin phenols (unambiguous tracers of vascular plant derived organic matter) and dissolved black carbon (dissolution products of thermogenic DOM produced on land during biomass burning and subsequently delivered to the sea [Jaffé *et al.*, 2013]), suggesting that their distribution is related to gradients in DOM associated with terrigenous versus oceanic inputs [Medeiros *et al.*, 2015b].

The Amazon River is thought to be representative of tropical rivers and rivers draining forested catchments [Hedges *et al.*, 1997], with total organic carbon content, DOC/particulate organic carbon

ratio and suspended sediment load near global averages for large rivers [Meybeck, 1982]. However, since we are interested in molecular formulae that are broadly related to terrigenous input (i.e., not only from the Amazon River), we looked for those that were observed not only in all samples from the Amazon River mouth [Medeiros *et al.*, 2015b], but also in FT-ICR MS spectra of samples from other rivers worldwide that have been reported in the literature. We found a total of 184 molecular formulae (Table S1) that were observed in all samples from the Amazon River (riverine collections occurred in three different years covering both high and low discharge conditions [Medeiros *et al.*, 2015b]), from the Congo River in the equatorial Africa (see Supporting Table of Stubbins *et al.* [2010]), from the Kolyma River in the Siberian Arctic (see Table S1 of Spencer *et al.* [2015]), and in all samples collected in the Altamaha River in the southeastern U.S. [Medeiros *et al.*, 2015c], which covered different seasons in multiple years and included a severe drought as well as a high-discharge event. Although it is not possible to affirm that these 184 formulae have a terrigenous source based on FT-ICR MS analysis alone, we emphasize that their relative abundances were enriched in the Amazon River [Medeiros *et al.*, 2015b] and that they were observed in all samples from four rivers with drastically different landscapes and vegetation coverage, spanning equatorial (Amazon and Congo Rivers), subtropical (Altamaha River), and Arctic (Kolyma River) regions. We also note that the aromaticity index (a measure of the aromaticity of the molecules [Koch and Dittmar, 2006, 2016]) of these 184 molecular formulae is high at 0.53 ± 0.10 (Table S1 and Figure S1 in the supporting information). This value is consistent with these formulae being indicators of riverine inputs, since rivers are known to be important sources of polycyclic aromatic compounds to the ocean [e.g., Mannino and Harvey, 2004; Stubbins *et al.*, 2010; Ziolkowski and Druffel, 2010]. Lastly, the percent contribution of these molecular formulae to the sum of the magnitude of all peaks with a molecular formula assigned in the FT-ICR MS spectrum in each sample analyzed in this study is highly correlated with bulk $\delta^{13}\text{C}$ SPE-DOC (Figure 2). As such, we assess these 184 molecular formulae as plausibly indicative of riverine inputs, referring to them hereafter as t-Peaks, where t-Peaks are formulae taken to be of terrigenous origin.

2.3.2. An Additional Metric of Terrigenous Input to the Ocean

Although the t-Peaks were observed in four rivers from vastly different regions, we cannot affirm at this point that these formulae are observed in other rivers worldwide. It is possible that as samples from other rivers are analyzed, the list of formulae indicative of riverine inputs will be further constrained. It is useful therefore to use an additional metric to further constrain terrigenous input to the ocean based on FT-ICR MS analysis.

We used an approach analogous to that presented by Flerus *et al.* [2012], who computed the degradation state of DOM based on the normalized intensity of FT-ICR MS peaks. Specifically, they selected five formulae with a particularly high positive correlation and five formulae with a particularly high negative correlation with $\Delta^{14}\text{C}$ SPE-DOC. They found that although the absolute value of the ratio of the sum of the magnitudes of those peaks is dependent on instrument and extraction technique, samples processed similarly allow for consistent and comparable results. Here since the interest was to identify the potential influence of compounds of terrigenous origin, we computed the correlations between the normalized intensity of FT-ICR-MS peaks and bulk $\delta^{13}\text{C}$ SPE-DOC. Specifically, we selected only molecular formulae that were observed

in all 171 samples from the North Atlantic and North Pacific (there are a total of 1122 such formulae) and computed the correlation between their relative abundance and the bulk $\delta^{13}\text{C}$ SPE-DOC of each sample. This yielded 1122 correlation coefficients, one associated with each molecular formula. We then selected the 40 formulae with the highest negative correlation (i.e., formulae relatively enriched in samples characterized by lighter $\delta^{13}\text{C}$ values; *Terr*) that are also part of the pool of 184 t-Peaks, and the 40 formulae with the highest positive correlation (i.e., formulae relatively enriched in samples characterized by heavier $\delta^{13}\text{C}$ values; *Mar*) that are also part of the “island of stability” (a set of 361 molecular formulae associated with dissolved organic compounds with the most stable combination of elements, i.e., compounds with very long residence time because they are mostly chemically invariant to degradation processes [Lechtenfeld *et al.*, 2014]) (Table S2 and Figure S2). The ratio of the sum of the normalized intensity of these FT-ICR MS peaks (sum magnitudes *Terr*/sum magnitudes (*Terr* + *Mar*); referred to as I_{Terr}) was then calculated for each sample. The rationale for selecting molecular formulae that are part of the t-Peaks and part of the island of stability is that since these formulae are widely observed in riverine and oceanic samples analyzed by FT-ICR MS, they are suitable to be implemented in a versatile index (Table S2).

In theory, the ratio I_{Terr} should increase with the terrigenous signature of the sample. To evaluate that, we compared the ratio I_{Terr} with other geochemical tracers known to be influenced by gradients in organic matter source. The ratio is (by design) highly correlated negatively with bulk $\delta^{13}\text{C}$ SPE-DOC ($r = -0.97$, $p < 0.001$). Additionally, the ratio is highly correlated ($r = 0.98$, $p < 0.001$) with the percentage of molecular formulae in each sample that have condensed aromatic structures in the molecule (i.e., compounds with aromaticity index ≥ 0.67 [Koch and Dittmar, 2006, 2016], consistent with higher concentrations of aromatic compounds in rivers. Lastly, we correlated the ratio with independent measurements of dissolved black carbon in the Atlantic Ocean samples that have been previously reported by Medeiros *et al.* [2015b], since rivers are important sources of dissolved black carbon to the oceans [e.g., Dittmar and Paeng, 2009; Jaffé *et al.*, 2013; Stubbins *et al.*, 2015]. Correlations were once again high and statistically significant ($r = 0.96$, $p < 0.001$). We note that if the constraints described in the last paragraph are not used (i.e., if we do not require that the molecular formulae used in the computation of the index be part of the t-Peaks or of the island of stability) and we instead simply choose the 40 molecular formulae with the highest negative and positive correlation with $\delta^{13}\text{C}$ values, results are similar to those just described.

For several analyses presented here, samples were grouped according to their location: Amazon River mouth (R; salinity $S = 0$), Amazon River plume (P; $10 < S < 34$), surface tropical North Atlantic (sNA; $S > 34$, depth < 100 m), deep tropical North Atlantic (dNA; depth > 1000 m), deep northern North Pacific (dNP; depth > 2000 m), and surface northern North Pacific (sNP; depth < 100 m).

3. Results

DOC concentrations varied substantially between the regions. Concentrations were highest in the Amazon River mouth, and progressively decreased from the surface tropical North Atlantic to the deep northern North Pacific (Figure 3), in agreement with previous studies [e.g., Hansell *et al.*, 2009].

3.1. Injection of Terrigenous DOM Into the Deep Ocean

The 184 molecular formulae described in the previous section (t-Peaks) were used to identify and track the presence of terrigenous DOM in the deep ocean. We quantified both their frequency of occurrence (i.e., the fraction of the 184 t-Peaks observed in each sample) as well as their contribution to the total magnitude of all peaks in the spectrum with an assigned molecular formula (i.e., the sum of the relative intensity of all t-Peaks divided by the sum of the relative intensity of all peaks with molecular formula assigned in the spectrum) for each sample. The t-Peaks were observed in all samples from the Amazon River (by definition; Figure 4a), accounting for 13% of the total magnitude of all peaks in the DOM pool (as identified by FT-ICR MS) in those samples (Figure 4b). Approximately 70% of the t-Peaks were also observed in the surface tropical North Atlantic away from the Amazon River plume (Figure 4a), accounting for 2.6% of the total magnitude in the FT-ICR MS spectra (Figure 4b). The percentage of occurrence decreases in the deep North Atlantic to 55%, and about 35% of the molecular formulae are still observed in the deep northern North Pacific Ocean (Figure 4a). A similar pattern is observed for their relative contribution to the total magnitude of all peaks in the DOM (Figure 4b). We emphasize that the t-Peaks were observed in multiple rivers worldwide, including one from the Arctic. Since

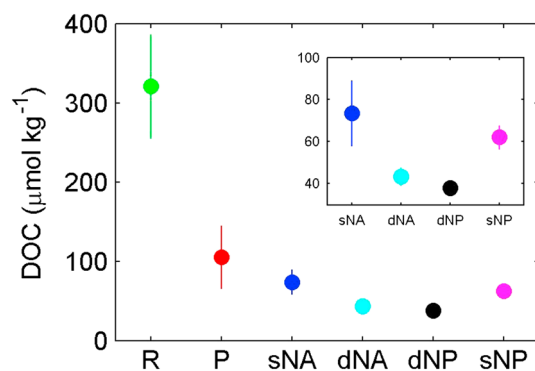


Figure 3. Distribution of average ± 1 standard deviation of dissolved organic carbon at different stages of the meridional overturning circulation. In some cases, standard deviation bars are smaller than the size of the symbols. Inset shows magnified DOC concentrations. R: Amazon River, P: Amazon River plume, sNA: surface North Atlantic, dNA: deep North Atlantic, dNP: deep North Pacific, sNP: surface North Pacific.

Arctic inputs contribute to the terrigenous signature in the deep North Atlantic [e.g., Benner *et al.*, 2005; Hernes and Benner, 2006], the presence of some of these molecular formulae in the deep ocean is likely to result from Arctic riverine inputs.

A pattern similar to that described for the t-Peaks was also observed for the distribution of bulk $\delta^{13}\text{C}$ SPE-DOC (Figure 4c) and for the ratio I_{Terr} (Figure 4d). Altogether, the progressive decreases in the percentage of occurrence of the t-Peaks (Figure 4a) and in their relative contribution to the total magnitude of all peaks in the DOM (Figure 4b), as well as the shift toward heavier $\delta^{13}\text{C}$ values (Figure 4c) and the decrease in the ratio I_{Terr} (Figure 4d) along the different stages of the overturning circulation captured by our sampling are consistent with the export of these compounds to the ocean by rivers and slow transformation, degradation, and/or dilution.

Despite the conservative approach used here to identify the t-Peaks (see section 2.3.1), we cannot rule out the possibility of nonterrigenous sources using FT-ICR MS data alone. Therefore, it is instructive to compare the patterns described above to the distribution of lignin. Lignin-derived phenol concentrations are generally higher in the deep North Atlantic than in the deep North Pacific [Opsahl and Benner, 1997; Hernes and Benner, 2006]. This appears to reflect the disproportionately larger share of global riverine discharge into the Atlantic relative to the Pacific [Opsahl and Benner, 1997], which amounts to a 3.6-fold higher input to the Atlantic on a *per volume* basis [Sverdrup *et al.*, 1942; Baumgartner and Reichel, 1975], and large-scale circulation patterns (i.e., deepwater formation in the North Atlantic, which can directly contribute to the injection of terrigenous organic matter into

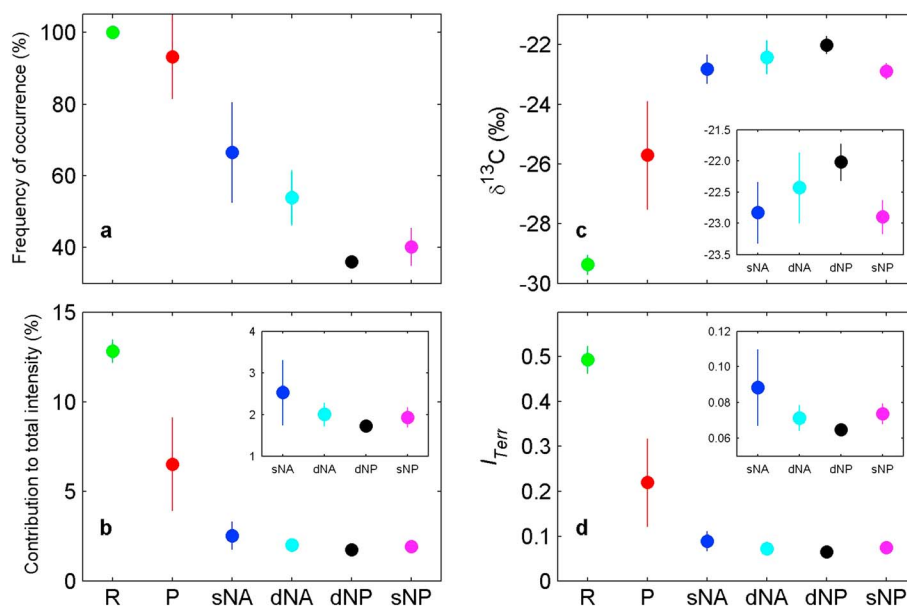


Figure 4. Distribution of average ± 1 standard deviation of (a) percentage of t-Peaks present in each region and (b) their percentage contribution to the sum of the magnitude of all peaks in FT-ICR MS spectra. (c) Bulk $\delta^{13}\text{C}$ SPE-DOC and (d) I_{Terr} , the ratio of relative abundance of molecular formulae negatively correlated with $\delta^{13}\text{C}$ (*Terr*) and the sum of the relative abundance of formulae negatively and positively correlated with $\delta^{13}\text{C}$ (*Terr* + *Mar*). In some cases, standard deviation bars are smaller than the size of the symbols. Insets show magnification of values for Atlantic and Pacific Ocean samples. R: Amazon River, P: Amazon River plume, sNA: surface North Atlantic, dNA: deep North Atlantic, dNP: deep North Pacific, sNP: surface North Pacific.

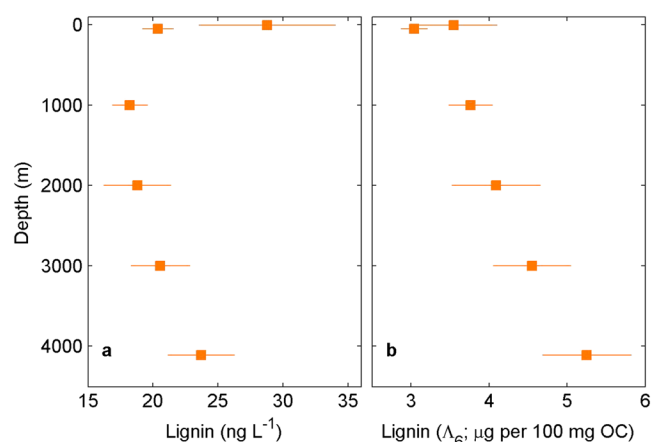


Figure 5. Vertical profiles of average ± 1 standard deviation of (a) dissolved lignin phenol concentration and (b) dissolved carbon-normalized lignin yields (A_6) in the northern North Pacific Ocean.

the deep ocean [Benner *et al.*, 2005]). The contribution of the t-Peaks is consistent with that being more significant in the deep tropical North Atlantic than in the deep northern North Pacific (Figures 4a and 4b). It is possible that the molecular formulae observed in the deep North Pacific are a result of direct vertical export (as sinking particles) from the surface North Pacific. The distribution of lignin in the North Pacific Ocean does not seem to support that interpretation, however. At the study site, far from the coast, dissolved lignin was relatively enriched near the bottom and near the surface, reaching a local minimum at about 1000 m below the surface (Figure 5a), which seems to be inconsistent with the interpretation that terrigenous material at depth is a result of direct vertical export from surface waters. Normalizing lignin concentrations by the amount of organic carbon (Figure 5b) also suggests a relative enrichment at depth compared to the upper water column in the North Pacific. Collectively, these results indicate that at least a fraction of the compounds associated with the t-Peaks reaches the deep northern North Pacific via the large-scale overturning circulation.

4. Discussion

A set of 184 molecular formulae has been identified here as plausible indicators of riverine carbon inputs (t-Peaks) to the ocean, based on their occurrence in four rivers spanning vastly different regions and on their correlation with known tracers of terrigenous input. However, mass spectrometric data suggest that a large set of compounds is ubiquitous in the marine environment. This is because they are the remainder of intensive degradation processes, and as such their composition and structure appear to be largely independent of their source [Reemtsma *et al.*, 2008]. This is consistent with the concept of the island of stability, a set of 361 molecular formulae associated with dissolved organic compounds having the most stable combination of elements that are widely observed in the marine environment [Lechtenfeld *et al.*, 2014]. Therefore, an alternative explanation for the occurrence of the t-Peaks in all samples from four different rivers is that these formulae could be associated with molecules that are quite stable, being observed in nearly all aquatic samples. That explanation does not seem to hold, however, since most of these molecular formulae were not observed in the deep ocean (see Figure 4a and section 3.1 for details). Additionally, the t-Peaks have different chemical characteristics from the formulae identified as the most stable in marine DOM (i.e., the island of stability) by Lechtenfeld *et al.* [2014]. While the molecular formulae from the island of stability have relatively high H/C ratios (1.17 ± 0.13) and low aromaticity indices (0.27 ± 0.09), the t-Peaks have high aromaticity indices (0.53 ± 0.10) and low H/C ratios (0.86 ± 0.14) (Figure S1). Terrigenous DOM has indeed been characterized by low H/C ratios [Sleighter and Hatcher, 2008]. There is no overlap between molecular formulae from the island of stability and the t-Peaks.

Although the distributions shown in Figure 4 are consistent with injection of terrigenous organic matter found in multiple rivers worldwide into the deep ocean by the overturning circulation, there are alternative explanations for the fact that some of the t-Peaks are observed at depth. First, although the compounds observed at depth have the same molecular formulae as those observed in the rivers, it is possible that they may have different structures and therefore are not the same compounds. Additionally, it is possible that although their relative abundance are correlated with concentrations of lignin phenols, dissolved black carbon, and $\delta^{13}\text{C}$ SPE-DOC [Medeiros *et al.*, 2015b] (see also Figures 2 and 4c), they may have additional nonterrigenous sources in the marine environment, which could explain their presence in the deep North Atlantic and deep North Pacific Oceans. If marine DOM contains compounds with these same formulae, however, some mechanism must be invoked to explain why they make a more important contribution to

the DOM pool in the deep North Atlantic than in the deep North Pacific. In other words, if the majority of the t-Peaks are in reality not characteristic of terrigenous input, but instead are widely present in marine DOM, why do they have a distribution that is consistent with the distribution of $\delta^{13}\text{C}$ SPE-DOC and of lignin phenols (as reported by *Opsahl and Benner* [1997]) in the ocean? Another alternative explanation is that the t-Peaks may have multiple sources and result from intense degradation/transformation processes. This scenario seems unlikely, however, since in that case one would expect their relative importance to be larger in the older DOM observed in the North Pacific than in the relatively younger DOM from the North Atlantic. As mentioned previously, there is no overlap between the t-Peaks and the molecular formulae recently reported to be extremely resistant to degradation (i.e., from the island of stability [*Lechtenfeld et al.*, 2014]), and those two pools have distinctive chemical characteristics (Figure S1). Therefore, despite the lack of structural information to unequivocally demonstrate that the molecules found in the deep North Pacific are the same as the t-Peaks and to demonstrate that they have a terrigenous origin, that interpretation is consistent with injection of terrigenous DOM into the deep ocean by the large-scale overturning circulation and with the distributions of bulk $\delta^{13}\text{C}$ SPE-DOC and dissolved lignin.

As a cautionary note, we emphasize that the fact that 35% of the t-Peaks are observed in the deep ocean (Figure 4a) does not mean that one third of the terrigenous material introduced into the ocean by rivers reaches the deep ocean. Since one of the criteria for identifying the t-Peaks was that they had to be present in all samples from four different large rivers, it is possible that a bias toward selecting formulae associated with compounds that are more resistant to degradation was introduced. This is because molecular formulae associated with riverine compounds that are highly resistant to degradation are more likely to be observed in multiple rivers than molecular formulae associated with riverine compounds that are highly degradable. If this is true, then the terrigenous pool represented by the t-Peaks (Figures 4a and 4b and Table S1) is likely more resistant to degradation than the terrigenous DOM pool as a whole.

The approach used here to identify the t-Peaks is very conservative, since it required formulae to have a relative abundance enriched in the Amazon River and be present in all samples from the four different rivers. This means that several molecular formulae may have been excluded solely due to small differences in the analytical procedures used in the different studies. For example, while samples from the Amazon and the Altamaha Rivers were analyzed using the same procedure and resulted in over 4000 molecular formulae being identified in each study [*Medeiros et al.*, 2015b, 2015c], samples from the Congo and the Kolyma Rivers were processed and analyzed slightly differently (e.g., using different magnets in the FT-ICR MS and different maximum mass accuracies), resulting in 2400 and 2000 molecular formulae being identified, respectively. As such, it is likely that many molecular formulae indicative of riverine inputs were not identified in all samples simply because of the different specifications and/or procedures used in these studies.

Riverine DOM can be removed rapidly and efficiently in many coastal regions [e.g., *Hedges et al.*, 1997; *Hernes and Benner*, 2003; *Fichot and Benner*, 2014]. The fact that some of the t-Peaks were observed in the deep North Pacific (Figure 4), holding the oldest DOM in the ocean, suggests that a fraction of the terrigenous DOM delivered by rivers may contribute to the DOM pool observed in the deep ocean and to the long-term carbon storage of terrigenous organic matter. As compounds associated with the t-Peaks are degraded during their transit in the deep ocean, it is possible that at least some of them are transformed to a more refractory state. In this case, their molecular formulae may not be recognizable as riverine in origin, but they contribute to a more stable DOM pool. To the extent that such transformations occur, they would contribute to the storage of terrigenous material on time scales much longer than that of the meridional overturning circulation.

The input of terrigenous DOM to the ocean can be and has been investigated using other tracers (e.g., lignin phenol concentrations, $\delta^{13}\text{C}$ values, and spectral slope of UV absorbance at certain wavelength bands [e.g., *Opsahl and Benner*, 1997; *Dittmar et al.*, 2006; *Fichot and Benner*, 2012]). The distribution of the t-Peaks and the ratio I_{terr} provides an additional set of tracers to identify the occurrence of terrigenous material in the ocean. This is especially useful because FT-ICR MS analysis is becoming increasingly frequent in studies characterizing the molecular composition of DOM in lakes, rivers, and the ocean [e.g., *Sleighter and Hatcher*, 2008; *Kujawinski et al.*, 2009; *Sleighter et al.*, 2010; *Stubbins et al.*, 2010; *Flerus et al.*, 2012; *Hertkorn et al.*, 2013; *Kellerman et al.*, 2014; *Lechtenfeld et al.*, 2014; *Osterholz et al.*, 2014; *Medeiros et al.*, 2015a, 2015b, 2015c]. Several of these studies were not designed to identify the presence of terrigenous DOM in the environment, and as such simultaneous measurements of specific tracers of terrigenous input (e.g., lignin phenols) were

not undertaken or are not available. Identifying the t-Peaks as plausible indicators of riverine inputs creates many new data mining opportunities: extensive FT-ICR MS data sets can be re-analyzed to identify the distribution of the t-Peaks and I_{Terr} , allowing the assessment of the distribution of terrigenous DOM in the environment even when lignin phenol concentrations or $\delta^{13}\text{C}$ values are not available. Similar to lignin [Opsahl and Benner, 1997], the t-Peaks can also be used to resolve a minor terrigenous component of DOM in oceanic waters that may not be detectable by stable carbon isotopic compositions alone.

5. Conclusions

A detailed investigation of DOM at the molecular level was used to identify 184 molecular formulae that are plausible indicators of riverine inputs (t-Peaks). The occurrence and relative abundance of these formulae were statistically significantly correlated with known tracers of terrigenous input, and they were also observed in all samples from four different major rivers characterized by vastly different landscapes and vegetation coverage spanning equatorial, subtropical, and Arctic regions. Tracking the percentage of the occurrence of the t-Peaks and their percentage contribution to the sum of the magnitude of all peaks in FT-ICR MS spectra reveals that terrigenous organic matter is injected into the deep ocean by the global meridional overturning circulation. That picture is consistent with the distribution of $\delta^{13}\text{C}$, dissolved lignin phenols, and I_{Terr} , an independent new ratio of the relative abundance of molecular formulae that have been found to be highly correlated negatively and positively with $\delta^{13}\text{C}$ SPE-DOC. These different tracers collectively indicate that although substantial removal occurs at the ocean surface, a fraction of the terrigenous DOM introduced by rivers worldwide contributes to the DOM pool observed in the deep ocean. Lastly, it is important to note that the 184 t-Peaks were identified based on the analyses of only four rivers (though covering multiple regions, from equatorial to Arctic environments). Therefore, we cannot affirm that those molecular formulae are observed in rivers worldwide or if for some reason those four rivers are unusual for having those formulae. Future investigations of DOM composition in other rivers detecting their presence or further constraining the number of molecular formulae would support their use as indicators of riverine inputs.

Acknowledgments

This research was supported by the Gordon and Betty Moore Foundation (MMI-2293 and 2928), by a University of Georgia Provost Summer Research Grant, and by the National Science Foundation (OCE 1356010, 1237140, 0934095, 1153930, 1234388, 1333157, ANT 1203885, and PLR 1500169). We acknowledge the two anonymous reviewers and the Editor for their thoughtful comments and suggestions that led to a much improved manuscript. We thank the officers and crew of the research vessels *Melville*, *Knorr*, and *Atlantis* for the highly successful operations on board. We also thank Katrin Klaproth for technical assistance with FT-ICR MS runs. The Brazilian government (Ministério da Marinha) is acknowledged for the opportunity to sample in the Brazil EEZ in 2012. Data used to produce the results of this manuscript can be obtained by contacting P.M.M.

References

- Aagaard, K., and E. C. Carmack (1989), Role of sea ice and other fresh water in the Arctic circulation, *J. Geophys. Res.*, *94*(C10), 14,485–14,498, doi:10.1029/JC094iC10p14485.
- Amon, R. M. W., et al. (2012), Dissolved organic matter sources in large Arctic rivers, *Geochim. Cosmochim. Acta*, *94*, 217–237.
- Anderson, L., and R. M. W. Amon (2015), DOC in the Arctic Ocean, 609–633, in *Biogeochemistry of Marine Dissolved Organic Matter*, 2nd ed., edited by D. Hansell and C. Carlson, pp. 693.
- Baumgartner, A., and E. Reichel (1975), *The World Water Balance*, Oldenbourg, Munich.
- Benner, R., and S. Opsahl (2001), Molecular indicators of the sources and transformations of dissolved organic matter in the Mississippi River plume, *Org. Geochem.*, *32*, 597–611.
- Benner, R., P. Louchouart, and R. M. W. Amon (2005), Terrigenous dissolved organic matter in the Arctic Ocean and its transport to surface and deep waters of the North Atlantic, *Global Biogeochem. Cycles*, *19*, GB2025, doi:10.1029/2004GB002398.
- Bianchi, T. S., T. Filley, K. Dria, and P. G. Hatcher (2004), Temporal variability in sources of dissolved organic carbon in the lower Mississippi River, *Geochim. Cosmochim. Acta*, *68*, 959–967.
- Carlson, C. A., and D. A. Hansell (2015), DOM sources, sinks, reactivity and budgets, in *Biogeochemistry of Marine Dissolved Organic Matter*, 2nd ed., edited by D. A. Hansell and C. A. Carlson, pp. 66–126, Academic Press, Elsevier Science, Waltham, Mass.
- Coynel, A., P. Seyler, H. Etcheber, M. Meybeck, and D. Orange (2005), Spatial and seasonal dynamics of total suspended sediment and organic carbon species in the Congo River, *Global Biogeochem. Cycles*, *19*, GB4019, doi:10.1029/2004GB002335.
- Dittmar, T., and A. Stubbins (2014), Dissolved organic matter in aquatic systems, in *Treatise on Geochemistry*, vol. 12, 2nd ed., edited by H. Holland and K. Turekian, pp. 125–156, Elsevier Science.
- Dittmar, T., and J. Paeng (2009), A heat-induced molecular signature in marine dissolved organic matter, *Nat. Geosci.*, *2*, 175–179.
- Dittmar, T., N. Hertkorn, G. Kattner, and R. J. Lara (2006), Mangroves, a major source of dissolved organic carbon to the oceans, *Global Biogeochem. Cycles*, *20*, GB1012, doi:10.1029/2005GB002570.
- Dittmar, T., B. P. Koch, N. Hertkorn, and G. Kattner (2008), A simple and efficient method for the solid-phase extraction of dissolved organic matter (SPE-DOM) from seawater, *Limnol. Oceanogr. Methods*, *6*, 230–235.
- Fichot, C. G., and R. Benner (2012), The spectral slope coefficient of chromophoric dissolved organic matter ($S_{275-295}$) as a tracer of terrigenous dissolved organic carbon in river-influenced ocean margins, *Limnol. Oceanogr.*, *57*, 1453–1466.
- Fichot, C. G., and R. Benner (2014), The fate of terrigenous dissolved organic carbon in a river-influenced ocean margin, *Global Biogeochem. Cycles*, *28*, 300–318, doi:10.1002/2013GB004670.
- Flerus, R., B. P. Koch, P. Schmitt-Kopplin, M. Witt, and G. Kattner (2011), Molecular level investigation of reactions between dissolved organic matter and extraction solvents using FT-ICR MS, *Mar. Chem.*, *124*, 100–107.
- Flerus, R., O. J. Lechtenfeld, B. P. Koch, S. L. McCallister, P. Schmitt-Kopplin, R. Benner, K. Kaiser, and G. Kattner (2012), A molecular perspective on the ageing of marine dissolved organic matter, *Biogeosciences*, *9*, 1935–1955.
- Follett, C. L., D. J. Repeta, D. H. Rothman, L. Xu, and C. Santinelli (2014), Hidden cycle of dissolved organic carbon in the deep ocean, *Proc. Natl. Acad. Sci.*, *111*, 16,706–16,711.

- Griffith, D. R., A. P. McNichol, L. Xu, F. A. McLaughlin, R. W. Macdonald, K. A. Brown, and T. I. Eglinton (2012), Carbon dynamics in the western Arctic Ocean: insights from full-depth carbon isotope profiles of DIC, DOC, and POC, *Biogeosciences*, *9*, 1217–1224.
- Hansell, D. A. (2005), Dissolved organic carbon reference material program, *EOS*, *86*, 318.
- Hansell, D. A., D. Kadko, and N. R. Bates (2004), Degradation of terrigenous dissolved organic carbon in the western Arctic Ocean, *Science*, *304*, 858–861.
- Hansell, D. A., C. A. Carlson, D. J. Repeta, and R. Schlitzer (2009), Dissolved organic matter in the ocean: New insights stimulated by a controversy, *Oceanography*, *22*, 52–61.
- Hedges, J. I., and J. R. Ertel (1982), Characterization of lignin by gas capillary chromatography of cupric oxide oxidation-products, *Anal. Chem.*, *54*, 174–178.
- Hedges, J. I., R. G. Keil, and R. Benner (1997), What happens to terrestrial organic matter in the ocean?, *Org. Geochem.*, *27*, 195–212.
- Hernes, P. J., and R. Benner (2002), Transport and diagenesis of dissolved and particulate terrigenous organic matter in the north Pacific Ocean, *Deep Sea Res., Part I*, *49*, 2119–2132.
- Hernes, P. J., and R. Benner (2003), Photochemical and microbial degradation of dissolved lignin phenols: Implications for the fate of terrigenous dissolved organic matter in marine environments, *J. Geophys. Res.*, *108*(C9), 3291, doi:10.1029/2002JC001421.
- Hernes, P. J., and R. Benner (2006), Terrigenous organic matter sources and reactivity in the North Atlantic Ocean and a comparison to the Arctic and Pacific oceans, *Mar. Chem.*, *100*, 66–79.
- Hertkorn, N., M. Harir, B. P. Koch, B. Michalke, and P. Schmitt-Kopplin (2013), High-field NMR spectroscopy and FTICR mass spectrometry: Powerful discovery tools for the molecular level characterization of marine dissolved organic matter, *Biogeosciences*, *10*, 1583–1624.
- Holmes, R. M., et al. (2012), Seasonal and annual fluxes of nutrients and organic matter from large rivers to the Arctic Ocean and surrounding seas, *Estuaries Coasts*, *35*, 369–382.
- Jaffé, R., Y. Ding, J. Niggemann, A. V. Vähätalo, A. Stubbins, R. G. M. Spencer, J. Campbell, and T. Dittmar (2013), Global charcoal mobilization from soils via dissolution and riverine transport to the oceans, *Science*, *340*, 345–347.
- Kellerman, A. M., T. Dittmar, D. N. Kothawala, and L. J. Tranvik (2014), Chemodiversity of dissolved organic matter in lakes driven by climate and hydrology, *Nat. Commun.*, *5*, doi:10.1038/ncomms4804.
- Koch, B. P., and T. Dittmar (2006), From mass to structure: An aromaticity index for high-resolution mass data of natural organic matter, *Rapid Commun. Mass Spectrom.*, *20*, 926–932.
- Koch, B. P., and T. Dittmar (2016), Erratum: From mass to structure: An aromaticity index for high-resolution mass data of natural organic matter, *Rapid Commun. Mass Spectrom.*, *30*, 250.
- Kuhlbrodt, T., A. Griesel, M. Montoya, A. Levermann, M. Hofmann, and S. Rahmstorf (2007), On the driving processes of the Atlantic meridional overturning circulation, *Rev. Geophys.*, *45*, RG2001, doi:10.1029/2004RG000166.
- Kujawinski, E. B. (2011), The impact of microbial metabolism on marine dissolved organic matter, *Ann. Rev. Mar. Sci.*, *3*, 567–599.
- Kujawinski, E. B., K. Longnecker, N. V. Blough, R. Del Vecchio, L. Finlay, J. B. Kitner, and S. J. Giovannoni (2009), Identification of possible source markers in marine dissolved organic matter using ultrahigh resolution electrospray ionization Fourier-transform ion cyclotron resonance mass spectrometry, *Geochim. Cosmochim. Acta*, *73*, 4384–4399.
- Lalonde, K., A. V. Vähätalo, and Y. Gélinas (2014), Revisiting the disappearance of terrestrial dissolved organic matter in the ocean: A $\delta^{13}\text{C}$ study, *Biogeosciences*, *11*, 3707–3719.
- Lechtenfeld, O. J., G. Kattner, R. Flerus, S. L. McCallister, P. Schmitt-Kopplin, and B. P. Koch (2014), Molecular transformation and degradation of refractory dissolved organic matter in the Atlantic and Southern Ocean, *Geochim. Cosmochim. Acta*, *126*, 321–337.
- Letscher, R., D. A. Hansell, and D. Kadko (2011), Rapid removal of terrigenous dissolved organic carbon over the Eurasian shelves of the Arctic Ocean, *Mar. Chem.*, *123*, 78–87.
- Mannino, A., and H. R. Harvey (2004), Black carbon in estuarine and coastal ocean dissolved organic matter, *Limnol. Oceanogr.*, *49*, 735–740.
- McCallister, S. L., J. E. Bauer, H. W. Ducklow, and E. A. Canuel (2006), Sources of estuarine dissolved and particulate organic matter: A multi-tracer approach, *Org. Geochem.*, *37*, 454–468.
- Medeiros, P. M., M. Seidel, L. C. Powers, T. Dittmar, D. A. Hansell, and W. L. Miller (2015a), Dissolved organic matter composition and photochemical transformations in the northern North Pacific Ocean, *Geophys. Res. Lett.*, *42*, 863–870, doi:10.1002/2014GL062663.
- Medeiros, P. M., M. Seidel, N. D. Ward, E. J. Carpenter, H. R. Gomes, J. Niggemann, A. V. Krusche, J. E. Richey, P. L. Yager, and T. Dittmar (2015b), Fate of the Amazon River dissolved organic matter in the tropical Atlantic Ocean, *Global Biogeochem. Cycles*, *29*, 677–690, doi:10.1002/2015GB005115.
- Medeiros, P. M., M. Seidel, T. Dittmar, W. B. Whitman, and M. A. Moran (2015c), Drought-induced variability in dissolved organic matter composition in a marsh-dominated estuary, *Geophys. Res. Lett.*, *42*, 6446–6453, doi:10.1002/2015GL064653.
- Menard, H. W., and S. M. Smith (1966), Hypsometry of ocean basin provinces, *J. Geophys. Res.*, *71*, 4305–4325, doi:10.1029/JZ071i018p04305.
- Meybeck, M. (1982), Carbon, nitrogen, and phosphorus transport by world rivers, *Am. J. Sci.*, *282*, 401–450.
- Moreira-Turcq, P., P. Seyler, J. L. Guyot, and H. Etcheber (2003), Exportation of organic carbon from the Amazon River and its main tributaries, *Hydro. Process.*, *17*, 1329–1344.
- Opsahl, S., and R. Benner (1997), Distribution and cycling of terrigenous dissolved organic matter in the ocean, *Nature*, *386*, 480–482.
- Opsahl, S., R. Benner, and R. M. W. Amon (1999), Major flux of terrigenous dissolved organic matter through the Arctic Ocean, *Limnol. Oceanogr.*, *44*, 2017–2023.
- Osterholz, H., T. Dittmar, and J. Niggemann (2014), Molecular evidence for rapid dissolved organic matter turnover in Arctic fjords, *Mar. Chem.*, *160*, 1–10.
- Pan, Y., et al (2011), A large and persistent carbon sink on the World's forests, *Science*, *333*, 988–993.
- Primeau, F. (2005), Characterizing transport between the surface mixed layer and the ocean interior with a forward and adjoint global ocean transport model, *J. Phys. Oceanogr.*, *35*, 545–564.
- Rahmstorf, S. (2002), Ocean circulation and climate during the past 120,000 years, *Nature*, *419*, 207–214.
- Raymond, P. A., and R. G. M. Spencer (2015), Riverine DOM, 509–533, in *Biogeochemistry of Marine Dissolved Organic Matter*, 2nd ed., edited by D. Hansell and C. Carlson, pp. 693, Academic Press, Oxford, U. K.
- Reemtsma, T., A. These, M. Linscheid, J. Leenheer, and A. Spitzzy (2008), Molecular and structural characterization of dissolved organic matter from the deep ocean by FTICR-MS, including hydrophilic nitrogenous organic molecules, *Environ. Sci. Technol.*, *42*, 1430–1437.
- Rossel, P. E., A. V. Vähätalo, M. Witt, and T. Dittmar (2013), Molecular composition of dissolved organic matter from a wetland plant (*Juncus effusus*) after photochemical and microbial decomposition (1.25 yr): Common features with deep sea dissolved organic matter, *Org. Geochem.*, *60*, 62–71.
- Seidel, M., M. Beck, T. Riedel, H. Waska, I. G. N. A. Suryaputra, B. Schnetger, J. Niggemann, M. Simon, and T. Dittmar (2014), Biogeochemistry of dissolved organic matter in an anoxic intertidal creek bank, *Geochim. Cosmochim. Acta*, *140*, 418–434.
- Seidel, M., P. L. Yager, N. D. Ward, E. J. Carpenter, H. R. Gomes, A. V. Krusche, J. E. Richey, T. Dittmar, and P. M. Medeiros (2015), Molecular-level changes of dissolved organic matter along the Amazon River-to-ocean continuum, *Mar. Chem.*, *177*, 218–231 doi:10.1016/j.marchem.2015.06.019.

- Sholkovitz, E. R. (1978), The flocculation of dissolved Fe, Mn, Al, Cu, Ni, Co and Cd during estuarine mixing, *Earth Planet. Sci. Lett.*, *41*, 77–86.
- Sleighter, R. L., and P. G. Hatcher (2008), Molecular characterization of dissolved organic matter (DOM) along a river to ocean transect of the lower Chesapeake Bay by ultrahigh resolution electrospray ionization Fourier transform ion cyclotron resonance mass spectrometry, *Mar. Chem.*, *110*, 140–152.
- Sleighter, R. L., Z. Liu, J. Xue, and P. G. Hatcher (2010), Multivariate statistical approaches for the characterization of dissolved organic matter analyzed by ultrahigh resolution mass spectrometry, *Environ. Sci. Technol.*, *44*, 7576–7582.
- Smethie, W. M., Jr., R. A. Fine, A. Putzka, and E. P. Jones (2000), Tracing the flow of North Atlantic Deep Water using chlorofluorocarbons, *J. Geophys. Res.*, *105*, 14,297–14,323, doi:10.1029/1999JC900274.
- Spencer, R. G. M., G. R. Aiken, K. P. Wickland, R. G. Striegl, and P. J. Hernes (2008), Seasonal and spatial variability in dissolved organic matter quantity and composition from the Yukon River Basin, Alaska, *Global Biogeochem. Cycles*, *22*, GB4002, doi:10.1029/2008GB003231.
- Spencer, R. G. M., et al. (2009), Photochemical degradation of dissolved organic matter and dissolved lignin phenols from the Congo River, *J. Geophys. Res.*, *114*, G03010, doi:10.1029/2009JG000968.
- Spencer, R. G. M., G. R. Aiken, R. Y. Dyda, K. D. Butler, B. A. Bergamaschi, and P. J. Hernes (2010), Comparison of XAD with other dissolved lignin isolation techniques and a compilation of analytical improvements for the analysis of lignin in aquatic settings, *Org. Geochem.*, *41*, 445–453.
- Spencer, R. G. M., P. J. Mann, T. Dittmar, T. I. Eglinton, C. McIntyre, R. M. Holmes, N. Zimov, and A. Stubbins (2015), Detecting the signature of permafrost thaw in Arctic rivers, *Geophys. Res. Lett.*, *42*, 2830–2835, doi:10.1002/2015GL063498.
- Stubbins, A., R. G. M. Spencer, H. Chen, P. G. Hatcher, K. Mopper, P. J. Hernes, V. L. Mwamba, A. M. Mangangu, J. N. Wabakghanzi, and J. Six (2010), Illuminated darkness: Molecular signatures of Congo River dissolved organic matter and its photochemical alteration as revealed by ultrahigh precision mass spectrometry, *Limnol. Oceanogr.*, *55*, 1467–1477.
- Stubbins, A., R. Spencer, P. J. Mann, R. M. Holmes, J. H. McClelland, J. Niggemann, and T. Dittmar (2015), Utilizing colored dissolved organic matter to derive dissolved black carbon export by Arctic rivers, *Front. Earth Sci.*, *3*, 63, doi:10.3389/feart.2015.00063.
- Sverdrup, H. U., J. W. Johnson, and R. H. Fleming (1942), *The Oceans*, Prentice-Hall, Englewood Cliffs, N. J.
- Walther, J. V. (2013), Understanding the Earth's natural resources: An introduction, 1–27, in *Earth's Natural Resources*, 1st ed., 428 pp., Jones & Bartlett Learning, Mass.
- Williams, P. M., and E. R. M. Druffel (1987), Radiocarbon in dissolved organic matter in the central North Pacific Ocean, *Nature*, *330*, 246–248.
- Ziolkowski, L. A., and E. R. M. Druffel (2010), Aged black carbon identified in marine dissolved organic carbon, *Geophys. Res. Lett.*, *37*, L16601, doi:10.1029/2010GL043963.



Environmental Drivers of Dissolved Organic Matter Molecular Composition in the Delaware Estuary

Helena Osterholz^{1*}, David L. Kirchman², Jutta Niggemann¹ and Thorsten Dittmar¹

¹ ICBM-MPI Bridging Group for Marine Geochemistry, Institute for Chemistry and Biology of the Marine Environment, Carl von Ossietzky University, Oldenburg, Germany, ² School of Marine Science and Policy, University of Delaware, Lewes, DE, USA

OPEN ACCESS

Edited by:

Nicholas David Ward,
University of Florida, USA

Reviewed by:

Yina Liu,
Pacific Northwest National Laboratory,
USA

Elizabeth Ann Canuel,
Virginia Institute of Marine Science,
USA

*Correspondence:

Helena Osterholz
helena.osterholz@uni-oldenburg.de

Specialty section:

This article was submitted to
Marine Biogeochemistry,
a section of the journal
Frontiers in Earth Science

Received: 26 August 2016

Accepted: 20 October 2016

Published: 17 November 2016

Citation:

Osterholz H, Kirchman DL,
Niggemann J and Dittmar T (2016)
Environmental Drivers of Dissolved
Organic Matter Molecular
Composition in the Delaware Estuary.
Front. Earth Sci. 4:95.
doi: 10.3389/feart.2016.00095

Estuaries as connectors of freshwater and marine aquatic systems are hotspots of biogeochemical element cycling. In one of the best studied temperate estuaries, the Delaware Estuary (USA), we investigated the variability of dissolved organic matter (DOM) over five sampling cruises along the salinity gradient in August and November of 3 consecutive years. Dissolved organic carbon (DOC) concentrations were more variable in the upper reaches of the estuary ($245 \pm 49 \mu\text{mol DOC L}^{-1}$) than at the mouth of the estuary ($129 \pm 14 \mu\text{mol L}^{-1}$). Bulk DOC decreased conservatively along the transect in November but was non-conservative with increased DOC concentrations mid-estuary in August. Detailed analysis of the solid-phase extractable DOM pool via ultrahigh resolution mass spectrometry (Fourier-transform ion cyclotron resonance mass spectrometry, FT-ICR-MS) revealed compositional differences at the molecular level that were not reflected in changes in concentration. Besides the mixing of terrestrial and marine endmember signatures, river discharge levels and biological activity impacted DOM molecular composition. DOM composition changed less between August and November than along the salinity gradient. Relative contributions of presumed photolabile DOM compounds did not reveal non-conservative behavior indicative of photochemical processing, suggesting that on the timescales of estuarine mixing photochemical removal of molecules plays a minor role in the turbid Delaware Bay. Overall, a large portion of molecular formulae overlapped between sampling campaigns and persisted during estuarine passage. Extending the analysis to the structural level via the fragmentation of molecular masses in the FT-ICR-MS, we found that the relative abundance of isomers along the salinity gradient did not change, indicating a high structural similarity of aquatic DOM independent of the origin. These results point toward a recalcitrant character of the DOM supplied by the Delaware River. We demonstrate that in addition to bulk DOC quantification, detailed information on molecular composition is essential for constraining sources of DOM and to identify the processes that impact estuarine DOM, thereby controlling amount and composition of DOM eventually discharged to the ocean through estuaries.

Keywords: dissolved organic matter, Delaware Estuary, FT-ICR-MS, discharge, conservative mixing, seasonal variation, collision-induced fragmentation

INTRODUCTION

Large amounts of terrigenous organic matter are channeled through rivers and estuaries into the oceans—approximately 0.25×10^{15} g are transported in the form of dissolved organic carbon (DOC) annually (Hedges et al., 1997). The true amount of the DOC exported from land is likely higher as some regions (for example northern high-latitude rivers, Holmes et al., 2011), diffuse flows and flood events (Cole et al., 2007; Raymond and Saiers, 2010) are not well constrained to date. During transit, the size and composition of the riverine dissolved organic matter (DOM) pool is transformed through a multitude of biotic and abiotic processes. Despite decades of research on estuarine and coastal DOM cycling, we still lack understanding of the mechanisms and magnitudes of these modifications, thereby possibly resulting in misinterpretation of characteristics of the riverine DOM discharged to the coastal seas and ultimately reaching the deep ocean (Bauer and Bianchi, 2011).

Generally, bulk DOC concentrations decrease along estuaries from the river to the ocean while at the same time, the composition of the DOM pool changes. On molecular level, the aromaticity of the DOM decreases (Abdulla et al., 2013), while molecular weight, carbohydrate content (Abdulla et al., 2010), heteroelement content (Sleighter and Hatcher, 2008) and lability increase (D'Andrilli et al., 2015) with increasing salinity. Positive and negative deviations from a conservative mixing line defined by high-DOC river water and the low-DOC marine endmember are frequently observed (Cadée, 1982; Middelburg and Herman, 2007; Sharp et al., 2009). Estuaries are complex systems where, in addition to mixing of fresh- and marine waters, diffuse sources such as subterranean groundwater discharge (Taniguchi et al., 2002), aeolian and anthropogenic input (Liu et al., 2005; Tzortziou et al., 2015) add to the intricacy of biogeochemical cycling. Abiotic processes shaping the DOM pool along the estuarine gradient of pH, ionic strength and turbidity include the adsorption on and desorption from mineral surfaces (Keil et al., 1994; Mayer, 1994), flocculation (Eisma, 1986), aggregation or precipitation. Loss of organic carbon from the dissolved phase in the estuarine turbidity maximum (e.g., Miller, 1999), where the concentration of particulate organic carbon is usually the highest, is accompanied by a loss in aromaticity and nitrogen-containing compounds, as these compounds are preferentially adsorbed (Aufdenkampe et al., 2001; Riedel et al., 2012). Photodegradation processes, although generally thought to be minor in riverine systems due to the low transmission (Spencer et al., 2009), exhibit the highest impact on aromatic moieties of terrestrial origin (Stubbins et al., 2010). By decreasing the average molecular weight and increasing the contribution of aliphatic compounds, the bioavailability of the DOM can increase through photochemically mediated breakdown of molecules especially in tropical regions (Medeiros et al., 2015b). Biological processes, in temperate regions influenced by seasonality, such as selective uptake and transformation by heterotrophic microbes (Azam et al., 1994; Bourgoin and Tremblay, 2010), as well as addition of compounds via autochthonous production (Pennock and Sharp, 1986) likewise shape the estuarine DOM pool. Medeiros et al. (2015b) for example showed that phytoplankton-derived

DOM inputs introduce saturated compounds in the tropical Amazon plume. DOM export by the Yukon River to the Bering Sea was highly stable over seasons, with enhanced DOM photo- and biolability in spring due to higher inputs of carbohydrates and aromatic moieties (Cao et al., 2016). Previous studies have furthermore shown that the DOC concentration in rivers increases with discharge (Schiff et al., 1998; Raymond and Saiers, 2010), superimposing the influence of most other environmental drivers. At high discharge, riverine DOM composition tends to carry a stronger terrigenous signal (Spencer et al., 2008). A similar observation was made by Medeiros et al. (2015a) who found strong seasonal variability in molecular DOM composition in the marsh-dominated Altamaha-Doboy-Sapelo estuary. This variability was driven mainly by river flow, leading to a stronger terrigenous signature at high discharge.

In our study, we investigate estuarine carbon cycling in the tidal Delaware River and Bay, located on the east coast of the USA. The freshwater flow into the estuary is dominated by the Delaware River, which supplies nearly 60% of the freshwater to the bay; the Schuylkill and other smaller rivers supply another 14% (Sutton et al., 1996). In total, these rivers account for >80% of freshwater input into the estuary. The water column of the Delaware Estuary is usually well-mixed, although stratification can build up near the mouth of the bay, particularly during summer (Garvine et al., 1992). The bay has an estimated flushing time of about 80 to 180 days (Ketchum, 1952; Sharp et al., 1982; Cifuentes et al., 1990). In parts heavily urbanized, its waters carry a high nutrient loading from the Philadelphia area and saline waters reach as far as ~125 km from the mouth (Biggs et al., 1983). The estuary has been extensively monitored over the last 30 years with a focus on carbon and nutrient fluxes (Sharp et al., 2009). Different sources of the DOM and particulate organic matter (POM) have been identified along the estuary: isotope and biomarker studies of ultrafiltered DOM have identified a terrestrial signal in the river and turbid middle estuary transitioning to a more algal and zooplankton-dominated signal in the lower estuary and coastal ocean (Mannino and Harvey, 1999, 2000b). Further compositional changes of the DOM pool have been examined at the level of chemical classes, e.g., total amino acids and polysaccharides (Hoch and Kirchman, 1995; Mannino and Harvey, 2000a; Kirchman and Borch, 2003), which in addition to mixing of marine and terrestrial signatures reveal a seasonal imprint as well as processing in the estuarine turbidity maximum. Of the rivers draining into the Middle Atlantic Bight, the Delaware River however carries a high proportion of allochthonous DOC and aged carbon (Hossler and Bauer, 2013).

We characterized the main drivers of DOM concentration and composition between August and November over 3 years (five sampling cruises) along the salinity gradient of the Delaware estuary, thereby allowing inferences about the modified terrestrial signal ultimately reaching the Atlantic Ocean. In addition to bulk DOC concentrations, we assessed the compositional variation of solid-phase extractable (SPE) DOM using ultrahigh resolution mass

spectrometry (Fourier-Transform Ion Cyclotron Resonance Mass Spectrometry, FT-ICR-MS), which allowed the assignment of thousands of different molecular formulae to a water sample (Stenson et al., 2003; Koch et al., 2005, 2007). Further, we applied collision-induced fragmentation to reveal possible structural changes within the SPE-DOM pool along the salinity gradient that might be hidden on molecular formula level. The different levels of analytical resolution provided unprecedented insight into the DOM cycling in the Delaware estuary. Overall, we used the new opportunities presented by FT-ICR-MS to build on the previous body of work in the Delaware and other study systems and to gain a more detailed understanding of DOM at the molecular level.

MATERIALS AND METHODS

Site Description and Sample Collection

Sampling was carried out from about 160 km upstream from the mouth of the estuary to a station just outside of the Delaware Bay during five cruises over three years (November 7–10 2011, August 9–13 2012, November 12–16 2012, August 3–7 2013, and November 18–21 2013). Water was obtained by a CTD rosette-mounted Niskin bottle from ~0.5 m depth. Ammonium, nitrate, phosphate, and silicate concentrations were measured with a SEAL Analytical AA3 Continuous Segmented Flow Analyzer using standard procedures (Sharp et al., 2009). The concentration of total chlorophyll *a* was estimated in acetone extracts by fluorometry. Light attenuation was estimated from the intensity of photosynthetically active radiance over a depth profile measured with a Biospherical PNF-210 radiometer. A microcentrifuge approach was used to estimate leucine incorporation (added concentration of 20 nM) (Kirchman, 2001). Sampling locations and environmental parameters are summarized in Table S1 and Figure S1.

River discharge at Trenton and Schuylkill gage stations was obtained from the USGS Water Information System (waterdata.usgs.gov). We calculated the sum of discharge for 7, 14, 28, 56, and 112 days before the start of each sampling campaign and found the same general trend (Figure S2). The summed discharge of 112 days was chosen for further calculations because it lies well within the residence time of the estuary which is between 80 to 180 days (Ketchum, 1952; Sharp et al., 1982; Cifuentes et al., 1990).

Dissolved Organic Matter Analysis

For quantification and molecular analysis of the DOM, water was filtered through precombusted glass fiber filters (GF/F, Whatman), acidified to pH 2 with 25% HCl (p.a. grade), and stored at 4°C in the dark before being shipped to Germany for analysis. Concentrations of DOC and total dissolved nitrogen (TDN) were measured via high temperature catalytic oxidation on a Shimadzu TOC-VCPH analyzer equipped with a TDN module. Accuracy and precision were monitored with consensus reference material (DSR, D. Hansell, University of Miami) and were better than 5%. DON was estimated by subtracting nitrate and ammonium concentrations from TDN. The DOM was solid-phase extracted according to Dittmar et al. (2008) using 1 g

PPL columns (Agilent Bond Elut), and the resulting methanol extracts were stored at –20°C in the dark. The concentration of extractable DOC was determined from the extracts after complete removal of the methanol and dissolution in ultrapure water. Methanol extracts were diluted to a DOC concentration of 20 mg C L⁻¹ in a methanol:water mixture of 1:1 (v/v) and submitted to Fourier Transform Ion Cyclotron Resonance Mass Spectrometry on a solarix FT-ICR-MS (Bruker Daltonik GmbH) equipped with an electrospray ionization source (Bruker Apollo II) applied in negative mode. 500 scans in a mass window from 150 to 2000 Da were accumulated and molecular formulae were calculated with the following restrictions: ¹²C_{1–130}¹H_{1–200}¹⁶O_{1–50}¹⁴N_{0–4}³⁴S_{0–2}³¹P_{0–1} to masses above the method detection limit after Riedel and Dittmar (2014). Additionally, masses detected in less than three samples were removed prior to further analysis.

Each sample was normalized to the sum of FT-ICR-MS signal intensities and corrected for dilution per sample. The modified aromaticity index (AI_{mod}, Koch and Dittmar, 2006 as corrected and reported in the erratum published in 2016), double bond equivalents (DBE) and weighted molar ratios were calculated for each sample. The molecular formulae were assigned to compound groups according to their O/C and H/C ratios as described in Seidel et al. (2014). Here, the seven main groups with their subcategories include (1) polycyclic aromatics (PCA, AI_{mod} > 0.66) subdivided into PCA containing more than 15 C atoms indicative of dissolved black carbon, PCA with less than 15 C atoms, or PCA containing a heteroelement; (2) polyphenols (0.5 < AI_{mod} ≤ 0.66) with high (O/C ≥ 0.5) or low oxygen (O/C < 0.5) content; (3) highly unsaturated aliphatics (AI_{mod} ≤ 0.5, H/C < 1.5, O/C < 0.9) with high (O/C ≥ 0.5) or low (O/C < 0.5) oxygen content; (4) unsaturated aliphatics (1.5 < H/C ≤ 2, O/C < 0.9, N = 0) with high (O/C ≥ 0.5) or low (O/C < 0.5) oxygen content; (5) saturated fatty acids (H/C > 2, O/C < 0.9) with or without heteroelements; (6) carbohydrate-like formulae (O/C > 0.9) with or without (N,S,P = 0) heteroelements; and (7) peptide-like molecular formulae (1.5 < H/C < 2, O/C < 0.9, N > 0). The assignment of a formula to a compound class is not unambiguous since the grouping does not take into account all possible isomers. Calculated and intensity-weighted molecular composition and molecular categories per sample are provided in Table S1.

In order to investigate the structural DOM composition along the salinity gradient, we fragmented six nominal masses of two homologous series (*m/z* 269, 283, 297, 341, 365, and 379 Da) of three samples from the sampling campaign in November 2012 (salinities 0.8, 14.7, and 30.7) via collision-induced fragmentation in the FT-ICR-MS. The nominal masses were chosen to compare to a previous publication using the same approach (Osterholz et al., 2015), to span a broad mass range and to have a high relative signal intensity suitable for fragmentation. The November 2012 cruise was chosen for the fragmentation experiment as the DOC concentrations behaved conservatively, being representative of the conditions in the estuary most of the time except for bloom or very high discharge conditions. For the fragmentation, methanol extracts were diluted to a DOC concentration of 60 mg C L⁻¹ in a methanol:water mixture of 1:1 (v/v). The collision voltage was chosen to yield similar signal intensities of the

most intense fragments and varied between 13 V and 18 V. 150 scans were accumulated for each analysis performed in duplicates. Molecular formula assignment to fragmentation mass spectra was done as described above. We identified 423 fragments resulting from the neutral losses of H₂O, CH₄O, 2H₂O, CO₂, CO₂+H₂O, CO₂+CH₄O, 2CO₂, 2CO₂+H₂O, 2CO₂+CH₄O, 3CO₂, 3CO₂+H₂O or 3CO₂+CH₄O. Only molecular formulae that were detected in the two replicate analyses were analyzed in further detail. The relative signal intensity of each fragment ion was divided by the sum of the intensities of all major fragment signal intensities plus the precursor ion signal intensity for better comparison between samples. The normalized fragment intensities were then grouped by neutral loss and compared between samples.

Statistical Analysis

Conservative mixing lines (Figures 1, 2) were constructed using the respective mean concentrations/values of the two samples of highest and lowest salinity. The deviation of each sample from the theoretical mixing line was then calculated and averaged over the whole transect. A high value therefore represents a high variability of the parameter in relation to the values expected for a conservative mixing scenario, similar as described in Seidel et al. (2015a).

Multivariate statistical analyses were performed using R (version 3.2.2) and the package *vegan* (Oksanen et al., 2015). All analyses were run on normalized intensities of signals with molecular formula assignment which were corrected for dilution. Four extraction efficiencies (on carbon basis) above 100 and below 40% were likely erroneous and were replaced by the average value of extraction efficiencies of other samples (67%). Principal coordinate analyses (PCoA) were performed on Bray Curtis distance matrices (Bray and Curtis, 1957). Environmental vectors were fitted to the respective PCoA scores using the *envfit* function in the *vegan* package. Spearman rank correlations were calculated between single molecular formulae intensities and environmental parameters. Only correlations between a formula and an environmental parameter with a $p < 0.01$ were considered in further analysis and discussion. The non-parametric Wilcoxon rank-sum test was used for comparisons between groups of samples.

RESULTS

Environmental Characterization of the Delaware Bay

DOC, TDN and nitrate concentrations as well as turbidity generally decreased along the salinity gradient (Figure 1, Figure S1). Several biological parameters influenced by water temperature and light availability varied greatly between the two months (August and November) we sampled. These parameters included microbial abundance, chlorophyll *a* concentration and leucine incorporation as well as silicate concentrations (Figure 2, Figure S1). Freshwater discharge did not vary consistently between the two seasons.

Most environmental parameters deviated from conservative mixing along the salinity gradient. Nitrate concentrations,

for example, were always high in the oligohaline zone, decreasing toward the ocean with a negative deviation from conservative mixing at intermediate salinities. Most of the total dissolved nitrogen in the Delaware estuary is inorganic. DON concentration did not vary consistently along the estuarine salinity gradient or with season.

Silicate concentrations were depleted at the freshwater end of the estuary in August, while in November concentrations were high because the river contributes large amounts of dissolved silicate into the estuary. Chlorophyll *a* concentration (Figure 2) and leucine incorporation (Figure S1) differed between the two campaigns that took place in August, yet covaried significantly ($\rho = 0.82$, $p < 0.01$) with highest values observed in the oligo- and polyhaline zones in August 2013 and overall high values during August 2012.

DOC concentrations decreased linearly (conservatively) during estuarine mixing in November (Figure 1). In August, however, changes in DOC concentrations were non-conservative; deviations from conservative mixing were significantly higher in August than in November (Wilcoxon rank-sum test, $p < 0.01$). Overall, DOC concentrations were more variable at the freshwater end; the coefficient of variation (CV) at low salinity was 20% (salinity < 1 , mean DOC $245 \pm 49 \mu\text{mol L}^{-1}$, $n = 14$) while it was 11% in marine waters (salinity > 30 , mean DOC $129 \pm 14 \mu\text{mol L}^{-1}$, $n = 14$). At salinities of less than 1, DOC concentrations were significantly lower in August than in November by 1.4-fold (Wilcoxon rank-sum test, $p < 0.01$). DOC concentrations in marine waters did not vary substantially between the 2 months. DOC concentrations at the high or low salinity extremes did not correlate significantly with discharge.

A turbidity maximum was apparent at salinities between 0 and 5 during all cruises; turbidity then decreased toward the ocean. Turbidity patterns were neither related to discharge nor revealed an impact on phytoplankton growth or DOC concentration.

Dissolved Organic Matter Molecular Composition

In the whole dataset consisting of 121 solid-phase extracted DOM samples, 12666 unique molecular formulae (MF) within the mass range of 154–885 Da were identified. Of those, 3093 MF (24%) were present in all 121 samples. Further, 78% of all MF were detected at least once during each of the five cruises. Considering each cruise separately, 34–45% of the MF were observed in every sample (November 2011: $n = 22$, August 2012: $n = 26$, November 2012: $n = 25$, August 2013: $n = 26$, November 2013: $n = 22$).

Principal coordinate analysis was performed on a Bray-Curtis dissimilarity matrix (Bray and Curtis, 1957) calculated using relative signal intensities of all samples (Figure 3). The two major axes of variation together encompassed almost 80% of the variability of the dataset. Salinity was highly positively correlated to principal coordinate PC1 ($\rho = 0.78$, $p < 0.001$, Figure 1), whereas silicate and DOC concentration were negatively correlated with PC1 ($\rho = -0.95$ and -0.57 , respectively, $p < 0.001$). Discharge was strongly associated

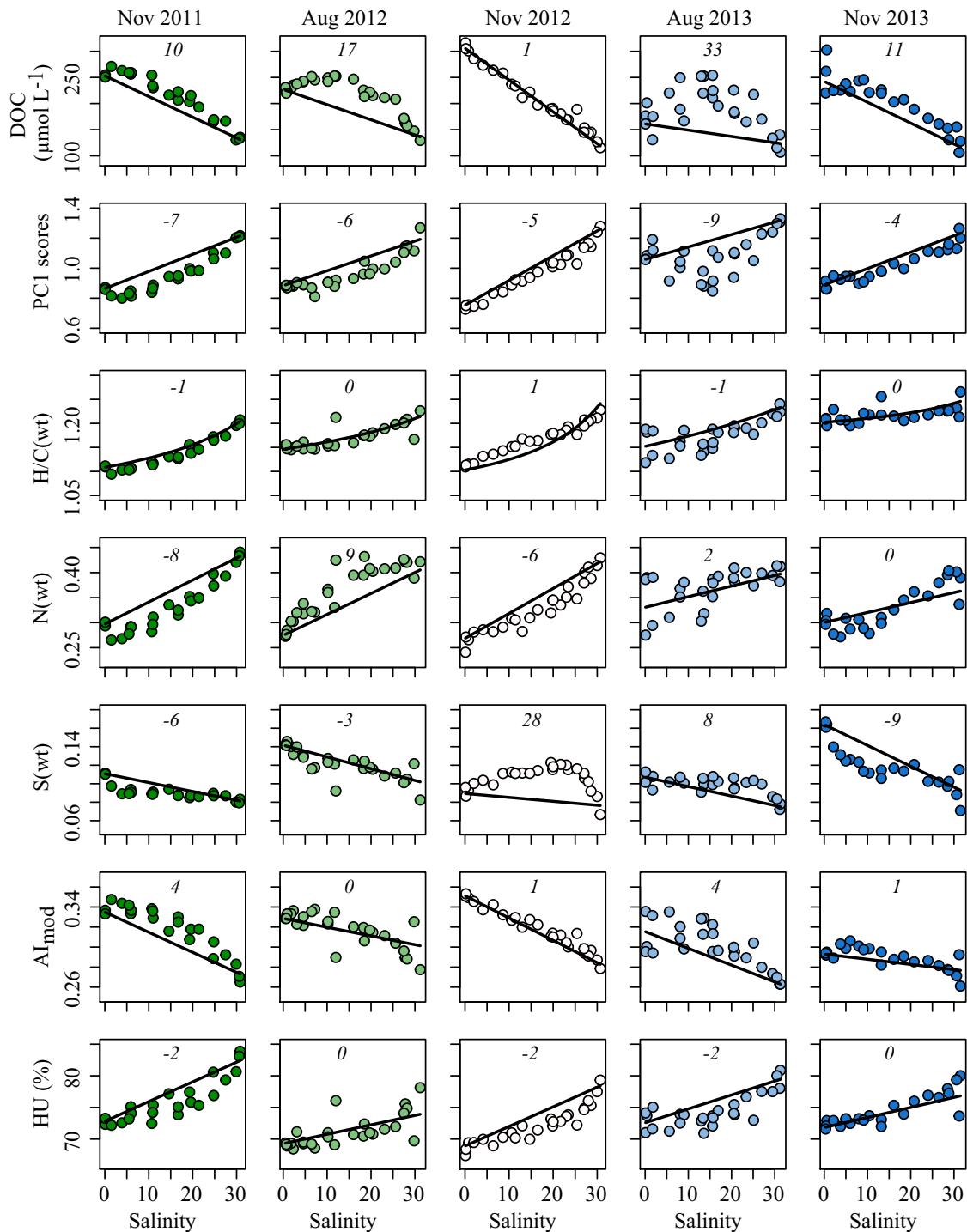
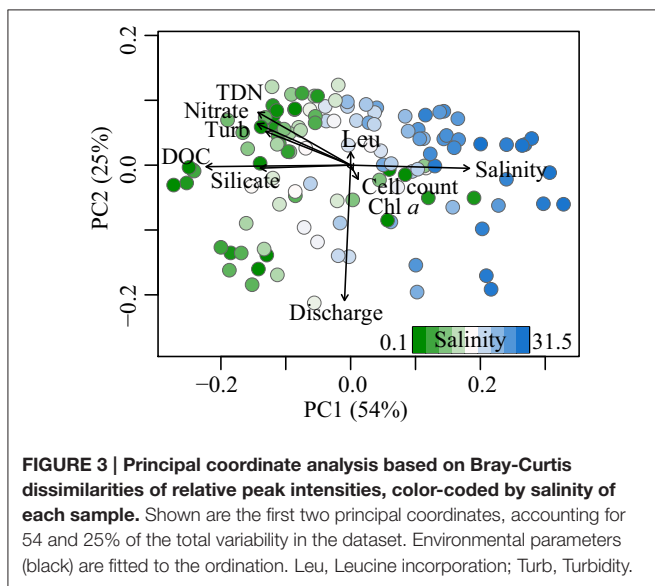
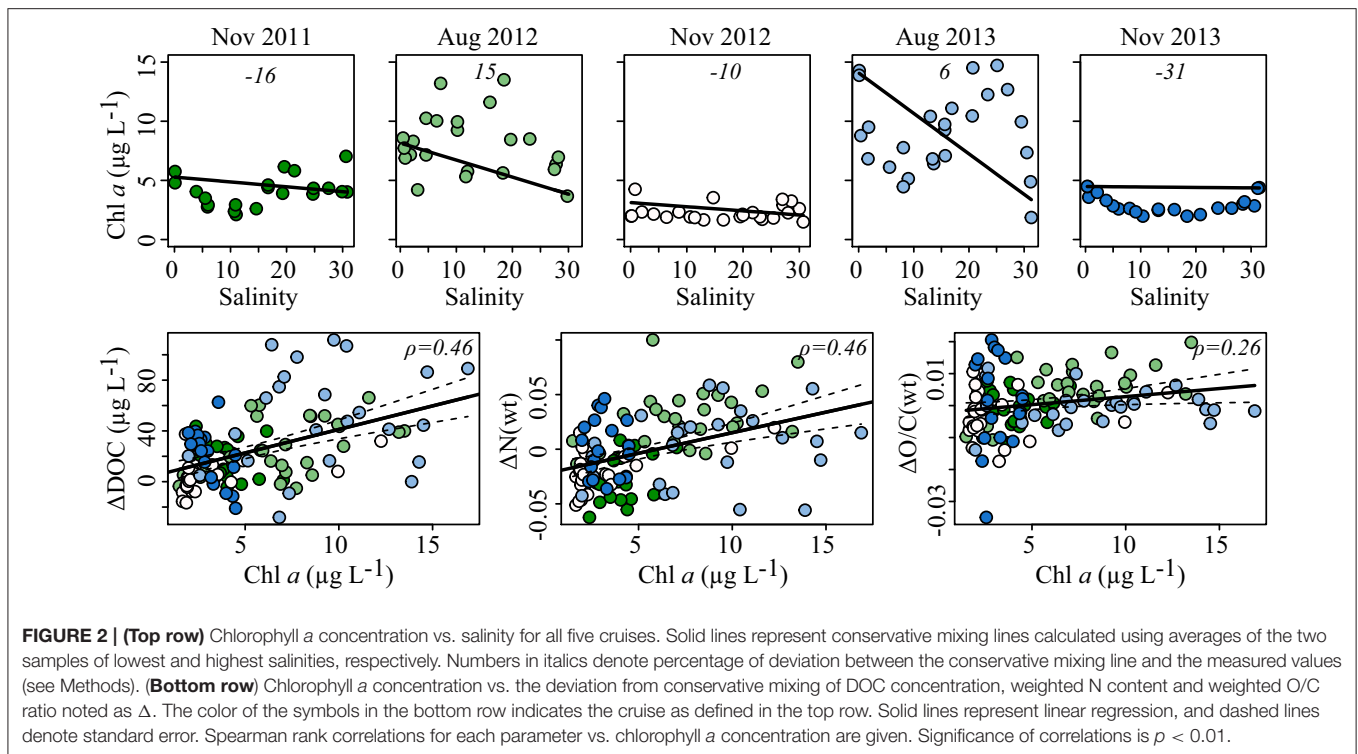


FIGURE 1 | DOC concentration and characteristics of DOM molecular composition (rows) vs. salinity for all five cruises (columns). PC1 scores are from **Figure 3** (1 was added to each score for data representation); H/C ratio, N- and S-content of molecular formulae were weighted by peak intensity; Al_{mod} , modified aromaticity index; HU, percentage of highly unsaturated compounds. Solid lines represent conservative mixing lines calculated using averages of the two samples of lowest and highest salinities, respectively. Numbers in italics denote percentage of deviation between the conservative mixing line and the measured values (see section Materials and Methods).

with PC2 ($\rho = -0.75$, $p < 0.001$, **Figure 4**), the second axis of variation comprising 25% of the variability of the DOM molecular data. Microbial abundance, bacterial production

(leucine incorporation) and chlorophyll *a* concentration were correlated with the third and/or fourth PCs, encompassing 6 and 3% of the variation in the data, respectively (Figures S3, S5E,F).



Three environmental parameters (salinity, discharge, chlorophyll *a* concentration) were chosen for a more detailed investigation of changes in molecular DOM composition. These three parameters each represent one group of co-correlating environmental variables identified via hierarchical clustering (Figure S4).

Almost half of all identified molecular formulae, capturing $85 \pm 5\%$ of the total signal intensity of each sample, decreased in intensity with increasing salinity. The overall aromaticity of the

SPE-DOM, assessed via the modified aromaticity index AI_{mod} , strongly decreased (Figure 1, Table 1). A molecular formulae based measure for terrigenous input, I_{terr} proposed by Medeiros et al. (2016), decreased from ~ 0.5 at the freshwater end to ~ 0.2 in the most marine waters and was highly negatively correlated with salinity ($\rho = -0.79$, $p < 0.001$). The relative contribution of sulfur to DOM molecular composition exhibited a weak relationship with salinity, overall decreasing toward the ocean. SPE-DOM N-containing molecular formulae, average molecular mass and H/C ratio all increased with increasing salinity (Figure 1, Figures S5A,B, Table S1). The relative abundance of highly unsaturated compounds, representing the largest compound class, likewise increased. The index for labile compounds above the molecular lability boundary (MLB) of H/C > 1.5 , the MLB_{wL} proposed by D'Andrilli et al. (2015), slightly increased toward the ocean for all cruises except in November 2012 ($\rho = 0.23$, $p < 0.05$).

At high discharge in the Delaware Bay, we found high values for O/C ratio, molecular mass and highly unsaturated compounds (Figure 4). The subgroup of oxygen-rich highly unsaturated compounds emphasizes this trend (Figure 4, Table 1, Figures S5C,D). We observed only a slight increase in aromaticity, while the I_{terr} did not correlate significantly with discharge ($p > 0.05$). The MLB_{wL} was highly negatively linked with discharge ($\rho = -0.80$, $p < 0.001$). About 2000 molecular formulae were positively affected by discharge and another 3000 were negatively affected, in total accounting for $\sim 60\%$ of total signal intensity (Table 1).

Chlorophyll *a* concentration and microbial activity were highly correlated; therefore only chlorophyll *a* was chosen for

TABLE 1 | Characteristics of molecular formulae correlating positively (POS) or negatively (NEG) with salinity, discharge and chlorophyll *a* concentration as well as of those molecules exhibiting no correlation to either one of the three environmental parameters.

	Salinity		Discharge		Chlorophyll <i>a</i>		No correlation
	NEG	POS	NEG	POS	NEG	POS	
MF	5690 ± 848	353 ± 96	2171 ± 180	2981 ± 999	162 ± 12	604 ± 258	471 ± 126
MW	371 ± 19	399 ± 10	302 ± 8	481 ± 13	334 ± 10	430 ± 27	414 ± 12
C	17.79 ± 0.81	17.69 ± 0.37	15.16 ± 0.44	21.56 ± 0.65	17.51 ± 0.47	18.04 ± 1.37	18.86 ± 0.68
H	20.40 ± 0.91	22.72 ± 0.55	20.18 ± 0.66	23.53 ± 1.30	22.45 ± 0.69	20.47 ± 2.32	25.33 ± 1.17
O	8.24 ± 0.62	8.54 ± 0.29	5.73 ± 0.21	12.04 ± 0.31	6.08 ± 0.26	10.66 ± 0.64	9.07 ± 0.26
N	0.21 ± 0.02	1.87 ± 0.04	0.33 ± 0.06	0.33 ± 0.05	0.22 ± 0.05	1.23 ± 0.08	0.82 ± 0.06
S	0.104 ± 0.021	0.065 ± 0.027	0.149 ± 0.037	0.059 ± 0.011	0.053 ± 0.023	0.201 ± 0.049	0.150 ± 0.031
P	0.001 ± 0.001	0.004 ± 0.004	0.004 ± 0.002	0.004 ± 0.002	0.007 ± 0.005	0.008 ± 0.006	0.057 ± 0.029
O/C	0.47 ± 0.02	0.48 ± 0.01	0.39 ± 0.01	0.57 ± 0.01	0.35 ± 0.01	0.60 ± 0.02	0.50 ± 0.01
H/C	1.15 ± 0.04	1.29 ± 0.01	1.32 ± 0.01	1.08 ± 0.05	1.27 ± 0.02	1.13 ± 0.08	1.34 ± 0.02
AI _{mod}	0.32 ± 0.02	0.18 ± 0.01	0.25 ± 0.01	0.30 ± 0.03	0.30 ± 0.01	0.26 ± 0.06	0.16 ± 0.02
DBE	8.7 ± 0.6	8.3 ± 0.1	6.2 ± 0.1	11.0 ± 0.6	7.4 ± 0.2	9.4 ± 0.8	7.6 ± 0.2
Compound classes (% of total)							
PCA	2.7 ± 0.8	0 ± 0	0.4 ± 0.2	2.9 ± 1.2	1.6 ± 0.7	0.9 ± 0.7	0.3 ± 0.2
PCA < C15	1.2 ± 0.4	0 ± 0	0.4 ± 0.2	0.6 ± 0.3	1.6 ± 0.7	0.0 ± 0.1	0 ± 0
PCA ≥ C15	1.4 ± 0.6	0 ± 0	0 ± 0	2.3 ± 1.0	0 ± 0	0.8 ± 0.6	0.3 ± 0.2
PCA-X	2.7 ± 0.7	0.1 ± 0.1	1.9 ± 0.4	1.2 ± 0.6	0.2 ± 0.2	11.5 ± 5.8	2.6 ± 1.5
PP	14.0 ± 2.4	1.0 ± 0.7	8.1 ± 0.9	11.7 ± 3.9	5.4 ± 1.6	8.2 ± 3.5	3.5 ± 1.2
PP O-rich	43 ± 1.4	0 ± 0	0.3 ± 0.1	8.0 ± 2.9	0.3 ± 0.1	5.9 ± 3.2	0.3 ± 0.2
PP O-poor	9.7 ± 1.4	1.0 ± 0.7	7.9 ± 0.9	3.7 ± 1.1	5.1 ± 1.6	2.2 ± 0.7	3.2 ± 1.2
HU	72.1 ± 3.3	95.0 ± 2.0	69.5 ± 2.0	83.1 ± 5.3	88.4 ± 3.3	69.2 ± 7.8	70.2 ± 3.3
HU O-rich	28.3 ± 3.8	35.0 ± 3.0	9.9 ± 1.3	59.9 ± 3.4	1.4 ± 0.4	61.7 ± 7.4	31.2 ± 3.0
HU O-poor	43.8 ± 4.0	59.9 ± 2.9	59.6 ± 2.5	23.2 ± 4.0	87.0 ± 3.7	7.5 ± 3.3	39.0 ± 2.6
UA	8.3 ± 1.9	1.2 ± 0.6	18.0 ± 1.5	0.7 ± 0.3	1.8 ± 0.7	3.9 ± 2.1	17.5 ± 2.6
UA O-rich	1.7 ± 0.4	1.0 ± 0.5	3.9 ± 0.5	0.4 ± 0.1	0 ± 0	2.2 ± 0.9	8.2 ± 1.0
UA O-poor	6.6 ± 1.6	0.2 ± 0.2	14.2 ± 1.4	0.3 ± 0.2	1.8 ± 0.7	1.7 ± 1.7	9.3 ± 2.1
FA-X	0.1 ± 0.0	0.0 ± 0.0	0.4 ± 0.3	0.1 ± 0.1	2.1 ± 1.4	0.7 ± 1.0	0.3 ± 0.4
Sugars	0.1 ± 0.0	0 ± 0	0 ± 0	0 ± 0	0 ± 0	0.1 ± 0.1	0.1 ± 0.1
Sugars-X	0 ± 0	0.3 ± 0.2	0 ± 0	0.1 ± 0.1	0.1 ± 0.2	0.5 ± 0.4	0.8 ± 0.3
Peptides	0.1 ± 0.0	2.4 ± 0.9	1.5 ± 0.4	0.1 ± 0.1	0.3 ± 0.1	5.1 ± 2.4	4.6 ± 1.3

Values represent formulae counts (MF), intensity-weighted molecular mass in Dalton (MW), element contribution (C, H, O, N, S, P), molar ratios (O/C, H/C), molecular indices (AI_{mod}, DBE) and relative contribution to compound classes (PCA, polycyclic aromatics; PCA < 15 or ≥ 15, PCA with less than or more/equal to 15 C atoms; -X, containing heteroelements (N, S, P); PP, polyphenols; HU, highly unsaturated compounds; UA, unsaturated aliphatics; FA, fatty acids).

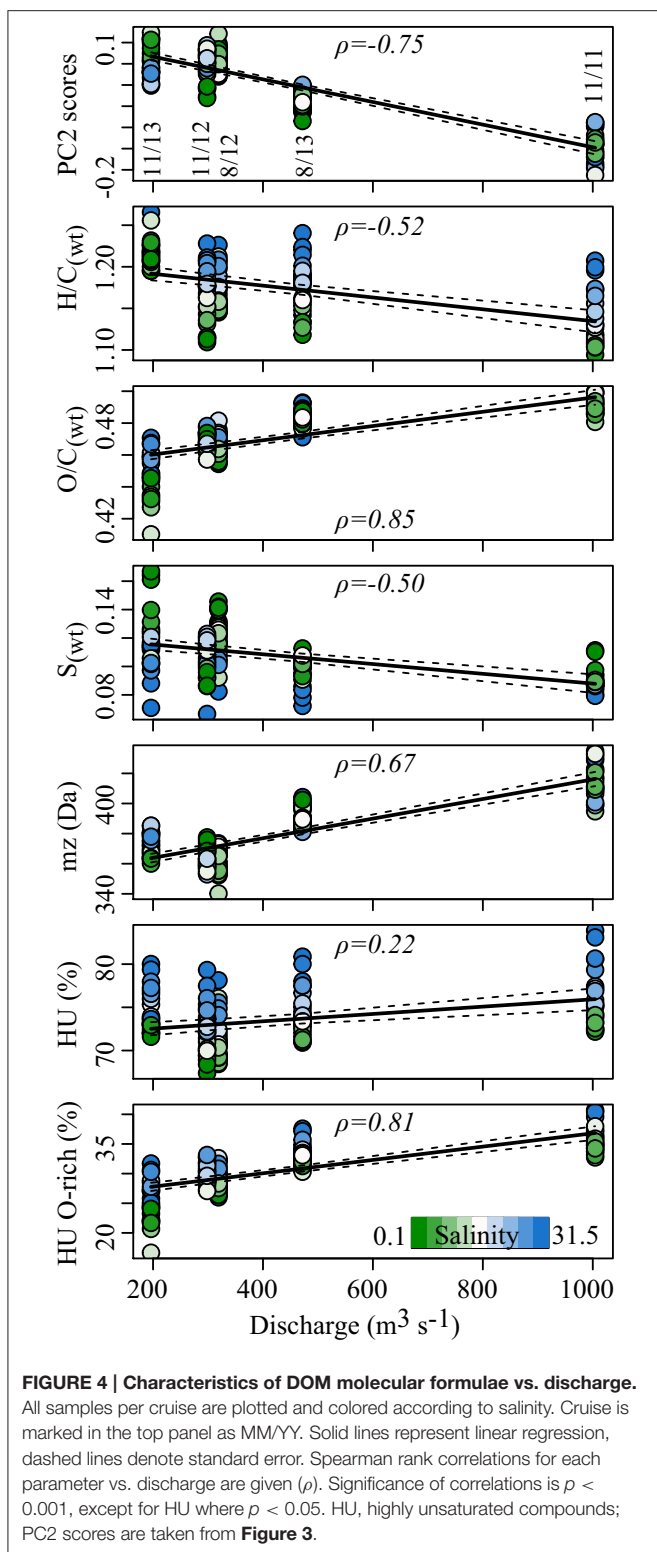
further investigation. Overall, chlorophyll *a* concentration was variable along the salinity gradient, but consistently displayed positive deviations from conservative mixing in August and negative deviations in November (Figure 2). Only a few molecules varied consistently with chlorophyll *a* concentration and accounted for ~6% of the total signal intensity (Figure S5E, Table 1). The molecular variation associated with the chlorophyll *a* gradient was, however, markedly different from random correlations as tested with a dataset of normally distributed, random variables (Figure S5H). During periods of high phytoplankton biomass and microbial production, DOM was enriched in N, S, O, unsaturated aliphatics, polyphenolic compounds as well as sugar- and peptide-like molecular formulae (Table 1). To explore the correlations in more detail, the deviations from conservative mixing of DOC concentrations and molecular parameters were calculated (Δ DOC, Δ N, Δ O/C);

significant increases are shown in Figure 2. The MLB_{wL} and I_{terr} did not correlate significantly with chlorophyll *a* concentrations ($p > 0.05$).

The 471 ± 126 molecular formulae that correlated with one of the three factors ($p > 0.01$) accounted for ~3% of the total signal intensity and were widely distributed over the van Krevelen space occupied by a typical DOM sample, but were less prevalent in the low-H/C and high-O/C region (Figure S5G).

Dissolved Organic Matter Structural Analysis

Fragmentation of six nominal masses from three samples along the salinity gradient in Nov 2012 was used to detect potential preferential removal or addition of DOM structural features along the salinity gradient of the Delaware Estuary. A total of



423 detected fragments were normalized and grouped by neutral loss (H_2O , CO_2 , CH_4O as well as combinations and multiples thereof). We did not detect any of the OCH_2 functionalities described by Liu et al. (2011). These neutral losses represent a

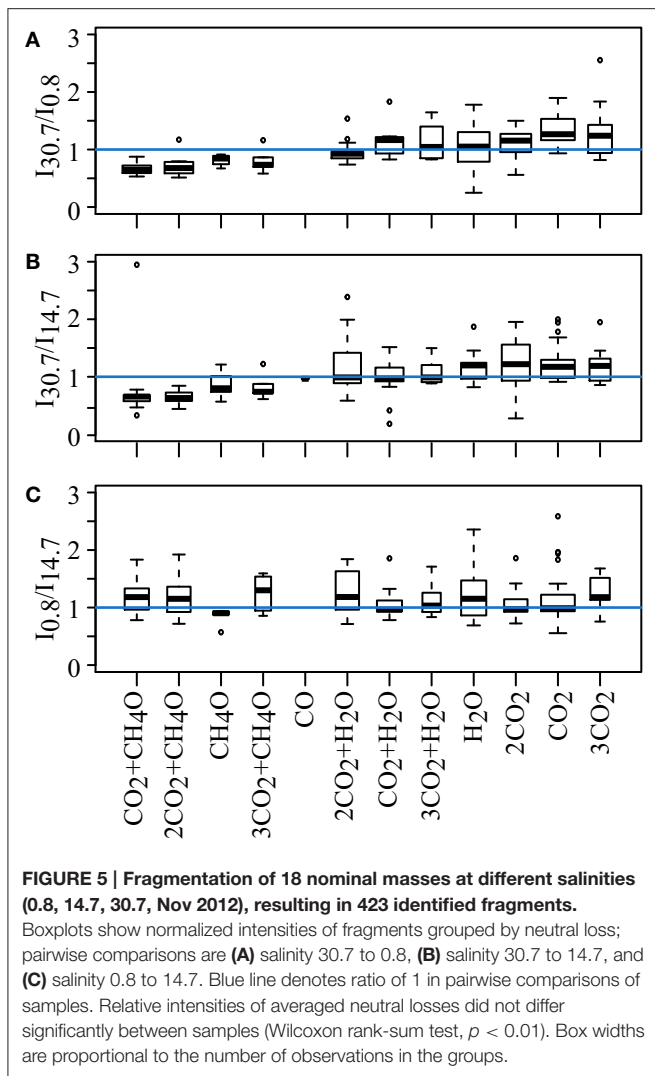
component of lignin biopolymers generated from wood extract and C18-extracted black waters and were thus presumed to occur in the terrigenous DOM. In pairwise comparisons of the relative signal intensities per neutral loss, a ratio of 1 indicates that no differences in neutral losses were observed between samples. This in turn suggests that a formula with the same molecular mass has a similar structure, regardless of its sampling location within the salinity gradient of the estuary. Although there were some deviations from the ratio of 1 among samples taken at different salinities, the fragmentation patterns did not differ significantly (Wilcoxon rank-sum test, $p > 0.05$, **Figure 5**).

DISCUSSION

In order to investigate the environmental drivers of DOM quantity and quality in a temperate estuarine system, we combined quantitative analysis of DOC concentrations with ultrahigh resolution mass spectrometric analysis of solid-phase extractable (SPE) DOM from samples from the entire salinity gradient of the Delaware estuary over 3 years. The analytical window provided by the combination of PPL-SPE and FT-ICR-MS allowed us to examine a large, otherwise inaccessible portion of the DOM pool; in this study on average $67 \pm 6\%$ of the DOC was captured with our solid-phase extraction method. The PPL columns used here poorly recover very small and polar compounds (Raeke et al., 2016), but absorb a wide range of compounds of varying polarity and are thought to provide a major fraction of the natural DOM (Green et al., 2014; Li et al., 2016). The extraction efficiency did not significantly change along the salinity gradient of the estuary, indicating that our method captured a reproducible fraction of the estuarine DOM pool. FT-ICR-MS analysis of our SPE-DOM samples allowed us to gain valuable information on molecular composition and explore variation with biogeochemical properties. Additional insights into DOM structural features were revealed with in-cell fragmentation.

Mixing of Terrigenous and Marine DOM along the Salinity Gradient

On its way from soils to the ocean margins, DOM can undergo transformations in molecular composition that are not reflected in the DOC concentrations along the salinity gradient. Besides a slight decrease in molecular formulae richness ($\rho = -0.29$, $p < 0.01$) and the Shannon diversity index ($\rho = -0.44$, $p < 0.001$) along the salinity gradient, condensed aromatic compounds, Al_{mod} , and polyphenols indicating DOM of terrigenous origin were higher in the low salinity region. Proportions of highly unsaturated compounds and molecular mass increased with increasing salinity, as did the contributions of nitrogen-containing molecular formulae and sugar- and peptide-like compounds that are thought to be products of more recent primary production (Amon et al., 2001). Our results are overall in line with previous studies applying ultrahigh resolution mass spectrometry to molecularly characterize DOM. These have shown that DOM tends to become more aliphatic, has a higher heteroelement content (N, S, P), and contains



lower abundances of oxygen-rich molecules along gradients of increasing salinity in temperate (Sleighter and Hatcher, 2008) and tropical estuaries (Medeiros et al., 2015b; Seidel et al., 2015b). Highly unsaturated compounds, however, are thought to mainly comprise soil-derived “humics” and other highly unsaturated compounds according to Šantl-Temkiv et al. (2013). It has to be kept in mind that FT-ICR-MS detects relative signal intensities and grouping into molecular classes is reported in proportions, i.e., if one compound class such as the polyphenols strongly decreases in a sample, another compound class or classes must increase. The less oxygenated polyphenols decrease more strongly with increasing salinity than the oxygen-rich subgroup (Table 1) which includes many phenolic acids. This finding illustrates that the classification into broad compound groups does not unambiguously identify the origin and fate of the molecules. Further, although unsaturated aliphatic compounds have previously been shown to be abundant in the ocean supposedly due to the DOM from marine organisms (Sleighter and Hatcher, 2008; Seidel et al., 2015a), they exhibited no relationship with salinity in our study.

Data on DON concentration and the molecular composition data give a different picture about sources of DOM in the estuary. DON concentrations were similar along the whole transect whereas increased DON concentrations have been observed previously in freshwater parts of estuaries (Badr et al., 2008). However, there was a strong positive correlation between relative intensities of N-containing molecular masses and salinity ($\rho = 0.77$, $p < 0.001$). This is consistent with the hypothesis that marine DOM is mainly derived from autochthonous production and contains more heteroelements than DOM from terrestrial sources (Sleighter and Hatcher, 2008). In addition to a higher N content of the SPE-DOM molecular formulae, we also observed a slightly positive correlation between the relative abundance of P in the assigned molecular formulae and salinity ($\rho = 0.18$, $p < 0.05$).

We propose that variation in the endmembers (river and ocean) is preserved more clearly in the DOM molecular composition than in DOC concentration. The coefficient of variation (CV) of DOC concentrations was 20% ($245 \pm 49 \mu\text{mol L}^{-1}$) in waters with salinities < 1 and 11% ($129 \pm 14 \mu\text{mol L}^{-1}$) in waters with salinity > 30 . In contrast, the CV of the Bray-Curtis dissimilarity of the SPE-DOM samples was similar for the low and high salinity samples (35 and 31%, respectively). Put differently, DOC concentrations decreased along the salinity gradient and reached similarly low levels in the marine waters while DOM molecular composition remained diverse among the five cruises. This discordance in trends of concentration and composition could be caused by the removal of DOM fractions not captured with our SPE-method. A more likely explanation is the consistent removal or dilution or both of SPE-DOM over the whole captured mass range, supported by the strong correlation of DOM molecular composition with salinity (e.g., Figures 1, 3).

The fact that few molecules increase in relative intensity toward the ocean indicates that dilution and/or degradation processes are by far more important than new production of DOM compounds in shaping DOM composition in this system. Many compounds present at the freshwater source were detected along the whole salinity gradient (34–45%, calculated separately for each cruise). Together with the high percentage of compounds that were detected repeatedly during each cruise (78%), these data indicate a common source of DOM from land that is preserved due to the recalcitrant nature of these compounds. Hossler and Bauer (2013) indeed report a high degree of allochthonous (40–96%) and aged DOC (1–23%) in the Delaware River and Bay. A second possibility is that some compounds are actually removed while others with different structures but the same molecular formulae are produced during the transit through the estuary, thus masking a lower-level DOM variability in the system (Sleighter and Hatcher, 2008). Since structure can be deduced from molecular formula only in extreme cases, i.e., for molecules with very low H/C ratios (Koch and Dittmar, 2006), we conducted fragmentation experiments applying FT-ICR-MS/MS to three samples along the salinity gradient at low, mid and high salinity of the November 2012 cruise. Collision-induced fragmentation has been shown to distinguish samples with similar molecular formulae fingerprints, but different structural

composition (Osterholz et al., 2015). The neutral losses of H₂O, CO₂, and CH₄O as well as combinations and multiples thereof are markedly different in relative intensity and exhibit ratios up to 4 when comparing relative fragment intensities of fresh, biologically produced and aged oceanic DOM. The same neutral losses were detected in the fragmentation experiments with Delaware Estuary DOM (Figure 5). However, none of the fragment intensities differed significantly between samples. This finding indicates that structures in aquatic DOM were highly similar, irrespective of their origin from marine or terrestrial sources. For our study, we infer that during estuarine mixing, there were no changes in DOM composition at the structural level that were overlooked at molecular formula level.

The Influence of Discharge Levels

During our five sampling campaigns we did not observe correlations between discharge regimes and DOC concentrations. This remained true even if only the low-salinity samples (salinity < 1, $n = 14$) were taken into account, which would be most directly affected by discharge. For forested streams in the eastern United States as well as the Amazon, high DOC concentrations at the onset of high discharge events and low DOC concentrations at low discharge have been reported (Raymond and Saiers, 2010; Ward et al., 2013). Other studies using a similar analysis approach to the one used here have detected positive correlations between DOC concentration and discharge (Raymond and Bauer, 2001; Medeiros et al., 2015b). The Delaware Estuary in general shows a weak axial salinity response to freshwater input, probably due to vertical shear flow dispersion and the action of lateral shear coupled to a strong lateral salinity gradient (Garvine et al., 1992). DOC, mostly exhibiting conservative behavior, accordingly showed no strong influence of discharge.

Although discharge did not affect DOC concentrations it affected DOM molecular composition. According to correlation analysis of the principal coordinates, discharge was identified as the second most important driver of DOM molecular composition responsible for about a quarter of the total variability. We observed a pronounced shift in DOM composition between low/normal discharge situations where the discharge was around or below the yearly mean flow of $\sim 400 \text{ m}^3 \text{ s}^{-1}$ provided by the Delaware and Schuylkill River (Polis and Kupferman, 1973) and high discharge regimes ($> 400 \text{ m}^3 \text{ s}^{-1}$, Figure 4). DOM associated with high river discharge was enriched in condensed aromatics, oxygen-rich polyphenols, oxygen-rich highly unsaturated compounds and a higher AI_{mod} , all indicative of higher terrigenous DOM input (Meyers-Schulte and Hedges, 1986; Koch et al., 2005). The specific positive correlation with oxygen-rich aromatic compounds presumably relates to the input of lignin- and tannin-like compounds with high O/C ratio (Table 1, Figure 4). Lignins are complex aromatic biopolymers that make up a major component of vascular plant biomass (Sarkanen and Ludwig, 1971). They are an important component of riverine DOM (Ertel et al., 1986). Tannins are produced by some algae but primarily are constituents of higher plant tissue (Hedges and Weliky, 1989). They are thought to be quickly removed from

aquatic environments via decomposition, precipitation, and sorption to sediments (Maie et al., 2008). Litterfall and plant debris are degraded in forest soils, from which rainfall events can mobilize tannins and lignin, leading to high concentrations in the Delaware River when discharge is high. The average mass of the compounds associated with discharge rates was higher than of those compounds negatively correlating with discharge. This is opposite of the expected trend as terrigenous SPE-DOM tends to have a lower molecular weight when compared to marine DOM analyzed via FT-ICR-MS (Koch et al., 2005; Medeiros et al., 2015b). Tannins, in molecular weight from 500 to 3000 Da (Bate-Smith, 1968), and lignin polymers of similar or higher molecular weight increased in abundance at high discharge and therefore could contribute to this increase in average molecular mass of the entire DOM pool. Forest and wetland coverage of the watershed decreases from the upper basin toward the bay but nevertheless accounts for the major land use of the Delaware basin (49 and 8%, respectively, Partnership for the Delaware Estuary, 2012). Forests and wetlands are possible sources for this terrigenous DOM. Another much debated source of DOC to the Delaware Estuary are the *Spartina alterniflora*-dominated wetlands surrounding especially the lower estuary. Hossler and Bauer (2012) reported a contribution of carbon originating from plants with a C₄-photosynthetic mechanism to DOC of up to 51% in the Delaware River. Since the production of maize, a C₄ plant, is low in the Delaware watershed, the salt marshes might be a large source of this C₄-organic matter. According to Benner et al. (1987) and Cifuentes (1991) and references therein, the marshes do not seem to export large quantities of organic matter to the estuarine water column. These sources, however, cannot be deciphered through the methods applied in our study.

Further, the river tended to carry more S-containing DOM to the freshwater end of the estuary at low to intermediate discharge scenarios ($\rho = -0.54$, $p < 0.001$, Figure 4, Table 1). The anthropogenically influenced portion of the Delaware River (land cover: 26% agriculture, 15% developed land, Partnership for the Delaware Estuary, 2012) especially in the central and lower watershed, may introduce dissolved organic sulfur (DOS) compounds originating from e.g., wastewater input and agriculture (Gonsior et al., 2011; Wagner et al., 2015), which would be less diluted at low river discharge. In the same manner, DOS compounds formed during early diagenesis in sediments could be released into the water column (Seidel et al., 2014) or be exported from the salt marshes surrounding the Delaware Bay (Luther et al., 1986). The Delaware Bay nevertheless carried SPE-DOS in ranges comparable to less anthropogenically influenced rivers such as Lena, Amazon and Congo (Wagner et al., 2015).

Seasonal DOM Imprint Due to Biological Processes

The impact of biological processes on DOM concentration and composition was assessed through chlorophyll *a* concentration as a proxy for phytoplankton biomass and bacterial activity measured via leucine incorporation. Due to their high correlation, these two factors cannot be distinguished in our correlative approach ($\rho = 0.82$, $p < 0.001$). There were

no significant correlations between DOC and chlorophyll *a* concentrations or with leucine incorporation rates.

Only a small portion of molecular formulae comprising about 6% of the total signal intensity correlated positively or negatively with chlorophyll *a* (Table 1). This number is similar to the percentage of molecular formulae attributed to phytoplankton and/or biodegradation-related processes in the Amazon (Medeiros et al., 2015b). The authors report selective removal of compounds with high O/C ratios via biodegradation (Sun et al., 1997; Kim et al., 2006) and input of phytoplankton-derived material of low O/C ratio (Landa et al., 2014). This was not observed for the Delaware system, where we found that oxygen-rich polyphenols and highly unsaturated compounds increased with chlorophyll *a* concentration. The higher heteroatom content and occurrence of saturated compounds are consistent with phytoplankton-derived DOM (Sleighter and Hatcher, 2008). Phytoplankton classes differed significantly not only between August and November sampling, but also between the different years (Kirchman et al., in press), possibly producing different DOM compounds and thereby hampering the detection of a uniform “biological signature.”

Abiotic Factors Influencing DOM Composition

At increasing ionic strength, abiotic processes such as flocculation and adsorption to particles may influence DOM composition (Hernes and Benner, 2003). Selective removal of terrestrially derived compounds such as humic acids (Fox, 1983; Ertel et al., 1986) has been reported during estuarine mixing, as well as sorption of amino acids and dissolved polysaccharides to particles in the turbidity maximum zone of the Delaware Estuary (Mannino and Harvey, 2000a). Flocculation with metal salts, for example, has been shown to selectively remove more aromatic compounds (Riedel et al., 2012). Cifuentes (1991) proposed the release of lignin phenols from resuspended sediments in the turbid regions of the Delaware Estuary. We were not able to attribute changes in DOC concentration or molecular DOM composition to adsorption processes in this zone through our correlative approach, i.e., correlating relative FT-ICR-MS signal intensities or bulk DOC concentrations with an environmental factor (here: turbidity). Likely, extensive DOM processing before it reaches the river and estuary (Goñi and Gardner, 2003), the small relative contribution of those compound classes to the total DOC pool, the low spatial resolution of the sampling points in and around the turbidity maximum and the strong superimposing signal of the mixing of fresh- and saltwater in combination all hinder the recognition of a turbidity maximum signal. In a recent publication, Hermes and Sikes (2016) showed that POC concentrations are highest in the bottom waters of the estuarine turbidity maximum and sampling at that depth might have revealed a stronger imprint of DOM-POM interaction that are not evident at the 0.5 m sampling depth chosen for our study.

Additionally, photochemical processes are known to shape the DOM pool by removing (condensed) aromatic structures, especially in rivers with watersheds dominated by forests and grassland (Hernes and Benner, 2003; Stubbins et al., 2010; Riedel et al., 2016). This process would yield a negative concave relationship of, for example, condensed aromatics and polyphenols, vs. salinity as both sunlight exposure potential and

time increase while the more colored freshwater is diluted along the estuary. As these compound classes decreased linearly along the salinity gradient, there was no evidence of a significant contribution of photochemical alteration to estuarine DOM processing in the Delaware Estuary. Further, we analyzed the relative contribution of molecular formulae identified as photolabile, photo-resistant and photo-produced by Stubbins et al. (2010) for the Congo River, but no pattern indicative of photochemical alteration emerged (data not shown).

In line with our findings, no large in situ sources or sinks of chromophoric DOM in the Delaware Estuary were reported by Del Vecchio and Blough (2004). These and other authors found photochemical processing to be more important in clearer waters offshore with higher light penetration depths for the Delaware, Amazon, and Mississippi river plumes (Hernes and Benner, 2003; Medeiros et al., 2015b; Seidel et al., 2015b). Indeed, an extensive photochemical DOM sink during August months was described also for the Delaware Estuary plume by Vodacek et al. (1997). The authors further assume oceanic and terrestrial DOM pools mixing in the estuary and on the shelf to originate from constant or very similar sources, which is consistent with a high overlap of detected molecular formulae described in this study.

CONCLUSION

In our study, we revealed DOM molecular-level variations that are masked by looking at DOC concentrations alone. Mixing of fresh- and marine waters, hydrological conditions, and also biological processes alter the composition of the DOM discharged through the Delaware Estuary into the Atlantic Ocean. For the first time, we applied collision-induced fragmentation to nominal masses along a salinity gradient, demonstrating that the chemical structures behind DOM molecular formulae exhibit a high similarity independent of their origin from marine or terrestrial environments.

Understanding the numerous processes occurring during land-to-ocean carbon transport is of utmost significance to the global carbon cycle as riverine discharge of DOC alone is sufficient to support the turnover of DOC throughout the entire marine environment (Williams and Druffel, 1987). Future increase in discharge due to increased precipitation and storm events projected by climate change scenarios and land use change reducing forest cover will most probably alter the signature of the DOM reaching the ocean, corroborating the need for further monitoring especially of such well-understood land-to-ocean connectors as the Delaware Estuary.

RESOURCE IDENTIFICATION INITIATIVE

CRAN: RRID:SCR_003005, vegan: RRID:SCR_011950.

AUTHOR CONTRIBUTIONS

DK, TD, and JN conceived the study. HO analyzed the samples and wrote the manuscript with considerable input of all coauthors.

FUNDING

This work was supported by NSF grants OCE-1030306 and OCE-1261359 to DK. HO, JN, and TD were funded by the University of Oldenburg, Germany.

ACKNOWLEDGMENTS

The field work was only possible with the help of Matt Cottrell, Monica Stegman, Thomas Lankiewicz, Katie Kalis, Raphaël Lami,

and Dave Kieber while Liying Yu was essential in the laboratory analyses. We are grateful to Matthias Friebe and Ina Ulber for DOC/TDN analysis and to Katrin Klapproth for FT-ICR-MS analysis.

SUPPLEMENTARY MATERIAL

The Supplementary Material for this article can be found online at: <http://journal.frontiersin.org/article/10.3389/feart.2016.00095/full#supplementary-material>

REFERENCES

- Abdulla, H. A. N., Minor, E. C., Dias, R. F., and Hatcher, P. G. (2013). Transformations of the chemical compositions of high molecular weight DOM along a salinity transect: using two dimensional correlation spectroscopy and principal component analysis approaches. *Geochim. Cosmochim. Acta* 118, 231–246. doi: 10.1016/j.gca.2013.03.036
- Abdulla, H. A. N., Minor, E. C., Dias, R. F., and Hatcher, P. G. (2010). Changes in the compound classes of dissolved organic matter along an estuarine transect: a study using FTIR and C-13 NMR. *Geochim. Cosmochim. Acta* 74, 3815–3838. doi: 10.1016/j.gca.2010.04.006
- Amon, R. M. W., Fitznar, H. P., and Benner, R. (2001). Linkages among the bioreactivity, chemical composition, and diagenetic state of marine dissolved organic matter. *Limnol. Oceanogr.* 46, 287–297. doi: 10.4319/lo.2001.46.2.0287
- Aufdenkampe, A. K., Hedges, J. I., Richey, J. E., Krusche, A. V., and Llerena, C. A. (2001). Sorptive fractionation of dissolved organic nitrogen and amino acids onto fine sediments within the Amazon Basin. *Limnol. Oceanogr.* 46, 1921–1935. doi: 10.4319/lo.2001.46.8.1921
- Azam, F., Smith, D. C., Steward, G. F., and Hagström, Å. (1994). Bacteria-organic matter coupling and its significance for oceanic carbon cycling. *Microb. Ecol.* 28, 167–179. doi: 10.1007/BF00166806
- Badr, E.-S. A., Tappin, A. D., and Achterberg, E. P. (2008). Distributions and seasonal variability of dissolved organic nitrogen in two estuaries in SW England. *Mar. Chem.* 110, 153–164. doi: 10.1016/j.marchem.2008.04.007
- Bate-Smith, E. C. (1968). The phenolic constituents of plants and their taxonomic significance. *J. Linn. Soc. Lond. Bot.* 60, 325–356. doi: 10.1111/j.1095-8339.1968.tb00094.x
- Bauer, J. E., and Bianchi, T. S. (2011). “Dissolved organic carbon cycling and transformation,” in *Treatise on Estuarine and Coastal Science*, Vol. 5, eds E. Wolanski and D. S. McLusky (Waltham, MA: Academic Press), 7–67.
- Benner, R., Fogel, M. L., Sprague, E. K., and Hodson, R. E. (1987). Depletion of ¹³C in lignin and its implications for stable carbon isotope studies. *Nature* 329, 708–710. doi: 10.1038/329708a0
- Biggs, R. B., Sharp, J. H., Church, T. M., and Tramontano, J. M. (1983). Optical properties, suspended sediments, and chemistry associated with the turbidity maxima of the Delaware Estuary. *Can. J. Fish. Aquat. Sci.* 40, 172–179. doi: 10.1139/f83-279
- Bourgoin, L.-H., and Tremblay, L. (2010). Bacterial reworking of terrigenous and marine organic matter in estuarine water columns and sediments. *Geochim. Cosmochim. Acta* 74, 5593–5609. doi: 10.1016/j.gca.2010.06.037
- Bray, J. R., and Curtis, J. T. (1957). An ordination of the upland forest communities of southern Wisconsin. *Ecol. Monogr.* 27, 326–349. doi: 10.2307/1942268
- Cadée, G. C. (1982). Tidal and seasonal variation in particulate and dissolved organic carbon in the western dutch Wadden Sea and Marsdiep tidal inlet. *Neth. J. Sea Res.* 15, 228–249. doi: 10.1016/0077-7579(82)90006-0
- Cao, X., Aiken, G. R., Spencer, R. G. M., Butler, K., Mao, J., and Schmidt-Rohr, K. (2016). Novel insights from NMR spectroscopy into seasonal changes in the composition of dissolved organic matter exported to the Bering Sea by the Yukon River. *Geochim. Cosmochim. Acta* 181, 72–88. doi: 10.1016/j.gca.2016.02.029
- Cifuentes, L. A. (1991). Spatial and temporal variations in terrestrially-derived organic-matter from sediments of the Delaware Estuary. *Estuaries* 14, 414–429. doi: 10.2307/1352266
- Cifuentes, L. A., Schemel, L. E., and Sharp, J. H. (1990). Qualitative and numerical analyses of the effects of river inflow variations on mixing diagrams in estuaries. *Estuar. Coast. Shelf Sci.* 30, 411–427. doi: 10.1016/0272-7714(90)90006-D
- Cole, J. J., Prairie, Y. T., Caraco, N. F., McDowell, W. H., Tranvik, L. J., Striegl, R. G., et al. (2007). Plumbing the global carbon cycle: integrating inland waters into the terrestrial carbon budget. *Ecosystems* 10, 172–185. doi: 10.1007/s10021-006-9013-8
- D’Andrilli, J., Cooper, W. T., Foreman, C. M., and Marshall, A. G. (2015). An ultrahigh-resolution mass spectrometry index to estimate natural organic matter lability. *Rapid Commun. Mass Spectrom.* 29, 2385–2401. doi: 10.1002/rcm.7400
- Del Vecchio, R., and Blough, N. V. (2004). Spatial and seasonal distribution of chromophoric dissolved organic matter and dissolved organic carbon in the Middle Atlantic Bight. *Mar. Chem.* 89, 169–187. doi: 10.1016/j.marchem.2004.02.027
- Dittmar, T., Koch, B., Hertkorn, N., and Kattner, G. (2008). A simple and efficient method for the solid-phase extraction of dissolved organic matter (SPE-DOM) from seawater. *Limnol. Oceanogr. Methods* 6, 230–235. doi: 10.4319/lom.2008.6.230
- Eisma, D. (1986). Flocculation and de-flocculation of suspended matter in estuaries. *Neth. J. Sea Res.* 20, 183–199. doi: 10.1016/0077-7579(86)90041-4
- Ertel, J. R., Hedges, J. I., Devol, A. H., Richey, J. E., and Ribeiro, M. D. N. G. (1986). Dissolved humic substances of the Amazon River system. *Limnol. Oceanogr.* 31, 739–754. doi: 10.4319/lo.1986.31.4.0739
- Fox, L. E. (1983). The removal of dissolved humic acid during estuarine mixing. *Estuar. Coast. Shelf Sci.* 16, 431–440. doi: 10.1016/0272-7714(83)90104-X
- Garvine, R. W., McCarthy, R. K., and Wong, K.-C. (1992). The axial salinity distribution in the Delaware Estuary and its weak response to river discharge. *Estuar. Coast. Shelf Sci.* 35, 157–165. doi: 10.1016/S0272-7714(05)80110-6
- Goñi, M. A., and Gardner, I. R. (2003). Seasonal dynamics in dissolved organic carbon concentrations in a Coastal Water-table aquifer at the forest-marsh interface. *Aquat. Geochem.* 9, 209–232. doi: 10.1023/B:AQUA.0000022955.82700.ed
- Gonsior, M., Zwartjes, M., Cooper, W. J., Song, W., Ishida, K. P., Tseng, L. Y., et al. (2011). Molecular characterization of effluent organic matter identified by ultrahigh resolution mass spectrometry. *Water Res.* 45, 2943–2953. doi: 10.1016/j.watres.2011.03.016
- Green, N. W., Perdue, E. M., Aiken, G. R., Butler, K. D., Chen, H., Dittmar, T., et al. (2014). An intercomparison of three methods for the large-scale isolation of oceanic dissolved organic matter. *Mar. Chem.* 161, 14–19. doi: 10.1016/j.marchem.2014.01.012
- Hedges, J. I., Keil, R. G., and Benner, R. (1997). What happens to terrestrial organic matter in the ocean? *Org. Geochem.* 27, 195–212.
- Hedges, J. I., and Weliky, K. (1989). Diagenesis of conifer needles in a coastal marine environment. *Geochim. Cosmochim. Acta* 53, 2659–2673. doi: 10.1016/0016-7037(89)90137-3
- Hermes, A. L., and Sikes, E. L. (2016). Particulate organic matter higher concentrations, terrestrial sources and losses in bottom waters of the turbidity maximum, Delaware Estuary, U.S.A. *Estuar. Coast. Shelf Sci.* 180, 179–189. doi: 10.1016/j.ecss.2016.07.005
- Hernes, P. J., and Benner, R. (2003). Photochemical and microbial degradation of dissolved lignin phenols: implications for the fate of terrigenous dissolved

- organic matter in marine environments. *J. Geophys. Res. Oceans* 108:3291. doi: 10.1029/2002JC001421
- Hoch, M. P., and Kirchman, D. L. (1995). Ammonium uptake by heterotrophic bacteria in the Delaware Estuary and adjacent coastal waters. *Limnol. Oceanogr.* 40, 886–897. doi: 10.4319/lo.1995.40.5.0886
- Holmes, R. M., McClelland, J. W., Peterson, B. J., Tank, S. E., Bulygina, E., Eglinton, T. L., et al. (2011). Seasonal and annual fluxes of nutrients and organic matter from large Rivers to the Arctic Ocean and surrounding Seas. *Estuar. Coasts* 35, 369–382. doi: 10.1007/s12237-011-9386-6
- Hossler, K., and Bauer, J. E. (2012). Estimation of riverine carbon and organic matter source contributions using time-based isotope mixing models. *J. Geophys. Res. Biogeosci.* 117, G03035. doi: 10.1029/2012jg001988
- Hossler, K., and Bauer, J. E. (2013). Amounts, isotopic character, and ages of organic and inorganic carbon exported from rivers to ocean margins: 1. Estimates of terrestrial losses and inputs to the Middle Atlantic Bight. *Global Biogeochem. Cycles* 27, 331–346. doi: 10.1002/gbc.20033
- Keil, R. G., Montlucon, D. B., Prahl, F. G., and Hedges, J. I. (1994). Sorptive preservation of labile organic matter in Marine Sediments. *Nature* 370, 549–552. doi: 10.1038/370549a0
- Ketchum, B. H. (1952). The distribution of salinity in the estuary of the Delaware River. *Woods Hole Oceanogr. Instit. Rep.* 52–103. doi: 10.1575/1912/5339
- Kim, S., Kaplan, L. A., and Hatcher, P. G. (2006). Biodegradable dissolved organic matter in a temperate and a tropical stream determined from ultrahigh resolution mass spectrometry. *Limnol. Oceanogr.* 51, 1054–1063. doi: 10.4319/lo.2006.51.2.1054
- Kirchman, D. L. (2001). “Measuring bacterial biomass production and growth rates from leucine incorporation in natural aquatic environments,” in *Methods in Microbiology*, ed J. H. Paul (St. Petersburg, FL: Academic Press), 227–237.
- Kirchman, D. L., and Borch, N. H. (2003). Fluxes of dissolved combined neutral sugars (polysaccharides) in the Delaware Estuary. *Estuaries* 26, 894–904. doi: 10.1007/BF02803348
- Koch, B. P., and Dittmar, T. (2006). From mass to structure: an aromaticity index for high-resolution mass data of natural organic matter. *Rapid Commun. Mass Spectrom.* 20, 926–932. doi: 10.1002/rcm.2386
- Koch, B. P., Dittmar, T., Witt, M., and Kattner, G. (2007). Fundamentals of molecular formula assignment to ultrahigh resolution mass data of natural organic matter. *Anal. Chem.* 79, 1758–1763. doi: 10.1021/ac061949s
- Koch, B. P., Witt, M. R., Engbrodt, R., Dittmar, T., and Kattner, G. (2005). Molecular formulae of marine and terrigenous dissolved organic matter detected by electrospray ionization Fourier transform ion cyclotron resonance mass spectrometry. *Geochim. Cosmochim. Acta* 69, 3299–3308. doi: 10.1016/j.gca.2005.02.027
- Landa, M., Cottrell, M. T., Kirchman, D. L., Kaiser, K., Medeiros, P. M., Tremblay, L., et al. (2014). Phylogenetic and structural response of heterotrophic bacteria to dissolved organic matter of different chemical composition in a continuous culture study. *Environ. Microbiol.* 16, 1668–1681. doi: 10.1111/1462-2920.12242
- Li, Y., Harir, M., Lucio, M., Kanawati, B., Smirnov, K., Flerus, R., et al. (2016). Proposed guidelines for solid phase extraction of suwannee River dissolved organic matter. *Anal. Chem.* 88, 6680–6688. doi: 10.1021/acs.analchem.5b04501
- Liu, W., Wang, Y., Russell, A., and Edgerton, E. S. (2005). Atmospheric aerosol over two urban–rural pairs in the southeastern United States: chemical composition and possible sources. *Atmos. Environ.* 39, 4453–4470. doi: 10.1016/j.atmosenv.2005.03.048
- Liu, Z., Sleighter, R. L., Zhong, J., and Hatcher, P. G. (2011). The chemical changes of DOM from black waters to coastal marine waters by HPLC combined with ultrahigh resolution mass spectrometry. *Estuar. Coast. Shelf Sci.* 92, 205–216. doi: 10.1016/j.ecss.2010.12.030
- Luther, G. W. III, Church, T. M., Scudlark, J. R., and Cosman, M. (1986). Inorganic and organic sulfur cycling in salt-marsh pore waters. *Science* 232, 746–749. doi: 10.1126/science.232.4751.746
- Maie, N., Pisani, O., and Jaffé, R. (2008). Mangrove tannins in aquatic ecosystems: their fate and possible influence on dissolved organic carbon and nitrogen cycling. *Limnol. Oceanogr.* 53, 160–171. doi: 10.4319/lo.2008.53.1.0160
- Mannino, A., and Harvey, H. R. (1999). Lipid composition in particulate and dissolved organic matter in the Delaware Estuary: sources and diagenetic patterns. *Geochim. Cosmochim. Acta* 63, 2219–2235. doi: 10.1016/S0016-7037(99)00128-3
- Mannino, A., and Harvey, H. R. (2000a). Biochemical composition of particles and dissolved organic matter along an estuarine gradient: Sources and implications for DOM reactivity. *Limnol. Oceanogr.* 45, 775–788. doi: 10.4319/lo.2000.45.4.0775
- Mannino, A., and Harvey, H. R. (2000b). Terrigenous dissolved organic matter along an estuarine gradient and its flux to the coastal ocean. *Org. Geochem.* 31, 1611–1625. doi: 10.1016/S0146-6380(00)00099-1
- Mayer, L. M. (1994). Relationships between mineral surfaces and organic carbon concentrations in soils and sediments. *Chem. Geol.* 114, 347–363. doi: 10.1016/0009-2541(94)90063-9
- Medeiros, P. M., Seidel, M., Dittmar, T., Whitman, W. B., and Moran, M. A. (2015a). Drought-induced variability in dissolved organic matter composition in a marsh-dominated estuary. *Geophys. Res. Lett.* 42, 6446–6453. doi: 10.1002/2015GL064653
- Medeiros, P. M., Seidel, M., Niggemann, J., Spencer, R. G. M., Hernes, P. J., Yager, P. L., et al. (2016). A novel molecular approach for tracing terrigenous dissolved organic matter into the deep ocean. *Global Biogeochem. Cycles* 30, 689–699. doi: 10.1002/2015GB005320
- Medeiros, P. M., Seidel, M., Ward, N. D., Carpenter, E. J., Gomes, H. R., Niggemann, J., et al. (2015b). Fate of the Amazon River dissolved organic matter in the tropical Atlantic Ocean. *Global Biogeochem. Cycles* 29, 677–690. doi: 10.1002/2015GB005115
- Meyers-Schulte, K. J., and Hedges, J. I. (1986). Molecular evidence for a terrestrial component of organic matter dissolved in ocean water. *Nature* 321, 61–63. doi: 10.1038/321061a0
- Middelburg, J. J., and Herman, P. M. J. (2007). Organic matter processing in tidal estuaries. *Mar. Chem.* 106, 127–147. doi: 10.1016/j.marchem.2006.02.007
- Miller, A. E. J. (1999). Seasonal investigations of dissolved organic carbon dynamics in the Tamar Estuary, U.K. *Estuar. Coast. Shelf Sci.* 49, 891–908. doi: 10.1006/ecss.1999.0552
- Oksanen, J., Blanchet, F. G., Kindt, R., Legendre, P., Minchin, P. R., O’Hara, R. B., et al. (2015). *Vegan: Community Ecology Package, R Package Version 2.3-1*. Available online at: <http://CRAN.R-project.org/package=vegan>
- Osterholz, H., Niggemann, J., Giebel, H. A., Simon, M., and Dittmar, T. (2015). Inefficient microbial production of refractory dissolved organic matter in the ocean. *Nat. Commun.* 6, 7422. doi: 10.1038/ncomms8422
- Partnership for the Delaware Estuary (2012). *Technical Report for the Delaware Estuary and Basin*. A complete section author list is available at the end of the report.
- Pennock, J. R., and Sharp, J. H. (1986). Phytoplankton production in the Delaware Estuary - Temporal and spatial variability. *Mar. Ecol. Prog. Ser.* 34, 143–155. doi: 10.3354/meps034143
- Polis, D., and Kupferman, S. L. (1973). *Physical Oceanography*. Newark, NJ: College of Marine Studies, University of Delaware.
- Raeke, J., Lechtenfeld, O. J., Wagner, M., Herzsprung, P., and Reemtsma, T. (2016). Selectivity of solid phase extraction of freshwater dissolved organic matter and its effect on ultrahigh resolution mass spectra. *Environ. Sci. Process. Impacts* 18, 918–927. doi: 10.1039/c6em00200e
- Raymond, P. A., and Bauer, J. E. (2001). DOC cycling in a temperate estuary: a mass balance approach using natural ¹⁴C and ¹³C isotopes. *Limnol. Oceanogr.* 46, 655–667. doi: 10.4319/lo.2001.46.3.0655
- Raymond, P. A., and Saiers, J. E. (2010). Event controlled DOC export from forested watersheds. *Biogeochemistry* 100, 197–209. doi: 10.1007/s10533-010-9416-7
- Riedel, T., Biester, H., and Dittmar, T. (2012). Molecular fractionation of dissolved organic matter with metal salts. *Environ. Sci. Technol.* 46, 4419–4426. doi: 10.1021/es203901u
- Riedel, T., and Dittmar, T. (2014). A Method detection limit for the analysis of natural organic matter via fourier transform ion cyclotron resonance mass spectrometry. *Anal. Chem.* 86, 8376–8382. doi: 10.1021/ac501946m
- Riedel, T., Zark, M., Vähätalo, A. V., Niggemann, J., Spencer, R. G. M., Hernes, P. J., et al. (2016). Molecular signatures of biogeochemical transformations in dissolved organic matter from ten World Rivers. *Front. Earth Sci.* 4:85. doi: 10.3389/feart.2016.00085

- Sarkanen, K., and Ludwig, C. (1971). *Lignins: Occurrence, Formation, Structure, and Reactions*. New York, NY: John Wiley and Sons, Inc.
- Schiff, S., Aravena, R., Mewhinney, E., Elgood, R., Warner, B., Dillon, P., et al. (1998). Precambrian shield Wetlands: hydrologic control of the sources and export of dissolved organic matter. *Clim. Change* 40, 167–188. doi:10.1023/A:1005496331593
- Seidel, M., Beck, M., Greskowiak, J., Riedel, T., Waska, H., Suryaputra, I. G. N. A., et al. (2015a). Benthic-pelagic coupling of nutrients and dissolved organic matter composition in an intertidal sandy beach. *Mar. Chem.* 176, 150–163. doi:10.1016/j.marchem.2015.08.011
- Seidel, M., Beck, M., Riedel, T., Waska, H., Suryaputra, I. G. N. A., Schnetger, B., et al. (2014). Biogeochemistry of dissolved organic matter in an anoxic intertidal creek bank. *Geochim. Cosmochim. Acta* 140, 418–434. doi:10.1016/j.gca.2014.05.038
- Seidel, M., Yager, P. L., Ward, N. D., Carpenter, E. J., Gomes, H. R., Krusche, A. V., et al. (2015b). Molecular-level changes of dissolved organic matter along the Amazon River-to-ocean continuum. *Mar. Chem.* 177, 218–231. doi:10.1016/j.marchem.2015.06.019
- Sharp, J. H., Culberson, C. H., and Church, T. M. (1982). The chemistry of the Delaware Estuary - General considerations. *Limnol. Oceanogr.* 27, 1015–1028. doi:10.4319/lo.1982.27.6.1015
- Sharp, J. H., Yoshiyama, K., Parker, A. E., Schwartz, M. C., Curless, S. E., Beauregard, A. Y., et al. (2009). A biogeochemical view of Estuarine Eutrophication: seasonal and spatial trends and correlations in the Delaware Estuary. *Estuar. Coasts* 32, 1023–1043. doi:10.1007/s12237-009-9210-8
- Sleighter, R. L., and Hatcher, P. G. (2008). Molecular characterization of dissolved organic matter (DOM) along a river to ocean transect of the lower Chesapeake Bay by ultrahigh resolution electrospray ionization Fourier transform ion cyclotron resonance mass spectrometry. *Mar. Chem.* 110, 140–152. doi:10.1016/j.marchem.2008.04.008
- Spencer, R. G. M., Aiken, G. R., Wickland, K. P., Striegl, R. G., and Hernes, P. J. (2008). Seasonal and spatial variability in dissolved organic matter quantity and composition from the Yukon River basin, Alaska. *Global Biogeochem. Cycles* 22, GB4002. doi:10.1029/2008GB003231
- Spencer, R. G. M., Stubbins, A., Hernes, P. J., Baker, A., Mopper, K., Aufdenkampe, A. K., et al. (2009). Photochemical degradation of dissolved organic matter and dissolved lignin phenols from the Congo River. *J. Geophys. Res. Biogeosci.* 114, G03010. doi:10.1029/2009JG000968
- Stenson, A. C., Marshall, A. G., and Cooper, W. T. (2003). Exact masses and chemical formulas of individual Suwannee River fulvic acids from ultrahigh resolution electrospray ionization fourier transform ion cyclotron resonance mass spectra. *Anal. Chem.* 75, 1275–1284. doi:10.1021/ac026106p
- Stubbins, A., Spencer, R. G. M., Chen, H., Hatcher, P. G., Mopper, K., Hernes, P. J., et al. (2010). Illuminated darkness: molecular signatures of Congo River dissolved organic matter and its photochemical alteration as revealed by ultrahigh precision mass spectrometry. *Limnol. Oceanogr.* 55, 1467–1477. doi:10.4319/lo.2010.55.4.1467
- Sun, L., Perdue, E. M., Meyer, J. L., and Weis, J. (1997). Use of elemental composition to predict bioavailability of dissolved organic matter in a Georgia River. *Limnol. Oceanogr.* 42, 714–721. doi:10.4319/lo.1997.42.4.0714
- Sutton, C., O'Herron, J., and Zappalorti, R. (1996). *The Scientific Characterization of the Delaware Estuary. Technical Report (DRBC Project No. 321; HA File No. 93.21)*. Delaware Estuary Program, U.S. Environmental Protection Agency, New York.
- Taniguchi, M., Burnett, W. C., Cable, J. E., and Turner, J. V. (2002). Investigation of submarine groundwater discharge. *Hydro. Process.* 16, 2115–2129. doi:10.1002/hyp.1145
- Šantil-Temkiv, T., Finster, K., Dittmar, T., Hansen, B. M., Thyraug, R., Nielsen, N. W., et al. (2013). Hailstones: a window into the microbial and chemical inventory of a storm cloud. *PLoS ONE* 8:e53550. doi:10.1371/journal.pone.0053550
- Tzortziou, M., Zeri, C., Dimitriou, E., Ding, Y., Jaffé, R., Anagnostou, E., et al. (2015). Colored dissolved organic matter dynamics and anthropogenic influences in a major transboundary river and its coastal wetland. *Limnol. Oceanogr.* 60, 1222–1240. doi:10.1002/lno.10092
- Vodacek, A., Blough, N. V., Degrandpre, M. D., Degrandpre, M. D., and Nelson, R. K. (1997). Seasonal variation of CDOM and DOC in the Middle Atlantic Bight: terrestrial inputs and photooxidation. *Limnol. Oceanogr.* 42, 674–686. doi:10.4319/lo.1997.42.4.0674
- Wagner, S., Riedel, T., Niggemann, J., Vähätalo, A. V., Dittmar, T., and Jaffé, R. (2015). Linking the molecular signature of heteroatomic dissolved organic matter to watershed characteristics in world rivers. *Environ. Sci. Technol.* 49, 13798–13806. doi:10.1021/acs.est.5b00525
- Ward, N. D., Keil, R. G., Medeiros, P. M., Brito, D. C., Cunha, A. C., Dittmar, T., et al. (2013). Degradation of terrestrially derived macromolecules in the Amazon River. *Nat. Geosci.* 6, 530–533. doi:10.1038/ngeo1817
- Williams, P. M., and Druffel, E. R. M. (1987). Radiocarbon in dissolved organic matter in the central North Pacific Ocean. *Nature* 330, 246–248. doi:10.1038/330246a0

Conflict of Interest Statement: The other authors declare that the research was conducted in the absence of any commercial or financial relationships that could be construed as a potential conflict of interest.

The handling Editor declared a past co-authorship with the author TD and states that the process nevertheless met the standards of a fair and objective review.

Copyright © 2016 Osterholz, Kirchman, Niggemann and Dittmar. This is an open-access article distributed under the terms of the Creative Commons Attribution License (CC BY). The use, distribution or reproduction in other forums is permitted, provided the original author(s) or licensor are credited and that the original publication in this journal is cited, in accordance with accepted academic practice. No use, distribution or reproduction is permitted which does not comply with these terms.

The Chemical Potential of Water in Soils and Sediments

Thomas Riedel*

Forschungsgruppe für Marine Geochemie
ICBM-MPI Brückengruppe
Carl von Ossietzky Universität
Carl-von-Ossietzky-Straße 9-11
26111 Oldenburg
Deutschland

Tobias K.D. Weber

Institut für Geoökologie
Technische Universität Braunschweig
Langer Kamp 19c
38106, Braunschweig
Deutschland

The chemical potential of water characterizes the thermodynamic state of the aqueous environment in soils and sediments. In the presence of clay minerals and other fines, such as organic matter and silt, it is lower than at standard state (less than $-237.18 \text{ kJ mol}^{-1}$). As a result, chemical reactions may proceed rather differently than in an ideal aqueous solution. This is currently not considered in biogeochemical models of soils and sediments. Therefore, we conducted a series of quantitative measurements of water's chemical potential in soils of various clay content. We can show that the amount of pore water in soils traditionally determined gravimetrically from water loss after drying at 105°C , overestimates the pore water that is thermodynamically at standard state. We discuss implications for biogeochemical processes in soils and sediments and give evidence that clay content is a good predictor for an estimate of chemical potential. Although the accurate chemical potential of water has so far received little attention, it may emerge as a useful tool in soils sciences, geochemistry, and other related disciplines.

Soils and sediments are complex mixtures of solid substances such as minerals and organic matter. However, if it was just this, no chemical reactions would occur and life would not exist in the earth's upper crust. The void volume between the solid compounds provides space for water, air, and organisms that thrive on the consumption of minerals and organic matter. The most important compound to sustain life is water which acts both as solvent and reactant. The chemical properties of soil pore water can be defined via various measures such as pH, redox state, or ionic strength. A property that is rarely considered in studies on soils and sediments is the chemical potential of water, $\mu_{\text{H}_2\text{O}}$. Assuming constant pressure, it is calculated from the activity of water, $a_{\text{H}_2\text{O}}$.

$$\mu_{\text{H}_2\text{O}} = \mu_{\text{H}_2\text{O}}^0 + RT \ln a_{\text{H}_2\text{O}} \quad [1]$$

where $\mu_{\text{H}_2\text{O}}^0$ is the standard chemical potential, R is the universal gas constant in $\text{J K}^{-1} \text{mol}^{-1}$, and T is absolute temperature of the system in K (Blandamer et al., 2005). Equation [1] defines the relationship between energy and activity of water. Because R is a constant, the chemical potential of water becomes a function of water activity and temperature.

In biogeochemical models, the chemical potential, $\mu_{\text{H}_2\text{O}}$, of the interstitial water in the pores of soils and sediments is commonly assumed to be that of bulk free water, $-237.18 \text{ kJ mol}^{-1}$ (e.g., Leal et al., 2014), thermodynamically the standard state. When dissolved ions are present, $\mu_{\text{H}_2\text{O}}$ is lower than at the standard state and needs to be adjusted (Pitzer, 1991), because the hydration of ions reduces $\mu_{\text{H}_2\text{O}}$. Upon hydration water molecules are removed from solution, resulting in a decrease of the fraction of solvent (free) water and an increase in the fraction of bound water as some water molecules arrange around the ions (Marcus, 2009). In the presence of charged mineral surfaces a similar behavior of water is observed. Literature data on water activity in soils and sediments indicates that $a_{\text{H}_2\text{O}}$ (and thus $\mu_{\text{H}_2\text{O}}$) is not unity for bulk

Core Ideas

- Measurements of the true chemical potential of water in soils are presented.
- The thermodynamic state of water is not uniform in up to 80% of the pore spaces of soils and sediments.
- Application of the chemical potential of water in biogeochemical studies of soils is discussed.

This article has supplemental material available online.

Soil Sci. Soc. Am. J.
doi:10.2136/sssaj2015.02.0085

Received 27 Feb. 2015.

Accepted 17 Oct. 2015.

*Correspondence author: (Thomas.riedel@uni-oldenburg.de).

© Soil Science Society of America, 5585 Guilford Rd., Madison WI 53711 USA. All Rights reserved.

Table 1 Soil type, particle-size distribution (in weight percentage), and organic matter content (OM) of the soils analyzed in this study.

Soil Type	Horizon	Sand	Silt	Clay	OM
		2–0.63 mm	0.63–0.002 mm	<0.002 mm	
Chernozem	Ap	7.0	74.1	18.9	4.2
Leptosolt†	–	93.0	2.0	5.0	0.6
Cambisol	Ap	64.7	28.9	6.4	2.1
Cambisol	Bw	79.1	17.5	3.4	0.6
Luvisol	Bt	2.9	78.4	18.7	1.9

† data taken from Rosenzweig et al. (2012).

pore water (cf. references given in Table S1). Especially in clay-rich soils and sediments this effect is more pronounced because of the permanent charge of clay surfaces and the large specific surface area (Petersen et al., 1996). Additionally, increasing clay mineral content reduces larger pores and increases the abundance of fine pores in which water is strongly bound by capillary forces (Freeze and Cherry, 1979). Further, the large specific surface area of clay minerals forces more water molecules to orientate themselves toward the charged mineral surfaces (Feibelman, 2010). The result is that less water is “free” in bulk solution and has a lower tendency to react chemically in solution as the additional binding energy lowers its activity (e.g., Huppert et al., 1982; Blandamer et al., 2005). Other soil properties also influence the adsorption of water, for example, organic matter content (Jury et al., 1991), as well as silt content as was recently shown (Jensen et al., 2015). Thus, the assumption that $\mu_{\text{H}_2\text{O}}$ is constant is not valid for all pore water in a soil. Strikingly, although the effect of salt ions on the chemical potential of water is long accepted (e.g., Kielland, 1937), the effect of charged mineral surfaces is so far merely acknowledged.

For the present study, we gathered data from literature combined with our own measurements to exemplarily estimate the chemical potential of pore water in soils and sediments. The discussion includes mostly clay content as this data was readily available in the literature used. However, as outlined above, $\mu_{\text{H}_2\text{O}}$ is also affected by several other soil properties (not only clay content) and has to be considered as an integrative parameter.

With the resulting data set, we like to raise awareness for the chemical potential of water as a property that is equally useful in soil sciences in addition to other parameters such as pH or redox potential.

Materials and Methods

Sample sites were located in the Northern German lowlands, close to the town of Braunschweig. The Leptosol sample was taken about 35 km north-northeast of Tel Aviv, Israel. Sampling was done with trowels; buckets were used for transport and storage. Aliquots of approximately 100 cm³ with no skeletal content were air dried in the laboratory and roots removed. Subsequently the samples were carefully ground to break up the soil aggregates. All subsequent analyses were done on the ground samples with particle size <2 mm. Samples were carbonate free allowing determination of organic matter (OM) content from loss on ignition on oven dried (105°C) samples after heating them in a muffle furnace at 400°C for 16 h (Nelson and Sommers, 1996).

Similarly to Lu et al. (2008), we added water to the ground air-dry soil samples and subsequently mixed them thoroughly. Three replicates of each sample type were prepared for the dew point measurement by placing them into sampling cups. To attain different water contents sampling cups were left uncovered at 20°C so that water could evaporate. After this, the covered samples were equilibrated for 24 h before $\mu_{\text{H}_2\text{O}}$ was determined. The samples were immediately weighed after each analysis. We repeated the drying, analysis, and weighing until the samples were air dry. Finally, all samples were oven dried and gravimetric water content could be determined for each measurement cycle. As only desiccation was performed, hysteresis effects are not considered.

For the laboratory estimate of $\mu_{\text{H}_2\text{O}}$, a WP4C Dewpoint Potentiometer (Decagon Devices, Inc., Pullmann, WA) was used. In a closed chamber the relative humidity (RH), in equilibrium with the samples moisture, is measured using the chilled mirror water vapor method (Gee et al., 1992) and from this $a_{\text{H}_2\text{O}}$ is calculated by $a_{\text{H}_2\text{O}} = \text{RH} \times 10^{-2}$. The WP4C measures both mirror and sample temperature with 0.001°C accuracy, resulting in an $a_{\text{H}_2\text{O}}$ reading accuracy of <0.001 in the 0.993 to 0.113 range. The chemical potential $\mu_{\text{H}_2\text{O}}$ was then calculated using Eq. [1] for standard conditions. All samples were run in triplicate.

The particle-size distribution was determined with the pipette method (Gee and Or, 2002).

We measured the gravimetric water content and the corresponding $\mu_{\text{H}_2\text{O}}$ in five samples of natural non saline soil (listed in Table 1) and of a pure sand sample consisting of homogenous grains where 0, 1, and 5% (w/w) of commercially available bentonite (Sigma Aldrich, St. Louis, MO) were added, respectively.

Additional data for 19 non saline soils was compiled from literature (see Table S1). The gravimetric water contents for the soils from the study presented by Lu et al. (2008) were calculated for $a_{\text{H}_2\text{O}} = 0.984$ ($\mu_{\text{H}_2\text{O}} = -274 \text{ kJ mol}^{-1}$) from parametric model fits describing the soil water retention curve of the Kholsi et al. Model (Kholsi et al., 2006). The datasets of Fink and Jackson (1973), Campbell and Shiozawa (1992), and Campbell et al. (1993) were used to fit a three parametric water adsorption isotherm for clay and silt (Fink and Jackson, 1973).

RESULTS

Accurate Chemical Potential of Water in Soils

All soil samples showed evidence for the abundance of pore water with chemical potentials lower than at standard state (Fig. 1), that is, the $\mu_{\text{H}_2\text{O}}$ of this pore water differs from that of water in an ideal solution. For example, considering the Luvisol sample in Fig. 1b, the $\mu_{\text{H}_2\text{O}}$ in up to 75 mg of H₂O per g of soil reveals to be less than $-237.18 \text{ kJ mol}^{-1}$ and may drop as low as $-1200 \text{ kJ mol}^{-1}$. When we assume a typical bulk density, ρ_{bulk} , of 1.2 g cm^{-3} and an average particle density, ρ_{part} , of 2.65 g cm^{-3} this soil has a porosity of ~ 0.55 (calculated as $1 - \rho_{\text{bulk}}/\rho_{\text{part}}$). Under fully saturated conditions, this equates to 550 mg H₂O per g soil. Thus, the 75 mg of H₂O correspond to $\sim 14\%$ of the pore space in this soil that contains water with $\mu_{\text{H}_2\text{O}} < -237.18 \text{ kJ mol}^{-1}$. Most importantly, the content of pore water with a $\mu_{\text{H}_2\text{O}}$ signifi-

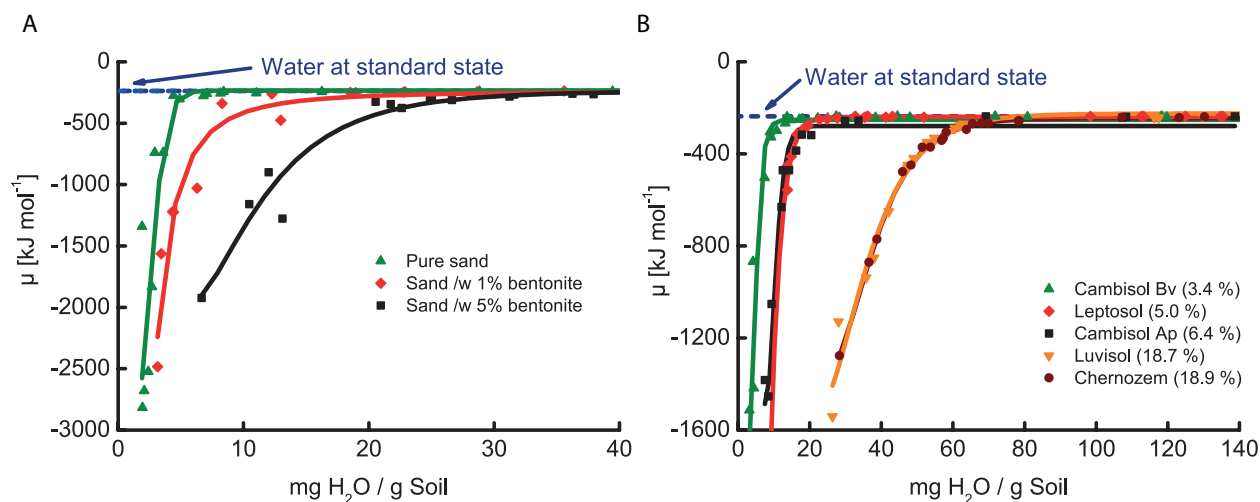


Fig. 1. Examples of chemical potential of total pore water, $\mu_{\text{H}_2\text{O}}$, as a function of gravimetric water content. (A) A pure sand with two additions of bentonite, (B) Five different soils with different clay content. Clay content is indicated in the figure legend after the soil name in parenthesis. The horizontal dashed line in blue depicts the chemical potential of free water at standard state ($-237.18 \text{ kJ mol}^{-1}$). Solid lines are fits only to illustrate the basic trends. Clay content (fraction with grain size diameter $< 2 \mu\text{m}$) is given as percentage of weight.

cantly lower than at standard state increased with increasing clay content. At a specific chemical potential the soil water content increases mainly as a function of clay (Fig. 2).

Discussion

Our data shows that the chemical potential of water in soils and sediments is not equivalent to that of free water. As the water content of a porous medium decreases, the fraction of adsorbed and more tightly bound water, mainly associated with mineral surfaces and small pores, remains constant while the fraction of free water decreases due to evaporative loss, hence, $\mu_{\text{H}_2\text{O}}$ drops. Soil (and sediment) water content is traditionally expressed as the ratio of the total mass of water present in a sample before drying to the mass of the sample after it has been dried to a constant mass at 105°C (Topp and Ferré, 2002). Thus the traditional methods that are used to evaluate soil water content overestimate the pore water content with $\mu_{\text{H}_2\text{O}} = -237 \text{ KJ mol}^{-1}$. Using published water activity data from the Trenton clay, a pure clay soil (Thomas, 1924), it may be estimated that $>80\%$ of the pore water is thermodynamically not at a standard state in this particular soil. Considering clay-rich sedimentary facies such as heavily weathered soils or marine deep sea deposits, this means that a large portion of the water in the pore space is thermodynamically different from a simple aqueous solution. We therefore argue that the commonly applied assumption in biogeochemical models of soil and sedimentary pore waters, that $\mu_{\text{H}_2\text{O}}$ is constant, is false and needs to be revised.

We report gravimetric rather than volumetric water content because our experiments were conducted with unconsolidated sediments. By doing so we neglect that soil structure, degree of aggregation, or bulk density may have some influence on our results. In closely packed sediments a larger proportion of water may be structurally bound than in loosely packed soils. Our approach may thus underestimate pore water content with $\mu_{\text{H}_2\text{O}}$ below standard state.

Note that the matric potential, which is used in soil physics to theoretically describe the state of water in porous geological media (e.g., Gee et al., 1992), is often determined similarly to the determination of $a_{\text{H}_2\text{O}}$. For this study, we therefore included works that measured or reported RH (or $a_{\text{H}_2\text{O}}$). We emphasize that the focus of the present work is on the chemical potential and that the matric potential is used to describe fluid flow and should not be confused with the chemical potential (Corey and Logsdon, 2005).

The effect of different clay mineralogy on $\mu_{\text{H}_2\text{O}}$ was not analyzed, but the different soil types used in this study likely exhibited mixed mineralogy, which suggests that the remarkable relationship between clay content and pore water of a specific $\mu_{\text{H}_2\text{O}}$ (Fig. 2) holds true for soils with different types of clay minerals. However, the small scatter of the data in Fig. 2 shows that other factors likely affect $\mu_{\text{H}_2\text{O}}$, for example, the heterogeneity of clay minerals and the presence of other fines such as organic matter and silt. The specific surface area that controls the adsorption of water (and thus the reduction of $\mu_{\text{H}_2\text{O}}$) depends on the type of clay mineral as well as the degree of weathering, silt content, and organic

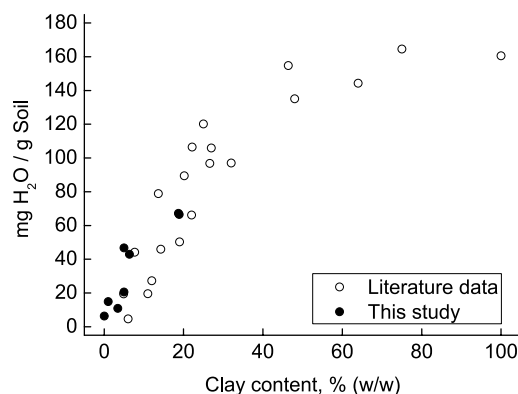


Fig. 2. Gravimetric content of water having a $\mu_{\text{H}_2\text{O}} < -274 \text{ kJ mol}^{-1}$ (amount of pore water in which microbial respiration turns thermodynamically unfavorable) as a function of clay content (fraction with grain size diameter $< 2 \mu\text{m}$) (Table S1).

matter (Jury et al., 1991; Petersen et al., 1996; Brady and Weil, 2008; Jensen et al., 2015). Especially in soils with low clay content, the role of organic matter may become increasingly important (Arthur et al., 2015) as well as in soils with very high OM content (Jensen et al., 2015). Some variation can therefore be expected for natural samples, although clay content seems to be a reasonably good predictor for an estimate of $\mu_{\text{H}_2\text{O}}$.

Effect of Chemical Potential on Other Solutes

The thermodynamics of aqueous solutions depend on the chemical potential of water. The thermodynamic activity of a solute is related to the activity of other solutes and the solvent via the Gibbs-Duhem equation:

$$\sum n_i d\mu_i = -SdT + Vdp \quad [2],$$

where S is entropy in J K^{-1} , V is volume in m^3 , p is pressure in Pa, n_i the number of moles to the i th component, and μ_i the chemical potential of the i th component. In a binary solution where p and T are kept constant Eq. [2] simplifies to

$$n_1 d\mu_1 + n_2 d\mu_2 = 0 \quad [3].$$

Thus, a change to μ_1 in a two-component system immediately influences μ_2 . The magnitude of change only depends on the molar ratio. Considering Component 1 as water, μ_2 for any given solute may be estimated via Eq. [3].

The chemical potential for a given solute dissolved in water with a chemical potential lower than at a standard state can be corrected via Eq. [3]. However, in geochemical models of clayey soils such corrections are not considered, albeit necessary for accurate thermodynamic calculations. In fact, biogeochemical studies do not determine the chemical potential of water and simply assume a value of $-237.18 \text{ kJ mol}^{-1}$. Therefore, this consideration is important to future research in soil biogeochemistry toward a better description and understanding of the chemical environment in soil pore waters. Using the Gibbs-Duhem equation may be a first theoretical approach, but can only be taken as an approximation, since it is not valid for inhomogeneous or small systems. In soils, where not only temperature and pressure, but also the adsorption of water influences $\mu_{\text{H}_2\text{O}}$, the validity of the Gibbs-Duhem equation either needs to be proven correctly or a new approach needs to be developed that is more appropriate.

Possible Relation between the Chemical Potential of Water and Microbial Activity in Soils and Sediments

When the thermodynamic activity of water falls below the standard state microbial processes, such as respiration, soon become unfavorable (Reid, 1980; Potts, 1994). Measurements of $\mu_{\text{H}_2\text{O}}$ (or the related water activity) can therefore be applied to quantify the amount of water that restricts microbial activity. In food control, for example, the thermodynamic state of water has found a wide application as an indicator for food stability since the 1970s because rates of chemical and biological reactions that degrade foods depend on this parameter (Labuza, 1971; Blandamer et al., 2005). For example, below a $\mu_{\text{H}_2\text{O}}$ of -260 kJ mol^{-1} ($a_{\text{H}_2\text{O}} = 0.99$) microbial growth becomes

limited and at lower $\mu_{\text{H}_2\text{O}}$ values of around -330 kJ mol^{-1} ($a_{\text{H}_2\text{O}} = 0.96$) microbial respiration ceases.

In soil and sediments, microbial activity has also been shown to be a function of $\mu_{\text{H}_2\text{O}}$, generally reported as the matric potential from which $\mu_{\text{H}_2\text{O}}$ can be calculated (Wilson and Griffin, 1975; Orchard and Cook, 1983; Fredrickson et al., 1989; Potts, 1994; Or et al., 2007). However, numbers vary slightly from those reported in food sciences. For example, in soils microbial respiration already ceases at $\mu_{\text{H}_2\text{O}} = -274 \text{ kJ mol}^{-1}$ ($a_{\text{H}_2\text{O}} = 0.984$; Wilson and Griffin, 1975). Figure 2 illustrates this point in more detail using our data as well as data from literature. Between 5 and 160 mg H_2O per g of soil had $\mu_{\text{H}_2\text{O}}$ of less than -274 kJ mol^{-1} (Fig. 2). In other words, up to 160 mg of H_2O per g of a soil or sediment appear to be thermodynamically unfavorable for microbial respiration. This pore water may be subtracted from the total pore water as it is not truly available for microbes. As soil carbon models are continuously improved the role of microorganisms is increasingly recognized (Wieder et al., 2013), because respiration to carbon dioxide links sedimentary organic matter mineralization to the atmospheric carbon pool (e.g., Schlesinger and Andrews, 2000). The quantification of the pore water fraction with $\mu_{\text{H}_2\text{O}} < -274 \text{ kJ mol}^{-1}$ may be useful for future endeavors to budget soil and sedimentary carbon cycles.

We note, however, that $\mu_{\text{H}_2\text{O}}$ only covers the thermodynamic state of the aqueous environment in a given soil or sediment. Other parameters such as redox conditions, the diversity of the microbial community or physical protection in organo-mineral complexes may also affect microbial respiration, but are not considered here. For example, pulses of carbon dioxide emissions from a soil during the first rain after a longer dry period are not only the result of an increase in the availability of free water, but a complex interplay of consecutively resuscitated microbial communities (Placella et al., 2012).

On a side note, suppression of microbial activity in fine-grained soils and sediments due to low $\mu_{\text{H}_2\text{O}}$ may serve as a tentative, yet unifying explanation for observations of why clay content correlates negatively with microbial activity (Fredrickson et al., 1989; Franzluebbers et al., 1996; McMahon and Chapelle, 1991), positively with organic carbon age (Wattel-Koekkoek et al., 2003), and positively with organic matter preservation (Keil et al., 1994; Kennedy et al., 2002).

CONCLUSIONS

Our main goal here is to raise the awareness that the thermodynamic state of water is not uniform in the pore spaces of soils and sediments. Current models of soils and sediments overestimate the amount of pore water thermodynamically at standard state with particularly strong effects at higher clay content. We therefore envisage the use of the chemical potential in addition to standard parameters such as redox potential, pH, or salinity for biogeochemical studies in soils and sediments. We further propose the need for new models that account for the reduced chemical potential of water which may reflect the physicochemical environment in the small pores of a soil or sediment more accurately. At the moment, popular geochemical tools such as PHREEQC

(Parkhurst and Appelo, 2013), do not allow one to adjust $\mu_{\text{H}_2\text{O}}$. The difficulty is that, as $\mu_{\text{H}_2\text{O}}$ drops, the chemical potential of other aqueous species in solution changes as well. As shown, this can theoretically be predicted using the Gibbs-Duhem equation. However, validation of this approach needs a new set of laboratory experiments designed to ultimately determine the effects of a reduced water chemical potential on biogeochemical reactions in unsaturated soils.

ACKNOWLEDGMENTS

We thank Ines Andrä for laboratory assistance and Wolfgang Durner for providing the analytical tools. Two anonymous reviewers provided helpful comments that greatly improved the manuscript.

REFERENCES

- Arthur, E., M. Tuller, P. Moldrup, D.K. Jensen, and L.W. de Jonge. 2015. Prediction of clay content from water vapour sorption isotherms considering hysteresis and soil organic matter content. *Eur. J. Soil Sci.* 66:206–217. doi:10.1111/ejss.12191
- Blandamer, M.J., J.B.F.N. Engberts, P.T. Gleeson, and J.C.R. Reis. 2005. Activity of water in aqueous systems; A frequently neglected property. *Chem. Soc. Rev.* 34:440–458. doi:10.1039/b400473f
- Brady, N.C., and R.R. Weil. 2008. *The nature and properties of soils*, 14th ed., Prentice Hall, Upper Saddle River, NJ.
- Campbell, G.S., and S. Shiozawa. 1992. Prediction of hydraulic properties of soils using particle-size distribution and bulk density data. In: M.T. van Genuchten et al., editors, *Proceedings of the International Workshop on Indirect Methods for Estimating Hydraulic Properties of Unsaturated Soils*, University of California, Riverside, CA. p. 317–328.
- Campbell, G.S., J.D. Jungbauer, Jr., S. Shiozawa, and R.D. Hungerford. 1993. A one-parameter equation for water sorption isotherms of soils. *Soil Sci.* 156:302–305. doi:10.1097/00010694-199311000-00002
- Corey, A.T., and S.B. Logsdon. 2005. Limitations of the chemical potential. *Soil Sci. Soc. Am. J.* 69:976–982. doi:10.2136/sssaj2004.0304
- Feibelman, P.J. 2010. The first wetting layer on a solid. *Phys. Today* 63:34–39. doi:10.1063/1.3326987
- Freeze, R.A., and J.A. Cherry. 1979. *Groundwater*: Prentice Hall Inc., Englewood Cliffs, NJ.
- Franzluebbers, A.J., R.L. Haney, F.M. Hons, and D.A. Zuberer. 1996. Active fractions of organic matter in soils with different texture. *Soil Biol. Biochem.* 28:1367–1372. doi:10.1016/S0038-0717(96)00143-5
- Fink, D.H., and R.D. Jackson. 1973. An equation describing water vapor adsorption isotherms of soils. *Soil Sci.* 116:256–261. doi:10.1097/00010694-197310000-00002
- Fredrickson, J.K., T.R. Garland, R.J. Hicks, J.M. Thomas, S.W. Li, and S.M. McFadden. 1989. Lithotrophic and heterotrophic bacteria in deep subsurface sediments and their relation to sediment properties. *Geomicrobiol. J.* 7:53–66. doi:10.1080/01490458909377849
- Gee, G.W., M.D. Campbell, G.S. Campbell, and J.H. Campbell. 1992. Rapid measurement of low soil water potentials using a water activity meter. *Soil Sci. Soc. Am. J.* 56:1068–1070. doi:10.2136/sssaj1992.03615995005600040010x
- Gee, G.W., and D. Or. 2002. Particle-size analysis. In: J.H. Dane and G.C. Topp, editors, *Methods of soil analysis*, Part 4. SSSA Book Ser. 5. SSSA, Madison, WI. p. 255–293.
- Huppert, D., E. Kolodney, M. Gutman, and E. Nachlielt. 1982. Effect of water activity on the rate of proton dissociation. *J. Am. Chem. Soc.* 104:6949–6953. doi:10.1021/ja00389a011
- Jensen, D.K., M. Tuller, L.W. de Jonge, E. Arthur, and P. Moldrup. 2015. A new two-stage approach to predicting the soil water characteristics from saturation to oven dryness. *J. Hydrol.* 521:498–507. doi:10.1016/j.jhydrol.2014.12.018
- Jury, W.A., W.R. Gardner, and W.H. Gardner. 1991. *Soil physics*. 5th ed., John Wiley & Sons, New York.
- Keil, R.G., D.B. Montlucon, F.B. Prah, and J.I. Hedges. 1994. Sorptive preservation of labile organic matter in marine sediments. *Nature* 370:549–552. doi:10.1038/370549a0
- Kennedy, M.J., D.R. Pevear, and D.J. Hill. 2002. Mineral surface control of organic carbon in black shale. *Science* 295:657–660. doi:10.1126/science.1066611
- Kielland, J. 1937. Individual activity coefficients of ions in aqueous solutions. *J. Amer. Chem. Soc.* 59:1675–1678.
- Khlosi, M., W.M. Cornelis, D. Gabriels, and G. Sin. 2006. Simple modification to describe the soil water retention curve between saturation and oven dryness. *Water Resour. Res.* 42:W11501.
- Labuza, T.P. 1971. Kinetics of lipid oxidation in foods. *Crit. Rev. Food Sci. Nutr.* 10:355–405.
- Leal, A.M.M., M.J. Blunt, and T.C. LaForve. 2014. Efficient chemical equilibrium calculations for geochemical speciation and reactive transport modelling. *Geochim. Cosmochim.* 131:301–322. doi:10.1016/j.gca.2014.01.038
- Lu, S., T. Ren, Y. Gong, and R. Horton. 2008. Evaluation of three models that describe soil water retention curves from saturation to oven dryness. *Soil Sci. Soc. Am. J.* 72:1542–1546. doi:10.2136/sssaj2007.0307N
- Marcus, Y. 2009. Effect of ions on the structure of water: Structure making and breaking. *Chem. Rev.* 109:1346–1370. doi:10.1021/cr8003828
- McMahon, P.B., and F.H. Chapelle. 1991. Microbial production of organic acids in aquitard sediments and its role in aquifer geochemistry. *Nature* 349:233–235. doi:10.1038/349233a0
- Nelson, D.W., and L.E. Sommers. 1996. Total carbon, organic carbon, and organic matter. In: D.L. Sparks et al., editors, *Methods of soil analysis*, Part 3. SSSA Book Series 5. SSSA, Madison, WI. p. 961–1010.
- Or, D., B.F. Smets, J.M. Wraith, A. Dechesne, and S.P. Friedman. 2007. Physical constraints affecting bacterial habitats and activity in unsaturated porous media a review. *Adv. Water Resour.* 30:1505–1527. doi:10.1016/j.advwatres.2006.05.025
- Orchard, V.A., and F.J. Cook. 1983. Relationship between soil respiration and soil moisture. *Soil Biol. Biochem.* 15:447–453. doi:10.1016/0038-0717(83)90010-X
- Parkhurst, D.L., and C.A.J. Appelo. 2013. Description of input and examples for PHREEQC version 3—A computer program for speciation, batch-reaction, one-dimensional transport, and inverse geochemical calculations: U.S. Geological Survey Techniques and Methods, 6, chap. A43. U.S. Geological Survey, Reston, VA.
- Petersen, L.W., P. Moldrup, O.H. Jacobsen, and D.E. Rolston. 1996. Relations between specific surface area and soil physical and chemical properties. *Soil Sci.* 161:9–21. doi:10.1097/00010694-199601000-00003
- Pitzer, K.S. 1991. *Activity coefficients in electrolyte solution*, CRC Press, Boca Raton, FL.
- Placella, S.A., E.L. Brodie, and M.K. Firestone. 2012. Rainfall-induced carbon dioxide pulses result from sequential resuscitation of phylogenetically clustered microbial groups. *Proc. Natl. Acad. Sci. USA* 109:10931–10936. doi:10.1073/pnas.1204306109
- Potts, M. 1994. Desiccation tolerance of prokaryotes. *Microbiol. Rev.* 58:755–805.
- Reid, D.S. 1980. Water activity as the criterion of water availability. In: D.C. Ellwood et al., editors, *Contemporary microbial ecology*. Academic Press Inc., London.
- Rosenzweig, R., U. Shavit, and A. Furman. 2012. Water retention curves of biofilm-affected soils using xanthan as an analogue. *Soil Sci. Soc. Am. J.* 76:61–69. doi:10.2136/sssaj2011.0155
- Schlesinger, W.H., and J.A. Andrews. 2000. Soil respiration and the global carbon cycle. *Biogeochemistry* 48:7–20. doi:10.1023/A:1006247623877
- Thomas, M.D. 1924. Aqueous vapor pressure of Soils: II. Studies in dry soils. *Utah Agric. Exp. Stn. Soil Sci.* 17:1–18. doi:10.1097/00010694-192401000-00001
- Topp, G.C., and P.A. Ferré. 2002. Water Content. In: J.H. Dane and G.C. Topp, editors, *Methods of soil analysis*, Part 4. SSSA Book Series No. 5. SSSA, Madison, WI. p. 417–545.
- Wattel-Koekkoek, E.J.W., P. Buurman, J. Van Der Plicht, E. Wattel, and N. Van Breemen. 2003. Mean residence time of soil organic matter associated with kaolinite and smectite. *Eur. J. Soil Sci.* 54:269–278. doi:10.1046/j.1365-2389.2003.00512.x
- Wieder, W.R., G.B. Bonan, and S.D. Allison. 2013. Global soil carbon projections are improved by modelling microbial processes. *Nat. Clim. Change* 3:909–912. doi:10.1038/nclimate1951
- Wilson, J.M., and D.M. Griffin. 1975. Water potential and the respiration of microorganisms in the soil. *Soil Biol. Biochem.* 7:199–204. doi:10.1016/0038-0717(75)90038-3



Molecular Signatures of Biogeochemical Transformations in Dissolved Organic Matter from Ten World Rivers

Thomas Riedel¹, Maren Zark¹, Anssi V. Vähätalo², Jutta Niggemann¹, Robert G. M. Spencer³, Peter J. Hernes⁴ and Thorsten Dittmar^{1*}

¹ Research Group for Marine Geochemistry (ICBM-MPI Bridging Group), Institute for Chemistry and Biology of the Marine Environment (ICBM), Carl von Ossietzky University, Oldenburg, Germany, ² Department of Biological and Environmental Science, University of Jyväskylä, Jyväskylä, Finland, ³ Department of Earth, Ocean and Atmospheric Science, Florida State University, Tallahassee, FL, USA, ⁴ Department of Land, Air and Water Resources—Hydrology, University of California, Davis, Davis, CA, USA

OPEN ACCESS

Edited by:

Samuel Abiven,
University of Zurich, Switzerland

Reviewed by:

Thibault Lambert,
University of Liège, Belgium
Lori Ziolkowski,
University of South Carolina, USA

*Correspondence:

Thorsten Dittmar
thorsten.dittmar@uni-oldenburg.de

Specialty section:

This article was submitted to
Biogeoscience,
a section of the journal
Frontiers in Earth Science

Received: 27 June 2016

Accepted: 30 August 2016

Published: 22 September 2016

Citation:

Riedel T, Zark M, Vähätalo AV, Niggemann J, Spencer RGM, Hernes PJ and Dittmar T (2016) Molecular Signatures of Biogeochemical Transformations in Dissolved Organic Matter from Ten World Rivers. *Front. Earth Sci.* 4:85. doi: 10.3389/feart.2016.00085

Rivers carry large amounts of dissolved organic matter (DOM) to the oceans thereby connecting terrestrial and marine element cycles. Photo-degradation in conjunction with microbial turnover is considered a major pathway by which terrigenous DOM is decomposed. To reveal globally relevant patterns behind this process, we performed photo-degradation experiments and year-long bio-assays on DOM from ten of the largest world rivers that collectively account for more than one-third of the fresh water discharge to the global ocean. We furthermore tested the hypothesis that the terrigenous component in deep-sea DOM may be far higher than biomarker studies suggest, because of the selective photochemical destruction of characteristic biomolecules from vascular plants. DOM was molecularly characterized by a combination of non-targeted ultrahigh-resolution mass spectrometry and quantitative molecular tracer analyses. We show that the reactivity of DOM is globally related to broad catchment properties. Basins that are dominated by forest and grassland export more photo-degradable DOM than other rivers. Chromophoric compounds are mainly vascular plant-derived polyphenols, and partially carry a pyrogenic signature from vegetation fires. These forest and grassland dominated rivers lost up to 50% of dissolved organic carbon (DOC) during irradiation, and up to 85% of DOC was lost in total if subsequently bio-incubated for 1 year. Basins covered by cropland, on the other hand, export DOM with a higher proportion of photo-resistant and bio-available DOM which is enriched in nitrogen. In these rivers, 30% or less of DOC was photodegraded. Consistent with previous studies, we found that riverine DOM resembled marine DOM in its broad molecular composition after extensive degradation, mainly due to almost complete removal of aromatics. More detailed molecular fingerprinting analysis (based on the relative abundance of >4000 DOM molecular formulas), however, revealed clear differences between degraded riverine and deep-sea DOM (molecular Bray-Curtis dissimilarity of ~50%). None of our experimental treatments enhanced the molecular similarity between the rivers and the

deep ocean. We conclude that terrigenous DOM retains a specific molecular signature during photo-degradation on much longer time scales than previously assumed and that substantial, thus far unknown, molecular transformations occur prior to downward convection into the deep oceanic basins.

Keywords: dissolved organic matter, world rivers, photo-degradation, bio-degradation, ultra-high resolution mass spectrometry, lignin, black carbon

INTRODUCTION

Rivers and streams transport large amounts of carbon to the oceans thereby connecting the terrestrial with the marine carbon cycle (Aufdenkampe et al., 2011; Raymond and Spencer, 2015). About 0.25 Pg of dissolved organic carbon (DOC) is carried annually via the riverine pathway into the global coastal ocean (Hedges et al., 1997; Dai et al., 2012). During transport of riverine dissolved organic matter (DOM), biotic and abiotic processes alter DOM concentration and composition (Cole et al., 2007). Mineralization turns large parts of DOM into dissolved inorganic carbon, part of which is evaded to the atmosphere as CO₂ (Lapierre et al., 2013; Raymond et al., 2013; Koehler et al., 2014).

Once released from soils into aqueous environments, a portion of DOM is quickly turned over by microorganisms (Ward et al., 2013), but some compounds resist immediate decomposition and are not degraded in year-long incubation experiments (Vähätalo and Wetzel, 2008). Many of the terrigenous compounds that escape fast microbial degradation are aromatic in nature. For instance, pyrogenic polycyclic aromatics are among the most resistant forms of organic matter in soils and aqueous environments (Santín et al., 2016). Most aromatic compounds absorb ultraviolet (UV) radiation and are thus susceptible to photo-degradation. Therefore, photo-degradation plays a major role in the fate of terrigenous DOM in sunlit surface waters (Osburn et al., 2009; Stubbins et al., 2010; Cory et al., 2014), and affects the quantity and composition of DOM. The oxidation of DOM yields inorganic carbon and nutrients such as ammonium (Miller and Zepp, 1995; Miller and Moran, 1997; Graneli et al., 1998; Vähätalo et al., 2003; Lapierre et al., 2013). Besides the direct terminal oxidation, the formation of low molecular weight compounds such as pyruvate, maleic or fumaric acid has also been observed (Mopper et al., 1991; Gerdes et al., 1997). As a result, the transformation of DOM into more bio-available substrates stimulates microbial growth thereby enhancing the effect of abiotic photo-chemical oxidation of DOM (Mopper et al., 1991; Lindell et al., 1995; Miller and Moran, 1997; Vähätalo and Wetzel, 2008; Aarnos et al., 2012). Exposure to UV radiation may also decrease microbial activity (Tranvik and Bertilsson, 2001), possibly due to radiation-induced damage to the organisms (Karentz et al., 1994), transformation of bio-labile DOM into recalcitrant forms (Obernosterer et al., 1999), photo-mineralization of bio-available DOM (Obernosterer and Benner, 2004) or the production of inhibitory substances (Lund and Hongve, 1994).

Exposure to sunlight and subsequent microbial decomposition particularly affect those compounds that are typical for a terrestrial origin, mainly polyphenols. Therefore,

after extensive photo- and microbial degradation, terrigenous DOM resembles marine DOM in its molecular composition (Dittmar et al., 2007; Stubbins et al., 2010; Rossel et al., 2013). The combined effect of photo- and microbial degradation seems to result in the accumulation of refractory molecules that share very similar molecular structures, independent of their original source (Jaffé et al., 2012). A universal, source-independent molecular character of the residuals of organic matter degradation in aquatic systems would have major implications. Degradation pathways, rather than the original source would determine the long-term fate of DOM in the ocean, and source assignment via molecular tracers would become more and more difficult in the progression of organic matter degradation.

Here, we address this topic by studying the impact of intense photo-degradation and year-long biodegradation on the molecular composition of DOM from ten of the largest world rivers. The results provide an overall pattern of DOM composition on a global scale that can be used to infer degradability and transformation of freshwater DOM and ultimately define the fate of riverine DOM in the sunlit hydrosphere. The studied rivers account for about one third of the global freshwater discharge to the oceans, and integrate characteristics of DOM from the watersheds covering 25% of global land area in five continents across contrasting biomes and latitudes. The DOM molecular composition of these large rivers varies systematically with land use (Wagner et al., 2015). In particular, the proportion of cropland has a major influence on the presence of nitrogen and sulfur in riverine DOM (Wagner et al., 2015). Here, we examined the same samples as in Wagner et al. (2015). Each river was sampled once during the season of peak discharge. Due to logistical reasons, the samples had to be transported to the laboratory unfiltered and at environmental temperature and had to be stored after filtration at 4°C for different time spans before they were further processed. The samples thus represent a snapshot in time, and at least a fraction of the most bio-labile DOM had been degraded prior to further experiments and analyses. Despite these inherent limitations, systematic variations of the molecular DOM composition as a function of land cover and land use had been preserved (Wagner et al., 2015).

In order to disentangle the molecular imprints of microbial and photo-degradation, sequential experiments were conducted with the 10 river samples. First, samples were irradiated with artificial sunlight to remove essentially all light-absorbing (chromophoric) DOM, and afterwards, the photo-irradiated samples were incubated for 1 year with natural riverine microbial communities. All experiments were accompanied with dark controls. In natural sunlit waters, microbial and photo-chemical

processes occur simultaneously, and the succession of microbial communities differs in nature compared to long-term laboratory incubations (Petersen and Kemp, 2010). The goal of this study was not the full reproduction of these natural processes, but instead reductionist experiments that aimed in resolving the following research questions:

- (1) Is the reactivity of riverine DOM, in terms of photo- and bio-degradability under defined laboratory conditions, related to land-cover and land use?
- (2) Do the molecular modifications induced by photo- and bio-degradation follow predictable patterns across the rivers?
- (3) Is there a universal molecular signature of resistant DOM across the major world rivers and the deep ocean?

To approach these questions we combined a non-targeted ultrahigh-resolution mass spectrometric approach with conventional quantitative molecular tracer analyses. Specifically, ultrahigh-resolution Fourier-transform ion cyclotron resonance mass spectrometry (FT-ICR-MS) resolved thousands of molecular formulas in DOM and, in conjunction with relative signal intensities for each of these formulas, most detailed molecular fingerprints were obtained for each sample. Lignin-derived phenols were quantified as a natural biomarker for vascular-plant derived DOM and benzenepolycarboxylic acids as tracer for pyrogenic DOM, i.e., dissolved black carbon (DBC).

MATERIALS AND METHODS

River Water Sampling

Ten major world rivers (for details see Lalonde et al., 2014) were sampled during the season of highest discharge. Water samples were taken by local operators at each river (see acknowledgments) following a standardized protocol by immersing pre-cleaned polyethylene containers (consecutively cleaned with detergent, acid, and ultrapure water). The sample named “Amazon” is a composite sample prepared from water of Rio Negro (25%) and Rio Solimoes (75%). All samples were kept in the dark and not filtered or poisoned prior to shipping. The containers were express-shipped to the laboratory in Helsinki. After arrival, the samples were filtered (1 μm Nucleopore QR 10IN or Graver Technologies VTEC 1-10PS) and stored at 4°C between 7 (Amazon) and 341 days (Yangtze). During transport and storage, microbial activity removed at least a fraction of bio-labile DOM prior to the start of the experiments. In the case of the St. Lawrence River this accounted for 19% of DOC (Lalonde et al., 2014). Additional information regarding sampling and sample preparation can be found in accompanying publications (Jaffé et al., 2013; Lalonde et al., 2014; Wagner et al., 2015).

Photo-Degradation and Bioassay

The experiment consisted of two phases as described in Lalonde et al. (2014): a photochemistry-phase followed by a bioassay-phase consisting of a 1-year long microbial incubation in the dark. Briefly, the irradiation experiment was designed to remove all chromophoric DOM through abiotic photochemical reactions. Direct photochemical reactions of DOM are possible only when DOM contains chromophores (i.e., chromophoric

dissolved organic matter, CDOM) that can absorb solar radiation at wavelengths >300 nm. The experimental conditions in the solar-simulator were chosen to remove $>96\%$ of CDOM (absorbance at 350 nm). Before the start of the radiation experiments samples were filtered through 0.2 μm filters (Cellulose Acetate, Sartorius). Samples were placed in acid-washed (HNO_3 , following copious rinsing with ion-exchanged Milli-Q water) and combusted (>2 h, 450°C) UV-transparent 750 mL quartz vials fitted with ground glass stoppers. A headspace corresponding to 10% of the vial internal volume was filled with oxygen gas, which was replenished after 4 days of irradiation to ensure complete oxidation of the UV-sensitive DOM fraction (Vähätalo and Wetzel, 2008). The samples were submerged (~ 1 cm) in a flow-through pool of tap water regulated to 25°C and irradiated for 10 days with metal halide lamps (Thorn OQ 1000) and fluorescent tubes (UVA-340, Q-Lab Corp.). The lamps simulated well the photo-chemically active part of natural solar radiation (Figure S1). The irradiance incident to the samples integrated from 280 to 350 nm was 28.9 W m^{-2} and 16.4 times higher than the corresponding global mean natural solar radiation at the sea surface. The ultraviolet radiation dose received by the samples over the 10-day experiment corresponded to an average of half-a-year dose of the natural solar radiation mentioned above (Lalonde et al., 2014). The high UV-irradiance kept the water samples sterile during the 10 days of irradiation. The sterility was additionally confirmed by the absence of bacterial cells in the samples prepared for epifluorescence microscopy (Aarnos et al., 2012). A second set of samples was treated as dark controls similar to the irradiated samples, but was kept in glass bottles wrapped in aluminum foil at room temperature.

After 10 days, irradiated samples as well as dark controls were sampled for analysis and subsequently received unfiltered water from each river as a microbial inoculum (10 mL inoculum to 1000 mL of treated sample) along with the addition of KH_2PO_4 to adjust the molar N to P ratio in the samples to approx. nine which is the typical ratio of bacterioplankton biomass (Goldman et al., 1987). Thus, phosphorus limitation of the microbial communities was eliminated. Samples were incubated at 22°C in the dark for 1 year.

We use the following abbreviations for the various experiments:

“initial”: untreated initial water (as in Wagner et al., 2015).

“D”: 10 days of dark incubation of sample “initial” without addition of inoculum and phosphate (dark control of the photo-degradation experiments).

“D+”: 1 year of dark incubation of sample “D” with addition of inoculum and phosphate.

“L”: 10 days of photo-degradation of sample “initial.”

“L+”: 1 year of dark incubation of sample “L” with addition of inoculum and phosphate.

DOC and CDOM Analysis

After the experiments, the irradiated and the dark control waters were sampled for the determination of DOC, CDOM, dissolved lignin, dissolved black carbon (DBC), and for molecular

characterization of DOM via FT-ICR-MS. The absorbance of CDOM was measured against ultrapure water and converted into absorption coefficients (Aarnos et al., 2012). The concentrations of DOC were measured as non-purgeable organic carbon in 0.2 μm filtered waters acidified to pH 2 (with HCl 32%, ultrapure) via high temperature catalytic oxidation using a Shimadzu TOC-V CPH carbon analyzer. Replicate analyses of a deep sea reference material (DSR, provided by D. Hansell, University of Miami, USA) yielded an accuracy and precision of <5.2%. Solid-phase extracted DOC (SPE-DOC, see below) was determined in the same way, after the methanol extracts were dried by evaporation and re-dissolved in ultra-pure water.

Sample Preparation for Molecular Analysis

All samples were solid phase extracted (SPE) prior to molecular analysis. SPE was performed according to Dittmar et al. (2008) using Varian Bond Elute PPL cartridges (100 mg) as solid phase. This is one of the most efficient methods available to date for the complete desalting of natural DOM samples, as it removes salt to undetectable traces and >50% of DOC is routinely recovered (Green et al., 2014). Cartridges were rinsed with 2 mL MeOH (analytical grade) prior to use. Samples were acidified to pH 2 with HCl (32 %, ultrapure) and allowed to pass through the cartridges under gravity. Cartridges were rinsed two times with 0.01 M HCl for removal of salt, dried with a stream of argon and immediately extracted with 1 mL of MeOH (analytical grade). Extraction efficiencies were determined on evaporated extracts, re-dissolved in ultrapure water, and were $56 \pm 12\%$ for initial and dark control samples and $35 \pm 12\%$ for irradiated samples on a carbon basis (this is further discussed below).

Black Carbon and Lignin Molecular Analysis

DBC was determined via benzenepolycarboxylic acids (BPCAs) released by hot nitric acid oxidation of SPE-DOM, according to Dittmar (2008) with the modification as described in Stubbins et al. (2015). Briefly, aliquots of the SPE-DOM samples were transferred into pre-combusted (400°C, 4 h) glass ampoules. The methanol was evaporated in a centrifugal vacuum evaporator (Christ RV2-18) and the samples re-dissolved in 0.5 mL nitric acid (65%, analytical grade). The ampoules were fire sealed and heated in a stainless steel pressure bomb at 170°C for 9 h. Afterwards, the nitric acid was evaporated in a centrifugal vacuum evaporator (Christ RV2-18) and the samples re-dissolved in the mobile phase of the liquid chromatography. BPCAs were then determined via ultra-performance liquid chromatography (Waters Acquity UPLC). Concentrations of BPCAs were converted into concentrations of DBC, according to Dittmar (2008), with the slight modification described in Stubbins et al. (2015). The analytical error (variability between replicate analysis) was <10%.

Lignin phenols were determined via the CuO oxidation method described by Hedges and Ertel (1982), with modifications as outlined by Spencer et al. (2010). In brief, SPE-DOM was transferred to Monel reaction vessels (Prime Focus) and dried under vacuum centrifugation. All samples were alkaline oxidized at 155°C in a stoichiometric excess of CuO, followed

by acidification to pH 1 (6 M H₂SO₄, analytical grade) and extracted three times with ethyl acetate (analytical grade), passed through Na₂SO₄ (analytical grade) drying columns and taken to dryness under a gentle stream of ultrapure nitrogen. After re-dissolution in pyridine (analytical grade), lignin phenols were silylated (with BSTFA, analytical grade), and quantified on a gas chromatography mass spectrometry system (Agilent 6890 gas chromatograph equipped with an Agilent 5973 mass selective detector and a DB5-MS capillary column; 30 m, 0.25 mm inner diameter, Agilent) using cinnamic acid as an internal standard and a five-point calibration scheme. Six lignin phenols were quantified for all samples, including three vanillyl phenols (vanillin, acetovanillone, vanillic acid), and three syringyl phenols (syringaldehyde, acetosyringone, syringic acid) (Spencer et al., 2010). The analytical error (variability between replicate analysis) was <10%. Lignin concentrations in river water are expressed as the sum of all detected phenols. The expression λ -lignin (%) is the sum of all lignin phenols ($\mu\text{g L}^{-1}$) divided by the concentration of DOC (mg L^{-1}).

FT-ICR-MS Analysis

FT-ICR-MS analyses were conducted on solid-phase extracted samples diluted with ultrapure water to 1:1 MeOH/water (v/v) to a DOC concentration of 20 mg L^{-1} . Samples were ionized in negative ionization mode using electrospray ionization (ESI) and analyzed on a Bruker Solarix 15 Tesla FT-ICR-MS at the University of Oldenburg (Germany).

The lower mass limit was set to m/z 150. 500 scans were accumulated per sample. Spectra were internally calibrated using an in-house reference mass list. After internal calibration the mass error was less than 100 ppb over the entire mass range. Molecular formulas considering the elements C, H, O, N, S, and P were assigned based on rules published in Koch et al. (2007). We used a method detection limit (MDL) based on the uncertainty of the noise derived from repeated analysis of blank samples (Riedel and Dittmar, 2014). This approach is superior to the commonly used fixed signal-to-noise ratio, as it filters noise peaks much more reliably from FT-ICR mass spectra (Riedel and Dittmar, 2014). All molecular formulas were detected as singly-charged negative ions.

The molecular formula of a molecule provides a wealth of information such as hetero-atom content, degree of oxidation, or saturation. With help of the aromaticity index [AI_{mod} , Koch and Dittmar (2006), as corrected and reported in the erratum (Koch and Dittmar, 2016)] and element ratios, formulas can be grouped into compound classes (Šantl-Temkiv et al., 2013; Riedel et al., 2014; Seidel et al., 2014). It is important to note that multiple structural isomers can exist for each molecular formula, but the following categories provide a helpful overview of likely structure behind a given molecular formula. They should not be interpreted as unambiguous structural assignments. Five categories were defined here and the molecular formulas in each sample were grouped into one of these categories. "Aliphatics" were defined as molecules with H/C ratios ≥ 1.5 . "Highly unsaturated compounds" that include also phenols with aliphatic side-chains, as well as carboxyl-rich alicyclic molecules (CRAM, Hertkorn et al., 2006) were defined as H/C < 1.5 and

$AI_{\text{mod}} \leq 0.5$. This group was further sub-divided into oxygen rich ($O/C > 0.5$) and oxygen poor ($O/C \leq 0.5$) compounds. "Polyphenols" contain polyphenolic as well as polycondensed aromatic compounds with aliphatic side-chains and were defined by $0.5 < AI_{\text{mod}} \leq 0.66$ (Koch and Dittmar, 2006). Accordingly, "polycondensed aromatics" were defined by $AI_{\text{mod}} > 0.66$. Unsaturated, polyphenolic and condensed aromatic compounds, albeit also present in marine DOM (Hertkorn et al., 2006), are particularly abundant in terrestrial systems, because vascular plants are the main producers of phenolic compounds on the planet.

Statistical Analysis

For all statistical analyses, the same number ($n = 1456$) of molecular formulas was considered for each river sample, resulting in a total number of 4048 different molecular formulas across all samples. For this selection, the 1456 molecular formulas with the highest FT-ICR-MS signal intensity were chosen for each sample; 1456 was the lowest number of molecular formulas detected in a single sample. The data were then normalized to the sum of signal intensities of the respective sample and finally used for statistical analysis. This data treatment ensured most robust statistical analysis, because the number of detected compounds is strongly influenced by minor analytical shifts or differences in SPE-DOC concentration since many compounds are detected at signal intensities close to the detection limit (Riedel and Dittmar, 2014). By considering the same number of the most intense signals in each sample, such analytical artifacts are avoided. Furthermore, statistical robustness is enhanced by using the same number of variables for each sample. Analytical reproducibility was assessed by analyzing a marine reference sample (see

below) eight times. This sample was included in all statistical analyses.

To relate bulk properties of the initial samples (e.g., bio- and photo-degradability) to the relative abundance of molecular formulas ($n = 2167$ molecular formulas in the initial river water sample set), linear correlation analyses (Pearson) were performed. In addition, a principle component analysis (PCA) was carried out to highlight the dominant patterns and trends in the FT-ICR-MS data. The PCA was calculated based on the relative signal intensities of the molecular formulas ($n = 4048$ different molecular formulas in the entire sample set). Furthermore, the molecular similarity of SPE-DOM between samples (with respect to the relative signal intensities of the molecular formulas) was assessed via a Bray Curtis dissimilarity analysis (Osterholz et al., 2015). As an alternative to these statistical analyses that considered the FT-ICR-MS signal intensities of each molecular formula, a simple presence / absence analysis was performed. A molecular formula was considered "present" if its signal intensity was above the MDL. Based on the presence and absence in the respective samples, molecular formulas were categorized as photo-stable, photo-labile, photo-produced and other categories (Table S2). Results are displayed in frequency plots (Figure 6 and Figure S6).

We added a sample from the North Equatorial Pacific Intermediate Water (NEqPIW, sampled at station NELHA off Big Island in Hawaii at 674 m water depth) in our comparison, which is considered to be one of the oldest water masses on Earth (Stuiver et al., 1983; Osterholz et al., 2015) that was extracted and measured by the same methods used in this study (Green et al., 2014). The sample was analyzed eight times, during the

TABLE 1 | The effects of simulated sunlight and microbial degradation on the concentration of riverine DOC.

		Amazon	Congo	Danube	Ganges Brahma.	Lena	Mekong	Mississippi	Paraná	St. Lawrence	Yangtze
DOC (mg L^{-1})	initial	4.4	6.7	2.4	0.8	5.8	1.6	3.4	2.5	3.8	1.7
Δ DOC (% of initial)	D+	-25	-15	-25	-25	-16	-25	-12	-24	-18	-24
	L	-36	-49	-33	-13	-28	-19	-24	-24	-18	-29
	L+	-80	-85	n. a.	-38	-62	-56	-68	-64	-63	-71
CDOM (m^{-1})	initial	13	26	3.0	0.89	9.1	2.3	4.8	3.6	5.3	2.0
Δ CDOM (% of initial)	L	-99	-100	-97	-96	-97	-99	-98	-97	-98	-97
DBC ($\mu\text{g L}^{-1}$)	initial	293	562	152	36	353	85	235	205	255	88
Δ DBC (% of initial)	D+	-20	-10	-39	-17	-20	-18	-17	-1	-35	-43
	L	-82	-93	-87	-53	-57	-88	-83	-68	-75	-84
	L+	-95	-96	n. a.	-83	-81	-84	-94	-90	-94	-92
CDOM/DOC ($\text{m}^2 \text{g}^{-1}$)	initial	3.1	3.9	1.2	1.1	1.6	1.4	1.4	1.5	1.4	1.2
L	0.05	0.04	0.05	0.06	0.07	0.05	0.04	0.06	0.04	0.04	0.05
DBC/DOC (% carbon)	initial	6.7	8.4	6.3	4.5	6.1	5.3	6.9	8.2	6.7	5.2
D+	7.1	8.8	5.1	5.0	5.8	5.8	6.5	10.6	5.4	3.8	
L	1.9	1.2	1.3	2.4	3.6	0.8	1.5	3.5	2.1	1.2	
L+	1.7	2.0	n. a.	1.2	3.0	2.0	1.3	2.2	1.1	1.4	

The delta notation (Δ DOC) refers to the induced change in concentration relative to the initial conditions ("initial"), i.e. the untreated samples of the ten rivers. The ratios of CDOM (absorption coefficient at 350 nm, m^{-1}) and DBC concentration, respectively, to DOC concentration in the initial samples are shown for comparison. A complete compilation of concentration data is in Table S1. For abbreviations, see material and methods, n.a.: data not available.

same period as the river samples. The eight replicate analyses of NEqPIW were used to assess analytical variability in all statistical analyses.

All statistics were performed using the software package R (Version 3.2.3, package “vegan” Oksanen et al., 2013).

RESULTS AND DISCUSSION

Is the Reactivity of Riverine DOM Related to Land Cover?

During the year-long dark microbial incubation of the untreated river samples (“D+”), 21% of DOC was lost on average ($\pm 5\%$ standard deviation, **Table 1**). This is comparable to the loss during the 10 days of intense photo-irradiation (“L”) where on average 27% ($\pm 11\%$) of DOC was removed. The microbial incubation of the photo-degraded sample (“L+”) was similarly efficient in DOC removal, and in sum 64% ($\pm 15\%$) of DOC was lost by sequential photo- and bio-degradation. This is consistent with photochemical transformation of DOC to CO_2 and biologically labile photoproducts, which are effectively assimilated by microbes (Miller and Zepp, 1995; Graneli et al., 1998; Vähätalo and Wetzel, 2008; Cory et al., 2014). The dark control of the photo-degradation experiment (“D”) did not significantly change in DOC concentration which is not surprising, given that it was filtered ($0.2 \mu\text{m}$) prior to incubation and much of the bio-labile DOM had presumably been removed prior to the experiment.

Pronounced differences in DOM reactivity were observed between the individual rivers (**Table 1** and Table S1). For instance, almost half of DOC was removed by photo-degradation from the Congo River, while only 13% of DOC was susceptible to photo-degradation in the Ganges-Brahmaputra River. Also bio-degradation varied strongly between rivers. Neither photo-, nor bio-degradability of any of the analyzed parameters was related to storage time of the samples prior to the experiment (student's *t*-test of Δ -values vs. storage time; $r^2 < 0.1$; $p > 0.1$; $n = 10$). Thus, differences in sample handling and processing were not the prime reason for the observed differences. Some watershed characteristics (data from Wagner et al., 2015), however, appeared to influence DOM reactivity (**Figure 1**). DOM from large basin areas with a high proportion of forests or grasslands was most susceptible to photo-degradation. For instance, in the Congo (90% of forest and grassland) almost 50% of DOC was removed by sterile irradiation (L), while in the Ganges-Brahmaputra (35% of forest and grassland) only about 10%. Agricultural use (large proportion of cropland) diminished photo-degradability, but was positively related to bio-degradability. For instance, in the Danube (almost 70% cropland) about 25% of DOC was biodegraded (D+), similar to Yangtze (almost 50% of cropland), while in the Congo or Lena (<10% cropland), only about 15% was removed. This observed trend is consistent with the finding that CDOM decreases with enhanced farming, while the amount of chromophores increases with wetland cover (Wilson and Xenopoulos, 2009). Compositional differences of DOM in rivers and lakes as a function of catchment properties have also been demonstrated by others (Mattsson et al., 2009; Jaffé et al., 2012; Lambert

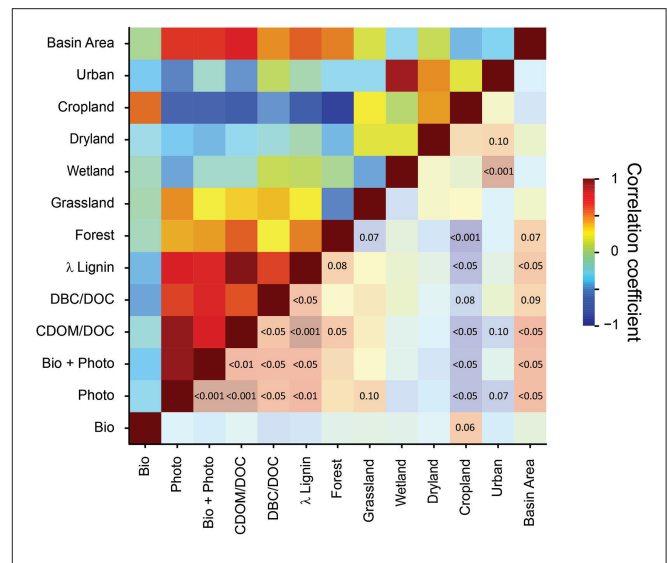


FIGURE 1 | Correlation matrix of catchment properties of the ten studied world rivers, molecular and optical properties of the untreated (“initial”) river samples, and the corresponding values of bio- and photo-reactivity of each samples (Δ DOC, % of initial, **Table 1). Data for land cover are from Wagner et al. (2015). Linear Pearson correlation was performed ($n = 10$). The color code represents the corresponding correlation coefficients (r). In the lower right triangle of the matrix, p -values are superimposed onto the same (but lighter) color scheme ($p > 0.1$ are omitted).**

et al., 2015; Wagner et al., 2015), and related to DOM reactivity (Remington et al., 2011). Our study now shows that the influence of land cover on DOM reactivity follows a globally consistent trend, across a wide range of world rivers. The studied rivers are from high-latitude to tropical rivers, and differ in catchment morphology. Despite these obvious differences, the influence of land cover on DOM composition and reactivity appears universal.

The CDOM/DOC ratio of the initial river samples was highly significantly correlated with photo-degradability of DOC ($p < 0.001$, $n = 10$; **Figure 1**), providing a good predictor for photo-degradability of DOM. Degradability is defined here as the loss of DOC due to the experimental treatment (Δ DOC in **Table 1**). CDOM is defined as the absorption coefficient at a wavelength of 350 nm (see methods). As a rule of thumb, a reduction of the CDOM/DOC ratio by 1 unit ($\text{m}^2 \text{g}^{-1}$), resulted in 10% less DOC removal due to irradiation (slope of linear regression in **Figure 1**, see also data in **Table 1**). A highly significant correlation between λ -lignin and CDOM/DOC ($p < 0.001$, $n = 10$; **Figure 1**) suggests that the main source of photodegradable CDOM in the forested and grassy basins is derived from vascular plant debris. The correlation with DBC/DOC indicates that DOM with high CDOM/DOC has also an elevated proportion of pyrogenic DOM. Bio-degradability, on the other hand, was inversely correlated with lignin, indicating that in the basins covered by cropland soft plant tissue with low content of lignin or non-vascular organisms are the main sources of bio-degradable DOM. Consistent with previous observations (Hernes and Benner, 2003; Benner and Kaiser, 2011; Fichot and Benner, 2012; Stubbins et al., 2015), the concentrations of

aromatic compounds (lignin and DBC) correlated with CDOM (Figure S2).

On a broader molecular level, thousands of molecular formulas detected in the initial river samples significantly correlated with bio- or photo-degradability of DOM (Figure 2). The molecular-level trends are consistent with that observed for CDOM, DBC and lignin. Overall, highly unsaturated compounds positively correlated with the photo-degradability of a given sample, while more saturated compounds inversely correlated with photo-degradability (Figure 2B). This is consistent with the molecular trends observed in other photo-degradation experiments (Opsahl and Benner, 1998; Gonsior et al., 2008; Spencer et al., 2009; Seidel et al., 2015). Bio-degradability, on the other hand, was related to degree of oxygenation (O/C) and nitrogen content (Figure 2A). The compounds with low oxygen numbers were more easily bio-degraded than others. At first view, this finding is in direct contradiction to short-term bio-incubation studies of DOM from the Amazon River and other streams (Kim et al., 2006; Seidel et al., 2015; Medeiros et al., 2015). In all these experiments, oxygen-rich molecules were preferentially degraded in the course of a few days, while compounds with low oxygen content were preferentially produced. One has to keep in mind, however, that these early stages of degradation occurred already prior to our experiment. In our study, the abundance of low-oxygen compounds in the bio-degradable samples may be an indication for bacterially produced biomass, which in turn is likely more bio-labile than vascular plant debris. Consistent with this explanation is the finding that many of the compounds that correlated positively with the bio-degradability of DOM contained nitrogen (Figure 2A), most of which fall in our category of “peptides.” For the same samples examined in this study, Wagner et al. (2015) pointed out that the use of nitrogen fertilizers in agricultural fields can lead to elevated content of nitrogen in DOM draining croplands.

In conclusion, bio- and photo-degradability of riverine DOM can globally be related to broad catchment properties. Independent of latitude, basins that are dominated by forest and grassland export photo-degradable DOM with a large proportion of chromophoric, phenolic compounds. Basins covered by cropland, on the other hand, export DOM with a relatively lower contribution of chromophores, but with more bio-available DOM which is enriched in nitrogen and likely of microbial origin. Thus, on a broad global scale land-use appears to be one of the main drivers for the reactivity and molecular composition of riverine DOM.

Molecular Modifications Induced by Photo- and Bio-Degradation

So far, we have discussed relationships between land cover, bulk DOM reactivity and molecular DOM composition in the rivers. In the following we relate these statistical relationships to the actual molecular changes induced by bio- and photo-degradation in our experiments.

The majority of molecular formulas did not disappear, but the photo-degradation experiment induced broad shifts in their

abundance distribution (Figures 3, 4). Consistent with the almost complete removal of chromophores (CDOM) and previous experiments (Gonsior et al., 2008; Stubbins et al., 2010; Seidel et al., 2015), aromatic and highly unsaturated oxygen-poor compounds were preferentially removed from all samples during photo-irradiation (Figures 3E, 4). At the same time, however, a significant fraction of polyphenolic and polycyclic aromatics, as well as DBC, was preserved consistently in all samples, despite almost entire removal of CDOM (Figures 4, 5). This trend was confirmed by quantitative DBC analysis (Figure 5, Table S1). The photo-production of aromatic compounds, as suggested by Waggoner et al. (2015), is unlikely the reason for the presence of aromatics after our experiments, because most of them were already detected prior to the experiment and did not increase in relative intensity. Few newly formed compounds with aromatic character were detected (low H/C in Figure S6). Similar observations were also reported by Stubbins et al. (2010) and Rossel et al. (2013), who argued that these compounds did not lose their basic aromatic structure, but were molecularly modified so that they moved from another molecular category into “aromatics,” possibly due to cleavage of aliphatic side-chains. A significant fraction of the polycyclic aromatics (and DBC) that remained after photo-incubation was bio-labile and removed in the following bio-incubation experiment (Figure 4E; Table S1). This enhanced bio-lability indicates major molecular transformations of the polycyclic aromatics during irradiation making them more accessible to microorganisms.

The reasons behind the observed photo-stability of some aromatics (as detected by FT-ICR-MS and as DBC) compared to almost complete loss of CDOM at 350 nm remains speculative at this point, but possibly some of the aromatic compounds in DOM absorb only UV-radiation at wavelengths <350 nm and even below 300 nm, which are almost absent in the spectrum of natural sunlight received at the Earth's surface (Figure S1). Furthermore, some aromatic moieties may also be protected from photo-degradation because of their molecular environment they are embedded in (McNally et al., 2005). The photo-chemical stability of an aromatic component in DOM is of major relevance, because it determines the long-term stability of terrigenous components in the ocean. For instance, DBC accumulates over ten-thousands of years in the ocean (Dittmar and Paeng, 2009; Ziolkowski and Druffel, 2010), despite being highly susceptible to photo-degradation (Stubbins et al., 2012). A minor photo-chemically resistant component in DBC would explain its long-term stability in the ocean.

Aside from the clear trend in aromaticity, photo-degradation caused a pronounced shift in molecular size. Larger molecules were preferentially removed over smaller molecules (Figures 3B, 4H), while smaller molecules preferentially accumulated. This is not because aromatic compounds had a higher molecular mass than non-aromatic compounds, since both effects of photo-degradation were clearly separated by the PCA (Figure 3). Cleavage of covalent bonds and the formation of low molecular weight compounds such as pyruvate, maleic or fumaric acid have been observed previously (Mopper et al., 1991; Gerdes et al., 1997). Many of these low-molecular mass compounds fall outside our analytical window defined largely by the solid

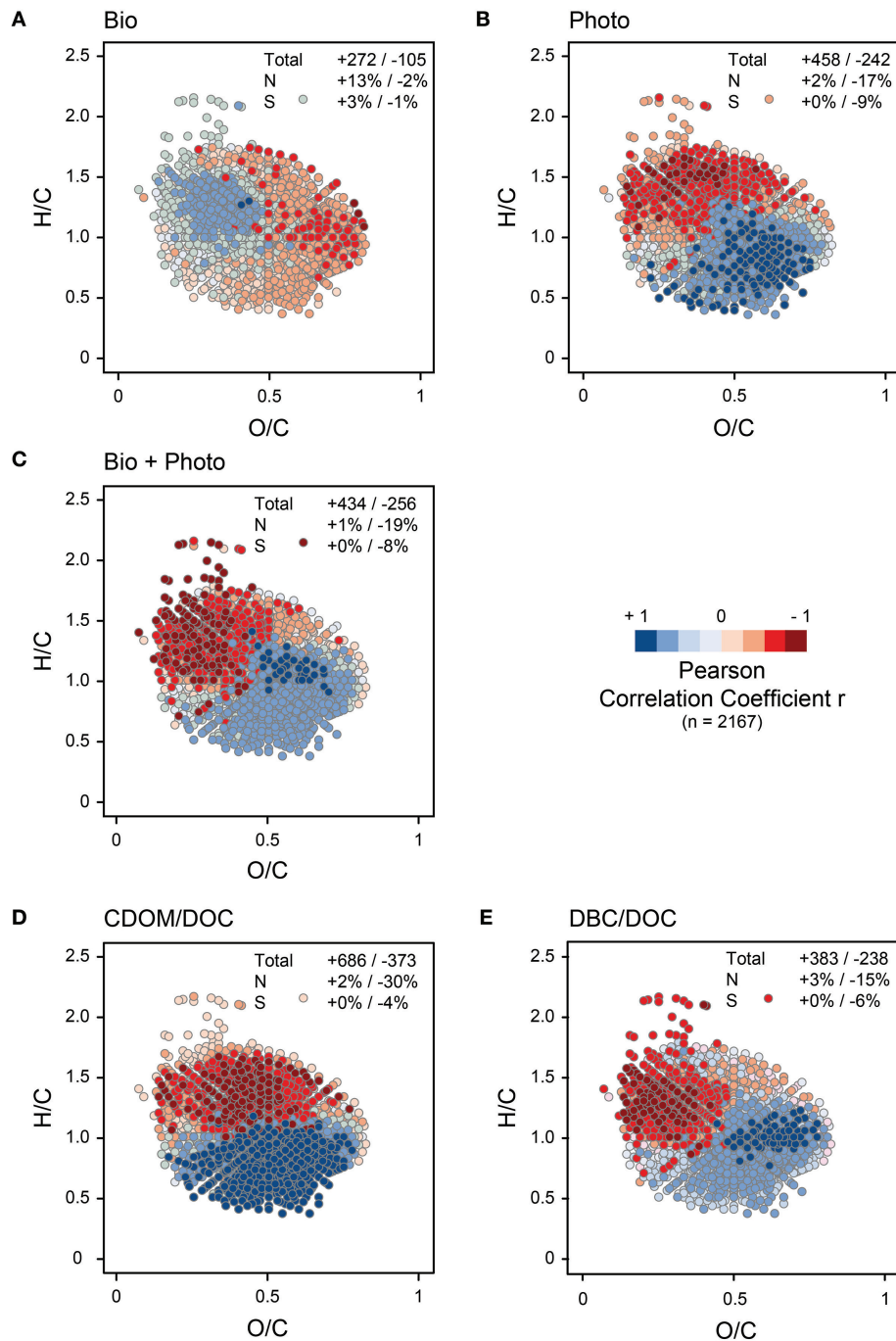


FIGURE 2 | Van Krevelen plots of the most intense molecular formulas from the 10 initial river samples (2167 formulas, see methods for details). Each dot represents one molecular formula. Color coded are correlation coefficients of the signal intensities of a given molecular formula vs. bio- and photo-reactivity of each sample (Δ DOC, % of initial, **Table 1**), optical and molecular properties, respectively. The numbers in the individual panels are the numbers of molecular formulas that correlated positively (+) and inversely (–) with the respective parameter, on a $p < 0.05$ ($n = 10$, $r > 0.54$) level, if not otherwise stated. The percentages show the proportion of nitrogen (N) or sulfur (S) containing molecular formulas that correlated positively (+) and inversely (–) with the respective parameter. Note, that for the reasons discussed in the main text, the correlation patterns of bio-degradation and DBC/DOC are very similar (but inverse), and there is a large similarity between photo-degradation and CDOM/DOC. **(A)** Δ DOC (% of initial) of the bio-degradation experiment (“D+”) vs. FT-ICR-MS signal intensity. To illustrate general trends despite the overall weak correlation, numbers in this panel are for a $p < 0.10$ significance level ($n = 10$, $r > 0.44$). **(B)** Δ DOC (% of initial) of the photo-degradation experiment (“L”) vs. FT-ICR-MS signal intensity. **(C)** Δ DOC (% of initial) of the bio-degradation experiment that followed photo-degradation (“L+”) vs. FT-ICR-MS signal intensity. **(D)** CDOM/DOC ratio vs. FT-ICR-MS signal intensity. **(E)** DBC/DOC ratio vs. FT-ICR-MS signal intensity.

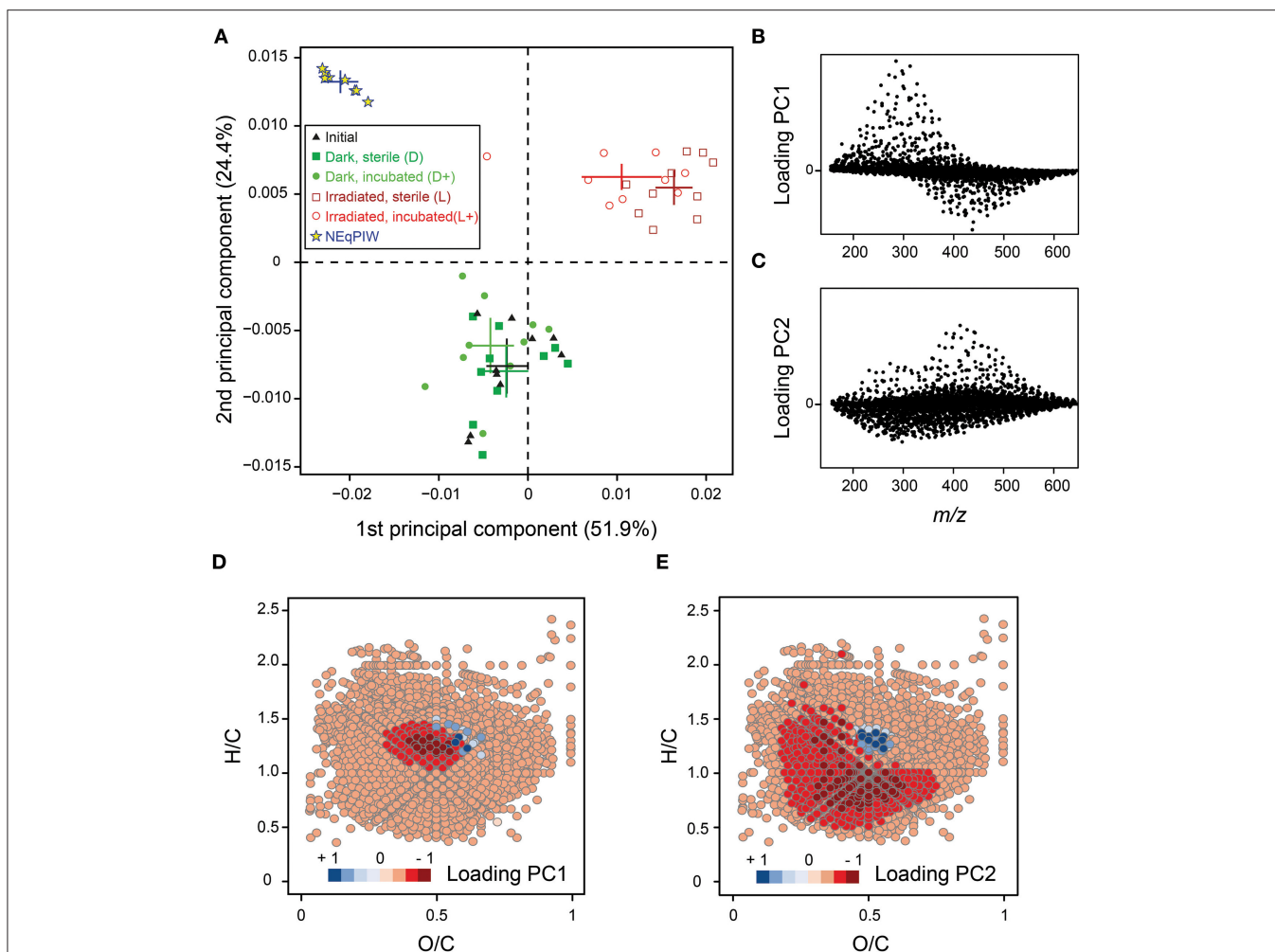


FIGURE 3 | Molecular compositional changes induced by bio- and photo-degradation. (A) Principle component analysis (PCA) score plot showing the first (52% variance explained) and second component (24% variance explained). Crosses represent average values ($\pm 95\%$ confidence interval) for the different experimental settings. Replicate analysis ($n = 8$) of DOM from North Equatorial Pacific Intermediate Water (NEqPIW) sample is included. (B) Loadings of PCA axis 1 plotted vs. mass to charge ratio (m/z) for each of the 4048 molecular formulas considered. (C) Loadings of PCA axis 2 plotted vs. mass to charge ratio (m/z) for each of the 4048 molecular formulas considered. (D) Loadings of PCA axis 1 plotted in van Krevelen space for each of the 4048 molecular formulas considered. (E) Loadings of PCA axis 2 plotted in van Krevelen space for each of the 4048 molecular formulas considered.

phase extraction (SPE) technique. While SPE via PPL adsorbers is one of the most efficient desalting techniques for natural DOM, in terms of carbon recovery ($>50\%$) and complete removal of salt (Green et al., 2014), small ionic molecules and colloidal matter are not efficiently retained and are thus lost from the analytical window (Hawkes et al., 2016). Accordingly, the DOC extraction efficiency dropped from an average of 56% for initial and dark control samples to 35% after photo-irradiation. After subsequent bio-incubation, close to 50% of DOC was again recovered via solid phase extraction. This provides clear evidence for the production of bio-labile, low-molecular mass compounds during the photo-degradation experiment. This is consistent with the observed production of bio-labile DOM of low molecular weight during photodegradation experiments (Bano et al., 1998; Remington et al., 2011) and in the field (Lambert et al., 2016). The consumption of low-molecular

mass compounds during bio-incubation was also evident on a molecular formula level. The shift in molecular size induced by photo-incubation was partially inverted during the subsequent bio-incubation (Figure 4H). Thus, low-molecular mass compounds were preferentially consumed over high-molecular mass compounds. This was observed in the incubation both with photo-irradiated and non-irradiated samples.

Different from a previous low-energy irradiation experiment with Amazon River water, where oxygen-rich aromatics were preferentially removed (Seidel et al., 2015), we observed the opposite trend (Figure 3E), i.e., low-oxygen compounds were preferentially destroyed, similar to Kujawinski et al. (2004). A major reaction pathway in the photo-oxidation of DOM is decarboxylation (Xie et al., 2004). In principle, this reaction should result in a lower O/C ratio of the residual DOM, but at the same time new oxygen-containing functional groups can

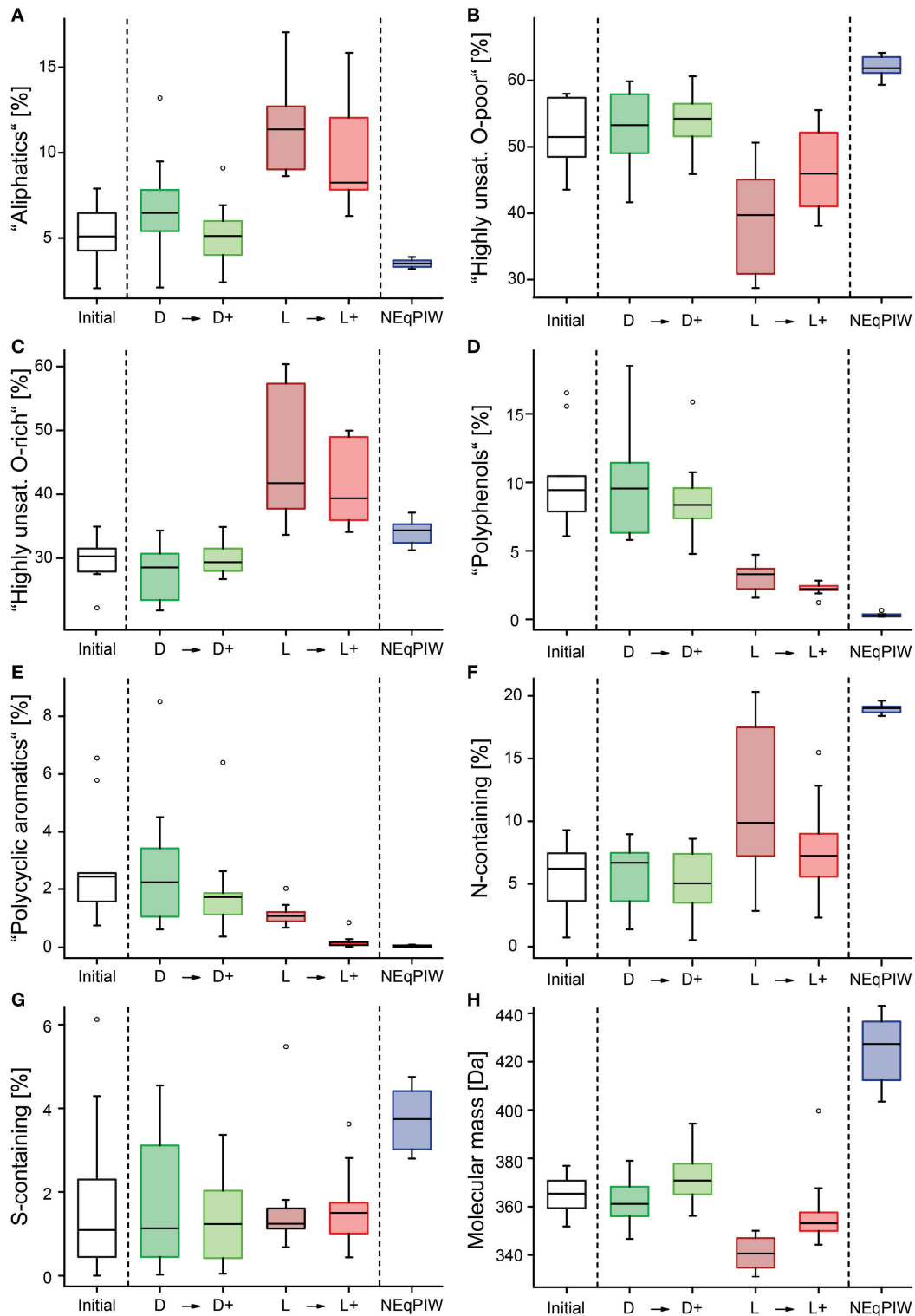


FIGURE 4 | Box-Whisker-Plots of the molecular composition after the experimental treatments of the ten river samples, including North Equatorial Pacific Intermediate Water (NEqPIW, $n = 8$ replicates). The percentages are the FT-ICR-MS signal-intensity weighted contributions of the various compound groups. The definition of the compound groups and abbreviations are given in the Material and Methods section. **(A–E)** Percentage of the various molecular compound groups, including all heteroelements (O, N, S, and P). **(F,G)** Percentage of those molecules that contained N or S. **(H)** Average molecular mass.

be produced during photo-oxidation (Xie et al., 2004). The labile compounds with low O/C that disappeared during our irradiation experiment likely received an oxygen substituent and became more oxidized. Kendrick mass defect analysis (Stenson et al., 2003) supports this explanation that addition of oxygen atoms indeed occurred, and that at the same time oxygen was removed from some compounds via decarboxylation reactions. More details on the Kendrick mass defect analysis are provided in the supplementary information (Figure S3). Apparently, decarboxylation occurs quickly during the first stages of photo-degradation (Seidel et al., 2015), whereas the addition of additional oxygen is a subsequent reaction, causing a net shift toward higher O/C ratios in DOM on the longer term (this study). Consistent with our observations from FT-ICR-MS, lignin-derived phenols are oxidized when exposed to sunlight, and an increase of the acid to aldehyde ratio of lignin phenols likely results from the incorporation of oxygen during irradiation (Hernes and Benner, 2003).

After irradiation, the relative abundance of N-containing compounds increased (Figure 4F). Photo-nitration is a possible explanation for this (Vione et al., 2014). For example, nitration of chlorophenols has been observed in the Rhone River delta as a result of the irradiation-induced formation of nitrogen dioxide radicals (Chiron et al., 2007). Photochemical reactions can also incorporate ammonium into dissolved organic forms (Kieber et al., 1997). Some of these photo-produced N-containing compounds were bio-labile and removed in the subsequent bio-incubation (Figure 4F).

Is There a Universal Molecular Signature of Resistant DOM across the Major World Rivers and the Deep Ocean?

Multiple studies have made the observation that photo-irradiation shifts the molecular signature of terrigenous DOM toward that of marine DOM (Dittmar et al., 2007; Stubbins et al., 2010; Rossel et al., 2013). The removal of characteristic terrigenous molecules by photo-degradation complicates the identification of terrestrial DOM in the ocean (Stubbins et al., 2010). Furthermore, it was suggested that the combined effects of photo- and microbial degradation may result in the accumulation of refractory molecules that share very similar molecular structures, independent of their original source (Jaffé et al., 2012). Convergence into a universal molecular composition in the course of degradation would imply that the long-term fate of DOM in the ocean is essentially source-independent.

At a first view, these previous observations were confirmed in our study. Overall trends in the molecular composition of DOM following irradiation with simulated sunlight were remarkably consistent between all ten rivers. Polyphenols (Figure 4D), condensed polycyclic aromatics (Figure 4E) and CDOM (Table 1) were preferentially removed over bulk DOC leaving behind DOM with a marine-like character, very similar to that of the old Pacific water mass (NEqPIW), included in our analysis. Also the frequency of molecular formulas on O/C and H/C scales in the photo-resistant component of DOM in the rivers was very similar to that of the marine sample

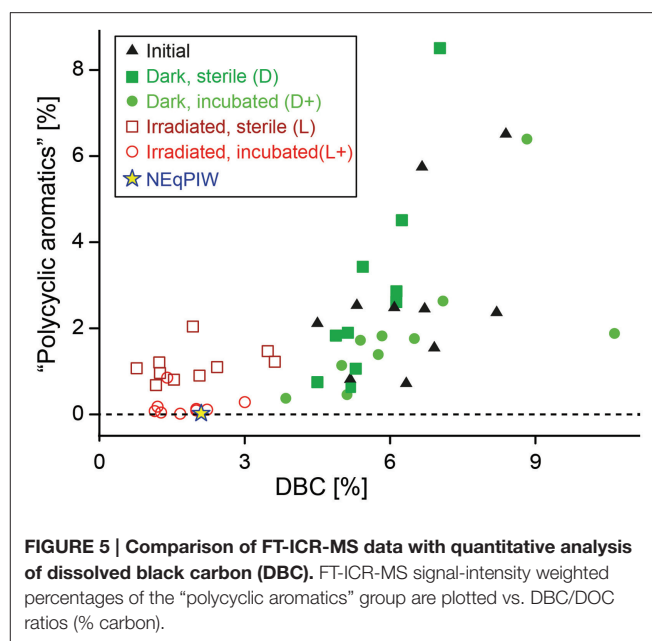
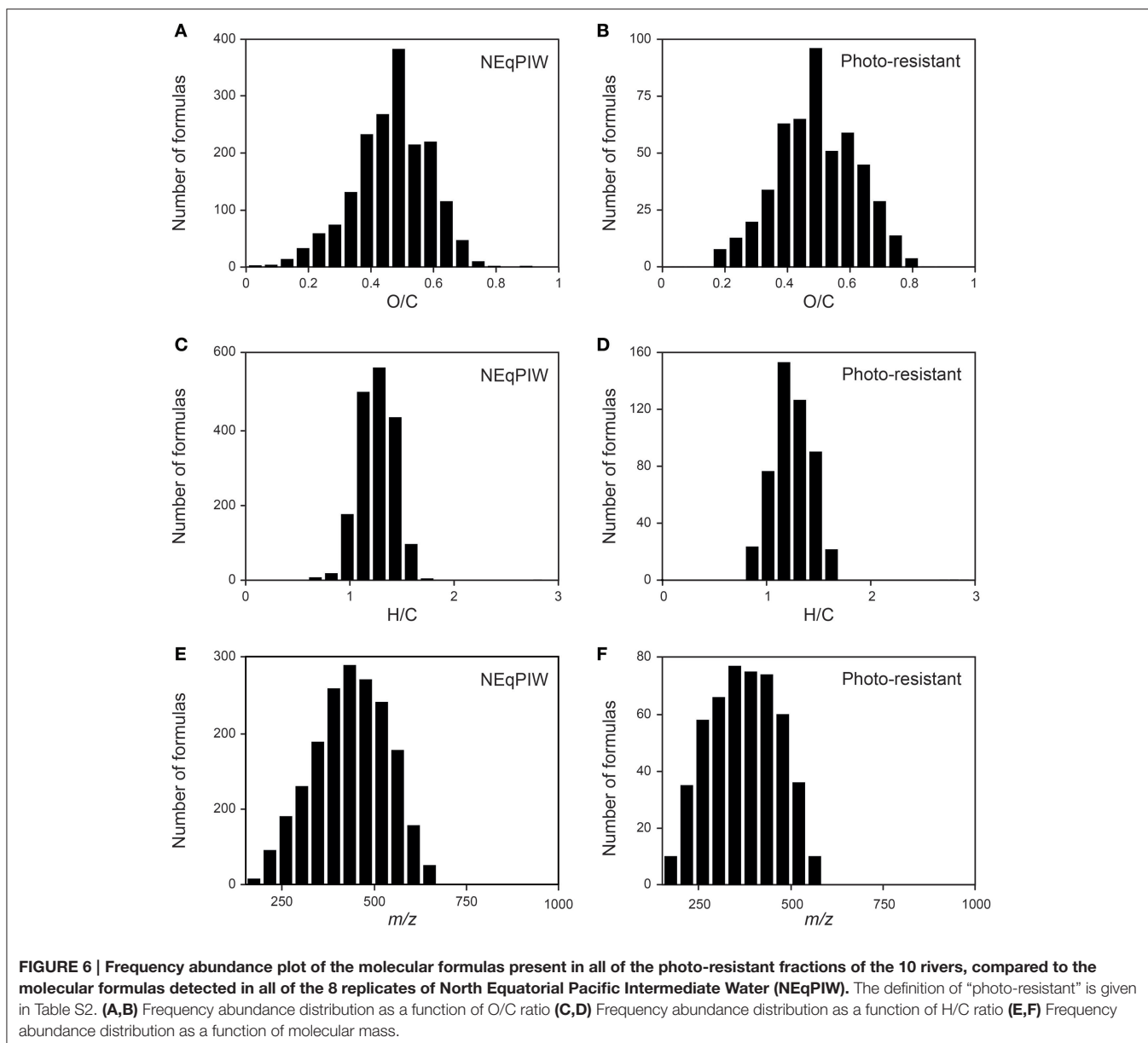


(Figure 6). An example of a single nominal mass (Figure S4) also suggests minimal differences between the photo-irradiated and marine DOM. Other molecular characteristics, however, showed a divergence of riverine and marine DOM due to the experimental treatment. Most notable, riverine compounds had on average much lower molecular masses than marine compounds (Figure 4H). Photo-degradation further increased this difference between riverine and marine (Figure 3), leaving a photo-resistant component behind that was more dissimilar to marine DOM in terms of molecular size. The rivers also contained much less nitrogen- and sulfur-containing compounds than the marine sample, and this difference only marginally changed due to the combined effect of photo- and bio-degradation (Figures 4E,G).

For a more quantitative evaluation of the molecular dissimilarities across the different samples, we performed a Bray-Curtis dissimilarity analysis. This approach takes into account the presence and absence of molecular formulas and their signal intensity distribution, i.e. the entire molecular fingerprint obtained by FT-ICR-MS. Replicate analysis of NEqPIW were dissimilar to about 5% on the Bray-Curtis scale. The initial river samples were dissimilar among each other to 17% (standard deviation $\pm 6\%$), and dissimilar to the marine NEqPIW sample by 48% ($\pm 5\%$). Surprisingly, the dissimilarity between samples remained unchanged at all stages of our experiments, and the bio- and photo-degraded samples (“L+”) were 20% ($\pm 6\%$) dissimilar among each other and 46% ($\pm 7\%$) dissimilar from marine NEqPIW. Even for the most recalcitrant compounds in our experiment, i.e. those compounds that were photo- and bio-resistant (Table S2), the level of dissimilarity was still identical ($19 \pm 7\%$ between rivers, and $42 \pm 7\%$ between rivers and NEqPIW).

The same picture emerges from PCA analysis (Figure 3A). Photo-degradation moved the river samples away from NEqPIW on axis 1, and toward NEqPIW on the axis 2. The second



axis represents largely the removal of aromatic compounds (**Figure 3E**), the first axis shifts in molecular mass (**Figure 3B**). To test whether the broad shift in molecular mass was the only reason for the differences between photo-irradiated and marine DOM, we repeated the PCA with a modified data set. This modification consisted of the removal of the broad molecular mass shift by normalizing each molecular formula to the sum of intensities of the respective nominal mass. In addition to this, only those molecular formulas were considered that co-occurred in all samples ($n = 852$). Even after this brute removal of variability between samples, the differences between riverine and marine DOM were preserved at all stages of experimental treatment (**Figure S5**). Thus, it is not only the molecular mass distribution, but all differences (as summarized in **Figure 4**, and

others) that contribute to the molecular dissimilarity between samples.

Despite this overall high level of molecular dissimilarity, there was a very clear relationship between molecular dissimilarity and reactivity (**Figure 7**). The reactive component in DOM was molecularly very dissimilar between the rivers and to NEqPIW (**Figures 7C,D**). In other words, each river had a unique group of compounds that was labile or produced, despite the clear overall trend discussed in the previous section. The only exceptions were the Congo and Amazon Rivers whose photo-labile component shared a high level of similarity (**Figure 7C**), possibly because of their similarity in climate and vegetation. In all rivers, the reactive components shared no molecular similarity with marine DOM (**Figures 7C,D**),

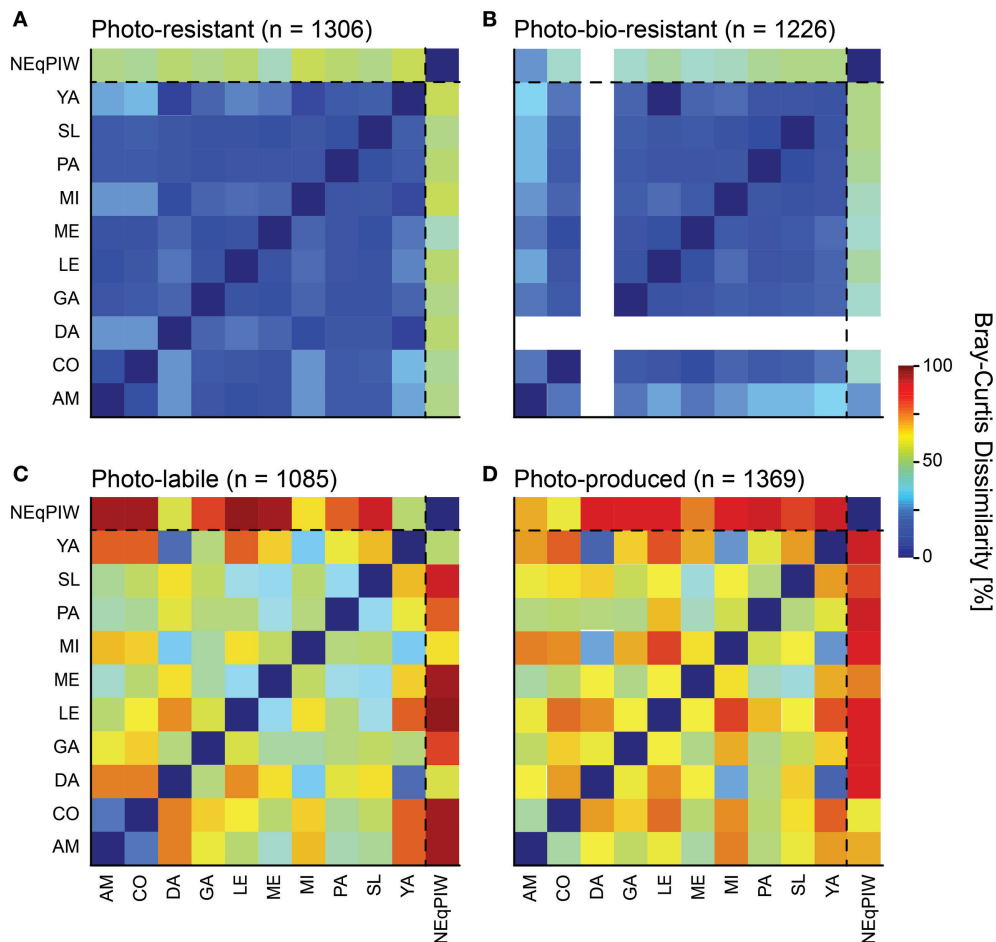


FIGURE 7 | Bray-Curtis dissimilarity matrices of the molecular formulas detected in the different reactivity fractions (for definition see Table S2) of the ten rivers, under consideration of FT-ICR-MS signal intensities. For comparison the marine sample was included, under consideration of the same molecular formulas as in each reactivity fraction. **(A)** Photo-resistant molecular formulas, signal intensities from experiment “L” were used. **(B)** Photo-bio-resistant molecular formulas, signal intensities from experiment “L+” were used. **(C)** Photo-labile molecular formulas, signal intensities from “initial” samples were used. **(D)** Photo-produced molecular formulas, signal intensities from experiment “L+” were used. Abbreviations: AM, Amazon River; CO, Congo River; DA, Danube River; GA, Ganges Brahmaputra River; LE, Lena River; ME, Mekong River; MI, Mississippi River; PA, Paraná River; SL, St. Lawrence River; YA, Yangtze River; NEqPIW, North Equatorial Pacific Intermediate Water. Note that the “L+” experiment was not performed with Danube River water.

indicating that these compounds had efficiently been removed on their long journey into intermediate depths of the North Pacific. Compared to the reactive component of DOM, the rivers shared a relatively high molecular similarity in their resistant component (Figures 7A,B). This component potentially resists large-scale transport in the ocean. However, the large molecular dissimilarity even of this resistant riverine fraction with the marine sample indicates substantial molecular transformation prior to downward convection into the deep basins of the oceans. Autochthonous marine DOM seems to dominate the molecular composition of NEqPIW. It is possible that the different microbial communities in fresh and marine waters may cause molecular transformations in DOM that remained uncovered in this study. Long-term molecular transformations in the ocean may also result in almost complete loss of terrigenous DOM (Opsahl and Benner, 1997). But if the hypothesis is

correct that the molecular composition of DOM converges in the course of degradation, irrespective of its original source, and that there is a universal molecular composition of recalcitrant DOM, different time scales and processes must be involved than considered in all experiments performed in this context to date.

AUTHOR CONTRIBUTIONS

AV designed sampling and performed photo- and bio-degradation experiments. Molecular analyses were done by JN, TR, TD (FT-ICR-MS and black carbon), RS and PH (lignin). Statistical analyses were done by MZ, TR, and TD. The manuscript was written under the lead of TD and TR, with the contribution of all authors.

FUNDING

RS was supported by the National Science Foundation through OCE-1333157/1464396. AV by the Academy of Finland (111761).

ACKNOWLEDGMENTS

We thank M. Friebe and I. Ulber for assistance in the lab and K. Klaproth for skilled technical support with the ESI-FT-ICR-MS. We would like to thank those who contributed to sampling: H. and K. Aarnos (shipping organizations), E. M. Paolucci

(Paraná), D. O. E. Musibono (Congo), A. Shantz (Mekong), S. R. Khan (Ganges-Brahmaputra), Q. Huang (Yangtze), W. Schneider and B. Heim (Lena), Y. Gélinas (St. Lawrence), and A. Rivas and C. E. Rezende (Amazon), E. Petrescu (Danube), and H. E. Reader (Mississippi).

SUPPLEMENTARY MATERIAL

The Supplementary Material for this article can be found online at: <http://journal.frontiersin.org/article/10.3389/feart.2016.00085>

REFERENCES

- Aarnos, H., Ylostalo, P., and Vähätalo, A. V., (2012). Seasonal phototransformation of dissolved organic matter to ammonium, dissolved inorganic carbon, and labile substrates supporting bacterial biomass across the Baltic Sea. *J. Geophys. Res.* 117:G01004. doi: 10.1029/2010jg001633
- Aufdenkampe, A. K., Mayorga, E., Raymond, P. A., Melack, J. M., Doney, S. C., Alin, S. R., et al. (2011). Riverine coupling of biogeochemical cycles between land, oceans, and atmosphere. *Front. Ecol. Environ.* 9:14. doi: 10.1890/100014
- Bano, N., Moran, M. A., and Hodson, R. E. (1998). Photochemical formation of labile organic matter from two components of dissolved organic carbon in a freshwater wetland. *Aquat. Microb. Ecol.* 16, 95–102. doi: 10.3354/ame016095
- Benner, R., and Kaiser, K. (2011). Biological and photochemical transformations of amino acids and lignin phenols in riverine dissolved organic matter. *Biogeochemistry* 102, 209–222. doi: 10.1007/s10533-010-9435-4
- Chiron, S., Minero, C., and Vione, D. (2007). Occurrence of 2,4-dichlorophenol and 2,4-dichloro-6-nitrophenol in the Rhone river delta (Southern France). *Environ. Sci. Technol.* 41, 3127–3133. doi: 10.1021/es0626638
- Cole, J. J., Prairie, Y. T., Caraco, N. F., McDowell, W. H., Tranvik, L. J., Striegl, R. G., et al. (2007). Plumbing the global carbon cycle: Integrating inland waters into the terrestrial carbon budget. *Ecosystems* 10, 171–184. doi: 10.1007/s10021-006-9013-8
- Cory, R. M., Ward, C. P., Crump, B. C., and Kling, G. W. (2014). Sunlight controls water column processing of carbon in arctic fresh waters. *Science* 345, 925–928. doi: 10.1126/science.1253119
- Dai, M., Yin, Z., Meng, F., Liu, Q., and Cai, W.-J. (2012). Spatial distribution of riverine DOC inputs to the ocean: an updated global synthesis. *Curr. Opin. Env. Sust.* 4, 170–178. doi: 10.1016/j.cosust.2012.03.003
- Dittmar, T. (2008). The molecular level determination of black carbon in marine dissolved organic matter. *Org. Geochem.* 39, 396–407. doi: 10.1016/j.orggeochem.2008.01.015
- Dittmar, T., Koch, B. P., Hertkon, N., and Kattner, G. (2008). A simple and efficient method for solid phase extraction of dissolved organic matter (SPE-DOM) from seawater. *Limnol. Oceanogr. Methods* 6, 230–235. doi: 10.4319/lom.2008.6.230
- Dittmar, T., and Paeng, J. (2009). A heat-induced molecular signature in marine dissolved organic matter. *Nat. Geosci.* 2, 175–179. doi: 10.1038/ngeo440
- Dittmar, T., Whitehead, K., Minor, L., and Koch, B. P. (2007). Tracing terrigenous dissolved organic matter and its photochemical decay in the ocean by using liquid chromatography / mass spectrometry. *Mar. Chem.* 107, 378–387. doi: 10.1016/j.marchem.2007.04.006
- Fichot, C. G., and Benner, R. (2012). The spectral slope coefficient of chromophoric dissolved organic matter (S275-295) as a tracer of terrigenous dissolved organic carbon in river-influenced ocean margins. *Limnol. Oceanogr.* 57, 1453–1466. doi: 10.4319/lo.2012.57.5.1453
- Gerdes, R., Döhrle, W., Spiller, W., Schneider, G., Schnurpfeil, G., and Schulz-Ekloff, G. (1997). Photo-oxidation of phenol and monochlorophenols in oxygen-saturated aqueous solutions by different photosensitizers. *J. Photochem. Photobiol.* 111, 65–74. doi: 10.1016/S1010-6030(97)00209-8
- Goldman, J. C., Caron, D. A., and Dennett, M. R. (1987). Regulation of gross growth efficiency and ammonium regeneration in bacteria by substrate C:N ratio. *Limnol. Oceanogr.* 32, 1239–1252. doi: 10.4319/lo.1987.32.6.1239
- Gonsior, M., Peake, B. M., Cooper, W. T., D'Andrilli, J., and Cooper, W. J. (2008). Photochemically induced changes in dissolved organic matter identified by ultrahigh resolution fourier transform ion cyclotron resonance mass spectrometry. *Environ. Sci. Technol.* 43, 698–703. doi: 10.1021/es8022804
- Graneli, W., Lindell, M., De Faria, B. M., and Esteves, F. D. A. (1998). Photoproduction of dissolved inorganic carbon in temperate and tropical lakes—dependence on wavelength band and dissolved organic carbon concentration. *Biogeochem.* 43, 175–195. doi: 10.1023/A:1006042629565
- Green, N. W., Perdue, E. M., Aiken, G. R., Butler, K. D., Chen, H., Dittmar, T., et al. (2014). An intercomparison of three methods for the large-scale isolation of oceanic dissolved organic matter. *Mar. Chem.* 161, 14–19. doi: 10.1016/j.marchem.2014.01.012
- Hawkes, J. A., Hansen, C. T., Goldammer, T., Bach, W., and Dittmar, T. (2016). Molecular alteration of marine dissolved organic matter under experimental hydrothermal conditions. *Geochim. Cosmochim. Acta* 175, 68–85. doi: 10.1016/j.gca.2015.11.025
- Hedges, J. I., and Ertel, J. R. (1982). Characterization of lignin by gas capillary chromatography of cupric oxide oxidation-products. *Anal. Chem.* 54, 174–178. doi: 10.1021/ac00239a007
- Hedges, J. I., Keil, R. G., and Benner, R. (1997). What happens to terrestrial organic matter in the ocean? *Org. Geochem.* 27, 195–212. doi: 10.1016/S0146-6380(97)00066-1
- Hernes, P. J., and Benner, R. (2003). Photochemical and microbial degradation of dissolved lignin phenols: Implications for the fate of terrigenous dissolved organic matter in marine environments. *J. Geophys. Res.* 108, 3291. doi: 10.1029/2002JC001421
- Hertkorn, N., Benner, R., Frommberger, M., Schmitt-Kopplin, P., Witt, M., Kaiser, K., et al. (2006). Characterization of a major refractory component of marine dissolved organic matter. *Geochim. Cosmochim. Acta* 70, 2990–3010. doi: 10.1016/j.gca.2006.03.021
- Jaffé, R., Ding, Y., Niggemann, J., Vähätalo, A. V., Stubbins, A., Spencer, R. G. M., et al. (2013). Global charcoal mobilization from soils via dissolution and riverine transport to the oceans. *Science* 340, 345–347. doi: 10.1126/science.1231476
- Jaffé, R., Yamashita, Y., Maie, N., Cooper, W. T., Dittmar, T., Dodds, W. K., et al. (2012). Dissolved organic matter in headwater streams: compositional variability across climatic regions of North America. *Geochim. Cosmochim. Acta* 94, 95–108. doi: 10.1016/j.gca.2012.06.031
- Karentz, D., Bothwell, M. L., Coffin, R. B., Hanson, A., Herndl, G. J., Kilham, S. S., et al. (1994). Impact of UV-B radiation on pelagic freshwater ecosystems: Report of working group on bacteria and phytoplankton. *Arch. Hydrobiol.* 43, 31–69.
- Kieber, R. J., Hydro, L. H., and Seaton, P. J., (1997). Photooxidation of triglycerides and fatty acids in seawater: implication toward the formation of marine humic substances. *Limnol. Oceanogr.* 42, 1454–1462. doi: 10.4319/lo.1997.42.6.1454
- Kim, S., Kaplan, L. A., and Hatcher, P. G., (2006). Biodegradable dissolved organic matter in a temperate and a tropical stream determined from ultra-high resolution mass spectrometry. *Limnol. Oceanogr.* 51, 1054–1063. doi: 10.4319/lo.2006.51.2.1054

- Koch, B. P., and Dittmar, T., (2006). From mass to structure: an aromaticity index for high-resolution mass data of natural organic matter. *Rapid Comm. Mass Spectrom.* 20, 926–993. doi: 10.1002/rcm.2386
- Koch, B. P., and Dittmar, T., (2016). Erratum: From mass to structure: an aromaticity index for high-resolution mass data of natural organic matter. *Rapid Comm. Mass Spectrom.* 30, 250. doi: 10.1002/rcm.7433
- Koch, B. P., Dittmar, T., Witt, M., and Kattner, G., (2007). Fundamentals of molecular formula assignment to ultrahigh resolution mass data of natural organic matter. *Anal. Chem.* 79, 1758–1763. doi: 10.1021/ac061949s
- Koehler, B., Landelius, T., Weyhenmeyer, G. A., Machida, N., and Tranvik, L. J. (2014). Sunlight-induced carbon dioxide emissions from inland waters. *Glob. Biogeochem.* 28, 696–711. doi: 10.1002/2014GB004850
- Kujawinski, E. B., Del Vecchio, R., Blough, N. V., Klein, G. C., and Marshall, A. G. (2004). Probing molecular-level transformations of dissolved organic matter: insights on photochemical degradation and protozoan modification of DOM from electrospray ionization Fourier transform ion cyclotron resonance mass spectrometry. *Mar. Chem.* 92, 23–37. doi: 10.1016/j.marchem.2004.06.038
- Lalonde, K., Vähätalo, A. V., and Gelinas, Y. (2014). Revisiting the disappearance of terrestrial dissolved organic matter in the ocean: a d13C study. *Biogeosciences* 11, 3707–3719. doi: 10.5194/bg-11-3707-2014
- Lambert, T., Darchambeau, F., Bouillon, S., Alhou, B., Jean-Daniel, M., Cristian, R., et al. (2015). Landscape control on the spatial and temporal variability of chromophoric dissolved organic matter and dissolved organic carbon in large African rivers. *Ecosystems* 18, 1224–1239. doi: 10.1007/s10021-015-9894-5
- Lambert, T., Bouillon, S., Darchambeau, F., Massicotte, P., and Borges, A. V. (2016). Shift in the chemical composition of dissolved organic matter in the Congo River network. *Biogeosci. Discuss.* 1–49. doi: 10.5194/bg-2016-240
- Lapierre, J.-F., Guillemette, F., Berggren, M., and del Giorgio, P. A. (2013). Increases in terrestrially derived carbon stimulate organic carbon processing and CO₂ emissions in boreal ecosystems. *Nat. Comm.* 4, 2972. doi: 10.1038/ncomms3972
- Lindell, M. J., Graneli, W., and Tranvik, L. J. (1995). Enhanced bacterial growth in response to photochemical transformation of dissolved humic matter. *Limnol. Oceanogr.* 40, 195–199. doi: 10.4319/lo.1995.40.1.0195
- Lund, V., and Hongve, D. (1994). Ultraviolet irradiated water containing humic substances inhibits bacterial metabolism. *Water Res.* 28, 1111–1116. doi: 10.1016/0043-1354(94)90197-X
- Mattsson, T., Kortelainen, P., Laubel, A., Evans, D., Pujo-Pay, M., Räike, A., et al. (2009). Export of dissolved organic matter in relation to land use along a European climatic gradient. *Sci. Total Environ.* 407, 1967–1976. doi: 10.1016/j.scitotenv.2008.11.014
- McNally, A. M., Moody, E. C., and McNeill, K. (2005). Kinetics and mechanism of the sensitized photodegradation of lignin model compounds. *Photochem. Photobiol. Sci.* 4, 268–274. doi: 10.1039/b416956e
- Medeiros, P. M., Seidel, M., Ward, N. D., Carpenter, E. J., Gomes, H. R., Niggemann, J., et al. (2015). Fate of the Amazon River dissolved organic matter in the tropical Atlantic Ocean. *Glob. Biogeochem. Cycles* 29, 677–690. doi: 10.1002/2015GB005115
- Miller, W. L., and Moran, M. A. (1997). Interaction of photochemical and microbial processes in the degradation of refractory dissolved organic matter from a coastal marine environment. *Limnol. Oceanogr.* 42, 1317–1324. doi: 10.4319/lo.1997.42.6.1317
- Miller, W. L., and Zepp, R. G. (1995). Photochemical production of dissolved inorganic carbon from terrestrial organic matter: Significance to the oceanic organic carbon cycle. *Geophys. Res. Lett.* 22, 417–420. doi: 10.1029/94GL03344
- Mopper, K., Zhou, X., Kieber, D. J., Sikorski, R. J., and Jones, R. N. (1991). Photochemical degradation of dissolved organic carbon and its impact on oceanic carbon cycle. *Nature* 353, 60–62. doi: 10.1038/353060a0
- Obernosterer, I., and Benner, R. (2004). Competition between biological and photochemical processes in the mineralization of dissolved organic carbon. *Limnol. Oceanogr.* 49, 117–124. doi: 10.4319/lo.2004.49.1.0117
- Obernosterer, I., Reitner, B., and Herndl, G. J. (1999). Contrasting effects of solar radiation on dissolved organic matter and its bioavailability to marine bacterioplankton. *Limnol. Oceanogr.* 44, 1645–1654. doi: 10.4319/lo.1999.44.7.1645
- Oksanen, J., Blanchet, F. G., Kindt, R., Legendre, P., Minchin, P. R., O'Hara, R. B., et al. (2013). *Vegan: Community Ecology Package*. R package version 2.0-10. Available online at: <http://CRAN.R-project.org/package=vegan>
- Opsahl, S., and Benner, R. (1997). Distribution and cycling of terrigenous dissolved organic matter in the ocean. *Nature* 386, 480–482. doi: 10.1038/386480a0
- Opsahl, S., and Benner, R. (1998). Photochemical reactivity of dissolved lignin in river and ocean waters. *Limnol. Oceanogr.* 43, 1297–1304. doi: 10.4319/lo.1998.43.6.1297
- Osburn, C. L., Retamal, L., and Vincent, W. F. (2009). Photoreactivity of chromophoric dissolved organic matter transported by the Mackenzie River to the Beaufort Sea. *Mar. Chem.* 115, 10–20. doi: 10.1016/j.marchem.2009.05.003
- Osterholz, H., Niggemann, J., Giebel, H. A., Simon, M., and Dittmar, T. (2015). Inefficient microbial production of refractory dissolved organic matter in the ocean. *Nat. Comm.* 6:7422. doi: 10.1038/ncomms8422
- Petersen, J. E., and Kemp, W. M. (2010). “Mesocosms: enclosed experimental ecosystems in ocean science,” in *Encyclopedia of Ocean Sciences, 2nd Edn.*, eds J. H. Steele, K. K. Turekian, and S. A. Thorpe (Amsterdam: Elsevier), 732–747.
- Raymond, P. A., Hartmann, J., Lauerwald, R., Sobek, S., McDonald, C., Hoover, M., et al. (2013). Global carbon dioxide emissions from inland waters. *Nature* 503, 355–359. doi: 10.1038/nature12760
- Raymond, P. A., and Spencer, R. G. M. (2015). “Riverine dissolved organic matter,” in *Biogeochemistry of Marine Dissolved Organic Matter, 2nd Edn.*, eds D. A. Hansell and C. A. Carlson (Amsterdam: Elsevier), 509–533.
- Remington, S., Krusche, A., and Richey, J. (2011). Effects of DOM photochemistry on bacterial metabolism and CO₂ evasion during falling water in a humic and a whitewater river in the Brazilian Amazon. *Biogeochemistry* 105, 185–200. doi: 10.1007/s10533-010-9565-8
- Riedel, T., Iden, S., Geilich, J., Wiedner, K., Durner, W., and Biester, H. (2014). Changes in the molecular composition of organic matter leached from an agricultural topsoil following addition of biomass-derived black carbon (biochar). *Org. Geochem.* 69, 52–60. doi: 10.1016/j.orggeochem.2014.02.003
- Riedel, T., and Dittmar, T. (2014). A method detection limit for the analysis of natural organic matter via fourier transform ion cyclotron resonance mass spectrometry. *Anal. Chem.* 86, 8376–8382. doi: 10.1021/ac501946m
- Rossel, P. E., Vähätalo, A. V., Witt, M., and Dittmar, T. (2013). Molecular composition of dissolved organic matter from a wetland plant (*Juncus effusus*) after photochemical and microbial decomposition (1.25 yr): Common features with deep sea dissolved organic matter. *Org. Geochem.* 60, 62–71. doi: 10.1016/j.orggeochem.2013.04.013
- Santín, C., Doerr, S. H., Kane, E. S., Masiello, C. A., Ohlson, M., Dittmar, J. M., et al. (2016). Towards a global assessment of pyrogenic carbon from vegetation fires. *Glob. Change Biol.* 22, 76–91. doi: 10.1111/gcb.12985
- Seidel, M., Beck, M., Riedel, T., Waska, H., Suryaputra, I. G. N. A., Schnetger, B., et al. (2014). Biogeochemistry of dissolved organic matter in an anoxic intertidal creek bank. *Geochim. Cosmochim. Acta* 140, 418–434. doi: 10.1016/j.gca.2014.05.038
- Seidel, M., Yager, P. L., Ward, N. D., Carpenter, E. J., Gomes, H. R., Krusche, A. V., et al. (2015). Molecular-level changes of dissolved organic matter along the Amazon River-to-ocean continuum. *Mar. Chem.* 177, 218–231. doi: 10.1016/j.marchem.2015.06.019
- Spencer, R. G. M., Aiken, G. R., Dyda, R. Y., Butler, K. D., Bergamaschi, B. A., and Hernes, P. J. (2010). Comparison of XAD with other dissolved lignin isolation techniques and a compilation of analytical improvements for the analysis of lignin in aquatic settings. *Org. Geochem.* 41, 445–453. doi: 10.1016/j.orggeochem.2010.02.004
- Spencer, R. G. M., Stubbins, A., Hernes, P. J., Andy, B., Kenneth, M., Anthony, K. A., et al. (2009). Photochemical degradation of dissolved organic matter and dissolved lignin phenols from the Congo River. *J. Geophys. Res.* 114:G03010. doi: 10.1029/2009JG000968
- Stenson, A. C., Marshall, A. G., and Cooper, W. T. (2003). Exact masses and chemical formulas of individual Suwannee River fulvic acids from ultrahigh resolution electrospray ionization Fourier transform ion cyclotron resonance mass spectra. *Anal. Chem.* 75, 1275–1284. doi: 10.1021/ac026106p
- Stubbins, A., Niggemann, J., and Dittmar, T. (2012). Photo-lability of deep ocean dissolved black carbon. *Biogeosciences* 9, 1661–1670. doi: 10.5194/bg-9-1661-2012
- Stubbins, A., Spencer, R. G. M., Chen, H., Hatcher, P. G., Mopper, K., Hernes, P. J., et al. (2010). Illuminated darkness: molecular signatures of Congo River dissolved organic matter and its photochemical alteration as revealed by ultrahigh precision mass spectrometry. *Limnol. Oceanogr.* 55, 1467–1477. doi: 10.4319/lo.2010.55.4.1467

- Stubbins, A., Spencer, R. G. M., Mann, P. J., Holmes, R. M., McClelland, J. W., Niggemann, J., et al. (2015). Utilizing colored dissolved organic matter to derive dissolved black carbon export by Arctic Rivers. *Front. Earth Sci.* 3:63. doi: 10.3389/feart.2015.00063
- Stuiver, M., Quay, P. D., and Ostlund, H. G. (1983). Abyssal Water Carbon-14 Distribution and the age of the world oceans. *Science* 219, 849–851. doi: 10.1126/science.219.4586.849
- Šantl-Temkiv, T., Finster, K., Dittmar, T., Hansen, B. M., Thyraug, R., Woetmann Nielsen, N., et al. (2013). Hailstones: a window into the microbial and chemical inventory of a storm cloud. *PLoS ONE* 8:e53550. doi: 10.1371/journal.pone.0053550
- Tranvik, L. J., and Bertilsson, S. (2001). Contrasting effects of solar UV radiation on dissolved organic sources for bacterial growth. *Ecol. Lett.* 4, 458–463. doi: 10.1046/j.1461-0248.2001.00245.x
- Vähätalo, A. V., and Wetzel, R. G. (2008). Long-term photochemical and microbial decomposition of wetland-derived dissolved organic matter with alteration of $^{13}\text{C}:^{12}\text{C}$ mass ratio. *Limnol. Oceanogr.* 53, 1387–1392. doi: 10.4319/lo.2008.53.4.1387
- Vähätalo, A. V., Salonen, K., Münster, U., Järvinen, M., and Wetzel, R. G. (2003). Photochemical transformation of allochthonous organic matter provides bioavailable nutrients in a humic lake. *Arch. Hydrobiol.* 156, 287–314. doi: 10.1127/0003-9136/2003/0156-0287
- Vione, D., Minella, M., Maurino, V., and Minero, C. (2014). Indirect photochemistry in sunlit surface waters: photoinduced production of reactive transient species. *Chem. A Eur. J.* 20, 10590–10606. doi: 10.1002/chem.201400413
- Waggoner, D. C., Chen, H., Willoughby, A. S., and Hatcher, P. G. (2015). Formation of black carbon-like and alicyclic aliphatic compounds by hydroxyl radical initiated degradation of lignin. *Org. Geochem.* 82, 69–76. doi: 10.1016/j.orggeochem.2015.02.007
- Wagner, S., Riedel, T., Niggemann, J., Vähätalo, A. V., Dittmar, T., and Jaffé, R. (2015). Linking the molecular signature of heteroatomic dissolved organic matter to watershed characteristics in world rivers. *Env. Sci. Technol.* 49, 13798–13806. doi: 10.1021/acs.est.5b00525
- Ward, N. D., Keil, R. G., Medeiros, P. M., Brito, D. C., Cunha, A. C., Richey, T., et al. (2013). Degradation of terrestrially derived macromolecules in the Amazon River. *Nat. Geosci.* 6, 530–533. doi: 10.1038/ngeo1817
- Wilson, H. F., and Xenopoulos, M. A. (2009). Effects of agricultural land use on the composition of fluvial dissolved organic matter. *Nat. Geosci.* 2, 37–41. doi: 10.1038/ngeo391
- Xie, H., Zafiriou, O. C., Cai, W.-J., Zepp, R. G., and Wang, Y. (2004). Photooxidation and its effects on the carboxyl content of dissolved organic matter in two coastal rivers in the southeastern United States. *Environ. Sci. Technol.* 38, 4113–4119. doi: 10.1021/es035407t
- Ziolkowski, L. A., and Druffel, E. R. M. (2010). Aged black carbon identified in marine dissolved organic carbon. *Geophys. Res. Lett.* 37:L16601. doi: 10.1029/2010GL043963

Conflict of Interest Statement: The authors declare that the research was conducted in the absence of any commercial or financial relationships that could be construed as a potential conflict of interest.

Copyright © 2016 Riedel, Zark, Vähätalo, Niggemann, Spencer, Hernes and Dittmar. This is an open-access article distributed under the terms of the Creative Commons Attribution License (CC BY). The use, distribution or reproduction in other forums is permitted, provided the original author(s) or licensor are credited and that the original publication in this journal is cited, in accordance with accepted academic practice. No use, distribution or reproduction is permitted which does not comply with these terms.



Dissolved organic matter in pore water of Arctic Ocean sediments: Environmental influence on molecular composition



Pamela E. Rossel^{a,b,c,*}, Christina Bienhold^{a,b}, Antje Boetius^{a,b}, Thorsten Dittmar^c

^a HGF-MPG Group for Deep Sea Ecology and Technology, Alfred Wegener Institute, Helmholtz Center for Polar and Marine Research, Am Handelshafen 12, 27570 Bremerhaven, Germany

^b Max Planck Institute for Marine Microbiology, Celsiusstr. 1, 28359 Bremen, Germany

^c Research Group for Marine Geochemistry (ICBM-MPI Bridging Group), Institute for Chemistry and Biology of the Marine Environment, University of Oldenburg, ICBM, D-26111 Oldenburg, Germany

ARTICLE INFO

Article history:

Received 8 January 2016
Received in revised form 16 March 2016
Accepted 2 April 2016
Available online 8 April 2016

Keywords:

Dissolved organic matter
Pore water
Fourier-transform ion cyclotron mass spectrometry
Arctic Ocean

ABSTRACT

Marine organic matter (OM) sinks from surface water to the seafloor via the biological pump. Benthic communities, which use this sedimented OM as an energy and carbon source, produce dissolved OM (DOM) in the process of degradation, enriching the sediment pore water with fresh DOM compounds. In the oligotrophic deep Arctic basin, particle flux is low but highly seasonal. We hypothesized that the molecular signal of freshly deposited, primary produced OM would be detectable in surface sediment pore water, which should differ in DOM composition from bottom water and deeper sediment pore water. The study focused on (i) the molecular composition of the DOM in sediment pore water of the deep Eurasian Arctic basins, (ii) the signal of marine vs. terrigenous DOM represented by different compounds preserved in the pore water and (iii) the relationship between Arctic Ocean ice cover and DOM composition. Composition based on mass spectrometric information, obtained via 15 T Fourier transform ion cyclotron resonance mass spectrometry, was correlated with environmental parameters with partial least square analysis. The fresh marine detrital OM signal from surface water was limited to pore water from <5 cm sediment depth. The productive ice margin stations showed a higher abundance of peptide, unsaturated aliphatic and saturated fatty acid molecular formulae, indicative of recent phytodetritus deposition, than the multiyear ice-covered stations, which had a stronger aromatic signal. The study contributes to the understanding of the coupling between Arctic Ocean productivity and its depositional regime, and how it may be altered in response to sea ice retreat and increasing river runoff.

© 2016 The Authors. Published by Elsevier Ltd. This is an open access article under the CC BY-NC-ND license (<http://creativecommons.org/licenses/by-nc-nd/4.0/>).

1. Introduction

Dissolved organic matter (DOM) dynamics in the deep ocean are rather poorly constrained, despite the relevance of this large global carbon reservoir of 700 Pg (Houghton, 2007). An unknown fraction of the ocean DOM originates from deposited marine particulate OM, which is produced in surface water and sinks to the seafloor via the biological pump. At the seafloor, this deposited OM is recycled by benthic animals and microorganisms on time-scales of weeks to months (Moodley et al., 2002; Witte et al., 2003). In the process of degradation, ca. 80% of the organic carbon (OC) is channeled into benthic respiration (Rowe and Deming, 1985; Deming and Yager, 1992), but a significant proportion is

hydrolyzed to DOM by extracellular digestive enzymes and the exudation of metabolites. Some smaller monomers such as fatty acids, sugars and amino acids are readily used by benthic microbial communities, leaving behind more recalcitrant organic compounds in the pore water. Part of this DOM, which represents an OC source comparable in magnitude to riverine input, is transported to the overlying bottom water and is mixed into the global ocean DOM pool, while another fraction diffuses to deeper sediment layers, delivering substrates to subsurface microbial communities (Burdige and Komada, 2015 and references therein).

The Arctic Ocean is one of the most oligotrophic seas on Earth, due to the limited availability of light for primary production for most of the season (Anderson and Dryssen, 1990). The flux of particulate OC (POC) in the central Arctic is low (ca. 2000 mmol C/m²/yr; Lalande et al., 2014), with the lowest values in the 100% ice-covered basins (100–400 mmol C/m²/yr; Lalande et al., 2014), compared with the areas along the ice margin (1000–3500 mmol C/m²/yr; Lalande et al., 2014). As in other

* Corresponding author at: HGF-MPG Group for Deep Sea Ecology and Technology, Alfred Wegener Institute, Helmholtz Center for Polar and Marine Research, Am Handelshafen 12, 27570 Bremerhaven, Germany.

E-mail address: prossel@mpi-bremen.de (P.E. Rossel).

oligotrophic seas, OM flux via sedimentation is the major force controlling the structure and activity of benthic communities in the Arctic (Boetius and Damm, 1998; Klages et al., 2004; Bienhold et al., 2012; Jacob et al., 2013; Kędra et al., 2015). Recently, in 2012, the sedimentation of large amounts of ice algae has been observed in the eastern central basins of the Arctic Ocean as a consequence of the record sea ice melt in summer 2012, representing a carbon deposition of 750 mmol C/m^2 within 1–2 months to a depth of 4000 m (Boetius et al., 2013).

Global warming is expected to further reduce Arctic ice cover, which – based on model predictions – may increase primary production, due to the effect of greater light availability (Walsh et al., 2005; Arrigo et al., 2008). However, in the long run, primary productivity may also decrease due to an increase in ocean stratification and a subsequent decline in nutrient availability (Wassmann et al., 2010; Zhang et al., 2010; Fernández-Méndez et al., 2015). With regard to the prediction that the Arctic Ocean will be ice-free in around 20–50 years from now (Wang and Overland, 2009), our understanding of it and how the system will respond to this environmental variation is limited, and baseline data are largely missing.

The input of particulate OM (POM) and subsequent diagenesis modulate the spatial distribution and composition of pore water DOM (Skoog and Benner, 1997; Amon et al., 2001). A detailed overview of the DOM molecular composition in sediment pore water has been achieved using ultra high resolution mass spectrometry via Fourier transform ion cyclotron resonance mass spectrometry (FT-ICR-MS) which, in contrast to traditional biomarker techniques (e.g. lignin phenol analysis), allows working with small sample volumes (30–50 ml; Schmidt et al., 2009; Seidel et al., 2014). It primarily addresses the component of DOM that cannot be resolved with conventional chromatographic separation techniques, and as such provides molecular fingerprints of DOM in previously unrepresented detail. As with any analytical technique, it has a defined analytical window and colloidal matter and low molecular

weight (MW) monomeric compounds are not fully recovered. In this study we have used it in order to characterize the DOM molecular composition of sediment pore water from the ice-covered eastern central basins of the Arctic Ocean. We hypothesized that the signal of the past season's primary production transferred to the sediment via the biological pump would be restricted to the surface sediment pore water. Furthermore, spatial patterns of DOM molecular signatures were evaluated in relation to environmental parameters, with a focus on (i) the molecular composition of the DOM in sediment pore water of Eurasian Arctic basins, (ii) the signal of fresh marine vs. terrigenous DOM in the sediment pore water and (iii) the relationship between ice cover and the DOM molecular composition.

2. Material and methods

2.1. Sampling sites and sample description

During the RV Polarstern cruise ARK-XXVII/3 to the Arctic Ocean in summer 2012, sea ice declined to a record minimum (Perovich et al., 2012) from an avg. of ca. 6.3 Mio km^2 between 1981 and 2010 to 3.3 Mio km^2 in 2012, based on sea ice remote sensing data (Spreen et al., 2008; www.meereisportal.de, checked on 4.04.2014). Bottom water and sediment pore water samples were collected with a TV guided multicorer at stations in the Nansen and Amundsen basins, between $83\text{--}89^\circ\text{N}$ and $18\text{--}130^\circ\text{E}$ (Fig. 1, Table 1). Stations 2–4 were south of 84°N , closer to the ice margin and characterized by first year sea ice (FYI), while stations 6–9 were north of 84°N below a sea ice cover of multiyear (MYI) and first year ice, which showed signs of surface and bottom melt (Boetius et al., 2013). During the expedition, seafloor deposits of sea-ice algal aggregates were observed at 3500–4400 m water depth, with the freshest deposits at the stations below multiyear ice cover (Boetius et al., 2013).

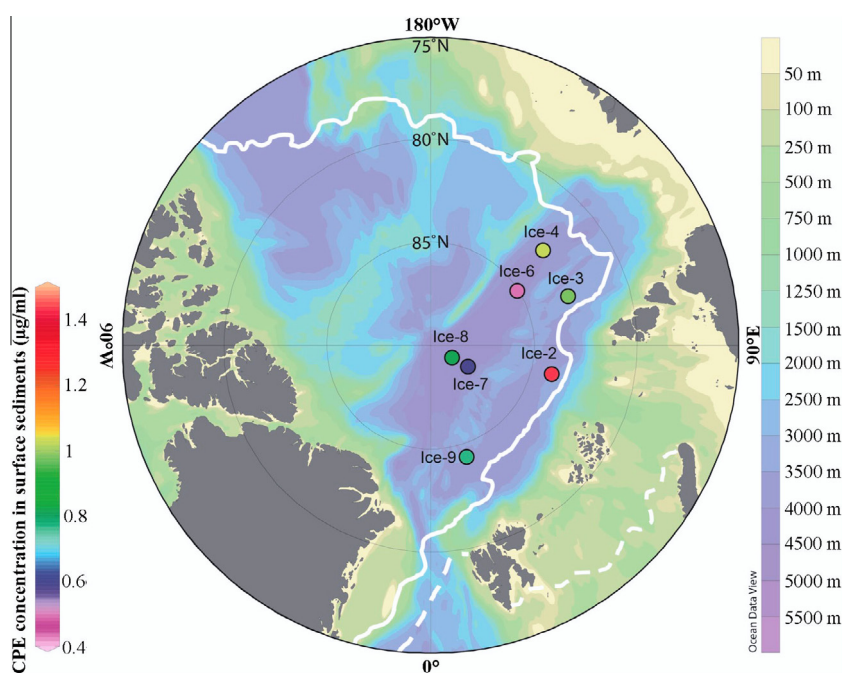


Fig. 1. Bathymetric map of the Arctic Ocean, indicating sampling stations in the Amundsen and Nansen basins. White line indicates monthly average of sea ice extent at the time of sampling in September 2012 (redrawn from www.meereisportal.de). White dashed line indicates maximum sea ice extent as monthly average in March 2012 (www.meereisportal.de), exceeding the map extract in the northern parts. Color of the dots indicates concentration of chlorophyll a equivalent (CPE) in surface sediments (0–1 cm in $\mu\text{g/ml}$ sediment), as indicated on the color bar to the left. (For interpretation of the references to color in this figure legend, the reader is referred to the web version of this article.)

Table 1
General information on samples. Stations 2, 3 and 4 are close to the ice edge and continental margin covered by FYI, while 6, 7, 8 and 9 are in the deep basins associated with strongly melted MYI (values separated by semicolon represent replicates).

Station, water depth (sampling date)	Lat., long.	Sea ice cover (%)	Ice thickness (m)	Depth (cm)	Sample #	DOC ($\mu\text{mol/l}$)	TDN ($\mu\text{mol/l}$)	DOC flux ($\text{mmol/m}^2/\text{yr}$) ^a	Chl <i>a</i> ($\mu\text{g/ml}$) ^b	Chl% ^b	Phaeopig. ($\mu\text{g/ml}$) ^b	CPE ($\mu\text{g/ml}$) ^b
Ice-2, 3446 m (15-08-12)	83°57.03'N, 76°48.31'E	80	1.2–2.0 ^c	0–1	1;2	197;172	26;23	134	0.24	17	1.19	1.43
				1–5	3;4	111;94	20;20		0.04	6	0.70	0.75
				5–10	5;6	108;90	18;23		0.02	6	0.35	0.37
				Bw. ^d	7;8	77;73	19;20					
Ice-3, 3591 m (21-08-12)	82°54.01'N, 109°48.78'E	70	0.7–1.2 ^c	0–1	9;10	346;242	32;30	265	0.21	22	0.76	0.97
				1–5	11;12	105;67	21;18		0.04	13	0.24	0.28
				5–10	13;14	74;78	19;21		0.02	12	0.13	0.14
				Bw. ^d	15;16	73;89	18;17					
Ice-4, 4166 m (25-08-12)	82°53.49'N, 129°57.54'E	80	0.7–0.9 ^c	0–1	17;18	199;114	48;25	68	0.22	22	0.80	1.02
				1–5	19;20	147;93	23;25		0.03	9	0.31	0.34
				5–10	21;22	49;51	20;18		0.01	9	0.14	0.15
				Bw. ^d	23;24	80;124	19;22					
Ice-6, 4354 m (08-09-12)	85°05.154'N, 122°29.43'E	50	0.9–1.7 ^c	0–1	29;30	81;102	19;19	19	0.07	14	0.42	0.49
				1–5	31;32	46;50	15;18		0.02	11	0.16	0.18
				5–10	33;34	39;72	15;16		0.01	6	0.10	0.11
				Bw. ^d	35;36; 37;38	75; ^e 71;75	17; ^e 17;18					
Ice-7, 4383 m (19-09-12)	87°55.92'N, 61°2.572'E	100	1.2–1.8 ^c	0–1	39;40	^e ;124	^e ;24	18	0.08	14	0.50	0.58
				1–5	41;42	82;53	22;16		0.02	7	0.19	0.21
				5–10	43;44	103;83	18;20		0.005	2	0.19	0.20
				Bw. ^d	45;46	97;123	20;44					
Ice-8, 4373 m (23-09-12)	88°49.22'N, 58°13.59'E	100	1.1–1.8 ^c	0–1	47;48	139;172	23;25	95	0.12	14	0.69	0.81
				1–5	49;50	85;81	19;19		0.02	8	0.21	0.23
				5–10	51;52	81;81	17;28		0.01	5	0.12	0.13
				Bw. ^d	53;54	73;84	17;47					
Ice-9, 4024 m (30-09-12)	84°20.739'N, 17°48.18'E	95	1.09 ^f	0–1	55;56	172;148	26;25	–44.39	0.05	7	0.71	0.76
				1–5	57;58	110;120	21;26		0.02	2	0.67	0.68
				5–10	59;60	106;122	21;24		0.01	1	0.71	0.71
				Bw. ^d	61;62	214;177	33;27					

^a Bottom water underlying sediment cores used for DOC efflux calculations.

^b Pigment analysis performed on cores from multicorer hauls different from the one used for pore water extraction but from the same station.

^c Sea ice cover and ice thickness from Boetius et al. (2013).

^d Bw, bottom water.

^e x, sample contaminated but did not affect the signal in the extract.

^f Data for sea ice observations available from the earth system database PANGAEA (Hendricks et al., 2012).

After retrieval of the multicorer and the transfer of cores to a 0 °C cold room, overlying bottom water was carefully collected from undisturbed cores. Sediment pore water was collected into 50 ml Sarstedt vials through rhizons (pore size 0.15 µm CSS, Rhizosphere Research Products,) using syringes without rubber on the piston at 0–1, 1–5 and 5–10 cm sediment depth. Up to 4 parallel cores were sampled at each station in order to obtain volumes of at least 50 ml per sediment depth (Table 1). Two pseudo replicates, prepared with the same pore water mixture collected from the cores at each depth, were analyzed separately in order to evaluate sampling variability and potential contamination during sample handling. All material had been rinsed with Milli-Q water and Milli-Q blanks were also prepared. Prior to analysis, all samples were stored at –20 °C. Data were submitted to the earth system database PANGAEA (Rossel et al., 2015a).

2.2. Pigment analysis

Samples for chlorophyll (chl) pigments, measured as a proxy for phytodetritus input to the seafloor, were retrieved from replicate multicorer cores from the same stations and were extracted from 1 ml sediment with 8 ml Me₂CO (90%). Glass beads were added and samples ground in a cell mill (Boetius and Damm, 1998). After centrifugation, the concentrations of chl *a* and phaeopigments in the supernatant (after addition of 250 µl HCl) were determined using fluorometric measurement with a Turner Trilogy fluorometer. The sum of chl *a* and phaeopigments is expressed as chloroplast pigment equivalent (CPE; Thiel, 1982). The ratio of chl *a* to CPE is expressed as a proportion (%) and provides an indication of the freshness of phytodetrital material.

2.3. DOM extraction, and dissolved OC (DOC) and total dissolved nitrogen (TDN) concentrations

Pore water samples were acidified with HCl (25% Carl Roth, Germany) to pH 2 and the OM was extracted with 100 mg styrene divinyl benzene polymer columns (Varian PPL) previously rinsed with MeOH (HPLC grade; Sigma–Aldrich, USA). The columns were then rinsed several times with ultrapure water at pH 2 to remove the salt from the cartridges, a procedure which is a prerequisite for MS analysis (Dittmar et al., 2008). Before DOM elution, the columns were dried under a stream of ultrapure N₂ and the solid phase-extracted (SPE)-DOM was eluted with 1 ml MeOH. SPE-DOM samples were stored at –20 °C until MS analysis. Additionally, 1 ml aliquots of each acidified pore water sample were used for analysis of DOC and TDN performed by hand injection via catalytic oxidation at high temperature with a TOC-VCPH Shimadzu instrument (Stubbins and Dittmar, 2012). To evaluate the accuracy of the pore water analysis, deep sea water material from the Consensus Reference Material Project (CRM; http://yyy.rsmas.miami.edu/groups/biogeochem/Table_1.htm) was also analyzed and was better than 5%.

2.4. DOC efflux from pore water gradients

DOC efflux from the sediment (J_{diff}) was calculated on the basis of Fick's first law of diffusion according to: $J_{\text{diff}} = D_{\text{sw}} \times dC/dz$, where J_{diff} = diffusive flux (mmol/m²/d), D_{sw} = diffusion coefficient in seawater (m²/s) corrected for temperature (Iversen and Jorgensen, 1993) and dC/dz = concentration gradient between the bottom water and a diffusive boundary layer of 1 mm according to in situ O₂ consumption profiles (Felden and Wenzhöfer, personal communication). For this, DOC concentration was obtained from overlying bottom water collected above the cores (Table 1). The relationship between diffusion coefficient and MW proposed by Burdige et al. (1992) was used to replace D_{sw} with D° in the J_{diff}

equation above according to: $\log D^\circ = 1.72 - 0.39 \times \log MW_{\text{wa}}$, where w_a is the intensity-weighted average obtained from the FT-ICR-MS analysis of the SPE-DOM from each sample. It is necessary to keep in mind that the MW_{wa} used is only indicative of those compounds amenable to electrospray ionization (Section 2.5). In order to constrain the time (t) for an avg. DOM molecule observed in our analytical window to diffuse into the sediment, we used the equation $t = L^2/2D$ (Jorgensen, 2006), where L is the distance (cm) and D is the diffusion coefficient (avg. from all stations) calculated after correction for porosity (θ) according to $D = D^\circ/1 - \ln(\theta^2)$. Although this is a rough estimation, it provides an avg. diffusion time for the length of the sediment column (sediment depth) at which the signal from recent phytodetritus deposits is observed.

2.5. Molecular analysis of DOM via FT-ICR-MS

DOM molecular analysis was performed with a Solarix FT-ICR-MS instrument equipped with a 15 T superconducting magnet (Bruker Daltonic). SPE-DOM aliquots were analyzed with an electrospray ionization source (Bruker Apollo II) in negative ion mode after dilution in 1:1 MeOH: ultrapure water to a final DOC concentration of 15–20 mg C/l, assuming extraction efficiency around 50% (due to limited volumes, SPE extracts were not analyzed for DOC concentration; Schmidt et al., 2009). Samples were infused at 120 µl/h using an ion accumulation of 0.4 s and a capillary voltage of 4 kV. Sample spectra were obtained after 600 individual scans. External and internal calibration were performed based on the arginine cluster and based on a list of >50 mass peaks of known formulae in the samples, respectively. Formula calculation for all samples was performed using an in-house Matlab (2010) routine that searches, with an error of <0.5 ppm, for all potential combinations of C, H, O, N, S and P. Calculation of formulae was performed for peaks with a signal to noise ratio (S/N) ≥ 4. Peaks in the Milli-Q water blanks were only retained in the data set if S/N was <20. The remaining peaks (9693) were used for formula calculation, including the elements C_∞, O_∞, H_∞, N ≤ 4; S ≤ 2 and P ≤ 1. In order to remove double assignments of formulae to the same mass, CH₂ homologous series extended to lower mass range were considered correct and the combination of the elements NSP, N₂S, N₃S, N₄S, N₂P, N₃P, N₄P, NS₂, N₂S₂, N₃S₂, N₄S₂, S₂P was not allowed. With this procedure, 5951 formulae were obtained for the whole data set, not considering isotopologues. Structural information was obtained from the aromaticity index (Almod; Koch and Dittmar, 2006, after correction by Koch and Dittmar, 2016) and the double bond equivalent (DBE, McLafferty and Turecek, 1994). Avg. values for DBE and Almod, as well as H/C and O/C elemental ratios were also calculated considering the intensity of the formulae peak in each sample (H/C_{wa}, O/C_{wa}, DBE_{wa} and Almod_{wa}).

In order to provide an overview of the formulae distribution and the potential compound groups present in pore water, molecular formulae were additionally associated with different molecular categories (Table 2). We used this approach because ≤6% of the DOM has so far been identified to the molecular level (Hedges et al., 2000; Dittmar and Stubbins, 2014). Furthermore, known molecular groups such as peptides, lignin phenols and tannins have specific element compositions, and can therefore be located in specific regions of the Van Krevelen diagram (VKD; e.g. Kim et al., 2003). Elemental ratios, heteroatom composition (N, S and P) and Almod were used to define these molecular categories. It is important to note that the classification of formulae within these categories does not necessarily indicate the presence of a specific structure or functional group; it only indicates that the formula is identical with a known molecule, although the structure may be different (e.g. Seidel et al., 2014). Furthermore, peptides in a strict sense should contain at least two Ns (dipeptides) but for simplification the category of peptide formulae also includes those

Table 2
Molecular categories evaluated (location of categories presented in a Van Krevelen diagram in Fig. 2).

	Saturated fatty acids formulae (Sat. fatty acids)	Saturated fatty acids with heteroatoms (Sat. fatty acids-CHOx)	Sugar formulae	Unsatur. aliphatic formulae		Peptide formulae	Highly unsatur. formulae		Polyphenol formulae (poly)		Dissolved black carbon formulae (BC)	
				O-rich	O-poor		O-rich	O-poor	O-rich	O-poor	<15C	≥ 15C
Almod	-	-	-	-	-	-	<0.5	<0.5	0.5 < x < 0.67	0.5 < x < 0.67	<15C	≥ 15C
H/C	>2	>2	-	1.5 < x < 2.0	1.5 < x < 2.0	1.5 < x < 2.0	<1.5	<1.5	0.5 < x < 0.67	0.5 < x < 0.67	≥ 0.67	≥ 0.67
O/C	<0.9	<0.9	>0.9	0.5 < x < 0.9	<0.5	<0.9	>0.5	<0.5	>0.5	>0.5	-	-
C atoms	-	-	-	-	-	-	-	-	-	-	<15	≥ 15
Heteroatoms (N, S, P)	0	Yes	-	-	-	N > 0	-	-	-	-	-	Yes

with one N but which are within the range of the H/C and O/C ratio of peptide groups (Kim et al., 2003; Table 2).

2.6. Statistical analysis

A conservative approach was used, where the minimum number of formulae detected in the whole data set was used as a top limit for each pore water sample, so only the 2316 most intense formulae for each sample were kept for further data normalization. For the normalization we defined a standardized detection limit according to published rules (Stubbins et al., 2014; Rossel et al., 2015b). After normalization and standardization of peak intensity, data were reduced from 5951 to 3707 formulae, the latter used for multivariate statistical analysis. Partial least square analysis (PLS; Unscrambler X v10.2 from Camo Software) considered the environmental data and the formulae along with their relative abundances in each sample, thereby allowing identification of formulae that were more strongly related to the environmental factors evaluated. In order to remove variability caused by different units, all environmental data were divided by their standard deviation prior to PLS analysis. PLS is especially suited for the analysis of FT-ICR-MS data, because the number of factors (several thousand formulae) can be much larger than the number of observations (samples; e.g. Tobias, 1995). It allows inclusion of environmental factors that may covary (e.g. Liu, 2011). The result of the PLS analysis is represented by scores and loadings, the latter for both the environmental (X loadings) and molecular data (Y loadings), so it provides a representation of a linear model relationship for samples (scores) and variables (loadings). Furthermore, molecular categories and calculated intensity-weighted ratios and indexes were also passively shown in the PLS model, so they do not influence it but their location in the model provides a better visualization of their correlation with other variables.

In order to visualize the formulae in Arctic pore water DOM samples that are better explained by the environmental factors variability, VKD with H/C ratio and O/C ratio using the PLS molecular loadings (Y loadings) in the z axis are presented. The formulae that contributed mainly to the positive and negative loadings of the most significant factors in the PLS analysis are discussed on the basis of significance levels. These are defined by values above or below a specific threshold for both loadings and H/C elemental ratio, the latter with values > 1.5 displaying molecular groups associated with fresh OM (e.g. peptides) and < 1.5 products of condensation reactions (e.g. Kim et al., 2003). For example, factor 1 > 0.25 or < -0.25 for positive (warm colors) or negative (cold colors) loadings and H/C > 1.5 or < 1.5 provides four possible combinations (loading > 0.25 with either H/C > 1.5 or H/C < 1.5 and loading < -0.25 with either H/C > 1.5 or H/C < 1.5). However, only significance levels are discussed if the combination displays a molecular category such as in Fig. 2 (see definition of molecular categories, Table 2).

3. Results and discussion

3.1. Pigment, pore water DOC and TDN concentrations

Chl *a* values were highest in surface sediments for all stations and higher at the ice margin stations (avg. at 0–1 cm $0.23 \pm 0.02 \mu\text{g/ml}$) than at the multiyear ice stations (avg. at 0–1 cm $0.08 \pm 0.03 \mu\text{g/ml}$). This difference in phytodetritus pigment accumulation between stations was also observed at deeper sediment depth (1–5 and 5–10 cm; Table 1). Similarly, phaeopigment concentration at the surface sediment was also higher at the ice margin (avg. $0.92 \pm 0.24 \mu\text{g/ml}$) than at multiyear ice stations (avg. $0.58 \pm 0.14 \mu\text{g/ml}$). Also, the proportion of chl *a* in surface

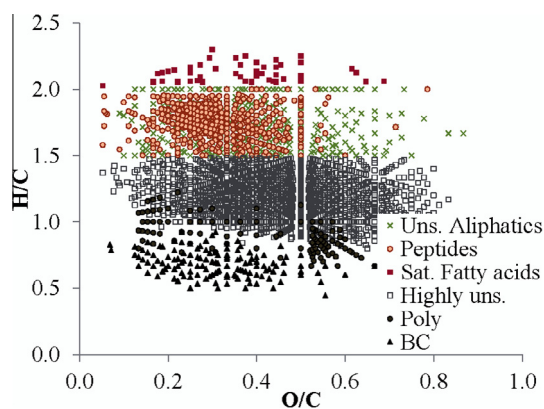


Fig. 2. VKD of H/C and O/C with different molecular categories. Formulae associated with the different molecular categories present in the whole data set. For definition of black carbon, polyphenols, highly unsaturated, unsaturated aliphatics, saturated fatty acids, sugars and peptides see the details in material and methods and Table 2.

sediments to chloroplast pigment equivalent CPE was higher at the ice margin (avg. $20.1 \pm 2.7\%$) than at the multiyear ice stations (avg. $12.1 \pm 3.7\%$). However, the variation indicating the deposition of freshly sedimented phytodetritus (e.g. within the same year) was not observed at deeper sediment depths. The observed ratios were higher than for previous measurements at similar water depth (Boetius and Damm, 1998). These variations indicate differences in both the quantity and quality of phytodetritus sedimentation, showing a higher recent productivity in the ice margin area. A similar decrease in chl *a* and CPE with increasing distance from the ice edge has been reported for sediments from the Fram Strait (Schewe and Soltwedel, 2003). According to pigment distribution with sediment depth, at the ice margin stations CPE decreased

from $1.14 \pm 0.25 \mu\text{g/ml}$ to 0.46 and $0.22 \mu\text{g/ml}$ at 1–5 cm and 5–10 cm, respectively, while at the multiyear ice stations a decrease from $0.66 \pm 0.15 \mu\text{g/ml}$ to 0.33 and $0.29 \mu\text{g/ml}$ was observed. Thus in both areas, CPE decreased one fold within the first 5 cm, to remain constant at multiyear ice stations, while at the ice margin it decreased two fold of surface values at 10 cm sediment depth. This trend is in agreement with the idea that OM in the sediment reaches an asymptotic value ca. 20% of surface OM concentration, which represents mainly refractory material (Emerson and Hedges, 1988). The strong decrease in CPE over the upper 5 cm suggests that bioturbation is restricted to the uppermost sediment horizons and is generally low, as reported for the bottom of the Laptev Sea slope (Boetius and Damm, 1998), and is in line with the low macrofauna density in the area (Degen et al., 2015).

DOC concentration in pore water also displayed a general decrease from surface to deeper sediment depth (Fig. S1a). Differences in DOC concentration among stations (Fig. S1a, Table 1) were observed only for surface sediment pore water, where it was higher at the ice margin (avg. $212 \pm 78 \mu\text{mol/l}$) than at the multiyear ice stations (avg. $134 \pm 34 \mu\text{mol/l}$). Previous DOC concentration values reported by Hulth et al. (1996) for surface sediment pore water from depths between 2000 and 2600 m for an area in Fram Strait close to Svalbard, varied between 1770 and $6470 \mu\text{mol/l}$, an order of magnitude higher than the values here. Although these depths are much shallower than for our sampling sites, this observation is in agreement with the substantially lower productivity in the central Arctic ($<80 \text{ mmol C/m}^2/\text{yr}$) than in shelf areas ($>2500 \text{ mmol C/m}^2/\text{yr}$; e.g. Gosselin et al., 1997; Romankevich and Vetrov, 2001; Anderson et al., 2003; Sakshaug, 2004; Wassmann et al., 2010).

Like DOC, TDN concentration in surface sediment pore water was higher at the ice margin (avg. $31 \pm 9 \mu\text{mol/l}$) than at the multiyear ice stations (avg. $23 \pm 3 \mu\text{mol/l}$; Fig. S1b, Table 1), in

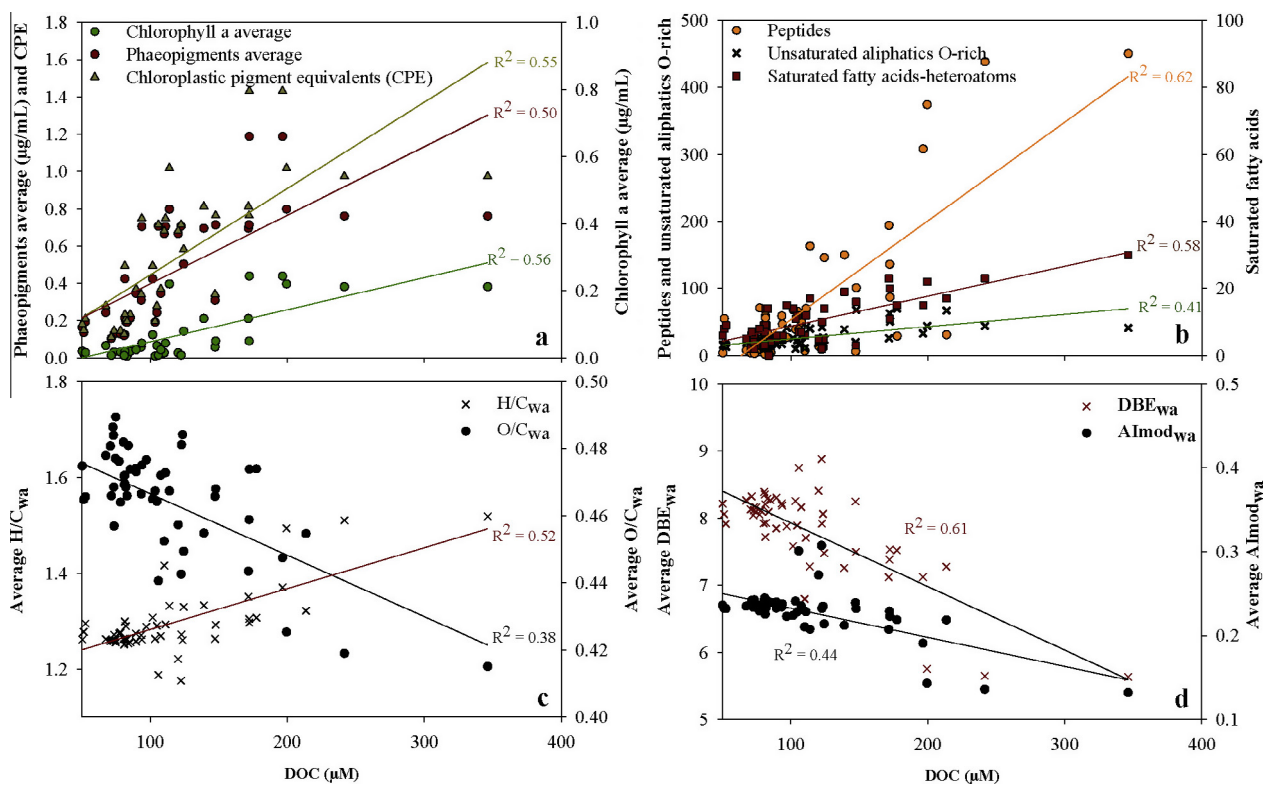


Fig. 3. DOC in relation to molecular groups and indexes evaluated in pore water samples. Significant correlations ($P < 0.0001$) based on model II regressions between (a) DOC and pigments (Chl *a*, phaeopigments and CPE), (b) DOC and number of formulae in the molecular categories of peptides, unsaturated aliphatic-O-rich, sat. fatty acids-CHOx (c) DOC and H/C_{wa} and O/C_{wa} and (d) DOC and DBE_{wa} and Almod_{wa} are indicated by their color coded correlation line and adjusted R^2 .

agreement with suggestions for the Svalbard area (Hulth et al., 1996). Hulth et al. (1996) found higher TDN concentration in pore water at the west than in the east of Svalbard and suggested that this was probably due to changes in production/import of particulate material and ice cover (Rachor, 1992). We suggest here that the trend also holds for much lower productivity regimes.

Porewater DOC concentration showed a significant positive linear correlation with chl pigments extracted from sediments, and the number of formulae in the compound groups related to fresh OM (Fig. 3a–c; Schmidt et al., 2011; Seidel et al., 2014) and negative correlations with common indicators of DOM decomposition (Fig. 3c and d; Seidel et al., 2014). Like DOC, TDN displayed significant correlation with most of these molecular indicators, except for phaeopigments, sat. fatty acids-CHOx, H/C_{wa} and Almod_{wa} (data not shown). Although FT-ICR-MS coupled to electrospray ionization is not a quantitative method due to differences in ionization efficiency for different compounds, variability in replicate analysis has been shown to be small and signal intensity has been linearly related to concentration (Soule et al., 2010; Seidel et al., 2015). Thus, the use of peak intensity (subscript in our calculations) provides semiquantitative information for a comparison of samples analyzed under the same instrumental conditions.

3.2. Bottom water DOM and DOC efflux

The melting event and subsequent sea ice minimum observed in 2012, when the samples for this study were collected, caused a large sedimentation of sea ice algae to the seafloor at all stations, with freshest deposits at the multiyear ice stations, but with a very patchy distribution of sea ice algae at the seafloor (Boetius et al., 2013). The sediment samples retrieved for pore water analysis here were not covered with algal aggregates, so the DOM molecular composition reflects more the decadal depositional environment of the central Arctic basins with low marine OM input (Lalande et al., 2014).

DOC concentration in bottom water siphoned off from above the cores was generally two- to threefold lower than in surface sediment pore water at the ice margin stations, while at the multiyear ice stations values were close to surface sediment concentration (except for station 8 that was twofold lower). DOC concentration in bottom water ranged from 71 to 214 $\mu\text{mol/l}$, with a maximum at station 9 (Table 1). These values are higher than reported values from the North Atlantic deep ocean (48 $\mu\text{mol/l}$, at ca. 400 m above ground; Hansell and Carlson, 1998) and the Amundsen and Nansen Basin (54 $\mu\text{mol/l}$ and 50 $\mu\text{mol/l}$, respectively at ca. 3000 m above ground) collected during a conductivity-temperature-depth (CTD) cast (Bussmann and Kattner, 2000). Such a gradient between the bottom water – sediment interface and the deep water reflects the diffusive boundary layer above the seafloor (Glud, 2008).

TDN in overlying bottom water varied from 17 to 47 $\mu\text{mol/l}$, with higher, although variable concentration at the multiyear ice stations (avg. $27 \pm 12 \mu\text{mol/l}$) compared with ice margin stations (avg. $19 \pm 2 \mu\text{mol/l}$; Table 1).

In bottom water DOM, a higher abundance of highly unsaturated formulae and lower contribution from those indicative of fresh OM (peptide, unsaturated aliphatics-O-rich and saturated fatty acids-CHOx) were observed, compared with surface sediment pore water samples. The difference was less pronounced at the multiyear ice stations than at the ice margin. Additionally, in bottom water the intensity-weighted averages of Almod_{wa} and DBE_{wa} were higher than at the surface sediment, except at station 9 where the values generally increased from bottom water to deeper sediment depth. These differences in composition and the overall increase in the number of *m/z* peaks from bottom water to surface sediment (Table S1) may result from higher hydrolytic activity in

response to fresh OM in surface sediments. Highly unsaturated compounds and aromatics from degradation of fresh OM appear to be released to the overlying bottom water.

The average DOC flux between seafloor and overlying water calculated from the DOC gradient at the different stations varied from 44 to 265 $\text{mmol/m}^2/\text{yr}$, with higher average values of 155 for the ice margin (range 68–265 $\text{mmol/m}^2/\text{yr}$) than at the multiyear ice stations with 22 (range 44 to 95 $\text{mmol/m}^2/\text{yr}$, Table 1). Negative values indicate an influx of DOC from bottom water into the surface sediment. The calculated DOC flux values represent a rough estimate and were at the lower end of values reported from the eastern Eurasian Basin and adjacent shelves (0–1314 $\text{mmol/m}^2/\text{yr}$; Hulth et al., 1997) and within the range for other deep-sea sediments (37 to 259 $\text{mmol/m}^2/\text{yr}$ and 66 $\text{mmol/m}^2/\text{yr}$ for Weddell Sea and Atlantic, respectively; Hulth et al., 1997; Hall et al., 2007). The calculated DOC efflux (positive values) are equivalent to ca. 0.2–0.9% of the POC export measured for near surface water layers (160–3300 $\text{mmol C/m}^2/\text{yr}$ for the multiyear and ice margin stations, respectively; Lalande et al., 2014), similar to proportions reported in previous investigations of deep-sea sediments (e.g. DOC efflux from sediments at >2000 m represented 0.25% of the POC export; Dunne et al., 2007). In comparison, respiration rate measured at the seafloor of the deep basins covered by 100% sea ice was 0.3–0.4 $\text{mmol O}_2/\text{m}^2/\text{day}$ (equivalent to ca. 100–150 $\text{mmol C/m}^2/\text{yr}$; Boetius et al., 2013). With a DOC efflux similar to or lower than the C respiration by benthic life, deposition of ca. 8–22% of surface POC could sustain seafloor communities, which is a reasonable assumption. Accordingly, the low DOC efflux here is consistent with the low POC export for the region (Lalande et al., 2014).

3.3. Molecular fingerprint of pore water DOM and its relationship with the environment

In the Arctic, at both the ice margin and at the multiyear ice stations, highly unsaturated formulae contributed $79 \pm 11\%$ and $83 \pm 7\%$, polyphenols $1.9 \pm 1.3\%$ and $3.6 \pm 4.4\%$ and dissolved BC $0.2 \pm 0.2\%$ and $0.6 \pm 1.2\%$ of the formulae. For comparison, in pore water from a tidal flat area, highly unsaturated formulae, polyphenols and dissolved BC contributed 58–75%, 12–17% and 2–10% of the formulae, respectively (Seidel et al., 2014). Thus, the highly unsaturated formulae contributed more to the Arctic pore water at both stations than to pore water in coastal areas. Because highly unsaturated formulae are represented mainly by carboxyl-rich alicyclic molecules (CRAM in the Arctic represents ca. 79% of the highly unsaturated formulae), known to be a major fraction of refractory DOM (Hertkorn et al., 2006), thereby indicating active degradation of OM in sediments of the central Arctic basins.

Regarding molecular indicators of fresh OM input to the sediments, contributions of <10% of peptide formulae to total N-containing compounds (Seidel et al., 2014) have been reported. In the Arctic Ocean, surface sediments (0–1 cm) have a greater contribution of peptides to the total N-containing compounds, with up to $39.9 \pm 18.7\%$ in the ice margin stations and $17.3 \pm 6.2\%$ at the multiyear ice stations. These contributions decrease to $7.1 \pm 3.6\%$ at the ice margin stations and $3.0 \pm 2.6\%$ at the multiyear ice stations at 5–10 cm sediment depth, thereby approaching the values reported by Seidel et al. (2014). The small contribution of peptides in previous work is also indicated by a low representation of this molecular category in the VKD (i.e. no clear pattern in the high H/C area of the diagram; Seidel et al., 2014). This may indicate that, although this compound group is associated with fresh input of OM, part of it may be better preserved in the detrital material of surface sediments of the Arctic Ocean than in other settings. The higher contribution of peptide formulae, especially at the ice margin stations compared with coastal areas does not appear to be

related to the sampling resolution (0–10 cm in Seidel et al., 2014 vs. 0–1 cm here). Combining the signal from 0–10 cm indicates that ice margin stations could still contribute >10% of peptide formulae to total N-compounds. Furthermore, the diffusion rate is very low in the clay-rich (Stein et al., 1994; Janssen et al., 2005) Arctic Ocean sediments, which could promote preservation of this compound group, in agreement with our results. Regardless of the processes leading to the greater presence of N-containing compounds in the region, their contribution, especially associated with peptide formulae, seems to be a characteristic molecular feature of Arctic pore water DOM compared with coastal areas (Schmidt et al., 2009; Seidel et al., 2014), coastal anoxic sediments (Jessen, 2015) and deep sea anoxic sediments (Schmidt et al., 2014). Together with the decrease in peptide formulae, carbohydrates were almost absent from the Arctic Ocean pore water, in agree-

ment with previous studies and with the expected rapid turnover of these compounds (Robador et al., 2010; Seidel et al., 2014).

In order to better understand the role of the environment for pore water DOM composition of the Arctic Ocean sediments, partial least square (PLS) analysis was performed with all pore water samples (Table 1). Based on the PLS, DOM molecular data variability in relation to the environment was explained mainly by two factors (Fig. 4). Factor 1 explained 51% of the environmental (X loadings) and 21% of the molecular data (Y loadings) variability, while factor 2 explained 12% and 21%, respectively. Pseudo replicates were displayed closely together, indicating no significant variability during sample handling (Figs. 5 and S2).

Factor 1 scaled with the phytodetritus proxies (% chl *a*, chl *a*, phaeopigments, CPE) correlated with DOC and TDN and correlated negatively with sediment and water depth (Fig. 4a and b),

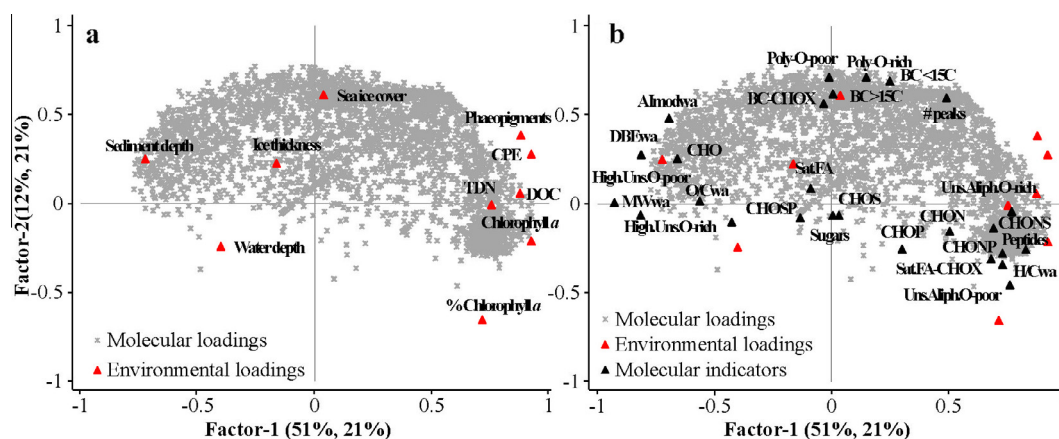


Fig. 4. PLS loadings for pore water samples with factor 1 explaining 51% and 21% of the environmental and molecular variability, respectively and factor 2 explaining 12% and 21%. (a) Correlation of environmental and molecular loadings (X and Y loadings) and (b) passively displaying the evaluated molecular categories, ratios and indexes (molecular indicators).

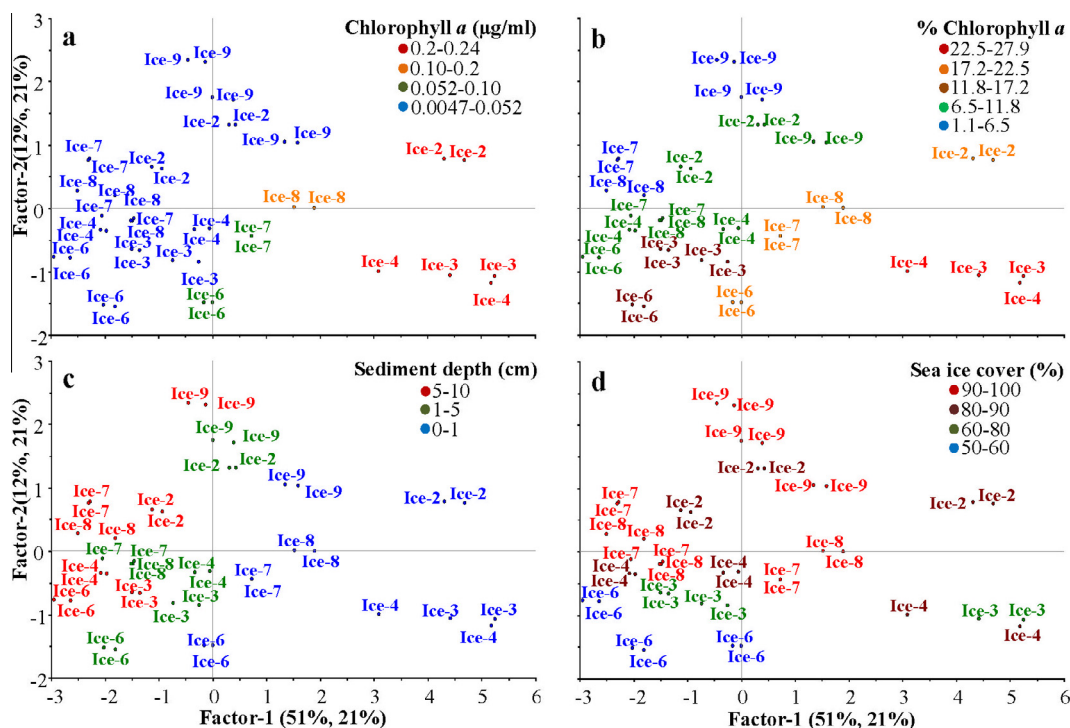


Fig. 5. PLS score plots for pore water samples. (a) Chl *a*, (b) % chl *a*, as examples of pigment data, (c) sediment depth and (d) ice cover. Samples in the score plots are indicated by the name of the station (Ice-#). A maximum of five color groups were allowed for each variable (except for sediment depth); if fewer groups are displayed this indicates that further separation based on the data was not possible.

distinguishing the ice margin from other stations. Molecular loadings used in the VKD of factor 1 (Fig. 6a and b, Table S3) indicate that phyto detritus input proxies, DOC and TDN (positive loadings from Fig. 4b) were associated mainly with N-containing compounds and the molecular categories of peptides, unsaturated aliphatics-O-poor, -O-rich, and sat. fatty acids-CHOx formulae (all with high H/C ratio, Fig. 6b). This is in agreement with the correlation of these categories with DOC prior to PLS analysis (Fig. 3a–c). The relationship of DOC, TDN and pigments with higher abundance of formulae of peptides, unsaturated aliphatics and sat. fatty acids-CHOx, is consistent with the association of these formulae with decomposition of algal material and microbes in pore water (Schmidt et al., 2011; Seidel et al., 2014) and the relationship of pigment and protein concentration in the Arctic continental slope (this study and Boetius and Damm, 1998). Therefore, these molecular categories are likely products of microbial degradation of sea ice algae and other sinking POM in the central Arctic.

Negative loadings of factor 1 (sediment and water depth in Fig. 4b) were associated with highly unsaturated O-poor and O-rich formulae (blue area in Fig. 6b, Table S3), in agreement with a generally lower contribution of these categories to surface sediments, and at the ice margin (Table S2). These compounds were also characterized by high $Almod_{wa}$, DBE_{wa} , MW_{wa} and O/C_{wa} . The increase in aromatic compounds (characterized by high $Almod$ and DBE) at the multiyear ice stations and at deeper sediment depth (Figs. 4–6) is consistent with their association with OM

decomposition (Seidel et al., 2014). Furthermore, these compounds, which commonly occur in river and coastal areas (e.g. Stenson et al., 2003; Tremblay et al., 2007) may reach the deep Arctic Ocean as POM transported with sea ice via the Transpolar Drift (Rudels et al., 1996). Particulate matter is trapped during sea ice formation on the Siberian shelves and transported across the Arctic through Fram Strait, providing an additional contribution of OM to the seafloor (Stein et al., 1994; Wassmann et al., 2004; Krumpen et al., 2011). Eventually, this matter sinks out from melting ice, sediments onto the seafloor and gets dissolved via benthic degradation, contributing to the DOM pool. Based on experimental incubation of DOC from the Yenisei river with its natural bacterial community, the refractory nature of this material has been confirmed, with a DOC loss of <4% after several years (Köhler et al., 2003). Hence, signals of the decomposition of POM derived from riverine input may accumulate in the pore water very slowly, with preservation on a much longer timescale than that of fresh marine OM. Although marine OM degradation can also produce aromatic compounds, a higher relative abundance of polyphenols has been shown to be a clear indicator of terrigenous OM (Seidel et al., 2015). Thus, the aromatic signal, represented mainly by polyphenols, in the Arctic pore water, is likely dominated by allochthonous OM sources.

MW_{wa} and O/C_{wa} values also displayed a general increase from surface sediment to 5–10 cm, with the latter generally higher at the surface sediments of the multiyear ice stations (Tables S1

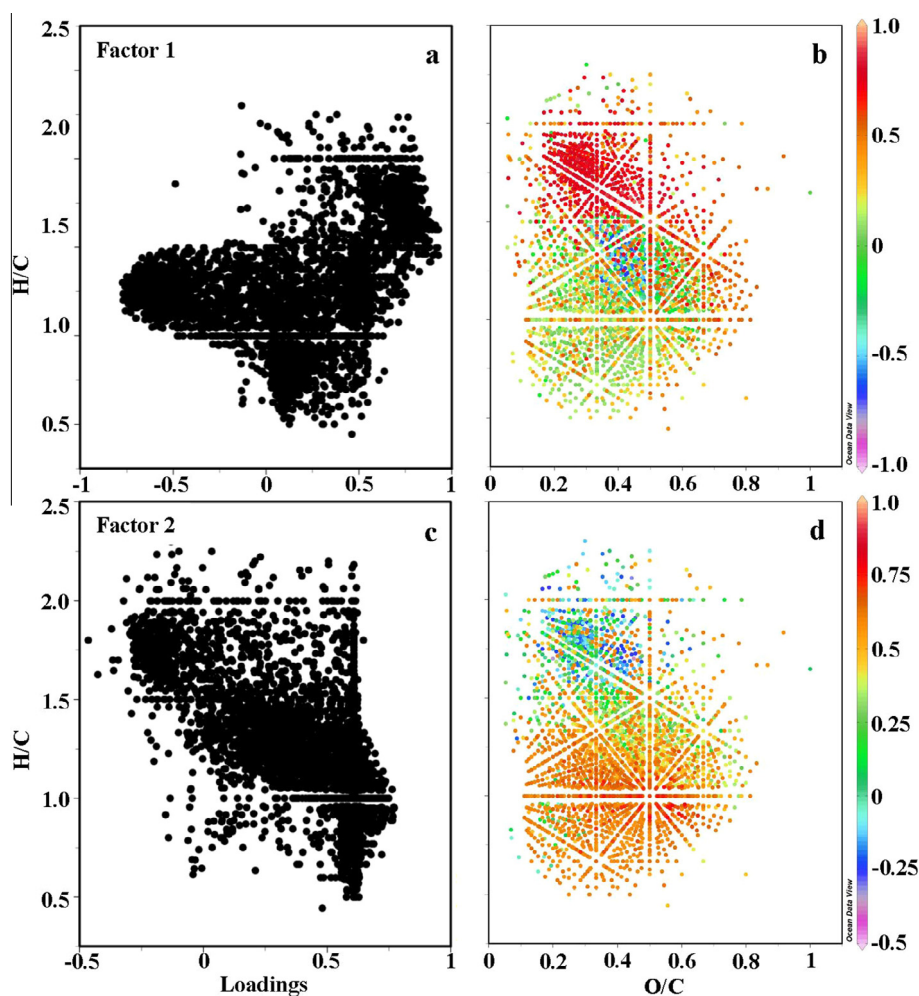


Fig. 6. VKD of H/C and O/C ratios using the PLS molecular loadings from Fig. 4. (a) H/C and factor 1 loadings, (b) VKD with factor 1 loadings on the z axis, (c) H/C and factor 2 loadings and (d) VKD with factor 2 loadings on the z axis. Positive and negative loadings of z axis indicated by warm and cold colors on the color bar to the right. (For interpretation of the references to color in this figure legend, the reader is referred to the web version of this article.)

and S2). This is contrary to the general decrease in MW and O/C related to decomposition of OM reported for pore water DOM (Seidel et al., 2014) and in other studies where DOM was exposed to degradation (Kim et al., 2006; Tremblay et al., 2007; Schmidt et al., 2009; Rossel et al., 2013, 2015b; Seidel et al., 2014; Jessen, 2015). The specific cause of the increase remains unclear, but may be related to the preferential preservation of terrigenous DOM, as it has been shown that river DOM has higher O/C and MW than marine pore water DOM (Schmidt et al., 2009). Nevertheless, the MW values from pore water were lower than those from bottom water and reported for Atlantic deep water DOM (Schmidt et al., 2009). In coastal sediments, MW values from pore water were also lower than for Atlantic deep water DOM (Table 3 of Schmidt et al., 2009) and displayed a decrease with increasing distance from the coast (Seidel et al., 2014).

The high contribution of terrigenous OM in the multiyear ice stations is also indicated by a higher O/C at these stations (0.46 ± 0.01) than at the ice margin (0.44 ± 0.03). However, these O/C values are lower than those reported for continental slope and shelf sediment pore water DOM (O/C_{wa} between 0.49 and 0.52; Schmidt et al., 2009), likely due to the distance of the stations from the coast.

Factor 2 was influenced mainly by the environmental variable ice cover (Fig. 4a and b), singling out multiyear ice station 9 (Fig. 5). Contrary to factor 2 negative loadings, positive loadings (same direction as ice cover) were highly populated with formulae (Fig. 4b) associated mainly with the categories highly unsaturated, poly-O-poor, black carbon (BC-CHOx, BC \geq 15C and BC < 15C) and poly-O-rich (Fig. 6c and red area of Fig. 6d; Tables S3 and S4). This is in agreement with the significant contribution of formulae associated with these categories at station 9 (Table S2). The high contribution of aromatics at station 9 may suggest deposition and diagenesis of ice rafted material via the transpolar drift, as discussed above (Table S2, Fig. 5d).

4. Conclusions

In the ice-covered Arctic Ocean, OM input to the deep seafloor at >3000 m water depth is influenced by both sedimentation of primary produced material and by terrigenous deposits, presumably with a substantial proportion originating from ice rafting and melting (Klages et al., 2004; Stein and Macdonald, 2004). This study shows for the first time that this is also reflected in the molecular composition of DOM, with regional differences in the deep Eurasian Arctic basins. The ice cover at the multiyear ice stations limits primary production and the subsequent export of OM to the sediment, resulting in a pore water signal dominated by terrigenous OM input (polyphenols and dissolved BC, indicated also by higher Almod_{wa} and DBE_{wa} values). However, recent indications of massive ice-algal falls from the melting Arctic sea ice may change this signature in the future. Accordingly, present day ice margin stations already show a stronger signature of phytodetrital matter, as indicated by higher amounts of peptides, unsaturated aliphatics-O-poor and -O-rich and sat. fatty acids-CHOx formulae, indicated also by higher H/C ratio values.

According to the DOM profiles, the signal of primary production transferred to the sediments via the biological pump is restricted to pore water from sediments shallower than 5 cm, representing the depth of mixing of recent phytodetritus supplied by bioturbation and an avg. DOC diffusion time of 0.17 yr. Deeper sediments do not reflect the signal of the surface, indicating a relatively fast turnover of the deposited material from the past season primary production. It remains to be further investigated if the observed accumulation of DOM in near-surface sediment horizons is already indicative of increasing primary productivity of the Arctic Ocean

due to the retreating sea-ice cover. Differences in the DOM molecular features between this and previous studies are attributed to environmental characteristics and factors that influence DOM distribution in pore water. Coastal areas have been shown to respond to gradients that varied with distance from the coast, while sediment depth had only a small influence on the variability (Seidel et al., 2014). In the Arctic Ocean, pore water organic chemistry reflects the low POM input from both marine and terrigenous matter, and both are influenced by ice cover variation and ice melting.

Acknowledgments

We thank M. Friebe, I. Ulber and K. Klapproth for support during sample analysis. We also acknowledge the captain and crew of the RV Polarstern expedition ARK27-3, R. Stiens and W. Stiens for sampling on board, and J. Felden for support during carbon flux calculations. Sea ice concentration data for the monthly averages in September and March 2012 were obtained from <http://www.meereisportal.de> (Grant: REKLIM-2013-04). This is a contribution to the European Research Council Advanced Investigator Grant 294757 to A.B. Two anonymous reviewers are acknowledged for constructive comments which improved the manuscript.

Appendix A. Supplementary data

Supplementary data associated with this article can be found, in the online version, at <http://dx.doi.org/10.1016/j.orggeochem.2016.04.003>.

Associate Editor—S. Wakeham

References

- Amon, R.M.W., Fitznar, H.-P., Benner, R., 2001. Linkages among the bioreactivity, chemical composition, and diagenetic state of marine dissolved organic matter. *Limnology and Oceanography* 46, 287–297.
- Anderson, L.G., Dryssen, D., 1990. An assessment of the transport of atmospheric CO₂ into the Arctic Ocean. *Journal of Geophysical Research* 95, 1703–1711.
- Anderson, L.G., Jones, E.P., Swift, J.H., 2003. Export production in the central Arctic Ocean evaluated from phosphate deficits. *Journal of Geophysical Research* 108. <http://dx.doi.org/10.1029/2001jc001057>.
- Arrigo, K.R., van Dijken, G., Pabi, S., 2008. Impact of a shrinking Arctic ice cover on marine primary production. *Geophysical Research Letters* 35, 1–6.
- Bienhold, C., Boetius, A., Ramette, A., 2012. The energy–diversity relationship of complex bacterial communities in Arctic deep-sea sediments. *ISME Journal* 6, 724–732.
- Boetius, A., Damm, E., 1998. Benthic oxygen uptake, hydrolytic potentials and microbial biomass at the Arctic continental slope. *Deep Sea Research Part I* 45, 239–275.
- Boetius, A., Albrecht, S., Bakker, K., Bienhold, C., Felden, J., Fernández-Méndez, M., Hendricks, S., Katlein, C., Lalonde, C., Krumpfen, T., Nicolaus, M., Peeken, I., Rabe, B., Rogacheva, A., Rybakova, E., Somavilla, R., Wenzhöfer, F., 2013. Export of algal biomass from the melting Arctic sea ice. *Science* 339. <http://dx.doi.org/10.1126/science.1231346>.
- Burdige, D.J., Komada, T., 2015. Sediment pore waters. In: Hansell, D.A., Carlson, C.A. (Eds.), *Biogeochemistry of Marine Dissolved Organic Matter*. Elsevier Inc. <http://dx.doi.org/10.1016/B978-0-12-405940-5.00012-1>.
- Burdige, D.J., Alperin, M.J., Homstead, J., Martens, C.S., 1992. The role of benthic fluxes of dissolved organic carbon in oceanic and sedimentary carbon cycling. *Geophysical Research Letters*. <http://dx.doi.org/10.1029/92GL02159>.
- Bussmann, I., Kattner, G., 2000. Distribution of dissolved organic carbon in the central Arctic Ocean: the influence of physical and biological properties. *Journal of Marine Systems* 27, 209–219.
- Degen, R., Vedenin, A., Gusky, M., Boetius, A., Brey, T., 2015. Patterns and trends of macrobenthic abundance, biomass and production in the deep Arctic Ocean. *Polar Research* 1, 1–18.
- Deming, J., Yager, P., 1992. Natural bacterial assemblages in deep-sea sediments: towards a global view. *Deep Food Chain Global Carbon Cycle*, 11–27.
- Dittmar, T., Stubbins, A., 2014. Dissolved organic matter in aquatic systems. In: Birrer, B., Falkowski, P., Freeman, K. (Eds.), *Treatise on Geochemistry*. Elsevier Ltd. <http://dx.doi.org/10.1016/B978-0-08-095975-7.01010-X>.
- Dittmar, T., Koch, B., Hertkorn, N., Kattner, G., 2008. A simple and efficient method for the solid-phase extraction of dissolved organic matter (SPE-DOM) from seawater. *Limnology and Oceanography Methods* 6, 230–235.

- Dunne, J.P., Sarmiento, J.L., Gnanadesikan, A., 2007. A synthesis of global particle export from the surface ocean and cycling through the ocean interior and on the seafloor. *Global Biogeochemical Cycles* 21, 1–16.
- Emerson, S., Hedges, J.L., 1988. Processes controlling the organic content of open ocean sediments. *Palaeogeography, Palaeoclimatology, Palaeoecology* 3, 621–634.
- Fernández-Méndez, M., Katlein, C., Rabe, B., Nicolaus, M., Peeken, I., Bakker, K., Flores, H., Boetius, A., 2015. Photosynthetic production in the central Arctic Ocean during the record sea-ice minimum in 2012. *Biogeosciences* 12, 3525–3549.
- Glud, R.N., 2008. Oxygen dynamics of marine sediments. *Marine Biological Research* 4, 243–289.
- Gosselin, M., Levasseur, M., Wheeler, P.A., Horner, R.A., Booth, B.C., 1997. New measurements of phytoplankton and ice algal production in the Arctic Ocean. *Deep Sea Research Part II* 44, 1623–1644.
- Hall, P.O.J., Brunnegård, J., Hulthe, G., Martin, W.R., Stahl, H., Tengberg, A., 2007. Dissolved organic matter in abyssal sediments: core recovery artifacts. *Limnology and Oceanography* 52, 19–31.
- Hansell, D.A., Carlson, C.A., 1998. Deep ocean gradients in the concentration of dissolved organic carbon. *Nature* 395, 263–266.
- Hedges, J.L., Eglinton, G., Hatcher, P.G., Kirchman, D.L., Arnosti, C., Derenne, S., Evershed, R.P., Kögel-Knabner, I., De Leeuw, J.W., Littke, R., Michaelis, W., Rullkötter, J., 2000. The molecularly-uncharacterized component of nonliving organic matter in natural environments. *Organic Geochemistry* 31, 945–958.
- Hendricks, S., Nicolaus, M., Schwegmann, S., 2012. Sea ice conditions during POLARSTERN cruise ARK-XXVII/3 (IceArc) in 2012. PANGAEA. <https://doi.pangaea.de/10.1594/PANGAEA.803221>.
- Hertkorn, N., Benner, R., Frommberger, M., Schmitt-Kopplin, P., Witt, M., Kaiser, K., Ketrup, A., Hedges, J.L., 2006. Characterization of a major refractory component of marine dissolved organic matter. *Geochimica et Cosmochimica Acta* 70, 2990–3010.
- Houghton, R.A., 2007. Balancing the global carbon budget. *Annual Review of Earth and Planetary Science* 35, 313–347.
- Hulth, S., Hall, P.O.J., Blackburn, T.H., Landen, A., 1996. Arctic sediments (Svalbard) pore water and solid phase distribution of C, N, P and Si. *Polar Biology* 16, 447–462.
- Hulth, S., Tengberg, A., Landen, A., Hall, P.O.J., 1997. Mineralization and burial of organic carbon in sediments of the southern Weddell Sea (Antarctica). *Deep Sea Research Part I* 44, 955–981.
- Hulthe, G., Hall, P., Damm, E., 1997. Benthic carbon fluxes – DOC versus ΣCO_2 in shelf, slope and deep-sea environments, and relation to oxygen fluxes. *Reports of Polar Research* 226, 115–116.
- Iversen, N., Jørgensen, B.B., 1993. Diffusion coefficients of sulfate and methane in marine sediments: influence of porosity. *Geochimica et Cosmochimica Acta* 57, 571–578.
- Jacob, M., Soltwedel, T., Boetius, A., Ramette, A., 2013. Biogeography of deep-sea benthic bacteria at regional scale (LTER HAUSGARTEN, Fram Strait, Arctic). *PLoS ONE* 8. <http://dx.doi.org/10.1371/journal.pone.0072779>.
- Janssen, F., Huettel, M., Witte, U., 2005. Pore-water advection and solute fluxes in permeable marine sediments: (II) Benthic respiration at three sandy sites with different permeabilities (German Bight, North Sea). *Limnology and Oceanography* 50, 779–792.
- Jessen, G.L., 2015. Structural and Functional Changes in Marine Microbial Communities Associated with Oxygen Dynamics (PhD thesis). University of Bremen, p. 196.
- Jørgensen, B.B., 2006. Bacteria and Marine Biogeochemistry. *Marine Geochemistry Volume*, pp. 169–206.
- Kędra, M., Moritz, C., Choy, E.S., David, C., Degen, R., Duerksen, S., Ellingsen, I., Górská, B., Grebmeier, J.M., Kirievskaia, D., van Oevelen, D., Piewosz, K., Samuelsen, A., Węśliński, J.M., 2015. Status and trends in the structure of Arctic benthic food webs. *Polar Research* 34, 1–23.
- Kim, S., Kramer, R.W., Hatcher, P.G., 2003. Graphical method for analysis of ultrahigh-resolution broadband mass spectra of natural organic matter, the Van Krevelen diagram. *Analytical Chemistry* 75, 5336–5344.
- Kim, S., Kaplan, L.A., Hatcher, P.G., 2006. Biodegradable dissolved organic matter in a temperate and a tropical stream determined from ultra-high resolution mass spectrometry. *Limnology and Oceanography* 51, 1054–1063.
- Klages, M., Boetius, A., Christensen, J., Deubel, H., Piepenburg, D., Schewe, I., Soltwedel, T., 2004. The benthos of Arctic seas and its role for the organic carbon cycle at the seafloor. In: Stein, R., Macdonald, R.W. (Eds.), *The Arctic Organic Carbon Cycle*. Springer Verlag, Heidelberg, pp. 139–167.
- Koch, B.P., Dittmar, T., 2006. From mass to structure: an aromaticity index for high-resolution mass data of natural organic matter. *Rapid Communications in Mass Spectrometry* 20, 926–932.
- Koch, B.P., Dittmar, T., 2016. Erratum of: from mass to structure: an aromaticity index for high-resolution mass data of natural organic matter. *Rapid Communications in Mass Spectrometry* 30. <http://dx.doi.org/10.1002/rcm.7433>.
- Köhler, H., Meon, B., Gordeev, V.V., Spitzky, A., Amon, R.M., 2003. Dissolved organic matter (DOM) in the rivers Ob and Yenisei and the adjacent Kara-Sea, Russia. In: Stein, R., Fahl, K., Fütterer, D., Galimov, E., Stepanets, O. (Eds.), *Siberian River Run-off in the Kara-Sea: Characterization, Quantification, Variability and Environmental Significance*. Elsevier, Amsterdam, pp. 281–308.
- Krumpen, T., Holemman, J.A., Willmes, S., Morales Maqueda, M.A., Busche, T., Dmitrenko, I.A., Gerdes, R., Haas, C., Heinemann, G., Hendricks, S., Kassens, H., Rabenstein, L., Schröder, D., 2011. Sea ice production and water mass modification in the eastern Laptev Sea. *Journal of Geophysical Research* 116, 1–17.
- Lalande, C., Nöthig, E.M., Somavilla, R., Bauerfeind, E., Shevchenko, V., Okolodkov, Y., 2014. Variability in under-ice export fluxes of biogenic matter in the Arctic Ocean. *Global Biogeochemical Cycles* 28, 571–583.
- Liu, J., 2011. Overview of Redundancy Analysis and Partial Linear Squares and their Extension to the frequency domain (MSc thesis). Dalhousie University, Halifax, Nova Scotia.
- McLafferty, F.W., Turecek, F., 1994. *Interpretation of Mass Spectra*, 1993. John Wiley & Sons Ltd., University Science Books, Mill Valley, California. <http://dx.doi.org/10.1002/bms.1200230614>.
- Moodley, L., Middelburg, J.J., Boschker, H.T.S., Duineveld, G.C.A., Pel, R., Herman, P. M.J., Heip, C.H.R., 2002. Bacteria and foraminifera: key players in a short-term deep-sea benthic response to phytodetritus. *Marine Ecology Progress Series* 236, 23–29.
- Perovich, D., Meier, W., Tschudi, M., Gerland, S., Richter-Menge, J., 2012. Sea ice (in Arctic report card 2012), <http://www.arctic.noaa.gov/report12/sea_ice.html>.
- Rachor, E., 1992. Scientific cruise report of the 1991 Arctic expedition ARK VIII/2 of RV Polarstern. *Reports of Polar Research* 115, 1–150.
- Robador, A., Brüchert, V., Steen, A.D., Arnosti, C., 2010. Temperature induced decoupling of enzymatic hydrolysis and carbon remineralization in long-term incubations of Arctic and temperate sediments. *Geochimica et Cosmochimica Acta* 74, 2316–2326.
- Romankevich, E., Vetrov, A., 2001. *Carbon Cycle in the Russian Arctic Seas*. Nauka, Moscow.
- Rossel, P.E., Vähätalo, A.V., Witt, M., Dittmar, T., 2013. Molecular composition of dissolved organic matter from a wetland plant (*Juncus effusus*) after photochemical and microbial decomposition (1.25 yr): common features with deep sea dissolved organic matter. *Organic Geochemistry* 60, 62–71.
- Rossel, P.E., Bienhold, C., Boetius, A., Dittmar, T., 2015a. Dissolved organic carbon in sediments of the central Arctic Ocean collected during POLARSTERN cruise ARK-XXVII/3 from August–September 2012. PANGAEA. <http://dx.doi.org/10.1594/PANGAEA.849056>.
- Rossel, P.E., Stubbins, A., Hach, P.F., Dittmar, T., 2015b. Bioavailability and molecular composition of dissolved organic matter from a diffuse hydrothermal system. *Marine Chemistry*. <http://dx.doi.org/10.1016/j.marchem.2015.07.002>.
- Rowe, G.T., Deming, J.W., 1985. The role of bacteria in the turnover of organic carbon in deep-sea sediments. *Journal of Marine Research* 43, 925–950.
- Rudels, B., Anderson, L.G., Jones, E.P., 1996. Formation and evolution of the surface mixed layer and halocline of the Arctic Ocean. *Journal of Geophysical Research*. <http://dx.doi.org/10.1029/96JC00143>.
- Sakshaug, E., 2004. Primary and secondary production in the Arctic Seas. In: Stein, T., Macdonald, R.W. (Eds.), *The Arctic Organic Carbon Cycle*. Springer Verlag, Heidelberg, pp. 57–81.
- Schewe, I., Soltwedel, T., 2003. Benthic response to ice-edge-induced particle flux in the Arctic Ocean. *Polar Biology* 26, 610–620.
- Schmidt, F., Elvert, M., Koch, B.P., Witt, M., Hinrichs, K.U., 2009. Molecular characterization of dissolved organic matter in pore water of continental shelf sediments. *Geochimica et Cosmochimica Acta* 73, 3337–3358.
- Schmidt, F., Koch, B.P., Elvert, M., Schmidt, G., Witt, M., Hinrichs, K.U., 2011. Diagenetic transformation of dissolved organic nitrogen compounds under contrasting sedimentary redox conditions in the black sea. *Environmental Science and Technology* 45, 5223–5229.
- Schmidt, F., Koch, B.P., Goldhammer, T., Zabel, M., Buttigieg, P., Ramette, A., Elvert, M., Witt, M., Lazar, M., Könneke, M., Heuer, V., Hinrichs, K.-U., Bach, W., 2014. Impact of biogeochemical zonation and depositional setting on molecular composition of dissolved organic matter in sediment pore waters. *Goldschmidt Abstracts*, 2212.
- Seidel, M., Beck, M., Riedel, T., Waska, H., Suryaaputra, I.G.N.A., Schnetger, B., Niggemann, J., Simon, M., Dittmar, T., 2014. Biogeochemistry of dissolved organic matter in an anoxic intertidal creek bank. *Geochimica et Cosmochimica Acta* 140, 418–434.
- Seidel, M., Yager, P.L., Ward, N.D., Carpenter, E.J., Gomes, H.R., Krusche, A.V., Richey, J.E., Dittmar, T., Medeiros, P.M., 2015. Molecular-level changes of dissolved organic matter along the Amazon River-to-ocean continuum. *Marine Chemistry* 177, 218–231.
- Skoog, A., Benner, R., 1997. Aldoses in various size fractions of marine organic matter: implications for carbon cycling. *Limnology and Oceanography* 42, 1803–1813.
- Soule, M.C.K., Longnecker, K., Giovannoni, S.J., Kujawinski, E.B., 2010. Impact of instrument and experiment parameters on reproducibility of ultrahigh resolution ESI FT-ICR mass spectra of natural organic matter. *Organic Geochemistry* 41, 725–733.
- Spren, G., Kaleschke, L., Heygster, G., 2008. Sea ice remote sensing using AMSR-E 89-GHz channels. *Journal of Geophysical Research* 113, C02S03.
- Stein, R., Macdonald, R.W., 2004. Geochemical proxies used for organic carbon source identification in Arctic Ocean sediments. In: Stein, R., Macdonald, R.W. (Eds.), *The Organic Carbon Cycle in the Arctic Ocean*. Springer Verlag, Heidelberg, pp. 24–30.
- Stein, R., Grobe, H., Wahsner, M., 1994. Organic carbon, carbonate, and clay mineral distributions in eastern central Arctic Ocean surface sediments. *Marine Geology* 119, 269–285.
- Stenson, A., Marshall, A., Cooper, W., 2003. Chemical formulas of individual Suwannee River fulvic acids from ultrahigh resolution electrospray ionization Fourier transform ion cyclotron resonance mass spectra. *Analytical Chemistry* 75, 1275–1284.
- Stubbins, A., Dittmar, T., 2012. Low volume quantification of dissolved organic carbon and dissolved nitrogen. *Limnology and Oceanography Methods* 10, 347–352.

- Stubbins, A., Lapierre, J.F., Berggren, M., Prairie, Y.T., Dittmar, T., Del Giorgio, P.A., 2014. What's in an EEM? Molecular signatures associated with dissolved organic fluorescence in Boreal Canada. *Environmental Science and Technology* 48, 10598–10606.
- Thiel, H., 1982. Zoobenthos of the CINECA area and other upwelling regions. *Rapp. Procès-Verbaux des Réunions. Conseil Permanent International pour l'Exploration de la Mer* 180, 323–334.
- Tobias, R.D., 1995. *An Introduction to Partial Least Squares Regression*. SAS institute, Cary, NC.
- Tremblay, L.B., Dittmar, T., Marshall, A.G., Cooper, W.J., Cooper, W.T., 2007. Molecular characterization of dissolved organic matter in a North Brazilian mangrove porewater and mangrove-fringed estuaries by ultrahigh resolution Fourier Transform-Ion Cyclotron Resonance mass spectrometry and excitation/emission spectroscopy. *Marine Chemistry* 105, 15–29.
- Walsh, J.J., Dieterle, D.A., Maslowski, W., Grebmeier, J.M., Whitledge, T.E., Flint, M., Sukhanova, I.N., Bates, N., Cota, G.F., Stockwell, D., Moran, S.B., Hansell, D.A., McRoy, C.P., 2005. A numerical model of seasonal primary production within the Chukchi/Beaufort Seas. *Deep Sea Research Part II* 52, 3541–3576.
- Wang, M.Y., Overland, J.E., 2009. A sea ice free summer Arctic within 30 years? *Geophysical Research Letters* 36. <http://dx.doi.org/10.1029/2009GL037820>.
- Wassmann, P., Bauerfeind, E., Fortier, M., Fukuchi, M., Hargrave, B., Moran, B., Noji, T., Nöthig, E.-M., Olli, K., Peinert, R., Sasaki, H., Shevchenko, V., 2004. Particulate organic carbon flux to the Arctic Ocean seafloor. In: Stein, R., MacDonald, R.W. (Eds.), *The Organic Carbon Cycle in the Arctic Ocean*. Springer, Verlag, pp. 101–122.
- Wassmann, P., Slagstad, D., Ellingsen, I., 2010. Primary production and climatic variability in the European sector of the Arctic Ocean prior to 2007: preliminary results. *Polar Biology* 33, 1641–1650.
- Witte, U., Aberle, N., Sand, M., Wenzhöfer, F., 2003. Rapid response of a deep-sea benthic community to POM enrichment: an in situ experimental study. *Marine Ecology Progress Series* 251, 27–36.
- Zhang, J., Spitz, Y.H., Steele, M., Ashjian, C., Campbell, R., Berline, L., Matrai, P., 2010. Modeling the impact of declining sea ice on the Arctic marine planktonic ecosystem. *Journal of Geophysical Research Oceanography* 115, 1–24.

Seasonal and spatial variability of dissolved organic matter composition in the lower Amazon River

Michael Seidel · Thorsten Dittmar · Nicholas D. Ward ·
Alex V. Krusche · Jeffrey E. Richey · Patricia L. Yager ·
Patricia M. Medeiros

Received: 2 April 2016 / Accepted: 14 November 2016 / Published online: 28 November 2016
© Springer International Publishing Switzerland 2016

Abstract We analyzed the molecular composition of dissolved organic matter (DOM) in the lower Amazon River (ca. 850 km from Óbidos to the mouth) using ultrahigh-resolution mass spectrometry and geochemical tracers. Changes in DOM composition along this lower reach suggest a transition from higher plant-derived DOM to more algal/microbial-derived DOM. This result was likely due to a combination of autochthonous production, alteration of terrigenous DOM as it transits down the river, and increased algal inputs from floodplain lakes and clearwater tributaries during high discharge conditions. Spatial gradients in dissolved organic carbon (DOC) concentrations varied

with discharge. Maximal DOC concentrations were observed near the mouth during high water, highlighting the importance of lateral inputs of DOM along the lower river. The majority of DOM molecular formulae did not change within the time it takes the water in the mainstem to be transported through the lower reach. This is indicative of molecules representing a mixture of compounds that are resistant to rapid alteration and reactive compounds that are continuously replenished by the lateral input of terrestrial organic matter from the landscape, tributaries, and floodplains. River water incubations revealed that photo- and bio-transformation alter at most 30% of the DOM molecular formulae. River discharge at the mouth differed from the sum of discharge measurements made at Óbidos and the main gauged tributaries in the lower Amazon. This indicates that changes in hydrology and associated variations in the source waters along the lower

Responsible Editor: Charles T. Driscoll

Electronic supplementary material The online version of this article (doi:[10.1007/s10533-016-0279-4](https://doi.org/10.1007/s10533-016-0279-4)) contains supplementary material, which is available to authorized users.

M. Seidel · P. L. Yager · P. M. Medeiros (✉)
Department of Marine Sciences, University of Georgia,
Athens, GA 30602, USA
e-mail: medeiros@uga.edu

M. Seidel · T. Dittmar
Research Group for Marine Geochemistry (ICBM-MPI
Bridging Group), Institute for Chemistry and Biology of
the Marine Environment (ICBM), Carl von Ossietzky
University of Oldenburg, 26129 Oldenburg, Germany

N. D. Ward · J. E. Richey
School of Oceanography, University of Washington,
Seattle, WA 98195, USA

A. V. Krusche
Centro de Energia Nuclear na Agricultura, Universidade
de São Paulo, Piracicaba, SP 13400-970, Brazil

Present Address:
N. D. Ward
Department of Geological Sciences, University of Florida,
Gainesville, FL 32611, USA

reach affected the molecular composition of the DOM that is being transported from the Amazon River to the coastal ocean.

Keywords Amazon River · Ultra-high resolution mass spectrometry · Dissolved organic matter

Introduction

The transport of organic matter from rivers to the oceans is an important pathway in the global carbon cycle (Aufdenkampe et al. 2011; Bianchi 2011). About 15% of global terrestrial primary production occurs in the Amazonian rainforests (Malhi et al. 2008) with the Amazon River contributing to roughly 20% of the global freshwater discharge to the ocean (Sioli 1984). The river drains an area of ca. 7×10^6 km² and its plume extends up to 1.3×10^6 km² in the tropical North Atlantic Ocean (Coles et al. 2013; Hedges et al. 1986). The Amazon River continuum (forest, watershed, floodplains, river, and plume) thus plays an important part in the global carbon cycle (Abril et al. 2014; Field et al. 1998; Mayorga et al. 2005; Raymond and Bauer 2001; Raymond et al. 2013). Although the Amazon River has been extensively studied, most efforts have been limited to stations near and upstream of the city of Óbidos, which is roughly 850 km upstream of the actual river mouth.

Óbidos is typically used as the downstream gauging station because tidal flow reversals complicate the measurement of discharge and geochemical components near the mouth. Yet, several large tributaries contribute to the flow below Óbidos and the geochemistry of the river is altered along the way. Understanding how geochemical constituents evolve along the lower reach of the river is vital for establishing comprehensive nutrient and carbon budgets for the tropical North Atlantic Ocean. Recently, studies were conducted in the downstream Amazon River and/or the adjacent coastal ocean (Medeiros et al. 2015b; Moreira-Turcq et al. 2013; Seidel et al. 2015b; Ward et al. 2013, 2015, 2016). Yet, there is still a lack of data concerning the composition of dissolved organic matter (DOM) in the lower reach of the river. This gap needs to be addressed because changes in river

DOM composition due to land use alteration (e.g., Wagner et al. 2015) will likely affect the carbon cycle on coastal and global scales. The Amazon basin is projected to experience an increase in extreme hydrologic patterns (e.g. flood/drought cycles) due to climate change (Manabe et al. 2004; Nohara et al. 2006). For example, the Amazon River experienced both a large drought and record flood during our study period (2010–2012).

Within the deep mainstem above Óbidos, low light penetration due to high turbidity and high chromophoric DOM concentrations is assumed to limit phytoplankton production. However, in situ primary production has been shown to be important in the main channel of other large tropical rivers, such as the Congo River (Descy et al. 2016). Considering that DOM derived from algal production is generally highly reactive (Duarte and Cebrián 1996; Stanley et al. 2012) and production is limited, most of the mainstem DOM is derived from vascular plants found both on land and in floodplains (Ertel et al. 1986; Hedges et al. 1986, 1994). The proportion of the wetlands was recently estimated to be ca. 14% of the total Amazon basin area (Hess et al. 2015), however, estimates of the exchange of water between the mainstem and floodplains vary considerably. Richey et al. (1989) proposed that up to 30% of the mainstem water has passed through floodplains while more recently, Alsdorf et al. (2010) concluded from satellite data that a smaller portion of ca. 5% of the total mainstem river discharge is exchanged with floodplains. Nonetheless, floodplains and associated lakes with higher light availability than the mainstem are important regions of high in situ primary production (Junk 1997; Melack and Forsberg 2001; Sioli 1984). Consequently, the extensive floodplains, floodplain lakes and tributaries represent considerable additional OM sources to the mainstem (Abril et al. 2014; Moreira-Turcq et al. 2013).

The composition of DOM in the lower Amazon River is further altered by processes such as microbial remineralization, sorption, photo-degradation, and lateral exchange with floodplains or soils (Amon and Benner 1996; Aufdenkampe et al. 2001; Hedges et al. 2000; Ward et al. 2013). Near the river mouth, semidiurnal tides have a maximum range of 5 m (Ferraz 1975). Analogous to saline/brackish mangrove forests further south (Kristensen et al. 2008), the

intertidal floodplain exchange is expected to alter the DOM composition within the freshwater-dominated Amazon estuary. Flocculation acts as an additional removal mechanism of terrigenous DOM along the estuarine salinity gradient (Sholkovitz et al. 1978).

It was proposed previously that the compositional uniformity of Amazon River DOM is the result of processes shaping these molecular imprints mainly outside of the river suggesting a recalcitrant character (e.g., Hedges et al. 2000). This idea sets up a conundrum, however, since the degradation of contemporary DOM (up to 5 years radiocarbon age) was found to be the main source for CO₂ outgassing in the Amazon River (Mayorga et al. 2005). The large fluxes of CO₂ therefore must be caused by high microbial respiration which indicates that high OM fluxes in the river are in dynamic balance with its degradation (Richey et al. 2002). Photo-degradation, although an important pathway for breakdown of terrestrially-derived DOM (Gonsior et al. 2009; Hernes and Benner 2003; Obernosterer and Benner 2004; Spencer et al. 2009; Stubbins et al. 2010), is diminished in the Amazon mainstem (Amaral et al. 2013; Amon and Benner 1996), and ultimately contributes less than 1% to basin-wide CO₂ outgassing (Remington et al. 2011).

Previous studies of the Amazon River DOM focused on molecular biomarkers such as lignin degradation products, amino acids and carbohydrates (e.g., Amon and Benner 1996; Aufdenkampe et al. 2007; Hedges et al. 1994, 2000; Ward et al. 2013). Despite the valuable information they provided on several processes, there is still a lack of data concerning the more detailed molecular composition of DOM. The recent advance of ultrahigh-resolution Fourier-transform ion cyclotron resonance mass spectrometry (FT-ICR-MS) allows resolving thousands of molecular formulae in complex DOM mixtures. Consequently, it has been applied to study the transformation of DOM in a wide range of aquatic habitats, including terrestrial to marine transition zones (Kujawinski et al. 2004; Medeiros et al. 2015b; Schmidt et al. 2009; Seidel et al. 2015a; Sleighter and Hatcher 2008).

Our study addresses the question of how the DOM molecular composition changes in the lower Amazon River, i.e. ca 850 km from Óbidos to the river mouth, during periods of high, falling, low and rising discharge conditions, i.e. wet to dry seasons. By

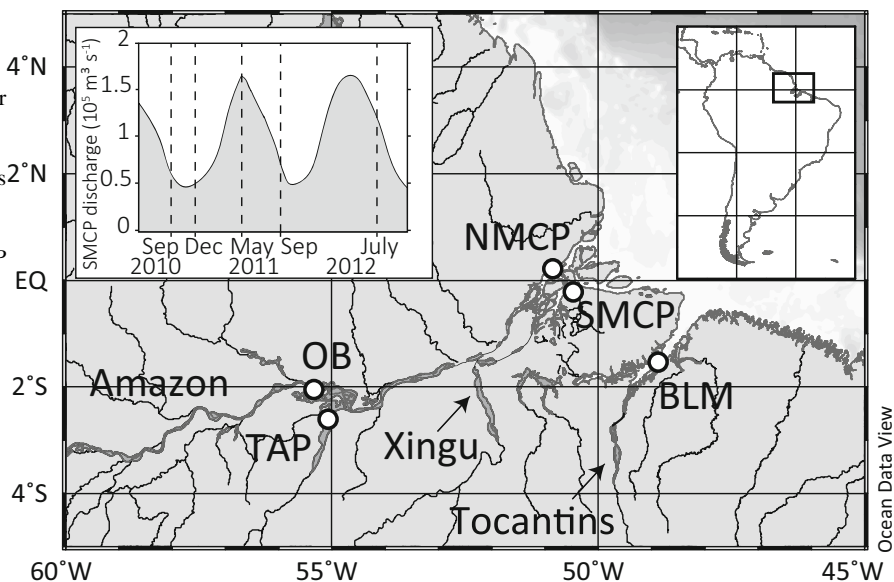
characterizing the molecular composition of DOM from the lower Amazon River and incubation experiments, we aim to answer the following set of questions: (i) What are the molecular characteristics of the various DOM sources and what is the molecular imprint of microbial and photochemical transformations in the river? (ii) Are these patterns consistent with observed spatial and seasonal trends in the molecular DOM composition from Óbidos to the river mouth? Incubation experiments with river water elucidated the influence of photo- and bio-degradation on the riverine DOM molecular composition. Samples from the upstream mainstem station at Óbidos were compared to the clearwater Tapajós River, a tributary ca. 80 km downstream of Óbidos, as well as to stations close to the river mouth in the vicinity at the cities of Macapá and Belém. The employed sampling strategy gave insights on how the discharge conditions influence the DOM composition in the mainstem.

Materials and methods

Study site, sampling and river incubations

In the central Amazon basin, precipitation ranges from 2000 to 2500 mm yr⁻¹, with rainy (December to May, peaking in austral summer) and dry seasons (June to December, peaking in austral winter) (e.g., McClain et al. 1997). Consequently, the river discharge varies seasonally (Fig. 1). At the gauging station at Óbidos (OB), the mean water level difference between low (around September) and high (around May) discharge is ca. 3 m, but can be more than 6 m during exceptional dry/wet periods (Casali et al. 2011). The average discharge at Óbidos was 176,000 ± 64,000 m³ s⁻¹ during the study period (Ward et al. 2015). The two main tributaries draining into the mainstem downstream of Óbidos are the clearwater Xingú and Tapajós (TAP) rivers, which contribute an additional 17,000 ± 18,000 m³ s⁻¹. The Tocantins River adds 10,000 ± 7000 m³ s⁻¹ of discharge, which flows through the channel south of the Marajó Island near Belém along with Amazon mainstem water exported through the Breves Channel (Ward et al. 2015). Roughly 80% of the total discharge to the ocean flows through the channels near Macapá (30% to the north channel, NMCP, and 50% to the south channel,

Fig. 1 Amazon River sampling transect with sampling stations (white circles). The insert at the upper left depicts the average river discharge through the South Macapá channel and the dashed lines indicate sampling time points (after Ward et al. 2015). BLM Belém, NMCP north Macapá, OB Óbidos, SMCP south Macapá, TAP Tapajós



SMCP), and 20% flows through the channel near Belém (BLM) (Ward et al. 2015).

Our sampling covered different discharge periods, i.e. low (September), rising (December), high (May), and falling (July/August) water level conditions. Samples were taken in the center of the river channel using a submersible pump at 50% river depth in 2010 (September—austral spring, and December—austral summer), 2011 (May—austral autumn, and September—austral spring), and 2012 (July/August—austral winter) at stations Belém, Macapá (north and south channels), Óbidos and Tapajós as described by Ward et al. (2015) (Fig. 1; Table 1). We chose 50% sampling depth because it is the location where total suspended sediment levels are roughly the average found throughout the water column (Meade et al. 1985; Ward et al. 2015). Bulk chemistry was measured at three equidistant cross-channel stations at both surface and 50% depth. We restricted the resource and time-intensive DOM characterization via ultra-high resolution mass spectrometry discussed here to the center of the river at mid depth because this best represents an average bulk DOM signal across the channel (Ward et al. 2015). The water samples were filtered with pre-combusted (5 h at 450 °C) glass fiber filters (GF/F 142 mm, 0.7 μm , Whatman) and 0.2 μm membrane filter (Supor, Pall) and the filtrates were acidified to pH 2 with HCl (p.a., Fisher Chemical).

Bio- and photo-incubation experiments were performed in triplicates (4 L of non-acidified water each) in the Amazon River mainstem at ambient water temperatures (ca. 30 °C), with river water from the North Macapá station during the September 2011 cruise (low discharge in austral spring) for 3 days. Bio-incubation experiments were performed using whole water in acid-washed, aluminum foil wrapped high-density polyethylene bottles, which were stored in dark coolers in the shade. Photo-incubation experiments were performed with water filtered through a 0.2 μm membrane filter into pre-combusted quartz glass bottles. The bottles were stored in a cooler without a lid in natural sunlight submerged in recirculating river water to the top of the bottle (34 cm). We did not measure photosynthetically reactive radiation during our experiments but a previous study found a quantum flux of up to 3000 $\mu\text{mol m}^{-2} \text{ s}^{-1}$ above surface water at noon near the equator (Furch and Junk 1997). It should also be noted that our photo-degradation experiment does not take into account water column mixing in the turbid mainstem with limited light penetration (e.g., Amon and Benner 1996).

Bulk geochemical and chemical tracer analyses

DOC and total dissolved nitrogen (TDN) concentrations in the filtered and acidified water samples were measured by high temperature catalytic oxidation on a

Table 1 Physical and chemical parameters at sampling sites along the lower Amazon River during different discharge conditions

Station ^a	Depth (m)	Temp (°C)	Year	Month	Discharge	DOC (μM)	δ ¹³ C (‰) ^b
OB	20	30.8	2010	Sept	Low	339	−28.7
	33	30.9	2011	Sept	Low	347	−29.9
	32	30.4	2010	Dec	Rising	346	−29.5
	33	28.4	2011	May	High	351	−29.6
	30	29.1	2012	Aug	Falling	359	−29.8
TAP	n.d. ^c	n.d.	2010	Sept	Low	125 ^d	n.d.
	15	31.3	2011	Sept	Low	122	−29.4
	16	30.6	2010	Dec	Rising	210	−29.5
	17	29.5	2011	May	High	176	−29.4
	18	31	2012	Aug	Falling	161	−29.7
NMCP	18	31.3	2010	Sept	Low	403	−29.0
	14	29.8	2011	Sept	Low	319	−29.6
	14	30.5	2010	Dec	Rising	293	−29.2
	n.d.	n.d.	2011	May	High	475 ^d	n.d.
	15	29.6	2012	Jul	Falling	252	−29.5
SMCP	15	30	2010	Sept	Low	352	−29.2
	10	30	2011	Sept	Low	305	−29.2
	20	30.3	2010	Dec	Rising	232	−29.7
	10	28.8	2011	May	High	451	−29.4
	10	29.2	2012	Jul	Falling	334	−29.8
BLM	n.d.	n.d.	2010	Sept	Low	n.d.	n.d.
	19	29.9	2011	Sept	Low	224	−28.5
	6	n.d.	2010	Dec	Rising	442 ^d	n.d.
	n.d.	n.d.	2011	May	High	492 ^d	n.d.
	18	29.5	2012	Aug	Falling	253	−28.8

^a *BLM* Belém, *NMCP* north Macapá, *OB* Óbidos, *SMCP* south Macapá, *TAP* Tapajós

^b δ¹³C SPE-DOM

^c Not determined

^d Value from Ward et al. (2015)

Shimadzu TOC-V_{CPH} instrument. It should be noted that the DOC concentrations values vary from those measured by Ward et al. (2015), because their samples were filtered only through a 0.7 μm GF/F and their measurements made at three cross-channel stations were averaged. Analytical accuracy and precision were tested against the deep-sea reference sample (D. Hansell, University of Miami, USA) and were better than 5%. TDN concentrations were reported previously by Ward et al. (2015).

DOM was extracted from 1 L of river water as described by Dittmar et al. (2008) using solid phase extraction (SPE) with cartridges filled with a styrene divinyl benzene polymer (Agilent Bond Elut PPL, 1 g). The extraction efficiencies (determined as amount of DOC in volume of original water sample versus amount of DOC in a defined evaporated volume of SPE-DOM extract that was re-dissolved in ultrapure water) were 60 ± 11% (*n* = 42). The methanol

extracts were stored frozen in the dark until further analysis.

The stable carbon isotope composition was determined on SPE-DOM by pipetting extracts containing ca. 20 μg of DOC into Sn caps (IVA, Germany) and subsequent drying at 40 °C in an oven. The isotopic composition was analyzed in duplicates on an isotope-ratio-monitoring mass spectrometer (Finnigan MAT 252, Bremen, Germany) via a Conflo II split interface. The stable carbon isotope ratios are reported in δ notation relative to the Vienna Pee Dee Belemnite. Precision and accuracy was <0.5‰ and procedural blanks did not yield detectable amounts of carbon isotope contamination.

The concentrations of chlorophyll *a* (for September 2011 and July/August 2012 collections), dissolved lignin (eight standard lignin phenols) of the river samples were reported previously by Ward et al. (2015). Dissolved lignin concentration of the photo-

Table 2 DOM molecular parameters (mean \pm SD) in Amazon-River samples that were significantly correlated to the respective environmental parameters (Spearman rank correlation, $p \leq 0.05$)

	River discharge		Water temperature		DOC concentration		Lignin concentration	
	Negative	Positive	Negative	Positive	Negative	Positive	Negative	Positive
Formula ^a	386 (10%)	350 (9%)	158 (4%)	181 (5%)	307 (8%)	209 (5%)	213 (6%)	308 (8%)
Mass (Da)	384.5 \pm 81.2	527.9 \pm 106.7*	436.7 \pm 136.4	418.7 \pm 79.4	377.5 \pm 82.4	543.6 \pm 93*	518.8 \pm 97.8	330.5 \pm 87.8*
C	17.7 \pm 3.5	25.8 \pm 4.8*	22.7 \pm 6.6	19.1 \pm 3.9*	17.8 \pm 3.6	26.8 \pm 4.1*	25.5 \pm 4.2	16.1 \pm 3.7*
H	21.6 \pm 5.2	25.9 \pm 8.3*	26.1 \pm 10.6	24.6 \pm 6.5	21.2 \pm 5.7	29.7 \pm 7.2*	30.4 \pm 5.9	16.4 \pm 5.8*
O	8.2 \pm 2.6	12 \pm 3.8*	8.4 \pm 3.8	8.9 \pm 2.5	7.7 \pm 2.5	11.9 \pm 3.6*	11.3 \pm 3.4	6.7 \pm 2.5*
N	1.4 \pm 0.8	0 \pm 0.2*	0.2 \pm 0.5	1.3 \pm 0.9*	1.4 \pm 0.7	0 \pm 0.2*	0.1 \pm 0.5	1 \pm 0.7*
S	0.01 \pm 0.12	0.04 \pm 0.2	0.06 \pm 0.23	0.05 \pm 0.24	0.03 \pm 0.2	0.08 \pm 0.3	0.03 \pm 0.17	0.01 \pm 0.13
P	0.03 \pm 0.16	0 \pm 0	0 \pm 0	0.1 \pm 0.3*	0.02 \pm 0.14	0 \pm 0	0.01 \pm 0.09	0 \pm 0
DBE	8.6 \pm 2.2	13.9 \pm 3.5*	10.7 \pm 3.7	8.5 \pm 2.4*	8.9 \pm 2.5	12.9 \pm 3.3*	11.4 \pm 2.7	9.4 \pm 2.9*
H/C	1.22 \pm 0.17	0.99 \pm 0.24*	1.12 \pm 0.29	1.28 \pm 0.19*	1.19 \pm 0.22	1.11 \pm 0.21*	1.19 \pm 0.15	1.02 \pm 0.26*
O/C	0.46 \pm 0.1	0.47 \pm 0.12	0.37 \pm 0.13	0.47 \pm 0.11*	0.43 \pm 0.1	0.45 \pm 0.11	0.44 \pm 0.1	0.41 \pm 0.1
Al _{mod}	0.26 \pm 0.14	0.41 \pm 0.14*	0.37 \pm 0.18	0.21 \pm 0.13*	0.29 \pm 0.15	0.33 \pm 0.12	0.28 \pm 0.1	0.44 \pm 0.17*
CHO ^b	29 (7.5%)	335 (95.7%)	136 (86.1%)	18 (9.9%)	14 (4.6%)	193 (92.3%)	211 (99.1%)	61 (19.8%)
CHON	344 (89.1%)	3 (0.9%)	13 (8.2%)	137 (75.7%)	281 (91.5%)	2 (1%)	11 (5.2%)	245 (79.5%)
CHOS	3 (0.8%)	12 (3.4%)	8 (5.1%)	4 (2.2%)	6 (2%)	14 (6.7%)	7 (3.3%)	2 (0.6%)

* Molecular parameters are significantly different comparing negatively to positively correlated formulae ($p < 0.001$, Wilcoxon–Whitney test)^a Number and relative proportion of total formulae (%)^b Number and relative proportion of correlated compounds (%)

degradation treatments with river water were measured for the present study in solid-phase extracts (Waters Oasis HLB cartridges) and analyzed after CuO oxidation and derivatization with BSTFA using a GC–ToF-MS (Agilent 7890A GC, Leco TruToF HT) as described in more detail by Ward et al. (2015). Dissolved lignin concentrations of the bio-degradation treatments with river water were reported previously by Ward et al. (2013).

FT-ICR-MS analysis

The methanol extracts were diluted 1:1 (v/v) with ultra-pure water to yield a DOC concentration of 15 mg L⁻¹ for the analysis with FT-ICR-MS. Samples were analyzed with a 15 Tesla solarix FT-ICR-MS (Bruker Daltonik GmbH, Bremen, Germany) equipped with an electrospray ionization source in negative mode. Instrument settings and molecular formulae assignments were as described in more detail by Seidel et al. (2014). In short, the capillary voltage was 4 kV in negative mode. Ions were accumulated in the hexapole for 0.3 s and data were acquired in broadband mode using 4 megaword data sets and a scanning range of 150–2000 Da with 500 scans accumulated per mass spectrum. Mass spectra were calibrated internally with a list of known compounds in the targeted mass range (achieved mass accuracy <0.1 ppm). Molecular formulae were assigned to peaks with a signal-to-noise ratio >4 applying the criteria described by Koch et al. (2007) with a mass tolerance of <0.5 ppm. The areas of peaks with assigned molecular formulae were normalized to the sum of all peak areas with identified molecular formulae in each sample and normalized peak intensities were multiplied by a factor of 10,000. The aromaticity and the degree of unsaturation of compounds were assessed using the modified aromaticity (AI_{mod}) and double bond equivalent (DBE) indexes (Koch and Dittmar 2006, 2016).

Changes in the DOM molecular composition were assessed in the triplicate incubation treatments by comparing the normalized relative peak heights of the molecular formulae at each time point considering only molecular formulae that were present/absent in each replicate of the individual treatments. Based on control measurements ($n = 36$) of an in-house standard (SPE-DOM from “North Equatorial Pacific

Intermediate Water”) we calculated a dynamic limit of quantification (LOQ) for all peaks with assigned molecular formulae (in percent of normalized peak heights). The dynamic LOQ takes into account that small peaks may fall below a fixed threshold in replicates measurements (false negatives because of large relative deviations of signal intensity) while large peaks are detected more reliably (small relative deviations of signal intensity). To avoid false negatives, changes were considered significant if they were >25% for small peaks (i.e., higher LOQ was used), and >5% for large peaks (lower LOQ because of lower probability for false negatives) following the exponential equation $y = 28.06698e^{-0.0603x}$ (where y is LOQ in %, and x is the normalized peak area). This approach eliminated inter-sample variability based on changing peak heights with low relative abundances that were close to the limit of the detection of the FT-ICR-MS.

The test for relative changes in normalized peak areas was also applied to measurements of the “North Equatorial Pacific Intermediate Water” DOM reference (Osterholz et al. 2014) which was run regularly in between samples to control for instrument variability of the FT-ICR-MS. Less than 5% of peaks changed in relative abundance in these measurements ($n = 36$) when the relative LOQ was applied. This result confirmed the robustness of the applied approach and it shows that the observed trends were not significantly influenced by analytical variability of the FT-ICR-MS.

Non-metric multidimensional scaling (NMDS) was used to determine the correlation of environmental parameters with the DOM molecular composition as described previously (Seidel et al. 2015b). The environmental data used for NMDS included the environmental parameters water temperature, sampling depth, river discharge, dissolved lignin concentrations, and TDN concentrations (Ward et al. 2015), DOC concentration, stable carbon isotope composition of SPE-DOM (this study), and chlorophyll a concentrations (for September 2011 and July/August 2012 collections) as reported previously (Ward et al. 2015). The environmental data were centered and scaled for NMDS ordination and the model was run on a Bray–Curtis distance matrix (based on normalized DOM data) using the vegan package (Oksanen et al. 2015) within the R statistical platform (R Core Team 2015). Spearman’s rank correlation analysis (α -level 0.05) was used to test for correlations between

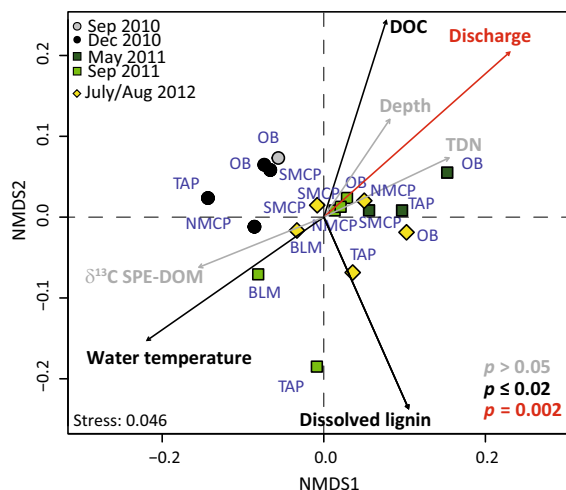


Fig. 2 Non-metric multidimensional scaling (NMDS) analysis based on the relative abundance of all DOM molecular formulae with environmental parameters shown as vectors. Colors of the vectors (environmental parameters) depict statistical significance of their correlations to the DOM molecular composition. (Color figure online)

environmental and geochemical parameters with DOM molecular formulae. The Wilcoxon–Mann–Whitney test was used to test for the significance of the differences in molecular parameters between compounds that increased or decreased during the incubation treatments, and between compounds that were correlated positively or negatively to environmental and geochemical parameters (α -level 0.001). Molecular compound groups were assigned to molecular formulae as described in Seidel et al. (2014): group (1) polycyclic aromatics (PCAs, $AI_{mod} > 0.66$), including condensed combustion-derived dissolved black carbon if $C > 15$ (Dittmar and Koch 2006), (2) highly aromatic compounds with aliphatic side chains (Koch and Dittmar 2006) ($0.66 \geq AI_{mod} \geq 0.50$), (3) highly unsaturated compounds, including lignin degradation products (Stenson et al. 2003) ($AI_{mod} < 0.50$ and $H/C < 1.5$), sub-divided into oxygen-poor (group 3a, $O/C \leq 0.5$) or oxygen-rich (group 3b, $O/C 0.5–0.9$) compounds, (4) unsaturated aliphatic compounds ($2.0 \geq H/C > 1.5$, $N = 0$), (5) saturated compounds, including lipids ($H/C > 2.0$ and $O/C < 0.9$), (6) saturated compounds ($H/C > 2.0$) with $O/C > 0.9$, including carbohydrate molecular formulae, and (7) unsaturated aliphatic compounds containing N, including peptide molecular formulae ($2.0 > H/C \geq 1.5$, $N > 0$). We note that the molecular

characterization by FT-ICR-MS is ambiguous because several different structures may exist for a single molecular formula. However, the molecular categorizing using ultrahigh-resolution MS provides insights to likely structures behind the identified molecular formulae. The assignment of compound groups based on molecular level composition obtained by FT-ICR-MS has therefore been successfully used to identify biogeochemical processing of DOM (e.g., Kim et al. 2003; Schmidt et al. 2009).

Results

River DOC concentration and stable carbon isotopic composition

DOC concentrations were in the range of 224–492 μM in the Amazon mainstem (Table 1). Lower DOC concentrations were observed in the Tapajós River throughout the sampling period (122–210 μM). At the sampling stations close to the river mouth, DOC concentrations were up to 140 μM (40%) above DOC values observed at Óbidos during high discharge in 2011 (Table 1). Seasonal changes of DOC concentrations were pronounced near the river mouth at the North and South channels near Macapá and Belém, with highest values observed during high discharge (Table 1). At the Macapá channels, DOC concentrations were second highest during low discharge in 2010. DOC concentrations at Óbidos exhibited small seasonal variability of ca. 5%.

Water discharge was correlated to DOC concentrations ($p < 0.001$, $\rho = 0.87$, $n = 23$) and water temperature ($p = 0.03$, $\rho = -0.50$, $n = 23$). Dissolved lignin concentrations were negatively correlated to DOC concentrations ($p = 0.02$, $\rho = -0.55$, $n = 18$).

The $\delta^{13}\text{C}$ SPE-DOM values were between -29.9 and -28.5‰ for all sampling while showing no significant trends downstream or with discharge conditions (Table 1).

River DOM molecular composition

In total, about 4700 molecular formulae were identified in the river SPE-DOM, consisting mostly of highly aromatic and highly unsaturated molecular formulae (groups 1 to 3 were up to ca. 90% of all molecular formulae, Supplementary Table S1). Highly

aromatic compounds (groups 1 and 2) were most abundant during high discharge. A minor proportion consisted of unsaturated aliphatic compounds (with/without N, groups 4 and 7) including peptide degradation products and saturated compounds including fatty acids and carbohydrate molecular formulae (groups 5 and 6, Supplementary Table S1).

In NMDS analysis, environmental factors correlated to DOM molecular variability were river discharge, DOC concentration, water temperature, and dissolved lignin concentrations (Fig. 2). A separate NMDS analysis with samples from the September 2011 and July 2012 collections revealed no correlation of the DOM molecular composition with concentrations of chlorophyll *a* (not shown).

Compared to the suite of all DOM molecular formulae (i.e., formulae that were observed in all river samples, Supplementary Table S2), we identified a pool of distinctively changing DOM compounds, i.e. formulae that were not present in all samples. These changing molecular formulae contributed 8–26% of the overall detected compounds (Supplementary Table S3). They were relatively enriched in the heteroatoms N, S and P (compare changing formulae in Supplementary Table S3 to all detected molecular formulae in Supplementary Table S2). They were also more saturated, i.e., changing formulae had higher H/C ratios, lower AI_{mod} and DBE values and O/C ratios (Supplementary Table S3) compared to the overall DOM molecular formulae (Supplementary

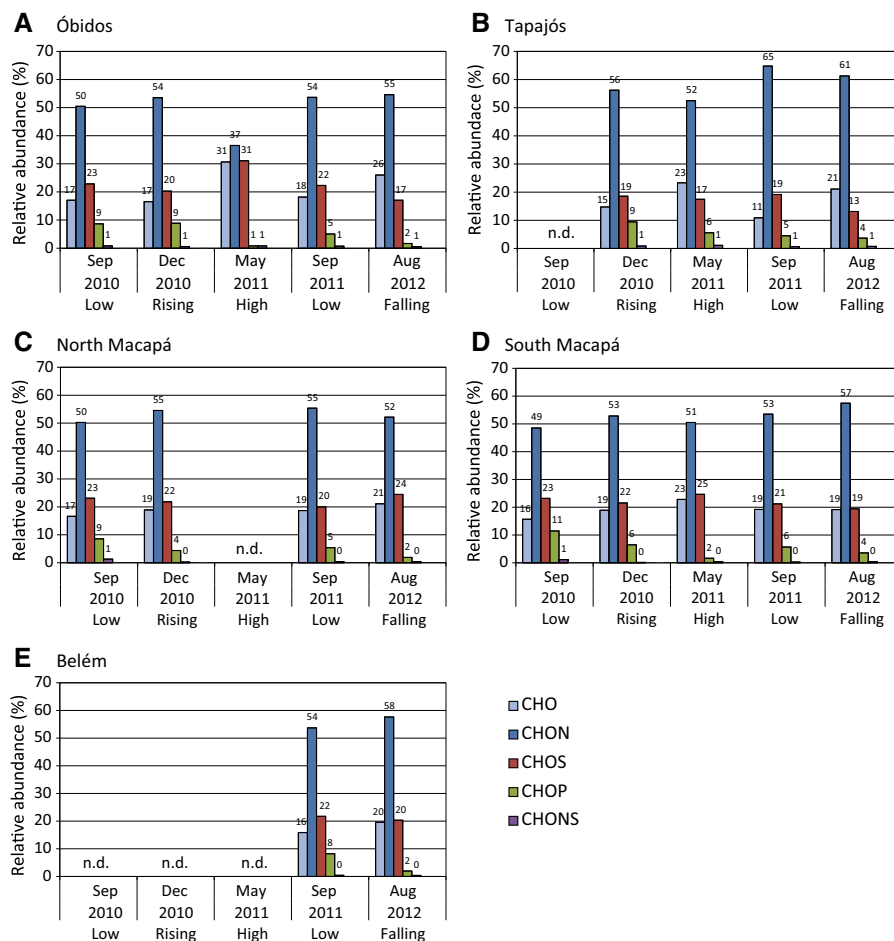


Fig. 3 Relative abundance of distinctively changing molecular formulae, i.e. formulae that were not present in all samples, in the Amazon River during different water discharge conditions. *ND* not determined

Table 3 Composition and changes (decrease/increase) of relative intensities of molecular formulae in the Amazon River mainstem comparing samples from Óbidos to Macapá (mean \pm SD) during different river discharge conditions

	Sep 2010—Low		Dec 2010—Rising		May 2011—High		Sep 2011—Low		Jul/Aug 2012—Falling	
	Decrease	Increase	Decrease	Increase	Decrease	Increase	Decrease	Increase	Decrease	Increase
Formulae ^a	167 (5%)	339 (10%)	141 (4%)	300 (9%)	222 (8%)	447 (16%)	80 (2%)	178 (5%)	227 (8%)	380 (13%)
Mass (Da)	424 \pm 101	434 \pm 112*	521 \pm 124	372 \pm 113*	451 \pm 150	435 \pm 118*	416 \pm 103	391 \pm 119*	416 \pm 124	472 \pm 121*
C	19 \pm 4	20 \pm 5*	24 \pm 5	18 \pm 5*	21 \pm 7	21 \pm 5*	20 \pm 4	18 \pm 5*	20 \pm 6	22 \pm 5*
H	22 \pm 7	24 \pm 7	27 \pm 8	23 \pm 7*	23 \pm 10	26 \pm 8	25 \pm 6	22 \pm 9*	26 \pm 8	24 \pm 8*
O	10 \pm 4	9 \pm 4*	12 \pm 5	7 \pm 3*	10 \pm 5	9 \pm 4*	8 \pm 4	9 \pm 4*	8 \pm 4	11 \pm 4
N	0.4 \pm 1	0.8 \pm 1*	0.6 \pm 1.3	0.8 \pm 0.9*	0.5 \pm 0.9	0.8 \pm 0.9*	0.9 \pm 1.2	0.6 \pm 1*	0.8 \pm 1.1	1.7 \pm 0.9
S	0.35 \pm 0.7	0.27 \pm 0.5	0.3 \pm 0.6	0.23 \pm 0.5	0.13 \pm 0.4	0.16 \pm 0.4	0.45 \pm 0.6	0.22 \pm 0.5*	0.19 \pm 0.5	1.14 \pm 0.3*
P	0.02 \pm 0.2	0.07 \pm 0.3	0.16 \pm 0.4	0 \pm 0*	0.01 \pm 0.1	0.02 \pm 0.1	0.01 \pm 0.1	0.05 \pm 0.2	0.02 \pm 0.1	1 \pm 0
H/C	1.2 \pm 0.3	1.2 \pm 0.3	1.2 \pm 0.3	1.2 \pm 0.3	1.1 \pm 0.4	1.3 \pm 0.2*	1.3 \pm 0.2	1.2 \pm 0.3	1.3 \pm 0.2	1.1 \pm 0.3*
O/C	0.6 \pm 0.2	0.4 \pm 0.1*	0.5 \pm 0.2	0.4 \pm 0.1*	0.5 \pm 0.1	0.4 \pm 0.1*	0.4 \pm 0.1	0.5 \pm 0.2	0.4 \pm 0.1	0.5 \pm 0.1
Al _{mod}	0.2 \pm 0.1	0.3 \pm 0.2	0.3 \pm 0.2	0.3 \pm 0.2	0.4 \pm 0.2	0.2 \pm 0.1*	0.2 \pm 0.1	0.2 \pm 0.2	0.2 \pm 0.1	0.3 \pm 0.2*
CHO ^b	99 (3%)	77 (2.3%)	64 (1.9%)	79 (2.3%)	125 (4.4%)	138 (4.9%)	13 (0.4%)	81 (2.5%)	87 (2.9%)	130 (4%)
CHON	28 (0.8%)	159 (4.7%)	27 (0.8%)	170 (5%)	67 (2.4%)	238 (8.4%)	34 (1%)	54 (1.6%)	99 (3.3%)	160 (5%)
CHOS	35 (1%)	76 (2.3%)	23 (0.7%)	50 (1.5%)	27 (1%)	62 (2.2%)	32 (1%)	34 (1%)	34 (1.2%)	86 (3%)

* Molecular parameters are significantly different comparing negatively to positively correlated formulae ($p < 0.001$, Wilcoxon–Whitney test)^a Number and relative proportion of total formulae (%)^b Number and relative abundance (% of total molecular formulae)

Table 4 Compositional DOM changes in river incubation treatments expressed as averages (of replicates) of molecular parameters (mean \pm SD)

	T ₀ ^a	Bio-incubation		Photo-incubation	
		Decrease	Increase	Decrease	Increase
Formulae ^b	4628	797 (17%)	629 (14%)	523 (11%)	715 (15%)
Mass	384.5 \pm 110.7	484 \pm 123	309 \pm 95*	523 \pm 103	295 \pm 91*
C	18.7 \pm 5.1	22.58 \pm 5.8	14.53 \pm 4.4*	24.46 \pm 4.8	13.68 \pm 4*
H	20.1 \pm 7.6	20.47 \pm 8.7	17.91 \pm 7.4*	23.64 \pm 7.3	16.97 \pm 7.4*
O	8.6 \pm 3.4	11.43 \pm 4	6.76 \pm 3.5*	12.23 \pm 3.9	6.51 \pm 3.4*
N	0.15 \pm 0.46	0.34 \pm 0.7	0.43 \pm 0.7*	0.35 \pm 0.8	0.4 \pm 0.7
S	0.04 \pm 0.21	0.1 \pm 0.4	0.06 \pm 0.3	0.09 \pm 0.4	0.14 \pm 0.4*
P	0.03 \pm 0.23	0.08 \pm 0.3	0.03 \pm 0.2	0.09 \pm 0.3	0.02 \pm 0.1*
H/C	1.1 \pm 0.3	0.9 \pm 0.3	1.23 \pm 0.3*	0.99 \pm 0.3	1.22 \pm 0.3*
O/C	0.5 \pm 0.1	0.51 \pm 0.1	0.48 \pm 0.2	0.5 \pm 0.1	0.49 \pm 0.2
AI _{mod}	0.37 \pm 0.20	0.46 \pm 0.2	0.28 \pm 0.2*	0.41 \pm 0.2	0.28 \pm 0.2*
CHO ^c	1608 (35%)	574 (12.4%)	397 (8.6%)	395 (8.5%)	421 (9.1%)
CHON	1471 (32%)	195 (4.2%)	203 (4.4%)	118 (2.5%)	204 (4.4%)
CHOS	565 (12%)	63 (1.4%)	35 (0.8%)	32 (0.7%)	96 (2.1%)
CHOP	227 (5%)	47 (1%)	16 (0.3%)	40 (0.9%)	13 (0.3%)

* Molecular parameters are significantly different comparing decreasing to increasing formulae ($p < 0.001$, Wilcoxon–Mann–Whitney test)

^a Initial sample from North Macapá station

^b Relative proportion of total formulae (%)

^c Number and relative proportion of total formulae (%)

Table S2). Prominent groups of the changing compounds were formulae containing C, H, O, and N (CHON, between 49 and 65%, Fig. 3) or S (CHOS, between 17 and 31%, Fig. 3).

CHO changing formulae were most abundant during high and falling discharge conditions (Fig. 3). CHON changing compounds were most abundant during low (2011), rising and falling discharge conditions, whereas CHOP changing compounds were generally most abundant during low and rising discharge conditions (Fig. 3).

The environmental and geochemical parameters river discharge, DOC concentrations, water temperature, and lignin concentrations were significantly correlated to 2130 molecular formulae (Table 2). Due to their co-correlation, DOC concentrations and river discharge shared a suite of 406 molecular formulae that were significantly correlated to both environmental factors. Likewise, 174 and 155 molecular formulae were co-correlated to river discharge and temperature or DOC and lignin concentrations,

respectively. During high discharge conditions with elevated river DOC concentrations, the positively correlated molecular formulae had significantly higher masses and higher numbers of C-atoms (compare compounds positively correlated to discharge and DOC concentration to negatively correlated compounds, Table 2). In addition, positively correlated compounds were significantly more aromatic during high discharge (higher AI_{mod} index positively correlated to discharge, Table 2). The input of CHON compounds was correlated to low discharge conditions (higher number of CHON compounds negatively correlated to discharge and DOC concentrations, Table 2). Compounds that were positively correlated to lignin concentrations had lower masses, lower C-numbers, were more aromatic (higher AI_{mod}) and contained more N than negatively correlated compounds (Table 2). Specifically, the positively correlated N-containing compounds were highly aromatic (group 2, 105 molecular formulae) and highly unsaturated compounds (group 3, 140 molecular formulae).

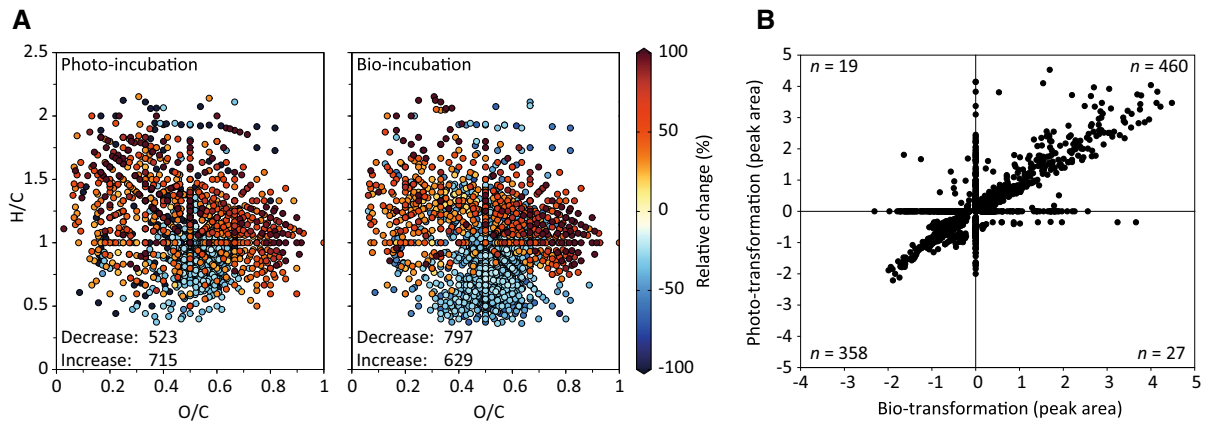


Fig. 4 **a** Van-Krevelen plots of DOM molecular formulae that changed in relative abundance in the incubation experiments with Amazon River water that was exposed to sunlight (photo-

incubation) or incubated in the *dark* (bio-incubation), **b** Scatter-plot of changes of normalized peak areas for molecular formulae in the bio- and photo-incubations treatments

The most distinct differences in the changing DOM molecular formulae were found between samples from the Tapajós River compared to stations at Óbidos and Macapá (Fig. 3). The DOM molecular formulae in the Tapajós River contained more N during most discharge conditions compared to the mainstem (Supplementary Tables S2 and S3).

Compared to Óbidos, the number of DOM compounds that relatively increased at the Macapá stations was higher than the number of relatively decreasing compounds (Table 3). The masses of the DOM compounds decreased downstream during rising, high and low (2011) discharge conditions (decreasing masses in Table 3) but increased downstream during low (2010) and falling discharge conditions (increasing masses in Table 3). Heavier and more aromatic DOM compounds relatively increased downstream during falling discharge conditions (significantly increasing compounds with higher averages of mass and AI_{mod} versus decreasing compounds with lower mass, and AI_{mod} , Table 3). Aromatic compounds and atomic masses decreased downstream during high discharge conditions (lower AI_{mod} and lower masses of increasing compounds, Table 3). The relative contribution of N-containing molecular formulae to the overall DOM compound pool increased from Óbidos to the river mouth during all studied discharge scenarios (between 2 and 8% of CHON compounds increased while only 1–3% decreased, Table 3). The CHOS compounds increased generally between 1 and

2% (Table 3) while the increase of CHOP compounds was <1% (not shown).

River water incubation experiments

Incubation experiments with river water from the North Macapá station were performed to decipher the DOM molecular signatures of microbial and photo-degradation. In the photo-degradation treatment, the standard eight dissolved lignin concentrations decreased at a rate of $0.26 \pm 0.03 \mu\text{g L}^{-1} \text{day}^{-1}$ ($n = 3$), whereas the decrease in the bio-degradation treatments was $0.72 \pm 0.09 \mu\text{g L}^{-1} \text{day}^{-1}$ ($n = 3$) (from Ward et al. 2013).

Bio- and photo-transformations altered ca. 26 and 31%, respectively of the molecular formulae detected via FT-ICR-MS (combined significantly decreasing/increasing molecular formulae, Table 4). The molecular trends were comparable, highlighting that a subset of molecular formulae was affected by both, photo- and bio-transformations (Fig. 4). In both treatments, decreasing molecular formulae exhibited significantly higher masses, higher number of C-atoms, and the compounds were less saturated (expressed by lower H/C and higher AI_{mod} values) than the increasing molecular formulae (Table 4). Increasing molecular formulae in the bio-degradation treatment were characterized by a significantly higher relative N content compared to the decreasing molecules, whereas in the photo-degradation treatments these changes were not significant (Table 4).

Comparing in situ river to DOM changes in the incubation experiments

The significantly decreasing/increasing compounds from the September 2011 campaign (Table 3) were not correlated to the significantly decreasing/increasing compounds from the photo- and bio-incubations (Table 4). We also compared the relative change of abundances of the individual molecular formulae from the incubation experiments (Table 4; Fig. 4) to the relative changes of the same molecular formulae in the Óbidos-to-Macapá transect (Fig. 5). The overlap revealed similar changes in the overall molecular composition, i.e. decreasing molecular formulae were less saturated (lower H/C ratios) than the increasing molecular formulae (higher H/C ratios, compare Figs. 4a–5a). The numbers of compounds that were potentially bio- and/or photo-produced in the Óbidos-to-Macapá transect were in the same range but more compounds were potentially bio- than photo-degraded (compare increasing to decreasing compounds in Fig. 5b, c).

We also compared the changing molecular formulae from the incubations experiments (Fig. 4) to the compounds from all river samples and correlated them to the environmental parameters (Supplementary Fig. S1). This approach was applied to capture how the relative abundance of potentially photo- and bio-

transformed molecular formulae is related to environmental factors. Overall, 372 and 349 photo- and bio-transformed compounds were found in the Óbidos-to-Macapá transect (considering all samples) and were significantly correlated to the environmental parameters (Supplementary Fig. S1). Photo- and bio-degraded compounds (mainly with H/C ratios <1) were positively correlated to river discharge and DOC concentrations (red in Supplementary Fig. S1), while photo- and bio-produced compounds (mainly with H/C ratios >1) were negatively correlated to river discharge and DOC concentrations (blue in Supplementary Fig. S1). These trends were not found for photo- and bio-transformed compounds that were correlated to water temperature and lignin concentrations.

Discussion

Bulk geochemical parameters and molecular composition of DOM in the lower Amazon River

The mainstem DOC concentrations of this study are comparable to previously reported values from stations further upstream (Hedges et al. 2000; Richey et al. 1980). The Tapajós River exhibited lower DOC concentrations than the mainstem (Table 1). The Tapajós River is one of the major clearwater rivers

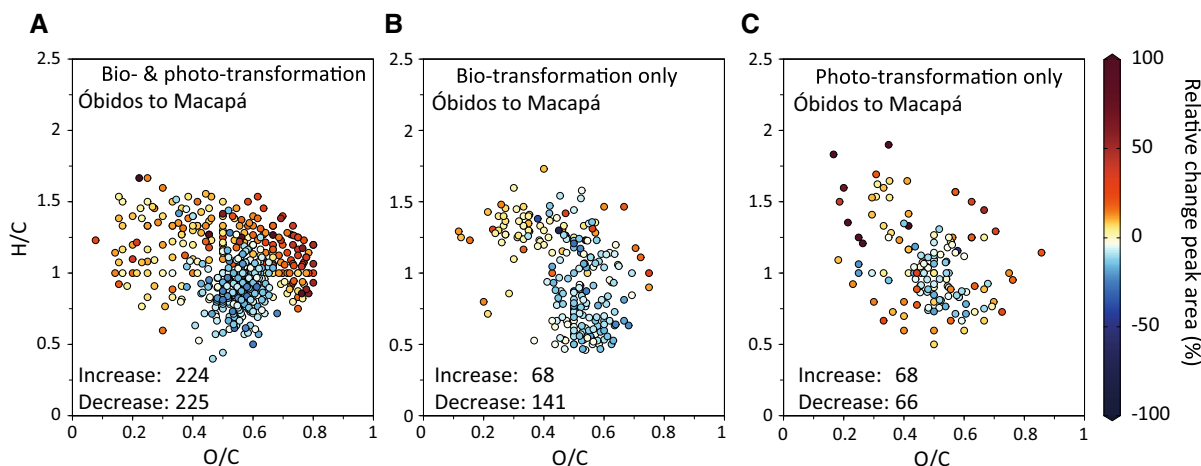


Fig. 5 Van-Krevelen plots of DOM compounds that increased (decreased) relatively in intensity in the river water incubation experiments matched with compounds that also increased (decreased) relatively along the river transect from Óbidos to Macapá, **a** molecular formulae changing in treatments with photo- and bio-transformations alike, and molecular formulae

exclusively changing in treatments with **b** bio-transformation or **c** photo-transformation. The color scale depicts the relative increase (red) or decrease (blue) of the normalized peak area of the molecular formulae from station Óbidos to the river mouth. (Color figure online)

in the Amazon Basin that drains lowland rainforest and savannas (Sioli 1984), and has high algal biomass as indicated by chlorophyll *a* concentrations (Ward et al. 2015). The biological degradation rate of vascular plant-derived DOM is significantly higher in the Tapajós River compared to the mainstem, resulting in a lower abundance of terrestrial biomarkers compared to the Amazon River (Ward et al. 2016). This, along with less DOM input from the watershed compared to black water rivers such as the Negro River, results in relatively low DOC concentrations, which are primarily derived from in situ primary production. This source difference is identifiable in the DOM molecular fingerprint (see discussion below).

The increase of DOC concentrations from Óbidos to the river mouth during high discharge (north and south Macapá stations) and rising discharge (station Belém) highlight additional OM sources compared to the mainstem such as water runoff from floodplains and wetlands and mobilized OM from soils (Field et al. 1998; Moreira-Turcq et al. 2013). At the Macapá channels though, DOC concentrations were also high during low discharge conditions in September 2010, when the Amazonian region was affected by severe drought conditions (Lewis et al. 2011). Because the input of allochthonous DOC to the mainstem is low during low discharge conditions (Ward et al. 2015), additional DOC sources within the river continuum, such as enhanced in situ primary production and the microbial degradation of particulate and suspended matter, are needed to explain the high observations. Microbial degradation, for example, has been shown to increase the transfer of particulate OM into the dissolved phase (Aufdenkampe et al. 2007).

A loss of water due to evapotranspiration is another process that could potentially concentrate DOC along the continuum. This is likely to be most relevant during high and falling water periods considering that river discharge measured at the mouth was 11 and 6% lower, respectively, compared to the sum discharge of the major tributaries and the Amazon River at Óbidos (Ward et al. 2015). The loss of volatile compounds due to evapotranspiration could also change the DOM composition. Water loss due to groundwater recharge is not likely to affect either DOM concentration or composition. In contrast, river discharge at the mouth during low and rising water was between 24 and 38% higher compared to upstream, indicating other potential water sources such as groundwater and the

numerous ungauged tributaries that enter the Amazon River from the north. Since endmember samples were not collected from groundwater or northern tributaries, it is difficult to speculate on how this would alter the DOM composition.

At Tapajós, DOC concentrations were highest during rising and high discharge (Table 1), whereas the concentration of dissolved lignin was lowest during these times (Ward et al. 2015). This finding likely indicates an increased contribution of DOC from autochthonous production and fringing flood plains (Guyot and Wasson 1994), which has been shown to be high during rising and high water periods in the central Amazon basin (Ellis et al. 2012; Moreira-Turcq et al. 2013). At Óbidos, seasonal variations of the quantity of OM input appear to be less pronounced compared to the Tapajós River and stations close to the river mouth, because the DOC concentrations at Óbidos did not change considerably in the course of the sampling. This difference suggests that the lower reach integrates a suite of diverse inputs and transformations, enhancing the expression of variability in bulk DOC concentrations that is discharged to the ocean.

The $\delta^{13}\text{C}$ SPE-DOM values were comparable to the stable carbon isotopic composition of contemporary C3 plants reported previously (Bernardes et al. 2004; Hedges et al. 1986; Mayorga et al. 2005; Quay et al. 1992). Bulk DOM had similar values, with a slightly larger range (−26.1 to −30.4‰), and particulate OM had an even larger range of values from −22.4 to −36.0‰ during the same study period (Ward et al. 2015). Based on these values, degraded tree leaves and woods thus appear to be a main DOM source to the mainstem, whereas C4 grasses or algal material in clearwater tributaries appear to contribute more to particulate OM (Quay et al. 1992; Ward et al. 2015). It is likely that the signature of C4 grasses is not expressed in DOM because grass-derived DOM may be remineralized faster than wood-derived DOM since it has been shown that up to 40% of the organic matter being respired in the river is C4 plant material derived from floodplain grasses (Quay et al. 1992). In fact, ^{13}C -labeled DOM leachates derived from grass were degraded 2.3 times faster than wood-derived leachates along the same study boundaries (Ward et al. 2016). Assuming that C3 plants are a main source for the DOM is consistent with earlier studies (Ertel et al. 1986; Hedges et al. 1994) and is supported by our

finding that most of the river DOM consisted of highly aromatic and highly unsaturated molecular formulae which include lignin degradation products (Stenson et al. 2003), polyphenols (Koch and Dittmar 2006), and combustion-derived compounds (Dittmar and Koch 2006). Molecular formulae with a relatively low hydrogen content (low H/C ratios) are commonly observed in terrestrial DOM due to the high content of aromatic compounds such as degraded lignins and tannins (Schmidt et al. 2009; Sleighter and Hatcher 2008) and mobilized black carbon (Dittmar et al. 2012; Jaffé et al. 2013).

DOM molecular changes in the river water incubation experiments

In both, bio- and photo-transformation treatments, the trends in the overall molecular composition of river DOM were comparable (Fig. 4), highlighting that smaller and more saturated molecular formulae were relatively enriched (lower masses and higher H/C ratios of increasing molecular formulae in Table 4). The breakdown of the eight standard lignin phenols in the photo-incubation treatments in the present study was roughly one third of the rate of biological lignin breakdown previously observed by Ward et al. (2013). While the rate of lignin photo-oxidation was slower than biological degradation, the results of the FT-ICR-MS analyses suggest that a subset of terrigenous compounds is sensitive to both photochemical and biological breakdowns (Fig. 4b). Furthermore, the relative increase of the N-content in compounds of the bio-degradation treatments suggests microbial sources because microbial DOM is relatively enriched in N compared to terrestrial DOM (higher average N content in Table 4) (Kujawinski et al. 2004; Schmidt et al. 2011; Sleighter and Hatcher 2008). The relative enrichment of the smaller DOM molecules after exposure to bio-degradation confirms previous findings of the microbial breakdown of a fraction of the dissolved terrigenous macromolecules within days to weeks (Fasching et al. 2014; Ward et al. 2013).

The relative increase of more saturated compounds (higher H/C ratios of increasing molecular formulae in Table 4) in our photo-degradation treatments supports previous findings that photo-degradation transforms (terrigenous) aromatic compounds into more aliphatic compounds (Medeiros et al. 2015a; Stubbins and Dittmar 2015; Stubbins et al. 2010). Surprisingly, the

decrease of aromaticity of the molecular formulae that were bio- and photo-degradable were comparable in the treatments (increasing compounds with lower average AI_{mod} values in Table 4). Photo- and bio-degradation are important sinks for terrigenous aromatic and polyphenolic compounds in rivers, lakes and the ocean (Fasching et al. 2014; Gonsior et al. 2009; Hernes and Benner 2003; Obernosterer and Benner 2004; Stubbins et al. 2010; Ward et al. 2013). On a single molecular formulae level, our data demonstrate that both processes can be important in shaping the composition of reactive river DOM. In reality, DOM may not be photo-transformed as quickly in the Amazon River. This is because water column mixing in the turbid mainstem with limited light penetration will remove photo-degradable DOM from the surface water thus causing bio-degradation to be potentially more important (Amon and Benner 1996). However, as sediments begin to settle along the lower river and near-shore plume, the potential for photo-oxidation increases (Medeiros et al. 2015b; Seidel et al. 2015b). In line with that we found distinct differences in the DOM composition after photo- and bio-incubations with Amazon River and plume water that were performed in previous studies for longer time periods (Medeiros et al. 2015b; Riedel et al. 2016; Seidel et al. 2015b). In these previous experiments, the shift from higher (pre-incubation) to lower (post-incubation) O/C ratios was more pronounced (Medeiros et al. 2015b; Seidel et al. 2015b) than in the present study (Fig. 4a). Furthermore, after a yearlong incubation it was observed that these molecular trends were reversed: in the late stages of photo- and bio-degradation, compounds with low oxygen numbers were more easily degraded than oxygen-rich compounds (Riedel et al. 2016). The combined results of the studies suggest that photo- and bio-transformation leave different molecular imprints in estuarine and plume DOM, i.e. compounds that escaped degradation and transformations in the river, even allowing to distinguish between photo- and bio-transformations in the plume (Medeiros et al. 2015b).

Seasonal variability of Amazon River DOM

Changes of summer wet and winter dry seasons are important drivers of the Amazon River DOM fingerprints because these were strongly affected by the seasonal changes of the river discharge and DOC

concentrations. Interestingly, the bulk ^{13}C isotopic composition of SPE-DOM was not correlated to its molecular composition (Fig. 2) which is probably due to the strong isotopic imprint of terrigenous DOM from the C3 plants of the forest. Yet, the low seasonal variability of $\delta^{13}\text{C}$ SPE-DOM values does not necessarily imply an invariable input of autochthonous and allochthonous OM. Algae in rivers may grow using isotopically depleted dissolved inorganic carbon, resulting from the mineralization of terrigenous OM (Vuorio et al. 2006). The ^{13}C isotopic composition of SPE-DOM alone therefore appears not to be a reliable predictor for seasonal changes of the allochthonous and autochthonous DOM sources in the Amazon River.

During high discharge conditions (i.e., the wet season around May), the relative abundance of highly aromatic compounds was highest (groups 1 and 2, Supplementary Table S1), highlighting their input from the flooded forest soils and surface runoff. In addition, during high discharge conditions, compounds exhibited higher masses and a higher number of C-atoms and consisted mainly of C, H, and O (molecular formulae positively correlated to discharge and DOC concentrations, Table 2). The elevated DOC concentrations during high discharge were thus probably largely driven by the input of these compounds that were flushed into the river. This finding is likely a result of the greater surface runoff and leaching of organic-rich soil horizons and surface litter during the rainy season. Generally, lignin-enriched plant-detritus or particles from lateral inputs to rivers during high discharge scenarios are a source of dissolved lignin due to desorption, dissolution, and mobilization processes (Hernes et al. 2007).

It is noteworthy that in our study, lignin concentrations were negatively correlated to DOC concentrations taking into account both, mainstem and tributary stations. A separate analysis revealed that dissolved lignin concentrations were highest during high water conditions of the wet season in the mainstem, whereas in the clearwater Tapajós River, lignin concentrations peaked during falling water (Ward et al. 2015). These findings suggest that during high discharge, the mainstem DOM was driven by the input of terrigenous material that is being flushed into the river, while during falling discharge conditions, the input of terrigenous material from tributaries became more important. Likewise, the ratio of dissolved cinnamyl to vanillyl phenols was highest

during low and falling water, indicating an enhanced contribution of macrophytes, which are typically found in floodplains and flushed into the mainstem during falling water (Ward et al. 2015).

Compounds containing N or P were most abundant during low, rising and/or falling discharge conditions (Fig. 3) and they were negatively correlated to discharge and DOC concentrations (Table 2). Higher N- and P-contents are typical for OM derived from phytoplankton and microbial biomass compared to higher land plant material and soils (Burkhardt et al. 1999; Cleveland and Liptzin 2007; Hedges et al. 1986). A recent study has shown higher in situ primary production in the Amazon mainstem and flood plain lakes during low water levels (Vidal et al. 2015). Accordingly, our data indicate a relatively higher input of algal and microbial DOM, mainly during low and falling discharge conditions (i.e., during the seasons with less precipitation).

A relative enrichment of N-containing molecular formulae was observed in our incubation experiments with river water that was exposed to bio-degradation (Table 4). In the river samples, we observed a positive correlation of N-containing molecular formulae with water temperature (Table 2). Although in tropical systems, air and water temperatures exhibit only small seasonal variability, we found slightly higher water temperatures (ca. 3 °C) during low discharge (Table 1). Higher water temperatures during low discharge conditions of the dry seasons were shown to stimulate growth of autochthonous biomass and bacterial production in the Amazon River (Benner et al. 1995; Vidal et al. 2015; Ward et al. 2013). In our study, chlorophyll *a* concentrations were not correlated to the DOM composition during low (September 2011) and falling (July/August 2012) discharge conditions. Our data thus suggest an increased contribution of the N- and P-containing compounds from other sources, for example, release during degradation of particles and from microbial biomass during the dry seasons with lower water discharge (e.g., in September). This conclusion is supported by previously reported quantitative trends of C-to-N ratios of the dissolved phase which were lowest during low discharge conditions in the Amazon River (Ward et al. 2015). In the following, we propose that the seasonally changing molecular imprints can also be used to track the fate of the DOM in the river water during its travel downstream to the river mouth.

Spatial trends in DOM molecular composition

DOM molecular formulae from station Tapajós were distinctly different compared to the mainstem stations at Óbidos and Macapá (e.g., Fig. 3). Clearwater rivers such as the Tapajós exhibit a much lower turbidity than the mainstem hence allowing deeper light penetration supporting more algal growth (Ward et al. 2015). Molecular formulae from diatoms and cyanobacteria are, compared to terrestrial DOM, particularly enriched in N (Landa et al. 2014; Sleighter and Hatcher 2008). Thus, the high abundance of N-containing compounds in the Tapajós tributary compared to the mainstem suggests autochthonous source for these molecules.

We determined the DOM compounds that were relatively enriched (or depleted) as the water is transported from station Óbidos to the river mouth and compared them with molecular formulae that were also enriched (or depleted) in the incubation treatments (Fig. 5). Molecular formulae with H/C ratios >1 that increased relatively in treatments with photo- and bio-transformations also increased at the river mouth (Macapá) compared to station Óbidos (224 increasing compounds in Fig. 5a). This pattern suggests that they have been bio- and/or photo-produced, while compounds with H/C ratios <1 were potentially bio- and/or photo-degraded (225 decreasing compounds in Fig. 5a). In line with the lignin degradation rates from the river water incubations, FT-ICR-MS analyses showed that photo-degradation potentially affected fewer compounds than the biological breakdown of DOM compounds along the Óbidos-to-Macapá transect (exclusively photo-degradable compounds were roughly half the amount of exclusively bio-degradable compounds, Fig. 5b, c). The diminished potential for photo-degradation is likely a result of the high turbidity in the deep Amazon mainstem.

It is important to emphasize that the observed downstream molecular trends such as the relative increase of CHON and CHOS compounds (Table 3) could not be explained by photo- and bio-transformation alone, demonstrating that additional processes affect the river DOM composition. For example, compared to the upriver regions in the more populated areas close to the Amazon River mouth, the relative increase of dissolved organic sulfur- and nitrogen-containing compounds may also be explained by the inflow of wastewater effluent (Gonsior et al.

2011, 2016; Wagner et al. 2015). It can also be expected that a part of the observed trends in the DOM composition (e.g., increase of CHON compounds) is related to the tidally enhanced water exchange in the river estuary (i.e., close to Macapá and Belém). In mangroves, for example, DOC concentration and composition exhibited a pronounced tidal pattern, depending on the regular tidal flooding and draining of the surrounding landscape (Kristensen et al. 2008). The discharge of porewater from downstream wetlands and sulfidic intertidal sediments may also be a source for sulfur- and nitrogen-containing DOM (Seidel et al. 2014; Sleighter et al. 2014). In addition, several molecular formulae from the incubation treatments were correlated to river discharge conditions and DOC concentrations (Supplementary Fig. S1) suggesting a seasonality for these processes.

We note that the incubations were performed with water from near Macapá. A part of the compounds that seasonally changed during the downstream transit in the mainstem may thus have been relatively enriched in the river mouth sample compared to river water near Óbidos. However, the comparable molecular trends (particularly the changes in H/C ratios) highlight the importance of photo-, and probably largely, bio-transformation within the mainstem. Consistent with the results from the bio- and photo-degradation treatments, the average masses of the DOM compounds decreased downstream during high and rising discharge conditions underscoring bio-degradation of DOM along the river (Table 3). Metagenomic and metatranscriptomic inventories along the study boundaries showed an increase in the gene expression ratio, an indicator of per cell activity, from Óbidos to the mouth (Satinsky et al. 2015). Furthermore, during high discharge in 2011, roughly 70% of the bulk bacterial respiration rates were found to be due to dissolved lignin phenol degradation (Ward et al. 2013). However, the downstream changes of the abundance of aromatic DOM compounds varied during the different discharge scenarios. For example, we found a significant increase of molecular masses and aromaticity during falling discharge conditions (Table 3). It was recently shown that during low discharge scenarios only a small proportion (ca. 30%) of the ca. 2-fold higher bulk bacterial respiration rates (compared to high discharge) were due to terrestrial phenol degradation in the Amazon mainstem (Ward et al. 2013). This indicates that during low discharge with higher

bacterial respiration rates, other organic substrates (e.g., from autochthonous sources) than dissolved terrestrial phenols are degraded preferably which may also explain the relative increase of terrestrial aromatic molecular formulae during falling discharge conditions in our study. In contrast, during high discharge, we found a significant decrease of aromatic molecular formulae (increasing compounds with lower AI_{mod} compared to decreasing compounds in Table 3). This highlights that terrestrial phenolic compounds were being more bio-degraded downstream which is supported by the higher lignin phenol degradation rates during high discharge scenarios that were reported by Ward et al. (2013).

We also observed distinct DOM molecular fingerprints that were likely associated with seasonally changing inputs of adjacent tributaries to the mainstem. For example, the percentage of increasing CHON and CHOS molecular formulae increased downstream from Óbidos towards the river mouth (Table 3). It is interesting to note that CHON compounds that were positively correlated to lignin concentrations were mainly aromatic and highly unsaturated compounds (Table 2) suggesting non-protein-like sources. Lignin phenols do not contain nitrogen and therefore these compounds may represent intermediates of the microbial degradation of land-plant material. The highest increase of CHON compounds found during flood scenarios when DOC concentrations increased downstream suggests input from allochthonous sources, because primary production in the mainstem is inhibited during high discharge when the suspended matter load is highest (Moreira-Turcq et al. 2003). It is therefore possible that these spatial changes were driven by inputs from clearwater tributaries (e.g. the Tapajós and Xingú Rivers) and floodplain lakes, where algal biomass is up to an order of magnitude higher compared to the mainstem (Moreira-Turcq et al. 2013; Vidal et al. 2015; Ward et al. 2015). This assumption is supported by the fact that the relative abundance of CHON compounds was always higher in the Tapajós tributary compared to Óbidos with algal- and microbial OM being a likely source for these compounds. The N-containing compounds were also particularly affected by microbial DOM transformations as illustrated by the results of the bio-incubation treatments, thus suggesting advanced bio-alteration of DOM downstream of Óbidos. CHON compounds may also be derived from

desorption of OM from suspended particles since the increase of the N-content of DOM has previously been ascribed to biophysical processes such as solubilization, sorption, and degradation of particulate matter (Aufdenkampe et al. 2007). Consequently, the relative increase of intensities of CHON compounds from Óbidos to the river mouth suggests two main sources and processes contributing to the suite of compounds with heteroatoms. These are, (i) the downstream transition of higher land plant-derived DOM (depleted in heteroatoms) to more algal and microbial DOM (i.e., spatial changes), and (ii) autochthonous production as well as bio-alteration of terrigenous DOM, and likely to a greater extent during high water conditions (i.e., seasonally), due to inputs from floodplain lakes and clearwater tributaries.

Conclusions

In the lower reach of the Amazon River, spatial changes in the DOM molecular composition are mainly the result of changes of the lateral input of allochthonous OM from tributaries, soils, and floodplains as well as the bio- and photo-degradation of DOM. We found that these factors strongly depend on the discharge conditions thus linking spatial and seasonal changes of allochthonous OM input that was found to be highest during flood conditions in the mainstem. The data from photo- and bio-degradation experiments highlight a pool of up to 30% of changing DOM molecular formulae (particularly enriched in heteroatoms N, S, and P) that are likely involved in the active processing of DOM in the river. At the same time, the majority of the riverine (non-changing) DOM molecular formulae (relatively depleted in N, S, and P heteroatoms) appear to be constantly replenished by the input of allochthonous OM from lateral sources and/or less susceptible to rapid alteration within the days it takes water to be transported to the river mouth. Up to 26% of the molecular formulae are subject to seasonal and spatial (downstream) changes possibly representing the more bio- and photo-reactive DOM that fuels the high respiratory CO_2 fluxes which were observed previously (Mayorga et al. 2005; Richey et al. 2002). This DOM pool includes land plant-derived DOM (highly aromatic and unsaturated CHO molecular formulae), but also heteroatom-enriched, more aliphatic DOM presumably from algal

and microbial sources which can be transported into the mainstem from floodplain lakes and clearwater tributaries. The present work extends our previous studies of the Amazon plume (Medeiros et al. 2015b; Seidel et al. 2015b). The results show that, in the Amazon River-to-ocean continuum, extent and locations of the patterns of biogeochemical processes influencing the DOM composition close to the mouth differ from those described previously for upstream at Óbidos and strongly depend on the river discharge conditions. Changes in catchment land use have been previously shown to alter the DOM composition of streams (e.g., Wagner et al. 2015). These connections must be taken into account in global carbon models and future scenarios considering the vast biogeochemical cycles that will be affected if the river hydrology and land use is to change.

Acknowledgements We thank Katrin Klaproth (University of Oldenburg, Germany) for technical assistance. We gratefully acknowledge funding provided by the Gordon and Betty Moore Foundation (ROCA, GBMF-MMI-2293 and 2928) and FAPESP (#08/58089-9). We are also very thankful to the associate editor and the three anonymous reviewers for their detailed and thoughtful comments that greatly improved an earlier version of this manuscript. We further thank the Brazilian government for the opportunity to sample in the Amazon River.

References

- Abril G, Martinez J-M, Artigas LF, Moreira-Turcq P, Benedetti MF, Vidal L, Meziane T, Kim J-H, Bernardes MC, Savoye N, Deborde J, Souza EL, Alberic P, Landim de Souza MF, Roland F (2014) Amazon River carbon dioxide outgassing fuelled by wetlands. *Nature* 505:395–398
- Alsdorf D, Han S-C, Bates P, Melack J (2010) Seasonal water storage on the Amazon floodplain measured from satellites. *Remote Sens Environ* 114:2448–2456
- Amaral J, Suhett A, Melo S, Farjalla V (2013) Seasonal variation and interaction of photodegradation and microbial metabolism of DOC in black water Amazonian ecosystems. *Aquat Microb Ecol* 70:157–168
- Amon RMW, Benner R (1996) Photochemical and microbial consumption of dissolved organic carbon and dissolved oxygen in the Amazon River system. *Geochim Cosmochim Acta* 60:1783–1792
- Aufdenkampe AK, Hedges JI, Richey JE, Krusche AV, Llerena CA (2001) Sorptive fractionation of dissolved organic nitrogen and amino acids onto fine sediments within the Amazon Basin. *Limnol Oceanogr* 46:1921–1935
- Aufdenkampe AK, Mayorga E, Hedges JI, Llerena C, Quay PD, Gudeman J, Krusche AV, Richey JE (2007) Organic matter in the Peruvian headwaters of the Amazon: compositional evolution from the Andes to the lowland Amazon mainstem. *Org Geochem* 38:337–364
- Aufdenkampe AK, Mayorga E, Raymond PA, Melack JM, Doney SC, Alin SR, Aalto RE, Yoo K (2011) Riverine coupling of biogeochemical cycles between land, oceans, and atmosphere. *Front Ecol Environ* 9:53–60
- Benner R, Opsahl S, Chin-Leo G, Richey JE, Forsberg BR (1995) Bacterial carbon metabolism in the Amazon River system. *Limnol Oceanogr* 40:1262–1270
- Bernardes MC, Martinelli LA, Krusche AV, Gudeman J, Moreira M, Victoria RL, Ometto JPHB, Ballester MVR, Aufdenkampe AK, Richey JE, Hedges JI (2004) Riverine organic matter composition as a function of land use changes, southwest Amazon. *Ecol Appl* 14:263–279
- Bianchi TS (2011) The role of terrestrially derived organic carbon in the coastal ocean: a changing paradigm and the priming effect. *Proc Natl Acad Sci USA* 108:19473–19481
- Burkhardt S, Zondervan I, Riebesell U (1999) Effect of CO₂ concentration on C:N:P ratio in marine phytoplankton: a species comparison. *Limnol Oceanogr* 44:683–690
- Casali S, Calijuri MDC, Barbarisi B, Renó VF, Affonso AG, Barbosa C, Silva TSF, Novo EMLDM (2011) Impact of the 2009 extreme water level variation on phytoplankton community structure in Lower Amazon floodplain lakes. *Acta Limnol Bras* 23:260–270
- Cleveland CC, Liptzin D (2007) C:N:P stoichiometry in soil: is there a “Redfield ratio” for the microbial biomass? *Biogeochemistry* 85:235–252
- Coles VJ, Brooks MT, Hopkins J, Stukel MR, Yager PL, Hood RR (2013) The pathways and properties of the Amazon River Plume in the tropical North Atlantic Ocean. *J Geophys Res* 118:6894–6913
- Descy J-P, Darchambeau F, Lambert T, Stoyneva-Gaertner MP, Bouillon S, Borges AV (2016) Phytoplankton dynamics in the Congo River. *Freshw Biol*. doi:10.1111/fwb.12851
- Dittmar T, Koch BP (2006) Thermogenic organic matter dissolved in the abyssal ocean. *Mar Chem* 102:208–217
- Dittmar T, Koch B, Hertkorn N, Kattner G (2008) A simple and efficient method for the solid-phase extraction of dissolved organic matter (SPE-DOM) from seawater. *Limnol Oceanogr Methods* 6:230–235
- Dittmar T, de Rezende CE, Manecki M, Niggemann J, Coelho Ovalle AR, Stubbins A, Bernardes MC (2012) Continuous flux of dissolved black carbon from a vanished tropical forest biome. *Nat Geosci* 5:618–622
- Duarte CM, Cebrián J (1996) The fate of marine autotrophic production. *Limnol Oceanogr* 41:1758–1766
- Ellis EE, Richey JE, Aufdenkampe AK, Krusche AV, Quay PD, Salimon C, da Cunha HB (2012) Factors controlling water-column respiration in rivers of the central and southwestern Amazon Basin. *Limnol Oceanogr* 57:527–540
- Ertel JR, Hedges JI, Devol AH, Richey JE, Ribeiro MDNG (1986) Dissolved humic substances of the Amazon River system. *Limnol Oceanogr* 31:739–754
- Fasching C, Behounek B, Singer GA, Battin TJ (2014) Microbial degradation of terrigenous dissolved organic matter and potential consequences for carbon cycling in brown-water streams. *Sci Rep* 4:4981
- Ferraz LADC (1975) Tidal and current prediction for the Amazon’s north channel using a hydrodynamical-numerical model. Master Thesis, Naval Postgraduate School, Monterey

- Field CB, Behrenfeld MJ, Randerson JT, Falkowski P (1998) Primary production of the biosphere: integrating terrestrial and oceanic components. *Science* 281:237–240
- Furch K, Junk WJ (1997) Physicochemical conditions in the floodplains. In: Junk WJ (ed) *The Central Amazon Floodplain*. Springer, Berlin, pp 69–108
- Gonsior M, Peake BM, Cooper WT, Podgorski D, D'Andrilli J, Cooper WJ (2009) Photochemically induced changes in dissolved organic matter identified by ultrahigh resolution Fourier transform ion cyclotron resonance mass spectrometry. *Environ Sci Technol* 43:698–703
- Gonsior M, Zwartjes M, Cooper WJ, Song W, Ishida KP, Tseng LY, Jeung MK, Rosso D, Hertkorn N, Schmitt-Kopplin P (2011) Molecular characterization of effluent organic matter identified by ultrahigh resolution mass spectrometry. *Water Res* 45:2943–2953
- Gonsior M, Valle J, Schmitt-Kopplin P, Hertkorn N, Bastviken D, Luek J, Harir M, Bastos W, Enrich-Prast A (2016) Chemodiversity of dissolved organic matter in the Amazon Basin. *Biogeosciences* 13:4279–4290
- Guyot JL, Wasson JG (1994) Regional pattern of riverine dissolved organic carbon in the Amazon drainage basin of Bolivia. *Limnol Oceanogr* 39:452–458
- Hedges JI, Clark WA, Quay PD, Richey JE, Devol AH, Santos UDM (1986) Compositions and fluxes of particulate organic material in the Amazon River. *Limnol Oceanogr* 31:717–738
- Hedges JI, Cowie GL, Richey JE, Quay PD, Benner R, Strom M, Forsberg BR (1994) Origins and processing of organic matter in the Amazon River as indicated by carbohydrates and amino acids. *Limnol Oceanogr* 39:743–761
- Hedges JI, Mayorga E, Tsamakis E, McClain ME, Aufdenkampe A, Quay P, Richey JE, Benner R, Opsahl S, Black B, Pimentel T, Quintanilla J, Maurice L (2000) Organic matter in Bolivian tributaries of the Amazon River: a comparison to the lower mainstream. *Limnol Oceanogr* 45:1449–1466
- Hernes PJ, Benner R (2003) Photochemical and microbial degradation of dissolved lignin phenols: implications for the fate of terrigenous dissolved organic matter in marine environments. *J Geophys Res* 108:3291
- Hernes PJ, Robinson AC, Aufdenkampe AK (2007) Fractionation of lignin during leaching and sorption and implications for organic matter “freshness”. *Geophys Res Lett* 34:L17401
- Hess LL, Melack JM, Affonso AG, Barbosa C, Gastil-Buhl M, Novo EM (2015) Wetlands of the lowland Amazon basin: extent, vegetative cover, and dual-season inundated area as mapped with JERS-1 Synthetic Aperture Radar. *Wetlands* 35:745–756
- Jaffé R, Ding Y, Niggemann J, Vähätalo AV, Stubbins A, Spencer RGM, Campbell J, Dittmar T (2013) Global charcoal mobilization from soils via dissolution and riverine transport to the oceans. *Science* 340:345–347
- Junk WJ (1997) General aspects of floodplain ecology with special reference to Amazonian floodplains, *The Central Amazon Floodplain*. Springer, Berlin
- Kim S, Kramer RW, Hatcher PG (2003) Graphical method for analysis of ultrahigh-resolution broadband mass spectra of natural organic matter, the van Krevelen diagram. *Anal Chem* 75:5336–5344
- Koch BP, Dittmar T (2006) From mass to structure: an aromaticity index for high-resolution mass data of natural organic matter. *Rapid Commun Mass Spectrom* 20:926–932
- Koch BP, Dittmar T (2016) From mass to structure: an aromaticity index for high-resolution mass data of natural organic matter. *Rapid Commun Mass Spectrom* 30:250
- Koch BP, Dittmar T, Witt M, Kattner G (2007) Fundamentals of molecular formula assignment to ultrahigh resolution mass data of natural organic matter. *Anal Chem* 79:1758–1763
- Kristensen E, Bouillon S, Dittmar T, Marchand C (2008) Organic carbon dynamics in mangrove ecosystems: a review. *Aquat Bot* 89:201–219
- Kujawinski EB, Del Vecchio R, Blough NV, Klein GC, Marshall AG (2004) Probing molecular-level transformations of dissolved organic matter: insights on photochemical degradation and protozoan modification of DOM from electrospray ionization Fourier transform ion cyclotron resonance mass spectrometry. *Mar Chem* 92:23–37
- Landa M, Cottrell MT, Kirchman DL, Kaiser K, Medeiros PM, Tremblay L, Batailler N, Caparros J, Catala P, Escoubeyrou K, Oriol L, Blain S, Obernosterer I (2014) Phylogenetic and structural response of heterotrophic bacteria to dissolved organic matter of different chemical composition in a continuous culture study. *Environ Microbiol* 16:1668–1681
- Lewis SL, Brando PM, Phillips OL, van der Heijden GMF, Nepstad D (2011) The 2010 Amazon drought. *Science* 331:554
- Malhi Y, Roberts JT, Betts RA, Killeen TJ, Li W, Nobre CA (2008) Climate change, deforestation, and the fate of the Amazon. *Science* 319:169–172
- Manabe S, Milly PCD, Wetherald R (2004) Simulated long-term changes in river discharge and soil moisture due to global warming/Simulations à long terme de changements d'écoulement fluvial et d'humidité du sol causés par le réchauffement global. *Hydrol Sci J* 49:4–642
- Mayorga E, Aufdenkampe AK, Masiello CA, Krusche AV, Hedges JI, Quay PD, Richey JE, Brown TA (2005) Young organic matter as a source of carbon dioxide outgassing from Amazonian rivers. *Nature* 436:538–541
- McClain ME, Richey JE, Brandes JA, Pimentel TP (1997) Dissolved organic matter and terrestrial-lotic linkages in the Central Amazon basin of Brazil. *Glob Biogeochem Cycles* 11:295–311
- Meade RH, Dunne T, Richey JE, Santos UD, Salati E (1985) Storage and remobilization of suspended sediment in the lower Amazon river of Brazil. *Science* 228:488–490
- Medeiros PM, Seidel M, Powers LC, Dittmar T, Hansell DA, Miller WL (2015a) Dissolved organic matter composition and photochemical transformations in the Northern North Pacific Ocean. *Geophys Res Lett* 42:863–870
- Medeiros PM, Seidel M, Ward ND, Carpenter EJ, Gomes HR, Niggemann J, Krusche AV, Richey JE, Yager PL, Dittmar T (2015b) Fate of the Amazon River dissolved organic matter in the tropical Atlantic Ocean. *Glob Biogeochem Cycles* 29:677–690
- Melack J, Forsberg B (2001) *Biogeochemistry of Amazon floodplain lakes and associated wetlands. The biogeochemistry of the Amazon basin and its role in a changing world*. Oxford University Press, Oxford, pp 235–276

- Moreira-Turcq P, Seyler P, Guyot JL, Etcheber H (2003) Exportation of organic carbon from the Amazon River and its main tributaries. *Hydrol Process* 17:1329–1344
- Moreira-Turcq P, Bonnet M-P, Amorim M, Bernardes M, Lagane C, Maurice L, Perez M, Seyler P (2013) Seasonal variability in concentration, composition, age, and fluxes of particulate organic carbon exchanged between the floodplain and Amazon River. *Glob Biogeochem Cycles* 27:119–130
- Nohara D, Kitoh A, Hosaka M, Oki T (2006) Impact of climate change on river discharge projected by multimodel ensemble. *J Hydrometeorol* 7:1076–1089
- Obernosterer I, Benner R (2004) Competition between biological and photochemical processes in the mineralization of dissolved organic carbon. *Limnol Oceanogr* 49:117–124
- Oksanen J, Blanchet FG, Kindt R, Legendre P, Minchin PR, O'Hara RB, Simpson GL, Solymos P, Stevens MHH, Wagner H (2015) Vegan: community ecology package. R package version 2.3-0. <http://CRAN.R-project.org/package=vegan>
- Osterholz H, Dittmar T, Niggemann J (2014) Molecular evidence for rapid dissolved organic matter turnover in Arctic fjords. *Mar Chem* 160:1–10
- Quay PD, Wilbur DO, Richey JE, Hedges JJ, Devol AH (1992) Carbon cycling in the Amazon River: implications from the ^{13}C compositions of particles and solutes. *Limnol Oceanogr* 37:857–871
- R Core Team (2015) R: a language and environment for statistical computing. R foundation for statistical computing, Vienna. <http://www.R-project.org/>
- Raymond PA, Bauer JE (2001) Riverine export of aged terrestrial organic matter to the North Atlantic Ocean. *Nature* 409:497–500
- Raymond PA, Hartmann J, Lauerwald R, Sobek S, McDonald C, Hoover M, Butman D, Striegl R, Mayorga E, Humborg C, Kortelainen P, Durr H, Meybeck M, Ciais P, Guth P (2013) Global carbon dioxide emissions from inland waters. *Nature* 503:355–359
- Remington S, Krusche A, Richey J (2011) Effects of DOM photochemistry on bacterial metabolism and CO_2 evasion during falling water in a humic and a whitewater river in the Brazilian Amazon. *Biogeochemistry* 105:185–200
- Richey JE, Brock JT, Naiman RJ, Wissmar RC, Stallard RF (1980) Organic carbon: oxidation and transport in the Amazon River. *Science* 207:1348–1351
- Richey JE, Mertes LAK, Dunne T, Victoria RL, Forsberg BR, Tancredi ACNS, Oliveira E (1989) Sources and routing of the Amazon River flood wave. *Glob Biogeochem Cycles* 3:191–204
- Richey JE, Melack JM, Aufdenkampe AK, Ballester VM, Hess LL (2002) Outgassing from Amazonian rivers and wetlands as a large tropical source of atmospheric CO_2 . *Nature* 416:617–620
- Riedel T, Zark M, Vähätalo A, Niggemann J, Spencer R, Hernes P, Dittmar T (2016) Molecular signatures of biogeochemical transformations in dissolved organic matter from ten World Rivers. *Front Earth Sci* 4:85. doi:10.3389/feart.2016.00085
- Satinsky B, Fortunato C, Doherty M, Smith C, Sharma S, Ward N, Krusche A, Yager P, Richey J, Moran M, Crump B (2015) Metagenomic and metatranscriptomic inventories of the lower Amazon River, May 2011. *Microbiome* 3:39
- Schmidt F, Elvert M, Koch BP, Witt M, Hinrichs K-U (2009) Molecular characterization of dissolved organic matter in pore water of continental shelf sediments. *Geochim Cosmochim Acta* 73:3337–3358
- Schmidt F, Koch BP, Elvert M, Schmidt G, Witt M, Hinrichs K-U (2011) Diagenetic transformation of dissolved organic nitrogen compounds under contrasting sedimentary redox conditions in the Black Sea. *Environ Sci Technol* 45:5223–5229
- Seidel M, Beck M, Riedel T, Waska H, Suryaputra IGNA, Schnetger B, Niggemann J, Simon M, Dittmar T (2014) Biogeochemistry of dissolved organic matter in an anoxic intertidal creek bank. *Geochim Cosmochim Acta* 140:418–434
- Seidel M, Beck M, Riedel T, Waska H, Suryaputra IGNA, Schnetger B, Greskowiak J, Niggemann J, Simon M, Dittmar T (2015a) Benthic-pelagic coupling of nutrients and dissolved organic matter composition in an intertidal sandy beach. *Mar Chem* 176:150–163
- Seidel M, Yager PL, Ward ND, Carpenter EJ, Gomes HR, Krusche AV, Richey JE, Dittmar T, Medeiros PM (2015b) Molecular-level changes of dissolved organic matter along the Amazon river-to-ocean continuum. *Mar Chem* 177:218–231
- Sholkovitz ER, Boyle EA, Price NB (1978) The removal of dissolved humic acids and iron during estuarine mixing. *Earth Planet Sci Lett* 40:130–136
- Sioli H (1984) The Amazon: limnology and landscape ecology of a mighty tropical river and its basin. *Monogr Biol* 56:763
- Sleighter RL, Hatcher PG (2008) Molecular characterization of dissolved organic matter (DOM) along a river to ocean transect of the lower Chesapeake Bay by ultrahigh resolution electrospray ionization Fourier transform ion cyclotron resonance mass spectrometry. *Mar Chem* 110:140–152
- Sleighter RL, Chin Y-P, Arnold WA, Hatcher PG, McCabe AJ, McAdams BC, Wallace GC (2014) Evidence of incorporation of abiotic S and N into prairie wetland dissolved organic matter. *Environ Sci Technol Lett* 1:345–350
- Spencer RGM, Stubbins A, Hernes PJ, Baker A, Mopper K, Aufdenkampe AK, Dyda RY, Mwamba VL, Mangangu AM, Wabakanghanzi JN, Six J (2009) Photochemical degradation of dissolved organic matter and dissolved lignin phenols from the Congo River. *J Geophys Res.* doi:10.1029/2009JG000968
- Stanley EH, Powers SM, Lottig NR, Buffam I, Crawford JT (2012) Contemporary changes in dissolved organic carbon (DOC) in human-dominated rivers: is there a role for DOC management? *Freshw Biol* 57:26–42
- Stenson AC, Marshall AG, Cooper WT (2003) Exact masses and chemical formulas of individual Suwannee River fulvic acids from ultrahigh resolution electrospray ionization Fourier transform ion cyclotron resonance mass spectra. *Anal Chem* 75:1275–1284
- Stubbins A, Dittmar T (2015) Illuminating the deep: molecular signatures of photochemical alteration of dissolved organic matter from North Atlantic Deep Water. *Mar Chem.* doi:10.1016/j.marchem.2015.06.020

- Stubbins A, Spencer RGM, Chen HM, Hatcher PG, Mopper K, Hernes PJ, Mwamba VL, Mangangu AM, Wabakanghanzi JN, Six J (2010) Illuminated darkness: molecular signatures of Congo River dissolved organic matter and its photochemical alteration as revealed by ultrahigh precision mass spectrometry. *Limnol Oceanogr* 55:1467–1477
- Vidal LO, Abril G, Artigas LF, Melo ML, Bernardes MC, Lobão LM, Reis MC, Moreira-Turcq P, Benedetti M, Tornisielo VL, Roland F (2015) Hydrological pulse regulating the bacterial heterotrophic metabolism between Amazonian mainstems and floodplain lakes. *Front Microbiol* 6:1054
- Vuorio K, Meili M, Sarvala J (2006) Taxon-specific variation in the stable isotopic signatures ($\delta^{13}\text{C}$ and $\delta^{15}\text{N}$) of lake phytoplankton. *Freshw Biol* 51:807–822
- Wagner S, Riedel T, Niggemann J, Vähätalo AV, Dittmar T, Jaffé R (2015) Linking the molecular signature of heteroatomic dissolved organic matter to watershed characteristics in world rivers. *Environ Sci Technol* 49:13798–13806
- Ward ND, Keil RG, Medeiros PM, Brito DC, Cunha AC, Dittmar T, Yager PL, Krusche AV, Richey JE (2013) Degradation of terrestrially derived macromolecules in the Amazon River. *Nat Geosci* 6:530–533
- Ward ND, Krusche AV, Sawakuchi HO, Brito DC, Cunha AC, Moura JMS, da Silva R, Yager PL, Keil RG, Richey JE (2015) The compositional evolution of dissolved and particulate organic matter along the lower Amazon River—Óbidos to the ocean. *Mar Chem* 177:244–256
- Ward ND, Bianchi TS, Sawakuchi HO, Gagne-Maynard W, Cunha AC, Brito DC, Neu V, de Matos Valerio A, da Silva R, Krusche AV, Richey JE, Keil RG (2016) The reactivity of plant-derived organic matter and the potential importance of priming effects along the lower Amazon River. *J Geophys Res* 121:1522–1539



Biodegradation of crude oil and dispersants in deep seawater from the Gulf of Mexico: Insights from ultra-high resolution mass spectrometry



Michael Seidel^{a,b}, Sara Kleindienst^{a,1}, Thorsten Dittmar^b, Samantha B. Joye^a, Patricia M. Medeiros^{a,*}

^a Department of Marine Sciences, University of Georgia, Athens, GA 30602, USA

^b Research Group for Marine Geochemistry (ICBM-MPI Bridging Group), Institute for Chemistry and Biology of the Marine Environment (ICBM), Carl von Ossietzky University of Oldenburg, 26129 Oldenburg, Germany

ARTICLE INFO

Available online 30 May 2015

Keywords:

Oil-biodegradation
Dispersants
Ultra-high resolution mass spectrometry
Corexit
Gulf of Mexico

ABSTRACT

During the 2010 Deepwater Horizon oil spill in the Gulf of Mexico, three million liters of chemical dispersants (Corexit 9500 and 9527) were directly applied at the discharging wellhead at 1500 m water depth. Such a deep-water large-scale application was unprecedented and the effect of dispersants on oil biodegradation is not yet completely understood. The present study explores the biodegradation of oil, dispersant, dispersed oil or dispersed oil and nutrients at the molecular level using ultra-high resolution Fourier-transform ion cyclotron resonance mass spectrometry (FT-ICR-MS) following a laboratory experiment with Gulf deep water. Oil-derived molecular formulae exhibited a specific molecular fingerprint and were mainly observed in the mass range < 300 Da. The relative abundance of heteroatom-containing (N, S, and P) compounds decreased over time in the oil-only treatments, indicating that they may have served as nutrients when oil-derived hydrocarbons were metabolized. Relative changes over time in the molecular composition were less pronounced in the dispersed oil treatments compared to the oil-only treatments, suggesting that dispersants affected the metabolic pathways of organic matter biodegradation. In particular, dispersant addition led to an increase of S-containing organic molecular formulae, likely derived from the surfactant di-octyl sulfosuccinate (DOSS). DOSS and several dispersant-derived metabolites (with and without S) were still detectable after six weeks of incubation, underscoring that they were not rapidly biodegraded under the experimental conditions. FT-ICR-MS fragmentation studies allowed tentatively assigning structures to several of these molecules, and we propose that they are degradation products of DOSS and other dispersant components. The present study suggests preferential degradation, transformation and enrichment of distinct dispersant molecules, highlighting the need to include these compounds when tracking Corexit-derived compounds in the environment.

© 2015 Elsevier Ltd. All rights reserved.

1. Introduction

Between April and July 2010, about 790 million liters of oil were released at a depth of 1500 m during the Deepwater Horizon (DWH) blowout in the northern Gulf of Mexico (hereafter Gulf) (McNutt et al., 2012). During the discharge, 7 million liters of chemical dispersants were used, mostly Corexit 9500A, of which ca. 3 million liters were applied directly to the discharging wellhead (National Response Team, 2011), and smaller amounts of Corexit 9527, which was mainly applied

at the sea surface (Graham et al., 2011; Kujawinski et al., 2011). The deep ocean application of dispersant was unprecedented. Many of the biological and physical factors that determine the distribution and degradation of chemically dispersed oil at sea remain poorly constrained (National Research Council, 2005). For example, there is insufficient knowledge about the rates at which dispersed oil binds to sediments, how quickly it is degraded in the ocean, whether and how it is taken up by organisms, and what (final) products are created during the degradation processes (National Research Council, 2005). The long-term fate of dispersant-derived products in the environment is a subject of ongoing research (White et al., 2014).

Chemical dispersants are applied after oil-spills to emulsify the hydrophobic oil-derived molecules in water and to stimulate biodegradation (National Research Council, 2005). Their primary

* Corresponding author. Tel.: +1 706 542 6744.

E-mail address: medeiros@uga.edu (P.M. Medeiros).

¹ Present address: Center for Applied Geosciences, Eberhard-Karls-University Tuebingen, 72074 Tuebingen, Germany.

purpose is to prevent the formation of thick surface oil slicks by enhancing the solution of oil in water and microbial oil degradation by increasing the bioavailability of the oil in the water column. While dispersants are generally assumed to be less toxic than oil (National Research Council, 2005), the increased oil-in-water solubility could make chemically dispersed oil more toxic to aquatic organisms (George-Ares and Clark, 2000; National Research Council, 2005), including algae (Lewis and Pryor, 2013), micro-zooplankton (Almeda et al., 2014) and fish (Ramachandran et al., 2004). Dispersants can also affect microbial degradation of oil-derived hydrocarbons (Lindstrom and Braddock, 2002). The commercially available dispersants Corexit 9500A and Corexit 9527 contain ca. 10% and 17% mass fraction (w/w%) of the anionic surfactant di-octyl sulfosuccinate (DOSS; Kujawinski et al., 2011), respectively, which has been shown to persist for more than four years after application in the deep ocean (Kujawinski et al., 2011; White et al., 2014).

Quantifying the chemical composition of petroleum remains an analytical challenge (Marshall and Rodgers, 2008). Gas-chromatography (GC) is capable of resolving only a small fraction of oil-derived molecules and most of the molecules that remain at oil-contaminated sites after weathering fall outside the GC-amenable analytical window (Aeppli et al., 2012). Almost 60% of the total mass of organics in Macondo crude oil is not detectable by conventional GC analyses (McKenna et al., 2013). Ultra high-resolution mass spectrometry is an analytical method that is capable of determining the primary molecular composition of oil (Marshall and Rodgers, 2003; Ruddy et al., 2014). The high mass accuracy of Fourier-transform ion cyclotron resonance mass spectrometry (FT-ICR-MS) allows the determination of thousands of molecular formulae in petroleum and dissolved organic matter (DOM; Marshall and Rodgers, 2008). While petroleum characterization via FT-ICR-MS has been the subject of several studies, the molecular characterization of the water-accommodated fraction (WAF) of oil or dispersant-derived compounds has received less attention, and previous studies on oil weathering and biodegradation focused mainly on oil-derived molecules from particulate organic matter (McKenna et al., 2013; Ruddy et al., 2014).

The present study extends the work of Kleindienst et al. (2015b) who explored the effects of dispersants on the activity and composition of oil-degrading microorganisms in a laboratory experiment. In their study, Kleindienst et al. (2015b) found that the application of dispersant significantly changed the microbial community composition within a week and did not enhance rates of hydrocarbon degradation (determined by ¹⁴C-hydrocarbon tracer experiments) or overall microbial activity (estimated by ³H-leucine incorporation rates). Here, we address the molecular compositional changes of the WAF of oil during biodegradation in more detail aiming to answer the following questions: how does the application of dispersant influence the biodegradation of individual compounds in the WAF of oil? Which oil- and dispersant-derived compounds are degraded and which accumulate in the DOM pool? To address these questions, we simulated an oil-in-fusion into deep seawater from the Gulf using laboratory microcosms and applied FT-ICR-MS including collision-induced fragmentation of single molecular formulae to reveal the transformations of DOM on the molecular formula and structural level, including a multitude of dispersant- and oil-derived compounds.

2. Experimental methods

2.1. Experimental design

Experimental microcosms were established using seawater collected from ca. 1200 m water depth at an active natural hydrocarbon seep located at the Green Canyon, block 600 (GC600) in

the Gulf of Mexico in March 2013. All treatments and controls were prepared and sampled in triplicate as described in detail by Kleindienst et al. (2015b). In short, Gulf deep water samples were amended with oil-only (Macondo surrogate from the Marlin platform), dispersant-only (Corexit 9500), dispersed oil, and dispersed-oil+nutrients (ammonium, nitrate, phosphate, and trace metals). Oil-only WAFs were prepared with 0.85 L of sterile seawater amended with 0.15 L Macondo surrogate oil and dispersed oil WAFs were additionally amended with 0.015 L of Corexit 9500. These treatments were mixed on a magnetic stirrer for 48 h at room temperature in the dark. The mixtures were allowed to settle for 1 h and afterwards, the aqueous phase was sub-sampled avoiding the oil or dispersant phases. Seawater controls were either incubated abiotically (0.2 μm filtered and pasteurized, abiotic control) or as biotic control without any nutrient, oil or dispersant addition. All treatments were employed in triplicate in 2 L pre-combusted glass bottles, placed on a roller table, and incubated under oxic conditions (oxygen concentrations were measured at each sampling point) at 8 °C in the dark, which matched the *in situ* temperature for these samples (Kleindienst et al., 2015b). Incubations were performed at atmospheric pressure since the majority of deep sea and seafloor prokaryotes appear to be able to grow at atmospheric pressure with little difference in community composition and incubation pressure (Jannasch et al., 1982; Parkes et al., 2009). Sampling was conducted at 8 °C in the cold room where the incubations were performed. Aliquots (200 mL) for DOM characterization via FT-ICR-MS analysis were collected at the start of the experiment (time zero = T_0), after one week (sampling point 1 = T_1) and after six weeks (sampling point 4 = T_4).

2.2. FT-ICR-MS analysis

Experimental bottles were sampled by inverting the bottles several times to mix them and then withdrawing the necessary volume of water for a given analysis (Kleindienst et al., 2015b). For DOM analysis, a filtered (0.7 μm pre-combusted glass fiber filters, Whatman) seawater sample (ca. 200 ml) was acidified to pH 2 (HCl, p.a.) and DOM was extracted using cartridges filled with a modified styrene divinyl benzene polymer (Agilent Bond Elut PPL, 0.2 g) (Dittmar et al., 2008). The extraction efficiencies were determined as the dissolved organic carbon (DOC) content of an extracted volume of original sample vs. the DOC content in the SPE-DOM (by evaporating an aliquot of methanol extract at 40 °C and re-dissolving the dried extract in ultrapure water). The methanol extracts were stored frozen to avoid esterification reactions between the SPE-DOM and methanol (Flerus et al., 2011). Methanol extracts were diluted 1:1 (v/v) with ultra-pure water to yield a DOC concentration of 12 mg L⁻¹ for the analysis with FT-ICR-MS. Samples were analyzed with a 15 Tesla solarix FT-ICR-MS (Bruker Daltonik GmbH, Bremen, Germany) equipped with an electrospray ionization source (ESI) in negative mode. This mode was chosen because anionic surfactants such as DOSS are readily analyzable by negative ESI-MS (e.g., Kujawinski et al., 2011; Place et al., 2010, 2016). Instrument settings and molecular formulae assignments are described in detail in Seidel et al. (2014). In short, the capillary voltage was 4 kV in negative mode. Ions were accumulated in the hexapole for 0.3 s and data were acquired in broadband mode using 4 megaword data sets and a scanning range of 150–2000 Da with 500 scans accumulated per mass spectrum. Mass spectra were calibrated internally with a list of known CHO compounds in the targeted mass range (achieved mass accuracy < 0.1 ppm). Molecular formulae were assigned to peaks with a signal-to-noise ratio > 4 applying the criteria described by Koch et al. (2007) with a mass tolerance of < 0.5 ppm. The areas of peaks with assigned molecular formulae were

normalized to the sum of all peak areas with identified molecular formulae in each sample and normalized peak intensities were multiplied by a factor of 10,000. The aromaticity and the degree of unsaturation of compounds were assessed using the modified aromaticity (Almod) and double bond equivalent (DBE) indexes, respectively (Koch and Dittmar, 2006).

Collision induced dissociation (CID) fragmentation experiments with the FT-ICR-MS were performed to confirm the presence of selected dispersant-related molecular formulae in the dispersed oil treatments. The quadrupole filter (Q1 mass) of the FT-ICR-MS was set to the nominal mass of each targeted ion (mass window of 1.0 Da). The isolated ions were then fragmented in the hexapole collision cell using Ar with the voltage in the collision cell (8–17 V) and ion accumulation time (0.5–1.0 s) adjusted to obtain optimum ratios of parent ion to fragment ions for each targeted compound. The resulting CID mass spectra were calibrated externally with full scan mass spectra of the same samples. Structures were tentatively assigned based on exact masses and calculated elemental composition of their parent and fragment ions and neutral losses (mass tolerance < 0.3 ppm).

Changes in the DOM molecular composition were assessed in the triplicate samples by applying a paired Student's *t*-test (after confirming normal distribution using Shapiro–Wilk's test of normality) comparing the normalized peak heights of the molecular formulae at each time point considering only molecular formulae that were present in each triplicate of the individual treatments. Changes were considered significant if $p < 0.01$. This approach eliminated inter-sample variability based on peaks with low relative abundances that were close to the limit of the detection of the FT-ICR-MS. Molecular formulae associated with the addition of dispersant were identified using differential mass spectra (Osterholz et al., 2014), i.e., by subtracting the averaged normalized peak intensity of each identified molecular formulae (means of triplicates for each treatment) in dispersant-containing incubations from dispersant-free incubations, i.e., abiotic control vs. dispersant-only, oil-only vs. dispersed oil, and oil-only vs. dispersed-oil-nutrients. Taking this approach, negative differences highlight molecular formulae that were relatively enriched in the three dispersant-amended treatments in comparison to the three non-dispersant-amended treatments and, consequently, these molecular formulae were tentatively identified as being associated with the dispersant addition (Supplementary Table S3, Fig. S4).

We note that ESI-FT-ICR-MS is not a quantitative tool for complex natural DOM mixtures due to the lack of standards and potential differences in the ionization efficiencies for different compounds. Nonetheless, under similar analytical conditions the analysis yields reproducible results (Kido Soule et al., 2010) even allowing for the quantification of known organic contaminants in seawater incubation experiments, for instance, by performing standard addition (Schwedt et al., 2015). In the present study, we used normalized peak areas to assess changes in the molecular DOM composition, i.e., by calculating peak intensity-weighted averages of Almod, DBE, molar ratios (H/C, O/C) and the number of heteroatoms (N, S, and P). The relative enrichment and/or depletion of DOSS and mono-octyl sulfosuccinate (MOSS, both determined by FT-ICR-MS) was substantiated by quantitative measurements using liquid chromatography tandem mass spectrometry (Place et al., 2016) and these quantitative data are reported elsewhere (Kleindienst et al., 2015b).

Correspondence analysis (CA) was performed using the vegan package (Oksanen et al., 2013) within the R statistical platform (R core team, 2014). CA is an ordination method maximizing the correspondence between species scores (i.e., molecular formulae) and sample scores (i.e., incubation treatments) (e.g., Ramette, 2007). CA is particularly useful if the analyzed species show an unimodal relationship within the samples, e.g., when certain

species show peak abundances under certain conditions (ter Braak, 1985), such as oil-derived molecular formulae in oil-only incubations. Only molecular formulae that were present in all triplicates of the individual incubation treatments were taken into account and normalized peak intensities were averaged and used as relative species abundances for CA.

3. Results and discussion

3.1. Extraction efficiencies

Solid-phase extraction (SPE) using PPL cartridges with styrene divinyl benzene polymer resins was applied to extract di-octyl sulfosuccinate (DOSS) from seawater samples in a previous study (Kujawinski et al., 2011). In our samples, the overall DOM extraction efficiencies based on organic carbon yield in the dispersant-amended treatments were lower (ca. 20–30%) than the oil-only (ca. 65%) or seawater-only (ca. 70%) treatments (Fig. S1). The reduced recoveries of dispersant-amended samples suggest that the dispersant affected adsorption of DOM to the PPL resin. Styrene-divinyl-benzene-based sorbents (such as PPL) retain organic analytes due to hydrophobic interactions (Fontanals et al., 2005). However, micelle formation *via* oil-dispersant interaction increases the polarity of oil-components so that micelle-entrapped oil-derived DOM becomes more hydrophilic (Campo et al., 2013). It is possible that in the dispersant-amended treatments micelle-formation reduced the amount of oil-derived DOM that adsorbed to the SPE resin, resulting in the lower observed extraction efficiencies. Compounds with O/C < 0.3 and H/C > 1 were less efficiently extracted from the dispersed oil treatments (with/without nutrients) compared to the abiotic (seawater-only) controls and the oil-only treatments (both treatments not being affected by micelle formation). For example, oil molecular formulae exhibited particularly low O/C ratios (intensity-weighted average of oil O/C 0.3 ± 0.2 , Supplementary Table S1, vs. seawater O/C 0.4 ± 0.1 , Supplementary Table S2). Hence, oil-derived compounds were readily identifiable because they clustered in a specific region in van-Krevelen space of oil-only treatments. Oil molecular formulae were less abundant in the dispersed oil treatments (missing molecular formulae with O/C < 0.3 and H/C > 1 in van-Krevelen space in dispersed oil treatments in Fig. 1). In the oil-only treatments, molecular formulae that were derived from oil (“Oil SPE-DOM” in Fig. 2C and E) also had noticeably higher relative intensities than marine DOM (compare “Seawater SPE-DOM” in Fig. 2A with C and E). The same molecular formulae had lower intensities in the dispersed oil treatments where seawater SPE-DOM compounds exhibited higher relative intensities (see small insets in Fig. 3A and C). On the one hand, the high peak intensities of oil-derived molecular formulae in the oil-only treatments (“Oil SPE-DOM” in Fig. 2C and E) and dispersant-derived molecular formulae in the dispersant-amended oil treatments (e.g., DOSS and MOSS in Fig. 3A and C) indicate that these compounds compete more efficiently for the negative charges in the electrospray source hence suppressing the intensity of the natural DOM ions (“Seawater SPE-DOM” in Fig. 2C and E and Fig. 3A and C). On the other hand, the lower relative abundances of oil-derived ions in the dispersed-oil treatments also suggest that the poorly retained suite of molecules were mainly oil-derived. Micelle formation therefore appears to be a likely reason for the lower DOM extraction efficiencies in the dispersed oil samples. Thus, direct comparison of the SPE-DOM molecular composition of oil samples with the dispersed oil samples may be hampered due to those differences in PPL extraction efficiencies. However, the DOM extraction efficiencies were consistent for the individual treatments over the course of the experiment (Supplementary Fig. S1). Thus, the SPE-DOM

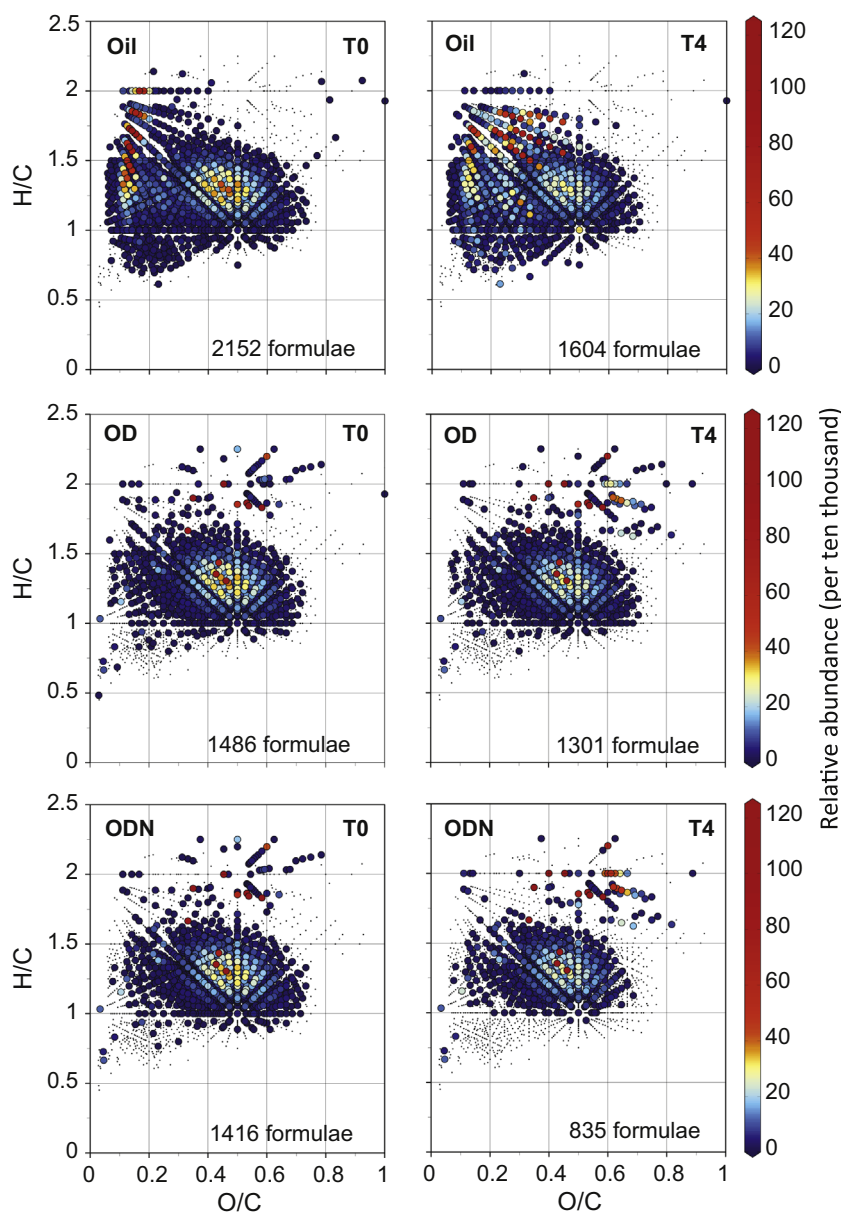


Fig. 1. Van-Krevelen-plots (O/C, oxygen-to-carbon and H/C, hydrogen-to-carbon ratios) containing all assigned molecular formulae in the abiotic seawater control (abiotic), oil-only (Oil), oil-dispersants (OD) and oil-dispersants-nutrients (ODN) treatments at the initial time point (T_0) and after six weeks of incubation (T_4). Each circle represents one molecular formula. The color scale illustrates the relative abundance of compounds (normalized to the sum of the peak areas with assigned molecular formulae in the triplicates $\times 10,000$). Grey dots depict molecular formulae not present in respective treatment but detected in other treatments.

molecular compositions of different time points for each treatment are comparable to each other.

3.2. Molecular composition of oil-derived DOM

We assigned molecular formulae to $74 \pm 2\%$ of the peaks in the FT-ICR-MS measurements ($n=52$) across the treatments (not taking into account ^{13}C isotope peaks). In total, 4176 molecular formulae were assigned to the DOM molecules across the experimental treatments. The t -test was applied to the FT-ICR-MS measurements of the abiotic control treatments and to control measurements of North Equatorial Pacific Intermediate Water (NEqPIW) reference (Osterholz et al., 2014), which was run frequently in between samples to assess instrument variability. Of the molecular formulae, $\leq 1\%$ changed if $p < 0.01$ when comparing T_0 to T_4 of the abiotic control. Changes of the relative abundance of

molecular formulae in NEqPIW reference (i.e., analytical variability of the FT-ICR-MS) were $\leq 3\%$ at $p < 0.01$. This confirms the robustness of the applied statistical approach.

The DOM composition was distinctly different in the oil-only treatments compared to the dispersant-amended treatments (Fig. 1). For instance, less molecular formulae were identified in the dispersed oil incubations (Supplementary Table S1), likely because of variability in extraction efficiencies and due to dispersant-derived ions suppressing the intensity of natural seawater and oil-derived ions. Comparing the results from the seawater-only and the oil-only treatments, which were characterized by similar extraction efficiencies (Supplementary Fig. S1) indicated strong differences in the molecular composition of the treatments (Fig. 2). Through correspondence analysis (CA), the oil incubations separated clearly from the seawater samples along the second CA axis (CA2, Supplementary Fig. S2A). Molecular formulae in the

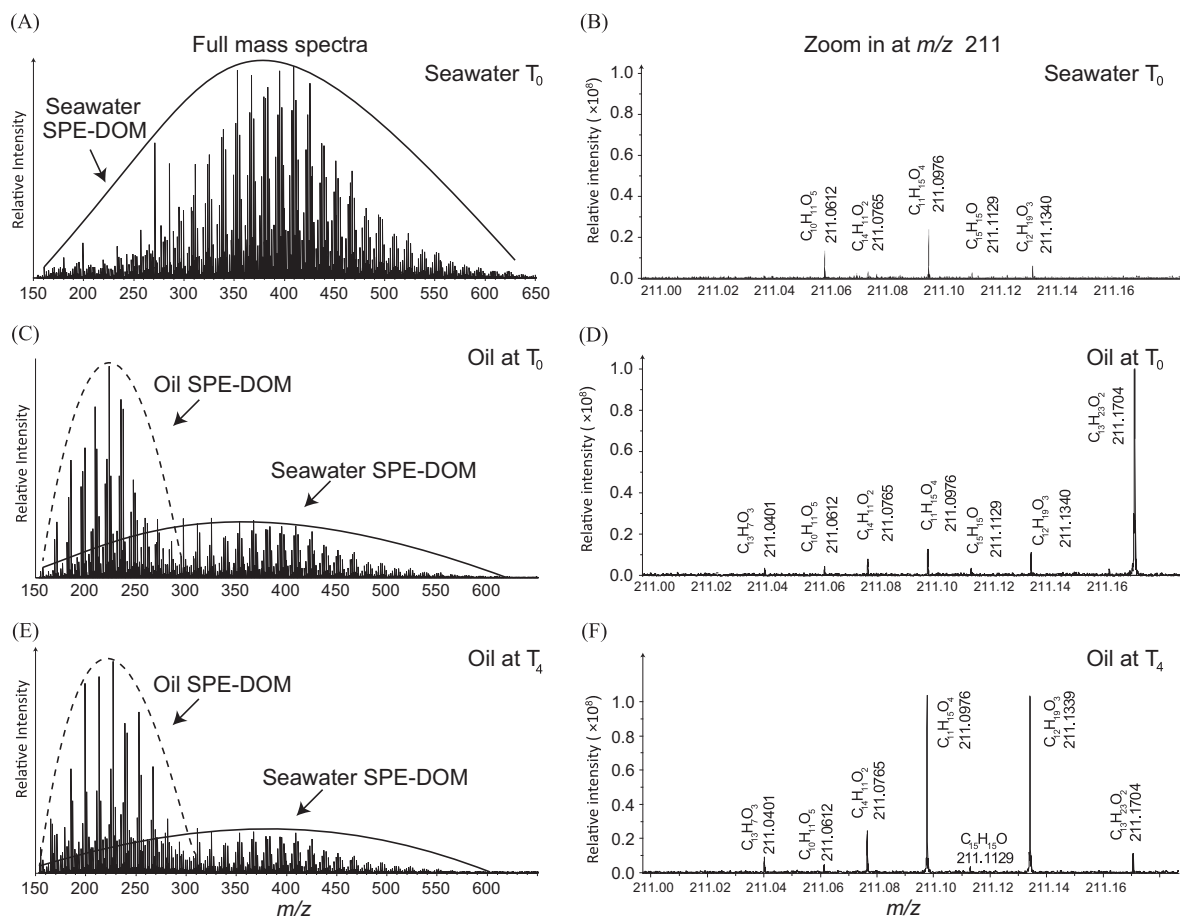


Fig. 2. ESI-FT-ICR mass spectra (mass range 150–650 Da, A, C, and E) and expanded mass range at 211 Da (B, D, and F) of the initial seawater samples (A and B, seawater T_0), initial and final oil-only incubations (C and D, oil T_0 , initial time point; E and F, oil T_4 , after six weeks of incubation). Highest relative intensities of oil-derived molecular formulae (“Oil SPE-DOM”) were found in the mass range < 300 Da whereas marine DOM (“Seawater DOM”) peaked in the 400 Da mass range. Note that the relative intensity scales in the right panel are in the same range to illustrate the higher relative intensities of oil-derived compounds in the oil-only treatments vs. marine DOM in the seawater-only sample.

oil-only incubations had a lower molecular weight (intensity-weighted average mass ca. 337 Da, Supplementary Table S1) than compounds in the seawater-only samples (ca. 400 Da, Supplementary Table S2; compare blue circles plotting close to oil samples to yellow and red circles plotting close to biotic control and seawater sample in Supplementary Fig. S2A). Thus, the WAF of oil-derived SPE-DOM (Fig. 2C and E) was of smaller molecular size than the natural marine SPE-DOM (Fig. 2A). In addition, more molecular formulae with higher relative intensities were found in the mass range < 300 Da in mass spectra of the oil-only treatments in comparison to the seawater samples (Fig. 2B, D, and F). This is consistent with previous ESI-FT-ICR-MS analyses of crude oil which showed high relative abundances of molecular formulae in the ≤ 300 Da mass range (Corilo et al., 2013). In the present study, the WAF of oil molecular formulae clustered in specific areas in van-Krevelen space: molecular formulae with negative loadings on CA2, which were most abundant in the oil-only incubations, exhibited lower O/C ratios than the natural marine SPE-DOM (blue circles in Supplementary Fig. S2C). The intensity-weighted average oil O/C ratios were ca. 0.3 whereas abiotic and biotic treatments with seawater had O/C ratios between 0.4 and 0.5, respectively (Supplementary Tables S1 and S2). Thus, the WAF of the analyzed oil exhibited a specific molecular fingerprint which can be used to track the fate of these compounds during incubation. In fact, the oil molecular fingerprint can be useful to identify future oil spill sources in the environment (Corilo et al., 2013).

3.3. Biodegradation of oil-derived DOM

In the oil-only treatments, biodegradation led to a large decrease in the molecular weight and in the number of carbon atoms of DOM molecular formulae (Supplementary Table S1). In these treatments, the relative intensity of molecular formulae in the mass range < 300 Da increased with time (Fig. 2D and F). Molecular weight changes in the other treatments were generally much smaller. In all treatments, on average more compounds were degraded than produced (Table 1), implying their mineralization and/or incorporation into biomass.

We grouped the molecular formulae across the treatments into three categories: compounds containing CHO only and compounds containing N or S (CHON or CHOS, respectively, Fig. 4). In the oil-only incubations, the relative decrease of molecular formulae was pronounced in all three compound groups (CHO, CHON, CHOS in Fig. 4A–C). Except for CHOS molecular formulae (Fig. 4C), compounds that increased in relative abundance were generally less oxygenated and thus had lower O/C ratios than the ones that were degraded (Table 1). The CHO molecular formulae that increased over the course of the incubation clustered in two specific areas in van-Krevelen space, (i) $H/C > 1.5$ and $O/C < 0.4$ and (ii) $H/C \approx 1$ and $O/C < 0.4$ (Fig. 4A–C). Thus, in the oil-only incubation, biodegradation led to an increase of the relative abundance of smaller (lower mass and lower number of C), more saturated (lower DBE values) and slightly less oxygenated (lower O/C ratios) molecular formulae (Table 1).

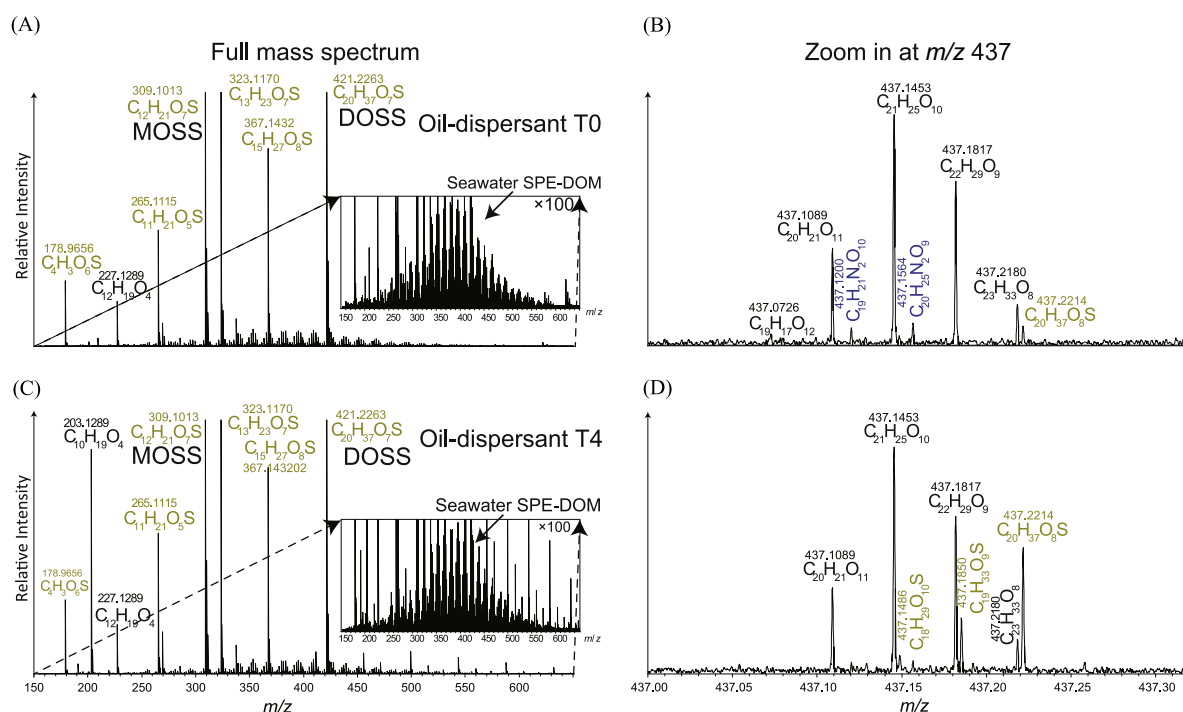


Fig. 3. ESI-FT-ICR mass spectra (mass range 150–650 Da, A and C) and expanded mass range at 437 Da (B and D) of the dispersant-amended oil incubations with selected CHO (black), CHON (blue) and CHOS (yellow) molecular formula assignments at different incubation time points (A and B, T_0 initial time point; C and D, T_4 after six weeks). DOSS and MOSS molecular formulae are marked in A and C. The small insets show the distribution of oil- and seawater-derived DOM peaks in the expanded intensity range (magnification 100x, compare to Fig. 2A). The mass spectra on the right panel were magnified at 437 Da because a pronounced relative increase of S-containing molecular formulae was observed in that mass range. (For interpretation of the references to color in this figure legend, the reader is referred to the web version of this article.)

Table 1

Compositional DOM changes in the oil-amended incubation treatments expressed as intensity-weighted averages (of triplicates) of molecular parameters for compounds that significantly increased or decreased over the course of the incubations.

	Oil		Dispersed oil		Dispersed-oil-nutrients	
	Decreasing ^a	Increasing	Decreasing	Increasing	Decreasing	Increasing
Formulae	534	105	71	21	145	17
Mass	386.5 ± 57.7	215.7 ± 36.4	374.1 ± 81.8	248.2 ± 135	385.7 ± 52.5	444.9 ± 61.7
C	19.1 ± 2.8	11.9 ± 2.2	18.1 ± 4.3	11.4 ± 4.8	18 ± 2.7	18.7 ± 3.1
H	24.9 ± 4.3	18.3 ± 5.2	24.1 ± 6.8	22.1 ± 8.3	23.1 ± 4	33.8 ± 7.5
O	8.1 ± 2.2	3.4 ± 0.9	8 ± 2.2	5.4 ± 3.9	9 ± 1.5	11 ± 2.4
N	0.1 ± 0.4	0 ± 0.1	0.2 ± 0.5	0 ± 0.4	0.1 ± 0.4	0.2 ± 0.7
S	0.03 ± 0.2	0.02 ± 0.1	0.11 ± 0.3	0.1 ± 0.4	0.05 ± 0.2	0.3 ± 0.5
P	0 ± 0.02	0 ± 0	0 ± 0	0.002 ± 0.059	0 ± 0	0.011 ± 0.113
H/C	1.3 ± 0.1	1.5 ± 0.3	1.3 ± 0.2	2 ± 0.2	1.3 ± 0.1	1.8 ± 0.2
O/C	0.4 ± 0.1	0.3 ± 0.1	0.4 ± 0.1	0.5 ± 0.2	0.5 ± 0	0.6 ± 0.1
DBE	7.7 ± 1.5	3.7 ± 2.1	7.1 ± 1.8	1.4 ± 1.6	7.5 ± 1.3	2.9 ± 2.8
AI_{mod}	0.24 ± 0.08	0.2 ± 0.19	0.22 ± 0.1	0 ± 0.04	0.22 ± 0.07	0.03 ± 0.12

^a Changes were significant with $p \leq 0.01$. Intensity-weighted averages were calculated using the normalized peak intensities that were averaged across triplicates. The intensity-weighted standard deviation (\pm value) represents the range of molar ratios in the respective group (increasing or decreasing compounds) and does not represent the analytical deviation of replicate measurements.

The relative decrease of the molecular size of compounds with advancing degradation is consistent with earlier reports about oil-degradation (Lemkau et al., 2014). However, previous studies of oil-weathering reported a relative increase of oxygenated organic compounds (Aeppli et al., 2012; Hall et al., 2013; Lemkau et al., 2014), whereas we observed only small changes in O/C ratios of DOM (Table 1). A reason for this difference may be that the previous studies reported the weathering of solid oil residues that were exposed to combined photo- and biodegradation, whereas the incubations of the present study involved biodegradation in the absence of light. Photo-oxidation has been shown to increase the relative abundance of oxygen in weathered oil (Garrett et al., 1998), which could explain why previous studies observed a

relative increase of O-content in light-exposed samples.

In general, the infusion of bioavailable organic carbon substrates can cause nutrient limitation which in turn may reduce accumulation of microbial biomass and limit carbon mineralization rates (Chapman, 1997). Specifically, the degradation of organic carbon substrate such as oil is often limited by the availability of inorganic substrates such as N, S and P (Atlas and Bartha, 1972; Chapman, 1997; Röling et al., 2002). We found that the relative abundance of several N- and S-containing formulae decreased substantially in the oil-only incubations (Fig. 4A–C) and molecular formulae that decreased contained more N and S than those which increased (Table 1). The decrease of P-containing compounds was less pronounced (Table 1) but still noticeable as the overall P

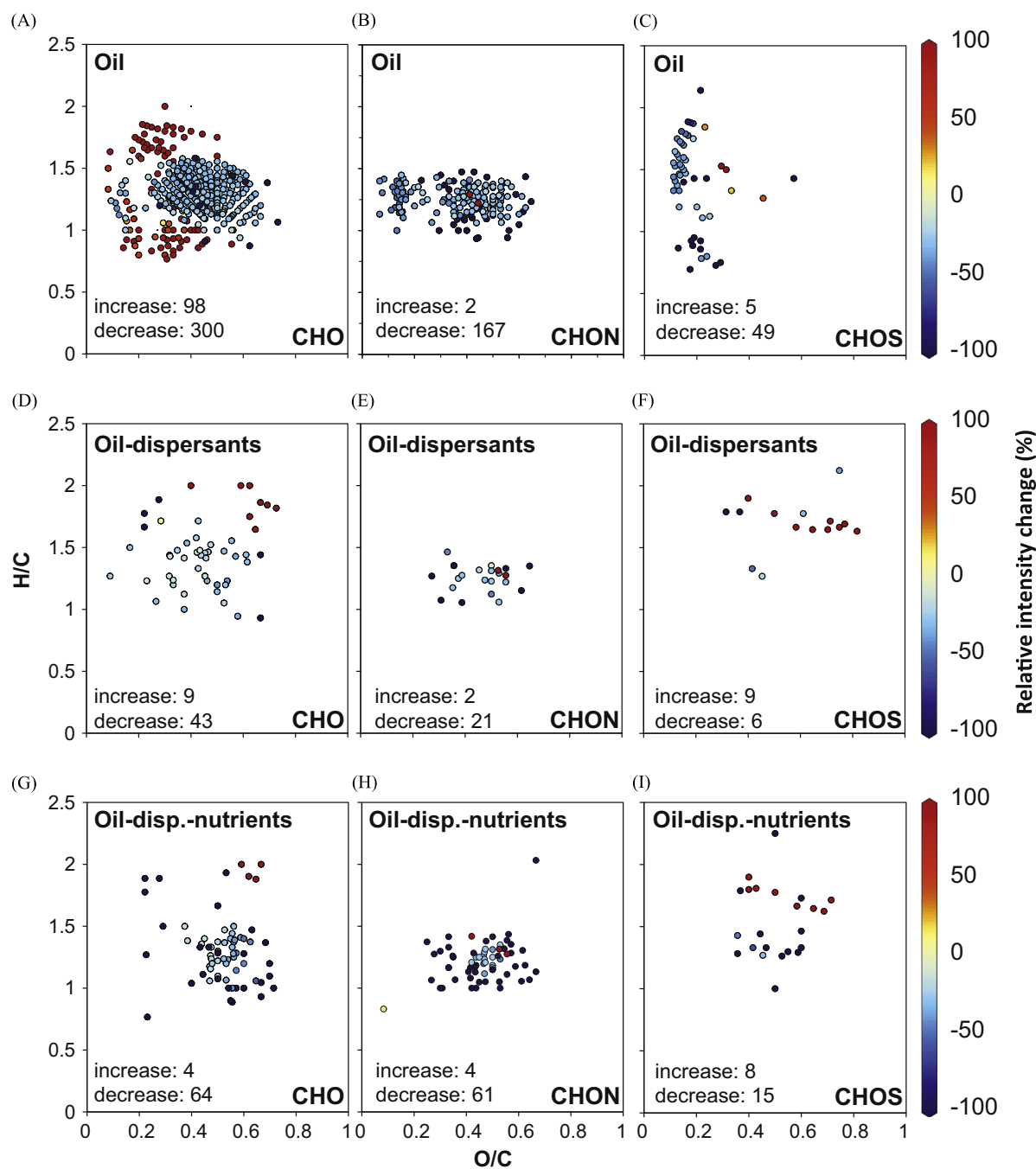


Fig. 4. Van-Krevelen plot of molecular formulae that changed significantly ($p < 0.01$, $n=3$) in relative abundance in the three oil-containing treatments (A–C oil-only, D–F dispersed oil, G–I dispersed oil + nutrients) over the course of the incubation considering all molecular formulae in each treatment. Molecular formulae were grouped according to their heteroatom content, i.e., no heteroatoms (CHO, left panel), N-containing (CHON, middle panel) or S-containing (CHOS, right panel). The color-scales represent a relative increase (red) or a relative decrease (blue) in peak intensity (in %) over the course of the incubation. (For interpretation of the references to color in this figure legend, the reader is referred to the web version of this article.)

content of the detected molecular formulae decreased in the oil-only and dispersed-oil treatments (Supplementary Table S1). It is possible that oil-derived and seawater DOM served as N, S and P sources to the microorganisms growing in the oil-amended treatments and that these nutrients fueled the observed accumulation of biomass when CHO compounds were metabolized. In particular, N-containing oil compounds were proposed to serve as substrate for microbes when N assimilation is stimulated during oil degradation (Lu et al., 2012) and several N-compound oil classes have been shown to undergo significant degradation (Corilo et al., 2013). The data presented here argue strongly for

microbial assimilation of both seawater and oil-derived nitrogen to support their growth.

In all dispersed-oil incubations, fewer molecular formulae were identified in comparison to the oil-only treatment (Supplementary Table S1), which was most likely because a range of molecules was trapped in micelles and thus not extractable *via* SPE. Nonetheless, the extraction efficiencies in each treatment did not vary significantly in the course of the incubations (Supplementary Fig. S1), indicating that the relative molecular changes are comparable for the dispersant-containing treatments. Despite the difference in extraction efficiencies, relative changes in the molecular composition were less

pronounced in the dispersed oil treatments, both with nutrients (145 decreasing formulae out of 1416 at T_0 , ca. 10%) and without nutrients (71 decreasing formulae out of 1486 at T_0 , ca. 5%), than in the oil-only treatments (534 decreasing formulae out of 2152 at T_0 , ca. 26%). This indicates that the microbial turnover of oil-derived compounds was higher in the oil-only treatments compared to the dispersed oil treatments (Kleindienst et al., 2015b). These findings point towards a negative impact of dispersants or dispersant-oil mixtures on microbial hydrocarbon degradation (reviewed in Kleindienst et al., 2015a). Furthermore, in the dispersed oil incubations molecular formulae that increased had a lower molecular weight (ca. 248 ± 135 Da, Table 1) than the decreasing molecular formulae (ca. 374 ± 82 Da, Table 1), while the opposite was the case in the oil-dispersant-nutrients treatment (compounds increasing ca. 445 ± 62 Da and decreasing ca. 386 ± 53 Da, respectively, Table 1). This infers that the nutrient supply in the oil-amended treatments affected which organic molecules were microbially metabolized. In both dispersed-oil treatments (with/without nutrient addition), increasing compounds were more saturated compared to increasing compounds of the oil-only treatments, i.e., they were characterized by lower DBE and aromaticity (Almod) indexes (Table 1). These differences in the transformation and mineralization of DOM between the treatments are probably due to the significant changes in the microbial community compositions and the potential ability of certain microbes to utilize dispersants-derived compounds as growth substrates (Kleindienst et al., 2015b).

Dispersants can serve as additional growth substrates in oil-contaminated environments (Atlas and Bartha, 1972; Foght and Westlake, 1982; Röling et al., 2002). Nutrient addition can decrease substrate limitation caused by insufficient supply of inorganic N

and P for oil-degrading microbes when dispersant is applied (Foght and Westlake, 1982). The number of compounds decreasing in relative abundance was higher in the dispersed oil incubations with nutrient amendment (145 out of 1416 molecular formulae at T_0 , ca. 10%) than in the dispersed oil incubations lacking nutrient addition (71 out of 1486 molecular formulae at T_0 , ca. 5%, Table 1). These data underscore that the addition of nutrients to the dispersed oil treatment stimulated the degradation of oil-derived DOM in comparison to the dispersed oil treatment, which lacked nutrient amendment. Nutrient addition is frequently used as a bioremediation strategy, e.g., for cleanup of petroleum-contaminated groundwater (Chapelle, 1999). Based on these findings, it appears that addition of nutrients stimulated the biodegradation of oil in the presence of dispersants. More studies are required to fully assess the utility of a combined dispersant-nutrients application as a response to an oil spill event.

3.4. Sulfur compounds in the dispersant-amended treatments

The surfactant DOSS (m/z 421) is a component of both Corexit 9500A and Corexit 9527 (Kujawinski et al., 2011), and it can quickly hydrolyze to MOSS (m/z 309) in water (Campo et al., 2013). Therefore, the presence of S-containing molecular formulae in the dispersant-amended treatments was expected, since these compounds contain sulfonyl moieties (Supplementary Table S1; for molecular structures see Fig. 5).

In correspondence analysis (CA) ordination, all three dispersant-amended treatments were separated from the non-dispersed samples (oil-only, biotic control) along the first CA axis (CA1, Supplementary Fig. S2A) due to the relatively high

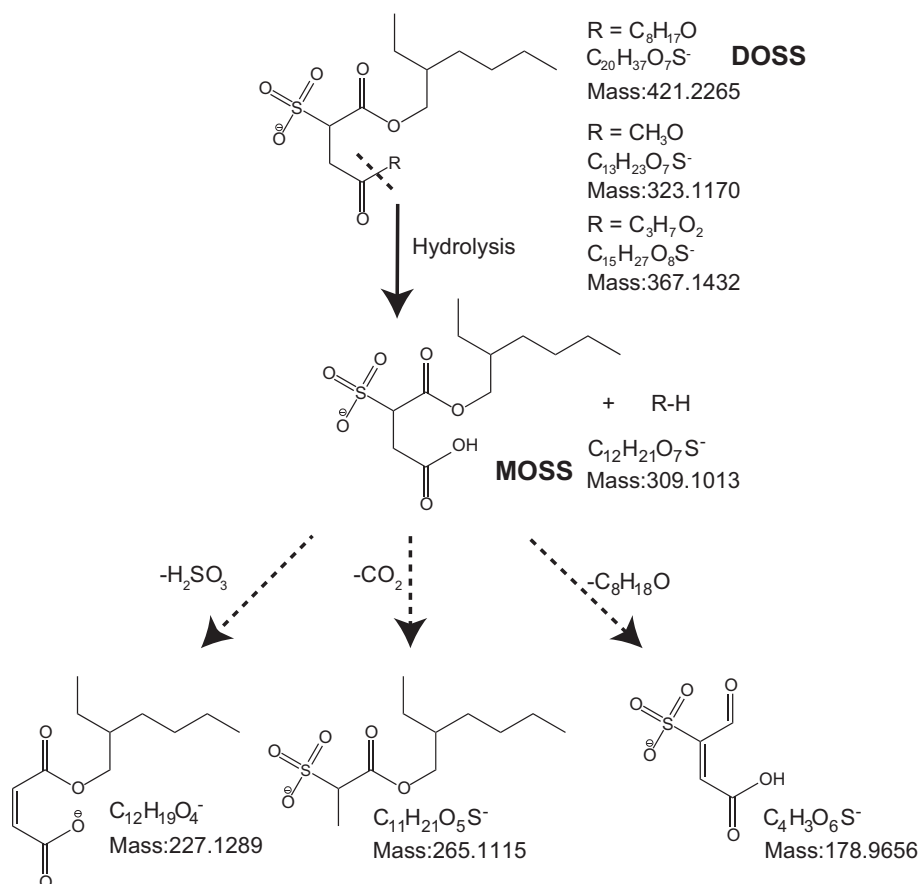


Fig. 5. Hydrolysis of di-octyl sulfosuccinate (DOSS) and tentatively identified dispersant-related molecules with different side chains (R) to mono-octyl sulfosuccinate (MOSS) (solid arrow) and proposed structures of compounds that were detected in the dispersant-amended treatments via ESI-FT-ICR-MS. Tentatively assigned structures are based on FT-ICR-MS collision-induced dissociation fragmentation spectra and exact molecular masses. Proposed degradation pathways are depicted with dashed arrows.

abundance of molecular formulae which were absent in the samples that did not contain dispersants (red circles in van-Krevelen plot of CA1 species scores in Supplementary Fig. S2B). Furthermore, we observed a relatively high abundance of S-containing compounds other than DOSS and MOSS in the dispersant-amended treatments (Fig. 3A and C). The intensity-weighted average S-content was also higher in the dispersant-amended treatments ($S=0.4 \pm 0.5$ at T_0 , compared to $S=0.1 \pm 0.2$ in oil-only treatment, Supplementary Tables S1), highlighting that, besides DOSS and MOSS, several S-containing compounds were added at T_0 or created following dispersant addition (Supplementary Table S3). The S-containing compounds that were transformed in the dispersed oil incubations (with/without nutrient addition, Fig. 4F and I) had a different molecular composition than the ones transformed in the oil-only incubations (Fig. 4C), i.e., they occupied different regions in van Krevelen space, suggesting that the microbial transformation of CHOS compounds in the dispersed oil samples was affected by the addition of the S-containing dispersant.

Previous studies have reported that DOSS was not readily biodegradable in the deep water plume after the DWH blow-out since it was still detectable several kilometers away from the actively flowing wellhead (Kujawinski et al., 2011), and persisted for up to four years in samples from Gulf beaches (White et al., 2014). DOSS is a major component of several Corexit formulations (Mathew et al., 2012; Ramirez et al., 2013) and it can therefore be used as a chemical marker compound for these dispersants in the environment (Kujawinski et al., 2011). DOSS and MOSS are readily analyzable by ESI-MS (e.g., Kujawinski et al., 2011; Place et al., 2010, 2016), and both molecular formulae were detected in the dispersant-amended treatments even at the end of the incubation experiment (Fig. 3A and C). The relative intensity of DOSS decreased only slightly in the oil-dispersant-nutrient (ca. 5%) and oil-dispersant treatment (11%, Supplementary Fig. S3). MOSS, in contrast, became relatively enriched (Supplementary Fig. S3). MOSS is an intermediate during DOSS biodegradation, but it can also form *via* abiotic hydrolysis (Campo et al., 2013), which explains why it was detected in all initial (Time 0) dispersant-amended treatments. The relative enrichment of MOSS was particularly pronounced in the dispersant-only and dispersant-oil treatments (Supplementary Fig. S3A and B), confirming the quantitative results obtained by liquid chromatography tandem mass spectrometry which showed the highest increase of MOSS in these treatments (Kleindienst et al., 2015b). Thus, one important (intermediate) degradation product of DOSS appeared to be MOSS. In accordance with the quantitative data (Kleindienst et al., 2015b), the relative abundance of MOSS increased only slightly in the dispersant-oil-nutrients treatments suggesting that the transformation of DOSS into other compounds than MOSS was more pronounced in this treatment.

We also detected 71 molecular formulae that were enriched in the initial time point of all dispersant-amended samples (40 degraded and 31 unchanged molecular formulae in Supplementary Table S3) compared to the dispersant-free samples. Of these, 23 molecular formulae were S-containing (8 degraded and 15 unchanged in Supplementary Table S3 and Fig. S4), including DOSS and MOSS. The elevated relative abundance of S-containing compounds at the initial time point of the dispersant-containing treatments (but not in the seawater-only and oil-only treatments) underscore that these compounds were added with the dispersant solution, for example as by-products, impurities, additives and/or intermediates of the synthesis of DOSS (Place et al., 2016).

The relative abundance of DOSS (m/z 421) decreased in the mass spectra when comparing the initial and final time points of the incubations (Supplementary Fig. S3). DOSS and related compounds with different molecular composition were presumably

further degraded to smaller sulfur-containing (e.g., m/z 265 or m/z 178) and non-sulfur-containing compounds (e.g., m/z 227, Fig. 5). However, the fact that DOSS was still detectable after six weeks of incubation supports earlier findings suggesting relatively slow biodegradation at low temperatures (Campo et al., 2013; Kujawinski et al., 2011). Dispersant-derived compounds such as $C_{12}H_{19}O_4^-$ (m/z 227) and $C_{11}H_{21}O_5S^-$ (m/z 265, Supplementary Fig. S3) became relatively enriched in the dispersant-only and dispersed-oil treatments in the course of the incubations which implicated that they were not readily bio-degradable under the experimental conditions (8 °C and absence of light) and on the studied time scales (weeks). We tentatively assigned structures to these compounds and we propose that they are intermediates of the degradation of DOSS and DOSS-related compounds (Fig. 5). Two of these related compounds resembled the core structure of DOSS but with a modified side chain (m/z 323 and m/z 367 in Fig. 5). Their fragmentation patterns, i.e., the characteristic fragment ion m/z 227 in the CID mass spectra (Supplementary Fig. S5C and D) confirmed that these compounds were structurally related to DOSS. They may be impurities or by-products from the synthesis of DOSS or they may result from re-esterification of MOSS with alcohols from the dispersant solution. It should be noted that re-esterification in the SPE-DOM (methanol) extracts can be assumed to be minimal because the extracts were stored frozen immediately after extraction (Flerus et al., 2011). Hence, these compounds were more likely derived from the dispersant solution.

We also observed 12 sulfur-containing compounds in the dispersant-amended treatments that were present after six weeks of incubation (T_4) but not at time zero (Supplementary Table S3, produced CHOS compounds in Supplementary Fig. S4). These compounds were particularly abundant in the ca. 400 Da mass range in the mass spectra of dispersed-oil treatments (e.g., increasing S-containing molecular formulae in Fig. 3D vs. Fig. 3B). It was not possible to obtain unambiguous CID mass spectra of these compounds due to the presence of several other molecules with the same nominal mass (m/z 437, Fig. 3D). However, the presence of these compounds suggests that they were newly formed in the course of the incubation, possibly due to the microbial transformation of dispersant-derived compounds. An enhanced expression of genes involved in the processing of sulfur-containing organic compounds was observed in deepwater plume samples with an elevated relative abundance of *Colwelliaceae* during the DWH oil spill (Rivers et al., 2013). The genome of *Colwellia psychrerythraea* 34H shows a remarkable potential for an enhanced sulfur metabolism (Méthé et al., 2005). It was therefore hypothesized that the observed selective enrichment of *Colwelliaceae* in the dispersed oil treatments may result from their enhanced capability to metabolize sulfur-containing (dispersant-derived) compounds (Kleindienst et al., 2015b).

4. Conclusions

Compositional changes of the WAF of oil, dispersant and dispersed oil (with/without nutrient amendment) were documented during biodegradation laboratory incubations of Gulf deep water. The WAF of the analyzed oil exhibited a specific molecular fingerprint. Oil-derived molecular formulae were of smaller molecular size than the natural marine SPE-DOM. This molecular fingerprint may therefore be useful to identify oil spill sources in the environment. In the oil-only treatments, biodegradation decreased the molecular weight and the number of carbon atoms of DOM molecular formulae that were also more saturated and slightly less oxygenated than the initially detected molecular formulae. The relative abundance of heteroatom-containing (N, S, and P) molecular formulae decreased in the oil-only incubations and it is likely

that these compounds served as nutrient sources in the oil-amended treatments for the build-up of biomass when hydrocarbons were metabolized. Relative changes in the DOM molecular composition were less pronounced in the dispersed oil treatments compared to the oil-only treatments indicating that the microbial turnover of oil-derived DOM was higher in the latter treatments. Furthermore, in the dispersed oil incubations, compounds that increased had a lower molecular weight than the decreasing molecular formulae, while the opposite was the case in the oil-dispersant-nutrients treatment. This infers that, in the dispersed oil treatments, the nutrient supply affected the type of organic compounds that were microbially metabolized.

The relative intensity of DOSS decreased in all dispersant-amended treatments whereas MOSS relatively increased, highlighting MOSS as an important intermediate during DOSS degradation. DOSS and related compounds were probably further degraded to smaller S- and non-S-containing metabolites. However, DOSS was still detectable after six weeks of incubation supporting earlier reports about its relatively slow biodegradation at low temperatures. Dispersant-derived metabolites (with/without S) became relatively enriched in all dispersant-amended treatments in the course of the incubation. Several S-containing molecular formulae were exclusively detected in the dispersant-amended treatments after six weeks of incubations, implying that they were formed in the course of the incubation, possibly due to the microbial transformation of dispersant-derived compounds. These data underscore the utility of DOSS and MOSS as chemical markers to track dispersant movement in the environment. However, we also observed several other S-containing compounds and the formation of new S-containing molecular formulae that was probably stimulated by the addition of the dispersants. Screening for DOSS and MOSS may thus not fully reveal how dispersants affect biogeochemical cycles in the ocean. Since some of these molecules increased relatively in the dispersant-amended samples, they may not be readily biodegradable on time scales of weeks to months at the low temperatures in the deep sea. The fate of these compounds, e.g., whether or not and on what time scales they accumulate, as well as their potential effects on organisms should therefore be subject of future research.

Acknowledgments

We thank K. Klapproth for technical assistance. The officers and crew of *R/V Pelican* (PE 13-21) are acknowledged for the successful operations on board. We are thankful to the reviewers and the editor for their detailed and thoughtful comments which greatly improved this manuscript. This research was supported by the Gulf of Mexico Research Initiative by funding provided to the consortium 'Ecosystem Impacts of Oil and Gas Inputs to the Gulf' (ECOGIG). This is ECOGIG contribution #356 and the data is archived at GRIIDC R1.x132.138:0003.

Appendix A. Supplementary material

Supplementary data associated with this article can be found in the online version at <http://dx.doi.org/10.1016/j.dsr2.2015.05.012>.

References

- Aeppli, C., Carmichael, C.A., Nelson, R.K., Lemkau, K.L., Graham, W.M., Redmond, M.C., Valentine, D.L., Reddy, C.M., 2012. Oil weathering after the Deepwater Horizon disaster led to the formation of oxygenated residues. *Environ. Sci. Technol.* 46, 8799–8807.
- Almeda, R., Hyatt, C., Buskey, E.J., 2014. Toxicity of dispersant Corexit 9500A and crude oil to marine microzooplankton. *Ecotoxicol. Environ. Saf.* 106, 76–85.
- Atlas, R.M., Bartha, R., 1972. Degradation and mineralization of petroleum in sea water: limitation by nitrogen and phosphorous. *Biotechnol. Bioeng.* 14, 309–318.
- Campo, P., Venosa, A.D., Suidan, M.T., 2013. Biodegradability of Corexit 9500 and dispersed South Louisiana crude oil at 5 and 25 °C. *Environ. Sci. Technol.* 47, 1960–1967.
- Chapelle, F.H., 1999. Bioremediation of petroleum hydrocarbon-contaminated ground water: the perspectives of history and hydrology. *Ground Water* 37, 122–132.
- Chapman, S.J., 1997. Carbon substrate mineralization and sulphur limitation. *Soil Biol. Biochem.* 29, 115–122.
- Corilo, Y.E., Podgorski, D.C., McKenna, A.M., Lemkau, K.L., Reddy, C.M., Marshall, A.G., Rodgers, R.P., 2013. Oil spill source identification by principal component analysis of electrospray ionization Fourier transform ion cyclotron resonance mass spectra. *Anal. Chem.* 85, 9064–9069.
- Dittmar, T., Koch, B., Hertkorn, N., Kattner, G., 2008. A simple and efficient method for the solid-phase extraction of dissolved organic matter (SPE-DOM) from seawater. *Limnol. Oceanogr.* – Methods 6, 230–235.
- Flerus, R., Koch, B.P., Schmitt-Kopplin, P., Witt, M., Kattner, G., 2011. Molecular level investigation of reactions between dissolved organic matter and extraction solvents using FT-ICR MS. *Mar. Chem.* 124, 100–107.
- Foght, J.M., Westlake, D.W.S., 1982. Effect of the dispersant Corexit 9527 on the microbial degradation of Prudhoe Bay oil. *Can. J. Microbiol.* 28, 117–122.
- Fontanals, N., Marcé, R.M., Borrull, F., 2005. New hydrophilic materials for solid-phase extraction. *Trends Anal. Chem.* 24, 394–406.
- Garrett, R.M., Pickering, I.J., Haith, C.E., Prince, R.C., 1998. Photooxidation of crude oils. *Environ. Sci. Technol.* 32, 3719–3723.
- George-Ares, A., Clark, J.R., 2000. Aquatic toxicity of two Corexit® dispersants. *Chemosphere* 40, 897–906.
- Graham, B., Reilly, W.K., Beinecke, F., Boesch, D.F., Garcia, T.D., Murray, C.A., Ulmer, F., 2011. National commission on the BP Deepwater Horizon oil spill and offshore drilling: the use of surface and subsea dispersants during the BP Deepwater Horizon oil spill. Staff working paper. Updated January 11, p. 4.
- Hall, G.J., Frysinger, G.S., Aeppli, C., Carmichael, C.A., Gros, J., Lemkau, K.L., Nelson, R.K., Reddy, C.M., 2013. Oxygenated weathering products of Deepwater Horizon oil come from surprising precursors. *Mar. Pollut. Bull.* 75, 140–149.
- Jannasch, H.W., Wirsén, C.O., Taylor, C.D., 1982. Deep-sea bacteria: isolation in the absence of decompression. *Science* 216, 1315–1317.
- Kido Soule, M.C., Longnecker, K., Giovannoni, S.J., Kujawinski, E.B., 2010. Impact of instrument and experiment parameters on reproducibility of ultrahigh resolution ESI FT-ICR mass spectra of natural organic matter. *Org. Geochem.* 41, 725–733.
- Kleindienst, S., Paul, J.H., Joye, S.B., 2015a. Using dispersants after oil spills: impacts on the composition and activity of microbial communities. *Nat. Rev. Microbiol.* 13, 388–396. [10.1038/nrmicro3452](https://doi.org/10.1038/nrmicro3452).
- Kleindienst, S., Seidel, M., Ziervogel, K., Grim, L.S., Loftis, K.M., Harrison, S., Malkin, S., Perkins, M.J., Field, J., Sogin, M.L., Dittmar, T., Passow, U., Medeiros, P.M., Joye, S.B., 2015b. Chemical dispersants can suppress the activity of natural oil-degrading microorganisms. *Proc. Natl. Acad. Sci.* 112, 14900–14905.
- Koch, B.P., Dittmar, T., 2006. From mass to structure: an aromaticity index for high-resolution mass data of natural organic matter. *Rapid Commun. Mass Spectrom.* 20, 926–932.
- Koch, B.P., Dittmar, T., Witt, M., Kattner, G., 2007. Fundamentals of molecular formula assignment to ultrahigh resolution mass data of natural organic matter. *Anal. Chem.* 79, 1758–1763.
- Kujawinski, E.B., Kido Soule, M.C., Valentine, D.L., Boysen, A.K., Longnecker, K., Redmond, M.C., 2011. Fate of dispersants associated with the Deepwater Horizon oil spill. *Environ. Sci. Technol.* 45, 1298–1306.
- Lemkau, K.L., McKenna, A.M., Podgorski, D.C., Rodgers, R.P., Reddy, C.M., 2014. Molecular evidence of heavy-oil weathering following the M/V Cosco Busan spill: insights from Fourier transform ion cyclotron resonance mass spectrometry. *Environ. Sci. Technol.* 48, 3760–3767.
- Lewis, M., Pryor, R., 2013. Toxicities of oils, dispersants and dispersed oils to algae and aquatic plants: Review and database value to resource sustainability. *Environ. Pollut.* 180, 345–367.
- Lindstrom, J.E., Braddock, J.F., 2002. Biodegradation of petroleum hydrocarbons at low temperature in the presence of the dispersant Corexit 9500. *Mar. Pollut. Bull.* 44, 739–747.
- Lu, Z., Deng, Y., Van Nostrand, J.D., He, Z., Voordeckers, J., Zhou, A., Lee, Y.-J., Mason, O.U., Dubinsky, E.A., Chavarría, K.L., Tom, L.M., Fortney, J.L., Lamendella, R., Jansson, J.K., D'Haeseleer, P., Hazen, T.C., Zhou, J., 2012. Microbial gene functions enriched in the Deepwater Horizon deep-sea oil plume. *ISME J.* 6, 451–460.
- Marshall, A.G., Rodgers, R.P., 2003. Petroleomics: the next grand challenge for chemical analysis. *Acc. Chem. Res.* 37, 53–59.
- Marshall, A.G., Rodgers, R.P., 2008. Petroleomics: chemistry of the underworld. *Proc. Natl. Acad. Sci. USA* 105, 18090–18095.
- Mathew, J., Schroeder, D.L., Zintek, L.B., Schupp, C.R., Kosempa, M.G., Zachary, A.M., Schupp, G.C., Wesolowski, D.J., 2012. Diocetyl sulfosuccinate analysis in near-shore Gulf of Mexico water by direct-injection liquid chromatography–tandem mass spectrometry. *J. Chromatogr. A* 1231, 46–51.
- McKenna, A.M., Nelson, R.K., Reddy, C.M., Savory, J.J., Kaiser, N.K., Fitzsimmons, J.E., Marshall, A.G., Rodgers, R.P., 2013. Expansion of the analytical window for oil spill characterization by ultrahigh resolution mass spectrometry: beyond gas chromatography. *Environ. Sci. Technol.* 47, 7530–7539.

- McNutt, M.K., Camilli, R., Crone, T.J., Guthrie, G.D., Hsieh, P.A., Ryerson, T.B., Savas, O., Shaffer, F., 2012. Review of flow rate estimates of the Deepwater Horizon oil spill. *Proc. Natl. Acad. Sci. USA* 109, 20260–20267.
- Méthé, B.A., Nelson, K.E., Deming, J.W., Momen, B., Melamud, E., Zhang, X., Moul, J., Madupu, R., Nelson, W.C., Dodson, R.J., Brinkac, L.M., Daugherty, S.C., Durkin, A.S., DeBoy, R.T., Kolonay, J.F., Sullivan, S.A., Zhou, L., Davidsen, T.M., Wu, M., Huston, A.L., Lewis, M., Weaver, B., Weidman, J.F., Khouri, H., Utterback, T.R., Feldblyum, T.V., Fraser, C.M., 2005. The psychrophilic lifestyle as revealed by the genome sequence of *Colwellia psychrerythraea* 34H through genomic and proteomic analyses. *Proc. Natl. Acad. Sci. USA* 102, 10913–10918.
- National Research Council, 2005. *Oil Spill Dispersants: Efficacy and Effects*. The National Academies Press, United States.
- National Response Team, 2011. *On Scene Coordinator report, Deepwater Horizon oil spill*, submitted to the National Response Team, September 2011. United States Coast Guard.
- Oksanen, J., Blanchet, F.G., Kindt, R., Legendre, P., Minchin, P.R., O'Hara, R.B., Simpson, G.L., Solymos, P., Stevens, M.H.H., Wagner, H., 2013. *Vegan: Community Ecology Package*. R package version 2.0-10. <http://CRAN.R-project.org/package=vegan>.
- Osterholz, H., Dittmar, T., Niggemann, J., 2014. Molecular evidence for rapid dissolved organic matter turnover in Arctic fjords. *Mar. Chem.* 160, 1–10.
- Parkes, R.J., Sellek, G., Webster, G., Martin, D., Anders, E., Weightman, A.J., Sass, H., 2009. Culturable prokaryotic diversity of deep, gas hydrate sediments: first use of a continuous high-pressure, anaerobic, enrichment and isolation system for subsurface sediments (DeepSoBUG). *Environ. Microbiol.* 11, 3140–3153.
- Place, B., Anderson, B., Mekebri, A., Furlong, E.T., Gray, J.L., Tjeerdema, R., Field, J., 2010. A role for analytical chemistry in advancing our understanding of the occurrence, fate, and effects of Corexit oil dispersants. *Environ. Sci. Technol.* 44, 6016–6018.
- Place B.J., Perkins M.J., Sinclair E., Barsamian A.L., Blakemore P.R., Field J.A., 2016. Trace analysis of surfactants in Corexit oil dispersant formulations and seawater. *Deep-Sea Res. II*, 129, 273–281. <http://dx.doi.org/10.1016/j.dsr2.2014.01.015>.
- R Core Team, 2014. *R Foundation for Statistical Computing*. R foundation for statistical computing, Vienna, Austria <http://www.R-project.org/>.
- Ramachandran, S.D., Hodson, P.V., Khan, C.W., Lee, K., 2004. Oil dispersant increases PAH uptake by fish exposed to crude oil. *Ecotoxicol. Environ. Saf.* 59, 300–308.
- Ramette, A., 2007. Multivariate analyses in microbial ecology. *FEMS Microbiol. Ecol.* 62, 142–160.
- Ramirez, C., Batchu, S., Gardinali, P., 2013. High sensitivity liquid chromatography tandem mass spectrometric methods for the analysis of dioctyl sulfosuccinate in different stages of an oil spill response monitoring effort. *Anal. Bioanal. Chem.* 405, 4167–4175.
- Rivers, A.R., Sharma, S., Tringe, S.G., Martin, J., Joye, S.B., Moran, M.A., 2013. Transcriptional response of bathypelagic marine bacterioplankton to the Deepwater Horizon oil spill. *ISME J.* 7, 2315–2329.
- Röling, W.F.M., Milner, M.G., Jones, D.M., Lee, K., Daniel, F., Swannell, R.J.P., Head, I.M., 2002. Robust hydrocarbon degradation and dynamics of bacterial communities during nutrient-enhanced oil spill bioremediation. *Appl. Environ. Microbiol.* 68, 5537–5548.
- Ruddy, B.M., Huettel, M., Kostka, J.E., Lobodin, V.V., Bythell, B.J., McKenna, A.M., Aeppli, C., Reddy, C.M., Nelson, R.K., Marshall, A.G., Rodgers, R.P., 2014. Targeted petroleomics: analytical investigation of Macondo well oil oxidation products from Pensacola Beach. *Energy Fuels* 28, 4043–4050.
- Schwedt, A., Seidel, M., Dittmar, T., Simon, M., Bondarev, V., Romano, S., Lavik, G., Schulz-Vogt, H.N., 2015. Substrate use of *Pseudovibrio* sp. growing in ultra-oligotrophic seawater. *PLoS ONE* 10, e0121675.
- Seidel, M., Beck, M., Riedel, T., Waska, H., Suryaputra, I.G.N.A., Schnetger, B., Niggemann, J., Simon, M., Dittmar, T., 2014. Biogeochemistry of dissolved organic matter in an anoxic intertidal creek bank. *Geochim. Cosmochim. Acta* 140, 418–434.
- ter Braak, C.J.F., 1985. Correspondence analysis of incidence and abundance data: properties in terms of a unimodal response model. *Biometrics* 41, 859–873.
- White, H.K., Lyons, S.L., Harrison, S.J., Findley, D.M., Liu, Y., Kujawinski, E.B., 2014. Long-term persistence of dispersants following the Deepwater Horizon oil spill. *Environ. Sci. Technol.* 1, 295–299.



Comparing molecular composition of dissolved organic matter in soil and stream water: Influence of land use and chemical characteristics



Anne-Gret Seifert^{a,*}, Vanessa-Nina Roth^b, Thorsten Dittmar^c, Gerd Gleixner^b, Lutz Breuer^d, Tobias Houska^d, Jürgen Marxsen^{a,e}

^a University Giessen, Animal Ecology & Systematic Zoology, Heinrich Buff Ring 29, D-35392 Giessen, Germany

^b Max Planck Institute for Biogeochemistry, POB 100164, 07701 Jena, Germany

^c Research Group for Marine Geochemistry (ICBM-MPI Bridging Group), Univ. of Oldenburg, Institute for Chemistry and Biology of the Marine Environment (ICBM), Carl-von-Ossietzky-Str. 9-11, 26111 Oldenburg, Germany

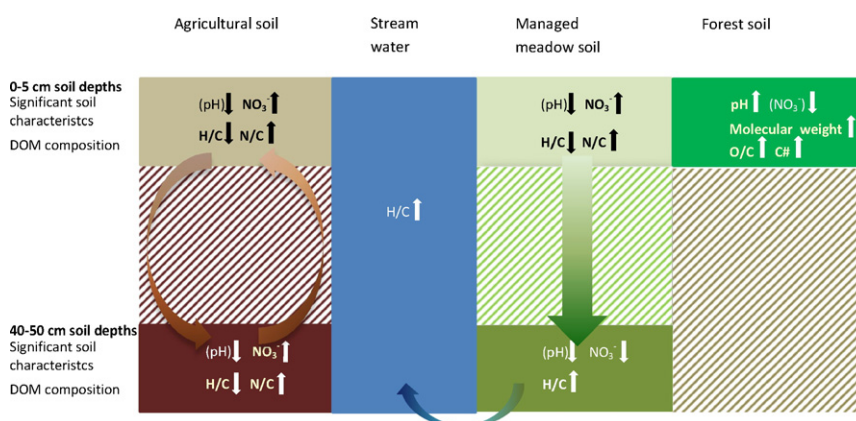
^d University Giessen, Landscape Ecology & Resources Management, Res Ctr BioSyst Land Use & Nutr IFZ, Heinrich-Buff-Ring 26-32, D-35392 Giessen, Germany

^e Limnological River Station of the Max Planck Institute for Limnology, Schlitz, Germany

HIGHLIGHTS

- Environmental parameters as pH and nitrate significantly affect chemical composition of DOM
- DOM molecular composition variation was apparent in the vertical stratification of undisturbed soils
- DOM became less aromatic with depth in undisturbed soils
- Stream DOM is mainly of allochthonous origin and predominantly derived from alongside stream subsoil/groundwater

GRAPHICAL ABSTRACT



ARTICLE INFO

Article history:

Received 27 May 2016

Received in revised form 1 July 2016

Accepted 5 July 2016

Available online 26 July 2016

Editor: J Jay Gan

Keywords:

Dissolved organic matter

Ion cyclotron resonance mass spectrometry

Land use

ABSTRACT

Electrospray ionization Fourier transform ion cyclotron resonance mass spectrometry (ESI-FT-ICR-MS) was used to examine the molecular composition of dissolved organic matter (DOM) from soils under different land use regimes and how the DOM composition in the catchment is reflected in adjacent streams. The study was carried out in a small area of the Schwingbach catchment, an anthropogenic-influenced landscape in central Germany. We investigated 30 different soil water samples from 4 sites and different depths (managed meadow (0–5 cm, 40–50 cm), deciduous forest (0–5 cm), mixed-coniferous forest (0–5 cm) and agricultural land (0–5 cm, 40–50 cm)) and 8 stream samples. 6194 molecular formulae and their magnitude-weighted parameters ((O/C)_w, (H/C)_w, (N/C)_w, (Al-mod)_w, (DBE/C)_w, (DBE/O)_w, (DBE-O)_w, (C#)_w, (MW)_w) were used to describe the molecular composition of the samples.

The samples can be roughly divided in three groups. Group 1 contains samples from managed meadow 40–50 cm and stream water, which are characterized by high saturation compared to samples from group 2 including

* Corresponding author.

E-mail addresses: anne-gret.seifert@allzool.bio.uni-giessen.de (A.-G. Seifert), vroth@bgc-jena.mpg.de (V.-N. Roth), thorsten.dittmar@uni-oldenburg.de (T. Dittmar), gerd.gleixner@bgc-jena.mpg.de (G. Gleixner), lutz.breuer@umwelt.uni-giessen.de (L. Breuer), tobias.houska@umwelt.uni-giessen.de (T. Houska), juergen.marxsen@allzool.bio.uni-giessen.de (J. Marxsen).

agricultural samples and samples from the surface meadow (0–5 cm), which held more nitrogen containing and aromatic compounds. Samples from both forested sites (group 3) are characterized by higher molecular weight and O/C ratio. Environmental parameters vary between sites and among these parameters pH and nitrate significantly affect chemical composition of DOM. Results indicate that most DOM in streams is of terrestrial origin. However, 120 molecular formulae were detected only in streams and not in any of the soil samples. These compounds share molecular formulae with peptides, unsaturated aliphatics and saturated FA-CHO/FA-CHOX. Compounds only found in soil samples are much more aromatic, have more double bonds and a much lower H/C ratio but higher oxygen content, which indicates the availability of fresh plant material and less microbial processed material compared to stream samples.

© 2016 Elsevier B.V. All rights reserved.

1. Introduction

Dissolved organic matter (DOM) is an important constituent of terrestrial and aquatic ecosystems. In most eco-regions worldwide, DOM is produced during decomposition and solubilization of either recent plant biomass or from soil organic matter (SOM) and serves as a link between terrestrial and aquatic systems. Since streams are net heterotrophic, they consume more energy than they create, a large proportion of DOM in river ecosystems is derived from terrestrial sources (Rasilo et al., 2015; Houser et al., 2005). Consequently, processes controlling DOM composition and concentration in fluvial systems are largely determined by conditions in the catchment area (Houser et al., 2005; Strayer et al., 2003; Hury et al., 2002).

DOM pools in terrestrial ecosystems are small compared to pools of soil organic matter (SOM) but they are considered to be a key indicator of soil quality (Jones et al., 2014) due to their rapid response to land use and vegetation change. Previous studies showed that land use and vegetation can affect DOM composition e.g. DOM leachates from humified organic soils often are dominated by highly aromatic high-molecular-weight compounds (Wickland et al., 2007). Land use changes and vegetation also affect soil properties such as pH, moisture, temperature and nutrient availability (Cohen et al., 2008). DOM is the primary energy source for microorganisms and affects their activity and abundance in soils. Both soil properties and microbial activity interact with DOM composition. Components of DOM differ in decomposability. For example, hydrophobic acids, rich in aromatic structures, are difficult to decompose for microorganisms, whereas leachates from living vegetation and fresh litter have a high contribution of low-molecular-weight carbohydrates, which are easy to decompose (Marschner and Kalbitz, 2003). However, fresh plant organic carbon is only available in the upper soil horizons and lost in the upper 20 cm. DOM at greater depths of mineral soils is mainly a product of SOM and only to a minor extent derived from fresh plant organic carbon (Malik and Gleixner, 2013; Steinbeiss et al., 2008; Fröberg et al., 2007). This might be of importance, when the quality of DOM transported to inland waters is considered, because different carbon pools are activated during base- and overland-/interflow. DOM derived from fresh plant material which is restricted to the upper part of the soil is transported to inland waters mainly during overland-/interflow caused by heavy precipitation events, whereas mainly old and highly processed deep DOM are transported to the aquatic systems during baseflow (Fellman et al., 2009; Sanderman et al., 2009). This will result in low concentrations of highly altered DOM in stream water (Sanderman et al., 2009) which reaches streams during most times of the year and thus, is the dominant pool for DOM in streams (Fiebig, 1995). Stream DOM concentration and chemistry reflect the combined influences of terrestrial biogeochemical cycling of organic matter and the discharge regime of the catchment, which is influenced by abiotic factors such as hydrology, precipitation and temperature. Low-order-streams are the first important link in the transporting route of DOM from their soil sources to their sinks, because they integrate chemical compounds from groundwater, surrounding landscape and in-stream processes, whereas the molecular formulae diversity decreases with stream order (Mosher et

al., 2015). Spatial and seasonal patterns which affect soil biogeochemical cycling are supposed to determine the concentration and composition of DOM found in streams and rivers.

The objective of this study was to examine the composition of terrestrial DOM and its influence on stream water DOM in immediate vicinity. We compared DOM composition from different vegetation sites and two different depths within a small area of the catchment and at two nearby points in the streams. DOM was characterized using Fourier transform ion cyclotron resonance mass spectrometry (FT-ICR-MS). Analytical techniques such as FT-ICR-MS provide information about the molecular composition of DOM. Due to the high mass accuracy, molecular formulae can be assigned to individual detected masses within the complex DOM mixture (Koch et al., 2005; Kujawinski et al., 2004). Characteristic fingerprints, consisting of many thousand molecular formulae, allow the distinction of DOM of different origins (Koch et al., 2005) and to identify unique molecular formulae for different ecosystems including rivers (Roth et al., 2014).

2. Materials and methods

2.1. Study site and sampling

The study site is a small area inside the 23.4 km² Schwingbach catchment. Samples were taken close to the junction of the Vollnkirchner Bach and the Schwingbach (SI-Figure). The Schwingbach and its tributary the Vollnkirchner Bach are low-mountainous creeks located in Hüttenberg (50°30'0" N, 8°37'0" E, Hesse, Germany). The Schwingbach is 10.9 km long, with an altitude range from 233 to 415 m a.s.l. The Vollnkirchner Bach is 4.7 km long and drains a 3.7 km² subcatchment. Both creeks are part of the "Study landscape Schwingbachtal" of the Justus Liebig University Giessen (Orlowski et al., 2014; Lauer et al., 2013). Land use is dominated by forested sites (36.9%) and arable land (39%), whereas grassland sites (10.5%) are mainly distributed along the stream. Soils are forested Cambisols as well as agricultural Stagnosols with thick loess layers (Stagnic Luvisols). Gleysols can be found predominantly under grassland sites along the streams.

Meteorological data were recorded at a climate station at the catchment outlet of the Vollnkirchner Bach including air temperature and precipitation. The climate station is equipped with an automated weather station (Campbell Scientific Inc., AQ5, UK) including a CR1000 data logger. Soil moisture and temperature were measured in 10 cm depth and 40 cm depth in grassland, 20 cm depth and 40 cm depth in agriculture soils and in 5 cm depth in deciduous forest soils (only soil moisture). Soil moisture and temperature was measured with permanently installed EC-5 sensors at forested and 10 cm grassland sites and 5TM-sensors at agriculture and 40 cm grassland sites equipped with EM50 data logger. The climate is classified as temperate with a mean annual temperature of 10.5 °C and annual precipitation sum of 588 mm for the hydrological year 01.11.2013–31.10.2014 (fb09-pasig.umwelt.uni-giessen.de:8081). Data are shown in Fig. 1.

Soil samples were taken twice a month in February, April, June, August and October from a managed meadow (0–5 cm, 40–50 cm), deciduous forest (0–5 cm), mixed-coniferous forest (0–5 cm) and

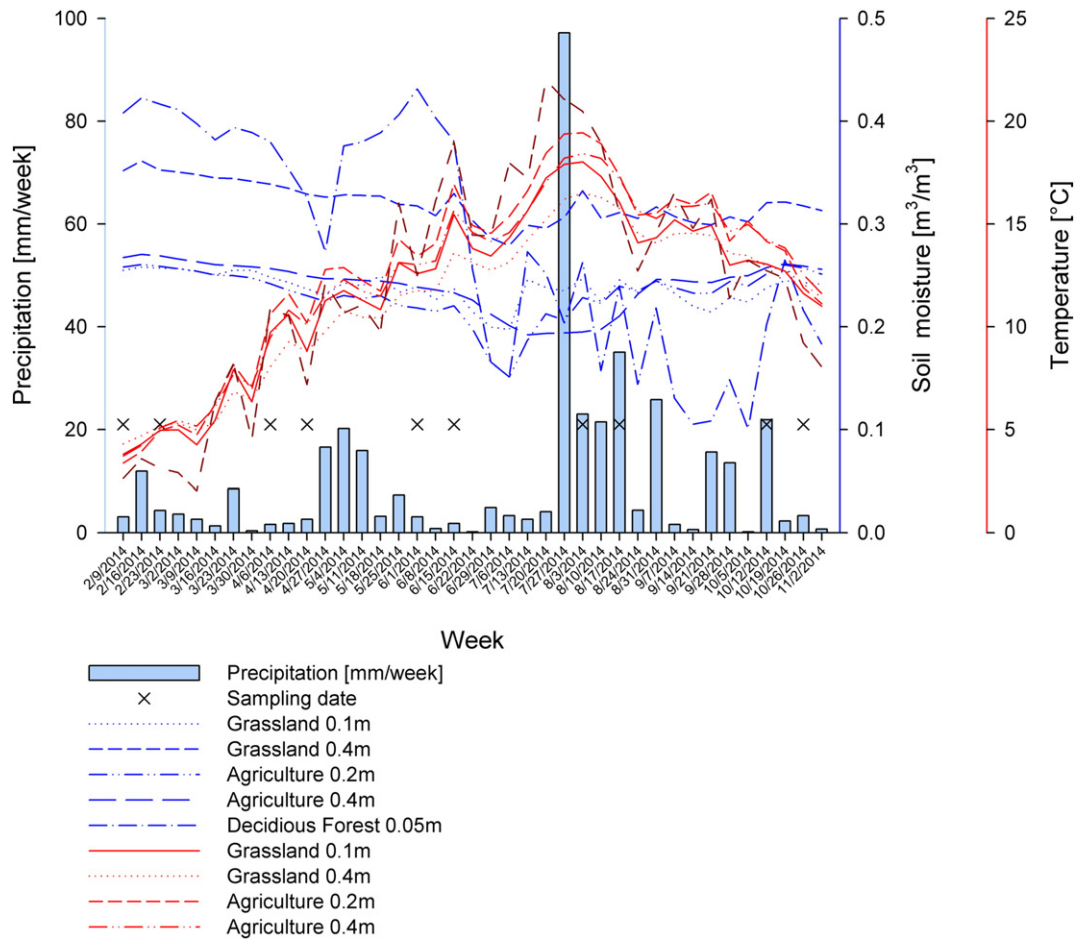


Fig. 1. Meteorological data recorded at the climate station at the catchment outlet near the test site and soil temperature and soil moisture measured with permanently installed sensors on the test site.

agricultural sites (0–5 cm, 40–50 cm). Meadow was cut once a year (01.05.2014) and grazed by sheep (02.–03.02. 2014, 01.09–02.09.2014). On the agricultural area the following activities took place: tillage 08.09.2014, manure 22.09.2014, planting 01.10.2014. Samples were taken at three different locations at each vegetation/depth within the specific area and at the specific sampling date and bulked together. Main plant species are given in Table 1. Each sample was kept in a labelled plastic bag and transported to a refrigerator where it was stored at 4 °C for no longer than 2 days until further processing. Green plant material was removed and soil samples were sieved through a 4.0 mm mesh and used for following analysis and experiments. Carbon content was determined from ball-milled subsamples using an elemental analyzer (Vario EL III[®], elemental, Germany).

2.2. Analyses of water extractable carbon

The water-extractable organic carbon fraction (WEOC) was isolated from soil samples as follows: 300 g (200 g from coniferous forest) of soil

Table 1
Main plant species on different test sites.

Land use	Main vegetation
Agriculture	Triticum
Managed meadow	<i>Dactylis glomerata</i> , <i>Bromus hordeaceus</i> , <i>Alopecurus pratensis</i> , <i>Ranunculus acris</i> , <i>Ajuga reptans</i> , <i>Rumex acetosa</i> , <i>Plantago lanceolata</i> , <i>Stellaria holostea</i> ,
Deciduous forest	<i>Quercus petraea</i> , <i>Carpinus betulus</i> , <i>Melica uniflora</i>
Mixed coniferous forest	<i>Pinus sylvestris</i> , <i>Picea abies</i> , <i>Carpinus betulus</i> , <i>Melica uniflora</i> , <i>Oxalis acetosella</i> , <i>Convallaria majalis</i>

were weighed into 2 L glass flask. 600 mL deionized water was added and the mixture was shaken for 2 h using an overhead shaker. The extracts were decanted and centrifuged (10 min, 3000 rpm) to accelerate the subsequent filtration through a fritted filter funnel with porosity 2 (16–40 μm) and 0.7 μm glass microfiber filters (GF/F, Whatman, England). This extraction method follows the procedure from Embacher et al. (2007). It is considered as a “relatively” weak procedure with minimized artifacts. Therefore, the extracted WEOC should reflect a water (or soil solution) soluble carbon fraction which is relatively close to the potential WEOC in situ (Embacher et al., 2007).

The soil solutions were analyzed for DOC, NO₃⁻, NO₂⁻, PO₄³⁻ and pH. The DOC concentration was measured using a TOC-5000A (Shimadzu). Soil solution pH was measured with a multi 3430 Set F (WTW, Germany). An ion chromatograph ICS-2000 (Dionex) was used to determine NO₃⁻, NO₂⁻, PO₄³⁻ concentration. As separating column AS18 2 × 250 mm with KOH as eluent was used. Statistical differences between soils and soil solutions were analyzed using Kruskal–Wallis following Mann–Whitney *U* test. Additionally, we tested correlation between environmental data with Spearman's rank *r_s* correlation. These tests were performed with SPSS 17.0 (SPSS Inc., Chicago, Illinois, United States).

To identify the molecular composition electrospray ionization Fourier transform ion cyclotron resonance was applied. For ESI-FT-ICR-MS, samples taken within a month were mixed. Thus, in total we had 30 soil samples, five within each sampling plot. Additionally, we had eight stream water samples taken at the same time as soil samples (except for February). The sampling plots are abbreviated with A0–5, A40–50, M0–5, M40–50, C0–5, D0–5 whereas A – agricultural area, M – managed meadow, C – mixed coniferous forest and D – deciduous forest. The numbers 0–5 and 40–50 indicate soil depth [cm]. The streams are

indicated with S = Schwingbach, V = Vollnkirchner Bach. The months are abbreviated with F – February, Ap – April, J – June, Ag – August and O – October. For ESI-FT-ICR-MS, in a first step, DOM was desalted and concentrated with solid phase extraction (SPE) (Varian PPL (0.1 g), Dittmar et al., 2008). The SPE cartridges were activated with methanol (MS grade) over night and conditioned with ultrapure water, methanol and finally with pH 2 ultrapure water. Specifically, DOC solutions were acidified with HCl (p.a.) to pH 2. Samples were passed through the cartridge by gravity, and were rinsed with pH 2 ultrapure water to remove any salt. The cartridge was dried using nitrogen, and DOC was eluted with 800 μ L methanol. For the ESI-FT-ICR-MS measurements the DOC concentrates were diluted with ultrapure water and methanol to 1:1 methanol/water (v/v) and 15 mg DOC/L. ESI-FT-ICR-MS measurements were accomplished in negative ionization mode at the Bruker Solarix 15 T FTICR-MS at the University of Oldenburg (Germany). The analytic solution was injected to the ESI source with 120 μ L/h and ESI needle voltage was set to -4 kV. 500 broadband scans were accumulated for each sample run. Spectra were calibrated using an in-house mass reference list.

Matlab R2012 (The MathWorks, Inc.) was used for data preparation. Further data handling was performed with Excel 2007 and Canoco 5 (Microcomputer Power, Ithaca, New York, United States). We used molecular formulae with a mass between 150 and 800 Da.

Molecular formula assignment was only performed for detected masses having a signal/noise ratio (S/N) above 5. Molecular formulae assignment considered the elements C, H, O, N, S, P ($N \leq 4$, $S \leq 2$, $P \leq 1$) (Herzprung et al., 2012; Riedel et al., 2012). Further, ultrapure water was treated similar to samples and was used as a procedural blank for extraction and FT-ICR-MS. Masses detected in blank samples were removed and only molecular formulae detected in more than one sample were used for data interpretation.

For statistical analyses the dataset with normalized peak intensities and their corresponding elemental composition was used. From this basic data set, a set of magnitude-weighted parameters were calculated based on each formula and relative intensity including aromaticity index (AI-mod, Koch and Dittmar, 2006), oxygen to carbon ratio (O/C), hydrogen to carbon ratio (H/C), nitrogen to carbon ratio (N/C), double bond equivalents (DBE), double bond equivalents to carbon ratio (DBE/C), double bond equivalents to oxygen ratio (DBE/O), the difference between DBE and number of oxygen (DBE-O), molecular weight (MW) and number of carbon atoms (C#) to characterize each sample. The magnitude-weighted parameters were calculated for each measurement as the sum of all of the products of chemical information and relative intensity (e.g., $(C\#)_w = \sum (C\#_n * M_n)$ with n for each individual elemental formula and M for the relative peak intensity (Roth et al., 2013; Sleighter et al., 2010). According to their O/C and H/C ratio individual molecular formulae can be plotted in van Krevelen (VK) diagrams and grouped based on established molar ratios, AI-mod and heteroatom content into BC (black carbon) with $C < 15$ or $C \geq 15$ (AI-mod > 0.666 , N, S or $P < 1$), BC-CHOX (AI-mod > 0.666 , N, S or $P \geq 1$), polyphenols ($0.5 < AI\text{-mod} \leq 0.666$) (Dittmar and Koch, 2006), highly unsaturated compounds (AI-mod < 0.5 , $H/C < 1.5$) (Stenson et al., 2003), unsaturated aliphatics ($1.5 \leq H/C \leq 2$, $N = 0$) (Seidel et al., 2014) saturated FA (fatty acids)-CHO ($H/C > 2$, $O/C < 0.9$, N, S or $P < 1$), saturated FA-CHOX ($H/C > 2$, $O/C < 0.9$, N, S or $P < 1$), sugars CHO ($O/C \geq 0.9$, N, S or $P < 1$), sugars CHOX ($O/C \geq 0.9$, N, S or $P \geq 1$) and peptides ($1.5 \leq H/C \leq 2$, $O/C < 0.9$; $N \geq 1$) (Seidel et al., 2014). Further polyphenols, highly unsaturated compounds and unsaturated aliphatics were divided according to their O/C ratio in O-poor and O-rich compounds groups (O-rich: $0.5 < O/C < 0.9$, O-poor: $O/C \leq 0.5$). It is important to note that with FT-ICR-MS we can only describe the molecular composition of formulae and not their molecular structure. Thus, one formula can represent numerous isomeric compounds.

We used principal component analysis (PCA) and redundancy analysis (RDA) with forward selection to compare our data and determine the relationship between samples, magnitude-weighted parameters

and/or environmental data. To describe the relative importance of different groups of environmental variables and their joint effects a variation partitioning analysis was performed. These tests were performed with Canoco 5.

Differences in DOM composition between both depths of meadow samples were evaluated by comparing the relative intensities in both depths. To determine which molecular formulae are more abundant, only molecular formulae which were detected in all five samples of each depth were used and the average values were compared. We considered only molecular formulae which increased/decreased their relative intensities by $>25\%$ by comparison to the other soil depth. We also examined molecular formulae which were detected in all five samples of M0–5 and in none of M40–50 samples and vice versa.

3. Results and discussion

3.1. Differences in molecular composition between samples

In all 38 investigated soil and stream samples 6194 different molecular formulae were identified and used to describe the molecular composition (SI, Table 1). 1196 molecular formulae were found in all 38 soil and stream samples (SI, Table 2). Most of these common molecular formulae were highly unsaturated compounds (O-poor, 53.7%, O-rich, 16.8%) and formulae indicating O-poor polyphenols (18.6%, SI, Table 3). These ubiquitous compounds are basics for lignin, a class of complex biopolymers in the support tissues of vascular plants, and tannins, astringent plant polyphenolic compounds.

Besides this overlap between samples, the chemical composition of DOM displays some site specific variation as shown in the PCA biplot (Fig. 2). The distribution of samples within the PCA is based on all detected molecular formulae. Differences between samples were more pronounced between mineral soils (agriculture and managed meadow) on one hand and organic soils (forest) on the other hand. Differences

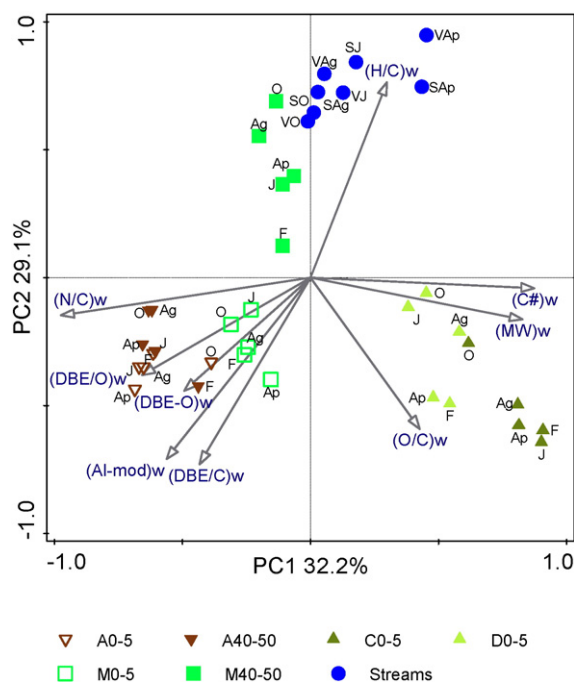


Fig. 2. Principal component analysis biplot of PC1 and PC2 based on all 6194 molecular formulae. Magnitude-weighted parameters that were calculated from the relative intensities of all 6194 formulae were added as supplementary variables. A0–5, A40–50, M0–5, M40–50, C0–5, D0–5 are abbreviations for A - agricultural area, M - managed meadow, C - mixed coniferous forest and D - deciduous forest. The numbers 0–5 and 40–50 indicate soil depth [cm]. The streams are indicated with S = Schwingbach, V = Vollnkirchner Bach. The months are abbreviated with F - February, Ap - April, J - June, Ag - August and O - October.

between surface and subsoil samples were found only in managed meadow samples, but not in the agricultural samples. Only modest differences were found between surface samples from managed meadow compared to arable soils as described also by Purton et al. (2015).

To interpret the variation of molecular formula composition of the samples, magnitude-weighted parameters (Table 3) were used as supplementary variables and plotted in Fig. 2. The supplements are not included in the PCA calculation and only show the direction of each gradient for all magnitude weighted parameter. PC1 and PC2 explain together 61.3% of the variance among the 38 samples. The samples can be roughly divided in three groups. Group 1 contains samples from M40–50 and stream water that are characterized by high saturation. To group 2 belong samples from A0–5, A40–50 and M0–5, which comprise more nitrogen containing and aromatic compounds indicated by higher $(DBE-O)_w$, $(DBE/O)_w$, $(AI-mod)_w$ and $(DBE/C)_w$ values. Both forest sites cluster as group 3 and are characterized by higher molecular weight and oxygenation ($(C\#)_w$, $(MW)_w$, $(O/C)_w$). The first principal component (PC1) explains 32.2% of the variation. Group 2 and 3 are divided by PC1. Samples of group 1 are divided from group 2 and 3 by PC2, which explains further 29.1% of the variation, but partly also by PC1. Within group 2, all M0–5 samples are separated along PC1 from both A0–5 and A40–50 samples, whereas M0–5 and M40–50 are mainly separated along PC2.

$(C\#)_w$, $(MW)_w$ and the $(N/C)_w$ ratio explain the sample correlation with PC1 (Fig. 2), whereas PC2 is related to saturation/aromaticity ($(H/C)_w$, $(AI-mod)_w$ and $(DBE/C)_w$). Samples with high $(H/C)_w$ values have positive PC2 scores and have higher values in stream water and M40–50 samples, whereas within group 1 the managed meadow samples are separated from stream samples by PC1 indicating higher molecular weights for stream samples. M40–50F differs from other samples in this group by having a lower $(DBE-O)_w$ value, which indicates a higher carbon saturation. Samples with high $(AI-mod)_w$, $(DBE/C)_w$, $(DBE/O)_w$, $(DBE-O)_w$ and $(N/C)_w$ values have negative PC1 and PC2 scores and are from A0–5, A40–50 and M0–5. Within this group, agricultural samples have a higher $(N/C)_w$ ratio compared to M0–5 samples.

Forest samples are described by a relative higher number of $(C\#)_w$, higher $(MW)_w$ and higher $(O/C)_w$ ratios compared to meadow and

agricultural samples. Within group 3, deciduous and coniferous forest samples are separated by PC1 with higher molecular weight and oxygenation for coniferous forest.

Analysis by RDA in combination with forward selection of magnitude-weighted parameters revealed that all magnitude-weighted parameters explain together 78.8% of the variability of the samples, whereas most variability was explained by $(N/C)_w$ ratio and aromaticity index. Our findings of the variability between forest at one hand and meadow/agriculture on the other hand can be only partly related to above ground vegetation and are in accordance with studies from Bu et al. (2010) and Traversa et al. (2008), where DOM differs as a function of plant litter and its degradation processes. We found only minor differences between managed meadow and agricultural samples. That agrees with investigations by Guggenberger et al. (1995) and Purton et al. (2015) on SOM who observed that broad land use categories are poor predictors of SOM chemistry, having only minor effects and that soil-scale processes have greater control over chemical composition.

3.2. Environmental data and their influence on DOM composition

The environmental variables used in the study consist of data to describe soil carbon content (soil C, DOC), nutrient input (nitrate, nitrite, phosphate), climate (soil temperature, soil moisture) and acidity (pH). Data are summarized in Table 2 and Fig. 1. If all six sites were compared, these environmental parameters vary significantly between sites. Soil C was significantly higher at both forest sites ($p = 0.008$ to all other sites/depths) and significantly lower at A40–50 and M40–50 compared to other sites/depths ($p = 0.008$ to all other sites/depths). There were no differences in soil C between M0–5 and A0–5 ($p = 0.56$) as well as between M40–50 and A40–50 ($p = 0.690$). At both forested sites pH was significantly lower compared to all other sites/depths ($p = 0.008$ to all other sites/depths), with no difference between the forested sites ($p = 0.56$). There was also a weak significant difference between A0–5 and M0–5 ($p = 0.32$). Soil C and pH as well as DOC and pH were significantly negatively correlated ($r_s = 0.733$, $p \leq 0.001$ for soil C and $r_s = 0.601$, $p = 0.001$ for DOC, Fig. 3). Differences in soil pH as measured in our

Table 2
Overview over available soil characteristics.

Land use	Depth	Month	C [%]	DOC [mg/L]	pH	NO ₃ -[ppm]	NO ₂ -[ppm]	PO ₄ ³⁻ -[ppm]
Agriculture	0–5 cm	February	1.69	8.92	6.47	11.12	0.08	0.43
		April	2.26	11.40	6.76	13.66	0.03	0.56
		June	2.01	10.30	6.72	7.07	0.05	0.40
		August	2.01	8.44	6.86	10.01	0.15	0.89
		October	1.73	10.47	6.97	7.24	0.26	2.93
	40–50 cm	February	0.75	6.67	6.43	9.71	0.19	0.13
		April	1.01	6.69	6.71	12.57	0.10	0.34
		June	0.74	5.77	7.01	4.61	0.04	0.09
		August	1.14	4.89	6.62	5.36	0.09	0.05
		October	0.97	6.02	7.07	7.10	0.16	0.47
Managed meadow	0–5 cm	February	2.17	9.02	6.47	7.54	0.23	0.22
		April	2.58	11.53	6.43	5.83	0.24	0.03
		June	2.14	7.29	6.54	8.08	0.06	0
		August	2.15	5.18	6.50	5.37	0.03	0
		October	2.57	7.27	6.20	5.35	0.05	0.02
	40–50 cm	February	0.97	3.13	6.22	2.36	0.11	0
		April	0.81	3.04	6.39	1.26	0.03	0
		June	0.88	4.22	6.71	1.86	0.01	0
		August	0.92	2.89	6.48	1.66	0.02	0
		October	0.76	2.37	6.67	1.21	0.04	0
Deciduous forest	0–5 cm	February	6.31	55.49	4.53	0	1.72	0.15
		April	5.67	34.33	5.12	0	0.86	0.33
		June	6.53	64.48	5.44	0	0.21	0.32
		August	11.70	82.16	4.76	0	0.12	0.16
		October	7.93	63.89	5.56	0	1.09	0.29
Mixed coniferous forest	0–5 cm	February	34.23	115.24	3.90	0	0.13	3.32
		April	16.95	93.94	4.50	0.03	1.23	0.13
		June	43.26	124.44	4.51	0	2.75	1
		August	19.88	120.56	4.78	0	0.64	0.04
		October	29.55	-	4.69	0.02	0.36	0.21

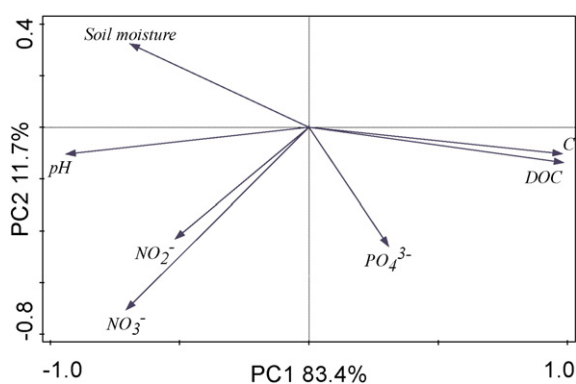


Fig. 3. Principal component analysis biplot of PC1 and PC2 shows the approximated correlation of environmental variables. A sharp angle indicates a positive correlation. The length of the arrow is a measure of fit for the environmental variable.

study can be related to aboveground vegetation since the initial pH varies among plant litter (Cornelissen et al., 2006). Especially woody debris has been shown to be more acidic than litter from leaf bodies, due to the production of organic acids (Ma et al., 2014). The release of these organic acids during accumulation in soils alters the pH of soil organic matter (Finzi et al., 1998), eventually leading to low pH values as measured in our forest samples. Moreover, our results reveal a negative correlation between pH and DOC concentration that might be explained by lower sorption at decreasing pH due to decreasing negative charge on the DOM itself (Kalbitz et al., 2000a). Nitrate concentration was significantly higher at both agricultural soil depths and M0–5 compared to forested sites and M40–50 ($p = 0.008$ to all other sites/depths) and significantly higher in M40–50 samples compared to forest samples ($p = 0.008$ to both forested sites).

Our results suggest that DOM composition depends to a large degree on environmental parameters. Testing chemical parameters showed that only pH and nitrate had significant effects (Fig. 4). Together they explain 75.3% of the variability. If pH is not selected using interactive forward selection test also DOC has significant effects. However, due to the negative correlation (Fig. 3; De Troyer et al., 2014; Roth et al., 2013) and thus, contradictory effects between pH and DOC in soil solutions, DOC content alone gives no further explanation to the variation in DOM composition if both environmental variables (pH and DOC) are considered. Soil pH is positively correlated to $(N/C)_w$ and negatively correlated to $(C\#)_w$, $(O/C)_w$ ratio and $(MW)_w$. Similar results were found by Roth et al. (2015). The nitrate content is positively correlated to all parameters related to aromaticity and $(N/C)_w$ and is negatively correlated to $(H/C)_w$ (Fig. 4). Influence of nutrient status on SOM composition was also described by Vancampenhout et al. (2012). We performed variation partitioning, which explains the variation by two groups of environmental variables (pH and nitrate). According to this analysis most of the explained variation in magnitude-weighted parameters was related to shared effects of pH and nitrate (46.4%). In addition, the independent effect of pH was considerable (20.7%), whereas nitrate alone explained only 6.3% of the variation.

These changes in environmental parameters namely pH and nitrate might be largely affected by land-use. The effects of forest ecosystems on pH and agriculture on nutrient status was shown in investigation by Rigueiro-Rodríguez et al. (2012) and Frink et al. (1999). Several studies investigated the effect of environmental variables like pH and nitrate concentration but also DOC content on carbon degradation and transport processes in soils (Andersson et al., 2000; Kalbitz et al., 2000b; Guggenberger et al., 1994). In general, inorganic nutrients like nitrate and phosphate e.g. stimulate microbial DOC consumption. We measured moderate nitrate concentration in the arable soil and in the surface samples of managed meadow soils in our study. Consequently, the relative higher abundance of aromatic compounds in these samples might be related to the depletion of easy degradable low-molecular

weight compounds like carbohydrates due to available nutrients. In contrast, inorganic nutrient and DOC content was low in M40–50 samples. Due to these limitations degradation processes might decrease in subsoil. Furthermore, according to Rumpel et al. (2004) the aromatic portion of partially degraded lignin- and tannin-derived compounds might be gradually adsorbed by mineral soil components, and thus are partly inaccessible to microbial degradation. These effects would further limit the degradation process in subsoils.

It has been shown that decreasing pH negatively affect DOM degradation through its effect on the activity and the composition of the microbial community (Marschner and Kalbitz, 2003) and the inhibition of phenol oxidase resulting in the accumulation of phenolic substances that constrain other enzymes (Freeman et al., 2001). Organic compounds like organic acids, inhibitory to bacterial activity may accumulate in the DOC pool and further lower biodegradation processes. We find that higher molecular size, higher oxygenation and carbon content and less nitrogen containing compounds occur with lower pH values as described also by Roth et al. (2015, 2013). Decreasing pH negatively affects net nitrogen mineralization (Szlavecz et al., 2006), whereas the higher degree of oxygenation might be partly related to the occurrence of phenolic tannin compounds in forest samples (Roth et al., 2015).

3.3. Vertical differences in DOM composition

The clustering of A0–5 and A40–50 in one region of the PCA (Fig. 2) suggests relatively homogenous DOM chemistry and may arise from agricultural use (e.g. tillage, ploughing). If environmental data were compared, both depths differ only in soil C/DOC concentration. In contrast, M0–5 and M40–50 samples differ significantly in soil C/DOC, nitrate concentration and soil moisture content, which is accompanied by different DOM composition. Fig. 5a shows all molecular formulae, which had a >25% higher relative intensity in M0–5 compared to M40–50 samples and vice versa (Fig. 5b). Fig. 6a, b shows molecular formulae which were either detected in all M0–5 samples, but in none of the M40–50 samples (Fig. 6a) or in all M40–50 samples and in none of the M0–5 samples (Fig. 6b). In general, molecular formulae with a relative higher intensity in M0–5 compared to M40–50 samples, where characterized by lower m/z values (M0–5: 375.3; M40–50: 417.6), higher aromaticity (AI-mod: M0–5: 0.55; M40–50: 0.27), lower H/C ratio (M0–5: 0.91; M40–50: 1.32) and higher O/C ratio (M0–5: 0.40; M40–50: 0.35). Similar trends were observed when evaluating depths trends in mineral soils (unpublished data by Roth et al.). These values indicate the input of fresh plant material, which is partly less microbially processed. M40–50 samples contain relatively more lipids, proteins, aminosugars and carbohydrates than M0–5 samples. These substances serve as main substrates and constituents of microorganisms. It is important to note that with ESI-FT-ICR-MS only trends and relative changes between samples can be detected. With this method we are not able to quantify the abundance of compounds because ionization efficiencies depend on the structure of molecules and the ionization efficiency can be suggested to be low for carbohydrates compared to many other component groups detected by FT-ICR-MS. Moreover, only few carbohydrates were detected, because carbohydrates are highly hydrophilic and hence not well recovered by solid phase extraction. The availability of these compounds in the subsoil can be attributed to decreased microbial activity as described also by Purton et al. (2015). Limited microbial activity might be partially attributable to low nutrient availability, but also to increased influence of organo-mineral associations, as the proportion of mineral-bound organic matter typically increases with depth (Kögel-Knabner et al., 2008). Besides decreasing microbial activity, the availability of easy degradable compounds in the subsoil might be also an indication of SOM recycling in deeper soil horizons as an important process in DOC production. After temporal immobilization by sorption to the mineral soil matrix or co-precipitation, DOC re-released into soil water might get altered or newly produced by microbial synthesis (Malik and Gleixner, 2013; Gleixner, 2013; Kaiser and Kalbitz, 2012)

Table 3
Magnitude-weighted parameters.

	(H/C) _w	(O/C) _w	(C#) _w	(DBE/O) _w	(DBE/C) _w	(DBE-O) _w	(Al-mod) _w	(N/C) _w	(M/W) _w
A0-5F	1.07	0.38	18.97	1.81	0.55	3.01	0.44	0.06	377.28
A0-5Ap	1.03	0.40	17.84	1.77	0.58	2.97	0.47	0.06	360.65
A0-5J	1.05	0.41	18.21	1.70	0.56	2.72	0.45	0.06	372.78
A0-5Ag	1.06	0.41	18.58	1.66	0.56	2.60	0.44	0.06	369.62
A0-5O	1.11	0.44	19.13	1.42	0.52	1.46	0.38	0.05	396.42
Average	1.06	0.41	18.55	1.67	0.55	2.55	0.44	0.06	375.35
Stddev	0.03	0.02	0.53	0.15	0.02	0.63	0.03	0.00	13.26
A40-50F	1.10	0.44	19.48	1.47	0.53	1.67	0.39	0.05	386.20
A40-50Ap	1.08	0.40	18.58	1.69	0.55	2.57	0.43	0.06	375.64
A40-50J	1.09	0.42	18.61	1.63	0.54	2.15	0.41	0.05	402.55
A40-50Ag	1.10	0.41	18.96	1.61	0.53	2.17	0.40	0.05	380.69
A40-50O	1.10	0.40	18.57	1.67	0.54	2.30	0.41	0.06	376.97
Average	1.09	0.41	18.84	1.61	0.54	2.17	0.41	0.05	384.41
Stddev	0.01	0.02	0.39	0.09	0.01	0.33	0.01	0.01	10.93
M0-5F	1.11	0.41	19.74	1.53	0.52	2.01	0.39	0.04	389.02
M0-5Ap	1.10	0.42	19.98	1.48	0.52	1.81	0.39	0.04	394.52
M0-5J	1.12	0.41	19.72	1.50	0.51	1.88	0.38	0.04	403.67
M0-5Ag	1.12	0.42	19.84	1.47	0.52	1.73	0.38	0.04	404.73
M0-5O	1.12	0.40	19.64	1.55	0.52	2.10	0.39	0.05	397.07
Average	1.11	0.41	19.78	1.51	0.52	1.91	0.39	0.04	397.80
Stddev	0.01	0.01	0.13	0.03	0.00	0.15	0.01	0.00	6.53
M40-50F	1.19	0.42	20.41	1.33	0.47	0.99	0.33	0.03	397.38
M40-50Ap	1.22	0.40	20.70	1.36	0.46	1.13	0.32	0.03	394.74
M40-50J	1.20	0.41	20.18	1.38	0.47	1.16	0.33	0.03	413.95
M40-50Ag	1.22	0.40	19.42	1.46	0.46	1.35	0.33	0.04	414.29
M40-50O	1.23	0.39	19.76	1.42	0.46	1.30	0.32	0.04	406.34
Average	1.21	0.40	20.09	1.39	0.46	1.19	0.33	0.03	405.34
Stddev	0.02	0.01	0.51	0.05	0.01	0.14	0.01	0.01	9.09
DF	1.07	0.41	20.73	1.56	0.53	2.30	0.40	0.02	442.42
DAp	1.13	0.44	21.00	1.33	0.50	1.08	0.35	0.02	440.74
DJ	1.15	0.42	20.22	1.47	0.49	1.50	0.35	0.02	446.60
DAg	1.16	0.43	21.24	1.32	0.48	0.97	0.33	0.02	437.98
DO	1.14	0.41	20.39	1.51	0.49	1.69	0.36	0.02	415.30
Average	1.13	0.42	20.72	1.44	0.50	1.51	0.36	0.02	436.61
Stddev	0.04	0.01	0.42	0.11	0.02	0.53	0.03	0.00	12.31
CF	1.11	0.47	21.28	1.28	0.50	0.78	0.34	0.01	428.35
CAp	1.12	0.46	21.41	1.26	0.50	0.75	0.34	0.01	427.36
CJ	1.10	0.46	21.84	1.29	0.50	1.02	0.35	0.01	410.11
CAg	1.13	0.45	21.74	1.31	0.49	0.98	0.34	0.01	403.43
CO	1.11	0.41	21.08	1.53	0.50	2.01	0.37	0.02	402.51
Average	1.11	0.45	21.47	1.33	0.50	1.11	0.35	0.01	414.35
Stddev	0.01	0.02	0.32	0.11	0.00	0.52	0.01	0.00	12.68
SAp	1.69	0.47	20.49	0.70	0.21	-4.92	0.14	0.01	436.47
SJ	1.27	0.38	20.44	1.39	0.43	1.10	0.29	0.03	401.18
SAg	1.24	0.39	20.09	1.37	0.45	1.16	0.31	0.03	398.32
SO	1.23	0.39	19.98	1.41	0.46	1.27	0.32	0.03	396.19
Average	1.36	0.41	20.25	1.22	0.39	-0.35	0.27	0.03	408.04
Stddev	0.22	0.04	0.25	0.35	0.12	3.05	0.08	0.01	19.06
VAp	1.51	0.35	18.62	1.27	0.32	-0.25	0.20	0.02	371.48
VJ	1.23	0.39	20.50	1.39	0.45	1.21	0.31	0.03	406.00
VAg	1.27	0.37	20.24	1.39	0.43	1.19	0.29	0.03	397.85
VO	1.22	0.39	20.26	1.41	0.46	1.30	0.32	0.03	402.45
Average	1.31	0.38	19.91	1.37	0.42	0.86	0.28	0.03	394.44
Stddev	0.14	0.02	0.86	0.06	0.06	0.74	0.05	0.01	15.67

and thus, can support a large microbial community (Gabor et al., 2014). Additionally, M40-50 are partly influenced by groundwater, thus water-logging might be also responsible for decreased degradation and the availability of easy degradable compounds.

Even though we found low-molecular-weight compounds like lipids, proteins, aminosugars and carbohydrates in the subsoil of M40-50 samples, in general, the averaged relative intensity of present low-molecular-substances ($200 < m/z < 300$) was higher in surface than in subsoil samples and beyond that higher in agricultural than in meadow samples (A0-5 = 3.45, SD = 0.72, A40-50 = 2.81, SD = 0.41, M0-5 = 2.42, SD = 0.15, M40-50 = 1.95, SD = 0.37, SI - Table 4). There were two exceptions (A-October and M-August), which might be related to tillage, manure and planting of Triticale on arable land in September/October and influence of high rainfall intensity in August (Fig. 1) and ensuing increased leaching in meadow samples during this month. In contrast, the averaged relative intensities of substances with

m/z values between 350 and 450 were similar in surface soils and subsoils and differed only slightly between arable soil and managed meadow soils (A0-5 = 2.48, SD = 0.10, A40-50 = 2.42, SD = 0.03, M0-5 = 2.55, SD = 0.05, M40-50 = 2.55, SD = 0.11). For $m/z > 500$, the averaged relative intensity was similar in subsoil and surface samples of agricultural samples and higher in subsoil compared to surface samples if the managed meadow soils were compared. Generally, the averaged intensity for $m/z > 500$ compounds was higher in managed meadow than in agricultural samples (A0-5 = 0.88, SD = 0.10, A40-50 = 0.94, SD = 0.11, M0-5 = 1.19, SD = 0.05, M40-50 = 1.42, SD = 0.04).

3.4. Soil water vs. stream water

We found 120 molecular formulae that were only detected in stream water and in none of the 30 soil samples. These stream compounds are mainly aliphatic, have a high H/C ratio and contain less oxygen (Fig. 7a).

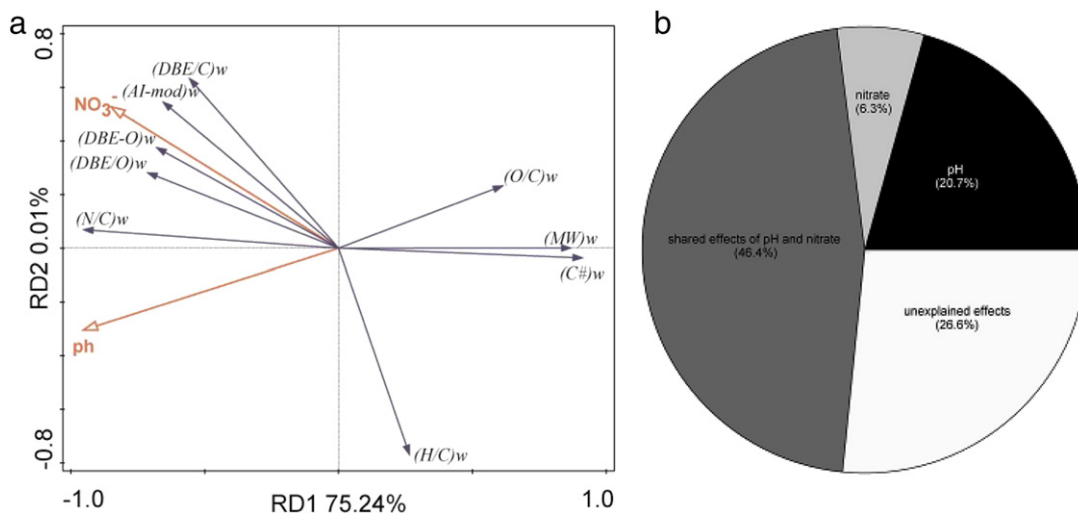


Fig. 4. a. Ordination biplot based on redundancy analyses of magnitude-weighted parameters and environmental parameters. Nitrate and pH were identified as significant factors and included in the model. b. Partitioning of the variation explained by the different sets (pH or nitrate) or combinations of sets (pH and nitrate) of explanatory variables.

In contrast, we detected 223 molecular formulae which were not detected in any stream sample, but were found in samples from all six sampling plots (M0–5, M40–50, A0–5, A40–50, D0–5, C0–5) and were additionally available at least in 50% of all soil samples. These

compounds are much more aromatic, have more double bonds and a much lower H/C ratio, which indicates the availability of fresh plant material and less microbial processed material, but higher oxygen content. There were only two compounds which were present in all 30 soil

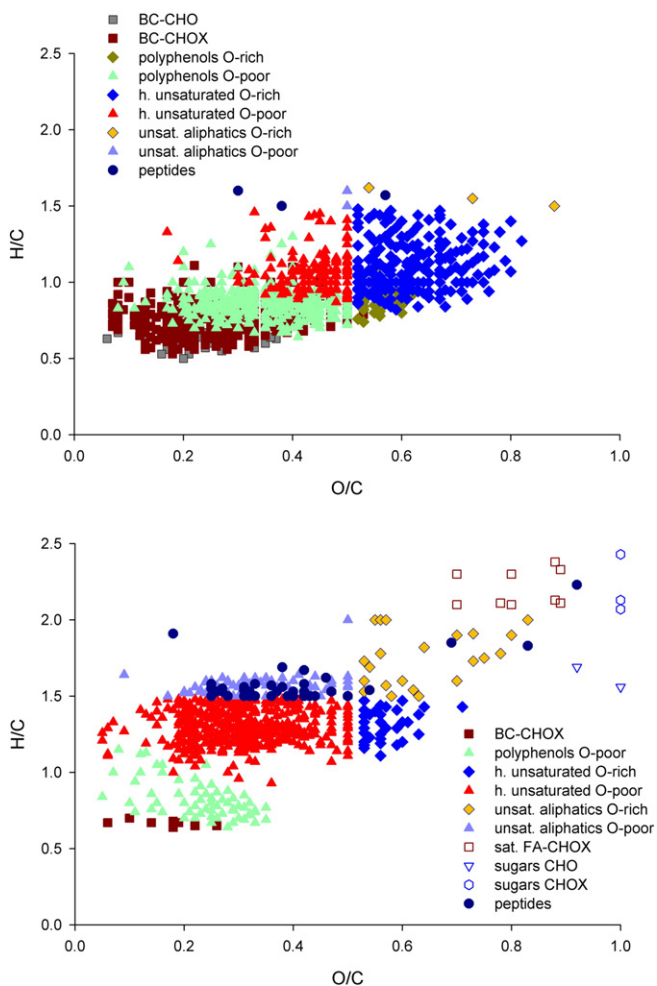


Fig. 5. The van Krevelen diagram shows the distribution of chemical components with a relative higher (>25%) intensity in a) all averaged M0-5 samples compared to averaged M40-50 and b) in all averaged M40-50 compared to averaged M0-5.

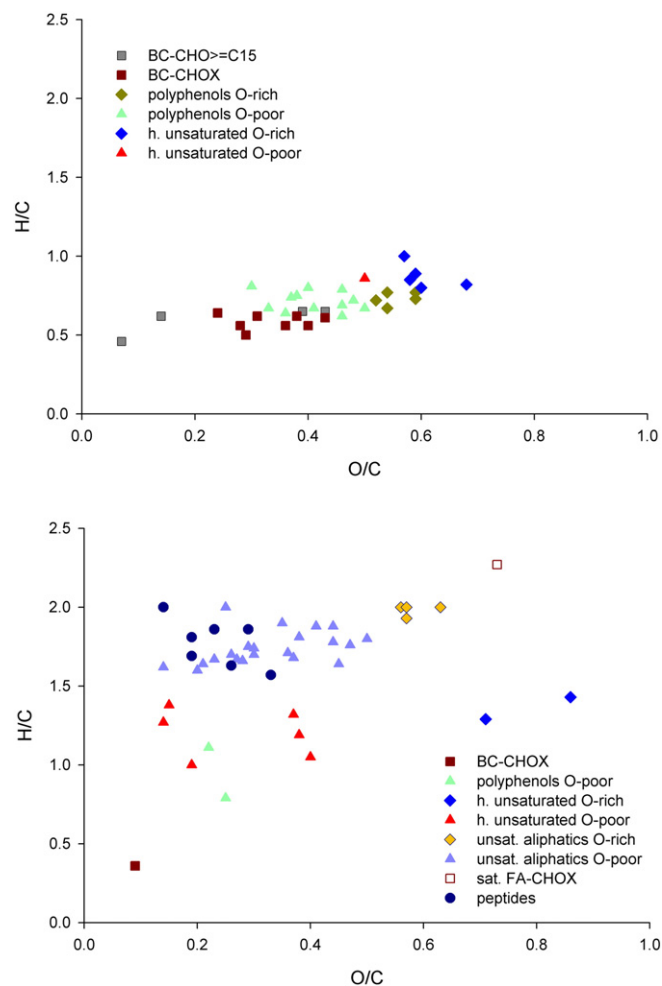


Fig. 6. The van Krevelen diagram shows the distribution of chemical components which were abundant either in a) all M0-5 samples and in non of the M40-50 samples or b) in all M40-50 samples and in non of the M0-5 samples.

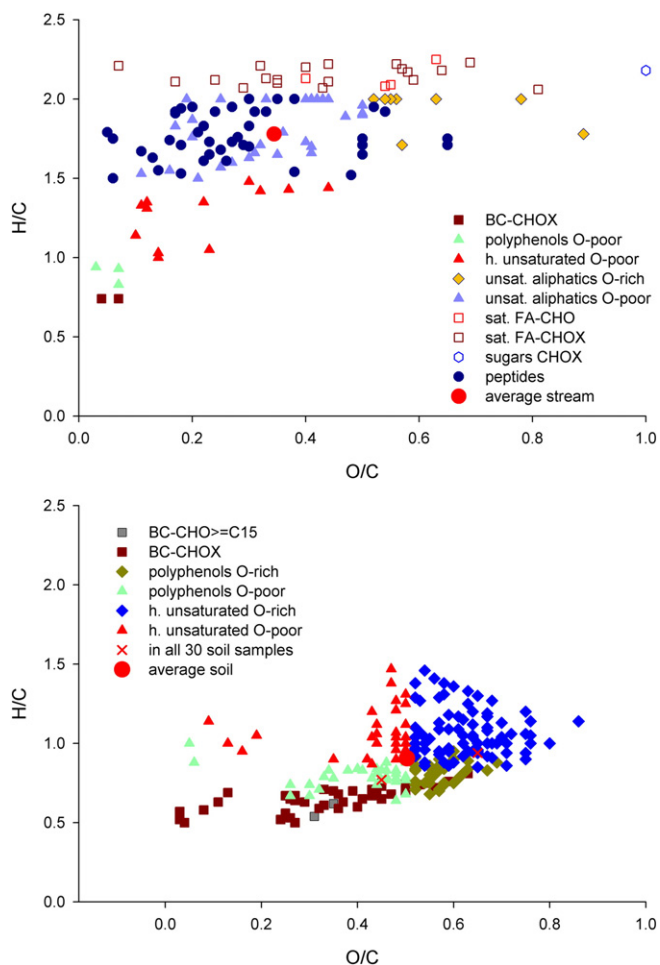


Fig. 7. Van Krevelen diagram showing the distribution of chemical components only present either in a) streams or in b) soil water. The components which represent streams were detected only in stream water but in none of the 30 soil samples. The soil components were found in samples from all six sampling plots (MO-5, M40-50, A0-5, A40-50, D0-5, C0-5) and were additionally available at least in >50% of all soil samples.

samples and in none of the eight stream samples (Fig. 7b). Large differences between compounds found either in streams or in soils are the lack of peptides, unsaturated aliphatics and saturated FA-CHO/FA-CHOX which were exclusively found in streams and the lack of highly unsaturated O-rich compounds and O-rich polyphenols which were exclusively found in soils. Other compounds like BC-CHOX and highly unsaturated O-poor compounds are detected in very low abundances in streams (Fig. 7a, b). We assume that most compounds found in streams, are not produced in the stream itself, but are of allochthonous origin. Besides flow from adjacent soils (including base flow, interflow and overland-flow, artificial drainage systems) allochthonous compounds can enter the stream via direct leachate of litter. The molecular formulae indicating O-poor polyphenols and highly unsaturated compounds might be a result of direct leachate and further modification and transformation processes in streams (Lu et al., 2013). In contrast to these allochthonous input, we assume that most peptides might be water-borne, because they were found in all streams and not in soils. Algal remains, for example, comprise a high percentage of peptide-like compounds (Knicker et al., 2004).

We found the largest overlap and similarity in chemical composition between stream and M40–50 cm (Fig. 2) assuming that soil water from deeper horizons and/or groundwater predominantly feeds the flow to the stream. This observation is well in agreement with another study recently performed in the Schwingbach catchment that showed similar isotopic composition for soil water from deeper

horizons/groundwater from managed meadow samples and stream surface water assuming as well that water from these vegetation site and horizons are primarily transported to the stream (Orlowski et al., 2015). It has been shown that stream DOC concentration is similar to concentrations found in soil water from deeper soil horizons despite high concentrations observed in leachate from surface soil (McDowell and Wood, 1984). However, organic-rich surface soils can contribute substantially to stream DOC when hydrologic conditions ensure connectivity of these DOC sources to the streams (Pacific et al., 2010; Hood et al., 2006; Prokushkin et al., 2005). Results of overland flow into the stream were not obvious from our measurements. Similar results were detected by Orlowski et al. (2015). Here, even during peak flow, isotopic signals of rainfall caused by increased runoff to the streams, did not contribute substantially to stream water isotopic composition although fast rainfall-runoff behaviors were observed (Orlowski et al., 2014). These observations are often made in small catchments where increased rainfall results in the discharge of “old” groundwater (Kirchner, 2003). The lack of evidence for overland- and/or interflow might further be related to only punctual measurements, because inputs to the streams are rapidly transported downstream. Our results show that chemical compounds which were available only in stream water, but not detected in any soil sample were much more aliphatic (Roth et al., 2015). Large molecules, condensed H/C and tannins were not found in streams. As already discussed, the complex soil structure adsorbed substances or they were degraded and thus, prevented them from being transported down the soil profile and further into the stream.

4. Summary and conclusion

We linked soil and stream DOM composition that were investigated with a method that allows us to resolve a high spectrum of compound classes on a molecular level. We compared molecular formulae of 30 soil samples from different sites characterized by different land use, vegetation cover and soil depth and eight stream samples. Most molecular formulae are not soil-ecosystem and/or season specific and were present at all sites and depths and during most seasons. System specific molecular formulae for soil samples were found in low number and low relative intensity and thus, could not be attributed to a specific land-use or vegetation scenario, even if only surface soil samples were compared. However, differences between soil samples were observed and seem to be more pronounced between mineral and organic soil surfaces and if vertical soil samples in non-disturbed profiles were compared. Managed meadow samples from surface and subsoil suggest a decline of aromatic structures with soil depth, which might indicate less fresh plant material in subsoils.

Land use is a key driver for changes in environmental conditions. These induced changes especially in pH and nitrate content are reflected in DOM composition of soil samples and might be more important than vegetation itself. Decreasing pH is linked to higher carbon and oxygen content of molecules and thus, greater molecular weight, which is probably related to inhibited microbial and enzymatic activity at low pH. Nitrate content is positively correlated to all parameters related to aromaticity and $(N/C)_w$ and negatively affects $(H/C)_w$, what probably reflects easy decomposable aboveground vegetation and thus, more fresh plant material in surface soils. Unique molecular formulae were only found when streams and overall soil samples were compared. Thus, results might either reflect the anthropogenic influence in this landscape what obliterates differences in DOM composition or only broad ecosystem categories like streams and soils contain noticeable unique molecular formulae. Since environmental characteristics and vertical soil profiles are important for DOM composition, future studies should focus on the influence of environmental data and consider vertical soil stratification and groundwater influence.

Supplementary data to this article can be found online at <http://dx.doi.org/10.1016/j.scitotenv.2016.07.033>.

Acknowledgments

Anne-Gret Seifert acknowledges financial support by the Deutsche Forschungsgemeinschaft (DFG)/German Research Foundation/Project SE 2313/1-1. We further like to thank the Justus Liebig University for grants provided to establish the Studienlandschaft Schwingbachtal. Vanessa-Nina Roth received financial support from the foundation “Zwillenberg-Tietz Stiftung” and Deutsche Forschungsgemeinschaft (DFG)/German Research Foundation as part of the collaborative research centre (CRC) 1076 “AquaDiva”.

Special thank to I. Ulber for general assistance in the lab and K. Klapproth for technical support with FT-ICR-MS.

References

- Andersson, S., Nilsson, S.J., et al., 2000. Leaching of dissolved organic carbon (DOC) and dissolved organic nitrogen (DON) in mor humus as affected by temperature and pH. *Soil Biol. Biochem.* 32 (1), 1–10.
- Bu, X.L., Wang, L.M., et al., 2010. Spectroscopic characterization of hot-water extractable organic matter from soils under four different vegetation types along an elevation gradient in the Wuyi Mountains. *Geoderma* 159 (1–2), 139–146.
- Cohen, M.J., Dunne, E.J., et al., 2008. Spatial variability of soil properties in cypress domes surrounded by different land uses. *Wetlands* 28 (2), 411–422.
- Cornelissen, J.H.C., Quested, H.M., et al., 2006. Foliar pH as a new plant trait: can it explain variation in foliar chemistry and carbon cycling processes among subarctic plant species and types? *Oecologia* 147 (2), 315–326.
- De Troyer, I., Merckx, R., et al., 2014. Factors controlling the dissolved organic matter concentration in pore waters of agricultural soils. *Vadose Zone J.* 13 (7).
- Dittmar, T., Koch, B.P., 2006. Thermogenic organic matter dissolved in the abyssal ocean. *Mar. Chem.* 102 (3–4), 208–217.
- Dittmar, T., Koch, B., et al., 2008. A simple and efficient method for the solid-phase extraction of dissolved organic matter (SPE-DOM) from seawater. *Limnol. Oceanogr. Methods* 6, 230–235.
- Embacher, A., Zsolnay, A., et al., 2007. The dynamics of water extractable organic matter (WDOM) in common arable topsoils: I. Quantity, quality and function over a three year period. *Geoderma* 139 (1–2), 11–22.
- Fellman, J.B., Hood, E., et al., 2009. Changes in the concentration, biodegradability, and fluorescent properties of dissolved organic matter during stormflows in coastal temperate watersheds. *J. Geophys. Res. Biogeosci.* 114.
- Fiebig, D.M., 1995. Groundwater discharge and its contribution of dissolved organic-carbon to an upland stream. *Arch. Hydrobiol.* 134 (2), 129–155.
- Finzi, A.C., Canham, C.D., et al., 1998. Canopy tree soil interactions within temperate forests: species effects on pH and cations. *Ecol. Appl.* 8 (2), 447–454.
- Freeman, C., Ostle, N., et al., 2001. An enzymic ‘latch’ on a global carbon store - a shortage of oxygen locks up carbon in peatlands by restraining a single enzyme. *Nature* 409 (6817), 149.
- Frink, C.R., Waggoner, P.E., et al., 1999. Nitrogen fertilizer: retrospect and prospect. *Proc. Natl. Acad. Sci. U. S. A.* 96 (4), 1175–1180.
- Fröberg, M., Kleja, D.B., et al., 2007. The contribution of fresh litter to dissolved organic carbon leached from a coniferous forest floor. *Eur. J. Soil Sci.* 58 (1), 108–114.
- Gabor, R.S., Eilers, K., et al., 2014. From the litter layer to the saprolite: chemical changes in water-soluble soil organic matter and their correlation to microbial community composition. *Soil Biol. Biochem.* 68, 166–176.
- Gleixner, G., 2013. Soil organic matter dynamics: a biological perspective derived from the use of compound-specific isotopes studies. *Ecol. Res.* 28 (5), 683–695.
- Guggenberger, G., Glaser, B., et al., 1994. Heavy-metal binding by hydrophobic and hydrophilic dissolved organic-carbon fractions in a Spodosol-a and Spodosol-B-horizon. *Water Air Soil Pollut.* 72 (1–4), 111–127.
- Guggenberger, G., Zech, W., et al., 1995. Lignin and carbohydrate alteration in particle-size separates of an oxisol under tropical pastures following native savanna. *Soil Biol. Biochem.* 27 (12), 1629–1638.
- Herzprung, P., von Tumpling, W., et al., 2012. Variations of DOM quality in inflows of a drinking water reservoir: linking of van Krevelen diagrams with EEMF spectra by rank correlation. *Environ. Sci. Technol.* 46 (10), 5511–5518.
- Hood, E., Gooseff, M.N., et al., 2006. Changes in the character of stream water dissolved organic carbon during flushing in three small watersheds, Oregon. *J. Geophys. Res. Biogeosci.* 111 (G1).
- Houser, J.N., Mulholland, P.J., et al., 2005. Catchment disturbance and stream metabolism: patterns in ecosystem respiration and gross primary production along a gradient of upland soil and vegetation disturbance. *J. N. Am. Benthol. Soc.* 24 (3), 538–552.
- Hury, A.D., Hury, V.M.B., et al., 2002. Catchment land-use, macroinvertebrates and detritus processing in headwater streams: taxonomic richness versus function. *Freshw. Biol.* 47 (3), 401–415.
- Jones, D.L., Simfukwe, P., et al., 2014. Evaluation of dissolved organic carbon as a soil quality indicator in national monitoring schemes. *PLoS One* 9 (3).
- Kaiser, K., Kalbitz, K., 2012. Cycling downwards - dissolved organic matter in soils. *Soil Biol. Biochem.* 52, 29–32.
- Kalbitz, K., Geyer, S., et al., 2000a. A comparative characterization of dissolved organic matter by means of original aqueous samples and isolated humic substances. *Chemosphere* 40 (12), 1305–1312.
- Kalbitz, K., Solinger, S., et al., 2000b. Controls on the dynamics of dissolved organic matter in soils: a review. *Soil Sci.* 165 (4), 277–304.
- Kirchner, J.W., 2003. A double paradox in catchment hydrology and geochemistry. *Hydrol. Process.* 17 (4), 871–874.
- Knicker, H., 2004. Stabilization of N-compounds in soil and organic-matter-rich sediments - what is the difference? *Mar. Chem.* 92 (1–4), 167–195.
- Koch, B.P., Dittmar, T., 2006. From mass to structure: an aromaticity index for high-resolution mass data of natural organic matter. *Rapid Commun. Mass Spectrom.* 20 (5), 926–932.
- Koch, B.P., Witt, M.R., et al., 2005. Molecular formulae of marine and terrigenous dissolved organic matter detected by electrospray ionization Fourier transform ion cyclotron resonance mass spectrometry. *Geochim. Cosmochim. Acta* 69 (13), 3299–3308.
- Kögel-Knabner, I., Guggenberger, G., et al., 2008. Organo-mineral associations in temperate soils: integrating biology, mineralogy, and organic matter chemistry. *J. Plant Nutr. Soil. Sci. (Zeitschrift Für Pflanzenernährung Und Bodenkunde)* 171 (1), 61–82.
- Kujawinski, E.B., Del Vecchio, R., et al., 2004. Probing molecular-level transformations of dissolved organic matter: insights on photochemical degradation and protozoan modification of DOM from electrospray ionization Fourier transform ion cyclotron resonance mass spectrometry. *Mar. Chem.* 92 (1–4), 23–37.
- Lauer, F., Frede, H.-G., et al., 2013. Uncertainty assessment of quantifying spatially concentrated groundwater discharge to small streams by distributed temperature sensing. *Water Resour. Res.* 49 (1), 400–407.
- Lu, Y.H., Bauer, J.E., et al., 2013. Photochemical and microbial alteration of dissolved organic matter in temperate headwater streams associated with different land use. *J. Geophys. Res. Biogeosci.* 118 (2), 566–580.
- Ma, Y.N., Filley, T.R., et al., 2014. Controls on wood and leaf litter incorporation into soil fractions in forests at different successional stages. *Soil Biol. Biochem.* 69, 212–222.
- Malik, A., Gleixner, G., 2013. Importance of microbial soil organic matter processing in dissolved organic carbon production. *FEMS Microbiol. Ecol.* 86 (1), 139–148.
- Marschner, B., Kalbitz, K., 2003. Controls of bioavailability and biodegradability of dissolved organic matter in soils. *Geoderma* 113 (3–4), 211–235.
- McDowell, W.H., Wood, T., 1984. Podzolization - soil processes control dissolved organic-carbon concentrations in stream water. *Soil Sci.* 137 (1), 23–32.
- Mosher, J.J., Kaplan, L.A., et al., 2015. Longitudinal shifts in dissolved organic matter chemogeography and chemodiversity within headwater streams: a river continuum reprise. *Biogeochemistry* 124 (1–3), 371–385.
- Orlowski, N., Lauer, F., et al., 2014. Linking spatial patterns of groundwater table dynamics and streamflow generation processes in a small developed catchment. *WaterSA* 6 (10), 3085–3117.
- Orlowski, N., Kraft, P., et al., 2015. Exploring water cycle dynamics through sampling multiple stable water isotope pools in a small developed landscape of Germany. *Hydrol. Earth Syst. Sci. Discuss.* 12, 1809–1853.
- Pacific, V.J., Jencso, K.G., et al., 2010. Variable flushing mechanisms and landscape structure control stream DOC export during snowmelt in a set of nested catchments. *Biogeochemistry* 99 (1–3), 193–211.
- Prokushkin, A.S., Kajimoto, T., et al., 2005. Climatic factors influencing fluxes of dissolved organic carbon from the forest floor in a continuous-permafrost Siberian watershed. *Can. J. For. Res. (Revue Canadienne De Recherche Forestiere)* 35 (9), 2130–2140.
- Purton, K., Pennock, D., et al., 2015. Will changes in climate and land use affect soil organic matter composition? Evidence from an ecotonal climosequence. *Geoderma* 253, 48–60.
- Rasilo, T., Ojala, A., et al., 2015. Concentrations and quality of DOC along the terrestrial-aquatic continuum in a boreal forested catchment. *Freshw. Sci.* 34 (2), 440–455.
- Riedel, T., Biester, H., et al., 2012. Molecular fractionation of dissolved organic matter with metal salts. *Environ. Sci. Technol.* 46 (8), 4419–4426.
- Rigueiro-Rodríguez, A., Mosquera-Losada, M.R., et al., 2012. Afforestation of agricultural land with *Pinus radiata* D. don and *Betula alba* L. in NW Spain: effects on soil pH, understorey production and floristic diversity eleven years after establishment. *Land Degrad. Dev.* 23 (3), 227–241.
- Roth, V.-N., Dittmar, T., et al., 2013. Latitude and pH driven trends in the molecular composition of DOM across a north south transect along the Yenisei River. *Geochim. Cosmochim. Acta* 123, 93–105.
- Roth, V.-N., Dittmar, T., et al., 2014. Ecosystem-specific composition of dissolved organic matter. *Vadose Zone J.* 13 (7).
- Roth, V.-N., Dittmar, T., et al., 2015. The molecular composition of dissolved organic matter in forest soils as a function of pH and temperature. *PLoS One* 10 (3).
- Rumpel, C., Eusterhues, K., et al., 2004. Location and chemical composition of stabilized organic carbon in topsoil and subsoil horizons of two acid forest soils. *Soil Biol. Biochem.* 36 (1), 177–190.
- Sanderman, J., Lohse, K.A., et al., 2009. Linking soils and streams: sources and chemistry of dissolved organic matter in a small coastal watershed. *Water Resour. Res.* 45.
- Seidel, M., Beck, M., et al., 2014. Biogeochemistry of dissolved organic matter in an anoxic intertidal creek bank. *Geochim. Cosmochim. Acta* 140 (2014), 418–434.
- Sleighter, R.L., Lie, Z.F., et al., 2010. Multivariate statistical approaches for the characterization of dissolved organic matter analyzed by ultrahigh resolution mass spectrometry. *Environ. Sci. Technol.* 44 (19), 7576–7582.
- Steinbeiss, S., Temperton, V.M., et al., 2008. Mechanisms of short-term soil carbon storage in experimental grasslands. *Soil Biol. Biochem.* 40 (10), 2634–2642.
- Stenson, A.C., Marshall, A.G., et al., 2003. Exact masses and chemical formulas of individual Suwannee River fulvic acids from ultrahigh resolution electrospray ionization Fourier transform ion cyclotron resonance mass spectra. *Anal. Chem.* 75 (6), 1275–1284.

- Strayer, D.L., Beighley, R.E., et al., 2003. Effects of land cover on stream ecosystems: roles of empirical models and scaling issues. *Ecosystems* 6 (5), 407–423.
- Szlavec, K., Placella, S.A., et al., 2006. Invasive earthworm species and nitrogen cycling in remnant forest patches. *Appl. Soil Ecol.* 32 (1), 54–62.
- Traversa, A., D'Orazio, V., et al., 2008. Properties of dissolved organic matter in forest soils: influence of different plant covering. *For. Ecol. Manag.* 256 (12), 2018–2028.
- Vancampenhout, K., De Vos, B., et al., 2012. Organic matter of subsoil horizons under broadleaved forest: highly processed or labile and plant-derived? *Soil Biol. Biochem.* 50, 40–46.
- Wickland, K.P., Neff, J.C., et al., 2007. Dissolved organic carbon in Alaskan boreal forest: sources, chemical characteristics, and biodegradability. *Ecosystems* 10 (8), 1323–1340.



Fe- and Cu-Complex Formation with Artificial Ligands Investigated by Ultra-High Resolution Fourier-Transform ion Cyclotron Resonance Mass Spectrometry (FT-ICR-MS): Implications for Natural Metal-Organic Complex Studies

Hannelore Waska^{1*}, Andrea Koschinsky² and Thorsten Dittmar¹

¹ Research Group for Marine Geochemistry (ICBM-MPI Bridging Group), Institute for Chemistry and Biology of the Marine Environment (ICBM), Carl von Ossietzky University Oldenburg, Oldenburg, Germany, ² Department of Physics and Earth Sciences, Jacobs University Bremen, Bremen, Germany

OPEN ACCESS

Edited by:

Kristen Nicolle Buck,
University of South Florida, USA

Reviewed by:

Martha Gledhill,
GEOMAR Helmholtz Centre for Ocean
Research Kiel, Germany
Rene Boiteau,
Woods Hole Oceanographic
Institution, USA

*Correspondence:

Hannelore Waska
hannelore.waska@uni-oldenburg.de

Specialty section:

This article was submitted to
Marine Biogeochemistry,
a section of the journal
Frontiers in Marine Science

Received: 31 March 2016

Accepted: 22 June 2016

Published: 12 July 2016

Citation:

Waska H, Koschinsky A and Dittmar T
(2016) Fe- and Cu-Complex
Formation with Artificial Ligands
Investigated by Ultra-High Resolution
Fourier-Transform ion Cyclotron
Resonance Mass Spectrometry
(FT-ICR-MS): Implications for Natural
Metal-Organic Complex Studies.
Front. Mar. Sci. 3:119.
doi: 10.3389/fmars.2016.00119

In recent years, electrospray-ionization mass spectrometry (ESI-MS) has been increasingly used to complement the bulk determination of metal-ligand equilibria, for example via competitive ligand exchange-adsorptive cathodic stripping voltammetry (CLE-ACSV). However, ESI-MS speciation analyses may be impacted by instrumental artifacts such as reduction reactions, fragmentation, and adduct formation at the ESI source, changes in the ionization efficiencies of the detected species in relation to sample matrix, and peak overlaps in response to increasing sample complexity. In our study, equilibria of the known artificial ligands citrate, ethylenediaminetetraacetic acid (EDTA), 1-nitroso-2-naphthol (NN), and salicylaldoxime (SA) with iron (Fe) and copper (Cu) were investigated by ultra-high resolution ESI-MS, Fourier-transform ion cyclotron resonance mass spectrometry (FT-ICR-MS), under a variety of sample matrix and ionization settings. The acquired mass spectra were compared with metal-ligand equilibrium data from the literature as well as an adapted speciation model. Overall, the mass spectra produced representative species mentioned in previous reports and predicted by the speciation calculations, such as Fe(Cit), Cu(Cit)₂, Fe(EDTA), Cu(EDTA), Fe(NN)₃, and Cu(SA)₂. The analyses furthermore revealed new species which had been hypothesized but not measured directly using other methods, for example ternary complexes of citrate with Fe and Cu, Cu(SA) monomers, and the dimer Fe(SA)₂. Finally, parallel measurements of a Cu+SA calibration series and a Cu+SA+EDTA competition series indicated that FT-ICR-MS can produce linear responses and low detection limits analogous to those of ACSV. We propose that ultra-high resolution FT-ICR-MS can be used as a representative tool to study interactions of trace metals with artificial as well as natural, unknown ligands at the molecular level.

Keywords: ligands, FT-ICR-MS, iron, copper, EDTA, citrate, salicylaldoxime, 1-nitroso-2-naphthol

INTRODUCTION

Electrospray-ionization mass spectrometry (ESI-MS) has become a promising new technique for the description of metal-ligand equilibria using known ligands. The advantage of ESI-MS resides in its easy application—samples in solution can be swiftly processed under a wide array of conditions—and its soft ionization procedure which allows for the detection of whole metal-organic compounds (Di Marco and Bombi, 2006). The ESI-MS measurements of known metal-ligand mixtures can be compared with speciation data acquired from other methods such as computational speciation modeling, crystallography, or complex affinity titrations. For example, the complexing behavior of citrate, an important natural metal chelator which forms highly diverse species with iron under different pH and stoichiometry conditions, has been studied by ESI-MS in comparison with complementary techniques, such as spectrophotometric titrations and chemical modeling (Gautier-Luneau et al., 2005; Nischwitz and Michalke, 2009; Silva et al., 2009; Bertoli et al., 2015). In parallel to these studies on artificial metal-organic compounds under well-constrained conditions, ESI-MS has recently been applied to identify unknown metal-binding ligands isolated from natural waters, which ubiquitously occur as a component of natural dissolved organic matter (DOM), and which govern the mobility and availability of bioactive trace metals such as iron (Fe) and copper (Cu) (McCormack et al., 2003; Ross et al., 2003; Mawji et al., 2008, 2011; Stenson, 2009; Velasquez et al., 2011). Although the number of studies in the field is scarce, they have shown that ESI-MS is currently the only technique with the potential to study a large number of metal-organic complexes simultaneously at the molecular level: ESI-MS and in particular ESI-FT-ICR-MS (Electrospray-ionization Fourier-transform ion cyclotron resonance mass spectrometry) are capable of resolving the high complexity of DOM, where thousands of unique compounds occur at pico- to nanomolar concentrations (Repeta, 2015). As such, they complement one of the most wide-spread methods currently applied to characterize the bulk metal-binding capacity of natural DOM, competitive ligand exchange-adsorptive cathodic stripping voltammetry (CLE-ACSV, Buck and Bruland, 2005; Buck et al., 2007). CLE-ACSV is highly sensitive (detection limits are usually at pico- to nanomolar levels), quantitative, and metal-ligand speciation can be investigated at near-natural conditions with regards to pH and sample matrix (including ionic strength). However, the high complexity of DOM is not sufficiently represented in CLE-ACSV measurements, even though metal-binding ligands within DOM are treated as a composite of multiple sub-classes defined by the analytical window (i.e., the amount of added artificial ligand for competition with the natural ligands). Furthermore, the natural ligands are investigated based on the response of the added competing artificial ligand, rather than by direct observation of their behavior. ESI-MS, and in particular high-resolution ESI-FT-ICR-MS, thus holds great potential to extend this field of research (Waska et al., 2015).

To complement CLE-ACSV by ESI-MS and ESI-FT-ICR-MS, potential instrument-specific artifacts of the ESI-MS technique have to be taken into account (Di Marco and Bombi, 2006;

Keith-Roach, 2010; Waska et al., 2015). Examples for such effects are:

- (1) **Speciation** changes of the sample, for example through reduction, adduct formation, and fragmentation at the ESI source or in the gas phase can impact metal-ligand equilibria and prevent the detection of target molecules.
- (2) **Signal intensities** of the different species are affected by their net charge in aqueous solutions, but also by **compound specific response factors** influenced by ionization mode and sample matrix (for example, the presence of other ions causing signal enhancement or suppression).
- (3) Sample requirements for the optimum performance of the instrument, such as low ionic strengths, and the addition of organic solvents for ionization enhancement, may prevent **quantitative and qualitative comparisons** of *in vitro* metal-ligand equilibria with those taking place in natural aqueous environments.

All of the above mentioned issues have been known for a while (Di Marco and Bombi, 2006), but only in recent years, systematic, and compound-specific investigations have been increasingly used to evaluate ESI-MS as a quantitative tool in metal-ligand equilibrium studies (Gledhill, 2001; Rellán-Álvarez et al., 2008; Keith-Roach, 2010; Reinoso-Maset et al., 2012). In this study, we aim to address the above mentioned analytical challenges, and report the applicability of ultra-high resolution ESI-FT-ICR-MS for the qualitative and quantitative investigation of metal-ligand equilibria. ESI-FT-ICR-MS is traditionally used to resolve complex mixtures of organic compounds such as natural DOM (Koch et al., 2005). Organic compounds show linear responses in FT-ICR-MS based on their relative abundance in a complex matrix (Seidel et al., 2015), but this approach is rarely used for quantitative studies of known target compounds in natural DOM. Compared to ESI-MS systems with lesser resolving power, the employment of ESI-FT-ICR-MS provides a higher degree of certainty in the detection of monoisotopic mass differences of metal-containing complexes (Waska et al., 2015), and furthermore enables the automatized assignment of molecular formulae based on the Kendrick mass defect (Koch et al., 2007). Both these advantages result in a swifter and more accurate detection of target compounds in known metal-ligand equilibria, and provide the additional opportunity to identify unknown molecules in complex natural mixtures such as DOM.

For our study, we chose two experimental approaches:

- (1) A baseline study of well-known metal-organic complexes in a fixed metal-ligand stoichiometry at fixed pH under different sample matrix and ionization conditions. The resulting qualitative speciation patterns and response factors were compared with speciation data from the literature.
- (2) A quantitative study where a known artificial ligand was titrated with increasing metal concentrations, once in the absence and once in the presence of another known competing ligand analogous to a CLE-ACSV calibration series. The resulting calibration curves were compared to

the results of simultaneous CLE-ACSV measurements of the same sample setup.

The experimental approaches were backed up by metal-ligand speciation calculations using the modeling program PHREEQC (PHREEQC for Windows, version 2.18.00, http://wwwbrr.cr.usgs.gov/projects/GWC_coupled/phreeqc/) with a default minteqv4 database designed to predict metal-ligand speciation in aqueous solutions. This database already included several known ligands, and was extended in the scope of this study to accommodate all investigated artificial ligands, by using conditional stability constants from the literature (e.g., Gledhill and van den Berg, 1994; Abualhaija et al., 2015).

The focus of our study lays on Fe - and Cu- complexes due to their bioactive nature and high affinity for organic ligands (Van den Berg, 1984; Rue and Bruland, 1995; Buck and Bruland, 2005; Buck et al., 2007). For the qualitative study, we chose a representative range of previously described ligands with different functional groups, binding stoichiometries, and binding strengths (**Table 1**): *Citrate* is a naturally occurring, physiologically important metal chelator which has been studied in-depth by ESI-MS and other speciation methods (Gautier-Luneau et al., 2005; Nischwitz and Michalke, 2009; Silva et al., 2009; Bertoli et al., 2015). Because it is a tricarboxylate chelator with an additional binding hydroxyl group, it could be seen as a representative of natural DOM which is largely composed of $C_xH_yO_z$ compounds and also contains a high density of carboxyl and hydroxyl functional groups as revealed by NMR analyses (Hertkorn et al., 2006; Repeta, 2015). *EDTA*, an artificial ligand produced for industrial and pharmaceutical applications, has gained recent interest due to its accumulation in the aquatic environment, where it impacts trace metal mobility (Nowack, 2002). It is a hexadentate ligand with two amine and four carboxylate functional groups and forms strong 1:1 or 1:2 complexes with transition metals and other cations (Chen et al., 2008; Reinoso-Maset et al., 2012). *1-nitroso-2-naphthol* (hereafter referred to as NN) is a hydrophobic metal chelator with a nitroso- and a hydroxyl group. Due to its ability to form strong, electroactive 1:3 complexes with Fe it is used for the determination of free (Van den Berg et al., 1991) and organically bound (Wu and Luther, 1995; Hawkes et al., 2013) Fe in natural water samples via adsorptive cathodic stripping voltammetry (ACSV) and CLE-ACSV, respectively. *Salicylaldehyde oxime* (SA), a salicylaldehyde oxime, is a chelator with an oxime and a hydroxyl functional group which forms 1:1 and 1:2 complexes with Cu and Fe, and is routinely used in the determination of Fe- and Cu-complexing capacities of DOM in natural water samples via CLE-ACSV (Campos and van den Berg, 1994; Rue and Bruland, 1995). For the quantitative study, we chose an SA-EDTA ligand system competing for Cu. This system has been extensively studied by CLE-ACSV under variations of matrix conditions such as pH and ionic strength (Campos and van den Berg, 1994; Buck and Bruland, 2005).

To the best of our knowledge, NN and SA have not been studied in detail by ESI-MS, and none of the abovementioned ligands have been investigated by ultra-high resolution ESI-FT-ICR-MS (Di Marco and Bombi, 2006; Keith-Roach, 2010). Our

study thus lays the foundation to describing the natural metal-DOM pool with two contrasting and complementary techniques (CLE-ACSV and ESI-FT-ICR-MS) in the future.

MATERIALS AND METHODS

Sample Preparation

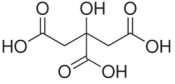
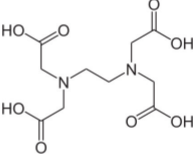
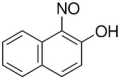
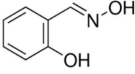
Baseline Setup

We produced a series of metal-ligand complex solutions by adding NIST traceable Fe and Cu standards (Alfa Aesar plasma standard solutions, original stock solutions in 5% HNO_3 , diluted in 0.01 M HCl suprapur for this study) to solutions of citrate (mono-sodium citrate, AppliChem), EDTA (EDTA tripotassium salt dihydrate, AppliChem), NN (1-nitroso-2-naphthol, 99%, Alfa Aesar), and SA (salicylaldehyde oxime $\geq 98\%$, Sigma Aldrich; **Table 1**). With the exception of NN, which was prepared using Optima LC-MS grade methanol (Fisher Chemicals), all ligand solutions were prepared with ultrapure water. The final metal-ligand solutions amounted to 20 μM metal (10 μM Fe and 10 μM Cu) and 100 μM ligand, producing a theoretical metal:ligand stoichiometry of 1:5 each. We chose this stoichiometry to provide sufficient ligands for both trace metals, thus preventing competition for binding sites and enabling simultaneous detection of free ligands as well as Fe- and Cu-complexes. The pH of the solutions was adjusted to $pH = 7.1 \pm 0.2$ in two setups using either sodium hydroxide or aqueous ammonia (both suprapur, Merck) and they were equilibrated overnight (>12 h) at room temperature. Thereafter, methanol (Optima LC-MS grade, Fisher Chemicals) was added to one set of solutions to produce a 1:1 methanol-water matrix, whereas the second set was kept in a water matrix. Both setups amounted to the same final ligand and trace metals concentrations. All solutions were filtered through 0.2 μm PTFE syringe filters prior to measurement.

Quantitative Setup

First, a calibration series was made by titrating increasing amounts of Cu (0–20 μM) to a constant amount of SA (200 μM) in 15 mL polytetrafluorethylene (PTFE) vials (VWR). The pH of the calibration solutions was adjusted to $pH = 7.5 \pm 0.2$ using sodium hydroxide. Subsamples were filtered through 0.2 μm PTFE syringe filters into acid-washed 2 mL Eppendorf safe-lock tubes, and Optima-grade methanol was added to each vial to produce a 1:1 (v:v) sample solution for FT-ICR-MS analysis. In a second treatment, we added 2 μM EDTA to each vessel of the same SA-Cu titration setup (0–20 μM Cu, 200 μM SA), and the samples were allowed to equilibrate overnight. Again, subsamples of the solutions were filtered into pre-cleaned safe-lock tubes and methanol was added prior to FT-ICR-MS measurements to produce a 1:1 (v:v) solution. The dilution with methanol resulted in final concentrations of 100 μM SA, 1 μM EDTA, and 0–10 μM Cu. Both setups (Cu + SA or Cu + EDTA + SA) were reproduced three times with the used reagent solutions being discarded after overnight equilibration, to condition all reaction vessels (PTFE and Eppendorf vials) before final sample preparations for the FT-ICR-MS measurement.

TABLE 1 | Properties of investigated ligands.

Ligand	Structure	logKCu(II)	logKFe(III)	Functional groups	Complex stoichiometry (for Fe and Cu)	References
Citric acid		6.1	11.85	3 carboxylate, 1 hydroxyl	1:2, 1:3 (Fe) 1:2, 1:3 (Cu)	Furia, 1972
EDTA		18.8	25.7	4 carboxylate, 2 amine	1:1 (Fe) 1:1 (Cu)	Furia, 1972
1-nitroso-2-naphthol		8.61	35.32*	1 nitroso, 1 hydroxyl	1:3 (Fe) 1:1 (Cu)	Sathe and Shetty, 1970 *Gledhill and van den Berg, 1994
Salicylaldoxime		11.97 Cu(SA)** 18.43 Cu(SA) ₂ **	6.66 Fe(SA)** 19.90 Fe(SA) ₂ **	1 oxime, 1 hydroxyl	1:1, 1:2 (Fe) 1:1, 1:2 (Cu)	**Abualhajja et al., 2015

All constants are for aqueous solutions with low salinity. *, ** had to be corrected for low salinity (calculated for the samples from this study to a salinity = 1×10^{-5}) based on the equations reported by the cited references.

FT-ICR-MS Analyses

The artificial metal-ligand solutions were analyzed in duplicates (qualitative setup) and triplicates (quantitative setup) on an ultra-high resolution 15 Tesla ESI-FT-ICR-MS (Solarix, Bruker Daltonics). All sample measurements were conducted in positive and negative ionization mode to compare speciation and ionization efficiencies of the complexes under the experimental pH and solvent settings. The measurement parameters were adapted from in-house tuning procedures commonly used for DOM analyses, in broadband scan mode with a syringe flow rate of $120 \mu\text{L h}^{-1}$ and an ion accumulation time of 0.20 s for negative and 0.25 s for positive ionization mode. For each sample, 100 mass scans were accumulated. Calibration was conducted internally using the Bruker DataAnalysis software with an error of <0.1 ppm, based on a specifically created mass list containing the calculated monoisotopic masses of the most dominant free ligands and complexes (Compass IsotopePattern, Bruker Daltonics), as well as known contaminations commonly found in ESI-MS spectra, such as fatty acids (Keller et al., 2008). The calibrated mass spectra were assembled to a common data table using a mass matching in-house Matlab script. To ensure reproducibility of the detected compounds and remove any noise, any detected mass had to occur in all replicate measurements of each setup to be considered for further data processing. Additionally, the acquired mass lists were processed with a Matlab search routine detecting $^{54/56}\text{Fe}$, $^{63/65}\text{Cu}$, $^{35/37}\text{Cl}$, $^{12/13}\text{C}$, and $^{39/41}\text{K}$ monoisotopic patterns based on the mass and abundance differences of the naturally occurring isotopes (Waska et al., 2015). This search routine was modified to detect peaks for up to three elements per molecule ($^{54/56}\text{Fe}$, $^{63/65}\text{Cu}$, $^{35/37}\text{Cl}$), and multiple ionization patterns ($^{12/13}\text{C}$). Thereafter, molecular formulae were assigned with the DataAnalysis software. A maximum mass error of 0.5 ppm was allowed, and the

elements $\text{C}_{1-50}\text{H}_{1-200}\text{O}_{1-100}\text{N}_{0-6}\text{Fe}_{0-3}\text{Cu}_{0-3}\text{Na}_{0-5}\text{Cl}_{0-5}$ were considered, allowing even and odd electron configurations where applicable (radicals with free electrons were not considered). Since EDTA had been added as potassium salt, K_{0-5} was included for the assignment of molecular formulae in the EDTA samples to account for potassium adducts. Only molecular formulae containing the molecular building blocks of the measured ligand (for example, C_6 and O_7 and their multiples for citrate) with a matching isotope pattern ($^{12/13}\text{C}$ plus the corresponding heteroatoms of the calculated molecular formulae) were taken into account. Thus, fragmented complexes or compounds with adducts other than NH_3^+ , Na^+ , K^+ , and Cl^- were not included.

CLE-ACSV Analyses

The Cu + SA ± EDTA titration setups were diluted 1:50 (Cu + SA only) and 1:25 (Cu + SA + EDTA) with ultrapure water and measured by ACSV (Campos and van den Berg, 1994; Waska et al., 2015). Immediately before the measurements, 100 μL of 3M KCl suprapur and 100 μL chelexed HEPES buffer (pH = 7.8) were added. The final solutions had a volume of 10 mL. Addition of KCl and HEPES buffer were included to (i) ensure enough ionic strength for the voltammetric cell, and (ii) achieve a stable pH for a reproducible location (and thus sensitivity) of the Cu-SA peak in the potential-current diagram. The instrument used was a Metrohm 757VA Computrace equipped with a hanging drop mercury electrode (HDME), a 3M KCl-filled reference electrode and a glassy carbon counter electrode. Samples were initially purged for 300 s with high purity Ar gas, then the salicylaldoxime-copper complex was deposited for 60 s at a potential of -50 mV. After an equilibration time of 5 s, the samples were scanned from -50 to -600 mV at a sweep rate of 20 mV s⁻¹. The measurement of each sample was repeated three times.

Speciation Calculations using PHREEQC

To predict ligand and metals speciation, thermodynamic equilibrium calculations were performed using the aqueous geochemical modeling program PHREEQC (Parkhurst and Appelo, 1999) with a minteqv4 database already containing conditional stability constants of EDTA and citrate with a variety of cations including Fe and Cu. Conditional stability constants were implemented into the minteqv4 database as follows: The conditional stability constant ($\log K$) for $\text{Cu}(\text{NN})_2$ was used directly from Sathe and Shetty (1970), whereas for $\text{Fe}(\text{NN})_3$, $\text{Cu}(\text{SA})$, $\text{Cu}(\text{SA})_2$, $\text{Fe}(\text{SA})$, and $\text{Fe}(\text{SA})_2$, $\log K'$ values were adjusted for an approximation of salinity ~ 0 (salinity = 1×10^{-5}) using the respective equations reported by Gledhill and van den Berg (1994) and Abualhaja et al. (2015) (Table 1). To calculate activity coefficients, by default a Davies equation was used by the program. The modified database is provided as Supplementary Information. Sample solutions for the calculations contained the adjusted pH and known added concentrations of Fe, Cu, and ligands. Only Fe(III) and Cu(II) were considered in the calculations, which were the main expected oxidation states of the NIST traceable standard solutions originally provided from Alfa Aesar in 5% HNO_3 . For oxygen and inorganic carbon contents, default concentrations of 64.5 and 0.49 μM , respectively, were incorporated from the PHREEQC examples database. Concentrations of K and Na corresponded to the added amounts of EDTA and citrate salts, respectively. In addition, concentrations of Cl, Na, and N(-3) corresponded to the added amounts of HCl (via the Fe and Cu spikes), NaOH, and aqueous ammonia (during pH adjustments). Because minteqv4 was created for aqueous solutions, the methanol content was not taken into account for the speciation calculations. This and other limitations of the speciation model (for instance, lack of data for complexes with yet unknown stoichiometries, metal valences, or cations such as Na^+ and K^+) may have impacted the outcome and should thus be kept in mind when considering the subsequent interpretations.

RESULTS

Speciation Patterns of the Target Compounds

In both ionization modes, the mass spectra of the investigated metal-ligand solutions were comprised mostly (86–90%) of singly ionized target compounds as revealed by the single charge $^{12/13}\text{C}$ isotope patterns opposed to those with double (9–14%) or triple (1–2%) charge. Moreover, all of the detected metal-ligand complexes were singly charged as well (Tables 2–5). The high mass resolution allowed the confirmation of the majority of the target compounds based on their unique isotopic patterns. For example, in negative ionization mode, the isotope mass differences of the detected complexes were (average of >10 measurements \pm standard deviation): $^{54/56}\text{Fe}$ (1.995329 \pm 0.00003 Da, natural difference: 1.995327 Da), $^{63/65}\text{Cu}$ (1.998198 \pm 0.000006 Da, natural difference: 1.99819 Da), $^{35/37}\text{Cl}$ (1.99705 \pm 0.00003 Da, natural difference: 1.99705 Da), $^{12/13}\text{C}$ (1.00337 \pm

0.00002 Da, natural difference: 1.00336 Da), and $^{39/41}\text{K}$ (1.99824 \pm 0.0002 Da, natural difference: 1.99812 Da). It should be noted that in complexes with a co-occurrence of K and Cu (found only in the solutions with EDTA), the isotope patterns of the two elements could not be resolved from each other due to their similar mass spacing: The overlap of the ^{65}Cu and ^{41}K signals changed the signal intensities of the apparent isotopologues, and prevented detection by the automated Matlab script.

For all investigated ligands and both ionization modes, adduct formation was observed: The dominant adduct was Na^+ , followed by K^+ (only for EDTA measurement setups) and Cl^- . Despite addition of aq. ammonia for pH adjustment in half of the experimental setups, NH_3^+ adducts were rarely found (Tables 2–5). In contrast to the numerous adduct-containing compounds detected via FT-ICR-MS, PHREEQC results had predicted that > 99% of Na^+ , K^+ , and Cl^- occurred as free ions in aqueous solution, while unbound ligand species differed only in their degree of protonation by free H^+ ions. Only sodium citrate species were calculated to occur in non-negligible amounts (732 nM), and only for the sample setup with NaOH as added base.

In the mass spectra, citrate compounds were mostly detected as mono-, di-, and trimers (Table 2), while mono- and dimers prevailed in the PHREEQC calculations. Three out of the four complexes predicted by the speciation calculations also occurred in the FT-ICR-MS spectra: a $\text{Fe}(\text{Cit})$ monomer, a $\text{Cu}(\text{Cit})_2$ dimer, and a $\text{Cu}_2(\text{Cit})_2$ dimer. A $\text{Cu}(\text{Cit})$ monomer predicted by PHREEQC was not detected in the mass spectra; instead, a 2:2 (metal:ligand) complex of Fe with citrate, and a ternary 2:2 complex of Fe and Cu with citrate, were found (Table 2). FT-ICR-MS and PHREEQC speciation results also overall agreed for the EDTA setups: Mostly monomers occurred, and Fe and Cu were exclusively complexed in 1:1 stoichiometries as well (Figure 1, Table 3). Although most detected metal-EDTA complexes in the mass spectra were with Fe(III) and Cu(II), three reduced Fe(II) complexes [$(\text{HEDTA})\text{Fe}(\text{II})^-$ ($m/z = 345.0026$), [$(\text{EDTA})\text{KFe}(\text{II})^-$ ($m/z = 382.9585$), and [$(\text{H}_2\text{EDTA})(\text{NH}_3)\text{Fe}(\text{II})^+$ ($m/z = 363.0361$)] occurred with small intensities (Table 3). NN generally occurred as mono- to trimers in negative, and mono- to pentamers in positive ionization mode. The Cu-NN ratio in the detected complexes was 1:2, while Fe was complexed by NN in 1:3, 1:4, and 1:5 stoichiometries. In negative ionization mode, these metal-NN complexes exclusively contained reduced Fe(II) and Cu(I), while in positive mode, $\text{Fe}(\text{III})(\text{NN})_3$ and $\text{Cu}(\text{II})(\text{NN})_2$ complexes were also detected (Table 4). In comparison, the speciation models predicted the occurrence of free NN exclusively as monomers, while for Fe and Cu, only the 1:3 and 1:2 stoichiometries, respectively, were calculated. Finally, all Cu and Fe were calculated in PHREEQC to be bound to SA in both 1:1 and 1:2 stoichiometries, and free SA was predicted to occur as monomer. Analogous to citrate, free SA also occurred in trimers in addition to the predicted mono-, and dimers in the mass spectra. It was bound to Fe in 1:1 and 1:2, and to Cu in 1:1, 1:2, and 1:3 stoichiometries. Both Cu(I) and Cu(II) were involved in the 1:1 complex formation with SA, while Fe was bound as Fe(III) (Table 5).

TABLE 2 | Detected citrate and citrate ± Fe ± Cu species (bold) in the four analytical setups at the FT-ICR-MS.

Ionization	Species	m/z	MeOH + H ₂ O + NH ₄	H ₂ O + NH ₄	MeOH + H ₂ O + Na	H ₂ O + Na
Negative	[(H ₃ Cit)] ⁻	191.0197	100	100	12.4	70.7
	[(H ₂ Cit)Na] ⁻	213.0017	2.3	1.7	6.8	14.2
	[(HCit)Na ₂] ⁻	234.9836	1.3	0.7	100	100
	[(Cit)Na ₃] ⁻	256.9655			22.2	10.1
	[(H ₂ Cit)Na ₂ Cl] ⁻	270.9603	3.1	1.8	1.2	9.5
	[(HCit)ClFe(III)]⁻	279.9078	1.7			
	[(HCit)Na ₃ Cl] ⁻	292.9423	0.4		21.8	22.3
	[(HCit)Na ₄ Cl ₂] ⁻	350.9008	0.2		10.3	13.7
	[(H ₄ Cit)(H ₃ Cit)] ⁻	383.0467	0.9	2.5		
	[(H ₃ Cit) ₂ Na] ⁻	405.0287	21.5	51.8	0.8	7.7
	[(H ₃ Cit)(H ₂ Cit)Na ₂] ⁻	427.0106	27.9	45.0	1.6	13.2
	[(H ₂ Cit) ₂ Na ₃] ⁻	448.9926	16.1	16.9	2.5	16.2
	[(H₂Cit)₂NaCu(II)]⁻	465.9427	1.5			
	[(H₂Cit)(HCit)Na₂Cu(II)]⁻	487.9246	0.5			
	[(HCit) ₂ Na ₅] ⁻	492.9565	0.1		57.9	39.7
	[(HCit)₂Cu(II)Fe(III)]⁻	496.8723	1.5			
	[(H₂Cit)(HCit)Cu(II)₂]⁻	504.8745	1.1			
	[(Cit)₂NaFe(III)₂]⁻	510.8517	0.9			
	[(HCit)(Cit)NaCu(II)Fe(III)]⁻	518.8542	1.8			
	[(HCit)₂NaCu(II)₂]⁻	526.8567	1.5			
[(H ₃ Cit) ₃ Na ₂] ⁻	619.0378	3.2	10.0			
[(H ₃ Cit) ₂ (H ₂ Cit)Na ₃] ⁻	641.0198	4.2	9.0			
[(H ₃ Cit)(H ₂ Cit) ₂ Na ₄] ⁻	663.0015	3.5	3.6		2.9	
Positive	[(H ₅ Cit)] ⁺	193.0343	10.0	11.5		
	[(H ₅ Cit)(NH ₃)] ⁺	210.0608	76.9	100		
	[(H ₄ Cit)Na] ⁺	215.0162	100	78.3		
	[(H ₃ Cit)Na ₂] ⁺	236.9982	15.1	10.4		
	[(H ₂ Cit)Na ₃] ⁺	258.9801	2.8	2.4		
	[HCitNa ₄] ⁺	280.9620			100	100
	[HCitNa ₅ Cl] ⁺	338.9210			25.5	22.3
	[(H ₄ Cit) ₂ Na] ⁺	407.0432	66.4	78.9		
	[(H ₄ Cit)(H ₃ Cit)Na ₂] ⁺	429.0252	13.1	13.7		
	[(H ₃ Cit) ₂ Na ₃] ⁺	451.0071	11.5	11.5		
	[(H ₃ Cit)(H ₂ Cit)Na ₄] ⁺	472.9891	8.3	8.2		
	[(H₂Cit)₂Cu(II)Fe(III)]⁺	498.8868	2.0			
	[(H₂Cit)(HCit)NaCu(II)Fe(III)]⁺	520.8687	0.9			
	[(H₃Cit)(H₂Cit)Cu(II)₂(NH₃)]⁺	523.9160	0.4			
	[(H₂Cit)₂NaCu(II)₂]⁺	528.8712	0.9			
	[(HCit)₂Na₂Cu(II)Fe(III)]⁺	542.8506	0.7			
	[(HCit)₂(NH₃)Na₂Cu(II)Fe(III)]⁺	559.8772	0.6			
	[(H ₄ Cit) ₂ (H ₃ Cit)Na ₂] ⁺	621.0523	0.9	1.2		
	[(H ₄ Cit)(H ₃ Cit) ₂ Na ₃] ⁺	643.0342	3.2	3.8		
	[(H ₃ Cit) ₃ Na ₄] ⁺	665.0162	3.9	5.1		
[(H ₃ Cit) ₂ (H ₂ Cit)Na ₅] ⁺	686.9981	2.2	3.0			
[(H ₃ Cit) ₄ Na ₅] ⁺	879.0252	0.8	1.8			

(C₆H₄O₇)⁴⁻ = molecular building block "Cit." m/z = mass-over-charge ratio of the detected compound in FT-ICR-MS. For each sample spectrum, the citrate (or citrate-metal) molecule with the highest relative FT-ICR-MS intensity was set to = 100%, and all other detected compounds are shown in relative intensity to this compound.

TABLE 3 | Detected EDTA and EDTA ± Fe ± Cu species (bold) in the four analytical setups at the FT-ICR-MS.

Ionization	Species	m/z	MeOH + H ₂ O + NH ₄	H ₂ O + NH ₄	MeOH + H ₂ O + Na	H ₂ O + Na
Negative	[(H ₃ EDTA)] ⁻	291.0834* [#]	100	100	12.6	35.6
	[(H ₂ EDTA)Na] ⁻	313.0653	0.8	0.7	13.3	40.2
	[(H ₂ EDTA)K] ⁻	329.0392	44.4	41.8	2.6	5.1
	[HEDTANa ₂] ⁻	335.0472			99.5	81.1
	[EDTAFe(III)]⁻	343.9948*	44.5	44.9	43.1	100
	[(HEDTA)Fe(II)]⁻	345.0026	0.7	0.8	0.1	1.3
	[(HEDTA)NaK] ⁻	351.0212	0.5	0.4	33.4	22.6
	[HEDTACu(II)]⁻	351.9973*	1.8	1.7	1.6	1.8
	[EDTANa ₃] ⁻	357.0292			100	69.5
	[(HEDTA)K ₂] ⁻	366.9951	7.8	6.9	1.2	1.1
	[(EDTA)Na ₂ K] ⁻	373.0033			39.5	24.5
	[(EDTA)NaCu(II)]⁻	373.9793	0.03		1.9	2.7
	[(EDTA)KFe(II)]⁻	382.9585	0.5	0.5	0.1	
	[(EDTA)NaK ₂] ⁻	388.9771			4.6	2.7
	[(EDTA)KCu(II)]⁻	389.9532	2.9	2.8	0.8	0.8
	[(EDTA)K ₃] ⁻	404.9511	1.3	1.0	0.1	
	[EDTANa ₄ Cl] ⁻	414.9878			10.8	8.2
	[EDTANa ₅ Cl ₂] ⁻	472.9464			3.3	2.3
	[(EDTA)Na ₄ KCl ₂] ⁻	488.9204			2.1	1.3
	[(EDTA)Na ₅ KCl ₃] ⁻	546.8791			0.6	
[(H ₃ EDTA)(H ₂ EDTA)K ₂] ⁻	659.0861	4.3	3.8			
[(H ₂ EDTA)(HEDTA)Na ₄] ⁻	671.1019			0.4	1.4	
Positive	[H ₅ EDTA] ⁺	293.0979	20.5	18.1		
	[H ₄ EDTANa] ⁺	315.0798 [#]	2.1	2.7		
	[(H ₄ EDTA)K] ⁺	331.0538	100	100		
	[H₂EDTAFe(III)]⁺	346.0094	1.2	1.2		
	[(H ₃ EDTA)Cu] ⁺	354.0119	0.7	0.7		
	[(H ₂ EDTA)Na ₃] ⁺	359.0437 [#]			2.5	26.5
	[(H₂EDTA)(NH₃)Fe(II)]⁺	363.0361	0.4	0.5		
	[(H ₃ EDTA)K ₂] ⁺	369.0097	2.2	2.3		
	[(H ₂ EDTA)KNa ₂] ⁺	375.0177			1.6	11.6
	[(HEDTA)Na ₄] ⁺	381.0258 [#]			100	100
	[(EDTA)Na₂Fe(III)]⁺	389.9732			12.5	97.9
	[(H₂EDTA)KCu(II)]⁺	391.9678	1.0	1.1		
	[(HEDTA)Na ₃ K] ⁺	396.9997			41.1	35.9
	[(EDTA)Na ₅] ⁺	403.0076			12.8	15.9
	[(EDTA)KNaFe(III)]⁺	405.9472	0.02	0.02	4.7	3.8
	[(H ₂ EDTA)K ₃] ⁺	406.9656	0.7	0.7		
	[(HEDTA)Na ₂ K ₂] ⁺	412.9736			6.4	4.9
	[(EDTA)Na ₄ K] ⁺	418.9816			5.4	4.2
	[(EDTA)Na₃Cu(II)]⁺	419.9577			18.3	22.9
	[(HEDTA)K₂Cu(II)]⁺	429.9237	0.7	0.8		
[(EDTA)Na₂KCu(II)]⁺	435.9317			9.9	10.3	
[(HEDTA)Na ₅ Cl] ⁺	438.9843			11.2	10.8	

(C₁₀H₁₂N₂O₈)⁴⁻ = molecular building block "EDTA." m/z = mass-over-charge ratio of the detected compound. For each sample spectrum, the EDTA (or EDTA-metal) molecule with the highest relative intensity was set to = 100%, and all other detected compounds are shown in relative intensity to this compound. *Described by Chen et al. (2008) and [#]described by Reinoso-Maset et al. (2012).

TABLE 4 | Detected NN and NN ± Fe ± Cu species (bold) in the four analytical setups at the FT-ICR-MS.

Ionization	Species	m/z	MeOH + H ₂ O + NH ₄	H ₂ O + NH ₄	MeOH + H ₂ O + Na	H ₂ O + Na
Negative	[(NN)] ⁻	172.0404	6.2	18.7	27.3	61.9
	[(NN)NaCl] ⁻	229.9990	0.03		5.0	0.4
	[(NN)Na ₂ Cl ₂] ⁻	287.9577			0.4	0.03
	[(NN) ₂ Na] ⁻	367.0700			2.3	4.7
	[(NN)₂Cu(I)]⁻	407.0099	1.4	0.9	14.8	
	[(NN) ₂ Na ₂ Cl] ⁻	425.0287			0.3	
	[(NN)₃Fe(II)]⁻	572.0551	100	100	100	100
[(NN)₃NaClFe(II)]⁻	630.0140	0.1		0.9	1.0	
Positive	[(H ₂ NN)] ⁺	174.0550	8.1	45.4		
	[(HNN)Na] ⁺	196.0369	0.7	3.3	39.2	60.3
	[N ₃ Na ₂] ⁺	218.0188			3.3	5.8
	[(HNN)Na ₂ Cl] ⁺	253.9955			0.4	0.3
	[(NN)Na ₃ Cl] ⁺	275.9775			0.3	0.6
	[(H ₂ NN)(HNN)] ⁺	347.1026	34.0	100		
	[(HNN) ₂ Na] ⁺	369.0846	1.1	5.8	100	100
	[(HNN)(NN)Na ₂] ⁺	391.0665			16.6	12.8
	[(HNN)(NN)Cu(II)]⁺	408.0166	48.7	36.6	0.8	
	[(NN) ₂ Na ₃] ⁺	413.0485			1.0	2.0
	[(HNN) ₂ Na ₂ Cl] ⁺	427.0433	0.02		0.8	0.4
	[(NN)₂Cu(I)Na]⁺	429.9985	0.3		27.0	
	[(H ₂ NN)(HNN) ₂ (NH ₃)] ⁺	537.1770	0.9	3.0		
	[(HNN) ₃ Na] ⁺	542.1323	0.02		1.0	0.8
	[(HNN) ₂ (NN)Na ₂] ⁺	564.1144			6.1	4.6
	[(HNN)(NN)₂Fe(III)]⁺	573.0619	14.9	19.6		
	[(HNN)₂(NN)Fe(II)]⁺	574.0698	100	95.1		
	[(HNN)(NN)₂NaFe(II)]⁺	596.0514	0.8	1.0	0.03	0.04
	[(NN)₃Fe(II)Na₂]⁺	618.0335			18.5	13.1
	[(NN)₃Cu(II)₂]⁺	641.9782	2.4			
	[(HNN) ₃ (NN)Na ₂] ⁺	737.1622			0.6	0.3
	[(HNN) ₂ (NN) ₂ Na ₃] ⁺	759.1442			0.8	0.9
[(HNN)₂(NN)₂NaFe(II)]⁺	769.0993	0.5		0.2	0.03	
[(HNN)(NN)₃Na₂Fe(II)]⁺	791.0813			29.5	13.0	
[(HNN)₂(NN)₃Na₂Fe(II)]⁺	964.1292			16.1	5.0	

(C₁₀H₆NO₂)⁻ = molecular building block "NN." m/z = mass-over-charge ratio of the detected compound. For each sample spectrum, the NN (or NN-metal) molecule with the highest relative signal intensity was set to = 100%, and all other detected compounds are shown in relative intensity to this compound.

Relative Abundances of the Target Compounds

The relative FT-ICR-MS signal intensities of the target species were generally highest when methanol was present in the samples (Figure 1). In sum, citrate and EDTA compounds had their highest intensities in positive ionization mode when aq. ammonia was the added base. Contrastingly, the NN compounds had highest (total) signal intensities in positive ionization mode after sodium hydroxide additions, and SA compounds had highest signal intensities with sodium hydroxide addition and measurement in negative ionization mode. The citrate speciation patterns were dominated by free uncomplexed ligands, both in relative intensity and number of detected species, particularly in positive ionization mode (Figure 1). In comparison, all detected metal-citrate complexes had much lower intensities

and were only found in the samples with methanol + water and aq. ammonia, albeit in both ionization modes (Table 2). The abundance patterns found in the mass spectra are in line with the PHREEQC-based speciation patterns for citrate, with uncomplexed citrate accounting for the highest concentrations (88 μM), Cu-citrate species contributing the second largest amount (10 μM), and Fe citrate species contributing the least (1.3 μM). Similar to citrate, the EDTA compounds detected in the mass spectra had the highest signal intensities in the samples with methanol + water and aq. ammonia compared to those samples with sodium hydroxide. Overall highest intensities were found for the free uncomplexed EDTA, particularly in positive ionization mode, again as predicted by the PHREEQC calculations (80 μM uncomplexed EDTA; Table 3). However, Fe was calculated to be complexed with EDTA at slightly lower

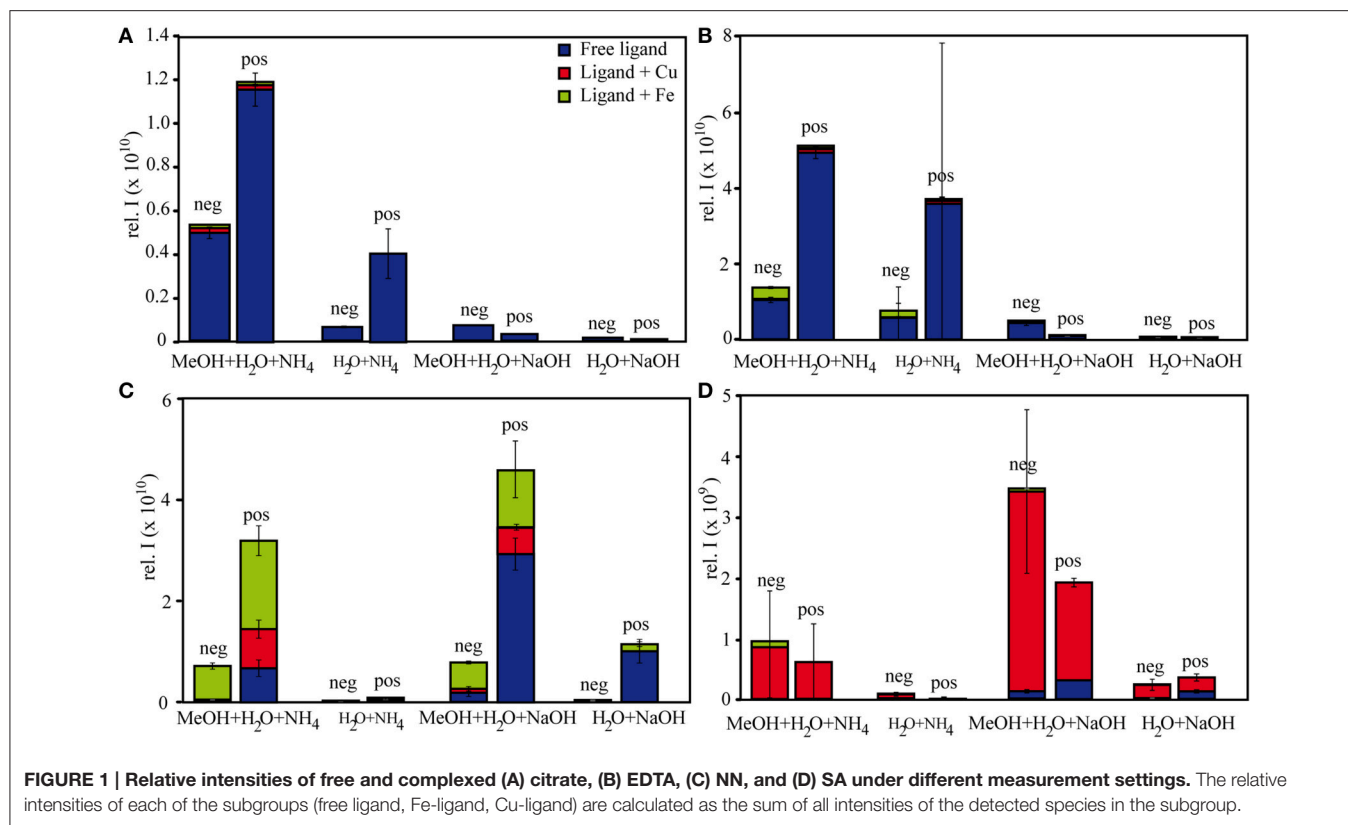
TABLE 5 | Detected SA and SA ± Fe ± Cu species (bold) in the four analytical setups in FT-ICR-MS.

Ionization	Species	m/z	MeOH + H ₂ O + NH ₄	H ₂ O + NH ₄	MeOH + H ₂ O + Na	H ₂ O + Na	
Negative	[(HSA)Na] ⁻	158.0224			1.4	2.5	
	[(H ₂ SA)NaCl] ⁻	193.9990			1.0	1.6	
	[(SA)Cu(II)]⁻	196.9544	9.4	12.1	2.6	3.4	
	[(HSA)Cu(I)]⁻	197.9622	32.2	37.1	9.4	12.5	
	[(HSA)Na ₂ Cl] ⁻	215.9810			1.2	2.2	
	[(HSA)Cl₂Fe(III)]⁻	260.9052	4.7	5.0			
	[(H ₂ SA) ₂ Na] ⁻	295.0700			0.8	1.4	
	[(HSA)₂Fe(III)]⁻	325.9996	11.8	18.5	1.8	3.6	
	[(H₂SA)(HSA)Cu(II)]⁻	334.0021	100	100	100	100	
	[(HSA)₂NaCu(II)]⁻	355.9840			7.0	6.9	
	[(H₂SA)₂(HSA)NaCu(II)]⁻	493.0318			2.0	1.6	
	Positive	[(H ₃ SA)Na] ⁺	160.0369			5.5	18.1
		[(H ₂ SA)Na ₂] ⁺	182.0188			6.0	24.9
[(HSA)Na ₃] ⁺		204.0008			2.3		
[(H ₂ SA)Na ₃ Cl] ⁺		239.9775			3.2	9.1	
[(HSA)Na ₄ Cl] ⁺		261.9594			1.3	4.9	
[(H ₃ SA) ₂ Na] ⁺		297.0846			2.4	9.1	
[(H ₃ SA)(H ₂ SA)Na ₂] ⁺		319.0665			0.9	2.1	
[(H₃SA)(H₂SA)Cu(II)]⁺		336.0166	100	100	0.3		
[(H ₂ SA) ₂ Na ₃] ⁺		341.0485			5.2	25.0	
[(H₂SA)₂NaCu(II)]⁺		357.9985			100	100	
[(H ₂ SA)(HSA)Na ₄] ⁺		363.0304			1.0	7.2	
[(H₂SA)(HSA)Na₂Cu(II)]⁺		379.9805			42.9	85.7	

(C₇H₄NO₂)³⁻ = molecular building block "SA." m/z = mass-over-charge ratio of the detected compound. For each sample spectrum, the SA (or SA-metal) molecule with the highest relative intensity was set to = 100%, and all other detected compounds are shown in relative intensity to this compound.

concentrations than Cu (8 and 10 μM, respectively), while the relative intensities of the detected species in the mass spectra decreased in the order EDTA > Fe(EDTA) > Cu(EDTA). This trend was consistent for all measurement settings, although a tendency of a relative Fe-EDTA decrease with relative Cu-EDTA increase was observed from negative to positive mode (Figure 1). Like EDTA and citrate, the NN and metal-NN compounds detected in the mass spectra had generally higher signal intensities in positive compared to negative ionization mode. In contrast to citrate and EDTA, only the relative intensities of the Fe-NN compounds were enhanced in the samples with methanol + water and aq. ammonia compared to those with sodium hydroxide. The uncomplexed ligands, as well as Cu-NN, always had their highest intensities in the samples with methanol + water measured in positive ionization mode, regardless of the added base (Figure 1). NN was the first ligand in the series for which the mass balances of the speciation calculations started to deviate substantially from the signal intensities of the corresponding compounds in the mass spectra: Calculations predicted free NN to be the major species (70 μM), while uncomplexed NN was only dominant in the FT-ICR-MS measurement settings where its signal intensities were enhanced due to Na adduct formation (Figure 1, Table 4). Furthermore, Cu was predicted to be bound only in low nanomolar concentrations (5 nM), but reached relatively higher signal intensities in the mass spectra, particularly under

conditions favoring ionization of free NN as well: There, the Cu(NN)₂ complex made up almost a third of the most abundant NN species (Table 4). Fe was calculated to occur exclusively as Fe(NN)₃ complex (10 μM) for both types of base addition, and was the dominant complex throughout the mass spectra. In the case of SA, differences between calculated concentrations and detected abundances were even more pronounced: The PHREEQC model predicted SA to occur primarily in its uncomplexed form (82 μM), but the uncomplexed ligand was almost undetectable in the mass spectra (Figure 1, Table 5). In the speciation calculations, Cu was fully complexed (2.7 μM for Cu(SA) and 7.3 μM for Cu(SA)₂), whereas Fe was mostly complexed as Fe(SA)₂ (118 nM), with very small amounts of Fe(SA) (8.2 fM). In line with these calculations, the Cu(SA)₂ peak was most prominent in the mass spectra, with more than 2-fold higher signal intensities than Cu(SA), and up to 50-fold higher signal intensities than the Fe(SA)₂ complex (Table 5). In general, the SA mass spectra also differed from those of the other ligand-metals solutions: The detected SA-compounds had overall lower intensities compared to those of the other metal-ligand solutions (up to one order of magnitude compared to NN, Figure 1), and the intensities of the detected compounds in the mass spectra were highest in samples with methanol+water matrix and sodium hydroxide as added base. Finally, the free, uncomplexed ligands were only detectable with sodium adducts in samples with added sodium hydroxide (Table 5), while Cu-SA



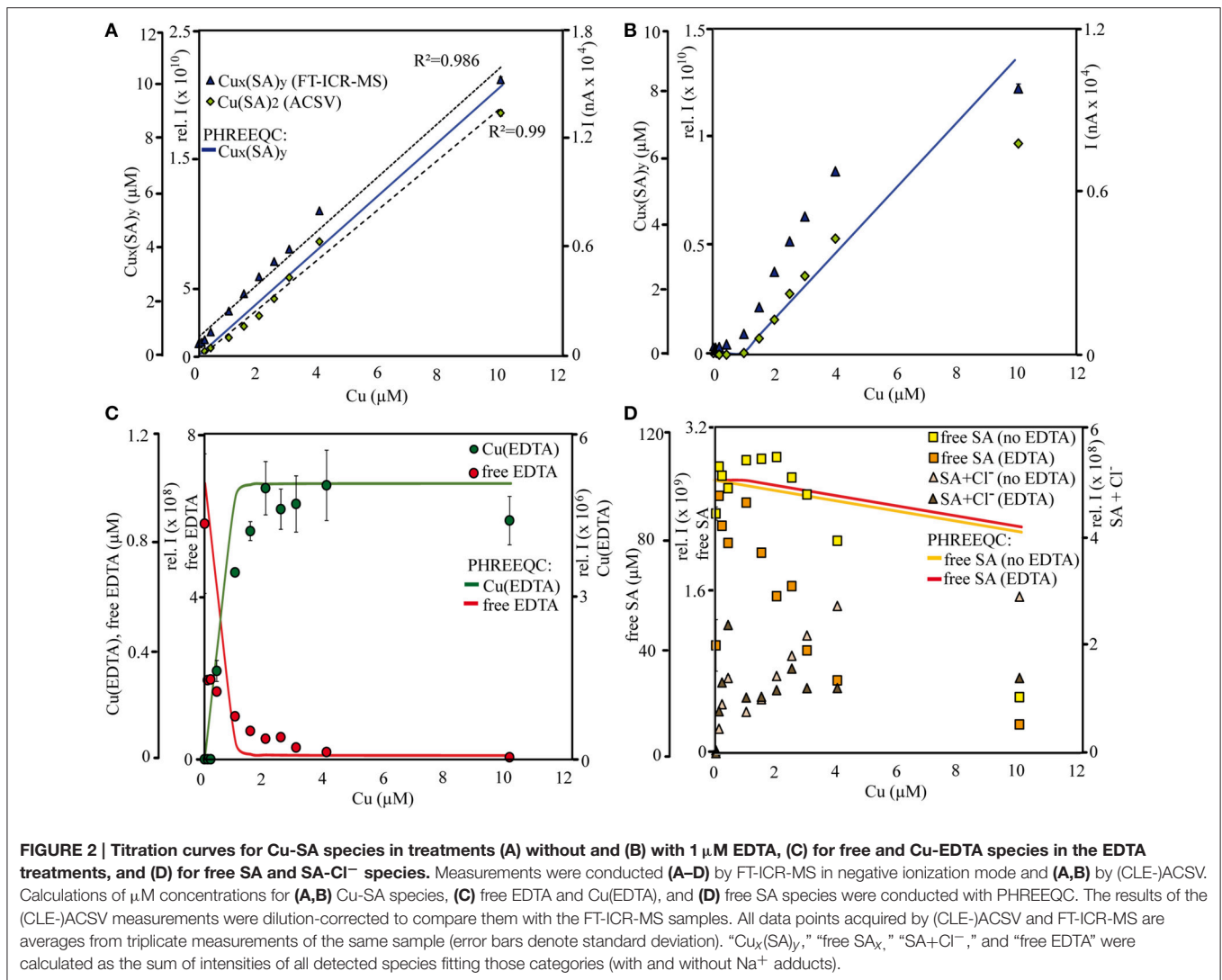
species had the highest signal intensities at all settings (Figure 1, Table 5).

Speciation and Abundances of the SA-Cu-titration Series

Overall, the distribution of the Cu-SA species in the calibration series resembled those of the qualitative SA sample solutions with the methanol + water matrix and sodium hydroxide as added base: Cu-SA mono-, di-, and trimers occurred, and the Cu(II)(SA)₂ complex had the highest signal intensities throughout the calibration series. Based on the results of the initial speciation and abundance experiments including all ligands, only the results from the ESI negative measurements were investigated in detail due to the higher signal intensities of the Cu-SA complexes with this ionization mode compared to ESI positive. In ESI negative mode, two new Cu₂(SA)₄ complexes occurred as well, most notably a [(H₂SA)₂(HSA)₂NaCu(II)₂]⁻ complex at *m/z* = 690.9938, which was detected at about ~ 10% of the signal intensity of the main Cu(II)(SA)₂ compound. The detected Cu-SA species all showed a linear increase in signal intensities when plotted against Cu concentrations, although the fit of the curve appeared to become worse at the highest amount of added Cu. In agreement with the FT-ICR-MS data, parallel measurements of dilutions of the SA-Cu-titration series via ACSV also resulted in linear response curves, although again the calibration curve seemed to decrease slightly at the highest added Cu concentration. Meanwhile, the combined Cu(SA) and Cu(SA)₂ complex concentrations calculated by

PHREEQC showed a linear increase throughout (Figures 2A,B after Cu concentrations >1 μM). In addition, the calculated relative contribution of the Cu(SA) monomer to the Cu_x(SA)_y pool was predicted to be in a similar magnitude (13–16% of the Cu(SA)₂ dimer) than what was derived from the relative signal intensities in the mass spectra (15–20%). The monomer was calculated to increase with increasing Cu concentrations by 2.7%, while FT-ICR-MS measurements revealed a slight decrease of Cu(SA) compared to Cu(SA)₂ species by 2.8%. Thus, the dominance of the Cu(SA)₂ dimer was more important than the relative contributions of the Cu(SA) monomer in instrumental setups and speciation calculations, despite the changes in the SA:Cu stoichiometries over the course of the titrations. As in the qualitative setup, PHREEQC and FT-ICR-MS results differed with regards to the abundance of the free ligand, which had overall lower signal intensities than expected from its concentration in solution, and for which the SA_x and SA_xNa_y⁺ intensities in the mass spectra initially increased upon addition of the first aliquot of the Cu calibration solution, but then decreased continuously over the rest of the titration series, and at much faster rates than the PHREEQC predictions for free SA concentrations (Figure 2D). Meanwhile, the signal intensities of SA species containing Cl⁻ adducts (SA_xNa_y⁺Cl_z⁻) in the mass spectra increased with increasing Cu solution additions (Figure 2D), but these species were likely adduct artifacts and not considered in the PHREEQC calculations.

The same Cu_x(SA)_y species occurred for the EDTA+SA+Cu equilibration titration as for that with SA and Cu alone; again,



Cu(SA)₂ was the species with the highest signal intensities, and free SA as well as SA_xNa_y⁺Cl_z⁻ compounds could be detected. In line with the Cu-SA-calibration series, we only report the ESI negative results here. In addition, several forms of uncomplexed EDTA, as well as one Cu(EDTA) complex ($[(\text{EDTA})\text{NaCu}(\text{II})]^-$, $m/z = 373.9793$) could be identified (Figure 2C). Compared to the calibration series without EDTA, the signal intensities for FT-ICR-MS and current peaks for CLE-ACSV of the Cu_x(SA)_y complexes were overall lower in this titration setup. They increased only from added Cu concentrations > 1 μM and leveled off again at Cu concentrations > 4 μM (Figure 2B). Again, the PHREEQC calculations predicted a similar amount of Cu(SA) compared to Cu(SA)₂ (13%, increasing to 15% at the highest Cu addition) as observed in the mass spectra (20.8%, decreasing to 14.8%). The PHREEQC-derived Cu_x(SA)_y curve did not show the decrease observed at Cu concentrations of 10 μM for the other two methods, and the free SA concentrations did not decrease as steeply in the speciation models as in the mass spectra (Figure 2D). Meanwhile, PHREEQC-calculated

patterns of steeply increasing Cu(EDTA) and sharply decreasing free EDTA concentrations mirrored signal intensity distribution changes recorded from the FT-ICR-MS, albeit with slightly differing curve slopes (Figure 2C). Finally, in the FT-ICR-MS spectra, free, uncomplexed SA, as well as SA_xNa_y⁺Cl_z⁻ again displayed similar increases and decreases, respectively, as in the setup with SA and Cu only (Figure 2D).

DISCUSSION

Metal-Ligand Speciation Patterns: Integrity and Reproducibility

Overall, our findings agreed well with those from other studies and the predictions from the speciation models: Most EDTA-compounds described by previous reports including uncomplexed EDTA and metal-EDTA were detected in this study as well as predicted by the PHREEQC calculations (Table 3, Chen et al., 2008; Reinoso-Maset et al., 2012). In addition, mostly

monomers, and only two dimers were detected, indicating that metal-EDTA equilibrium studies are likely to be comparable amongst different experimental and instrumental setups. Also, $\text{Fe}(\text{NN})_3$ was found to be the dominant metal-NN species in our mass spectra (**Table 4**) in line with our speciation data as well as reports from CLE-ACSV where it is used to study the Fe-complexing capacities of natural seawater samples (Gledhill and van den Berg, 1994; Wu and Luther, 1995; Hawkes et al., 2013). Furthermore, all $\text{Cu}_x(\text{SA})_y$ and $\text{Fe}_x(\text{SA})_y$ species predicted by the PHREEQC calculations and previous studies were found in our mass spectra under the tested conditions (Campos and van den Berg, 1994; Buck and Bruland, 2005; Abualhaija and van den Berg, 2014). One remarkable difference between the PHREEQC calculations and the mass spectra was the higher abundance of molecular assemblages such as tri-, tetra-, and even pentamers in the latter compared to the former (**Tables 2–5**). Analogous to (single ion) adduct formation, the formation of molecular assemblages is not uncommon in ESI. However, because data on the formation of the investigated complexes in aqueous solutions is not available, we also cannot exclude the possibility that such species also exist in aqueous solutions, but cannot be predicted because the thermodynamic equilibrium constants are not known.

Adduct formation in ESI may obscure compound identification (**Tables 2–5**): Na^+ - and K^+ -containing adducts were ubiquitous in positive ionization mode in those samples that contained Na^+ and K^+ in solution or potassium, even though PHREEQC speciation models did not predict significant concentrations of sodiated species in solution. Adduct formation in ESI was particularly pronounced for the metal-citrate solutions, where none of the metal-citrate species previously reported by others (Gautier-Luneau et al., 2005; Nischwitz and Michalke, 2009; Silva et al., 2009; Bertoli et al., 2015) could be found, although their pH and stoichiometry settings were in a comparable range to those in this study. These discrepancies can primarily be explained by a re-distribution of Na^+ , Cl^- , and H^+ (which occurred in the aqueous phase as free ions according to the PHREEQC calculations) during ionization and gas phase transfer. For example, a $\text{Fe}(\text{Cit})$ monomer ($m/z = 279.9078$) and two $\text{Cu}(\text{Cit})_2$ dimers ($m/z = 465.9427$ and 487.9246) had also been described by Bertoli et al. (2015), albeit without a Cl^- adduct for the former and without Na^+ adducts for the latter. Nischwitz and Michalke (2009) also observed a $\text{Cu}(\text{Cit})_2$ complex, but with a NH_3^+ instead of Na^+ adduct. In line with the results from the literature and our FT-ICR-MS data, the PHREEQC calculations predicted the occurrence of a $\text{Fe}(\text{Cit})$ monomer and a $\text{Cu}(\text{Cit})_2$ dimer in aqueous solution. Furthermore, in the case of both PHREEQC calculations and FT-ICR-MS measurements, $\text{Cu}_2(\text{Cit})_2$ complexes were reported to occur (**Table 2**). Finally, the $\text{Fe}_2(\text{Cit})_2$ complex ($m/z = 510.8517$) detected in our study was also listed by Gautier-Luneau et al. (2005) and Silva et al. (2009), there again containing H^+ instead of Na^+ adducts. Together with the FT-ICR-MS data and the PHREEQC speciation results, we conclude that the rearrangement of ions normally expected to freely occur in aqueous solutions, such as Na^+ , Cl^- , and H^+ , produces a wide variety of adducts during ionization. Adduct

formation in ESI is to be expected because ESI functions on this principle. In addition, e^- transfer for metal ions such as Fe and Cu, also takes place during negative ionization mode, as demonstrated especially for the complexes formed with NN (**Table 4**). Any adduct formation would be valid as long as the complex stoichiometry and net charge are preserved. The only compounds for which no literature or PHREEQC speciation data could be found were the $\text{FeCu}(\text{Cit})_2$ complexes (again, with varying amounts of Na^+ and Cl^- adducts, **Table 2**). PHREEQC predicted that <2% of the added Fe would form complexes with citrate, while $7.7 \mu\text{M}$ still occurred as $\text{Fe}(\text{OH})^{2+}$ ions. In principle, it is feasible that the remaining dissolved Fe became attached to $\text{Cu}(\text{Cit})_2$ complexes during ionization. On the other hand, to the best of our knowledge, this is the first ESI-MS study to be conducted with both metals and citrate in the same solution, and while the PHREEQC database does not contain stability constants for such a complex, the stoichiometry is theoretically possible in the aqueous environment considering the often described existence of $\text{Cu}_2(\text{Cit})_2$ and $\text{Fe}_2(\text{Cit})_2$ complexes.

As mentioned above, reduction at the ESI source produced reduced metal-ligand complexes for Fe-NN and Cu-NN, Fe-EDTA, and Cu-SA (Di Marco and Bombi, 2006; Rellán-Álvarez et al., 2008). Oddly, a reduced Fe-NN complex was also detected in positive ionization mode (**Table 4**). It is possible that partial reduction of $\text{Fe}(\text{III})(\text{NN})_3$ happened during equilibration of the aqueous samples, or that $\text{Fe}(\text{II})(\text{NN})_3$ was formed with traces of Fe(II) present in the NIST standard solution, and that this complex has a much higher response factor than $\text{Fe}(\text{III})(\text{NN})_3$, analogous to $\text{Fe}(\text{II})$ nicotianamide opposed to $\text{Fe}(\text{III})$ nicotianamide (Rellán-Álvarez et al., 2008). Changes in the oxidation state may influence the binding strength. For example, it has been suggested that reduction of Fe(III) to Fe(II) during photolysis of siderophores may increase its bioavailability (Barbeau et al., 2001). Nevertheless, the integrity of the $\text{Fe}(\text{II})(\text{NN})_3$ complex indicated that under the soft ionization conditions, the complex was still stable even if binding strengths had decreased. Incidentally, the methanol additions used for the increased ionization efficiencies could also decrease the metal-ligand binding strength, as has been demonstrated for EDTA (Xue and Traina, 1996). Within the parameters of our study, the relative intensity distributions of the samples with and without methanol do not indicate a decrease in complexing capacity with an increase of organic solvent (**Tables 2–5**), and subtle changes may have been masked by matrix-induced changes in response factors.

Metal-ligand equilibria, in particular those involving citrate, are sensitive to changes in pH (Gautier-Luneau et al., 2005; Silva et al., 2009). pH also influences ESI (Di Marco and Bombi, 2006; Van Berkel and Kertesz, 2007). During positive ionization of metal-bipyridyl complexes the pH of the ESI triplets can decrease by 4–5 units (Gatlin and Tureček, 1994) and can increase by 1–2 units during negative ionization of metal-NA complexes (Rellán-Álvarez et al., 2008). At higher pH mononuclear prevail over di- and trinuclear iron citrate complexes (Gautier-Luneau et al., 2005; Silva et al., 2009). Consistently, we found that mononuclear Fe- and Cu-citrate complexes were present in negative ionization

mode, while the samples measured in positive mode exclusively contained dinuclear metal-citrate species (Table 2). This may indicate a relative increase of the pH from positive to negative ionization settings. On the other hand, the relative intensities of the Cu(SA) species compared to those with a Cu(SA)₂ stoichiometry decreased from negative to positive mode in our study, although PHREEQC calculations over a pH range from 2 to 9 resulted in an opposite trend. It is not possible to judge whether any pH changes within the scope of our experiments may have been as dramatic as those reported by others (Gatlin and Tureček, 1994; Rellán-Álvarez et al., 2008). This is, because firstly, only near-neutral settings (7.1 ± 0.2 and 7.5 ± 0.2) were investigated, thus preventing the evaluation of artifacts based on changing ionization efficiencies with changing pH. Secondly, most tested ligands are known to form strong complexes with Fe and Cu above a pH threshold of ~ 5 , and thirdly, excess ligands were always present in solution, providing a certain buffering capacity (Rellán-Álvarez et al., 2008). It should be noted that the curves of the EDTA \pm SA⁺ titration series acquired by FT-ICR-MS matched those produced by (CLE-)ACSV, although the latter had a higher ionic strength and higher (HEPES buffered) pH (7.8) compared to the former, indicating a resilience of the tested metal-ligand equilibria toward the induced changes of the sample matrix. For studies of kinetically more labile metal-organic complexes, additional measures such as higher sample flow rates, generally low ionic strength, and/or the use of a buffer, may further prevent electrochemical interferences of the equilibria at the ESI source (Wang and Agnes, 1999; Van Berkel and Kertesz, 2007).

Relative Abundances of Detected Species: Impact of Response Factors

To a large extent, the observed abundance patterns in signal intensities depicted in Figure 1 can be explained by the relative abundances of the compounds: For example, citrate and EDTA formed 1:2 and 1:1 complexes with Fe and Cu, and thus a comparatively large proportion of free ligands still remained in solution. The high relative intensities of the free ligands corresponded to the results of the PHREEQC calculations as well (88 and 80 μM for unbound citrate and EDTA, respectively). SA formed complexes up to 1:3 stoichiometries, and NN even formed pentamer complexes with Fe, and this relative decrease in free ligands opposed to the relative increase of metal-ligand complexes is also reflected in the intensity distributions in Figure 1. However, the intensity distributions were also influenced by the different response factors (or ionization efficiencies) of the different species in the solution. For example, based on the metal-ligand stoichiometries of the detected complexes and the PHREEQC speciation calculations, SA still should have had a slightly higher amount of free ligands in solution (82 μM) compared to NN (70 μM), but the signal intensities of the free ligands were much smaller for the former compared to the latter (Figure 1). It has been previously proposed that the ionization efficiency of organic compounds increases with increasing pKa and molecular size (Oss et al., 2010). Although the pKa (which increases in the order

of citrate < EDTA < NN < SA) did not seem to have an influence on the relative ionization of the studied compounds, a slight trend of increasing signal intensities with increasing molecular weight was apparent over a wide range of compound types and measurement settings (Figure 3).

Most importantly, large differences in FT-ICR-MS signal intensities (absolute and relative) were found for all tested reagents between negative and positive ionization mode (Figures 1, 4). From Figure 4, it is evident that the signal intensities of all free ligands (citrate, EDTA, NN, and SA) increased through Na⁺ or K⁺ adduct formation in positive mode. This led to the effect that citrate and EDTA, which have net negative charges in aqueous solutions, displayed overall higher signal intensities for all compounds in positive rather than negative ionization mode (Figure 1). Citrate and EDTA solutions were prepared from sodium and potassium salts respectively, and an initial concentration of 100 μM Na⁺ was present in all sample setups for citrate, while all EDTA setups contained 300 μM K⁺. Consequently, adduct formation already occurred in the samples without added sodium hydroxide. In contrast, SA and NN had been prepared from pure ligand stock solutions, and Na adduct formation occurred mainly upon addition of sodium hydroxide, leading to overall higher response factors of the uncomplexed ligands (Figure 4). The additional input of sodium to the citrate and EDTA setups for pH adjustment did not enhance the ionization of sodiated species further, but had an opposite effect, with speciation changing drastically (Tables 2, 3, Figure 4) together with an overall sharp decrease in relative signal intensities of all (free and complexed) target compounds (Figure 1). Reinoso-Maset et al. (2012) demonstrated in their ESI-MS study on Mn-EDTA and Th-EDTA complexes, that ion suppression of EDTA occurred in negative mode as soon as metals salts were added, both through the salt additives Cl⁻ or NO₃⁻, as well as the metal ions themselves, and that signal intensities of target metal-ligand complexes could decrease up

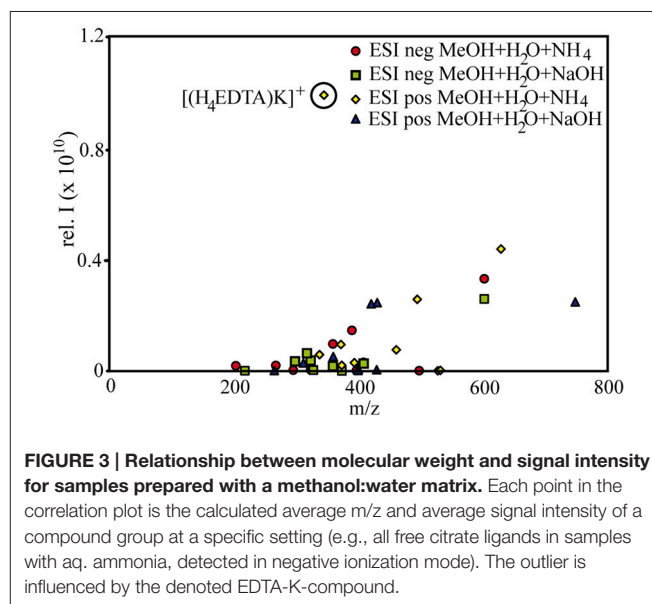


FIGURE 3 | Relationship between molecular weight and signal intensity for samples prepared with a methanol:water matrix. Each point in the correlation plot is the calculated average m/z and average signal intensity of a compound group at a specific setting (e.g., all free citrate ligands in samples with aq. ammonia, detected in negative ionization mode). The outlier is influenced by the denoted EDTA-K-compound.

to 72%. Based on our study, we suggest that small additions of cations can in fact increase the response factors in positive ionization mode, but ionization may be severely decreasing once a (sample-specific) threshold of ion concentrations has been crossed. In this respect, it is noteworthy that the added amounts of sodium hydroxide (~1 mM) in this study corresponded to the concentration ranges of the metal salts used in Reinoso-Maset et al. (2012).

In both Cu-SA-calibration series, the signal intensities of the free SA species increased after adding the first Cu aliquot, counterintuitive to the expectations that free ligand abundances should decrease with increasing Cu-SA species formation (Figure 2D). In line with our findings on EDTA and citrate, as well as the qualitative observations of free and Cu-SA ionization patterns upon addition of sodium hydroxide, this also indicates that the addition of (Na^+ , Cl^- , and Cu^{2+}) ions during the first titration had a beneficial effect on the ionization of these selected species (Figures 1, 2D). Nevertheless, the signal intensities of the free SA compounds decreased further on with increasing Cu concentrations, presumably due to scavenging by the added Cu. Overall, all acquired mass spectra had increasing signal intensities over the course of the titrations (as indicated by an increase in the sum of all signal intensities for each sample), because they were governed by the quantitative increase of the newly formed metal-ligand complexes. In fact, linear increases of signal intensities were also found for unknown compounds, for which SA-specific sum formulae could not be assigned a priori using our set criteria. The majority of these compounds were the ^{13}C or ^{65}Cu -containing masses corresponding to the detected species listed in Table 5. However, some new molecules could also be identified based on their linear increase. For example, for a compound with the $m/z = 168.9595$, which occurred in all 11 titration samples, was significantly positively correlated with Cu concentrations (Pearson's $\rho = 0.97$), and contained $^{12/13}\text{C}$ and $^{63/65}\text{Cu}$ isotopologues, we could assign the molecular formula $\text{C}_6\text{H}_4\text{CuNO}$, likely the complex of a by-product from the original SA solution with the added Cu. Thus, the titration series was a useful means to distinguish between non-related singular changes in ionization efficiencies, and actual quantitative responses of newly formed Cu-ligand complexes.

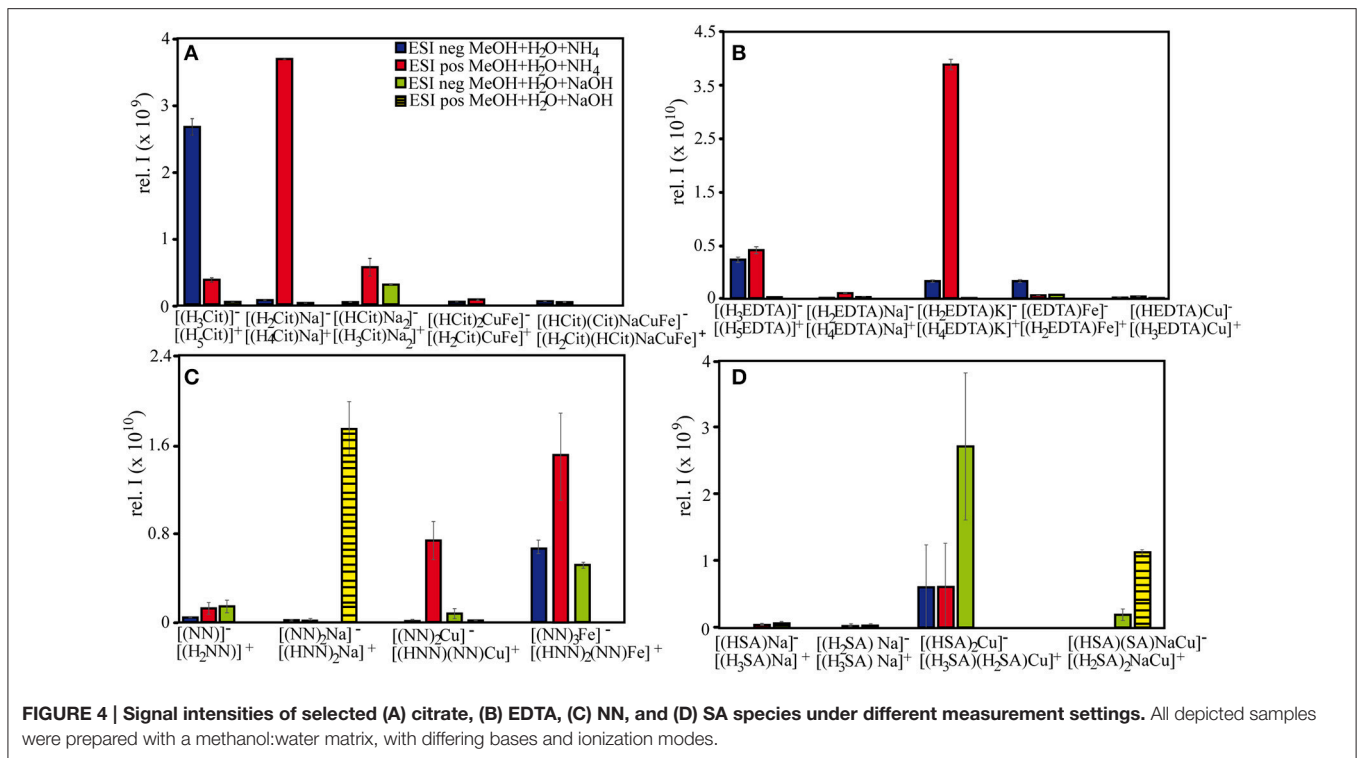
While ionization of free ligands was enhanced due to sodium or potassium adduct formation, signal intensities of metal-ligand complexes did not appear to be influenced by this process. Nevertheless, the relative abundances of the metal-ligand compounds in the mass spectra were not always representative of their thermodynamic equilibrium concentrations in aqueous solutions: For example, in the case of EDTA, the $\text{Fe}(\text{EDTA})$ signal intensities were up to 3-fold higher than expected, while $\text{Cu}(\text{EDTA})$ abundances were 3-fold lower (Figure 1, Table 3). Even more extreme were the discrepancies between free NN and free SA and their metal-ligand complexes, where the latter were up to three orders of magnitude higher than the former, despite the high thermodynamic equilibrium concentrations for the uncomplexed ligands. These patterns can partly be attributed to the relatively poor ionization efficiencies of the unbound ligands, even when their response factors were increased upon adduct formation (Figure 4). Furthermore, Cu in the speciation models was predicted to be fully >99% complexed with three

out of the four added ligands (citrate, EDTA, SA), whereas in solutions with NN, $7\ \mu\text{M}$ free Cu^{2+} were calculated to occur which may have formed adducts to the free ligand at the ESI source, thus increasing the $\text{Cu}(\text{NN})_2$ signature. For Fe, the dominant inorganic forms in aqueous solutions containing citrate and SA were $\text{Fe}(\text{III})\text{oxihydroxides}$, and $\text{Fe}_x(\text{Cit})_y$ and $\text{Fe}_x(\text{SA})_y$ complexes did occur mainly at ESI negative mode where reduction at the ESI source could cause Fe adduct formation as well. As mentioned before, the NN and SA data for the PHREEQC speciation models may not have been sufficient to explain all of the observed patterns; for example, the calculated $\text{Fe}(\text{SA})$ concentrations are very low considering that SA is used as a competitive ligand in CLE-ACSV to study the Fe-complexing capacity of natural DOM (Abualhaija and van den Berg, 2014). Probably, a combination of instrumental effects (different response factors, metal adduct, and molecular assembly formations), and lack of data for “unpredictable” compounds caused the discrepancies between the models and the measured abundance patterns.

Overall, citrate complexes with Fe and/or Cu had similar signal intensities in negative and positive ionization mode, whereas complexes of EDTA, NN, and SA with Fe appeared to ionize better in negative mode and those with Cu were relatively higher in positive mode. In line with our findings, Waska et al. (2015) showed that the desferrioxamine B (DFoB) complex with iron could be detected at concentrations as low as 1 nM via FT-ICR-MS, while DFoB-Cu was detected at the high end of the calibration series (150–300 nM), and only in positive ionization mode. In contrast, Chen et al. (2008) showed higher intensities of Cu-EDTA over Fe-EDTA at negative ionization in their study of a multi-metal-EDTA complex mixture. Finally, Rellán-Álvarez et al. (2008) found that in negative mode, the ionization efficiencies of Cu-complexes of the aminocarboxylate ligand nicotinic acid (NA) were more sensitive to changes in the capillary cone voltages of their ESI-MS(TOF) system, and more likely to decrease sharply with increasing voltages compared to those with Fe. However, all abovementioned trends in response factors of Fe-complexes and Cu-complexes during different ionization modes are empirically derived, and future studies will be necessary to explain the responsible mechanisms.

Qualitative and Quantitative Comparison of FT-ICR-MS with (CLE)-ACSV

The calibration curves of both the FT-ICR-MS and the ACSV measurements remained linear over the course of the titration series, although the curve leveled slightly off at the highest added Cu concentrations (Figure 2A). For ACSV, the limit of detection (LOD) was calculated as $\text{LOD} = 3s + a$ (a = average peak height, s = standard deviation) of the blank signal of the first sample in the titration series, where no Cu had been added. The resulting value corresponded to a Cu concentration of 1.45 nM, which is relatively high for this method (Campos and van den Berg, 1994). This is partly owed to a high Cu blank, and partly to the concentration of SA ($2\ \mu\text{M}$) in the diluted sample which decreases the sensitivity of the method by ~50% compared to the concentrations normally used for the determination of dissolved Cu (20–25 μM SA, Campos and van den Berg). In comparison, the signal intensity of the method detection limit



(MDL, Riedel and Dittmar, 2014) of the ESI-FT-ICR-MS was on average 1.01×10^6 , and corresponded to a LOD of 0.71 nM for the $\text{Cu}(\text{SA})_2$ complex with $m/z = 334.0021$. Thus, this complex is measured with a sensitivity comparable to that acquired by the ACSV method, as well as to iron-siderophore complexes, which had been reported to be detectable in the low nanomolar range for ESI-(FT-ICR)MS (Gledhill, 2001; Waska et al., 2015). If all identified $\text{Cu}_x(\text{SA})_y$ species are taken into account, the resulting calibration curve corresponds to an even lower LOD of 0.41 nM. Even though ACSV only captures the $\text{Cu}(\text{SA})_2$ complex and ESI-FT-ICR-MS revealed a multitude of $\text{Cu}_x(\text{SA})_y$ complexes, LODs in comparable orders of magnitude for the two methods were achieved in our study, and the acquired calibration curves were remarkably similar. We attribute this to the dominance of the $\text{Cu}(\text{SA})_2$ complexes (i.e., the sum of all detected $\text{Cu}(\text{SA})_2$ complexes, including Na^+ adducts) in the mass spectra, which constantly contributed the majority of the $\text{Cu}_x(\text{SA})_y$ signal intensities. The occurrence of several dimer compounds is an artifact of the FT-ICR-MS (due to adduct formation), and all dimers combined contribute to the ACSV signal as one $\text{Cu}_x(\text{SA})_y$ compound.

Analogous to the SA-Cu-calibration series, the detected Cu-complexes in the SA + EDTA + Cu competition series behaved similarly in both FT-ICR-MS and ACSV measurements (Figure 2B), and the $\text{Cu}_x(\text{SA})_y$ dimers dominated the mass spectra throughout (81.7–81.1% contribution to the total signal intensities). Furthermore, the decreasing signal intensities of the free SA and EDTA ligands with increasing Cu concentrations in the FT-ICR-MS mass spectra were similar to those of free SA in the titration series with SA and Cu alone, and indicative of ligand

scavenging of the added Cu (Figure 2D). Due to competition between EDTA and SA for free Cu, a slower increase of the SA-Cu complex signal intensities was found, especially in the low Cu concentration range (0–2 μM). Surprisingly, however, the Cu-SA complex signal intensities only increased linearly between Cu concentrations of 1.5–4 μM and then leveled off in both measurement modes, in contrast to the expectation that more, free SA and Cu should result in higher rates of Cu-SA complex formation (Figure 2B). Meanwhile, the PHREEQC calculations with the known $\text{Cu}_x(\text{SA})_y$ complex stoichiometries did not indicate a substantial equilibrium shift between the mono- and dimer, or a decrease in linearity of all accounted $\text{Cu}_x(\text{SA})_y$ complexes. In the SA + EDTA + Cu measurements *via* FT-ICR-MS, we also did not detect any new compounds in addition to the already described $\text{Cu}_x(\text{SA})_y$, $\text{Cu}(\text{EDTA})$, and free ligand types. Explanations for the decrease of the $\text{Cu}_x(\text{SA})_y$ complex intensities in both FT-ICR-MS and CLE-ACSV at the highest Cu concentration could be 2-fold: (1) through formation of yet unknown $\text{Cu} \pm \text{SA} \pm \text{EDTA}$ compounds which were undetectable in the mass spectra and/or removed from the sample solutions, for example through adsorption to the reaction vessel walls or the PTFE syringe filters before subsequent analyses; (2) due to matrix-dependent “constituent overload” of both ACSV and FT-ICR-MS: In the case of ACSV, through adsorption processes which exceed the surface capacity of the mercury drop of the working electrode (Campos and van den Berg), and in the case of FT-ICR-MS, through ion suppression (Rellán-Álvarez et al., 2008; Reinoso-Maset et al., 2012).

We calculated the concentrations and conditional stability constants of EDTA (**Figure 2B**) based on the two titration curves (the last titration point was omitted), by using the ProMCC software created for voltammetric titrations by Omanović et al. (2015). For the titration curves acquired by CLE-ACSV and FT-ICR-MS, the EDTA concentrations amounted to 1.11 ± 0.02 and $1.00 \pm 0.03 \mu\text{M}$, respectively, while the $\log K'_{\text{CuEDTA}}$ was calculated to be 17.33 ± 0.03 and 15.49 ± 0.04 , respectively. While the calculated concentrations of both methods agreed well with the added amounts of EDTA, the conditional stability constants deviated substantially from each other and from those obtained from the literature. Generally, EDTA binding constants (overall, as well as compared to SA) tend to increase with decreasing ionic strength (Campos and van den Berg, 1994), and thus one would expect a higher $\log K'_{\text{CuEDTA}}$ for the samples measured by FT-ICR-MS compared to those by CLE-ACSV, since the latter contained 0.06M KCl as additional electrolyte. K^+ and Na^+ were present in low amounts, however, and they do not provoke as strong side reactions for EDTA and SA as other salt ions usually found in seawater samples, such as Mg^{2+} or Ca^{2+} . In fact, we observed the opposite trend of a decreasing $\log K'_{\text{CuEDTA}}$ with decreasing ionic strengths of the samples, although it should be noted that they were in line with previous reports: The CLE-ACSV results are in the range of those found by Xue and Traina (1996) based on potentiometric titrations of Cu-EDTA in 50–60% methanol-water mixtures (17.35–17.87), while the FT-ICR-MS results are more similar to those calculated by Boija et al. (2014) for Cu-EDTA (15.0 ± 0.1), who used Ni as a competing metal ion and conducted measurements by ESI-MS. Thus, the acquired conditional stability constants may be subject to method-dependent artifacts (potentiometric vs. ESI-MS). Because PHREEQC calculations are always based on empirically derived parameters, the speciation models can be impacted as well, and this has to be taken into account when comparing models with instrument-derived speciation results.

Implications for Natural Metal-DOM Studies

As demonstrated by our study, FT-ICR-MS is able to capture the speciation of metal-organic complexes with a wide range of structures, binding stoichiometries, and binding strengths, and the detected species agree well with predictions from other analytical methods, earlier ESI-MS reports from the literature, and speciation calculations (**Tables 1–5**). Nevertheless, even simple artificial metal-ligand solutions can produce mass spectra of high complexity due to adduct formation or dimerization during ionization, and care must be taken in the interpretation of the results when true metal-ligand complexes present in aqueous solution are sought to be identified. Based on the signal intensities of the detected compounds (**Figures 1, 2**), we can identify several common trends for all tested ligand types: Overall, highest FT-ICR-MS signal responses were found for methanol-water mixtures, and selective ionization of metal-organic complexes in pure water solutions did not play an important role. In contrast to Stenson (2009), and in line with Silva et al. (2009), we suggest that for metal-ligand measurements, the enhanced

ionization efficiency due to the methanol matrix outweighs any potential advantage of a selective ionization of metal-containing compounds predicted for samples made up with pure water only. Furthermore, it appears that Fe-ligand complexes benefitted most from the addition of aq. ammonia rather than sodium hydroxide, and had highest signal intensities in negative ionization mode. Cu-ligands and free ligand species were overall preferentially ionized in positive mode, and the addition of a base enhanced the free ligand response factors through adduct formation, also particularly in positive ionization mode.

Although only a few specific compounds were investigated, the abovementioned observations may also be applicable to unknown natural ligands found in DOM. Traditionally, DOM is desalinated and pre-concentrated by solid-phase extraction (SPE-DOM), and FT-ICR-MS analyses of the extracts are routinely used for DOM fingerprinting of water masses as well as exometabolome studies (Dittmar et al., 2008). It has been shown that metal-organic complexes, as well as free Fe- and Cu-binding ligands, can be solid-phase extracted together with DOM (Macrellis et al., 2001; McCormack et al., 2003; Mawji et al., 2008, 2011; Velasquez et al., 2011; Waska et al., 2015). For example, in the scope of this study, we tested artificial ligands with a variety of metal-binding functional groups, including carboxylate and hydroxyl groups, as well as N-containing groups such as oximes and amines (**Table 1**). NMR analyses of marine SPE-DOM indicate that it predominantly contains carboxylic groups (Hertkorn et al., 2006; Repeta, 2015), demonstrating that functional groups such as those tested here may also occur in natural ligands. Furthermore, catecholate and hydroxamate groups typical for siderophores have been found in marine SPE-DOM using spectrophotometric methods (Macrellis et al., 2001). CLE-ACSV of natural seawater samples as well as SPE extracts also revealed that uncomplexed SPE-ligands (1) have binding strengths in the range of those found for natural seawater ($\log K'_{\text{FeL}} \sim 12$, Macrellis et al., 2001, $\log K'_{\text{CuL}} \sim 13$ –14, Waska et al., 2015) and (2) are extracted at efficiencies similar to total DOM and higher than those of intact metal-organic complexes (Waska et al., 2015). Therefore, SPE-ligands may represent a near-natural ligand population, and based on the range of the binding strengths tested in this study, we would expect the majority of metal-organic complexes with natural ligands to stay intact during ESI-MS analyses. It should be noted that the conditional stability constants from Waska et al. (2015) were derived from CLE-ACSV titrations of SPE-DOM re-dissolved in artificial seawater to correct for side reactions of SA with salt ions. For FT-ICR-MS analyses, SPE-ligands in the original desalinated extracts have to be used, and as seen from our SA-EDTA-Cu competitive titration, binding strengths may differ substantially depending on matrix and used methodology, especially when side reactions affect some ligand types in DOM to a greater extent than others (Campos and van den Berg, 1994). Thus, conditional stability constants derived from FT-ICR-MS measurements likely do not capture the complexation properties of the original water sample, although they can be used in several other ways, for example to determine ligand concentrations, intercalibrate FT-ICR-MS and CLE-ACSV, or link metal binding of SPE-ligands to other SPE-DOM characteristics such as elemental composition of

detected molecules. SPE-ligands can also be spiked with excess trace metals concentrations, and in past studies, compounds, which newly occurred in DOM mass spectra after metal salt additions, have been identified as metal-organic complexes, and confirmed by isotopic pattern recognition and/or molecular formulae assignment (“presence-absence check,” (McCormack et al., 2003; Mawji et al., 2008; Stenson, 2009; Velasquez et al., 2011)). However, the study presented here confirms previous reports (e.g., Reinoso-Maset et al., 2012) that the response factors of metal-organic compounds, as well as uncomplexed ligands, can be selectively sensitive toward changes in the sample matrix, for example through additives in trace metals solutions (for example NO_3^- , Na^+ , or Cl^-), the trace metals themselves, and enhancement/suppression effects of bases such as aq. ammonia and sodium hydroxide. Thus, simple presence-absence patterns of newly detected compounds have to be treated with caution, particularly when considering that even state-of-the-art ultra-high resolution mass spectrometry still contains uncertainties hampering isotope pattern recognition and molecular formulae assignments, for example due to peak overlaps (Waska et al., 2015). Based on the results from our study, we propose that presence-absence studies could be conducted as titrations within the range of the natural ligand pool instead of excess equilibrations, to track linear increases in signal intensities. This approach still includes uncertainties due to metal adduct formation as opposed to the production of “real” aqueous metal-ligand complexes, and for it to be a valid knock-out criterion, we suggest a co-evaluation of the sample complexing capacity using CLE-ACSV, and/or the employment of a competing ligand such as SA or NN to scavenge excess metals. In addition, molecular formulae assignments and isotope pattern recognition in sample scans at high resolution (for example, through mass window isolation) may aid in the unambiguous identification of metal-organic target compounds in SPE-DOM.

CONCLUSION

In this study, we applied a soft ionization mass spectrometric technique with ultra-high resolution (FT-ICR-MS) to characterize equilibria of the model ligands citrate, EDTA, 1-nitroso-2-naphthol, and salicylaldehyde with iron (Fe) and copper (Cu). In general, methanol-containing samples had much higher sensitivities compared to those only containing water. We also suggest that easily ionized ligands, such as citrate and EDTA (and possibly, carboxylic-rich DOM), produce better results with aqueous ammonia as added base, while less polar ligands such as NN and SA may profit from an ionization-enhancing base like sodium hydroxide. In comparison with a PHREEQC speciation model, the predicted metal-ligand complex stoichiometries all were found in the tested sample solutions, although the patterns were sometimes obscured by

REFERENCES

Abualhaija, M. M., and van den Berg, C. M. G. (2014). Chemical speciation of iron in seawater using catalytic cathodic stripping voltammetry with

instrument-based dimerization or adduct formation. The signal intensities of some compounds (for example, unbound NN and SA, or $\text{Cu}(\text{NN})_2$ and $\text{Fe}(\text{SA})$ complexes) differed from predicted concentrations, indicating that ionization efficiencies may impact the abundance distribution patterns of some metal-ligand equilibria. An intercomparison between CLE-ACSV and FT-ICR-MS revealed that FT-ICR-MS-derived complex formation is a quantitative process which can be used to (1) identify unknown compounds based on their linear increase with increasing added metal concentrations, and (2) calculate the concentration of a titrated free ligand (in the case of this study, EDTA). Although no conclusive evidence was found for an impact of pH or organic solvent (methanol) on the overall integrity of the compounds or their linear increase with increasing concentrations, FT-ICR-MS- and CLE-ACSV-calculated conditional stability constants differed. Thus, we conclude that FT-ICR-MS-derived conditional stability constants can only be compared between similarly processed sample types such as SPE-DOM measured by MS. We finally suggest that CLE-ACSV should be used for an a priori characterization of the natural sample and corresponding SPE-DOM ligand pool, with FT-ICR-MS being applied for subsequent molecular characterizations, for example, based on the methods described in this paper. This approach will provide novel insights into the large, yet unknown pool of small organic ligands still hidden in DOM.

AUTHOR CONTRIBUTIONS

HW planned and conducted this study and wrote the manuscript. TD, AK contributed to data interpretation and writing of the manuscript.

FUNDING

This work was funded by a DFG “Eigene Stelle” fellowship to HW (WA3067/2-1).

ACKNOWLEDGMENTS

We would like to thank Katrin Klaproth, Heike Simon, Andrea Mentges, and Jeff Hawkes for technical assistance and insightful comments on the study. Furthermore, we are indebted to David Turner and Janek Greskowiak for their valuable advice on PHREEQC speciation modeling.

SUPPLEMENTARY MATERIAL

The Supplementary Material for this article can be found online at: <http://journal.frontiersin.org/article/10.3389/fmars.2016.00119>

ligand competition against salicylaldehyde. *Mar. Chem.* 164, 60–74. doi: 10.1016/j.marchem.2014.06.005

Abualhaija, M. M., Whitby, H., and van den Berg, C. M. G. (2015). Competition between copper and iron for humic ligands in estuarine

- waters. *Mar. Chem.* 172, 46–56. doi: 10.1016/j.marchem.2015.03.010
- Barbeau, K., Rue, E. L., Bruland, K. W., and Butler, A. (2001). Photochemical cycling of iron in the surface ocean mediated by microbial iron(III) binding ligands. *Nature* 413, 409–413. doi: 10.1038/35096545
- Bertoli, A. C., Carvalho, R., Freitas, M. P., Ramalho, T. C., Mancini, D. T., Oliveira, M. C., et al. (2015). Structural determination of Cu and Fe-citrate complexes: theoretical investigation and analysis by ESI-MS. *J. Inorg. Biochem.* 144, 31–37. doi: 10.1016/j.jinorgbio.2014.12.008
- Bojja, S., Almesäker, A., Hedenström, E., Bylund, D., Edlund, H., and Norgren, M. (2014). Determination of conditional stability constants for some divalent transition metal ion-EDTA complexes by electrospray ionization mass spectrometry. *J. Mass Spectrom.* 49, 550–556. doi: 10.1002/jms.3372
- Buck, K. N., and Bruland, K. W. (2005). Copper speciation in San Francisco Bay: a novel approach using multiple analytical windows. *Mar. Chem.* 96, 185–198. doi: 10.1016/j.marchem.2005.01.001
- Buck, K. N., Lohan, M. C., Berger, C. J. M., and Bruland, K. W. (2007). Dissolved iron speciation in two distinct river plumes and an estuary: implications for riverine iron supply. *Limnol. Oceanogr.* 52, 843–855. doi: 10.4319/lo.2007.52.2.0843
- Campos, M. L. A. M., and van den Berg, C. M. G. (1994). Determination of copper complexation in sea water by cathodic stripping voltammetry and ligand competition with salicylaldehyde. *Anal. Chim. Acta* 284, 481–496. doi: 10.1016/0003-2670(94)85055-0
- Chen, Z., Sun, Q., Xi, Y., and Owens, G. (2008). Speciation of metal-EDTA complexes by flow injection analysis with electrospray ionization mass spectrometry and ion chromatography with inductively coupled plasma mass spectrometry. *J. Sep. Sci.* 31, 3796–3802. doi: 10.1002/jssc.200800292
- Di Marco, V. B., and Bombi, G. G. (2006). Electrospray mass spectrometry (ESI-MS) in the study of metal-ligand solution equilibria. *Mass Spectrom. Rev.* 25, 347–379. doi: 10.1002/mas.20070
- Dittmar, T., Koch, B., Hertkorn, N., and Kattner, G. (2008). A simple and efficient method for the solid-phase extraction of dissolved organic matter (SPE-DOM) from seawater. *Limnol. Oceanogr. Methods* 6, 230–235. doi: 10.4319/lo.2008.6.230
- Furia, T. E. (1972). “Sequestrants in food,” in *CRC Handbook of Food Additives*, ed T. E. Furia (Boca Raton, FL: CRC Press), 271–294.
- Gatlin, C. L., and Tureček, F. (1994). Acidity determination in droplets formed by electrospraying methanol-water solutions. *Anal. Chem.* 66, 712–718. doi: 10.1021/ac00077a021
- Gautier-Luneau, I., Merle, C., Phanon, D., Lebrun, C., Biaso, F., Serratrice, G., et al. (2005). New trends in the chemistry of iron(III) citrate complexes: correlations between X-ray structures and solution species probed by electrospray mass spectrometry and kinetics of iron uptake from citrate by iron chelators. *Chem. Eur. J.* 11, 2207–2219. doi: 10.1002/chem.200401087
- Gledhill, M. (2001). Electrospray ionization-mass spectrometry of hydroxamate siderophores. *Analyst* 126, 1359–1362. doi: 10.1039/b101268l
- Gledhill, M., and van den Berg, C. M. G. (1994). Determination of complexation of iron(III) with natural organic complexing ligands in seawater using cathodic stripping voltammetry. *Mar. Chem.* 47, 41–54. doi: 10.1016/0304-4203(94)90012-4
- Hawkes, J. A., Gledhill, M., Connelly, D. P., and Achterberg, E. P. (2013). Characterisation of iron-binding ligands in seawater by reverse titration. *Anal. Chim. Acta* 766, 53–60. doi: 10.1016/j.aca.2012.12.048
- Hertkorn, N., Benner, R., Frommberger, M., Schmitt-Kopplin, P., Witt, M., Kaiser, K., et al. (2006). Characterization of a major refractory component of marine dissolved organic matter. *Geochim. Cosmochim. Acta* 70, 2990–3010. doi: 10.1016/j.gca.2006.03.021
- Keith-Roach, M. J. (2010). A review of recent trends in electrospray ionization-mass spectrometry for the analysis of metal-organic ligand complexes. *Anal. Chim. Acta* 678, 140–148. doi: 10.1016/j.aca.2010.08.023
- Keller, B. O., Sui, J., Young, A. B., and Whittall, R. M. (2008). Interferences and contaminants encountered in modern mass spectrometry. *Anal. Chim. Acta* 627, 71–81. doi: 10.1016/j.aca.2008.04.043
- Koch, B. P., Dittmar, T., Witt, M., and Kattner, G. (2007). Fundamentals of molecular formula assignment to ultrahigh resolution mass data of natural organic matter. *Anal. Chem.* 79, 1758–1763. doi: 10.1021/ac061949s
- Koch, B. P., Witt, M., Engbrodt, R., Dittmar, T., and Kattner, G. (2005). Molecular formulae of marine and terrigenous dissolved organic matter detected by electrospray ionization Fourier transform ion cyclotron resonance mass spectrometry. *Geochim. Cosmochim. Acta* 69, 3299–3308. doi: 10.1016/j.gca.2005.02.027
- Macrellis, H. M., Trick, C. G., Rue, E. L., Smith, G., and Bruland, K. W. (2001). Collection and detection of natural iron-binding ligands from seawater. *Mar. Chem.* 76, 175–187. doi: 10.1016/S0304-4203(01)00061-5
- Mawji, E., Gledhill, M., Milton, J. A., Tarran, G. A., Ussher, S., Thompson, A., et al. (2008). Hydroxamate siderophores: occurrence and importance in the Atlantic Ocean. *Environ. Sci. Technol.* 42, 8675–8680. doi: 10.1021/es801884r
- Mawji, E., Gledhill, M., Milton, J. A., Zubkov, M. V., Thompson, A., Wolff, G. A., et al. (2011). Production of siderophore type chelates in Atlantic Ocean waters enriched with different carbon and nitrogen sources. *Mar. Chem.* 124, 90–99. doi: 10.1016/j.marchem.2010.12.005
- McCormack, P., Worsfold, P. J., and Gledhill, M. (2003). Separation and detection of siderophores produced by marine bacterioplankton using high-performance liquid chromatography with electrospray ionization mass spectrometry. *Anal. Chem.* 75, 2647–2652. doi: 10.1021/ac0340105
- Nischwitz, V., and Michalke, B. (2009). Electrospray ionization with selected reaction monitoring for the determination of Mn-citrate, Fe-citrate, Cu-citrate, and Zn-citrate. *Rapid Comm. Mass Spectrom.* 23, 2338–2346. doi: 10.1002/rcm.4156
- Nowack, B. (2002). Environmental chemistry of aminocarboxylate chelating agents. *Environ. Sci. Technol.* 36, 4009–4016. doi: 10.1021/es025683s
- Omanović, D., Garnier, C., and PiZeta, I. (2015). ProMCC: an all-in-one tool for trace metal complexation studies. *Mar. Chem.* 173, 25–39. doi: 10.1016/j.marchem.2014.10.011
- Oss, M., Krueve, A., Herodes, K., and Leito, I. (2010). Electrospray ionization efficiency scale of organic compounds. *Anal. Chem.* 82, 2865–2872. doi: 10.1021/ac902856t
- Parkhurst, D. L., and Appelo, C. A. J. (1999). *User's Guide to PHREEQC (Version 2) – A Computer Program for Speciation, Batch-Reaction, One-Dimensional Transport, and Inverse Geochemical Calculations*. U. S. Geological Survey Water-Resources Investigations Report, 99-4259.
- Reinoso-Maset, E., Worsfold, P. J., and Keith-Roach, M. J. (2012). Evaluation of electrospray ionization mass spectrometry as a technique for the investigation of competitive interactions: a case study of the ternary Th-Mn-EDTA system. *Rapid. Comm. Mass Spectrom.* 26, 2755–2762. doi: 10.1002/rcm.6404
- Rellán-Álvarez, R., Abadía, J., and Álvarez-Fernández, A. (2008). Formation of metal-nicotianamine complexes as affected by pH, ligand exchange with citrate and metal exchange. A study by electrospray ionization time-of-flight mass spectrometry. *Rapid. Comm. Mass Spectrom.* 22, 1553–1562. doi: 10.1002/rcm.3523
- Repeta, D. (2015). “Chemical characterization and cycling of dissolved organic matter,” in *Biogeochemistry of Dissolved Organic Matter*, eds D. A. Hansell and C. A. Carlson (Boston, MA: Academic Press), 21–63.
- Riedel, T., and Dittmar, T. (2014). A method detection limit for the analysis of natural organic matter via Fourier transform ion cyclotron resonance mass spectrometry. *Anal. Chem.* 86, 8376–8382. doi: 10.1021/ac501946m
- Ross, A. R. S., Ikononou, M. G., and Orians, K. J. (2003). Characterization of copper-complexing ligands in seawater using immobilized copper(II)-ion affinity chromatography and electrospray ionization mass spectrometry. *Mar. Chem.* 83, 47–58. doi: 10.1016/S0304-4203(03)00095-1
- Rue, E. L., and Bruland, K. W. (1995). Complexation of iron(III) by natural organic ligands in the Central North Pacific as determined by a new competitive ligand equilibration/adsorptive cathodic stripping voltammetric method. *Mar. Chem.* 50, 117–138. doi: 10.1016/0304-4203(95)00031-L
- Sathe, R. M., and Shetty, S. Y. (1970). Potentiometric studies of the complexes of Be²⁺ and Cu²⁺ with some naphthalene derivatives. *J. Inorg. Nucl. Chem.* 32, 1383–1386. doi: 10.1016/0022-1902(70)80140-3
- Seidel, M., Yager, P. L., Ward, N. D., Carpenter, E. J., Gomes, H. R., Krusche, A. V., et al. (2015). Molecular-level changes of dissolved organic matter along the Amazon River-to-ocean continuum. *Mar. Chem.* 177, 218–231. doi: 10.1016/j.marchem.2015.06.019
- Silva, A. M., Kong, X.-L., Parkin, M. C., Cammack, R., and Hider, R. C. (2009). Iron(III) citrate speciation in aqueous solution. *Dalton Trans.* 40, 8616–8625. doi: 10.1039/b910970f

- Stenson, A. C. (2009). Fourier transform ion cyclotron resonance mass spectral characterization of metal-humic binding. *Rapid. Comm. Mass Spectrom.* 23, 465–476. doi: 10.1002/rcm.3889
- Van Berkel, G. J., and Kertesz, V. (2007). Using the electrochemistry of the electrospray ion source. *Anal. Chem.* 79, 5510–5520. doi: 10.1021/ac071944a
- Van den Berg, C. M. G. (1984). Determination of the complexing capacity and conditional stability constants of complexes of copper(II) with natural organic ligands in seawater by cathodic stripping voltammetry of copper-catechol complex ions. *Mar. Chem.* 15, 1–18. doi: 10.1016/0304-4203(84)90035-5
- Van den Berg, C. M. G., Nimmo, M., Abollino, O., and Mentasi, E. (1991). The determination of trace levels of iron in seawater using adsorptive cathodic stripping voltammetry. *Electroanalysis* 3, 477–484. doi: 10.1002/elan.1140030606
- Velasquez, I., Nunn, B. L., Ibisamni, E., Goodlett, D. R., Hunter, K. A., and Sander, S. G. (2011). Detection of hydroxamate siderophores in coastal and Sub-Antarctic waters off the South Eastern Coast of New Zealand. *Mar. Chem.* 126, 97–107. doi: 10.1016/j.marchem.2011.04.003
- Wang, H., and Agnes, G. R. (1999). Kinetically labile equilibrium shifts induced by the electrospray process. *Anal. Chem.* 71, 4166–4172. doi: 10.1021/ac981375u
- Waska, H., Koschinsky, A., Ruiz Chanchos, M. J., and Dittmar, T. (2015). Investigating the potential of solid-phase extraction and Fourier-transform ion cyclotron resonance mass spectrometry (FT-ICR-MS) for the isolation and identification of dissolved metal-organic complexes from seawater. *Mar. Chem.* 173, 78–92. doi: 10.1016/j.marchem.2014.10.001
- Wu, J., and Luther, G. W. (1995). Complexation of Fe(III) by natural organic ligands in the Northwest Atlantic Ocean by a competitive ligand equilibration method and a kinetic approach. *Mar. Chem.* 50, 159–177. doi: 10.1016/0304-4203(95)00033-N
- Xue, Y., and Traina, S. J. (1996). Stability of metal-organic complexes in acetone- and methanol-water mixtures. *Environ. Sci. Technol.* 30, 3177–3183. doi: 10.1021/es950740l

Conflict of Interest Statement: The authors declare that the research was conducted in the absence of any commercial or financial relationships that could be construed as a potential conflict of interest.

Copyright © 2016 Waska, Koschinsky and Dittmar. This is an open-access article distributed under the terms of the Creative Commons Attribution License (CC BY). The use, distribution or reproduction in other forums is permitted, provided the original author(s) or licensor are credited and that the original publication in this journal is cited, in accordance with accepted academic practice. No use, distribution or reproduction is permitted which does not comply with these terms.